IRON COMPLEXES WITH TERDENTATE LIGANDS: PREPARATION, ELECTRONIC STRUCTURE DETERMINATION, AND UTILITY AS CATALYST PRECURSORS

A Dissertation

Presented to the Faculty of the Graduate School

of Cornell University

In Partial Fulfillment of the Requirements for the Degree of

Doctor of Philosophy

by

Ryan J. Trovitch

January 2009

© 2009 Ryan J. Trovitch

IRON COMPLEXES WITH TERDENTATE LIGANDS: PREPARATION, ELECTRONIC STRUCTURE DETERMINATION, AND UTILITY AS CATALYST PRECURSORS

Ryan J. Trovitch, Ph. D.

Cornell University 2009

A series of bis(imino)pyridine iron complexes bearing monoanionic ligands, (PDI)Fe-X (PDI = 2,6-$(ArN=CMe)_2C_5H_3N$; X = halide, alkyl, alkoxide, carboxylate) has been prepared and the electronic structure of each compound investigated. Combining spectroscopic, X-ray crystallographic, and magnetic data, the electronic structure of the halide, alkoxide, and carboxylate complexes has been described as having a high-spin ferrous center that is antiferromagnetically coupled to a bis(imino)pyridine radical. Magnetic and Mössbauer spectroscopic data collected on the carboxylate complexes revealed a lower degree of antiferromagnetic coupling for due to a weaker ligand field. The electronic structure of the alkyl complexes appeared highly dependent on field strength of the hydrocarbyl group; sp^3-alkyls were found to have high-spin ferrous centers while acetylides had intermediate spin centers. The electronic structure of the alkyl complex, (^{iPr}PDI)Fe-(η^3-C_3H_5), was best described as having an intermediate-spin ferric center antiferromagnetically coupled to two chelate radicals. The preparation of bis(imino)pyridine iron alkyl complexes possessing β-hydrogen atoms was accomplished from the substoichiometric addition of alkyl bromides to (^{iPr}PDI)Fe$(N_2)_2$. Because the electronic structure of the alkyl and halide complexes was elucidated, this reaction has been described as a one-electron oxidative addition, where oxidation occurs at the bis(imino)pyridine ligand rather than the metal. For these alkyls, the kinetic stability of each complex at ambient temperature was inversely proportional to the number of β-hydrogen atoms present. A series of

deuterium labeling experiments confirmed fast and reversible β-hydrogen elimination and that transfer dehydrogenation of chelate isopropyl groups was a main decomposition pathway. Additionally, the scope of (^{iPr}PDI)Fe(N_2)$_2$ mediated olefin hydrogenation has been expanded to include amine, ether, ketone, and ester containing substrates. Conducting stoichiometric experiments between each substrate and (^{iPr}PDI)Fe(N_2)$_2$ in the absence of 4 atmospheres of dihydrogen revealed important catalyst degradation pathways. The C-O bond cleavage of allylic and vinylic ethers was observed over the course of hours at ambient temperature while ester addition to (^{iPr}PDI)Fe(N_2)$_2$ often resulted in C-O bond cleavage to form the corresponding alkyl and carboxylate complexes. Although the redox-active bis(imino)pyridine chelate is known to stabilize a reducing ferrous center, one electron processes have often resulted in catalyst decomposition.

BIOGRAPHICAL SKETCH

Ryan James Trovitch was born and raised in the small coal-mining town of Hazleton, located in Northeastern Pennsylvania. He attended middle and high school at MMI Preparatory School (Mining and Mechanical Institute of Freeland) and developed a penchant for competitive sports and mischievous behavior. Of equal importance, he received a solid introduction to many academic fields but found the instruction of chemistry from Dr. David W. Stiller to be the most fascinating. After graduating high school in 2000, Ryan stayed in NEPA to attend King's College and was extremely fortunate to take general chemistry from and do research with Prof. Robert L. LaDuca. While learning to use a glove box as a freshman, he characterized a series of copper and nickel metal-organic frameworks and was hooked on inorganic chemistry upon realizing that he possessed the "world's supply" of those coordination polymers. In 2003, he spent a summer in the laboratory of Prof. Mark M. Banaszak-Holl at the University of Michigan investigating germylene mediated C-H bond activation as an REU Fellow. Ryan graduated *summa cum laude* from the King's College Honors Program in 2004 and decided to continue studying inorganic chemistry at Cornell University. After hesitantly shunning the recommendations of Professors LaDuca and Banaszak-Holl to join the Wolczanski group, he commenced his graduate work in the laboratory of Prof. Paul J. Chirik immediately thereafter. During his time at Cornell, Ryan acquired an immeasurable amount of knowledge pertaining to the ever-expanding field of iron chemistry, met an incredible woman, and learned an awful lot about himself in the process. Ryan hopes to address the world's energy concerns while conducting postdoctoral research at Los Alamos National Laboratory under the guidance of Dr. Kevin John and Dr. R. Tom Baker, starting in September of 2008. Without leaving behind his scientific background, he hopes to pursue a career in academia, business, or politics and positively influence society in any way possible.

Terence and Jean Trovitch

Ida Kimock

Brittany Held

ACKNOWLEDGMENTS

During my time at Cornell, many different people have helped to make this manuscript a reality. First and foremost, I would like to thank my advisor, Prof. Paul Chirik, for his continuous scientific input and mentorship. His dedication to the chemistry presented in this dissertation has never waivered. On a personal level, his advisement has forced me to mature in ways I never thought possible and has helped me realize the level of intellectual rigor required to become a professional scientist.

The direct work of a few other highly talented scientists is presented in this work, for which they must be acknowledged. I would like to thank Prof. Suzanne Bart for her assistance in acquiring SQUID and EPR data on a few of the complexes presented in Chapter 1 and Appendix A. Similarly, I would like to thank her advisor, Prof. Karsten Meyer, for his collaborative interest in studying the electronic structure of these iron compounds. I am grateful for the groundbreaking chemistry Suzanne discovered during her time at Cornell, as it helped form the backdrop of my project. I would also like to thank a second pair of German collaborators, Prof. Karl Wieghardt and Dr. Eckhard Bill, for their assistance in collecting Mössbauer spectroscopic data on a few of the complexes discussed in Chapters 1 and 3. During my last few years at Cornell, I was also fortunate to work with Prof. Bradley Wile on a few of the complexes presented in Chapter 1 and Appendix A.

There are also quite a few scientists at Cornell that I would like to acknowledge for their help over the years. The X-ray crystallographic data collected by Emil Lobkovsky has been invaluable in determining the electronic structure of many of the complexes discussed in detail throughout this manuscript. Without his work, many of the scientific claims made in this dissertation would remain in question. I would like to thank Pete Wolczanski, one of my special committee members, for his insights regarding my research and for helping me to develop scientifically. In the

process of sitting through four graduate classes taught by Pete, I have learned an enormous amount of fundamental inorganic and organometallic chemistry that I will carry with me throughout my career. I would like to thank the Abruña group, especially Samuel Flores-Torres and Neus Vila-Cusco, for their assistance in collecting electrochemical data. I would also like to thank the Freed group for their help in collecting the EPR data presented in Appendix B. Ivan Keresztes and Tony Condo were helpful in answering an endless number of NMR related questions that have come up. John Terry, Tom McCarrick, Dave Wise, Ralph Personius, and many other Cornell University Department of Chemistry and Chemical Biology staff members were extremely helpful in addressing the day-to-day problems that came up over the years. Finally, I would like to thank Prof. Geoff Coates for acting as the third member of my special committee.

Since joining the Chirik group, I have been blessed to work alongside some of the best and brightest organometallic chemists of my generation. In acknowledging past and present group members, there is no one better to start with than Wes Bernskoetter. Had he not taken me under his wing in the beginning of my second year, I may have gotten replaced by a Chinese post-doc (though the smell of dried fish would have nauseated Paul to no end). Wes always had the time to help me figure out new laboratory or NMR techniques, regardless of how busy he was. Suzanne, along with Eric and Marco, spent a significant amount of time showing me the ropes and teaching me how to interpret paramagnetic NMR spectra, a skill that proved extremely important throughout my time at Cornell. Foreign post-docs Ignacio and Brad were great coworkers and both provided tremendous scientific and personal advice (along with a few laughs) in the short time they spent at Cornell.

I would like to thank all of the other past and present Chirik group members for their help and support over the years. I am particularly indebted to the people I've

spent the most time with in the group (besides Scott), Doris and Mandy. Without their help running the group the last few years, things definitely wouldn't have run as smoothly as they did.

Most importantly, I would like to dedicate this dissertation to those that have provided me with an endless amount of support throughout graduate school and the course of my education. Brittany has been a stabilizing force in my life and she deserves a *big* medal for the number of times she has willingly listened to me talk (or complain) about my research. I will always be grateful for her desire to follow me to the Land of Enchantment. Ever since I was little, my parents have always pushed me to do work with my head, rather than my hands. Although life has not proven to be quite so simple (I still need both), their encouragement throughout my years of education has been invaluable. I would also like to dedicate this dissertation to my Grandma, Ida Kimock. She is at least partially responsible for the person I have become and I will never forget the years of wisdom and advice she has shared with me.

TABLE OF CONTENTS

Biographical Sketch iii

Dedication iv

Acknowledgements v

Table of Contents viii

List of Figures xi

List of Tables xv

Chapter 1: Preparation and Electronic Structure Elucidation of Bis(imino)pyridine Iron Complexes Bearing X-Type Ligands

1.1 Abstract 1

1.2 Introduction 2

1.3 Monohalide Complexes 4

1.4 Preparation and Electronic Structure of Monoalkyl Complexes 15

1.5 Other X-type PDI Complexes 31

1.6 Mössbauer Spectroscopy 37

1.7 Conclusion 41

1.8 Experimental Procedures 42

References 54

Chapter 2: *β*-Hydrogen Containing Bis(imino)pyridine Iron Alkyl Complexes: Preparation, Kinetic Stability, and Decomposition Pathways

2.1 Abstract 56

2.2 Introduction 57
2.3 Preparation and Characterization of β-Hydrogen Containing Alkyls 60
2.4 Stability and Decomposition Products 66
2.5 Deuterium Labeling Studies 68
2.6 Discussion 75
2.7 Conclusion 78
2.8 Experimental Procedures 78
References 84

Chapter 3: Bis(imino)pyridine Iron Catalyzed Olefin Hydrogenation: Substrate Scope, Functional Group Tolerance, and Identification of Catalyst Resting States

3.1 Abstract 87
3.2 Introduction 88
3.3 Scope of Hydrogenation 91
3.4 Catalyst Resting States 96
3.5 Electronic Structure of Neutral Ligand Complexes 104
3.6 Discussion 110
3.7 Conclusion 110
3.8 Experimental Procedures 111
References 128

Chapter 4: Carbon-Oxygen Bond Cleavage with Bis(imino)pyridine Iron

4.1 Abstract 130
4.2 Introduction 131

4.3 Ether Bond Cleavage 133
4.4 Cleavage of Ester C-O Bonds 137
4.5 Deuterium Labeling Experiments 150
4.6 Discussion 153
4.7 Conclusion 160
4.8 Experimental Procedures 161
References 170

Chapter 5: Bis(diisopropylphosphino)pyridine Iron Complexes: Preparation, Reactivity, and Assessment of Catalytic Hydrogenation Activity

5.1 Abstract 173
5.2 Introduction 174
5.3 Preparation of PNP Iron Complexes 175
5.4 Evaluation of Catalytic Activity 190
5.5 Discussion 194
5.6 Conclusions 195
5.7 Experimental Procedures 196
References 204

Appendix A: Preliminary Investigations 207

Appendix B: Investigation of PDI Iron Complexes by EPR Spectroscopy 248

Appendix C: Crystal Structure Data 257

LIST OF FIGURES

1.1 One electron reduction of PDI iron dihalide precursors. 4

1.2 Solid state magnetic susceptibility data for **1-Br**. 5

1.3 ^{1}H NMR spectrum of **1-Br**. 6

1.4 Temperature dependent ^{1}H NMR shifts of **1-Br** resonances. 7

1.5 Molecular structure of **1-Br(THF)**. 8

1.6 Molecular structure of **2-Cl(Et_2O)**. 10

1.7 Molecular structure of **1-(FBF_3)(Et_2O)**. 12

1.8 Alkylation of bis(imino)pyridine iron monohalides with MeLi. 16

1.9 Alkylation of bis(imino)pyridine iron halide complexes with neosilyllithium. 17

1.10 Preparation of bis(imino)pyridine iron neopentyl complexes. 19

1.11 Solid state structure of **2-Np**. 19

1.12 Synthesis of 4-coordinate ^{iPr}PDI iron acetylide complexes. 21

1.13 Molecular structure of **1-CC^{t}Bu**. 22

1.14 Molecular structure of **1-CCPh.** 23

1.15 Solid state magnetic susceptibility data for **1-Np**. 27

1.16 Preparation of **1-Allyl** from Grignard addition to **1-Br**. 28

1.17 Molecular structure of **1-Allyl.** 30

1.18 Preparation of bis(imino)pyridine iron carboxylate complexes. 34

1.19 Molecular structure of **1-OBz**. 35

1.20 Molecular structure of **1-H_2CIN**. 36

1.21 Mössbauer spectrum of **1-H_2CIN** at 80 K. 38

1.22 Qualitative molecular orbital calculated for **1-Cl**. 39

1.23 Proposed electronic structure of (PDI)Fe-X complexes. 41

2.1 Reaction of isobutyllithium with **1-Br**. 60

2.2 Addition of ethyl bromide to **1-$(N_2)_2$**. 62

2.3 Preparation of **1-^{n}Bu** and **1-^{i}Bu**. 63

2.4 Evidence for radical cyclization by formation of **1-$CH_2{}^c$Pent**. 63

2.5 ^{1}H NMR spectrum of **1-Et**. 65

2.6 Decomposition of **1-Et** by way of transfer hydrogenation. 66

2.7 Thermal stability of bis(imino)pyridine iron alkyl complexes. 67

2.8 Bis(imino)pyridine deuterium incorporation from bromoethane-d_5. 69

2.9 Isotopic exchange observed for **1-Et-d_5**. 70

2.10 Facile ligand exchange between **1**-Br** and **1-$(N_2)_2$**. 72

2.11 Observation of deuterated butane and butenes from **1*-^{n}Bu** degradation. 73

2.12 Transfer hydrogenation of 1-hexene. 74

2.13 Alkyl group exchange through fast β-hydrogen elimination. 74

2.14 Ligand based oxidative addition of alkyl bromides to **1-$(N_2)_2$**. 75

2.15 Mechanism of **1-Et** degradation and transfer hydrogenation. 76

3.1 α,β-Unsaturated ketones that induce decomposition of **1-$(N_2)_2$** under catalytic hydrogenation conditions. 93

3.2 Catalytic deuteration of allylamine and 5-hexen-2-one with **1-$(N_2)_2$**. 96

3.3 Preparation of bis(imino)pyridine iron amine complexes. 97

3.4 Amine exchange at bis(imino)pyridine iron. 98

3.5 Preparation of bis(imino)pyridine iron ketone complexes. 99

3.6 Ketone exchange at bis(imino)pyridine iron. 101

3.7 Ester and amide TIP complexes of bis(imino)pyridine iron. 102

3.8 Ground and excited state electronic structure of bis(imino)pyridine iron neutral ligand complexes. 104

3.9 ^{1}H NMR spectrum of **1-OC(Ph)$_2$** in benzene-d_6 at 293 K. 105

3.10 Solid state structure of **1-OC(Ph)$_2$** at 30 % probability ellipsoids. 106

3.11 ^{57}Fe Mössbauer spectra of **1-OC(Me)Ph** and **1-OC(Ph)$_2$**. 108

4.1 Substrate dependent catalytic activity of **1-(N$_2$)$_2$**. 132

4.2 Scope of ether C-O bond cleavage with **1-(N$_2$)$_2$**. 134

4.3 Vinyl bromide addition to **1-(N$_2$)$_2$**. 135

4.4 Theromolytic preparation of **1-Aryl** from **1-(N$_2$)$_2$**. 136

4.5 C-O bond cleavage of *trans*-methyl cinnamate with **1-(N$_2$)$_2$**. 138

4.6 Synthesis of **1-(OAc)(Vinyl)** and **1-(OBz)(Vinyl)**. 139

4.7 Solid-state structure of **1-(OAc)(Vinyl)**. 141

4.8 Formation of **1-OAc** by ester C-O bond cleavage. 142

4.9 Solid-state structure of **1-(OAc)**. 143

4.10 Oxidation of the bis(imino)pyridine chelate accompanying ester cleavage. 144

4.11 Oxidation of one ligand and one metal center upon allyl acetate cleavage with **1-(N$_2$)$_2$**. 145

4.12 Acyl C-O bond cleavage of phenyl acetate at **1-(N$_2$)$_2$**. 146

4.13 Cleavage of ethyl acetate at 65 °C. 147

4.14 Cleavage of ethyl benzoate with **1-(N$_2$)$_2$** and observation of **1-Et**. 148

4.15 Scope of ester and acyl C-O bond cleavage with **1-(N$_2$)$_2$**. 149

4.16 Utilization of formates for the preparation of ^{iPr}PDI iron alkoxide complexes. 150

4.17 Formation of **1-OAc-*d$_3$*** and **1-CD$_3$** from cleavage of methyl acetate-d_6. 151

4.18 Deuterium exchange at the methylene position of ethyl acetate. 152

4.19 Deuterium labeling of ethyl acetate. 152

4.20 Mechanism of ether cleavage with **1-(N$_2$)$_2$**. 157

4.21 Proposed mechanism of ester C-O bond cleavage mediated by **1-$(N_2)_2$**. 158

4.22 Proposed mechanism of deuterium exchange observed for **1-EtOAc**. 159

5.1 Preparation of ^{iPr}PNP iron dihalide starting materials and the reduction of **4-Br_2** under 1 atmosphere of CO. 176

5.2 ^{1}H NMR spectra of **4-Cl_2** and **4-Br_2** at 293 K in chloroform-*d*. 177

5.3 Molecular structure of **4-$(CO)_2$** at 30 % probability ellipsoids. 178

5.4 Preparation of **4-Cl(Me)** by salt metathesis. 180

5.5 ^{1}H NMR spectra of **4-Cl(Me)** at 293 K in benzene-d_6. 181

5.6 Synthetic routes to **4-$H_2(N_2)$** and **4-H(SiH_2Ph)N_2**. 182

5.7 Routes of hydride exchange for **4-$H_2(N_2)$**. 183

5.8 Molecular structure of **4-H(SiH_2Ph)N_2** with 30% probability ellipsoids. 185

5.9 Reactivity of **4-$H_2(N_2)$** and **4-H(SiH_2Ph)N_2** towards carbon monoxide. 187

5.10 Molecular structure of **4-H(SiH_2Ph)(CO)** with 30% probability ellipsoids. 188

5.11 Ligand substitution to prepare **4-H(SiH_2Ph)(PMe_3)**. 190

5.12 Formation of **4-$H_2(H_2)$** along with iron-hydride equilibration. 192

5.13 Conversion of **4-H(SiH_2Ph)N_2** to **4-H(SiH_2Ph)(H_2)** under 4 atmospheres of H_2 in benzene-d_6. 193

5.14 Proposed pathway for isotopic exchange in **4-H(SiH_2Ph)N_2** upon treatment with D_2 gas. 194

LIST OF TABLES

1.1 Selected bond distances (Å) and angles (°) for **1-Br(THF)**. 8

1.2 Selected bond distances (Å) and angles (°) for **2-Cl(Et_2O)**. 10

1.3 ^{1}H NMR resonances of bis(imino)pyridine iron monohalide complexes. 11

1.4 Selected bond distances (Å) and angles (°) for **1-(FBF_3)(Et_2O)**. 13

1.5 ^{1}H NMR resonances of bis(imino)pyridine iron monoalkyl complexes. 16

1.6 Selected bond distances (Å) and angles (°) for **2-Np**. 20

1.7 Selected bond distances (Å) and angles (°) for **1-CC^{t}Bu**. 22

1.8 Selected bond distances (Å) and angles (°) for **1-CCPh**. 24

1.9 Solution magnetic susceptibility of bis(imino)pyridine iron alkyl complexes 26

1.10 Selected bond distances (Å) and angles (°) for **1-Allyl**. 30

1.11 Selected bond distances (Å) and angles (°) for **1-OBz**. 35

1.12 Selected bond distances (Å) and angles (°) for **1-H_2CIN**. 36

1.13 Mössbauer parameters ($mm \cdot s^{-1}$) for (PDI)Fe-X complexes at 80 K. 38

2.1 ^{1}H NMR resonances for bis(imino)pyridine iron alkyl complexes. 65

3.1 Catalytic hydrogenation of ether-substituted substrates, fluorinated styrenes, and trans-β-methylstyrene with **1-(N_2)$_2$**. 92

3.2 Hydrogenation of carbonyl containing substrates with **1-(N_2)$_2$**. 94

3.3 Catalytic hydrogenation of amino-substituted olefins and 4-methyl-1-pentene with **1-(N_2)$_2$**. 95

3.4 Diagnostic benzene-d_6 ^{1}H NMR shifts of newly prepared bis(imino)pyridine complexes that exhibit temperature independent paramagnetism. 100

3.5 Selected bond distances (Å) and angles (°) for **1-OC(Ph)$_2$**. 107

4.1 Selected bond distances (Å) and angles (°) for **1-(OAc)(Vinyl)**. 141

4.2 Selected bond distances (Å) and angles (°) for **1-(OAc)**. 144

5.1 Selected bond distances (Å) and angles (°) for **4-$(CO)_2$**. 179

5.2 Metrical parameters for **4-H(SiH_2Ph)N_2**. 186

5.3 Selected metrical parameters for **4-H(SiH_2Ph)(CO)**. 189

CHAPTER 1

PREPARATION AND ELECTRONIC STRUCTURE ELUCIDATION OF BIS(IMINO)PYRIDINE IRON COMPLEXES BEARING X-TYPE LIGANDS*

1.1 Abstract

A series of bis(imino)pyridine iron monohalide complexes (^{Ar}PDI)FeX (X = Cl, Br; ^{Ar}PDI = 2,6-(*Ar*N=CMe)$_2$C$_5$H$_3$N; *Ar* = 2,6-^{i}Pr$_2$-C$_6$H$_3$ (^{iPr}PDI), 2,6-Et$_2$-C$_6$H$_3$ (^{Et}PDI), 2,4,6-Me$_3$-C$_6$H$_2$ (^{Mes}PDI)) have been prepared by treatment of the corresponding dihalide with 1 equivalent of NaBEt$_3$H. The reactivity of these complexes towards σ-donors has been investigated and the molecular structure of several resulting 5-coordinate complexes have been determined by single crystal X-ray diffraction. Attempts to prepare an iron monofluoride from reaction of (^{iPr}PDI)Fe(N$_2$)$_2$ and BF$_3$·Et$_2$O resulted in the formation of (^{iPr}PDI)Fe(FBF$_3$)(Et$_2$O), a 5-coordinate square pyramidal complex in which a monoanionic η^1-BF$_4$ ligand occupies the apical coordination site. Treatment of the monohalide halide complexes with alkyllithium reagents resulted in isolation of the corresponding bis(imino)pyridine iron alkyl complexes. In cases where a 5-coordinate iron dialkyl could not be isolated (R = Me, Np, C≡C^{t}Bu, C≡CPh), preparation of the monoalkyl complexes was achieved from the reductive alkylation of the corresponding dihalide with 2 equivalents of the alkyllithium reagent. Addition of either alcohols or carboxylic acids to (^{iPr}PDI)Fe(N$_2$)$_2$ resulted in immediate formation of the corresponding iron alkoxide or carboxylate complex, respectively. The electronic structure of representative 4- and 5-coordinate complexes has been investigated by X-ray crystallography, Mössbauer spectroscopy,

* Parts of this chapter have been taken from (a) Bouwkamp, M. W.; Bart, S. C.; Hawrelak, E. J.; Trovitch, R. J.; Lobkovsky, E.; Chirik, P. J. *Chem. Commun.* **2005**, 3406-3408. Reproduced by permission of The Royal Society of Chemistry. (b) Fernández, I. F.; Trovitch, R. J.; Lobkovsky, E.; Chirik, P. J. *Organometallics* **2008**, *27*, 109-118. Copyright 2008 American Chemical Society.

SQUID magnetometry. Many complexes have been described as having a high-spin iron(II) center antiferromagnetically coupled to a monoanionic bis(imino)pyridine chelate. In the case of the acetylide complexes, an increase in field strength was observed and the electronic structure has been described as having an intermediate-spin ferrous center antiferromagnetically coupled to a chelate radical. One complex, the bis(imino)pyridine iron allyl complex, exhibited spectral and structural data consistent with a ferric metal center and doubly reduced ^{iPr}PDI ligand.

1.2 Introduction

Over the last decade, aryl-substituted bis(imino)pyridine ligands, ^{Ar}PDI (2,6-(*Ar*N=CMe)$_2$C$_5$H$_3$N; *Ar* = 2,6-^{i}Pr$_2$-C$_6$H$_3$ (^{iPr}PDI), 2,6-Et$_2$-C$_6$H$_3$ (^{Et}PDI), 2,4,6-Me$_3$-C$_6$H$_2$ (^{Mes}PDI)) have become a heavily utilized class of ligands due to their ease of synthesis,[1,2] electronic modularity,[3] and their ability to coordinate to a wide range of transition and alkali metal ions.[4] The π-accepting capability of these ligands is well established: bis(imino)pyridine ligands have been found to stabilize iron complexes in which the metal center is *formally* in the 2- oxidation state.[5] Electronically, the bis(imino)pyridine ligands appear to be as π-acidic as carbon monoxide;[3] however, these ligands are not limited to two electron reduction and tend to participate in facile one electron redox events.[6,7]

One example that vividly highlights this ligand property is the stepwise reduction of (^{iPr}PDI)FeCl$_2$.[8] On route to (^{iPr}PDI)Fe(N$_2$)$_2$,[9] aliquots of the dihalide reduction in the presence of excess of 0.5 % sodium amalgam at early reaction times allowed observation of the iron monochloride intermediate, (^{iPr}PDI)FeCl.[10] Isolation of this complex in high yield was accomplished by treating the dihalide with one equivalent of NaBEt$_3$H.[10] A comprehensive investigation into the electronic structure of (^{iPr}PDI)FeCl utilizing spectroscopic, crystallographic, and computational data

established that the bis(imino)pyridine ligand is monoreduced and antiferromagnetically coupled to a high spin ferrous center.[8] One electron reduction of (^{iPr}PDI)FeCl to (^{iPr}PDI)Fe(N_2)$_2$ occured at the ^{iPr}PDI ligand rather than the metal center and the ground state of the latter complex has been described as having a doubly reduced ligand that antiferromagnetically couples to an intermediate spin Fe(II) center.[8]

Monohalide complexes other than (^{iPr}PDI)FeCl have also been reported. The preparation of (^{iPr}PDI)FeBr and (^{Mes}PDI)FeCl has been accomplished by addition of one equivalent of $NaBEt_3H$ to the respective dihalide.[10] Alkylation of (^{iPr}PDI)FeCl or (^{iPr}PDI)$FeCl_2$ with one or two equivalents of MeLi, respectively, resulted in the isolation of (^{iPr}PDI)FeMe.[10] Subsequently, reductive alkylation of (^{iPr}PDI)$FeCl_2$ with 2 equivalents of PhLi yielded (^{iPr}PDI)FePh.[11] Interest in isolating well-defined bis(imino)pyridine iron alkyl and dialkyl[10-14] complexes stems from the observation that, upon activation with methylaluminoxane (MAO), (PDI)FeX_2 complexes are highly active for the polymerization of α-olefins.[15,16] Cationic iron(II) and dicationic iron (III) alkyl complexes have been proposed to be the active species for this transformation;[17,18] however, it remains likely that the active species has a chemically modified ligand as a result of MAO addition to the iron dihalide complex.[12] Examples of cationic bis(imino)pyridine iron alkyl complexes were later isolated from treatment of (^{iPr}PDI)Fe(CH_2SiMe_3)$_2$ with a borate reagent and shown to polymerize ethylene, but this result was independent of MAO activation.[19] Over-reduction to form anionic bis(imino)pyridine iron alkyl complexes has been reported[11,20] and these complexes were found to be active for ethylene polymerization upon treatment with MAO.[20]

Understanding the reversible electron transfer capabilities of the bis(imino)pyridine ligand framework remains a fundamental task and is crucial to the design of catalysts bearing redox-active ligands. Because reduction of

bis(imino)pyridine iron halide complexes occurs at the ligand, the oxidation of (^{iPr}PDI)Fe(N_2)$_2$ was anticipated to be a viable way to prepare new PDI iron complexes. In this chapter, the electronic structure of several bis(imino)pyridine iron halide, alkyl, alkoxide, and carboxylate complexes has been investigated and comparisons made to the initial electronic structure description reported for (^{iPr}PDI)FeCl.[8]

1.3 Monohalide Complexes

In an attempt to expand the number of bis(imino)pyridine (PDI) monohalide precusors that could be employed for the preparation of iron alkyl complexes, (^{Et}PDI)$FeCl_2$ (**2-Cl$_2$**) [^{Et}PDI = 2,6-(2,6-$Et_2C_6H_3N$=CMe)$_2C_5H_3N$],[21] and (^{Mes}PDI)$FeBr_2$ (**3-Br$_2$**) [^{Mes}PDI = 2,6-(2,4,6-$Me_3C_6H_2N$=CMe)$_2C_5H_3N$][16] were prepared by stirring the appropriate ligand and iron dihalide in tetrahydrofuran. The reduction of these dihalide precursors with one equivalent of $NaBEt_3H$ resulted in the isolation of the respective PDI iron monohalide complexes (Figure 1.1).

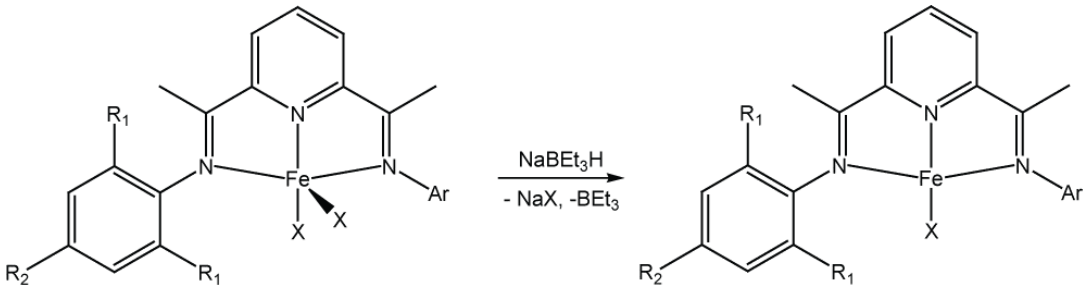

Figure 1.1. One electron reduction of PDI iron dihalide precursors.

Magnetic moments determined by Evans method solution magnetometry[22] (benzene-d_6, 20 °C) for **2-Cl** and **3-Br** were 4.0(2) μ_B and 3.8(2) μ_B, respectively. While this data is consistent with an overall $S = 3/2$ spin state, investigating the

magnetic susceptibility of **1-Br** by variable temperature SQUID magnetometry produced a plot with μ_{eff} values ranging from 3.6 to 4.5 μ_B (5 – 300 K) (Figure 1.2, top). Plotting the inverse of χ over this range produced a linear fit, confirming that **1-Br** behaves as a simple paramagnet (Figure 1.2, bottom). The ambient temperature value of 4.5 μ_B, which was effectively reproduced from four independently prepared samples of **1-Br**, suggests that the experimental Evans method values obtained for the monohalide complexes [**1-Br**: μ_{eff} = 3.9(2) μ_B (benzene-d_6, 20 °C)] are systematically low but remain within error. A spin-Hamiltonian simulation of the magnetic data yielded the following values: g = 2.429, $|D|$ = 9.3 cm^{-1}, and E/D = 0.

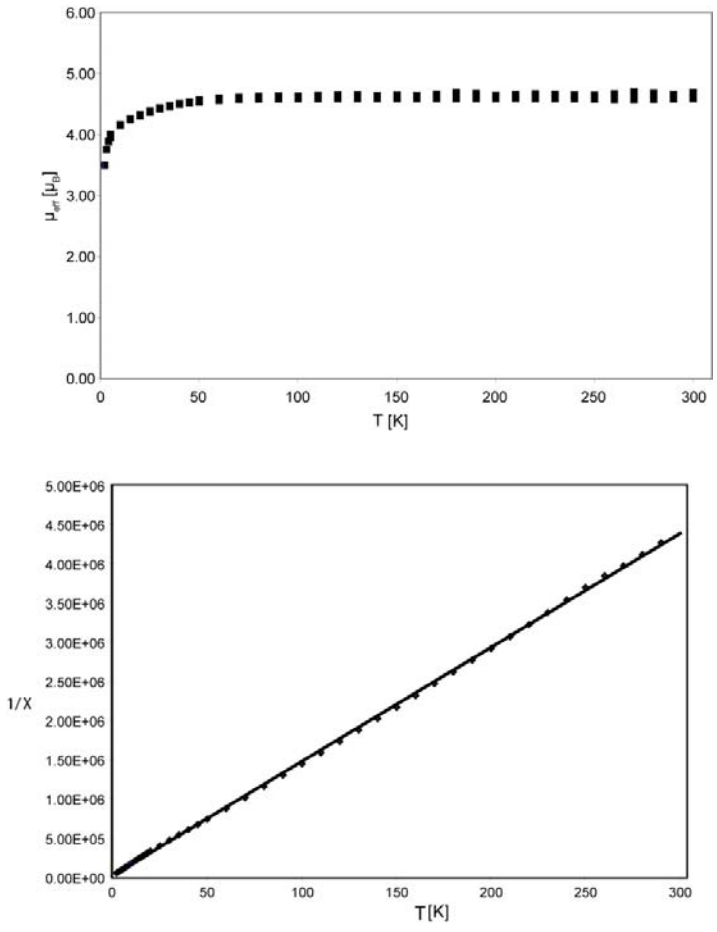

Figure 1.2. Solid state magnetic susceptibility data for **1-Br** (top, four trials) and Curie plot from 5 K to 300 K (bottom).

The ^{1}H NMR spectrum of **1-Br** (Figure 1.3, top) at 20 °C exhibits paramagnetically broadened resonances over a 600 ppm range, with the hydrogen atoms in the chelate plane experiencing the greatest shift from their diamagnetic reference values.[23] For example, the imine methyl resonance appears at -212.71 ppm while the *p*-pyridine peak is at 388.94 ppm, a direct function of being in conjugation with the iron center. The isopropyl methine resonance is shifted significantly upfield due to a through-space interaction with the metal center. The spectrum of **1-Br** was monitored upon cooling to 193 K and movement of the resonances towards the diamagnetic region followed Curie behavior (Figure 1.4). However, these linear fits did not accurately extrapolate to the diamagnetic reference value of the resonances.[23]

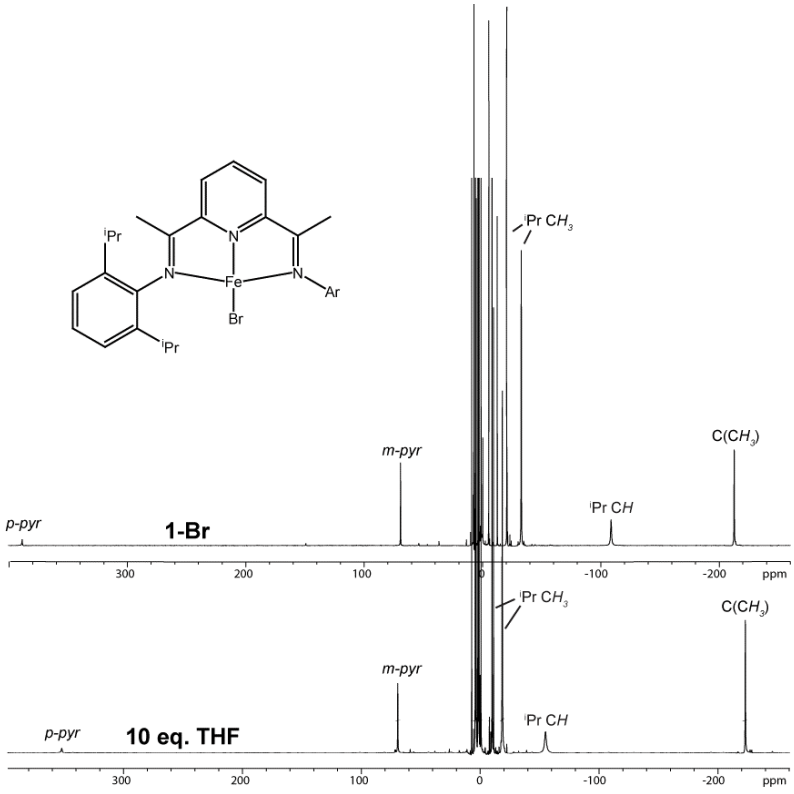

Figure 1.3. ^{1}H NMR spectrum of **1-Br** (top) and **1-Br** in the presence of 10 equivalents of tetrahydrofuran (bottom). Both spectra recorded in benzene-d_6 at 20 °C.

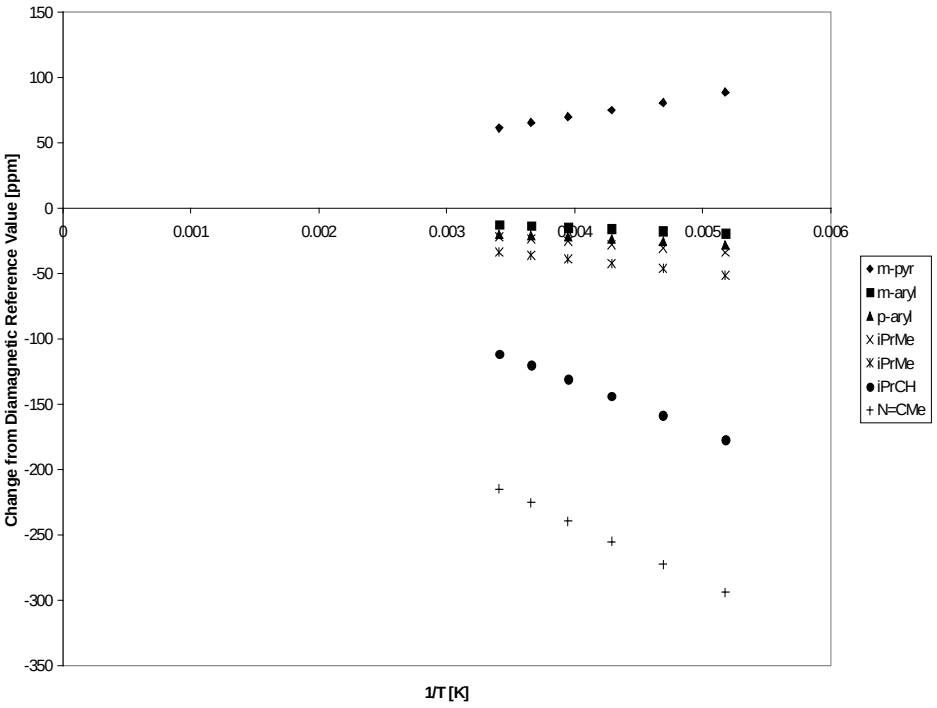

Figure 1.4. Temperature dependent ^{1}H NMR shifts of select **1-Br** resonances in toluene-d_8.

Addition of 10 equivalents of tetrahydrofuran to a benzene-d_6 solution of **1-Br** resulted in dramatic shifting of these resonances, with the imine methyl and *p*-pyridine resonances moving 37 ppm and 10 ppm upfield, respectively (Figure 1.3, bottom). The *m*-pyridine resonance generally appears around 68 ppm and is less sensitive to the nature of the X-type ligand or substrate coordination than the other chelate backbone resonances. The isopropyl methine resonance shifts the most upon tetrahydrofuran coordination, as this interaction shields the through space interaction between this position and the iron center. Recrystallization of concentrated pentane solutions of **1-Br** in the presence of tetrahydrofuran at -35 °C afforded crystals of **1-Br(THF)** suitable for X-ray diffraction. The solid state structure of **1-Br(THF)** is presented in Figure 1.5 with selected bond distances (Å) and angles (°) tabulated in Table 1.1. Dissolving this complex in benzene-d_6 afforded ^{1}H NMR resonances that are slightly shifted for **1-Br** along with broad tetrahydrofuran peaks.

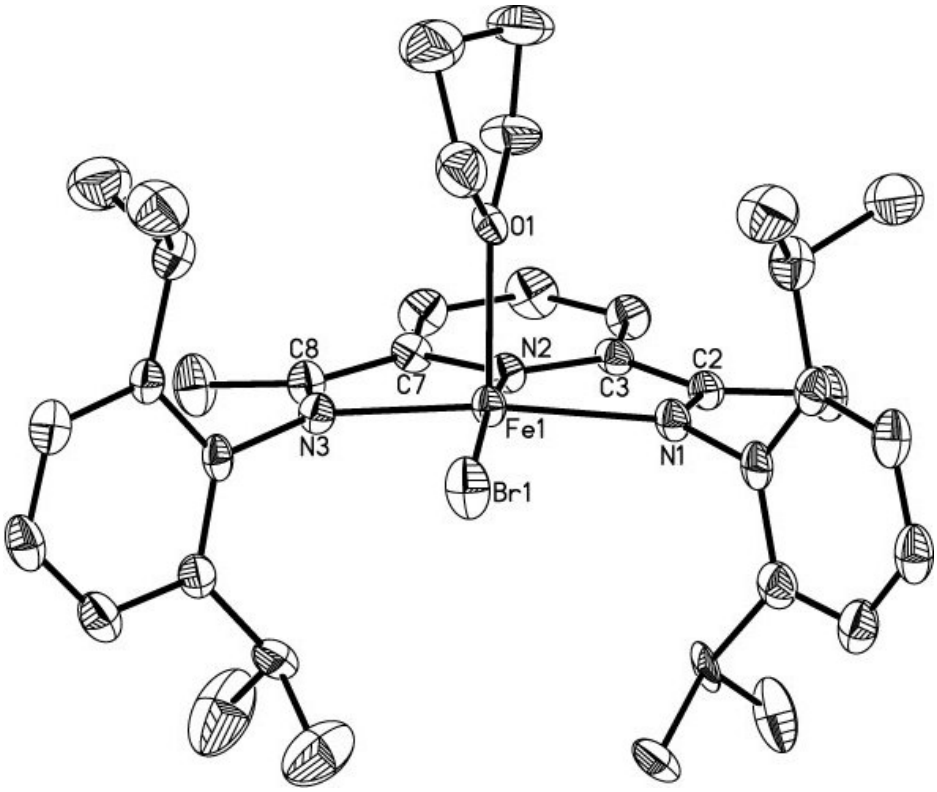

Figure 1.5. Molecular structure of **1-Br(THF)** at 30 % probability ellipsoids. Hydrogen atoms omitted for clarity.

Table 1.1. Selected bond distances (Å) and angles (°) for **1-Br(THF)**.

Fe(1)-N(1)	2.172(3)	N(3)-C(8)	1.306(4)
Fe(1)-N(2)	2.008(3)	C(2)-C(3)	1.446(5)
Fe(1)-N(3)	2.150(3)	C(7)-C(8)	1.433(5)
Fe(1)-O(1)	2.166(5)	N(2)-Fe(1)-O(1)	92.64(15)
Fe(1)-Br(1)	2.4165(6)	N(2)-Fe(1)-Br(1)	167.89(9)
N(1)-C(2)	1.299(4)		

The overall molecular geometry of **1-Br(THF)** is close to idealized square pyramidal with an N(2)-Fe(1)-Br(1) bond angle of 167.89(9)°. The disordered tetrahydrofuran ligand, for which two rotamers were successfully modeled, occupies the apical position of the coordination sphere with an N(2)-Fe(1)-O(1) bond angle of 92.64(15)°. Additionally, one aryl isopropyl substituent was successfully modeled for positional disorder. Inspection of the bis(imino)pyridine N_{imine}-C_{imine} and C_{imine}-C_{ipso} bond distances has been established as a valuable metric to evaluate the degree of ligand reduction for crystallographically characterized complexes.[6] The metrical parameters (Table 1.1) reveal chelate distances suggestive of one electron reduction with contracted C_{imine}-C_{ipso} distances of 1.446(5) Å and 1.433(5) Å. The N_{imine}-C_{imine} bond lengths of 1.299(4) Å and 1.306(4) Å observed for this complex are slightly elongated from the free ligand values of 1.274(3) Å[8] and between the values of 1.28 Å and 1.32 Å associated with an unreduced and monoreduced chelate, respectively.[6] A qualitative molecular orbital diagram highlighting the electronic structure of each complex prepared in this Chapter is presented in Section 1.6.

Cooling a concentrated diethyl ether solution of **2-Cl** to -35 °C yielded X-ray quality green crystals of **2-Cl(Et_2O)**. The molecular structure of **2-Cl(Et_2O)** (Figure 1.6) reveals a similar distorted square pyramidal geometry about the metal center, where diethyl ether occupies the apical position. Similar to **1-Br(THF)**, dissolving crystals of **2-Cl(Et_2O)** in benzene-d_6 resulted in immediate loss of diethyl ether and observation of **2-Cl** as judged by ^{1}H NMR spectroscopy. The metrical parameters reported in Table 1.2 reveal that the chlorine atom is displaced from the iron chelate plane to a greater extent than the bromine atom in **1-Br(THF)**, with an N(2)-Fe(1)-Cl(1) angle of 150.96(6)°. Although less pronounced, deviation from square pyramidal geometry is also highlighted by the N(2)-Fe(1)-O(1) bond angle of 108.99(8)°. The N(1)-C(2) and N(3)-C(8) bond lengths of 1.313(3) Å and 1.301(3) Å observed for **2-**

Cl(Et$_2$O) are elongated from the free ligand reference value of 1.274(3) Å.[8] The C_{imine}-C_{ipso} distances, which are often a more diagnostic metric for PDI reduction than the imine bond lengths, *vide infra*, are contracted to 1.443(4) Å and 1.453(4) Å for C(2)-C(3) and C(7)-C(8), respectively, and are consistent with a monoreduced chelate.

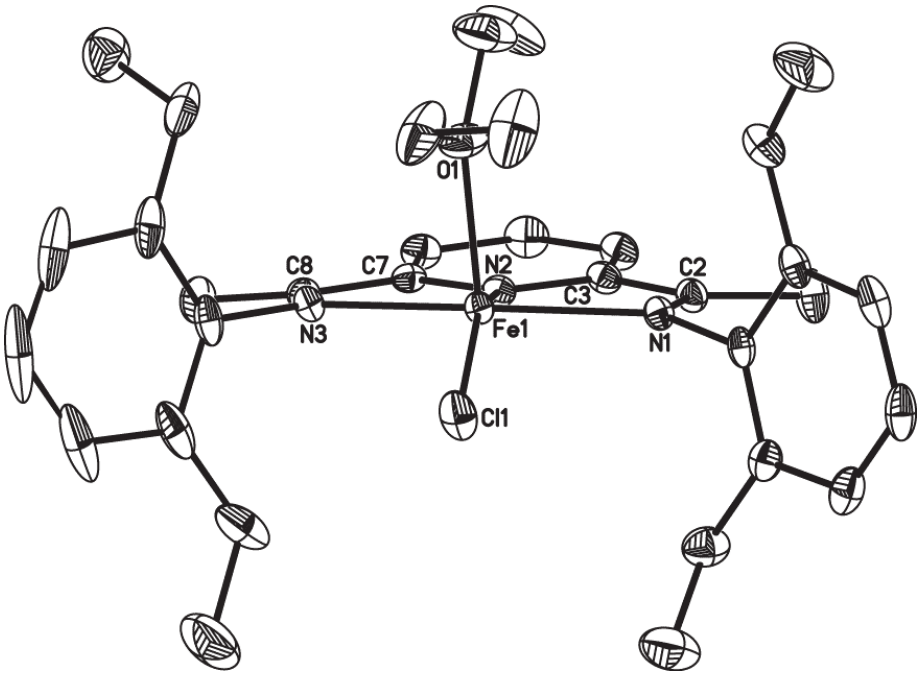

Figure 1.6. Molecular structure of **2-Cl(Et$_2$O)** at 30 % probability ellipsoids. Hydrogen atoms omitted for clarity.

Table 1.2. Selected bond distances (Å) and angles (°) for **2-Cl(Et$_2$O)**.

Fe(1)-N(1)	2.181(2)	N(3)-C(8)	1.301(3)
Fe(1)-N(2)	2.009(2)	C(2)-C(3)	1.443(4)
Fe(1)-N(3)	2.209(2)	C(7)-C(8)	1.453(4)
Fe(1)-Cl(1)	2.2668(8)	N(2)-Fe(1)-O(1)	108.99(8)
Fe(1)-O(1)	2.213(2)	N(2)-Fe(1)-Cl(1)	150.96(6)
N(1)-C(2)	1.313(3)		

Table 1.3. In-plane chelate hydrogen resonances of bis(imino)pyridine iron monohalide complexes observed by ^{1}H NMR spectroscopy in benzene-d_6 at 20 °C.

Complex	*p-pyr* (ppm)	*m-pyr* (ppm)	N=C*Me* (ppm)
1-Cl	385.6	68.1	-212.9
1-Br	388.9	69.2	-212.7
1-Cl(py)	328.2	97.8	-240.5
1-Br(py)	325.9	101.8	-241.3
2-Cl	369.3	68.1	-214.0
2-Br	365.5	70.0	-214.9
3-Cl	357.1	63.9	-209.1
3-Br	354.0	65.8	-209.7

Contrasting the coordination of tetrahydrofuran to **1-Br**, stoichiometric addition of pyridine to either **1-Cl** or **1-Br** resulted in the immediate formation of the 5-coordinate complexes, **1-Cl(py)** or **1-Br(py)**, respectively, as judged by ^{1}H NMR spectroscopy (Table 1.3). The imine methyl and *p*-pyridine resonances for these compounds appear at -240.46 and 328.18 ppm or -241.30 ppm and 325.93 ppm, respectively. Repeated cycles of hydrocarbon solvent removal and dissolution did not change the ^{1}H NMR spectrum of either **1-Cl(py)** or **1-Br(py)**, confirming a preference for pyridine over diethyl ether coordination. Addition of 1 equivalent of pyridine-d_5 to **1-Cl** resulted in the formation of **1-Cl(py)-*d*$_5$**, and upon investigation by ^{1}H and ^{2}H NMR spectroscopy, revealed that the pyridine resonances appear at 120.75, 40.10, and 24.20 ppm. The solid state structure of **1-Cl(py)** has been reported[11] and the N_{imine}-C_{imine} and C_{imine}-C_{ipso} distances of 1.3020(3)/1.2844(3) Å and 1.4533(36)/1.4773(32) Å, respectively, are reasonable for a one electron reduction of the PDI ligand.[6] Although both measurements are consistent with an $S = 3/2$ complex with contributions from spin-orbit coupling, a disparity between the solution and solid state magnetic susceptibility was observed for the 5-coordinate monohalides; a moment of

3.9(2) μ_B was observed for **1-Br(py)** in benzene-d_6 and a solid state value of 4.5(1) μ_B was obtained for **1-Br(THF)** at ambient temperature using a magnetic susceptibility balance.

In an attempt to prepare a bis(imino)pyridine iron monofluoride complex (**1-F**), one equivalent of $BF_3 \cdot Et_2O$ was added to ^{iPr}PDIFe$(N_2)_2$ (**1-$(N_2)_2$**). Rather than yielding **1-F**, this reaction resulted in the formation of **1-$(FBF_3)(Et_2O)$**, consistent with previously observed reactivity of this reagent with a reducing iron center.[24] In addition to the ^{1}H NMR spectrum of this complex, which suggested ether coordination in solution, crystals of **1-$(FBF_3)(Et_2O)$** suitable for X-ray crystallography were obtained by cooling a saturated ether/pentane solution to -35 °C. The molecular structure of **1-$(FBF_3)(Et_2O)$** (Figure 1.7) confirmed a 5-coordinate iron center and selected metrical parameters are reported in Table 1.4. The preparation of **1-F(py)** was ultimately accomplished by addition of py·HF to **1-OTMS**, *vide infra*.[25]

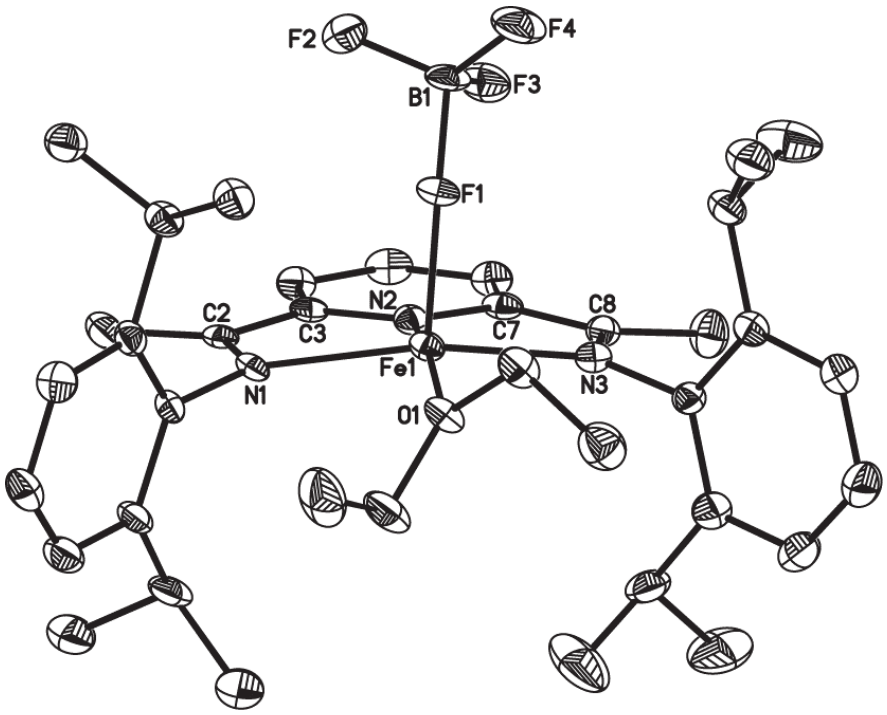

Figure 1.7. Molecular structure of **1-$(FBF_3)(Et_2O)$** at 30 % probability ellipsoids. Hydrogen atoms omitted for clarity.

Table 1.4. Selected bond distances (Å) and angles (°) for **1-(FBF_3)(Et_2O)**.

Fe(1)-N(1)	2.177(2)	N(1)-C(2)	1.312(3)
Fe(1)-N(2)	1.977(2)	N(3)-C(8)	1.330(3)
Fe(1)-N(3)	2.169(2)	C(2)-C(3)	1.454(3)
Fe(1)-F(1)	2.0890(16)	C(7)-C(8)	1.437(4)
Fe(1)-O(1)	2.1027(18)	N(2)-Fe(1)-F(1)	105.62(7)
F(1)-B(1)	1.484(3)	N(2)-Fe(1)-O(1)	165.93(8)

In striking contrast to the solid state structures of **2-Cl(Et_2O)**, **1-Cl(py)**,[11] and **1-Br(THF)**, **1-(FBF_3)(Et_2O)** exhibits a distorted square pyramidal geometry where the anionic BF_4 ligand occupies the *apical* coordination site. This contrasts the C_{2v}-symmetry observed in the ^{1}H NMR spectrum of this complex, which is likely derived from reversible ether binding. The measured bond angles of 105.62(7)° and 165.93(8)° for N(2)-Fe(1)-F(1) and N(2)-Fe(1)-O(1), respectively, closely resemble the distortions from square pyramidal geometry that were observed for **2-Cl(Et_2O)**. The Fe(1)-F(1) bond distance of 2.0890(16) Å appears reasonable for an inner-sphere anionic BF_4 ligand and is close to the distance of 2.0672(10) Å reported by Holland and co-workers.[24] As expected, the F(1)-B(1) bond length of 1.484(3) Å is significantly longer than the other B-F bonds (1.362 Å average). The chelate distances observed in **1-(FBF_3)(Et_2O)** are also consistent with one electron bis(imino)pyridine reduction.

The electronic structure of **1-Cl** was investigated in a comprehensive structural, spectroscopic, and computational study.[8] The assignment of this complex as a high spin ferrous center antiferromagnetically coupled to a monoreduced

bis(imino)pyridine chelate relied on broken symmetry calculations and the comparison of experimental Mössbauer parameters to those computed for each electronic structure possibility. X-ray crystallographic data were collected for **1-Cl**; unfortunately, however, the metrical parameters proved to be unreliable due to the crystallization of two different rotamers of a single diisopropylaryl substituent.[2] Consequentially, the bond distances computed for each electronic structure description were compared to those experimentally determined for **2-Cl(Et_2O)** without investigating the magnetic or spectral data observed for these structurally different complexes.[8]

Nevertheless, compilation of the newly acquired data for both structural types, (^{iPr}PDI)FeX and (^{iPr}PDI)FeX(L), provides validation and greater insight into the computationally determined electronic structure of these complexes. Investigation of tetrahydrofuran coordination to **1-Br** by ^{1}H NMR spectroscopy revealed that shifting of the chelate resonances was proportional to the amount of substrate added. Adding a stoichiometric amount of pyridine resulted in more favorable substrate coordination and immediate formation of **1-Br(py)**. Because **1-Br(THF)** and **1-Br(py)** have magnetic moments consistent with $S = 3/2$ complexes at 20 °C, 4.5(1) and 3.9(2) μ_B, respectively, the extrapolation of these 5-coordinate complexes to fit the electronic structure described for **1-Cl** is valid. In fact, the solid state magnetic susceptibility determined for **1-Br** and **1-Br(THF)** (4.5 μ_B) is higher than expected for the $S = 3/2$ spin only value of 3.87 μ_B and is consistent with an expected orbital contribution.[26] A lower solid state magnetic susceptibility was expected, but not observed, for **1-Br(THF)** and **1-Br(py)** because greater spacial overlap between the PDI localized electron and the metal center may have occurred with an increase of ligand field.[8]

1.4 Preparation and Electronic Structure of Monoalkyl Complexes

With a series of 4- and 5-coordinate monohalide complexes in hand, the reactivity of these compounds towards Grignard and alkyllithium reagents was investigated for two reasons. First, structural characterization of a series of monoalkyl complexes would allow for a proper discussion of bis(imino)pyridine chelate reduction for 4-coordinate bis(imino)pyridine iron complexes bearing only X-type ligands. One example of this type, **1-Me**, was structurally characterized at the commencement of this study and found to exhibit parameters consistent with an idealized square planar geometry and one electron ligand reduction.[10] Additionally, studying the reactivity of these complexes could provide information regarding the properties of the propagating species in bis(imino)pyridine iron dichloride mediated α-olefin polymerization and other catalytic bond forming reactions. Although an iron alkyl cation has been proposed as the active species,[17,18] preparing and studying the neutral counterparts of these complexes may contribute to the discussion.

In a similar manner to that used for **1-Me**, the preparation of **2-Me** and **3-Me** was accomplished by slow, stoichiometric addition of methyllithium to a cold solution (-35 °C) of either **2-Cl** or **3-Br** in diethyl ether (Figure 1.8). Importantly, these complexes display ^{1}H NMR spectra with paramagnetically broadened resonances spread over a 400 ppm shift range (Table 1.5). Although the range of peaks observed for these monomethyl complexes is significantly narrower than what was observed for the monohalide complexes (Table 1.3), it is important to note that the diagnostic in-plane chelate resonances are shifted in the same direction and general location from their diamagnetic reference values.[23] For example, the imine methyl resonances appear around -165 ppm, while the *p*-pyridine resonances were located between 210 and 270 ppm, respectively. Notably, the Fe-CH_3 resonance was not located for any of the three complexes.

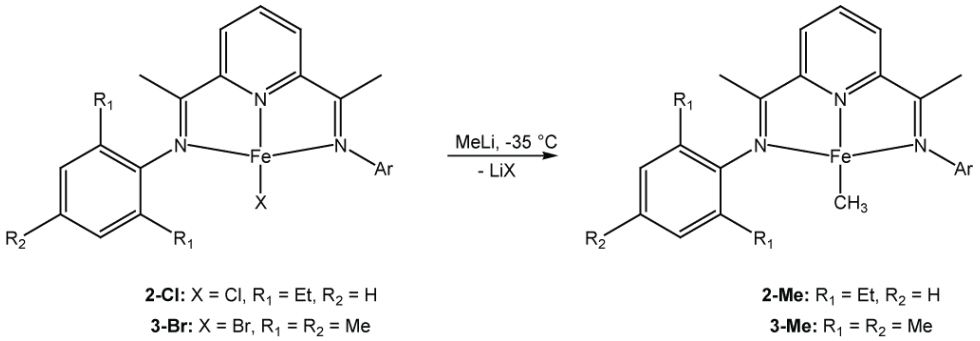

Figure 1.8. Alkylation of bis(imino)pyridine iron monohalides with MeLi.

Table 1.5. Diagnostic ^{1}H NMR resonances of bis(imino)pyridine iron monoalkyl complexes in benzene-d_6 at 20 °C.

Complex	*p-pyr* (ppm)	*m-pyr* (ppm)	N=C*Me* (ppm)
1-Me	216.5	58.9	-163.8
2-Me	264.7	63.2	-167.8
3-Me	264.5	61.5	-161.5
1-Ns	369.3	66.9	-206.8
2-Ns	341.5	67.9	-194.0
3-Ns	334.8	66.9	-189.3
1-Np	374.1	63.8	-200.0
2-Np	347.8	67.4	-192.6
1-Ph	216.6	64.4	-153.7
1-CC^{t}Bu	133.1	45.5	-130.7
1-CCPh	117.3	39.8	-121.9

In the initial report of **1-Me**, it was observed that this complex could also be prepared from the addition of 2 equivalents of methyllithium to **1-Cl$_2$**.[10] Similarly, **3-Me** was prepared in this fashion from **3-Br$_2$**. Care was taken to add only two equivalents of methyllithium, as over-reduction to form the corresponding alkyl anion has been observed.[20] Although this method appears to be a straightforward way to prepare a series of monoalkyl complexes directly from the dihalide, the observed reactivity is highly dependent on the alkyllithium reagent and (^{iPr}PDI)FeX$_2$ precursor.

For example, addition of two equivalents of neosilyllithum to **1-Cl$_2$** resulted in the formation of the resulting PDI iron dialkyl complex, **1-Ns$_2$**,[10,12] while conducting the same reaction with **2-Cl$_2$** resulted in the formation of a 4:1 ratio of **2-Ns** and **2-Ns$_2$** (Figure 1.9, top). Obviously, a cleaner and more general route to prepare bis(imino)pyridine iron mononeosilyl complexes was desired. Fortunately, alkylation of either **1-Cl**, **2-Cl**, or **3-Br** with one equivalent of $LiCH_2Si(CH_3)_3$ resulted in formation of the desired mononeosilyl complex (Figure 1.9, bottom), as judged by ^{1}H NMR spectroscopy (Table 1.5).

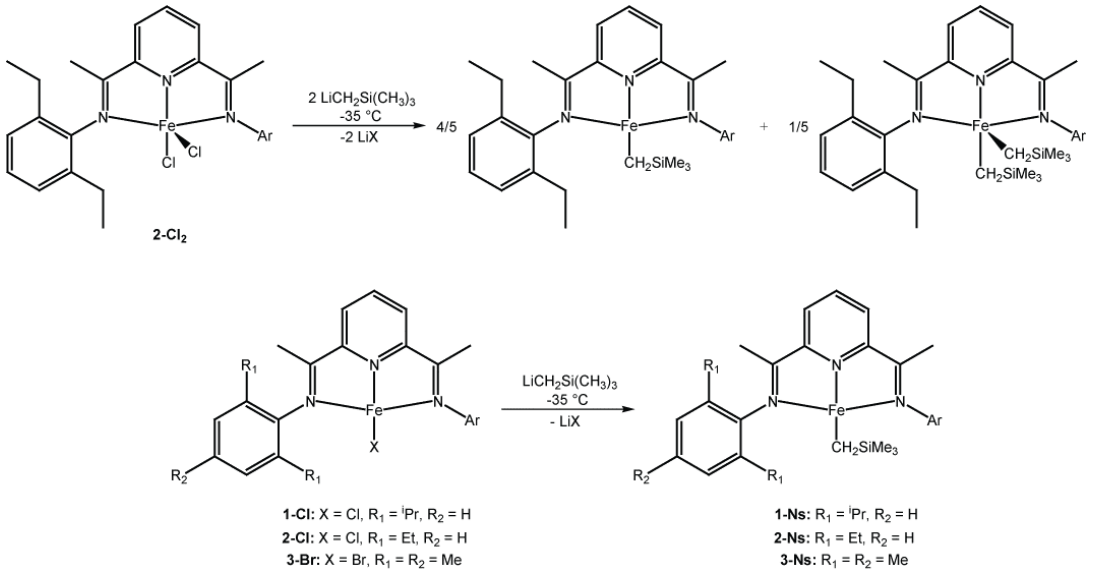

Figure 1.9. Alkylation of bis(imino)pyridine iron halide complexes with neosilyllithium.

The solid state structure of **2-Ns** was also determined by X-ray diffraction.[11] The N_{imine}-C_{imine} bond distances of 1.3177(17) Å and 1.3188(17) Å, along with the C_{imine}-C_{ipso} distances of 1.4397(16) Å and 1.4388(19) Å are indicative of one-electron chelate reduction.[6] In contrast to the idealized square planar geometry that was observed for **1-Me**,[10] this complex is greatly distorted from square planar geometry, as the neosilyl group is bent out of the chelate plane with an N(2)-Fe(1)-C(30) bond

angle of 147.40(5)°. This deviation could be due to a steric interaction between the bulky neosilyl ligand and the aryl ethyl groups that lie above and below the metal-chelate plane. The metrical parameters of these complexes, taken alongside the observed magnetic moments of these compounds, *vide infra*, gave an initial glimpse that these monoalkyl complexes could be described as having high-spin ferrous centers that are antiferromagnetically coupled to monoreduced bis(imino)pyridine chelates.[11]

Following the initial reports of **1-Ns$_2$** preparation, Cámpora and co-workers described the synthesis of this complex from the addition of free ^{iPr}PDI to a stoichiometric amount of $(py)_2Fe(CH_2Si(CH_3)_3)_2$.[13] This dialkyl precursor undergoes loss of both equivalents of pyridine in the presence of other bis(imino)pyridine ligands.[14] Reagents of this type remain relatively unexplored synthons for the preparation of organometallic iron alkyl complexes. This methodology was also used to gain insight into the stability of various bis(imino)pyridine iron neopentyl complexes. Adding either $(py)_2Fe(CH_2C(CH_3)_3)_2$ or $(py)_2Fe(CH_2C(CH_3)_3)Cl$ to ^{iPr}PDI resulted in pyridine substitution followed by neopentyl group mitration to the *para*-pyridine of the chelate.[11] Knowing that **1-Np$_2$** could not be prepared from this method, the addition of 2 equivalents of neopentyllithium to **1-Cl$_2$** was investigated as a route to prepare **1-Np**. This reaction, as well as the stoichiometric addition of NpLi to **1-Cl** or **2-Cl,** yielded clean bis(imino)pyridine iron neopentyl compound upon recrystallization of the crude reaction mixture from pentane (Figure 1.10). Both the neosilyl and neopentyl complexes display ^{1}H NMR resonances over a similar range (Table 1.5) and the Fe-C*H$_2$* resonance was not located for either class of compound. In the case of **2-Np**, single crystals suitable for X-ray diffraction were obtained and the solid state structure (Figure 1.11) was determined.

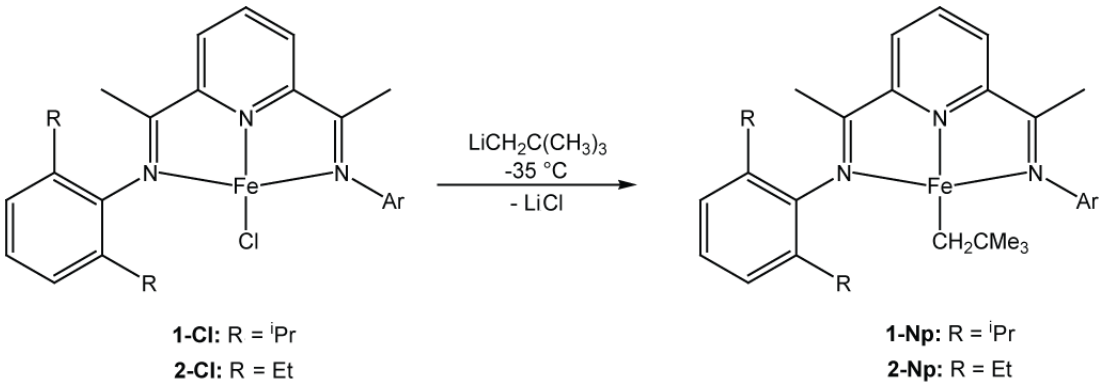

Figure 1.10. Preparation of bis(imino)pyridine iron neopentyl complexes.

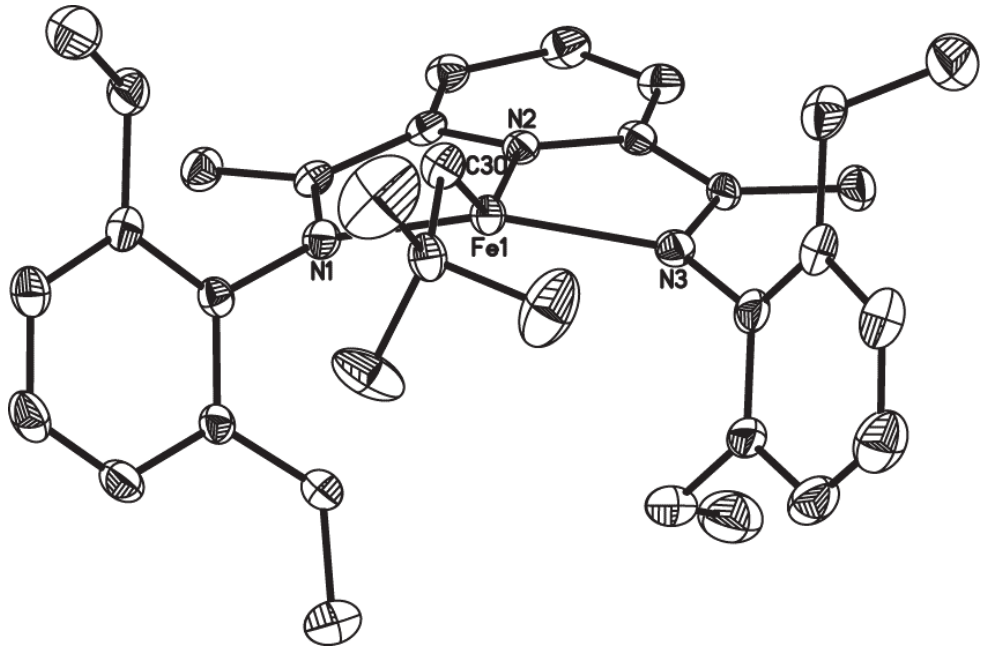

Figure 1.11. Solid state structure of **2-Np** at 30% probability ellipsoids. Hydrogen atoms omitted for clarity.

Selected metrical parameters for **2-Np** are tabulated in Table 1.6. The overall geometry of this complex is similar to that observed for **2-Ns**,[11] where the neopentyl group is bent out of the chelate plane at an N(2)-Fe(1)-C(30) angle of 142.24 °. The neopentyl methyl groups in this structure are rotationally disordered and the structure

is generally of lower quality than the one obtained for **2-Ns**. Even though the inherent low quality of this data set is reflected by the standard deviation values calculated for the metrical parameters in Table 1.5, the chelate bond lengths remain unmistakably representative of a singly reduced ligand.[6] The N_{imine}-C_{imine} bond distances of 1.314(4) Å and 1.329(17) Å and C_{imine}-C_{ipso} distances of 1.4397(16) Å and 1.4388(19) Å are well within the expected values,[6] even when error is considered.

Table 1.6. Selected bond distances (Å) and angles (°) for **2-Np**.

Fe(1)-N(1)	2.158(3)	N(3)-C(8)	1.329(4)
Fe(1)-N(2)	1.986(3)	C(2)-C(3)	1.446(5)
Fe(1)-N(3)	2.126(3)	C(7)-C(8)	1.428(5)
Fe(1)-C(30)	2.036(4)	N(2)-Fe(1)-C(30)	142.24(14)
N(1)-C(2)	1.314(4)	Fe(1)-C(30)-C(31)	123.0(2)

After preparing a series of iron alkyl complexes, the synthesis of bis(imino)pyridine iron complexes bearing either alkenyl, aryl, or alkynyl ligands was investigated to determine whether or not an increase in ligand field strength would result in a change of the electronic structure description. The synthesis of one aryl complex, **1-Ph**, was previously achieved from the addition of 2 equivalents of phenyllithium to **1-Br$_2$** at -35 °C in diethyl ether solution.[11] Preliminary investigation of this compound revealed ^{1}H NMR resonances over a slightly narrower range than those observed for the idealized square planar monomethyl complex **1-Me** (Table 1.5). However, impurities from undesired overreduction of **1-Ph**, mainly **[1-**

(Ph)N$_2$]Li(Et$_2$O)$_3$,[11] prevented characterization of this complex by X-ray crystallography and the acquisition of meaningful magnetic data.

Examples of stronger field *sp*–hybridized alkynyl complexes were also prepared. Addition of one equivalent of LiC≡CPh or LiC≡C^{t}Bu to **1-Cl** resulted in the formation of the respective acetylide complexes, **1-CCPh** and **1-CC^{t}Bu** (Figure 1.12). Additionally, **1-CC^{t}Bu** was prepared from 2 equivalents of the alkyllithium reagent with **1-Cl$_2$**. To determine if these complexes had a square planar geometry similar to **1-Me**, crystals of **1-CC^{t}Bu** suitable for X-ray diffraction were grown from a concentrated pentane solution at -35 °C and the solid state structure is presented in Figure 1.13.

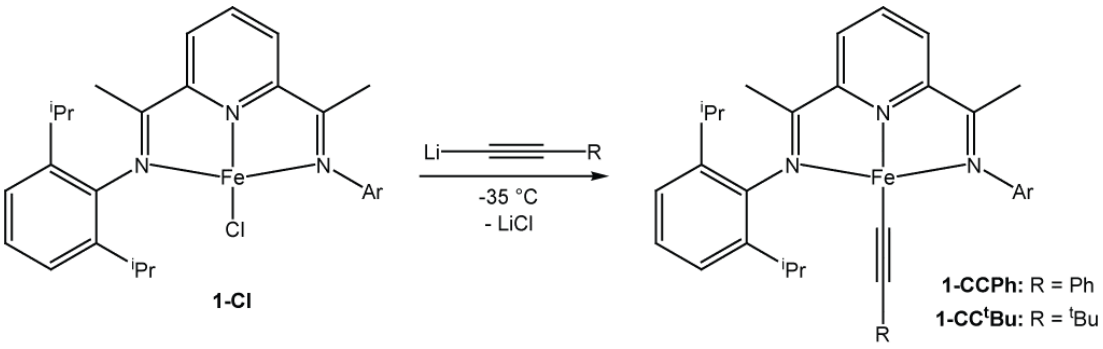

Figure 1.12. Synthesis of 4-coordinate ^{iPr}PDI iron acetylide complexes.

The metrical parameters of **1-CC^{t}Bu** (Table 1.7) are representative of a monoreduced bis(imino)pyridine ligand with average N_{imine}-C_{imine} and C_{imine}-C_{ipso} distances of 1.313(4) Å and 1.444(5) Å, respectively.[6] Similar to **1-Me**, this complex displays an idealized square planar geometry with an N(2)-Fe(1)-C(34) bond angle of 177.77(14)°C and the sum of the angles about iron is 359.91(12)°. As expected, the Fe(1)-C(34) bond distance of 1.902(4) Å is significantly shorter than the same distance found for the *sp*^{3}-hybridized monoalkyls; **1-Me** (2.001(6) Å), **2-Ns** (2.0343(14) Å),

and **2-Np** (2.036(4) Å). With the increase in ligand field, the ^{1}H NMR resonances for the in-plane ligand chelate hydrogens were observed over a narrower shift range at 20 °C in benzene-d_6; the imine methyl and *p*-pyridine resonances were detected at -133.1 ppm and 130.7 ppm, respectively (Table 1.5).

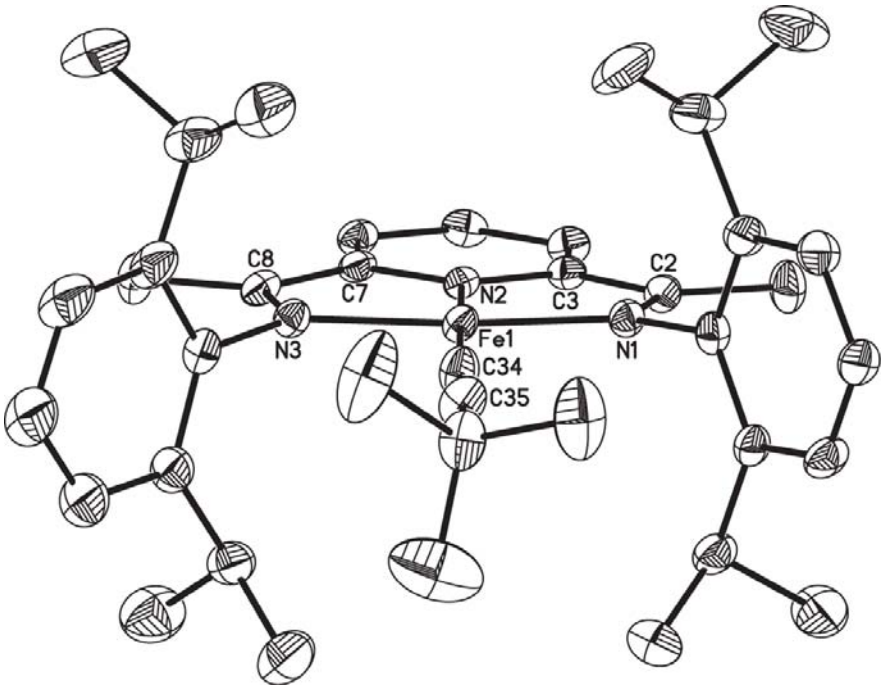

Figure 1.13. Molecular structure of **1-CC^{t}Bu** shown at 30% probability ellipsoids. Hydrogen atoms and one set of rotationally disordered *tert*-butyl carbons omitted for clarity.

Table 1.7. Selected bond distances (Å) and angles (°) for **1-CC^{t}Bu**.

Fe(1)-N(1)	1.921(3)	N(3)-C(8)	1.325(4)
Fe(1)-N(2)	1.855(2)	C(2)-C(3)	1.451(4)
Fe(1)-N(3)	1.948(3)	C(7)-C(8)	1.437(5)
Fe(1)-C(34)	1.902(4)	C(34)-C(35)	1.211(5)
N(1)-C(2)	1.301(4)	N(2)-Fe(1)-C(34)	177.77(14)

The other newly prepared bis(imino)pyridine iron acetylide complex, **1-CCPh**, was crystallographically characterized and was also found to have an idealized square planar geometry with the sum of angles about iron totaling 360.01(7) ° (Figure 1.14). For this complex, one aryl isopropyl substituent was positionally disordered and successfully modeled. As with **1-CC^{t}Bu**, the chelate metrical parameters (Table 1.8) are suggestive of a one electron reduction, with N_{imine}-C_{imine} and C_{imine}-C_{ipso} distances of 1.325(2)/1.330(2) Å and 1.429(3)/1.436(3) Å, respectively. The Fe(1)-C(34) bond in **1-CCPh** is similar to the one observed for **1-CC^{t}Bu** at 1.915(2) Å.

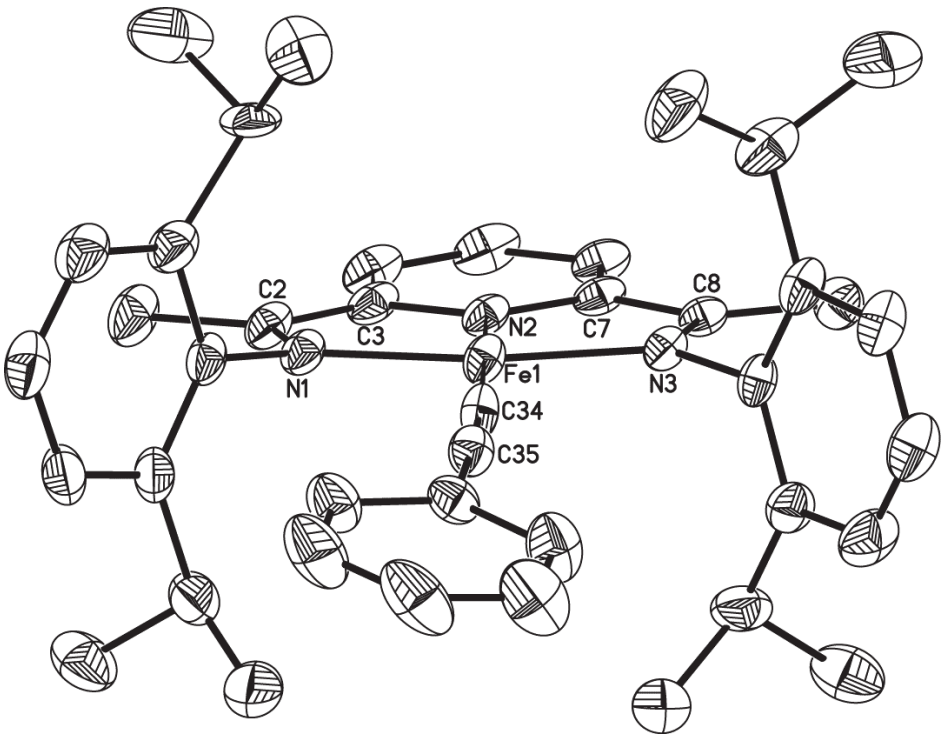

Figure 1.14. Molecular structure of **1-CCPh** shown at 30% probability ellipsoids. Hydrogen atoms and one positionally disordered isopropyl group omitted for clarity.

Table 1.8. Selected bond distances (Å) and angles (°) for **1-CCPh**.

Fe(1)-N(1)	1.9407(15)	N(3)-C(8)	1.330(2)
Fe(1)-N(2)	1.8401(14)	C(2)-C(3)	1.429(3)
Fe(1)-N(3)	1.9329(15)	C(7)-C(8)	1.437(5)
Fe(1)-C(34)	1.915(2)	C(34)-C(35)	1.436(3)
N(1)-C(2)	1.325(2)	N(2)-Fe(1)-C(34)	177.43(8)

When investigating reduction of bis(imino)pyridine,[6-8] or other redox active imine based ligands,[27] the analysis of crystallographically determined chelate bond lengths is the most straightforward method of discerning the degree of reduction. It has been established that N_{imine}-C_{imine} distances of approximately 1.32 Å are consistent with single electron reduction of the bis(imino)pyridine chelate.[6] This distance is significantly elongated from the free ligand value of 1.274 Å and the bond length approximation of an unreduced PDI ligand on a metal center, 1.28 Å. However, care must be taken not to overanalyze N_{imine}-C_{imine} distances that lie between 1.28 Å and 1.32 Å, as this bond distance is highly sensitive to the nature of the metal itself[7] and other ligands that surround the metal center.[23] The remote C_{imine}-C_{ipso} bond is less influenced by these factors and is therefore a much more reliable distance to consider for chelate reduction. Examination of this distance also provides greater distinction between an unreduced (1.50 Å) and singly reduced bis(imino)pyridine ligand (1.44 Å).[6] For a doubly reduced chelate, lengths of 1.36 Å and 1.40 Å for the N_{imine}-C_{imine} and C_{imine}-C_{ipso} bond distances, respectively, would be expected.[6,23]

Upon review of the bond lengths observed for **1-Me**,[10] **2-Ns**,[11] **2-Np** (Table 1.6), **1-CC^{t}Bu** (Table 1.7), and **1-CCPh** (Table 1.8), the bis(imino)pyridine chelate in

each of these complexes appears singly reduced in a similar manner to the aforementioned monohalide complexes. The C_{imine}-C_{ipso} distances found in these complexes range between 1.428 Å and 1.451 Å and are all within error of the accepted monoreduced value of 1.44 Å.[6] The somewhat less reliable N_{imine}-C_{imine} distances are all relatively close to 1.32 Å, with values ranging between 1.301 Å to 1.337 Å. Going forward, one-electron bis(imino)pyridine reduction in the alkyl complexes will be assumed.

Of all the crystallographically characterized iron alkyl complexes, the metrical parameters about the metal center stand out for the acetylide complexes. For **1-CC^{t}Bu** and **1-CCPh**, the average Fe-$N_{pyridine}$ and Fe-N_{imine} bond lengths are 1.848(2) Å and 1.936(3) Å, respectively. For bis(imino)pyridine iron alkyl complexes, the average Fe-$N_{pyridine}$ and Fe-N_{imine} bonds are considerably longer with distances of 1.958(4) Å and 2.072(4) Å, respectively. It has been reported that dicationic, high-spin iron bipyridine complexes have Fe-N bond lengths that are typically 0.16 to 0.22 Å longer than their low-spin counterparts.[28] In this case, the discrepancy in Fe-N bond distances observed between the acetylides and sp^3-hybridized alkyls hinted that the stronger field acetylide complexes have intermediate-spin rather than high-spin ferrous centers.

Investigation of the spectroscopic features and magnetic susceptibility of the 4-coordinate iron alkyls is also an important component of the electronic structure discussion of these complexes. All of the iron alkyl complexes displayed similar ^{1}H NMR spectroscopic features and the stronger field (**1-CCR** and **1-Ph**) and in-plane (**1-CCR**, **1-Me**) alkyls exhibited the narrowest shift ranges (Table 1.5). This spectroscopic observation bears little experimental weight, however, because it provides no direct information regarding the spin or oxidation state of the metal center. Confirmation that the ligand centered radical is antiferromagnetically coupled to both the high-spin and intermediate-spin iron centers was obtained by investigating

the magnetic susceptibility of each alkyl complex. The benzene-d_6 solution magnetic data for all of the discussed monoalkyl complexes at 20 °C is presented in Table 1.9. The iron alkyl complexes exhibit moments consistent with an $S = 3/2$ metal center and range from 3.5 μ_B to 4.2 μ_B. The solution magnetic susceptibility values of 2.0(2) μ_B and 2.5(2) μ_B observed for **1-CC^{t}Bu** and **1-CCPh**, respectively, along with the observation of shorter Fe-N bonds in the solid state structure, strongly suggest that the electronic structure of the acetylide complexes are best described as having intermediate-spin iron(II) metal centers that are antiferromagnetically coupled to the monoreduced PDI ligands. Additionally, the solid state magnetic moment of **1-CCPh** was determined to be 2.6(1) μ_B (Guoy balance). This value is once again slightly higher than the solution value but remains within experimental error.

Table 1.9. Solution magnetic susceptibility of bis(imino)pyridine iron alkyl complexes determined in benzene-d_6 at 20 °C.

Complex	μ_{eff} (μ_B)	Reference
1-Me	3.5	10
2-Me	4.1	10
3-Me	3.9	10
1-Ns	3.8	11
2-Ns	4.0	10
3-Ns	4.0	this work
1-Np	4.0	11
2-Np	4.2	11
1-Ph	4.2	11
1-CC^{t}Bu	2.0	this work
1-CCPh	2.5	this work

Variable temperature, solid-state magnetic susceptibility data was collected for **1-Np** and **2-Np**, to see whether or not these alkyls exhibit spin-crossover behavior upon cooling. In accordance with the data obtained for **1-Br**, the solid state magnetic susceptibility of **1-Np** ranged from 2.8 μ_B to 4.4 μ_B (5 – 300 K) (Figure 1.15), without evidence for spin-crossover. Similarly, the magnetic susceptibility of **2-Np** ranged from 3.6 μ_B to 4.7 μ_B over the same temperature range. The ambient temperature values of 4.4 μ_B and 4.7 μ_B observed for **1-Np** and **2-Np**, respectively, are higher than their determined solution values of 4.0(2) μ_B and 4.2(2) μ_B but remain within error. Overall the structural, spectral, and magnetic data acquired for **1-Np** and **2-Np** establish that these sp^3-hybridized alkyl complexes have the same electronic structure as the one calculated for **1-Cl**.[8] Without reliable variable temperature magnetic susceptibility data for **1-Me** and **1-Ph**, the spin-state of the iron center in these complexes remains ambiguous and may cross from high-spin to intermediate-spin at low temperatures.

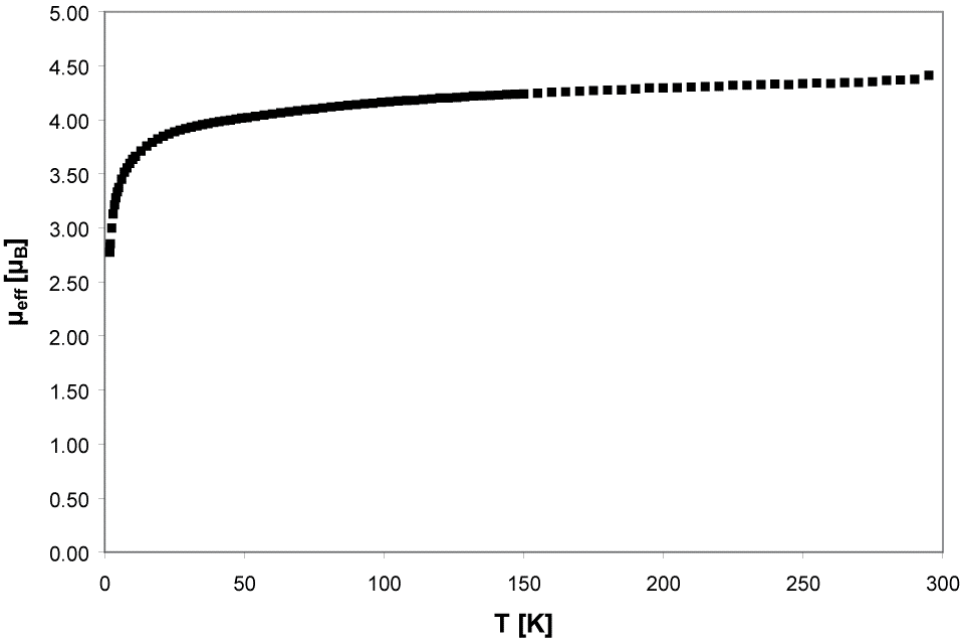

Figure 1.15. Solid state magnetic susceptibility data for **1-Np**.

During the preparation of bis(imino)pyridine iron alkyl complexes, one complex in particular had drastically different ^{1}H NMR spectroscopic properties. This complex, the bis(imino)pyridine iron allyl complex, **1-Allyl**, was prepared from the addition of allylmagnesium bromide to **1-Br** (Figure 1.16). This complex proved difficult to isolate because the allyl complex and magnesium bromide byproduct remained in equilibrium during workup.[29] The addition of excess 1,4-dioxane to aid $MgBr_2$ precipitation proved to be only marginally successful.

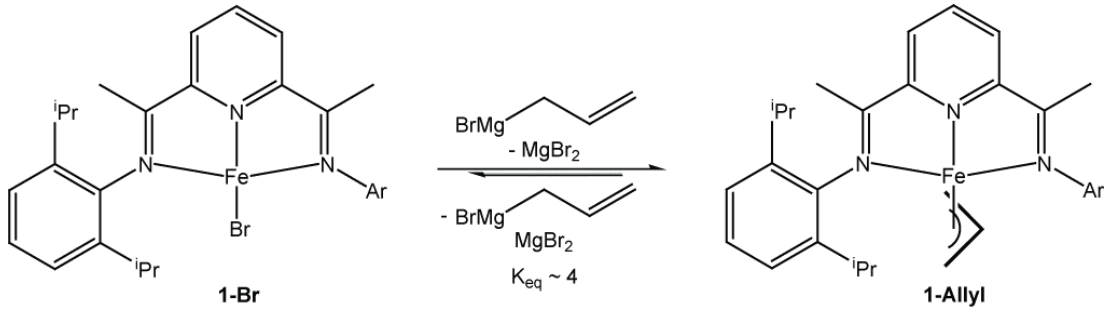

Figure 1.16. Preparation of **1-Allyl** from Grignard addition to **1-Br**.

All of the (PDI)Fe-X complexes previously discussed in this chapter exhibit resonances that are paramagnetically broadened and shifted over a 600 ppm chemical shift range (Tables 1.3 and 1.5). Importantly, the hydrogen atoms located in the chelate plane appear the most shifted from their diamagnetic reference values due to a Fermi contact interaction with the high- or intermediate-spin, d^6 metal center. Additionally, the isopropyl methine resonances are shifted significantly upfield (to around -110 ppm) due to a through space interaction with the metal center. For the alkyl complexes, the resonances associated with the alkyl chain (other than the hydrogens on the α-carbon) show up downfield of 20 ppm, consistent with a directly delocalized through-bond interaction.

For **1-Allyl**, the paramagnetically broadened ^{1}H NMR resonances are dispersed over a much narrower chemical shift range (175 ppm) with the imine methyl resonance appearing at -26.64 ppm and the *m*-pyridine resonance at 47.64 ppm. The narrow shift range of these peaks is likely due an η^3, rather than η^1, allyl ligand in solution. The observed C_{2v}-symmetry of **1-Allyl** could be the result of fast left-right flipping/rotation of the bound η^3-allyl ligand or an interconversion between η^1- and η^3-hapticity on the NMR timescale. Interestingly, the isopropyl methine resonances of this complex appear at 2.99 ppm; their dipolar interaction with the metal center is shielded by the η^3-allyl ligand. Unfortunately, the *p*-pyridine peak for **1-Allyl** was not located.

The solid-state structure of **1-Allyl** (Figure 1.17) revealed that the allyl ligand is coordinated in an η^3-fashion, with the three carbon plane oriented nearly perpendicular to the iron chelate plane and the methine carbon, C(35), directed toward an imine nitrogen. Notably, the central carbon atom is not in the iron chelate plane, providing a molecule with a more idealized square pyramidal rather than trigonal bipyramidal geometry. The allyl ligand was positionally disordered with nearly equal populations of the rotamer where the methine carbon is directed toward N(1) and the opposite rotamer where it is directed toward N(3). Although successfully modeled, the disorder compromises discussion of the metrical parameters of the allyl ligand itself.

The distortions observed in the bond distances of the bis(imino)pyridine ligand for **1-Allyl** (Table 1.10) clearly establish that this ligand is doubly reduced, with C_{imine}-$C_{pyridine}$ distances of 1.420(2) Å and 1.410(2) Å.[6] Although less convincing, the N_{imine}-C_{imine} distances are elongated to 1.3273(18) Å and 1.3369(18) Å and also suggest a doubly reduced bis(imino)pyridine. The iron-nitrogen distances for this complex of 1.9934(11) Å, 1.8418(11) Å, and 2.0017(12) Å suggest that this is an

intermediate rather than high-spin complex. This two electron chelate reduction is the likely explanation for the unusual ^{1}H NMR properties of **1-Allyl**.

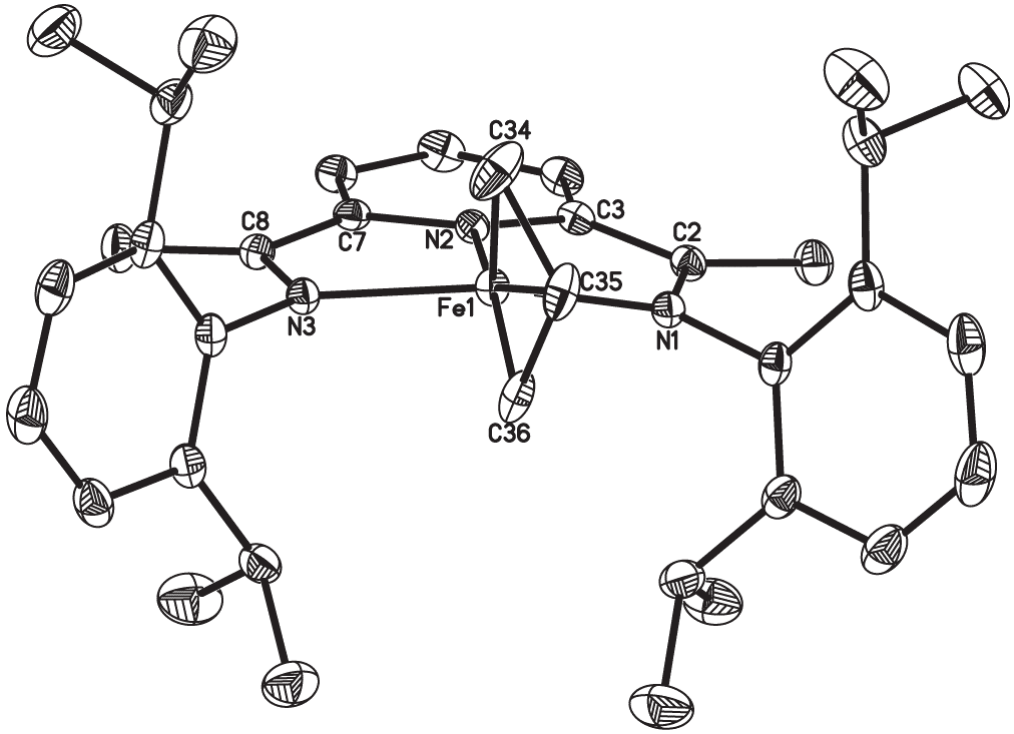

Figure 1.17. Molecular structure of **1-Allyl** at 30 % probability ellipsoids. Hydrogen atoms and one positionally disordered allyl ligand omitted for clarity.

Table 1.10. Selected bond distances (Å) and angles (°) for **1-Allyl**.

Fe(1)-N(1)	1.9934(11)	N(1)-C(2)	1.3273(18)
Fe(1)-N(2)	1.8418(11)	N(3)-C(8)	1.3369(18)
Fe(1)-N(3)	2.0017(12)	C(2)-C(3)	1.420(2)
Fe(1)-C(34)	2.115(4)	C(7)-C(8)	1.410(2)
Fe(1)-C(35)	2.074(3)	N(2)-Fe(1)-C(34)	124.24(13)
Fe(1)-C(36)	2.151(3)	N(2)-Fe(1)-C(36)	167.86(13)

Even though analytically pure samples of **1-Allyl** could not be obtained, the two electron bis(imino)pyridine chelate reduction sparked interest in determining the magnetic susceptibility of this complex. Two independently prepared samples of **1-Allyl** that each contained approximately 10 % **1-Br** were analyzed by Evans method[22] and determined to have an average magnetic susceptibility of 2.4(2) μ_B at 20 °C in benzene-d_6. While this is an unreliable way to assay the magnetic moment of this complex, the relatively low moment (especially with **1-Br** impurity, $S = 3/2$, $\mu_{eff} =$ 3.9(2) μ_B) does hint that the doubly reduced chelate antiferromagnetically couples to an intermediate spin, iron(III) center ($S = 1/2$). If a synthetic route to pure **1-Allyl** is discovered, a more detailed spectroscopic, magnetic, and computational study is required to describe the electronic structure of this compound indisputably.

1.5 Other PDI Iron Complexes with X-type Ligands

Because the electronic configuration of (PDI)Fe-X complexes appeared highly sensitive to the nature of the X group, as observed between the acetylide and sp^3-hybridized iron alkyl complexes, the preparation of complexes containing monoanionic ligands from each extreme of the spectrochemical series was desired. With the electronic structure of the weak field bis(imino)pyridine iron complexes in hand (X = Br, Cl), routes to the iron cyanide complex, **1-CN**, were explored. Unfortunately, both the addition of cyanogen to **1-$(N_2)_2$** and NaCN addition to either **1-Cl** or **1-Br** proved unsuccessful. Addition of a stoichiometric amount of trimethylsilyl isocyanide to **1-$(N_2)_2$** or **1-OEt** (Chapter 4), resulted in the formation of the bis(isocyanide) complex, **1-$(CNTMS)_2$**, rather than N-Si bond cleavage. The preparation of a strong field iron monohydride, **1-H**, or monosilyl, **1-SiR_3**, complex has also proven to be problematic. Addition of $PhSiH_3$ or SiH_4 to **1-$(N_2)_2$** resulted in the formation of the corresponding iron bis(η^2-silane) complex.[9] Attempts to

synthesize **1-H** from the addition of H_2 to **1-$(N_2)_2$** or an iron alkyl complex have resulted in the formation of the dihydrogen complex, **1-H_2**,[9] which rapidly loses hydrogen upon re-exposure to a nitrogen atmosphere.

Because oxidative addition was not observed for either dihydrogen or Si-H bonds with **1-$(N_2)_2$**, substrates containing weak O-H bonds were added to the reducing metal center in substoichiometric quantities. This strategy was first attempted with alcohols for two reasons; oxidative addition of the O-H bond could result in the formation of a five coordinate bis(imino)pyridine iron alkoxy hydride complex or occur across two metal centers, yielding both **1-OR** and **1-H**. The first alcohol added to **1-$(N_2)_2$** was allyl alcohol. The addition of 0.5 equivalents resulted in the formation of a new paramagnetic complex along with the observation of unreacted **1-$(N_2)_2$** and free bis(imino)pyridine ligand by ^{1}H NMR spectroscopy. This newly formed paramagnetic complex was identified as the iron alkoxide complex, **1-OAllyl**, by X-ray crystallography. The metrical parameters of the ligand in **1-OAllyl** were suggestive of one electron reduction with N_{imine}-C_{imine} and C_{imine}-C_{ipso} bond distances of 1.312(3)/1.306(2) Å and 1.459(3)/1.460(3) Å, respectively.[6] Similarly, this alkoxide complex displayed a ^{1}H NMR spectrum reminiscent of the aforementioned monohalide complexes with the imine methyl resonance at -219.87 ppm. The alcohol hydrogen atom was not located for this reaction and could account for the observation of free ligand.

A second bis(imino)pyridine iron alkoxide complex has also been characterized by X-ray crystallography, the iron silanolate complex, **1-OTMS**.[25] This compound was prepared from the stoichiometric addition of $NaOSiMe_3$ to **1-Br**. In an unrelated experiment, **1-OTMS** was isolated as a byproduct of wet (trimethylsilyl)acetylene addition to **1-$(N_2)_2$** and crystallographically characterized. One data set was fitted for a triclinic space group and had two equivalent iron

environments in the unit cell. The second data set was fit to a monoclinic space group and the unit cell contained two inequivalent iron environments. For this collection, one bis(imino)pyridine iron silanolate molecule had a positionally disordered isopropyl aryl substituent, while the other had a rotationally disordered trimethylsilyl group. The chelate metrical parameters for all three crystallographically determined examples of **1-OTMS** were consistent with a monoreduced ligand. The N_{imine}-C_{imine} bond lengths ranged between 1.2966(35) Å and 1.3051(17) Å, while the C_{imine}-C_{ipso} bond distances between were between 1.4406(36) Å and 1.4602(38) Å among the 3 molecules (2 data sets).[6] The average Fe-N_{py} and Fe-N_{imine} bond distances of 1.987(2) Å and 2.120(2) Å, respectively, are consistent with a high-spin metal center.

Additionally, pyridine has been added to **1-OTMS** and the resulting 5-coordinate complex, **1-OTMS(py)**, has been crystallographically characterized.[25] The overall geometry of this complex is distorted square pyramidal, similar to **1-Br(THF)** and **1-Cl(Et_2O)**, with N(2)-Fe(1)-O(1) and N(2)-Fe(1)-N(4) angles of 160.99(12) ° and 95.38 °, respectively. Importantly, the N_{imine}-C_{imine} and C_{imine}-C_{ipso} distances of 1.299(5)/1.322(5) Å and 1.454(6)/1.447(6) Å, respectively, are consistent with one electron bis(imino)pyridine reduction.

The chelate metrical parameters in the solid state structures of **1-OAllyl**, **1-OTMS**, and **1-OTMS(py)** are all consistent with a monoreduced chelate and the Fe-N distances suggest that the iron center for each complex is high spin. Each complex displays a ^{1}H NMR spectra suggestive of a high-spin ferrous center; peaks were observed over a 600 ppm range in analogy to the monohalide complexes. Solution magnetic moments collected for **1-OAllyl** (4.0(2) μ_B) and **1-OTMS** (4.0(2) μ_B) in benzene-d_6 solution at 20 °C confirmed the presence of a high-spin iron center in these complexes. Unfortunately, the magnetic susceptibility of **1-OTMS(py)** has not been investigated and the spin-state of this complex remains open for investigation.

The addition of carboxylic acids to **1-$(N_2)_2$** was also investigated as a way to prepare bis(imino)pyridine complexes with weak field carboxylate ligands. Stoichiometric, dropwise addition of either benzoic or hydrocinnamic acid to a dilute pentane solution of **1-$(N_2)_2$** resulted in the carboxylate complexes **1-OBz** (76% yield) and **1-H_2CIN** (41% yield), respectively (Figure 1.18). As observed for the alcohol addition, this method of preparation yielded reasonable amounts of free ligand (~20 %), which was readily removed from the product mixture upon crystallization from concentrated toluene solutions layered with pentane at -35 °C.

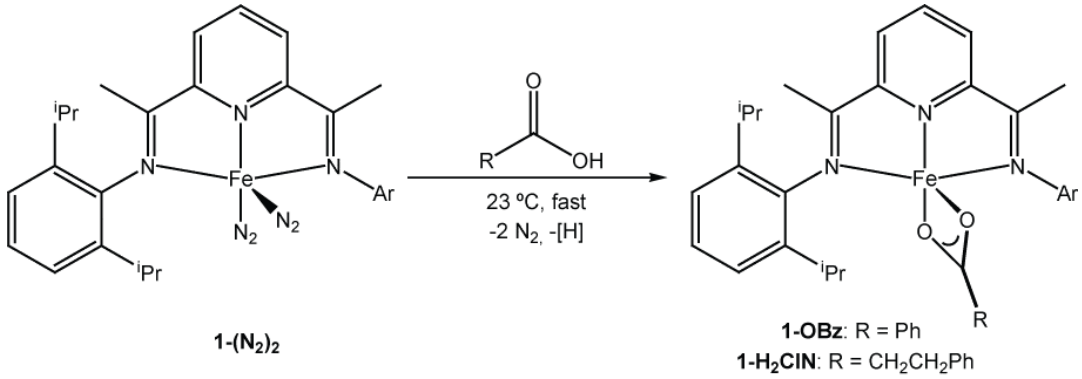

Figure 1.18. Preparation of bis(imino)pyridine iron carboxylate complexes.

Both iron carboxylate complexes, **1-OBz** and **1-H_2CIN**, were characterized by X-ray cyrstallographically. For both **1-OBz** (Figure 1.19) and **1-H_2CIN** (Figure 1.20), the κ^2-carboxylate ligand is nearly symmetrically disposed about the iron-chelate plane with N(2)-Fe(1)-O(1/2) bond angles of 158.21(6)/137.69(5) ° and 156.61(12)/140.23(12) °, respectively. In either case, the Fe(1)-C(34) bond is well outside the sum of the covalent radii of a high-spin iron center and an sp^2-hybridized carbon atom (2.25 Å)[30] at 2.437(2) Å (**1-OBz**) and 2.383(4) Å (**1-H_2CIN**). The chelate distances for both complexes are consistent with a one electron reduction, with average N_{imine}-C_{imine} and C_{imine}-C_{ipso} distances of 1.301 Å and 1.452 Å, respectively. In

metrical parameters of **1-OBz** (Table 1.11) suggest that the chelate reduction is delocalized, while the same distances in **1-H_2CIN** (Table 1.12) appear highly localized. This localization is likely an artifact of the lower quality crystallographic data collected for this carboxylate complex and further comment will be offered in Chapter 4 of this dissertation.

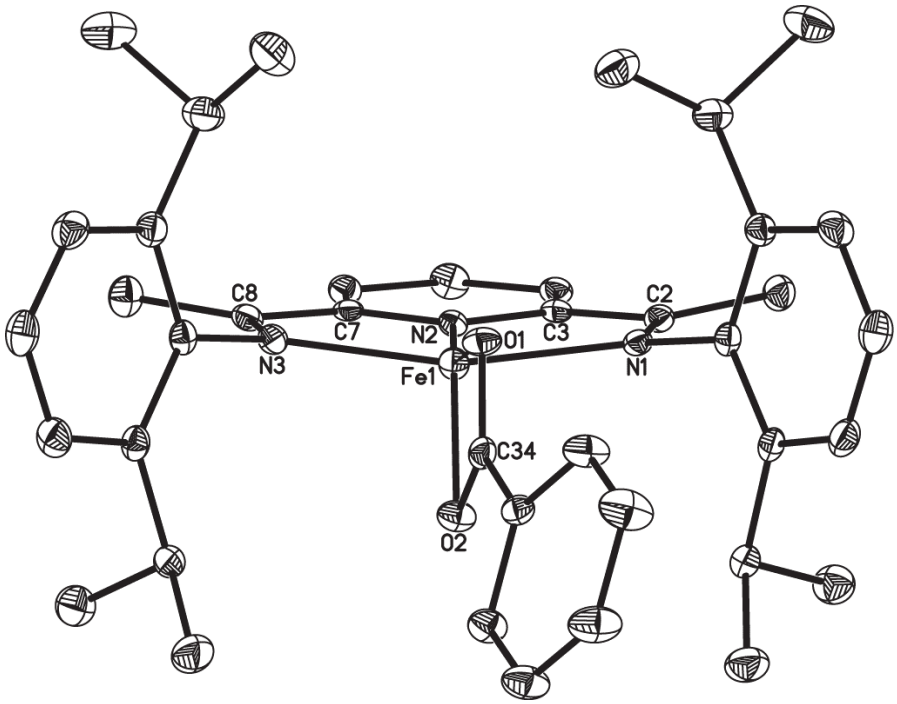

Figure 1.19. Molecular structure of **1-OBz** at 30 % probability ellipsoids. Hydrogen atoms omitted for clarity.

Table 1.11. Selected bond distances (Å) and angles (°) for **1-OBz**.

Fe(1)-N(1)	2.1678(14)	N(1)-C(2)	1.305(2)
Fe(1)-N(2)	1.9842(15)	N(3)-C(8)	1.308(2)
Fe(1)-N(3)	2.1269(15)	C(2)-C(3)	1.450(3)
Fe(1)-O(1)	2.1166(13)	C(7)-C(8)	1.410(2)
Fe(1)-O(2)	2.1033(13)	N(2)-Fe(1)-O(1)	158.21(6)

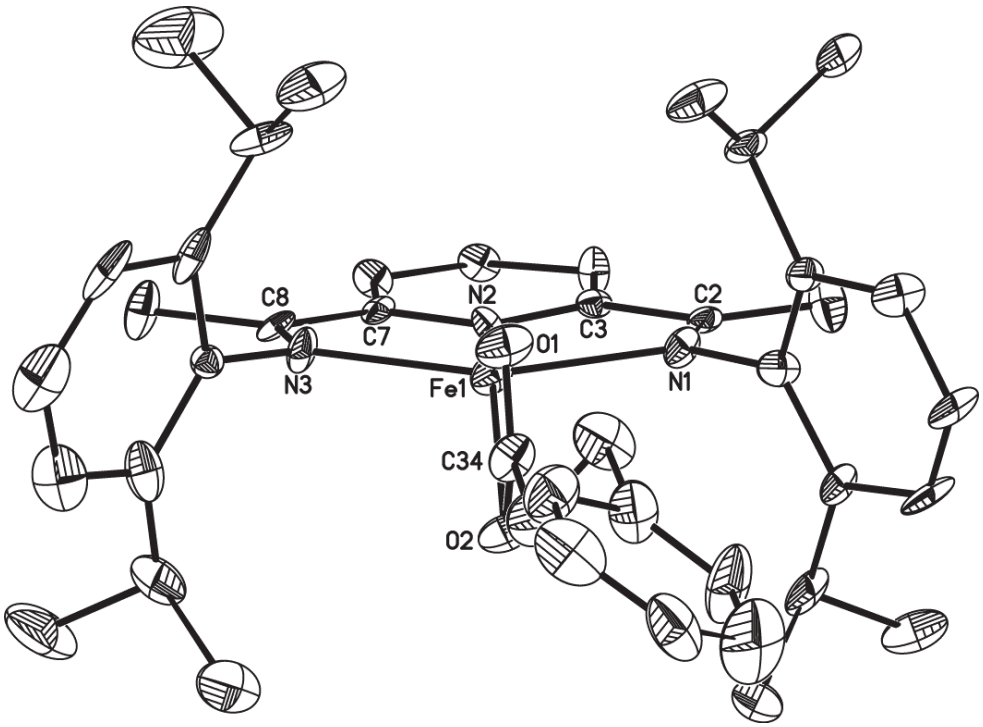

Figure 1.20. Molecular structure of **1-H_2CIN** at 30 % probability ellipsoids. Hydrogen atoms omitted for clarity.

Table 1.12. Selected bond distances (Å) and angles (°) for **1-H_2CIN**.

Fe(1)-N(1)	2.143(3)	N(1)-C(2)	1.264(4)
Fe(1)-N(2)	2.005(3)	N(3)-C(8)	1.327(4)
Fe(1)-N(3)	2.109(3)	C(2)-C(3)	1.494(5)
Fe(1)-O(1)	2.127(3)	C(7)-C(8)	1.408(5)
Fe(1)-O(2)	2.102(3)	N(2)-Fe(1)-O(1)	156.61(12)

The ^{1}H NMR spectra of **1-OBz** and **1-H_2CIN** display paramagnetically broadened resonances shifted over 650 ppm range, with the imine methyl resonance at -284.10 and -284.97 ppm, respectively. Even though this peak appears significantly

more upfield than for the monohalides or alkyls, the remaining resonances are shifted in the same direction and general range as these other compounds. The solution magnetic susceptibility measured for these complexes was found to be 4.9(2) μ_B for **1-OBz** and 4.4(2) μ_B for **1-H_2CIN**, confirming that the iron center is high-spin. These values are slightly higher than observed for the other high-spin (PDI)Fe-X complexes and may be due to a weaker degree of antiferromagnetic coupling (lower degree of covalency) between the chelate and high-spin metal center caused by the weak field κ^2-carboxylate ligand. Similar reactivity was observed when unprotected lactams such as δ-valerolactam, succinimide, and phthalimide were added to **1-(N_2)$_2$**; however, these κ^2-N,O complexes were not fully investigated because they displayed ^{1}H NMR shifts that were nearly identical to the carboxylates.

1.6 Mössbauer Spectroscopy

With a series of (PDI)Fe-X compounds in hand, a representative example for each type of complex described in this Chapter was chosen for investigation by Mössbauer spectroscopy. The spectrum obtained for **1-H_2CIN** is presented in Figure 1.21 as a representative example and the Mössbauer parameters (δ, ΔE_Q) determined for this complex, **1-Cl**, **1-Np** and **1-CCPh** are tabulated in Table 1.13. Additionally, the sample purity for each complex (%) is reported in Table 1.13. As expected, the complex with the weakest ligand field, **1-H_2CIN**, produced the highest isomer shift (δ = 0.96 mm·s^{-1}). This establishes a lower degree of covalency between the metal and bis(imino)pyridine ligand and explains the higher magnetic susceptibility of this complex as compared to the other high-spin complexes. The observed isomer shift decreases as the field strength increases for this set of complexes; **1-Cl** (δ = 0.77 mm·s^{-1}), **1-Np** (δ = 0.57 mm·s^{-1}), and **1-CCPh** (δ = 0.31 mm·s^{-1}).

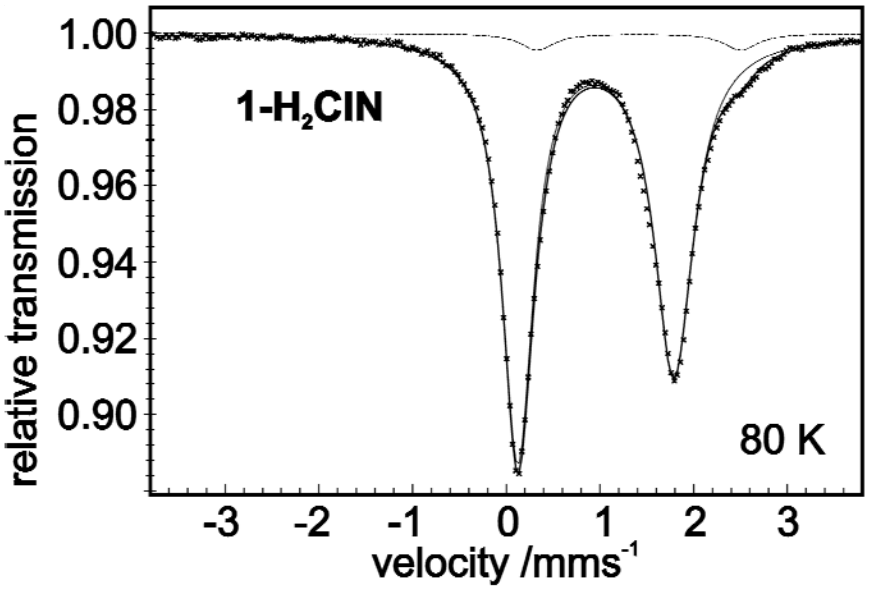

Figure 1.21. Zero-field Mössbauer spectrum of **1-H_2CIN** at 80 K.

Table 1.13. Mössbauer parameters ($mm \cdot s^{-1}$) for (PDI)Fe-X complexes at 80 K.

Complex	δ	ΔE_Q	%
1-H_2CIN	0.96	1.66	96
1-Cl	0.77	0.73	100
1-Np	0.57	1.16	100
1-CCPh	0.31	3.66	79

Although the zero-field Mössbauer spectrum of **1-CCPh** is contaminated with minor quantities of undesired iron containing species (13 %, 8 %), the isomer shift observed for this complex (δ = 0.31 $mm \cdot s^{-1}$) is more consistent with an intermediate rather than high-spin ferrous center.[31] Inspection of the quadrupole splitting values (ΔE_Q) obtained for this series of complexes further substantiates this claim. The values obtained for the high spin cases, **1-H_2CIN** (ΔE_Q = 1.66 $mm \cdot s^{-1}$), **1-Cl** (ΔE_Q = 0.73 $mm \cdot s^{-1}$), and **1-Np** (ΔE_Q = 1.16 $mm \cdot s^{-1}$), are all considerably lower than the quadrupole splitting of ΔE_Q = 3.66 $mm \cdot s^{-1}$ observed for **1-CCPh**. Based on the relative

d-orbital energies determined for **1-Cl** (Figure 1.22) with a (4,1) B3LYP broken symmetry calculation that placed four unpaired electrons on the metal and one on the chelate,[8] an increase in quadrupole splitting would be expected when going from a high to an intermediate-spin metal center. Placement of the $d_{x^2-y^2}$ based electron into any of the other SOMOs (d_{xy}, d_{xz}, or d_{z^2}) would greatly decrease the electric field gradient oriented in the xy-plane and increase the electron density along the z-axis. Increasing the charge along the z-axis, when the complex already has an electronic environment heavily oriented in that direction, would therefore produce a larger quadrupole splitting value.

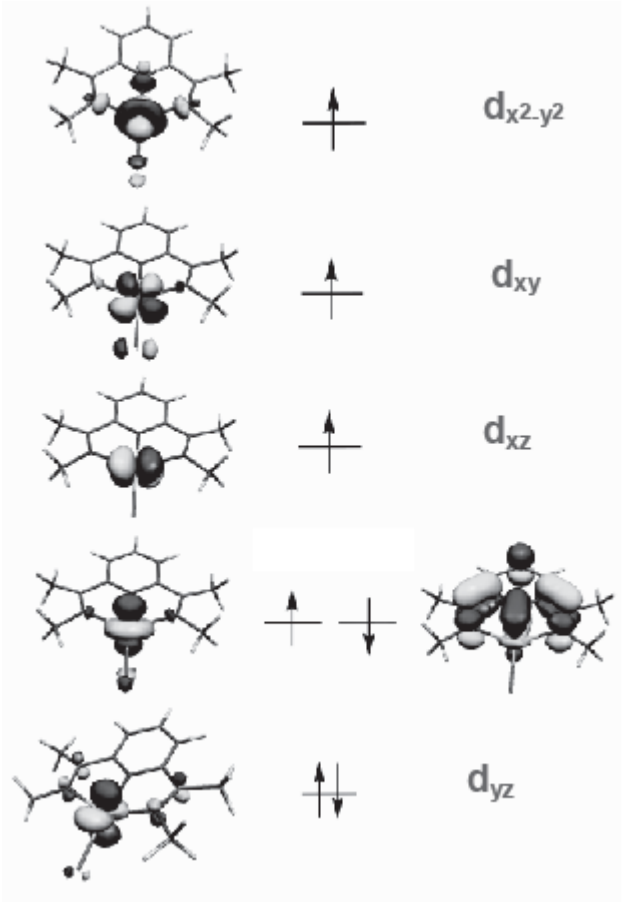

Figure 1.22. Qualitative molecular orbital calculated for **1-Cl**.

As presented in Figure 1.22, the electronic structure of **1-Cl** is best described as a high-spin ferrous center that is antiferromagnetically coupled to a singly reduced bis(imino)pyridine chelate. This electronic structure is also proposed for many of the complexes presented in this work (Figure 1.23, middle), including all of the newly prepared halide, alkoxide, and carboxylate complexes. The magnetic, structural, and Mössbauer spectroscopic data presented in this work establishes that **1-CC^{t}Bu, 1-CCPh** (Figure 1.23, left), and **1-Allyl** (Figure 1.23, right) do not fit this model. The electronic structure the acetylide complexes is best described as having an intermediate-spin ferrous center antiferromagnetically coupled to a chelate radical, while **1-Allyl** is proposed to have an intermediate spin ferric center that is antiferromagnetically coupled to two bis(imino)pyridine radicals. The parentage of each orbital has been labeled for the complexes with a high-spin ferrous center (Figure 1.23, middle), in analogy to **1-Cl**,[8] but the ordering of the low energy orbitals may be different for other complexes in this category. The parentage of each metal-based orbital in the electronic description of **1-CC^{t}Bu**, **1-CCPh**, and **1-Allyl** (Figure 1.23) is based on the computational data obtained for **1-Cl**. Definitive assignment of these orbitals is dependent on open shell, broken-symmetry DFT calculations. The iron center in **1-Me**, **2-Me**, **3-Me**, and **1-Ph** appears high-spin at 20 °C (Table 1.9); however, the ^{1}H NMR shifts observed for these complexes (Table 1.5) suggest that spin crossover may occur at a lower temperature. Additionally, EPR data has been collected for many of the complexes discussed in this Chapter and is presented in Appendix B.

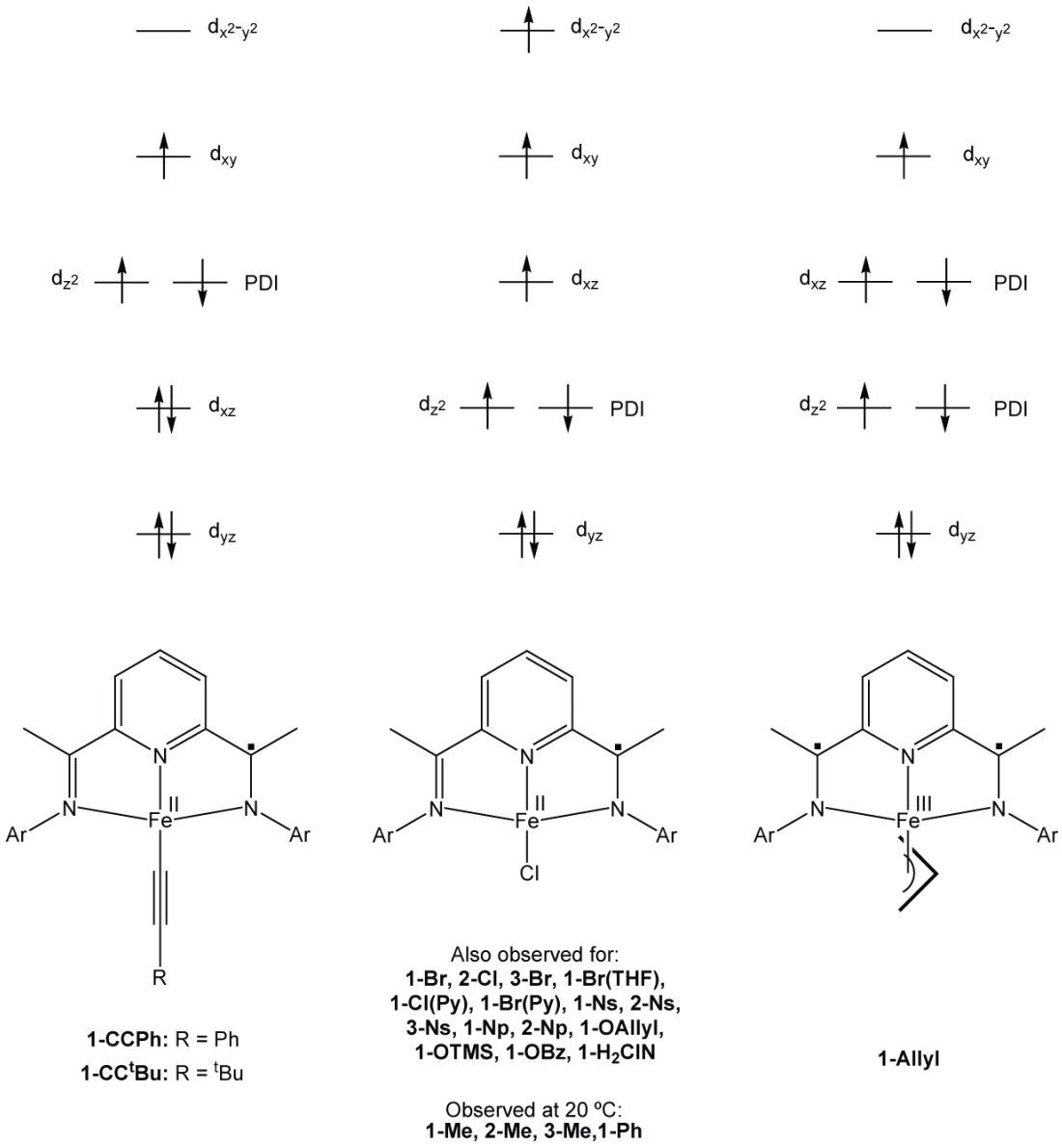

Figure 1.23. Proposed electronic structure of each compound prepared in this work.

1.7 Conclusion

The electronic structure of several bis(imino)pyridine iron monohalide complexes, with and without σ-donors in the fifth coordination site, was investigated and found to have high-spin ferrous centers that antiferromagnetically couple to singly reduced bis(imino)pyridine ligands. Similarly, four-coordinate iron monoalkyl

complexes were prepared and the electronic structure examined. For this class of compound, the spin state of the metal center is dependent on the field strength of the alkyl ligand. For example, the iron alkyls have an electronic structure similar to the monohalide complexes, while the bis(imino)pyridine iron acetylide complexes were found to have an intermediate-spin iron center. One alkyl complex in particular, **1-Allyl**, was found to have an entirely different electronic structure. Elucidation of the solid-state structure of this complex confirmed that the bis(imino)pyridine chelate in this complex was doubly reduced, leaving the metal center in the ferric oxidation state. The difference in electronic structure observed between the iron alkyl, alkynyl, and allyl complexes highlights the redox flexibility of the bis(imino)pyridine ligand. Preparation and electronic structure elucidation of bis(imino)pyridine iron alkoxide complexes revealed that these complexes are also best described as having a high-spin ferrous center that is antiferromagnetically coupled to the chelate. In an attempt to prepare weak field (PDI)Fe-X complexes, iron carboxylate complexes were targeted. The ^{1}H NMR properties and solid-state structure of these κ^2-carboxylate compounds suggested single reduction of the bis(imino)pyridine chelate and magnetic susceptibility measurements revealed a higher moment than observed for the other high-spin complexes. Investigation of this series by Mössbauer spectroscopy confirmed a lower degree of covalency for the carboxylates, as well as the intermediate-spin electronic configuration proposed for the iron acetylide complexes.

1.8 Experimental Procedures

General Considerations. All air- and moisture-sensitive manipulations were carried out using standard vacuum line, Schlenk, and cannula techniques or in an MBraun inert atmosphere dry box containing an atmosphere of purified nitrogen. Solvents for air- and moisture-sensitive manipulations were initially dried and deoxygenated using

literature procedures.[32] Hydrogen and deuterium gas were passed through a column containing manganese oxide supported on vermiculite and 4 Å molecular sieves before admission to the high vacuum line. Benzene-d_6 and toluene-d_8 were purchased from Cambridge Isotope Laboratories and dried over 4 Å molecular sieves or titanocene, respectively. The complexes **1-(N$_2$)$_2$**[9] and **1-Cl**[10] were prepared according to literature procedures.

Sodium triethylborohydride, boron trifluoride diethyl etherate, methyllithium, and allylmagnesium bromide were purchased from Aldrich and used as received. Neosilyllithium was purchased as a solution from Aldrich and the solvent was evacuated before use. Sodium cyanide (J. T. Baker), benzoic acid (Acros), and hydrocinnamic acid (Aldrich) were all dried on the high-vacuum line before use. Trimethylsilyl cyanide was purchased from Aldrich and dried over sieves before use. Allyl alcohol was obtained from Aldrich and carefully dried over a small amount of sodium before use. Cyanogen gas was purchased from Matheson and used as received. Similarly, silane was purchased from Voltaix and used as received. Neopentyllithium was prepared according to literature procedure.[33] Both LiCCPh and LiCC^{t}Bu were prepared by deprotonation of the respective acetylene with ^{n}BuLi in diethyl ether (LiCCPh) or tetrahydrofuran (LiCC^{t}Bu). The resulting solutions were evacuated, filtered through Celite with ether, and washed with pentane to obtain the desired reagent as a white solid.

^{1}H NMR spectra were recorded on Varian Mercury 300, Inova 400, 500, and 600 spectrometers operating at 299.76, 399.78, 500.62, and 599.78 MHz, respectively. All ^{1}H chemical shifts are reported relative to $SiMe_4$ using the ^{1}H (residual) shift of the solvent as a secondary standard. Solution magnetic moments were determined by Evans method[22] using a ferrocene standard and are the average value of at least two independent measurements. Gouy balance measurements were performed with a

Johnson Matthey instrument that was calibrated with $HgCo(SCN)_4$. Peak width at half height is given for paramagnetically broadened resonances. Elemental analyses were performed at Robertson Microlit Laboratories, Inc., in Madison, NJ.

Single crystals suitable for X-ray diffraction were coated with polyisobutylene oil in a drybox, transferred to a nylon loop and then quickly transferred to the goniometer head of a Bruker X8 APEX2 diffractometer equipped with a molybdenum X-ray tube (λ = 0.71073 Å). Preliminary data revealed the crystal system. A hemisphere routine was used for data collection and determination of lattice constants. The space group was identified and the data were processed using the Bruker SAINT+ program and corrected for absorption using SADABS. The structures were solved using direct methods (SHELXS) completed by subsequent Fourier synthesis and refined by full-matrix least-squares procedures.

Mössbauer data were collected on an alternating constant-acceleration spectrometer. The minimum experimental line width was 0.24 mm s^{-1} (full width at half height). A constant sample temperature was maintained with an Oxford Instruments Variox or an Oxford Instruments Mössbauer-Spectromag 2000 cyrostat. Reported isomer shifts (δ) are referenced to iron metal at 293 K.

Preparation of (^{Et}PDI)FeCl (2-Cl). A 250 mL round-bottom flask was charged with 0.500 g (0.906 mmol) of **2-Cl$_2$** and approximately 100 mL of diethyl ether. The resulting solution was cooled to -35 °C over the course of 20 minutes. A second solution containing 0.11 g (0.906 mmol) of sodium triethylborohydride (from 1.0 M solution in toluene) in 25 mL of diethyl ether was added dropwise to the cold solution. The resulting reaction mixture turned dark green in color immediately after the addition. After stirring for 3 hours, the solution was filtered through Celite. The solvent was removed *in vacuo* to afford 0.352 g (75 %) of a dark green solid identified

as **2-Cl**. Analysis for $C_{29}H_{35}N_3FeCl$: Calc. C, 67.38; H, 6.83; N, 8.13. Found C, 67.00; H, 6.50; N, 7.87. Magnetic susceptibility (benzene-d_6, 293 K) μ_{eff} = 4.0(2) μ_B. ^{1}H NMR (benzene-d_6, 293 K): δ = 369.3 (238 Hz, 1H, *p-pyr*), 68.1 (85 Hz, 2H, *m-pyr*), -6.5 (32 Hz, 4H, *m-aryl*), -15.3 (24 Hz, 2H, *p-aryl*), -31.9 (87 Hz, 12H, CH_2CH_3), -52.1 (197 Hz, 4H, CH_2CH_3), - 61.5 (236 Hz, 4H, CH_2CH_3), -214.0 (166 Hz, 6 H, $C(CH_3)$).

Preparation of (^{Mes}PDI)FeBr (3-Br). This complex was prepared in a manner similar to **2-Cl** with 0.500 g (0.86 mmol) of **3-Br$_2$** and 0.105 g of sodium triethylborohydride solution (0.86 mmol, 1.0 M in toluene) to yield 0.317 g (74%) of a dark green solid identified as **3-Br**. Analysis for $C_{27}H_{31}N_3FeBr$: Calc. C, 60.80; H, 5.87; N, 7.88. Found C, 60.47; H, 5.53; N, 7.48. Magnetic susceptibility (benzene-d_6, 293 K) μ_{eff} = 3.8(2) μ_B. ^{1}H NMR (benzene-d_6, 293 K): δ = 354.01 (258 Hz, 1H, *p-pyr*), 65.78 (113, 2H, *m-pyr*), 18.83 (14 Hz, 6H, *p-CH$_3$*), -6.44 (37 Hz, 4H, *m-aryl*), -41.44 (214 Hz, 12H, *o-CH$_3$*), -209.73 (233 Hz, 6H, C(C*H$_3$*)).

Addition of tetrahydrofuran to 1-Br. A J. Young tube was charged with 0.015 g (0.024 mmol) of **1-Br** and approximately 0.7 mL of benzene-d_6. Using a microsyringe, 0.017 g (20 μL, 0.240 mmol) of tetrahydrofuran was added. This solution was analyzed by ^{1}H NMR spectroscopy and a small deviation from the resonances of **1-Br** was observed. ^{1}H NMR (benzene-d_6, 293 K): δ = 351.87 (833 Hz, 1H, *p-pyr*), 69.27 (165 Hz, 2H, *m-pyr*), -0.75 (36 Hz, 4H, *m-aryl*), -10.05 (57 Hz, 12H, CH(CH_3)$_2$), -11.32 (26 Hz, 2H, *p-aryl*), -18.63 (173 Hz, 12H, CH(CH_3)$_2$), -54.96 (717 Hz, 4H, CH(CH$_3$)$_2$), -223.06 (194 Hz, 6H, C(CH_3)). Upon removing the solvent and redissolving the green solid in benzene-d_6, ^{1}H NMR spectroscopy revealed that a small amount of tetrahydrofuran remained and the resonances shifted towards free **1-Br**. ^{1}H

NMR (benzene-d_6, 293 K): δ = 383.05 (314 Hz, 1H, *p-pyr*), 68.97 (93 Hz, 2H, *m-pyr*), -4.75 (33 Hz, 4H, *m-aryl*), -12.29 (29 Hz, 2H, *p-aryl*), -19.51 (42 Hz, 12H, $CH(CH_3)_2$), -31.25 (141 Hz, 12H, $CH(CH_3)_2$), -102.92 (674 Hz, 4H, $CH(CH_3)_2$), -212.21 (156 Hz, 6H, $C(CH_3)$). Greenish-brown crystals of **1-Br(THF)** suitable for X-ray diffraction and Gouy balance magnetic susceptibility determination were obtained by chilling a concentrated solution of **1-Br** in pentane/tetrahydrofuran to -35 °C. Magnetic susceptibility (Gouy balance, 293 K) μ_{eff} = 4.5(1) μ_B.

Preparation of (^{iPr}PDI)FeBr(py) (1-Br(py)). A 20 mL scintillation vial was charged with 0.075 g (0.121 mmol) of **1-Br** and approximately 10 mL of diethyl ether and set to stir. A second solution of 0.011 g (11 μL, 0.134 mmol) of pyridine in approximately 5 mL of pentane was added slowly dropwise and the resulting greenish-brown solution was allowed to stir at ambient temperature for 18 hours. The reaction mixture was filtered through Celite with toluene and all solvent was removed *in vacuo* to yield a rust colored solid. Recrystallization from a concentrated toluene solution layered with pentane at -35 °C afforded 0.056 g (0.080 mmol, 66 %) of rust colored crystals identified as **1-Br(py)**. Analysis for $C_{38}H_{48}BrFeN_4$: Calc. C, 65.52; H, 6.95; N, 8.04. Found: C, 65.44; H, 7.19; N, 7.71. Magnetic susceptibility (benzene-d_6, 293 K): μ_{eff} = 3.9(2) μ_B. ^{1}H NMR (benzene-d_6, 293 K): δ = 325.93 (712 Hz, 1H, *p-pyr*), 114.75 (4301 Hz, 2H, *py*), 101.75 (174 Hz, 2H, *m-pyr*), 38.80 (400 Hz, 1H, *py*), 23.78 (312 Hz, 2H, *py*), 10.81 (239 Hz, 4H, $CH(CH_3)_2$), -0.30 (361 Hz, 12H, $CH(CH_3)_2$), -7.96 (620 Hz, 12H, $CH(CH_3)_2$), -8.63 (32 Hz, 2H, *p-aryl*), -241.30 (525 Hz, 6H, $C(CH_3)$), *m-aryl* resonance not located.

Preparation of (^{iPr}PDI)FeCl(py) (1-Cl(py)). This complex was prepared in a manner similar to **1-Br(py)** with 0.050 g (0.087 mmol) of **1-Cl** and 0.010 g (14 μL, 0.174

mmol) of pyridine to yield 0.11 g (20 %) of **1-Cl(py)** as a reddish-brown solid upon recrystallization. ^{1}H NMR (benzene-d_6, 293 K): δ = 328.18 (104 Hz, 1H, *p-pyr*), 120.75 (4670 Hz, 2H, *py*), 97.84 (181 Hz, 2H, *m-pyr*), 40.10 (275 Hz, 1H, *py*), 24.20 (211 Hz, 2H, *py*), -1.34 (768 Hz, 12H, CH(CH_3)$_2$), -6.58 (1437 Hz, 12H, CH(CH_3)$_2$), -8.85 (31 Hz, 2H, *m-aryl*), -10.11 (93 Hz, 1H, *p-aryl*), -240.46 (594 Hz, 6H, C(CH_3)), one resonance not located.

Preparation of (^{iPr}PDI)Fe(FBF$_3$)(Et$_2$O) (1-(FBF$_3$)(Et$_2$O)). A 20 mL scintillation vial was charged with 0.100 g (0.168 mmol) of **1-(N$_2$)$_2$** and approximately 10 mL of diethyl ether and set to stir. With a microsyringe, 0.018 g (16 μL, 0.168 mmol) of boron trifluoride diethyl etherate was added to the solution. The resulting green solution turned brown in color over the course of 18 hours while stirring. At that time, the solution was filtered through Celite and the solvent was removed *in vacuo*. Upon recrystallization of the resulting brown solid from diethyl ether at -35 °C, brown crystals identified as **1-(FBF$_3$)(Et$_2$O)** were isolated. Analysis for $C_{33}H_{43}N_3FeBF_4$ **1-(FBF$_3$)**: Calc. C, 63.48; H, 6.94; N, 6.73. Found C, 63.07, H, 6.83; N, 5.88. ^{1}H NMR (benzene-d_6, 293 K): δ = 114.47 (1769 Hz, *p-pyr* or *m-pyr*), -5.48 (140 Hz, *aryl*), -25.14 (567 Hz, 12H, CH(CH_3)$_2$), -35.55 (542 Hz, 12H, CH(CH_3)$_2$), -155.46 (1405 Hz, 4H, CH(CH$_3$)$_2$), -267.95 (186 Hz, 6H, C(CH_3)), several resonances not located.

Preparation of (^{Et}PDI)FeMe (2-Me). A 100 mL round-bottomed flask was charged with 0.500 g (0.971 mmol) of **2-Cl** and 50 mL of diethyl ether. The resulting brown solution was chilled to -35 °C in the dry box freezer. With stirring, 0.606 mL (0.971 mmol) MeLi (1.6 M in diethyl ether) was added forming a dark reddish-brown reaction mixture. The slurry was stirred for 30 minutes and then filtered through Celite. The filtrate was collected and the solvent removed *in vacuo* leaving a reddish-

purple solid. The product was washed twice with pentane to afford 0.374 g (78 %) of **2-Me**. Analysis for $C_{30}H_{33}N_3Fe$: Calc. C, 72.57; H, 7.71; N, 8.46. Found C, 72.43; H, 7.46; N, 8.63. Magnetic susceptibility (benzene-d_6, 293 K) μ_{eff} = 4.1(2) μ_B. ^{1}H NMR (benzene-d_6, 293 K): δ = 264.7 (123 Hz, 1H, *p-pyr*), 63.2 (58 Hz, 2H, *m-pyr*), -5.2 (19 Hz, 4H, *m-aryl*), -24.6 (52 Hz, 12H, CH_2CH_3), -32.6 (78 Hz, 2H, *p-aryl*), -48.1 (142 Hz, 4H, CH_2CH_3), -57.2 (198 Hz, 4H, CH_2CH_3), -167.8 (132 Hz, 6 H, C(CH_3)), Fe-CH_3 not located.

Preparation of (^{Mes}PDI)FeMe (3-Me). This compound was prepared using the same general procedure as **2-Me** but instead by addition of 0.3 mL (0.48 mmol) of 1.6 M methyllithium solution in diethyl ether to 0.160 g (0.25 mmol) of **3-Cl$_2$**. This procedure afforded 0.032 g (27 %) of a green solid identified as **3-Me**. Analysis for $C_{28}H_{29}N_3Fe$: Calc. C, 71.32; H, 7.32; N, 8.97. Found C, 71.32; H, 6.98; N, 8.52. Magnetic susceptibility (benzene-d_6, 293 K) μ_{eff} = 3.9(2) μ_B. ^{1}H NMR (benzene-d_6, 293 K): δ = 264.5 (150 Hz, 1H, *p-pyr*), 61.5 (54 Hz, 1H, *m-pyr*), 12.6 (10 Hz, 6H, *p*-CH_3), -6.2 (22 Hz, 4H, *m-aryl*), -41.7 (119 Hz, 12H, *o*-CH_3), -161.5 (142 Hz, 6H, C(CH_3)), Fe-CH_3 not located.

Preparation of (^{Et}PDI)FeCH$_2$SiMe$_3$ (2-Ns). A 20 mL scintillation vial was charged with 0.035 g (0.068 mmol) of **2-Cl** and approximately 5 mL of diethyl ether. After cooling to -35 °C for 25 minutes, 0.006 g (0.068 mmol) of $LiCH_2SiMe_3$ dissolved in a minimal amount of diethyl ether was added dropwise. The resulting dark green solution was stirred for 5 hours after which time it was filtered through Celite. Removal of the solvent *in vacuo* yielded 0.028 g (72 %) of a green solid identified as **2-Ns**. Analysis for $C_{33}H_{46}N_3SiFe$: Calc. C, 69.21; H, 8.10; N, 7.34. Found C, 68.92; H, 7.67; N, 7.06. Magnetic susceptibility (benzene-d_6, 293 K) μ_{eff} = 4.0(2) μ_B. ^{1}H NMR

(benzene-d_6, 293 K): δ = 341.5 (187 Hz, 1H, *p-pyr*), 67.9 (115 Hz, 2H, *m-pyr*), 42.3 (219 Hz, 9H, Si*Me*$_3$), -10.88 (57 Hz, 4H, *m-aryl*), -16.9 (50 Hz, 2H, *p-aryl*), -23.9 (83 Hz, 12H, CH_2CH_3), -61.9 (249 Hz, 4H, CH_2CH_3), -75.4 (315 Hz, 4H, CH_2CH_3), -194.0 (189 Hz, 6H, C(C*H*$_3$)), Fe-C*H*$_2$ not located.

Preparation of (^{Mes}PDI)FeCH$_2$SiMe$_3$ (3-Ns). A 20 mL scintillation vial was charged with 0.075 g (0.141 mmol) of **3-Br**, approximately 15 mL of diethyl ether, and a stir bar. After cooling at -35 °C for 20 minutes, a second solution composed of 0.010 g (0.141 mmol) of $LiCH_2Si(CH_3)_3$ in approximately 3 mL of diethyl ether was added dropwise over the course of 5 minutes. This solution was warmed to room temperature and allowed to stir for 5 hours. After filtering through Celite, the solvent was removed *in vacuo* to yield 0.054 g (71 %) of a dark green solid characterized as **3-Ns**. Analysis for $C_{31}H_{42}N_3SiFe$: Calc. C, 68.86; H, 7.85; N, 7.77. Found C, 68.65; H, 7.85; N, 7.46. Magnetic susceptibility (benzene-d_6, 293 K) μ_{eff} = 4.0(2) μ_B. ^{1}H NMR (benzene-d_6, 293 K): δ = 334.58 (183, 1H, *p-pyr*), 66.75 (88 Hz, 2H, *m-pyr*), 38.25 (200 Hz, 9H, Si*Me*$_3$), 14.87 (7 Hz, 6H, *p-CH*$_3$), -11.59 (23 Hz, 4H, *m-aryl*), -50.99 (169.52, 12H, *o-CH*$_3$), -189.43 (159 Hz, 6H, C(C*H*$_3$)), Fe-C*H*$_2$ not located.

Preparation of (^{iPr}PDI)FeCH$_2$CMe$_3$ (1-Np). A 250 mL round-bottomed flask was charged with 0.100 g (0.175 mmol) of **1-Cl** and approximately 100 mL of diethyl ether. The resulting solution was placed in a liquid nitrogen chilled cold well for approximately 20 minutes. A second diethyl ether solution containing 0.014 g (0.175 mmol) of neopentyllithium in 15 mL of solvent was prepared and added dropwise to the cold stirring solution of **1-Cl**. The solution changed color slightly over the course of 2 hours from bright green to brownish-green. At this time, the solution was filtered through a Celite fitted frit and the solvent was removed in vacuo to yield 0.090 g

(85%) of a dark olive colored powder identified as **1-Np**. Analysis for $C_{38}H_{54}N_3Fe$: Calcd C, 74.98; H, 8.94; N, 6.90. Found: C, 74.63; H, 9.19; N, 6.47. Magnetic susceptibility (benzene-d_6, 293 K): μ_{eff} = 4.0(2) μ_B ^{1}H NMR (benzene-d_6, 293 K): δ = 374.05 (169 Hz, 1H, *p-pyr*), 86.68 (367 Hz, 9H, C(CH_3)$_3$), 63.80 (67 Hz, 2H, *m-pyr*), -11.27 (23 Hz, 4H, *m-aryl*), -16.21 (20 Hz, 2H, *p-aryl*), -19.56 (29 Hz, 12H, CH(CH_3)$_2$), -33.94 (87 Hz, 12H, CH(CH_3)$_2$), -118.94 (371 Hz, 4H, CH(CH$_3$)$_2$), -199.95 (143 Hz, 6H, C(CH_3)), Fe-CH_2C(CH$_3$)$_3$ resonance not located.

Preparation of (^{Et}PDI)FeCH$_2$CMe$_3$ (2-Np). This complex was prepared in a manner similar to **1-Np** with 0.250 g (0.484 mmol) of **2-Cl** and 0.045 g (0.484 mmol) of neopentyllithium to yield 0.143 g (54%) of a dark green powder identified as **2-Np**. Analysis for $C_{34}H_{46}N_3Fe$: Calcd C, 73.90; H, 8.39; N, 7.60. Found: C, 73.84; H, 8.03; N, 7.28. Magnetic susceptibility (benzene-d_6, 293 K): μ_{eff} = 4.2(2) μ_B. ^{1}H NMR (benzene-d_6, 293 K): δ = 347.84 (235 Hz, 1H, *p-pyr*), 91.06 (443 Hz, 9H, C(CH_3)$_3$), 67.38 (87 Hz, 2H, *m-pyr*), -11.90 (37 Hz, 4H, *m-aryl*), -16.09 (31 Hz, 2H, *p-aryl*), -27.70 (68 Hz, 12H, CH$_2$CH_3), -66.10 (257 Hz, 2H, CH_2CH$_3$), -82.35 (308 Hz, 2H, CH_2CH$_3$), -192.59 (62 Hz, 6H, C(CH_3)), Fe-CH_2C(CH$_3$)$_3$ resonance not located.

Preparation of (^{iPr}PDI)FeCC^{t}Bu (1-CC^{t}Bu). A 200 mL round-bottomed flask was charged with 0.150 g (0.262 mmol) of **1-Cl** and approximately 100 mL of diethyl ether and placed in the cold well for 20 minutes. A second solution of 0.023 g (0.262 mmol) of LiCC^{t}Bu in approximately 10 mL of diethyl ether was added slowly dropwise and within minutes the solution became brownish-red in color. After stirring for 18 hours, the solution was filtered through Celite and the solvent was removed in vacuo. Recrystallization from concentrated ether/pentane solution at -35 °C allowed collection of 0.055 g (20 %) analytically pure **1-CC^{t}Bu**. Analysis for $C_{39}H_{52}N_3Fe$:

Calcd C, 75.71; H, 8.47; N, 6.79. Found: C, 75.32; H, 8.72; N, 7.00. Magnetic susceptibility (benzene-d_6, 293 K): μ_{eff} = 2.5(1) μ_B. ^{1}H NMR (benzene-d_6, 293 K): δ = 132.26 (201 Hz, 1H, *p-pyr*), 44.22 (44 Hz, 2H, *m-pyr*), 23.12 (32 Hz, 9H, ^tBu), -1.03 (12 Hz, 4H, *m-aryl*), -8.77 (23 Hz, 12H, CH(CH_3)$_2$), -11.57 (87 Hz, 12H, CH(CH_3)$_2$), -64.99 (338 Hz, 4H, CH(CH$_3$)$_2$), -130.68 (241 Hz, 6H, C(CH_3)), one resonance not located.

Preparation of (^{iPr}PDI)FeCCPh (1-CCPh). This complex was prepared in a manner similar to **1-CC^{t}Bu** with 0.200 g (0.349 mmol) of **1-Cl** and 0.038 g (0.349 mmol) of LiCCPh to yield 0.055 g (35 %) **1-CCPh** as a crystalline brown solid. Analysis for $C_{41}H_{48}N_3Fe$: Calcd C, 77.10; H, 7.57; N, 6.58. Found: C, 76.77; H, 7.58; N, 6.58. Magnetic susceptibility (Gouy Balance, 293 K): μ_{eff} = 2.6(2) μ_B. ^{1}H NMR (benzene-d_6, 293 K): δ = 117.29 (249 Hz, 1H, *p-pyr*), 39.75 (13 Hz, 2H, *m-pyr*), 18.78 (20 Hz, 2H, *phenyl*), 17.58 (27 Hz, 2H, *phenyl*), 14.91 (23 Hz, 1H, *phenyl*), -0.62 (25 Hz, 4H, *m-aryl*), -8.05 (25 Hz, 12H, CH(CH_3)$_2$), -10.66 (83 Hz, 12H, CH(CH_3)$_2$), -61.45 (397 Hz, 4H, CH(CH$_3$)$_2$), -121.27 (219 Hz, 6H, C(CH_3)), one resonance not located.

Preparation of (^{iPr}PDI)Fe(C_3H_5) (1-Allyl). This compound was directly synthesized by the slow addition of 0.053 g of allylmagnesium bromide (362 μL of a 1.0 M solution in ether, 0.362 mmol) to a cold stirring pentane solution containing 0.175 g (0.283 mmol) of **1-Br**. Approximately 1 mL of 1,4-dioxane was added to the reaction mixture to aid $MgBr_2$ precipitation. After stirring for 1 hour, the reddish-brown solution was filtered through a Celite and the solvent was removed *in vacuo* to yield a reddish-brown solid. This residue was washed with approximately 2 mL of pentane 5 times and the resulting concentrated pentane solution was chilled to -35 °C for days. Recrystallization yielded 0.035 g (21 %) of a brown solid identified as **1-Allyl**.

Analysis for $C_{36}H_{48}FeN_3$: Calcd C, 74.73; H, 8.36; N, 7.26. Found: C, 74.66; H, 8.49; N, 6.90. Magnetic susceptibility (benzene-d_6, 293 K): μ_{eff} = 2.4(2) μ_B. ^{1}H NMR (benzene-d_6, 293 K): δ = 148.64 (770 Hz, 2H, *allyl*), 98.47 (795 Hz, 1H, *allyl*), 72.80 (619 Hz, 2H, *allyl*), 47.64 (42 Hz, 2H, *m-pyr*), 8.07 (39 Hz, 2H), 2.99 (59 Hz, 4H, C*H*(CH_3)$_2$), 0.09 (48 Hz, 12H, CH(C*H*$_3$)$_2$), -0.46 (50 Hz, 12H, CH(C*H*$_3$)$_2$), -26.64 (184 Hz, 6H, C(C*H*$_3$)), two peaks not located.

Preparation of (^{iPr}PDI)Fe(OCH$_2$CH=CH$_2$) (1-OAllyl). A 20 mL scintillation vial was charged with 0.050 g (0.084 mmol) of **1-(N$_2$)$_2$** and approximately 15 mL of pentane. Using a microsyringe, 0.005 g (6 μL, 0.084 mmol) of allyl alcohol was added to 5 mL of pentane and this mixture was added slowly to the stirring **1-(N$_2$)$_2$** solution. After one hour, the resulting solution was filtered through Celite and the solvent was removed *in vacuo* to yield 0.026 g (52%) of a dark brown solid identified as **1-OCH$_2$CH=CH$_2$**. Analysis for $C_{35}H_{48}FeN_3O$: Calcd C, 72.15; H, 8.30; N, 7.21. Found: C, 71.94; H, 8.30; N, 6.99. Magnetic susceptibility (benzene-d_6, 293 K): μ_{eff} = 4.0(2) μ_B. ^{1}H NMR (benzene-d_6, 293 K): δ =112.09 (190 Hz, 1H), 92.59 (298 Hz, 1H), 73.61 (73 Hz, 2H), 54.76 (52 Hz, 1H), -8.90 (28 Hz, 2H, *m-aryl*), -14.82 (24 Hz, 1H, *p-aryl*), -24.26 (29 Hz, 12H, CH(C*H*$_3$)$_2$), -38.47 (149 Hz, 12H, CH(C*H*$_3$)$_2$), -118.79 (394 Hz, 4H, C*H*(CH_3)$_2$), -219.87 (131 Hz, 6H, C(C*H*$_3$)), one peak not located.

Preparation of (^{iPr}PDI)Fe(O$_2$CPh) (1-OBz). Preparation of (^{iPr}PDI)Fe(O$_2$CPh) (1-OBz). This complex was prepared from the addition of 0.031 g (0.253 mmol) of benzoic acid to 0.150 g (0.253 mmol) of **1-(N$_2$)$_2$** in toluene solution. After approximately 1 hour, the solvent was evacuated *in vacuo*. Crystallization and removal of ^{iPr}PDI impurity was accomplished by recrystallization from a toluene and pentane solution at -35 °C. Recrystallization of the remaining material from a concentrated

diethyl ether and pentane solution yielded 0.127 g (76%) of a brownish-green solid identified as **1-OBz**. Analysis for $C_{40}H_{48}FeN_3O_2$: Calcd C, 72.94; H, 7.35; N, 6.38. Found: C, 72.71; H, 7.65; N, 6.16. Magnetic susceptibility (benzene-d_6, 293 K): μ_{eff} = 4.9(2) μ_B. ^{1}H NMR (benzene-d_6, 293 K): δ = 373.68 (355 Hz, 1H, *p-pyr*), 119.63 (113 Hz, 2H, *m-pyr*), 69.35 (165 Hz, 2H, *o-phenyl*), 34.43 (25 Hz, 2H, *m-phenyl*), 19.99 (17 Hz, 1H, *p-phenyl*), -3.16 (25 Hz, 2H, *m-aryl*), -16.87 (21 Hz, 1H, *p-aryl*), -20.10 (26 Hz, 12H, CH(C*H*$_3$)$_2$), -30.10 (102 Hz, 12H, CH(C*H*$_3$)$_2$), -117.12 (516 Hz, 4H, C*H*(CH$_3$)$_2$), -284.10 (214 Hz, 6H, C(C*H*$_3$)).

Preparation of (^{iPr}PDI)Fe($O_2CCH_2CH_2Ph$) (1-H_2CIN). This compound was prepared in a manner similar to **1-OBz** with 0.250 g (0.421 mmol) of **1-$(N_2)_2$** and 0.063 g (0.421 mmol) of hydrocinnamic acid to yield 0.120 g (41%) of a dark green solid identified as **1-H_2CIN**. Analysis for $C_{42}H_{52}FeN_3O$: Calcd C, 73.46; H, 7.63; N, 6.12. Found: C, 73.38; H, 7.47; N, 5.81. Magnetic susceptibility (benzene-d_6, 293 K): μ_{eff} = 4.4(2) μ_B. ^{1}H NMR (benzene-d_6, 293 K): δ = 372.36 (116 Hz, 1H, *p-pyr*), 181.60 (379 Hz, 2H, COC*H*$_2$), 119.57 (124 Hz, 2H, *m-pyr*), 65.59 (159 Hz, 2H, C*H*$_2$(C_6H_5)), 33.60 (42 Hz, 2H, *o-phenyl*), 17.34 (16 Hz, 2H, *m-phenyl*), 15.08 (16 Hz, 1H, *p-phenyl*), -3.05 (27 Hz, 2H, *m-aryl*), -16.55 (23 Hz, 1H, *p-aryl*), -19.89 (29 Hz, 12H, CH(C*H*$_3$)$_2$), -30.04 (118 Hz, 12H, CH(C*H*$_3$)$_2$), -117.26 (533 Hz, 4H, C*H*(CH$_3$)$_2$), -284.97 (270 Hz, 6H, C(C*H*$_3$)).

REFERENCES

[1] (a) Kleigrewe, N.; Steffen, W.; Blömker, T.; Kehr, G.; Fröhlich, R.; Wibbeling, B.; Erker, G.; Wasilke, J.-C.; Wu, G.; Bazan, G. C. *J. Am. Chem. Soc.* **2005**, *127*, 13955. (b) Bianchini, C.; Giambastiani, G.; Rios, I. G.; Mantovani, G.; Meli, A.; Segarra, A. M. *Coord. Chem. Rev.* **2006**, *250*, 1391.

[2] Bart, S. C.; Ph.D. Thesis, Cornell University, 2006.

[3] Zhu, D.; Budzelaar, P. H. M. *Organometallics* **2008**, *27*, 2699.

[4] Blackmore, I. J.; Gibson, V. C.; Hitchcock, P. B.; Rees, C. W.; Williams, D. J.; White, A. J. P. *J. Am. Chem. Soc.* **2005**, *127*, 6012.

[5] Scott, J.; Vidyaratne, I.; Korobkov, I.; Gambarotta, S.; Budzelaar, P. H. M. *Inorg. Chem.* **2008**, *47*, 896.

[6] Knijnenburg, Q.; Gambarotta, S.; Budzelaar, P. H. M. *Dalton Trans.* **2006**, 5442.

[7] de Bruin, B.; Bill, E.; Bothe, E.; Weyhermüller, T.; Wieghardt, K. *Inorg. Chem.* **2000**, *39*, 2936.

[8] Bart, S. C.; Chlopek, K.; Bill, E.; Bouwkamp, M. W.; Lobkovsky, E.; Neese, F.; Wieghardt, K., Chirik, P. J. *J. Am. Chem. Soc.* **2006**, *128*, 13901.

[9] Bart, S. C.; Lobkovsky, E.; Chirik, P. J. *J. Am. Chem. Soc.* **2004**, *126*, 13794.

[10] Bouwkamp, M. W.; Bart, S. C.; Hawrelak, E. J.; Trovitch, R. J.; Lobkovsky, E.; Chirik, P. J. *Chem. Commun.* **2005**, 3406.

[11] Fernández, I.; Trovitch, R. J.; Lobkovsky, E.; Chirik, P. J. *Organometallics* **2008**, *27*, 109.

[12] Scott, J.; Gambarotta, S.; Korobkov, I.; Budzelaar, P. H. M. *J. Am. Chem. Soc.* **2005**, *127*, 13019.

[13] Cámpora, J.; Naz, A. M.; Palma, P.; Álvarez, E.; Reyes, M. L. *Organometallics* **2005**, *24*, 4878.

[14] Tondreau, A. M.; Lobkovsky, E.; Chirik, P. J. *Org. Lett.* **2008**, *10*, 2789.

[15] Small, B. L.; Brookhart, M.; Bennett, A. M. A. *J. Am. Chem. Soc.* **1998**, *120*, 4049.

[16] Britovsek, G. J. P.; Bruce, M.; Gibson, V. C.; Kimberley, B. S.; Maddox, P. J.; Mastroianni, S.; McTavish, S. J.; Redshaw, C.; Solan, G. A.; Strömberg, S.; White, A. J. P.; Williams, D. J. *J. Am. Chem. Soc.* **1999**, 121, 8728.

[17] (a) Deng, L.; Margl, P.; Ziegler, T. J. *J. Am. Chem. Soc.* **1999**, *121*, 6479. (b) Griffiths, E. A. H.; Britovsek, G. J. P.; Gibson, V. C.; Gould, I. R. *Chem. Commun.* **1999**, 1333. (c) Khoroshun, D. V.; Musaev, D. G.; Vreven, T.; Morokuma, K. *Organometallics* **2001**, *20*, 2007.

[18] Raucoules, R.; de Bruin, T.; Raybaud, P.; Adamo, C. *Organometallics* **2008**, *27*, 3368.

[19] Bouwkamp, M. W.; Lobkovsky, E.; Chirik, P. J. *J. Am. Chem. Soc.* **2006**, *128*, 9660.

[20] Scott, J.; Gambarotta, S.; Korobkov, I.; Budzelaar, P. H. M. *Organometallics* **2005**, *24*, 6298.

[21] Schmidt, R.; Welch, M. B.; Palackal, S. J.; Alt, H. G. *J. Mol. Cat. A* **2002**, *179*, 155.

[22] Sur, S. K. *J. Magn. Res.* **1989**, *82*, 169.

[23] Bart, S. C.; Lobkovsky, E.; Bill, E.; Wieghardt, K.; Chirik, P. J. *Inorg. Chem.* **2007**, *46*, 7055.

[24] Vela, J.; Smith, J. M.; Yu, Y.; Ketterer, N. A.; Flaschenriem, C. J.; Lachicotte, R. J.; Holland, P. L. *J. Am. Chem. Soc.* **2005**, *127*, 7857.

[25] Wile, B. M.; Lobkovsky, E.; Chirik, P. J. *Unpublished results*.

[26] Crabtree, R. H. *The Organometallic Chemistry of the Transition Metals*; John Wiley & Sons: Hoboken, NJ 2005, p. 465.

[27] Muresan, N.; Lu, C. C.; Ghosh, M.; Peters, J. C.; Abe, M.; Henling, L. M.; Weyhermöller, T.; Bill, E.; Wieghardt, K. *Inorg. Chem.* **2008**, *47*, 4579.

[28] Daku, L. M. L.; Vargas, A.; Hauser, A.; Fouqueau, A.; Casida, M. E. *Chem. Phys. Chem.* **2005**, *6*, 1393.

[29] Shriver, D.; Atkins, P. *Inorganic Chemistry*; W. H. Freeman and Company: New York, 1999, p. 514.

[30] Cordero, B.; Gómez, V.; Platero-Prats, A. E.; Revés, M.; Echeverría, J.; Cremades, E.; Barragán, F.; Alvarez, S. *Dalton Trans*. **2008**, 2832.

[31] Dickson, D. P. E.; Barry, F. J. *Mössbauer Spectroscopy*, Cambridge University Press: Cambridge, 1986.

[32] Pangborn, A. B.; Giardello, M. A.; Grubbs, R. H.; Rosen, R. K.; Timmers, F. J. *Organometallics* **1996**, *15*, 1518.

[33] Schrock, R. R.; Fellman, J. D. *J. Am. Chem. Soc.* **1978**, *100*, 3359.

CHAPTER 2

β-HYDROGEN CONTAINING BIS(IMINO)PYRIDINE IRON ALKYL COMPLEXES: PREPARATION, KINETIC STABILITY, AND DECOMPOSITION PATHWAYS*

2.1 Abstract

Bis(imino)pyridine iron alkyl complexes bearing β-hydrogen atoms, (^{iPr}PDI)FeR ((^{iPr}PDI = 2,6-(2,6-$^{i}Pr_2$-C_6H_3N=CMe)$_2C_5H_3N$; R = Et, ^{n}Bu, ^{i}Bu, $CH_2{}^{c}C_5H_{11}$; **1-R**), were synthesized either by direct alkylation of (^{iPr}PDI)FeCl (**1-Cl**) with the appropriate Grignard reagent or more typically by oxidative addition of the appropriate alkyl bromide to the iron bis(dinitrogen) complex, (^{iPr}PDI)Fe$(N_2)_2$ (**1-$(N_2)_2$**). In the latter method, the formal oxidative addition reaction produced (^{iPr}PDI)FeBr (**1-Br**), along with the desired iron alkyl, **1-R**. Because both compounds are known to contain high spin ferrous centers that are antiferromagnetically coupled to a singly reduced chelate, the oxidative process is bis(imino)pyridine ligand-based (one electron is formally removed from each chelate, not the metal center). The kinetic stability of each **1-R** compound was assayed in benzene-d_6 solution and found to produce a mixture of the corresponding alkane and alkene upon decomposition. The stability of each alkyl complex was inversely correlated with the number of β-hydrogens present. For example, the iron ethyl complex, (^{iPr}PDI)FeEt (**1-Et**), underwent clean loss of ethane over the course of 3 hours at 23 °C, while the corresponding isobutyl complex, (^{iPr}PDI)Fe^{i}Bu (**1-^{i}Bu**), had a half-life of over 12 hours under identical conditions. The mechanism of decomposition was studied with a series of deuterium labeling experiments and supports a pathway involving initial β-

* Parts of this chapter have been reproduced with permission from Trovitch, R. J.; Lobkovsky, E.; Chirik, P. J. *J. Am. Chem. Soc.* **2008**, ASAP (DOI: 10.1021/ja803296f). Copyright 2008 American Chemical Society.

hydrogen elimination followed by cyclometalation of an aryl isopropyl substituent, demonstrating an overall transfer hydrogenation pathway. The relevance of such pathways to chain transfer in bis(imino)pyridine iron catalyzed olefin polymerization reactions is also presented.

2.2 Introduction

When activated with methylalumoxane (MAO), aryl-substituted bis(imino)pyridine iron and cobalt dihalide compounds exhibit productivities for ethylene polymerization that rival the most efficient group 4 metallocene catalysts.[1-3] Accordingly, this class of compounds has attracted considerable attention from both academic and industrial laboratories.[4] Systematic evaluation of aryl substituent effects has established structure-reactivity relationships that allow tuning of the polymerization activity by straightforward manipulation of ligand architecture.[5] For example, bis(imino)pyridine iron dihalide pre-catalysts bearing two large 2,6-substituents on the aryl ring are known to produce linear polyethylene whereas those with only a single *ortho* aryl substituent are selective for α-olefin production with near ideal Schultz-Flory distributions.[1,2,6-8]

Despite the tremendous successes with bis(imino)pyridine iron catalysts, short catalyst lifetimes and formation of large amounts of 1-butene during ethylene oligomerization to α-olefins have been identified as potential obstacles to commercialization.[7] Ideally, new catalyst discovery would be guided by well-understood mechanistic principles – an approach that has proven invaluable in group 4 metallocene catalyst development and implementation.[9] For example, an understanding of counter ion effects, the nature of the transition structure and the influence of cyclopentadienyl substituents has resulted in the formulation of improved catalysts with remarkable selectivities, productivities, and lifetimes.[10]

In contrast, few mechanistic details are known for bis(imino)pyridine iron catalyzed polymerizations. The mode of propagation and the oxidation state of the active species remain matters of controversy. Initial theoretical studies assumed formation of cationic monoalkyl iron(II) compounds upon activation with methylalumoxane (MAO),[11,12,13] which has been experimentally supported by both NMR spectroscopy[14] and ESI mass spectrometry.[15] Alternatively, Mössbauer spectroscopic and EPR studies suggested that the iron(II) pre-catalysts are oxidized to iron(III) upon treatment with MAO.[16] Studies into the MAO-activation of bis(imino)pyridine iron dihalides by optical spectroscopy revealed gross spectral changes and a decrease of the *d-d* transitions as a function of time, temperature, and activator concentration and were interpreted as an iron centered spin transition.[17] Both the paramagnetism of the iron center and well-established redox and chemical participation of the bis(imino)pyridine ligand complicate characterization of the active species.[18,19]

In principle, these ambiguities could be resolved by preparation of well-defined, single component bis(imino)pyridine iron catalysts. Bis(imino)pyridine iron alkyl cations are worthy targets as these compounds may allow study of fundamental transformations related to chain initiation, growth and termination. For many years, however, the requisite bis(imino)pyridine iron dialkyl species remained elusive.[20] During the initial investigation of bis(imino)pyridine iron alkyl chemistry, which is discussed in detail in Chapter 1, the preparation of **1-Ns$_2$** was achieved from the addition of two equivalents of $LiCH_2SiMe_3$ to **1-Cl$_2$** followed by recrystallization from cold pentane.[21] Shortly thereafter, Gambarrotta and coworkers described a more detailed investigation into this reaction and provided evidence for chemical participation of the bis(imino)pyridine chelate.[22] Cámpora and coworkers later described a more versatile synthetic method whereby addition of free

bis(imino)pyridine to (pyridine)$_2$Fe(CH_2SiMe_3)$_2$ furnished the corresponding iron dialkyls in high yield.[23] This methodology was also utilized to explore the relative stability of neosilyl and neopentyl bis(imino)pyridine iron alkyl complexes.[24] With synthetic routes to **1-Ns$_2$** in hand, the bis(imino)pyridine iron alkyl cations, [(^{iPr}PDI)Fe-R]$^+$X$^-$ (R = CH_2SiMe_3, X$^-$ = BPh_4^-; R = $CH_2SiMe_2CH_2SiMe_3$, X$^-$ = $MeB(C_6F_5)_3^-$), were synthesized and shown to be active for ethylene polymerization.[25] While these results demonstrate the catalytic competency of a formally iron(II) alkyl cation as the propagating species, they by no means validate that such compounds are formed from MAO-activation of a bis(imino)pyridine iron dihalide. In fact, studies by Budzelaar,[26] Gambarotta[22,27,28] and Kissin[29] with bis(imino)pyridine ferrous dihalide-aluminum alkyl mixtures establish that ligand alkylation and transmetallation to aluminum are likely during polymerization.

Despite these complexities, preparation of well-defined bis(imino)pyridine iron alkyl compounds may provide insight into fundamental transformations related to catalytic olefin oligomerization and polymerization and allow for a deeper understanding of empirically established structure-reactivity relationships. In addition, these compounds allow evaluation of the chemical and electronic participation of the bis(imino)pyridine chelate and its role during catalysis. All of the bis(imino)pyridine iron alkyl complexes that are discussed in Chapter 1 are protected from β-hydrogen elimination and are persistent at ambient temperature in benzene-d_6 solution. While these compounds have proven useful in determining the stability of the iron-carbon bond and as synthons to certain iron alkyl cations, the lack of β-hydrogen atoms limits relevance to the propagating species during olefin polymerization. In addition, preliminary studies concerning the cationic iron alkyl complexes indicated slow initiation relative to propagation.[25] Seeking to expand the number of well-defined, single component iron pre-catalysts and better mimic the potential propagating

species, the synthesis, characterization, and thermal stability of bis(imino)pyridine iron alkyl complexes bearing *β*-hydrogens are described in this chapter. Investigation of alkyl bromide oxidative addition to **1-$(N_2)_2$**[30] established the loss of one electron from two different bis(imino)pyridine ligands. The mechanism of iron alkyl complex decomposition was studied and found to proceed by transfer dehydrogenation of the bis(imino)pyridine chelate.

2.3 Preparation and Characterization of β-Hydrogen Containing Alkyls

The bis(imino)pyridine iron isobutyl complex, (^{iPr}PDI)FeCH_2CHMe_2 (**1-^{i}Bu**), was the initial synthetic target of an iron alkyl complex bearing *β*-hydrogen atoms. Because the synthesis of *β*-hydrogen stabilized bis(imino)pyridine iron alkyls (Chapter 1) was accomplished by straightforward salt metathesis of **1-Cl** or **1-Br** with the appropriate alkyl lithium reagent (*e.g.* $LiCH_3$, $LiCH_2SiMe_3$, $LiCH_2CMe_3$), this route was initially explored. Stirring a diethyl ether solution of **1-Br** with one equivalent of ^{i}BuLi under a dinitrogen atmosphere for less than 30 minutes furnished only a small amount (~ 10 %) of a paramagnetic compound identified as **1-^{i}Bu** (*vide infra*). Examination of the diamagnetic region of the ^{1}H NMR spectrum established that the major iron product was the bis(dinitrogen) complex, **1-$(N_2)_2$**, formed from the reduction of **1-Br** (Figure 2.1).[30]

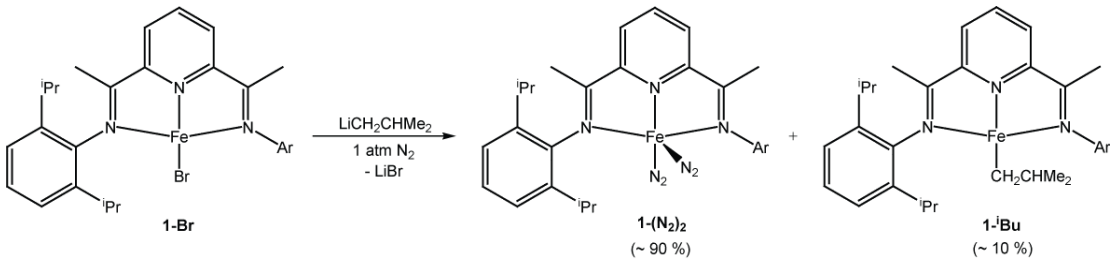

Figure 2.1. Reaction of isobutyllithium with **1-Br**.

In Chapter 1, the preparation of **1-Allyl** was accomplished from reaction of allylmagnesium bromide with **1-Br**; however, this procedure failed to result in complete consumption of the starting material, even when excess Grignard reagent was added. Because reduction, rather than alkylation, was observed for isobutyllithium addition to the iron monohalide, the less reducing isobutylmagnesium chloride was explored as a potential synthetic route to **1-^{i}Bu**. Addition of ^{i}BuMgCl to a diethyl ether solution of **1-Cl** furnished the desired iron monoalkyl in greater yield and purity than by the corresponding lithiation. Only small (~ 10%) quantities of **1-$(N_2)_2$** were obtained using this procedure. However, the kinetic instability of the compound (*vide infra*) complicated isolation of **1-^{i}Bu** on a preparative scale.

Because other bis(imino)pyridine iron alkyl complexes may be shorter lived than **1-^{i}Bu**, a more reliable synthetic method that obviated the complications of work up, titration of Grignard reagents, and the possibility of competing reduction reactions was targeted. In an attempt to expand upon the one electron oxidation of **1-$(N_2)_2$** observed upon reaction with alcohols or carboxylic acids (Chapter 1), oxidative addition of alkyl halides to **1-$(N_2)_2$** was explored as a possible synthetic route to bis(imino)pyridine iron alkyls bearing β-hydrogens. This approach remains of interest because the electronic structure of **1-$(N_2)_2$** has been described as an intermediate spin ferrous complex with a bis(imino)pyridine diradical dianion.[31] Thus, oxidative transformations can result in formal electron loss either at the metal center or the bis(imino)pyridine ligand.[32]

Studies into the oxidative addition of alkyl halides to **1-$(N_2)_2$** began with ethyl bromide. Preparation of a neutral bis(imino)pyridine iron ethyl complex was of interest given the significance of this class of compound in ethylene polymerization. Treatment of a benzene-d_6 solution of **1-$(N_2)_2$** with 0.5 equivalents of CH_3CH_2Br resulted in immediate formation of two new paramagnetic products. The first was

readily identified as the previously reported bis(imino)pyridine iron bromide, **1-Br**, while the second compound was assigned as the desired iron ethyl species, **1-Et** (Figure 2.2). The latter compound was characterized using a combination of ^{1}H NMR spectroscopy as well as degradation studies. Full details of the spectral assignment and the relative stability of each prepared *β*-hydrogen containing iron alkyl complex will be discussed.

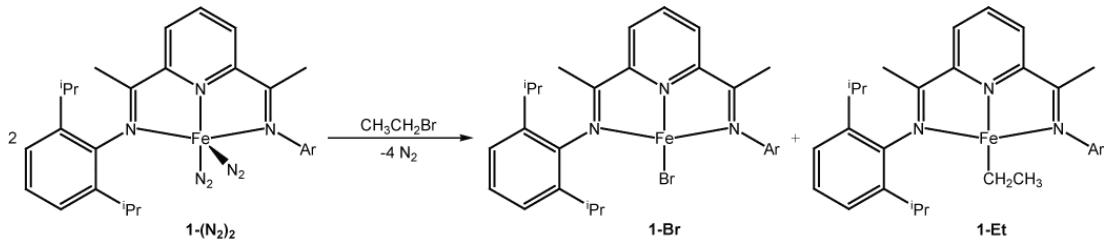

Figure 2.2. Addition of ethyl bromide to **1-$(N_2)_2$**.

The identification of **1-Et** following addition of ethyl bromide to **1-$(N_2)_2$** suggested that alkyl halide addition was an effective method for the synthesis of bis(imino)pyridine iron alkyl complexes bearing *β*-hydrogens. Addition of one equivalent of either *n*-butyl bromide or isobutyl bromide to a benzene-d_6 solution of two equivalents of **1-$(N_2)_2$** yielded **1-Br** in both cases and the bis(imino)pyridine iron *n*-butyl and *i*-butyl compounds, **1-^{n}Bu** and **1-^{i}Bu**, respectively (Figure 2.3). Vacuum transfer of the volatiles immediately following each of the aforementioned alkyl bromide addition reactions and analysis by ^{1}H NMR spectroscopy revealed formation of small amounts (25 % for *n*-BuBr, 12 % for *i*-BuBr) of alkane along with trace amounts of alkene immediately following mixing of the reagents. Addition of more than 0.5 equivalents of alkyl bromide to **1-$(N_2)_2$** furnished a detectable quantity of **1-Br_2** along with other unidentified products. Again, analysis of the volatile components by ^{1}H NMR spectroscopy following vacuum transfer established formation of the corresponding alkane and alkene.

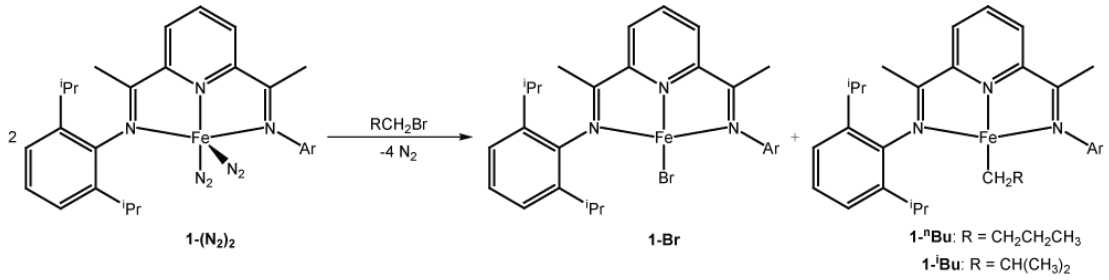

Figure 2.3. Preparation of **1-^{n}Bu** and **1-^{i}Bu**.

Because these results suggested the intermediacy of radicals during the formal oxidative addition event, the addition of 6-bromo-1-hexene to **1-$(N_2)_2$** was studied as the free 5-hexenyl radical is known to cyclize at a rate of approximately 10^5 sec^{-1}.[33] This probe has been used previously by Schwartz to assay radical chain involvement in the addition of R-X to [(η^5-$C_5H_5)_2Zr$].[34] Treatment of a benzene-d_6 solution of **1-$(N_2)_2$** with 0.5 equivalents of 6-bromo-1-hexene yielded **1-Br** along with the bis(imino)pyridine iron methylcyclopentyl complex, **1-$CH_2{}^{c}$Pent**, as the sole iron alkyl product (Figure 2.4). Analysis of the volatile components immediately following addition yielded 27 % of organic byproducts (86 % methylene cyclopentane, 14 % methyl cyclopentane) that likely arise from inefficient capture of the alkyl radical. It is also possible that **1-$CH_2{}^{c}$Pent** arises from alkylation of the metal followed by olefin insertion.

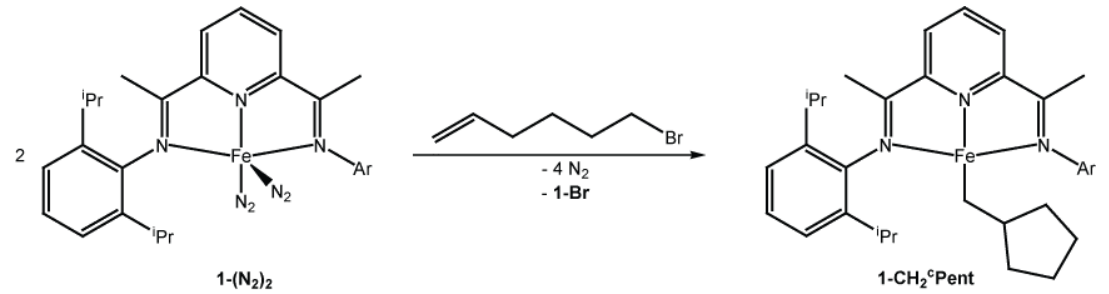

Figure 2.4. Evidence for radical cyclization by formation of **1-$CH_2{}^{c}$Pent**.

The oxidative addition of secondary and tertiary alkyl bromides to **1-(N_2)$_2$** was also explored. Addition of one equivalent of 2-bromobutane to a benzene-d_6 solution of two equivalents of **1-(N_2)$_2$** furnished **1-Br** along with small quantities (~ 5 %) of the bis(imino)pyridine iron *n*-butyl complex, **1-^{n}Bu**. Analysis of the volatile products of the reaction mixture by ^{1}H NMR spectroscopy established formation of *cis*- (4 %) and *trans*-2-butene (12 %) as the sole alkene products along with butane (84 %). The results implicate fast and irreversible β-hydrogen elimination from secondary iron alkyls along with radical formation (*vide infra*). In an analogous experiment, addition of *tert*-butyl bromide to a benzene-d_6 solution of **1-(N_2)$_2$** yielded **1-Br** along with **1-^{i}Bu**. Collection and examination of the volatiles from this reaction (before significant decomposition of the iron alkyl, *vide infra*) by ^{1}H NMR spectroscopy revealed that a near equimolar ratio of isobutene and isobutane accompanies oxidative addition, consistent with involvement of *tert*-butyl radical.

Each of the bis(imino)pyridine iron alkyl complexes bearing β-hydrogens was kinetically unstable and handled carefully - and sometimes quickly - in solution under an inert atmosphere. As a result, characterization of these compounds has relied primarily on ^{1}H and ^{2}H NMR spectroscopy augmented by degradation studies. The complete assignment of the ^{1}H NMR spectrum of **1-Br**, and the other alkyl complexes described in Chapter 1, have proven valuable for the spectroscopic characterization of the bis(imino)pyridine iron alkyl complexes bearing β-hydrogens. Selected assignments for each iron alkyl complex presented in this Chapter are given in Table 3.1. A representative benzene-d_6 ^{1}H NMR spectrum of **1-Et** recorded at 23 ºC is presented in Figure 2.5. As the spectroscopic properties of each alkyl compound are similar, only **1-Et** will be discussed in detail. For **1-Et**, the imine methyl group appears the most upfield at –172.74 ppm while the *p*-pyridine hydrogen is the most downfield at 263.35 ppm. Other diagnostic resonances with large isotropic shifts are

the *m*-pyridine hydrogens located at 63.75 ppm and the isopropyl methine centered at –89.75 ppm. Unfortunately, the hydrogens on the carbon attached directly to the iron have not been located by ^{1}H NMR spectroscopy for any iron alkyl compound prepared in this dissertation.

Table 2.1. Selected ^{1}H NMR resonances for bis(imino)pyridine iron alkyl complexes bearing *β*-hydrogen atoms. All values reported in ppm in benzene-d_6 at 23 ºC.

Complex	*p-pyr*	*β-Alkyl*	*m-pyr*	N=C*Me*
1-Et	263.4	149.7	63.8	-172.7
1-^{n}Bu	284.5	142.5	64.8	-175.4
1-^{i}Bu	350.0	200.4	66.3	-185.6
1-CH$_2$^{c}Pent	338.9	197.2	67.4	-182.3

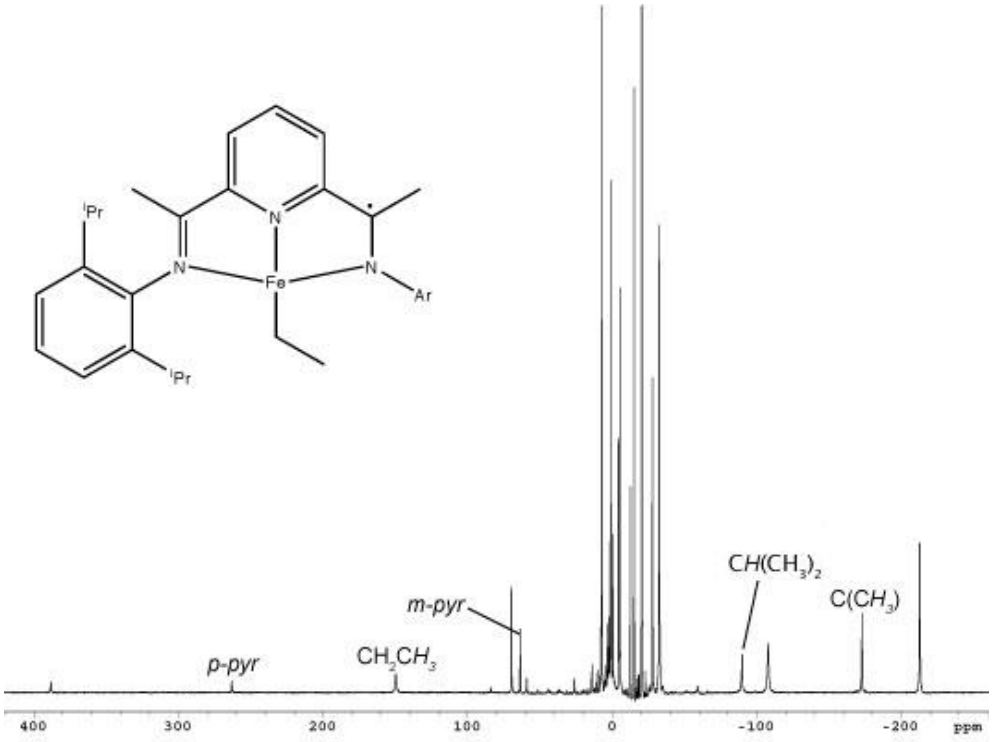

Figure 2.5. ^{1}H NMR spectrum of **1-Et** (labeled resonances) along with **1-Br** (unlabeled) in benzene-d_6 at 23 ºC.

2.4 Stability and Decomposition Products

With a family of neutral bis(imino)pyridine iron alkyls with *β*-hydrogens in hand, the relative stability of each compound was assayed in benzene-d_6 solution at 23 ºC. After 18 hours, **1-Et** undergoes exclusive loss of ethane and formation of two new iron products (Figure 2.6). One of the iron products was identified as the diamagnetic bis(imino)pyridine dinitrogen complex, **1-(N_2)** (or **1-(N_2)$_2$**, depending on the amount of N_2 present).[30] The second iron compound, **1-DH**, was detected after hydrolysis of the organometallic products and analysis of the free chelate by ^{1}H NMR spectroscopy as well as by D_2 addition experiments. This molecule was previously observed and characterized following the decomposition of a bis(imino)pyridine iron diazoalkane complex.[35] Thus, the decomposition of **1-Et** can be viewed as a transfer dehydrogenation from the ligand to the iron alkyl, liberating ethane and forming an equimolar mixture of **1-N_2** and **1-DH**. In the case of **1-Et**, the liberated ethane was quantified with a Toepler pump and 92 % of the expected gas was obtained.

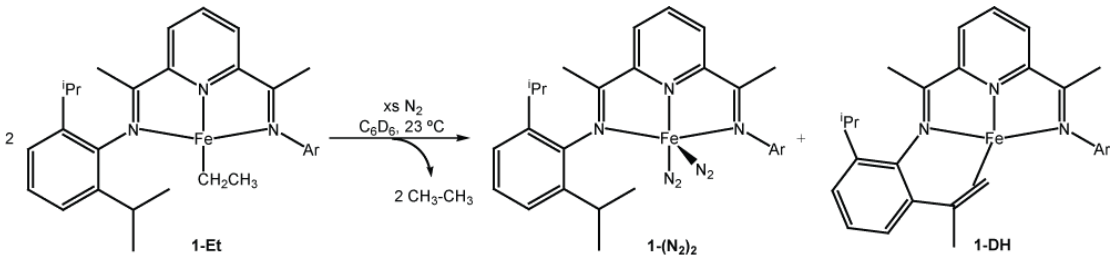

Figure 2.6. Decomposition of **1-Et** by way of transfer hydrogenation.

The thermal stability and half-lives of the bis(imino)pyridine iron alkyls with β-hydrogens prepared in this study were also assayed at 23 ºC in benzene-d_6. The organic products released following disappearance of the iron alkyl were identified by ^{1}H NMR spectroscopy and are reported in Figure 2.7. In addition, the half-life for each reaction is also reported in Figure 2.7. In each case, a mixture of iron products, **1-$(N_2)_n$** and **1-DH**, was observed and is denoted as "[Fe]" for simplicity. The iron *n*-butyl compound, **1-^{n}Bu**, exhibited a significantly longer half-life than **1-Et** but produced predominantly butane with small amounts of 2-butene. No 1-butene was detected by ^{1}H NMR spectroscopy from these experiments.

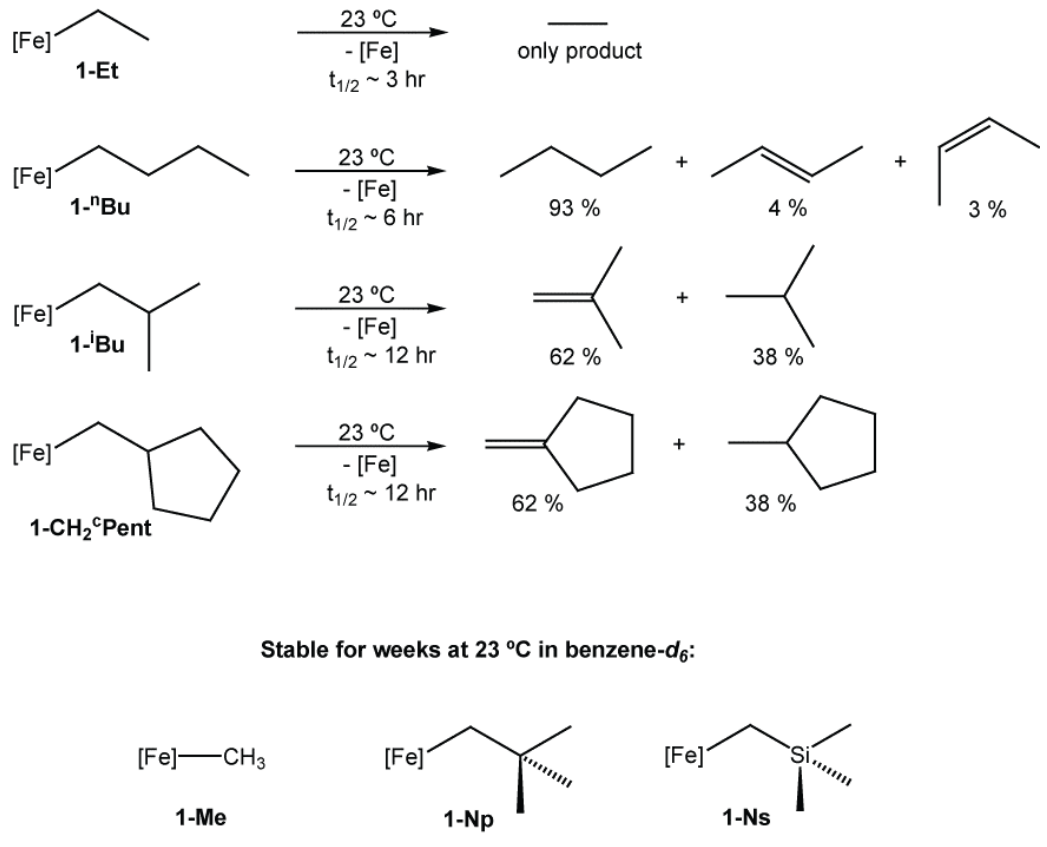

Figure 2.7. Thermal stability of bis(imino)pyridine iron alkyl complexes.

Bis(imino)pyridine iron alkyls bearing only one β-hydrogen, **1-^{i}Bu** and **1-$CH_2{}^{c}$Pent**, were longer lived than either **1-Et** or **1-^{n}Bu** and produced significantly higher fractions of olefins upon disappearance of the iron alkyl, demonstrating a reduced propensity for transfer hydrogenation with more sterically demanding alkyls. The relatively long lifetime of **1-^{i}Bu** versus **1-^{n}Bu** and **1-Et**, established that stability of the iron alkyls decreased as the number of β-hydrogens increase.

The loss of alkane from the compounds presented in Figure 2.7 prompted reinvestigation of the thermal stability of **1-Me**, **1-Ns** and **1-Np**. It is possible that iron-carbon bond homolysis,[36] not β-hydrogen elimination, is responsible for the kinetic instability of the iron-alkyls prepared in this work. Allowing benzene-d_6 solutions of **1-Me**, **1-Ns** or **1-Np** to stand at 23 ºC produced no detectable change by ^{1}H NMR spectroscopy. Because the iron-carbon bond strengths for **1-Et**, **1-^{n}Bu**, **1-^{i}Bu** and **1-Np** are expected to be similar,[37] the relative stability of the compounds is believed to be a result of the presence or absence of β-hydrogens. In fact, if iron bond homolysis were indeed operative, the more hindered **1-Np** may be expected to be the least, not most, kinetically persistent.

2.5 Deuterium Labeling Studies

The loss of alkane and formation of **1-DH** from the bis(imino)pyridine iron alkyl complexes prompted more detailed studies into the mechanism of thermal decomposition for these compounds. Understanding these pathways may provide insight into chain transfer processes related to bis(imino)pyridine iron-catalyzed olefin oligomerizations and polymerizations. Previous studies with MAO-activated metal dihalides indicate that chain transfer by β-hydrogen elimination is more prominent for cobalt than for iron catalysts,[38] although in single component iron cases, β-hydrogen elimination was indeed observed.

A series of deuterium labeling experiments were conducted to verify the origin of the hydrogen atoms in the alkane products. Treatment of a benzene solution of **1-$(N_2)_2$** with 0.5 equivalents of CD_3CD_2Br yielded a mixture of **1*-Et-d_n** and **1*-Br** as judged by ^{2}H NMR spectroscopy (Figure 2.8). The "*" designates deuterium incorporation into an isopropyl methyl group. Analysis of the mixture by ^{2}H NMR spectroscopy within 15 minutes of alkyl halide addition revealed the presence of peaks centered at 36.4 and 149.7 ppm, corresponding to the Fe-CD_2CD$_3$ and Fe-CD$_2$CD_3 deuterons, respectively. The resonance for the methylene positions was only observed by ^{2}H NMR spectroscopy; no corresponding peak has been located in the ^{1}H NMR spectrum of natural abundance **1-Et**. Observation of ^{2}H but not ^{1}H NMR peaks is due to better resolution of deuterium spectra for paramagnetic compounds; a phenomenon that is a result of the difference in magnetogyric ratios of the two nuclei.[39] Interestingly, the ^{2}H NMR spectrum of the product mixture also contained four additional peaks corresponding to deuterium labeling of the isopropyl methyl groups of *both* **1-Br** and **1-Et**.

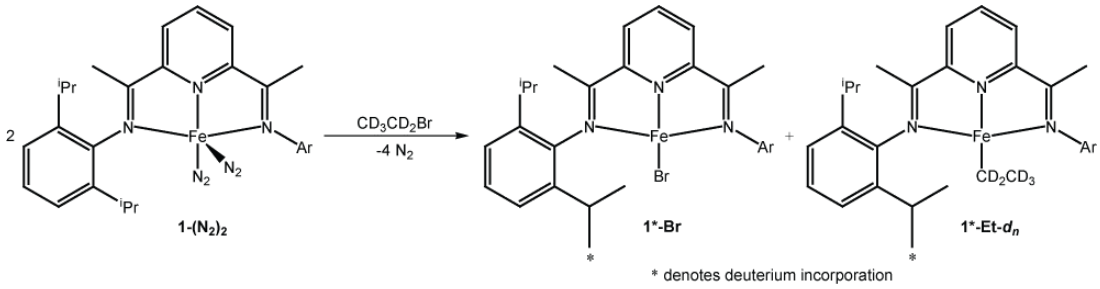

Figure 2.8. Bis(imino)pyridine deuterium incorporation from bromoethane-d_5.

Monitoring the stability of **1*-Et-d_n** by ^{2}H NMR spectroscopy at 23 ºC in benzene-d_6 revealed smooth disappearance of the resonances for the ethyl chain over the course of 3.5 hours. Throughout this experiment, the peaks for the isopropyl methyl positions of **1*-Et-d_n** remain, demonstrating deuterium depletion from the

ethyl chain *before* alkane loss (Figure 2.9). After 18 hours at 23 ºC, no ^{2}H NMR signals assigned to **1*-Et** remained, consistent with the lifetime measured previously for natural abundance **1-Et** determined by ^{1}H NMR spectroscopy. Because of the complexities associated with isotopic scrambling into the ligand, kinetic isotope effects for the loss of ethane from isotopologues of **1-Et** were not determined (Figure 2.9).

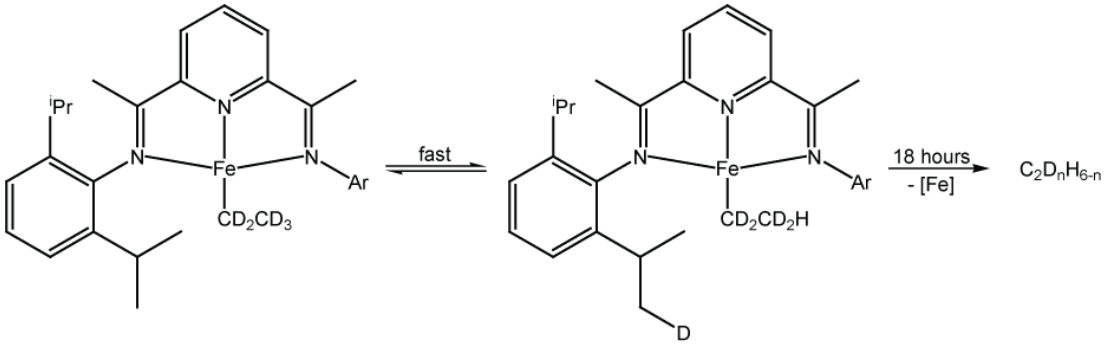

Figure 2.9. Isotopic exchange observed for **1-Et-d_5**.

Evidence for isotopic exchange within the ethyl chain prior to ethane loss was also obtained from ^{1}H NMR spectroscopy. A ^{1}H NMR resonance was observed at 149.7 ppm approximately 20 minutes following addition of CD_3CD_2Br to **1-$(N_2)_2$**. It is likely that hydrogen was also incorporated into the iron methylene position, however, the inability to observe a signal for this position by ^{1}H NMR spectroscopy prohibits obtaining definitive experimental evidence. These experiments definitively establish "chain walking" – reversible β-hydrogen elimination followed by olefin rotation (or loss) and reinsertion – prior to cyclometalation and reductive elimination of ethane.

A benzene solution of **1-$(N_2)_2$** was also treated with 0.5 equivalents of CH_3CD_2Br. After 30 minutes at 23 ºC, the ^{2}H NMR spectrum of the product mixture established formation of **1*-Br** along with **1*-Et-d_n**. At this time interval, the alkyl region of the ^{2}H NMR spectrum contained a prominent peak at 38 ppm for the Fe-CD_2CH$_3$ position and a very small peak, barely above the detection limit of the

experiment (≤5 %), at 145 ppm, suggesting that only a minimal amount of deuterium was present in the *β*-methyl group and that the two positions are not rapidly exchanging. Continued monitoring of the compound by ^{2}H NMR spectroscopy over the course of 18 hours revealed disappearance of the ethyl complex with continued observation of the peaks for **1*-Br**.

The incorporation of deuterium into the isopropyl methyl groups of both the iron alkyl and the iron bromide compounds clearly establishes chemical participation of the bis(imino)pyridine chelate. Additional experiments were carried out to determine the origin of the deuterium in **1*-Br**. Because it is known that the isopropyl methyl groups of **1-(N$_2$)$_2$** are rapidly deuterated upon exposure to four atmospheres of D_2 gas, an analogous experiment was conducted with isolated **1-Br**. No deuterium incorporation was observed over the course of 24 hours at 23 ºC, demonstrating that isopropyl methyl group cyclometalation is not operative in this compound.

One possibility for the formation of **1*-Br** involves ligand exchange from **1*-R**. Because **1*-Br** was observed immediately following addition of bromoethane-d_5 to **1-(N$_2$)$_2$**, the product iron alkyl must undergo rapid *β*-hydrogen (deuterium) elimination and cyclometalation to form **1*-(N$_2$)**, which then would participate in ligand exchange. Crossover experiments were conducted to evaluate this possibility (Figure 2.10). The imine methyl groups of the bis(imino)pyridine ligand were deuterium-labeled to track the chelate compounds by ^{1}H and ^{2}H NMR spectroscopy. The compounds with deuterium-labeled imine methyl groups are designated by "**". Thus, **1**-Br** was prepared in a straightforward manner from $NaBEt_3H$ reduction of **1**-Br$_2$**.[21]

Preparation of a benzene solution containing an equimolar mixture of **1**-Br** and **1-(N$_2$)$_2$** at 23 ºC resulted in immediate formation of **1**-(N$_2$)$_2$** as judged by ^{2}H NMR spectroscopy (Figure 2.10). Performing a similar experiment with **1**-Br** and **1-Np** produced no evidence for formation of **1**-Np**, suggesting that ligand exchange

does not occur between iron halide and iron alkyl complexes. Thus, observation of **1*-Br** from addition of either CD_3CD_2Br or CH_3CD_2Br to **1-$(N_2)_2$** is likely due to rapid cyclometalation and isotopic exchange from the iron alkyl followed by ligand exchange to form **1*-Br**. The ligand undergoing exchange could either be the bromide or the bis(imino)pyridine chelate. Although our experiments do not distinguish these two possibilities (or a combination of the two), the bromide exchange process is tentatively favored. Recall that **1-$(N_2)_n$** (n = 1, 2) is formed from the thermal decomposition of **1-Et** and thus ligand exchange can occur throughout the process of ethylene dissociation and ethane formation.

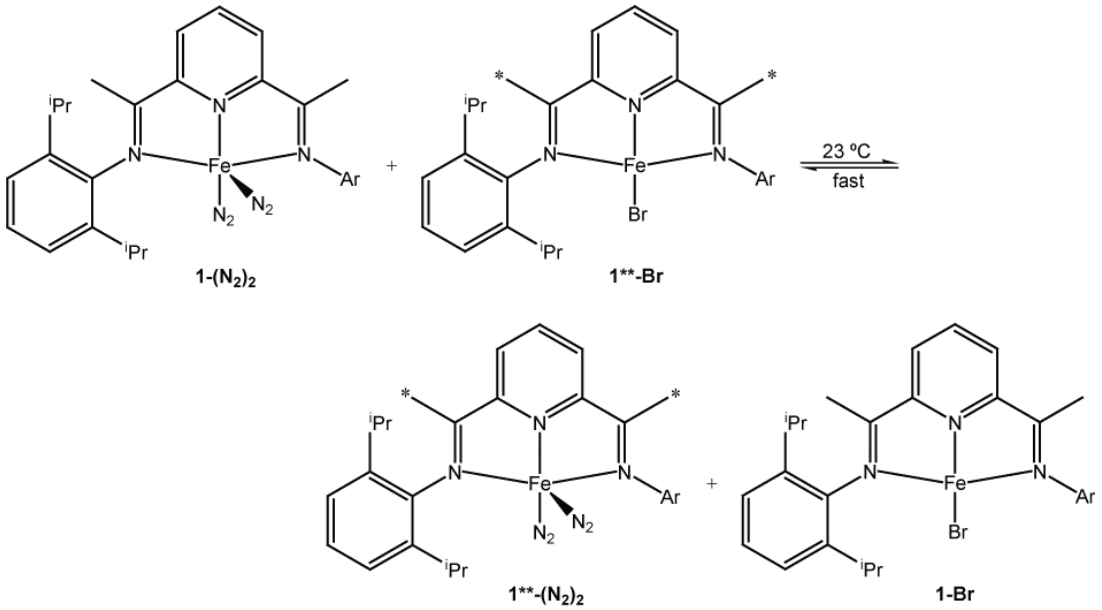

Figure 2.10. Facile ligand exchange between **1**-Br** and **1-$(N_2)_2$**.

Deuterium labeling experiments were also carried out with **1-^{n}Bu** to assay the possibility of alkyl chain running and confirm bis(imino)pyridine participation. The deuterium labeled iron dinitrogen complex, **1*-$(N_2)_2$**, was prepared by addition of excess D_2 gas to **1-$(N_2)_2$**.[30] Addition of 0.5 equivalents of $CH_3CH_2CH_2CH_2Br$ to a benzene solution of **1*-$(N_2)_2$** resulted in rapid formation of **1*-Br** along with **1*-^{n}Bu**.

Monitoring the disappearance of **1*-^{n}Bu** by ^{2}H NMR spectroscopy established deuterium incorporation into all positions of the butane and 2-butenes (Figure 2.11). Thus, alkyl isomerization (chain walking) is operative concomitant with alkane and alkene loss and chelate cyclometalation.

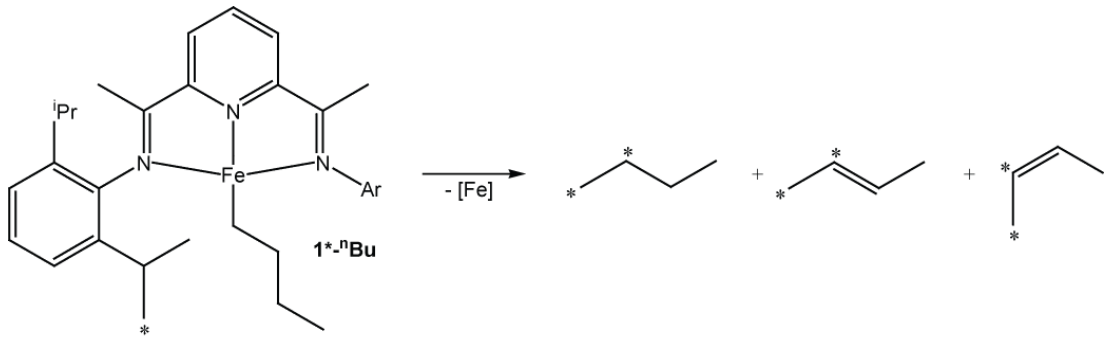

Figure 2.11. Observation of deuterated butane and butenes from **1*-^{n}Bu** degradation.

The oxidative addition of CD_3OTf to **1-$(N_2)_2$** was also studied as a control experiment to verify that the β-carbon position was the source of deuterium during competing cyclometalation. Treatment of **1-$(N_2)_2$** with 0.5 equivalents of CD_3OTf cleanly furnished the deuterated isotopologue of the previously reported iron methyl complex, **1-CD_3**,[21] along with the bis(imino)pyridine iron triflate, **1-OTf**. The latter complex was independently prepared by addition of Me_3SiOTf to **1-$(N_2)_2$** and has been fully characterized and displays diagnostic ^{1}H NMR shifts, similar to the iron acetate complexes described in chapter 1. Importantly, analysis of the product mixture by ^{2}H NMR spectroscopy provided no evidence for deuterium incorporation into the isopropyl methyl groups of either **1-CD_3** or **1-OTf**, confirming the β-position of the alkyl as the source of isotopic exchange.

Additionally, olefins were added to **1-$(N_2)_2$** to further assay cyclometalation and the transfer hydrogenation step. Addition of one equivalent of 1-hexene to a

benzene-d_6 solution of **1-$(N_2)_2$** at 23 ºC resulted in clean and quantitative formation of **1-DH** and hexane over the course of five days (Figure 2.12). The iron-olefin compound, **1-DH**, and ethane were also obtained following treatment of **1-$(N_2)_2$** with excess ethylene. In this case, an unidentified insoluble red precipitate was formed, that upon degradation yielded ethane. Despite this complication, these experiments clearly establish the role of the chelate isopropyl methyl groups in transfer hydrogenation of the iron alkyl.

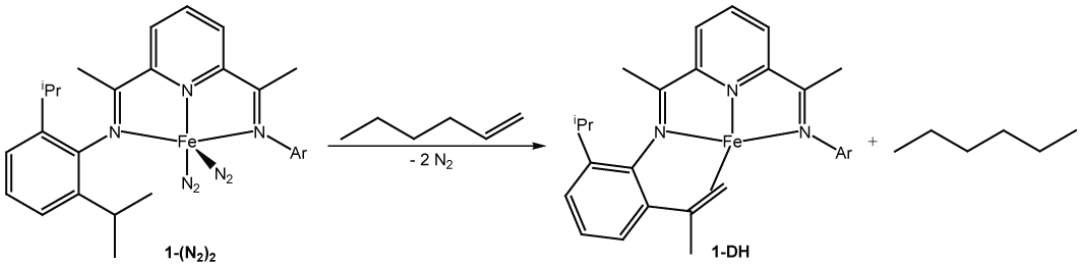

Figure 2.12. Transfer hydrogenation of 1-hexene.

To further substantiate the claim of facile β-hydrogen elimination and olefin dissociation prior to alkane formation, olefin for iron alkyl exchange studies were also conducted. Addition of one equivalent of isobutene to a benzene-d_6 solution of **1-$CH_2{}^cPent$** resulted in a near equimolar mixture of **1-^{i}Bu** and **1-$CH_2{}^cPent$** along with the corresponding free olefins (Figure 2.13). Similar exchange reactions were observed in related bis(imino)pyridine cobalt complexes where treatment of (PDI)CoR (R = ^{n}Pr, ^{n}Bu) with ethylene yielded the corresponding cobalt ethyl and free olefins.[40]

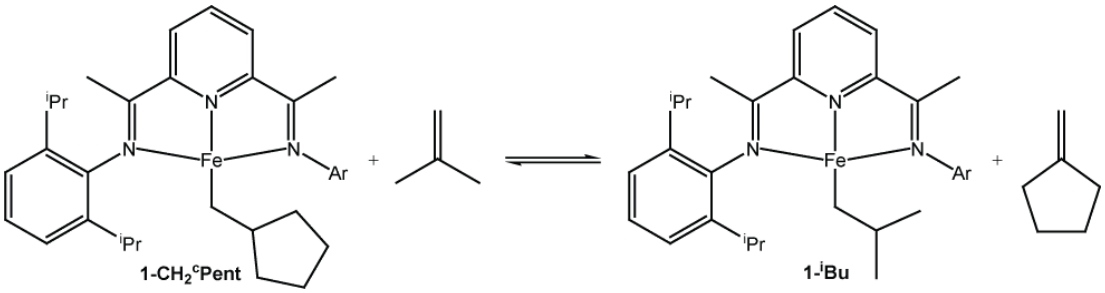

Figure 2.13. Alkyl group exchange through fast β-hydrogen elimination.

2.6 Discussion

The electronic structure of **1-Br**, in combination with the magnetic and structural data for the isolated iron alkyls **1-Me** and **1-Ns** (presented in Chapter 1), provides additional insight on the oxidative addition of alkyl bromides to **1-$(N_2)_2$**. The sp^3 hybridized bis(imino)pyridine iron alkyls have an identical electronic structure to **1-Br**; overall $S = 3/2$ ground states arising from high spin ($S_{Fe} = 2$) ferrous centers antiferromagnetically coupled to bis(imino)pyridine radical anions ($S_{PDI} = 1/2$). Thus, oxidative addition of alkyl bromides to **1-$(N_2)_2$** is formally *ligand*, rather than metal, based. The two electron reduced bis(imino)pyridine chelate in **1-$(N_2)_2$** is oxidized by one electron to produce two new iron products where the iron(II) oxidation state is preserved (Figure 2.14).[41] Notably, a spin change from intermediate to high spin occurs at the iron center upon chelate oxidation.

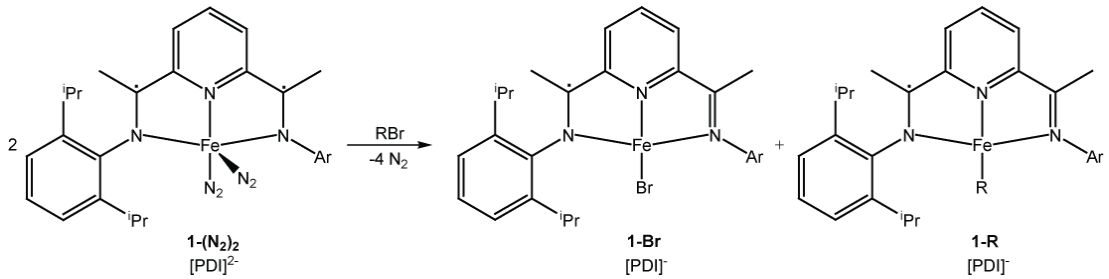

Figure 2.14. Ligand based oxidative addition of alkyl bromides to **1-$(N_2)_2$**.

Based on all of the experimental data, a mechanism for alkane loss from bis(imino)pyridine iron alkyl complexes is presented in Figure 2.15, using **1-Et** as a representative example. β-hydrogen elimination from the iron alkyl forms the bis(imino)pyridine iron olefin hydride compound. Olefin dissociation and reinsertion (or olefin rotation) is fast relative to subsequent steps, as isotopic exchange between the β-CH_3 and α-CH_2 positions is faster than liberation of alkane. If ethylene loss occurs, a putative bis(imino)pyridine iron hydride is formed, which is known to

undergo rapid loss of H_2 to form either the iron dihydrogen or N_2 complex, depending on the relative concentration of the respective gases.[30] Formal oxidative addition of an isopropyl methyl C-H bond affords the bis(imino)pyridine cyclometalated hydride. A similar species has been implicated in H/D exchange in the preparation of **1*-$(N_2)_2$** from D_2 gas.[30] Insertion of ethylene into the iron hydride bond yields the cyclometalated ethyl compound, which can undergo reversible or productive β-hydrogen elimination to furnish ethane and **1-DH**.

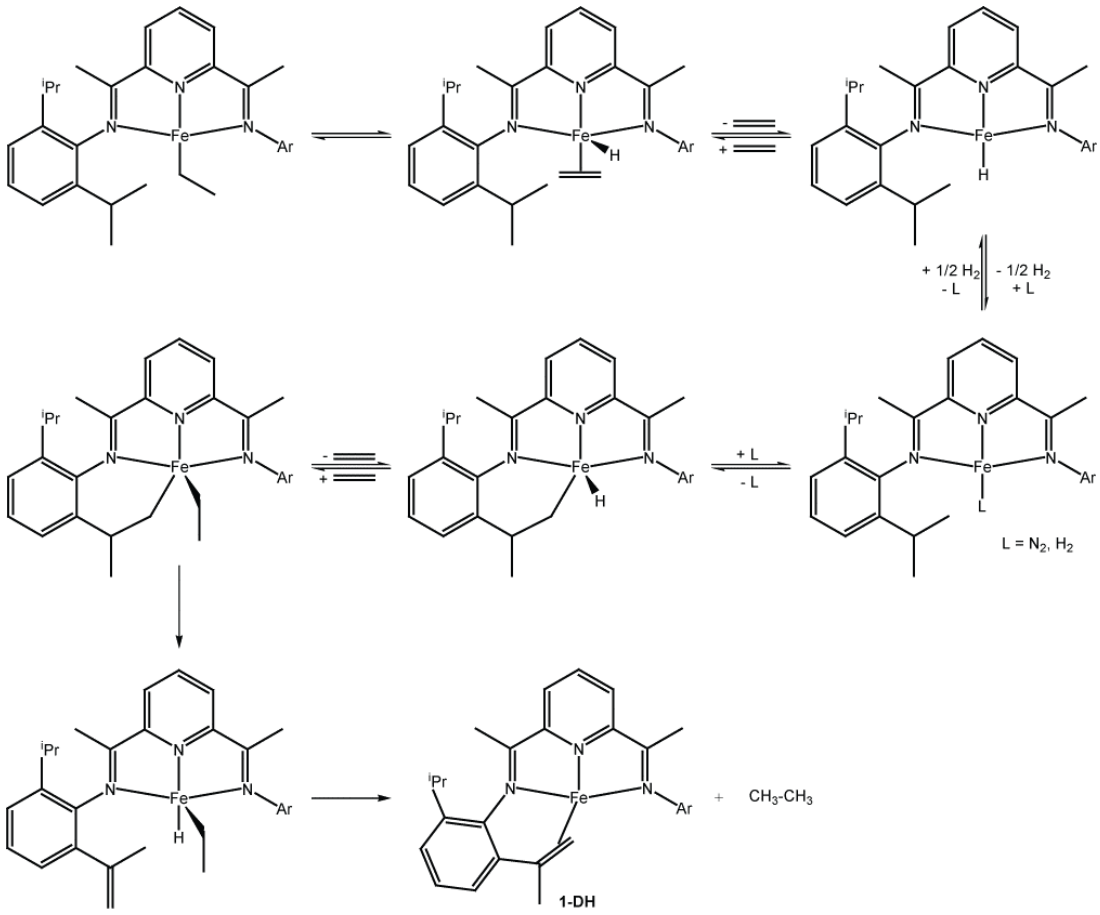

Figure 2.15. Mechanism of **1-Et** degradation and transfer hydrogenation.

It is interesting to compare the relative stability of the bis(imino)pyridine iron alkyl compounds studied in this work to the three coordinate β-diketiminate (BDI)

iron alkyls reported by Holland and coworkers.[37] Because the **1-R** series of compounds are best described as containing high spin ferrous ions antiferromagnetically coupled to bis(imino)pyridine chelate radical anions, both classes of molecules contain a high spin (S_{Fe} = 2) iron coordinated to a mononanionic ligand. Furthermore, both ligand environments possess orthogonal 2,6-diisopropyl aryl substituents and to a first approximation (ignoring differences in chelate bite angles), have similar steric environments.

In a comprehensive study of iron(II) alkyl stability, Holland and co-workers prepared a broad spectrum of (BDI)Fe-R compounds bearing β-hydrogens, including secondary and tertiary iron alkyls.[37] Isomerization of the iron alkyl and olefin for alkyl exchange reactions were observed, demonstrating that reversible β-hydrogen elimination is operative. Irreversible formation or decomposition of these compounds by alkane loss was not reported. This difference in reactivity may be traced to the competing cyclometalation in the bis(imino)pyridine compounds. The instability of the putative product of β-hydrogen elimination, **1-H**, is due to H_2 loss and formation of formally low-valent [(^{iPr}PDI)Fe] compounds. This enables ligand C-H activation and provides a pathway to irreversible alkane formation and hence decomposition of the iron alkyl. No analogous compound or pathway has been reported in the β-diketiminate chemistry and hence kinetically persistent iron alkyls result. It should be noted that in the bis(imino)pyridine examples, chain walking via β-hydrogen elimination, olefin dissociation (or rotation) followed by reinsertion is operative followed by a slower cyclometalation-insertion sequence.

2.7 Conclusion

Neutral bis(imino)pyridine iron alkyl complexes bearing *β*-hydrogen atoms have been synthesized either by salt metathesis reactions or by oxidative addition of an appropriate alkyl bromide to **1-$(N_2)_2$**. Studies into the electronic structures of both **1-R** and **1-Br** establish that formal electron loss occurs from the bis(imino)pyridine ligand, not the metal. Evaluation of the kinetic stability of the iron alkyl species revealed decomposition by transfer hydrogenation of an isopropyl methyl substituent on the chelate aryl rings. The ability to access reduced iron compounds, stabilized by a redox active bis(imino)pyridine chelate, promotes C-H bond oxidative addition leading to cyclometalation and irreversible formation of alkane. These studies demonstrate the viability of this process as a chain termination pathway in bis(imino)pyridine iron catalyzed olefin polymerization reactions.

2.8 Experimental Procedures

General Considerations. All air- and moisture-sensitive manipulations were carried out using standard vacuum line, Schlenk, and cannula techniques or in an MBraun inert atmosphere dry box containing an atmosphere of purified nitrogen. Solvents for air- and moisture-sensitive manipulations were initially dried and deoxygenated using literature procedures.[42] Hydrogen and deuterium gas were passed through a column containing manganese oxide supported on vermiculite and 4 Å molecular sieves before admission to the high vacuum line. Benzene-d_6 and toluene-d_8 were purchased from Cambridge Isotope Laboratories and dried over 4 Å molecular sieves or titanocene, respectively. **1-$(N_2)_2$** and **1-Br** were prepared according to literature procedures.[30,21] Isobutyllithium and isobutylmagnesium chloride were purchased from Aldrich and used as received. Methyl trifluoromethanesulfonate, methyl trifluoromethanesulfonate-d_3, and trimethylsilyl trifluoromethanesulfonate were

purchased from Aldrich and vacuum transferred from 4 Å molecular sieves. Bromoethane and bromoethane-d_5 were purchased from Aldrich and dried over calcium hydride before use. 1-Bromo-2-methylpropane was purchased from Acros and dried in a similar fashion. 6-Bromo-1-hexene was obtained from Alfa Aesar and dried over calcium hydride. 2-Bromobutane was purchased from Eastman and dried over calcium hydride before use. 2-Bromo-2-methylpropane and 1-bromobutane were dried over calcium hydride after being received from Fisher Scientific. 1-Hexene and 2-methylpropene were purchased from Aldrich and dried over lithium aluminum hydride. Bromoethane-1,1-d_2 was purchased from CDN Isotopes and dried over calcium hydride before use.

^{1}H NMR spectra were recorded on Varian Mercury 300, Inova 400, 500, and 600 spectrometers operating at 299.76, 399.78, 500.62, and 599.78 MHz, respectively. ^{2}H NMR spectra were recorded at 20 ºC on the Inova 400, 500, and 600 MHz spectrometers operating at 61.37, 76.85, and 92.07 MHz, respectively. All ^{1}H chemical shifts are reported relative to $SiMe_4$ using the ^{1}H (residual) shift of the solvent as a secondary standard. Approximate half-lives for the iron alkyl complexes were determined by following the disappearance of the imine methyl and isopropyl methyl resonances of this complex over time. Relative integrations of the imine methyl and isopropyl methyl ^{1}H NMR resonances of **1-Br** were used as benchmarks for comparison. Solution magnetic moments were determined by Evans method[43] using a ferrocene standard and are the average value of at least two independent measurements. Peak width at half height is given for paramagnetically broadened resonances. Elemental analyses were performed at Robertson Microlit Laboratories, Inc., in Madison, NJ.

Single crystals suitable for X-ray diffraction were coated with polyisobutylene oil in a drybox, transferred to a nylon loop, and quickly moved to the goniometer head

of a Bruker X8 APEX2 diffractometer equipped with a molybdenum X-ray tube (λ = 0.71073 Å). Preliminary data revealed the crystal system. A hemisphere routine was used for data collection and determination of lattice constants. The space group was identified and the data were processed using the Bruker SAINT+ program and corrected for absorption using SADABS. The structures were solved using direct methods (SHELXS) completed by subsequent Fourier synthesis and refined by full-matrix least-squares procedures.

Characterization of (^{iPr}PDI)Fe(CH_2CH_3) (1-Et). Using a calibrated gas bulb, 0.021 mmol of either bromoethane or bromoethane-d_5 was transferred to a J. Young Tube containing 0.025 mg (0.042 mmol) of **1-$(N_2)_2$** and approximately 0.7 mL of benzene-d_6. Upon sitting at room temperature for 20 min, the reaction mixture was found to contain **1-Br** and **1-Et** (or **1-Et-d_5**) by ^{1}H NMR spectroscopy. ^{1}H NMR (benzene-d_6, 293 K): δ = 263.35 (221 Hz, 1H, *p-pyr*), 149.69 (555 Hz, 3H, CH_2CH_3), 63.75 (103 Hz, 2H, *m-pyr*), -4.50 (100 Hz, 4H, *m-aryl*), -15.14 (64 Hz, 12H, $CH(CH_3)_2$), -27.88 (123 Hz, 12H, $CH(CH_3)_2$), -89.75 (308 Hz, 4H, $CH(CH_3)_2$), -172.74 (214 Hz, 6H, $C(CH_3)$), Fe-CH_2 and *p-aryl* resonance not located. Degradation of **1-Et** was monitored over the course of 24 hours at ambient temperature. Transfer of the volatiles and analysis by ^{1}H NMR spectroscopy confirmed a 15 % yield of solely ethane (based on bromoethane) as judged by integration against 1 μL of cyclohexane. A second degradation experiment yielded 92 % of the ethane expected by Toepler pump analysis.

Characterization of (^{iPr}PDI)Fe($CH_2CH_2CH_2CH_3$) (1-^{n}Bu). This complex was prepared in a manner similar to **1-Et** along with **1-Br** from the gas bulb addition of 0.017 mmol of 1-bromobutane to 0.020 g (0.034 mmol) of **1-$(N_2)_2$** in benzene-d_6. ^{1}H

NMR (benzene-d_6, 293 K): δ = 284.47 (106 Hz, 1H, *p-pyr*), 142.49 (3149 Hz, 2H, $FeCH_2CH_2CH_2CH_3$), 64.78 (76 Hz, 2H, *m-pyr*), 60.05 (86 Hz, *butyl*), 36.92 (64 Hz, *butyl*), -5.59 (65 Hz, 4H, *m-aryl*), -6.41 (59 Hz, 2H, *p-aryl*), -16.40 (65 Hz, 12H, $CH(CH_3)_2$), -28.85 (112 Hz, 12H, $CH(CH_3)_2$), -99.21 (255 Hz, 4H, $CH(CH_3)_2$), -175.37 (177 Hz, 6H, $C(CH_3)$), Fe-CH_2 resonance not located. Complete decomposition of **1-^{n}Bu** occurred within 72 hours at ambient temperature. Transfer of the volatiles and analysis by ^{1}H NMR spectroscopy confirmed a 41 % return of the alkyl derivative (93 % butane, 4 % *trans*-2-butene, and 3 % *cis*-2-butene) as judged by ^{1}H NMR integration against 1 μL of cyclohexane.

Characterization of (^{iPr}PDI)Fe(CH_2CHMe_2) (1-^{i}Bu). In a manner similar to bromoethane, gas bulb addition of 0.017 mmol of 1-bromo-2-methylpropane to 0.020 g of **1-$(N_2)_2$** yielded a mixture of **1-Br** and **1-^{i}Bu** in benzene-d_6, as judged by ^{1}H NMR spectroscopy. This complex was additionally observed by ^{1}H NMR spectroscopy, along with **1-Br**, from the addition of 0.002 g (2 μL, 0.017 mmol) of 2-bromo-2-methylpropane to 0.020 g (0.034 mmol) of **1-$(N_2)_2$** in benzene-d_6. A third method of preparation was achieved through the addition of 0.008 g (32 μL of a 2.0 M solution in ether, 0.065 mmol) of isobutylmagnesium chloride to a J. Young tube containing 0.025 g (0.044 mmol) of **1-Cl** in benzene-d_6. ^{1}H NMR (benzene-d_6, 293 K): δ = 350.03 (583 Hz, 1H, *p-pyr*), 200.42 (7533 Hz, 1H, $FeCH_2CH(CH_3)_2$), 73.34 (301 Hz, 6H, ^{i}Bu CH_3), 66.30 (85 Hz, 2H, *m-pyr*), -9.19 (42 Hz, 4H, *m-aryl*), -13.38 (38 Hz, 2H, *p-aryl*), -19.74 (54 Hz, 12H, $CH(CH_3)_2$), -31.10 (118 Hz, 12H, $CH(CH_3)_2$), -123.36 (336 Hz, 4H, $CH(CH_3)_2$), -185.63 (209 Hz, 6H, $C(CH_3)$), two peaks not located. As judged by ^{1}H NMR spectroscopy, a 55 % yield of the organic degradation products (52 % 2-methylpropene, 48% 2-methylpropane) was achieved upon vacuum transfer of the volatiles after 1 week and integration against 1 μL of cyclohexane.

Characterization of (^{iPr}PDI)Fe($CH_2{}^cPent$) (1-$CH_2{}^cPent$). This complex was observed by ^{1}H NMR spectroscopy upon addition of 0.003 g (2.25 μL, 0.017 mmol) of 6-bromo-1-hexene to 0.020 g (0.034 mmol) of **1-$(N_2)_2$** in benzene-d_6. ^{1}H NMR (benzene-d_6, 293 K): δ = 338.91 (175 Hz, 1H, *p-pyr*), 197.22 (662 Hz, 1H, $FeCH_2CHR_2$), 85.67 (543 Hz, ^{c}*Pentyl*), 67.37 (77 Hz, 2H, *m-pyr*), 52.53 (180 Hz, ^{c}*Pentyl*), 46.38 (57 Hz, ^{c}*Pentyl*), 34.62 (44 Hz, ^{c}*Pentyl*), -8.86 (27 Hz, 4H, *m-aryl*), -12.80 (24 Hz, 2H, *p-aryl*), -19.17 (32 Hz, 12H, $CH(CH_3)_2$), -30.62 (89 Hz, 12H, $CH(CH_3)_2$), -120.43 (563 Hz, 4H, $CH(CH_3)_2$), -182.34 (145 Hz, 6H, $C(CH_3)$), Fe-CH_2 not located. Decomposition of this mixture by hydrolysis and transfer of the volatiles resulted in the observation of both methylenecyclopentane and methylcyclopentane by ^{1}H NMR spectroscopy. Additionally, **1-$CH_2{}^cPent$** underwent complete degradation in benzene-d_6 over the course of 72 hours at ambient temperature. Transfer of the volatiles and analysis by ^{1}H NMR spectroscopy confirmed a 38 % return of the alkyl derivative (40 % methylenecyclopentane and 60 % methylcyclopentane) as judged by ^{1}H NMR integration against 1 μL of cyclohexane.

Preparation of (^{iPr}PDI)FeOTf (1-OTf). A 20 mL scintillation vial was charged with 0.100 g (0.168 mmol) of **1-$(N_2)_2$** and approximately 10 mL of diethyl ether. A second solution of 0.041 g (34 μL, 0.185 mmol) of trimethylsilyl trifluoromethanesulfonate in approximately 5 mL of ether was added slowly dropwise and the resulting olive green solution was allowed to stir for 18 hours. The reaction mixture was filtered through Celite with ether and the solvent was removed *in vacuo* to yield a greenish-brown solid. Recrystallization from a concentrated ether solution layered with pentane at -35 °C yielded 0.064 g (0.093 mmol, 55 %) of dark green crystals identified as **1-OTf**. Analysis for $C_{34}H_{43}F_3FeN_3O_3S$: Calcd C, 59.47; H, 6.31; N, 6.12. Found: C, 62.33; H,

6.92; N, 6.05. Magnetic susceptibility (benzene-d_6, 293 K): $\mu_{eff} = 4.3\ \mu_B$. ^{1}H NMR (benzene-d_6, 293 K): δ = 392.79 (213 Hz, 1H, *p-pyr*), 94.92 (106 Hz, 2H, *m-pyr*), -6.19 (39 Hz, 4H, *m-aryl*), -16.59 (32 Hz, 2H, *p-aryl*), -24.87 (55 Hz, 12H, $CH(CH_3)_2$), -38.45 (135 Hz, 12H, $CH(CH_3)_2$), -143.50 (415 Hz, 4H, $CH(CH_3)_2$), -242.75 (163 Hz, 6H, $C(CH_3)$).

REFERENCES

[1] Small, B. L.; Brookhart, M.; Bennett, A. M. A. *J. Am. Chem. Soc.* **1998**, *120*, 4049.

[2] Britovsek, G. J. P.; Gibson, V. C.; Kimberley, B. S.; Maddox, P. J.; McTavish, S. J.; Solan, G. A.; White, A. J. P.; Williams, D. J. *Chem. Commun.* **1998**, 849.

[3] Bianchini, C.; Giambastiani, G.; Rios, I. G.; Mantovani, G.; Meli, A.; Segarra, A. M. *Coord. Chem. Rev.* **2006**, *250*, 1391.

[4] Bennett, A. M. A. (DuPont) PCT Int. Appl. WO 9827124 A1, 1998, 68 pp. (b) Brookhart, M. S.; Small, B. L. PCT Int. Appl. WO 9902472 A1 1999, 54 pp.

[5] Gibson, V. C.; Redshaw, C.; Solan, G. A. *Chem. Rev.* **2007**, *107*, 1745.

[6] Britovsek, G. J. P.; Mastroianni, S.; Solan, G. A.; Baugh, S. P. D.; Redshaw, C.; Gibson, V. C.; White, A. J. P.; Williams, D. J.; Elsegood, M. R. J. *Chem. Eur. J.* **2000**, *6*, 2221.

[7] Ionkin, A. S.; Marshall, W. J.; Adelman, D. J.; Fones, B. B.; Fish, B. M.; Schiffhauer, M. F. *Organometallics* **2008**, *27*, 1147.

[8] Ionkin, A. S.; Marshall, W. J.; Adelman, D. J.; Fones, B. B.; Fish, B. M.; Schiffhauer, M. F.; Soper, P. D.; Waterland, R. L.; Spence, R. E.; Xie, T. *J. Polym. Sci. A.* **2008**, *46*, 585.

[9] (a) Mohring, P. C.; Coville, N. J. *Coord. Chem. Rev.* **2006**, *250*, 18. (b) Coates, G. W. *Chem. Rev.* **2000**, *100*, 1223. (c) Resconi, L.; Cavallo, L.; Fait, A.; Piemontesi, F. *Chem. Rev.* **2000**, *100*, 1253. (d) Ewen, J. A. *Sci. Am.* **1997**, *276*, 86.

[10] Miller, S. A.; Bercaw, J. E. *Organometallics* **2006**, *25*, 3576.

[11] Griffiths, E. A. H.; Britovsek, G. J. P.; Gibson, V. C.; Gould, I. R. *Chem. Commun.* **1999**, 1333.

[12] Khoroshun, D. V.; Musaev, T.; Vreven, T.; Morokuma, K. *Organometallics* **2001**, *20*, 2007.

[13] Raucoules, R.; de Bruin, T.; Raybaud, P.; Adamo, C. *Organometallics* **2008**, *27*, 3368.

[14] Bryliakov, K. P.; Semikolenova, N. V.; Zudin, V. N.; Zakaharov, V. A.; Talsi, E. P. *Catal. Commun.* **2004**, *5*, 45.

[15] Castro, P. M.; Lahtinen, P.; Axenov, K.; Viidanoja, J.; Kotiaho, T.; Leskela, M.; Repo, T. *Organometallics* **2005**, *24*, 3664.

[16] Britovsek, G. J. P.; Clentsmith, G. K. B.; Gibson, V. C.; Goodgame, D. M. L.; McTavish, S. J.; Pankhurst, Q. A. *Catal. Commun.* **2002**, 3, 207.

[17] Tellman, K. P.; Humphries, M. J.; Rzepa, H. S.; Gibson, V. C. *Organometallics* **2004**, *23*, 5503.

[18] Knijnenburg, Q.; Gambarotta, S.; Budzelaar, P. H. M. *Dalton Trans.* **2006**, *46*, 5442.

[19] de Bruin, B.; Bill, E.; Bothe, E.; Weyermüller, T.; Wieghardt, K. *Inorg. Chem.* **2000**, *39*, 2936.

[20] Britovsek, G. J. P.; Gibson, V. C.; Spitzmesser, S. K.; Tellmann, K. P.; White, A. J. P.; Williams, D. J. *Dalton Trans.* **2002**, *6*, 1159.

[21] Bouwkamp, M. W.; Bart, S. C.; Hawrelak, E. J.; Trovitch, R. J.; Lobkovsky, E.; Chirik, P. J. *Chem. Commun.* **2005**, 3406.

[22] Scott, J.; Gambarotta, S.; Korobkov, I.; Budzelaar, P. H. M. *J. Am. Chem. Soc.* **2005**, *127*, 13019.

[23] Cámpora, J.; Naz, A. M.; Palma, P.; Álvarez, E.; Reyes, M. L. *Organometallics* **2005**, *24*, 4878.

[24] Fernández, I.; Trovitch, R. J.; Lobkovsky, E.; Chirik, P. J. *Organometallics* **2008**, *27*, 109.

[25] Bouwkamp, M. W.; Lobkovsky, E.; Chirik, P. J. *J. Am. Chem. Soc.* **2005**, *127*, 9660.

[26] Knijnenburg, Q.; Smits, J. M. M.; Budzelaar, P. H. M. *Organometallics* **2006**, *25*, 1036.

[27] Scott, J.; Gambarotta, S.; Korobkov, I.; Budzelaar, P. H. M. *Organometallics* **2005**, *24*, 6298.

[28] Scott, J.; Gambarotta, S.; Korobkov, I.; Kninjenburg, Q.; de Bruin, B.; Budzelaar, P. H. M. *J. Am. Chem. Soc.* **2005**, *127*, 17204.

[29] Kissin, Y. V.; Qian, C.; Xie, G.; Chen, Y. *J. Poly. Sci. A.* **2006**, *44*, 6159.

[30] Bart, S. C.; Lobkovsky, E.; Chirik, P. J. *J. Am. Chem. Soc.* **2004**, *126*, 13794.

[31] Bart, S. C.; Chlopek, K.; Bill, E.; Bouwkamp, M. W.; Lobkovsky, E.; Neese, F.; Wieghardt, K.; Chirik, P. J. *J. Am. Chem. Soc.* **2006**, *128*, 13901.

[32] Bart, S. C.; Lobkovsky, E.; Bill, E.; Chirik, P. J. *J. Am. Chem. Soc.* **2006**, *128*, 5302.

[33] Lal, D.; Griller, D.; Husband, S.; Ingold, K. V. *J. Am. Chem. Soc.* **1974**, *96*, 6355.

[34] Williams, G. M.; Schwartz, J. *J. Am. Chem. Soc.* **1982**, *104*, 1122.

[35] Bart, S. C.; Bowman, A. C.; Lobkovsky, E.; Chirik, P. J. *J. Am. Chem. Soc.* **2007**, *129*, 7212.

[36] Lau, W.; Huffman, J. C.; Kochi, J. K. *Organometallics* **1982**, *1*, 155.

[37] Vela, J.; Vaddadi, S.; Cundari, T. R.; Smith, J. M.; Gregory, E. A.; Lachicotte, R. J.; Flaschenreim, C. J.; Holland, P. L. *Organometallics* **2004**, *23*, 5226.

[38] Britovsek, G. J. P.; Bruce, M.; Gibson, V. C.; Kimberly, B. S.; Maddox, P. J.; Mastroianni, S.; McTavish, S. J.; Redshaw, C.; Solan, G. A.; Stromberg, S.; White, A. J. P.; Williams, D. J. *J. Am. Chem. Soc.* **1999**, *121*, 8728.

[39] Holm, R. H.; Hawkins, C. J. in *NMR of Paramagnetic Molecules: Principles and Applications*; La Mar, G. N.; Horrocks, W. D.; Holm, R. H. Academic Press, New York, 1973 pp. 287.

[40] Gibson, V. C.; Tellmann, K. P.; Humphries, M. J.; Wass, D. F. *Chem. Commun.* **2002**, 2316.

[41] For related ligand-centered oxidation chemistry see: Ketterer, N. A.; Fan, H. J.; Blackmore, K. J.; Yang, X. F.; Ziller, J. W.; Baik, M. H.; Heyduk, A. F. *J. Am. Chem. Soc.* **2008**, *130*, 4364.

[42] Pangborn, A. B.; Giardello, M. A.; Grubbs, R. H.; Rosen, R. K.; Timmers, F. J. *Organometallics* **1996**, *15*, 1518.

[43] Sur, S. K. *J. Magn. Res.* **1989**, *82*, 169.

CHAPTER 3

BIS(IMINO)PYRIDINE IRON CATALYZED OLEFIN HYDROGENATION: SUBSTRATE SCOPE, FUNCTIONAL GROUP TOLERANCE, AND IDENTIFICATION OF CATALYST RESTING STATES[*]

3.1 Abstract

An investigation into the substrate scope of bis(imino)pyridine iron mediated alkene reduction revealed effective hydrogenation of olefinic substrates containing a wide array of functionality. Allylic or vinylic ethers, fluorinated aromatics, and amines were hydrogenated with turnover frequencies indistinguishable from analogous α-olefins. The hydrogenation of amide, ester, and ketone containing substrates was achieved but was highly substrate dependent. For these substrates, reduction was observed at the alkene without detectable carbonyl reduction. Decomposition of the iron compound was observed in the presence of α,β-unsaturated ketones. Stoichiometric experiments were conducted for a variety of substrates to probe the metal-substrate interaction and the functional group tolerance of bis(imino)pyridine iron. In many cases, neutral ligand complexes were observed and their electronic structures investigated. Examination by NMR spectroscopy, Mössbauer spectroscopy, and X-ray diffraction revealed that the ground state electronic structure of these complexes can best be described as having a four coordinate, intermediate spin iron(II) center antiferromagnetically coupled to a doubly reduced bis(imino)pyridine chelate. In cases where the monodentate ligand is a sufficiently strong π-acid, evidence for a third ligand reduction (at the pendant ligand) and a ferric metal center was observed by ^{1}H NMR spectroscopy and X-ray crystallography.

[*] Parts of this chapter have been reproduced with permission from Trovitch, R. J.; Lobkovsky, E.; Bill, E.; Chirik, P. J. *Organometallics* **2008**, *27*, 1470-1478. Copyright 2008 American Chemical Society.

3.2 Introduction

Ever since the advent of homogeneous olefin hydrogenation catalysts,[1] and their application to asymmetric reductions,[2] enantiopure hydrogenation catalysts have been used extensively in industry[3] and in academia.[4] The initial commercial application of this process, for which Knowles shared the Nobel Prize in chemistry with Noyori in 2001, was the production of enantiopure 3,4-dihydroxyphenylaniline (L-DOPA), a drug used for treatment of Parkinson's disease.[5] In the 1980s, Noyori greatly expanded upon this work, often employing [1,1'-binaphthalene]-diylbis[diphenylphosphine] (BINAP) derived ligands, which are still widely used in the production of pharmaceutical targets.[6] Today, asymmetric hydrogenation remains wildly popular in the pharmaceutical industry, as more than 1000 chiral ligand systems have been developed.[7] The industrial syntheses of recently launched drugs such as Tipranavir[8] and Rozerem[9] also rely on asymmetric hydrogenation.

Even though impressive levels of activity and specificity have been achieved in the aforementioned systems, one remaining drawback is their use of precious metals. The cost of precious metals continues to skyrocket and stringent requirements have been placed on the allowance of these toxic metal impurities in pharmaceutical products.[10] Research groups in academia and industry have focused on replacing these catalysts with first row transition metal surrogates in order to sidestep these inconveniences. Over the last few decades, the use of iron catalysts in oxidation and cross-coupling reactions has been studied thoroughly.[10,11]

Significant advances have also been made in the development of iron based hydrogenation catalysis. In the 1960s, Butterfield and co-workers discovered that under 400 psi of dihydrogen and at 180 °C, $Fe(CO)_5$ promoted the hydrogenation and isomerization of methyl linoleate[12] and was later expanded to include arene hydrogenation under water-gas shift conditions.[13] Using milder conditions, Wrighton

and co-workers reported a photocatalytic method for hydrogenating 1-hexene at ambient temperature under only 1 atmosphere of dihydrogen.[14,15] Similar methodology resulted in the formation of $(H_2C{=}CH_2)Fe(CO)_4$[16,17] and $(H_2C{=}CH_2)_2Fe(CO)_3$[18] which easily lose ethylene and generate the proposed catalytically active species, $Fe(CO)_3$.[14] Theoretical work by Weitz in 2005 further implicated $Fe(CO)_3$ as the catalytically active species.[19]

Two electron reduction of (^{iPr}PDI)$FeBr_2$ (^{iPr}PDI = 2,6-(2,6-$^{i}Pr_2$-$C_6H_3N{=}CMe)_2$-C_5H_3N, **1-Br$_2$**) under an atmosphere of nitrogen resulted in the formation of the corresponding bis(imino)pyridine iron bis(dinitrogen) complex, (^{iPr}PDI)$Fe(N_2)_2$ (**1-(N$_2$)$_2$**), which was found to be an effective precursor for the catalytic hydrogenation and hydrosilylation of olefins and alkynes.[20] Impressively, this complex catalyzes the hydrogenation of unactivated olefins in non-polar solvents at a rate comparable to commonly used precious metal catalysts.[21] For this transformation, efficient turnover was observed under only 4 atmospheres of hydrogen and catalyst loadings as low as 0.04 mol%.[21] The initial report of this catalyst focused primarily on the hydrogenation of simple, unfunctionalized olefins.[20]

When bound to bis(imino)pyridine iron, weak field σ-donating ligands produce intermediate spin iron(II) centers that antiferromagnetically couple to a doubly reduced chelate, $[PDI]^{2-}$.[22,23] These complexes, (^{iPr}PDI)Fe-L (L = pyridine, **1-Py**; 4-(dimethylamino)pyridine, **1-DMAP**; ammonia, **1-NH$_3$**; *tert*-butylamine, **1-NH$_2$^{t}Bu**), exhibit temperature independent paramagnetism due to excited state mixing of a triplet state which lies close in energy to the singlet ground state, as supported by DFT calculations.[22,23] Stronger field π-accepting ligands, such as carbon monoxide (**1-(CO)$_2$**) and *tert*-butylisocyanide (**1-(^{t}BuNC)$_2$**), stabilize the ground state singlet to form highly covalent, low-spin complexes ($S = 0$) that do not exhibit temperature independent paramagnetism. A similar observation has been made for the complex

(^{iPr}PDI)Fe(DEPE) (**1-DEPE**), where the 1,2-bis(diethylphosphino)ethane ligand is bound through both phosphines.[23]

In the last few years, other examples of iron catalyzed hydrogenation reactions have been reported. Casey and Guan have very recently described an iron transfer hydrogenation catalyst that is effective for the reduction of ketones.[24] Other groups have focused on employing phosphine ligands in catalytic iron systems. Bianchini and Oro were first to describe such a system, reporting the hydrogenation of alkynes to alkenes with the cationic complex $[P(CH_2CH_2PPh_2)_3FeH(H_2)][BPh_4]$.[25] This methodology was later expanded to include a zwitterionic tris(phosphino)borate iron(II) alkyl complex that was effective for the hydrogenation of unactivated olefins.[26] Groundbreaking work on the development of asymmetric iron hydrogenation catalysts was achieved in early 2008 by the groups of Morris[27] and Beller[28] and remains a rapidly growing area of research.

To have the broadest application, iron catalysts would need to perform asymmetric, late stage transformations on complex pharmaceutical precursors. Achieving this objective would avert the necessity for toxic precious metal catalysts towards the end of syntheses and significantly lower purification costs. Even with all of these recent breakthroughs, replacement of precious metal catalysts with iron surrogates can only occur when metal-substrate interactions with these catalysts are fully understood. In this Chapter, an in depth look at the tolerance of bis(imino)pyridine iron towards a variety of functional groups is explored.

3.3 Scope of Hydrogenation

Oxygenated alkenes were the first class of substrate explored in catalytic **1-$(N_2)_2$** promoted olefin hydrogenation. Each catalytic reaction was conducted under 4 atmospheres of dihydrogen with 5 mol % **1-$(N_2)_2$** in benzene-d_6 at 23 °C (Table 3.1). To avoid unwanted side reactions in the absence of H_2 (discussed in greater detail in Chapter 4), the catalyst solutions were frozen at liquid nitrogen temperature and thawed following the addition of substrate and gas. Conversions were determined at the desired time by ^{1}H NMR spectroscopy following quenching of the reaction by exposure to air or evacuation of hydrogen and vacuum transfer of the volatile reaction components. Ether functionality had little impact on the observed hydrogenation turnover frequencies (Table 3.1). Ethyl vinyl ether, allyl ethyl ether, and allyl ether were all hydrogenated at rates indistinguishable from the previously reported unactivated α-olefins.[20]

Substrates containing fluorinated aromatic substituents were also well tolerated by the iron catalyst. 4-Fluorostyrene and 2,3,4,5,6-pentafluorostyrene were hydrogenated at rates similar to those observed for styrene[20] and *trans*-β-methyl styrene (Table 3.1). In contrast to the reactivity presented in Chapter 2, introduction of the halogen substituent did not result in competitive iron C-F bond activation. Monitoring an equimolar solution of **1-$(N_2)_2$** and fluorobenzene at ambient temperature over the course of 24 hours in the absence of dihydrogen provided no evidence for bond activation under these conditions. The ability of bis(imino)pyridine iron to cleave C-F bonds that are not sp^2-hybridized has yet to be fully investigated.

Table 3.1. Catalytic hydrogenation of ether-substituted substrates, fluorinated styrenes, and trans-β-methylstyrene with **1-$(N_2)_2$**.

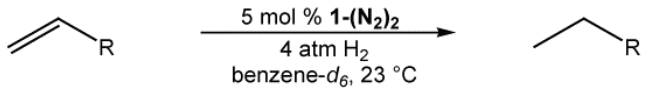

Substrate	Time (min)	% Conversion	TOF (hr^{-1})
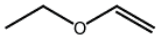	5	> 99	> 240
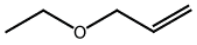	5	> 99	> 240
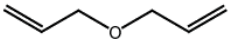	5	> 99	> 480
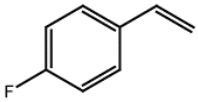	5	> 99	> 240
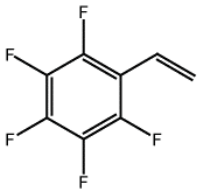	5	> 99	> 240
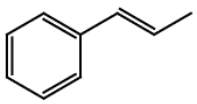	5	> 99	> 240

In contrast to ether substitution, the introduction of carbonyl groups had a deleterious effect on catalytic turnover (Table 3.2). Hydrogenation of 5-hexen-2-one required heating to 65 °C for reasonable turnover while (+)-dihydrocarvone was not hydrogenated even upon heating for 15 hours at the same temperature. The inability to partially hydrogenate the latter substrate at higher temperature is likely due to a reduced coordination affinity for the *gem*-disubstituted olefin as compared to the ketone substituent. Attempts to extend this transformation to the α-enones shown in Figure 3.1 have been unsuccessful. Hydrogenation of the alkene in *trans*-chalcone,

trans-4-hexen-3-one, *trans*-4-phenyl-3-buten-2-one, 2-cyclohexen-1-one, or (–)-carvone was unsuccessful with 10 mol % of **1-$(N_2)_2$** under 4 atmospheres of H_2. For these substrates, the brownish-green color of the catalyst solution faded almost immediately upon thawing and the ^{1}H NMR spectrum of the reaction mixture revealed free bis(imino)pyridine ligand.

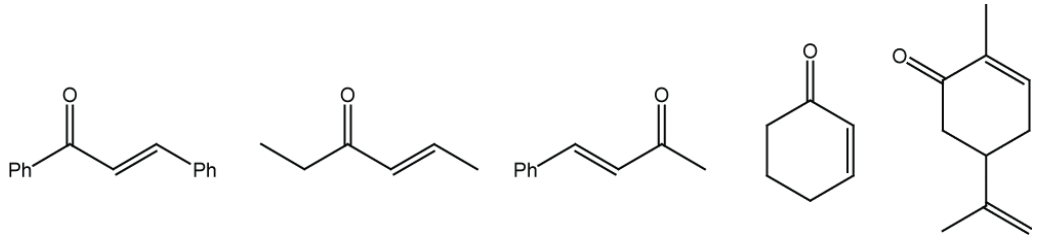

Figure 3.1. *α,β*-Unsaturated ketones that induce decomposition of **1-$(N_2)_2$** under catalytic hydrogenation conditions.

The ability of **1-$(N_2)_2$** to hydrogenate ester containing substrates appeared to be highly dependent on the position of this functional group relative to the olefin (Table 3.2). For example, the rate of *trans*-methylcinnamate conversion was indistinguishable from that of *trans*-*β*-methylstyrene (Table 3.1), while no conversion was observed for allyl acetate or vinyl acetate. Previous work revealed that dimethyl itaconate was readily hydrogenated with **1-$(N_2)_2$** under similar conditions.[20] In this study, internal and trisubstituted olefins were effectively hydrogenated when adjacent to an ethyl substituted ester. This result contrasts the inability of this catalyst to hydrogenate unactivated tri- or tetra-substituted olefins,[21] and highlights the observed activity difference between activated and unactivated alkenes.

The final class of substrates to be examined for catalytic **1-$(N_2)_2$** mediated reduction was a series of allylamines. Interest in hydrogenating amino-olefins stems from the numerous pharmaceutical targets that contain this functionality.[29] Similar conditions were employed; however, a 0.3 mol % catalyst loading was used for these

substrates to highlight the activity differences observed between different degrees of amine substitution (Table 3.3). Determining the conversion by ^{1}H NMR spectroscopy following vacuum transfer of the volatiles revealed that turnover frequencies for allyl group hydrogenation increased with alkylation of the amine group. The unprotected amine, allylamine, was by far the slowest, reaching only 20 % conversion after 24 hours. Highlighting the observed pattern, *N*,*N*-dimethylallylamine was hydrogenated at a rate indistinguishable from that of 4-methyl-1-pentene.

Table 3.2. Hydrogenation of carbonyl containing substrates with **1-$(N_2)_2$**.

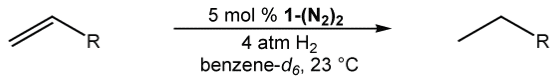

Substrate	Time (min)	% Conversion	TOF (hr^{-1})
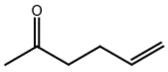	60[a]	93	19
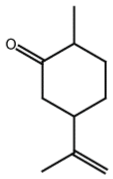	900[a]	0	0
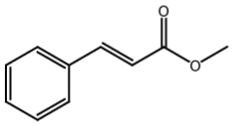	5	> 99	> 480
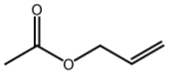	900	0	0
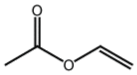	900	0	0
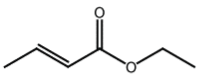	5	> 99	> 240
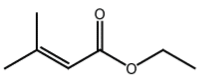	1440	50	0.4
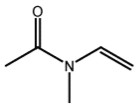	240	87	4.4

[a] Catalytic reaction conducted at 65 °C.

Table 3.3. Catalytic hydrogenation of amino-substituted olefins and 4-methyl-1-pentene with **1-$(N_2)_2$**.

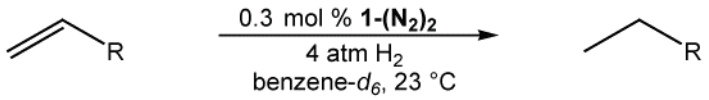

Substrate	Time (min)	% Conversion	TOF (hr^{-1})
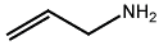	1440	20	3
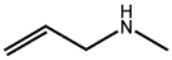	60	95	320
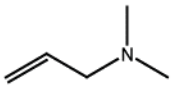	15	95	1270
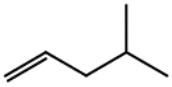	15	95	1270

Catalytic deuteration experiments were conducted to determine whether chain-walking processes were competitive with hydrogenation. Conducting the catalytic deuteration of allylamine under 4 atmospheres of D_2 with 1.5 mol % **1-$(N_2)_2$** at 65 °C resulted in exclusive deuterium incorporation into the 2 and 3 positions of the alkyl chain (Figure 3.2). Additionally, no deuterium incorporation was observed at the N-H positions, suggesting that oxidative addition of the N-H bond followed by H/D exchange is not operative under these conditions. Similarly, performing the previously described hydrogenation of 5-hexen-2-one under D_2 instead of H_2 resulted in isotopic incorporation into only the 5 and 6 positions of the chain (Figure 3.2).

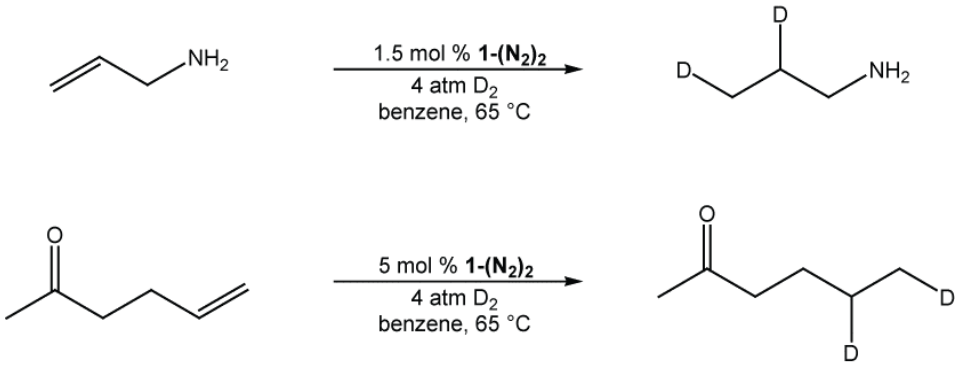

Figure 3.2. Catalytic deuteration of allylamine and 5-hexen-2-one with **1-$(N_2)_2$**.

3.4 Catalyst Resting States

To gain a deeper understanding of the interaction between the iron center and each type of functional group, stoichiometric reactions were conducted between **1-$(N_2)_2$** and a series of representative substrates. Initial interest in amine containing substrates stemmed from the different hydrogenation activities observed among various allyl amines. Addition of 1 equivalent of allyl amine to **1-$(N_2)_2$** in benzene-d_6 solution resulted in dinitrogen loss and the formation of (^{iPr}PDI)Fe($NH_2CH_2CH{=}CH_2$) (**1-$NH_2CH_2CH{=}CH_2$**) (Figure 3.3). In the same fashion, **1-$NH_2CH_2CH_2CH_3$**, **1-$NH_2CH_2C(Me)_2CH{=}CH_2$**, and **1-$NH(Me)CH_2CH{=}CH_2$** were prepared and characterized by multinuclear NMR spectroscopy and combustion analysis (Figure 3.3). Importantly, addition of either *N*,*N*-dimethylallylamine or *trans*-*β*-methylstyrene produced no detectable change in the ^{1}H NMR spectra of the iron compound. This lack of interaction between **1-$(N_2)_2$** and *N*,*N*-dimethylallylamine suggests that amine coordination to the metal center is responsible for the relatively low turnover frequencies observed for *N*-allylmethylamine and allylamine hydrogenation.

Characterization of these complexes by ^{1}H NMR spectroscopy allowed estimation of relative amine binding affinity to **1-$(N_2)_2$**. Adding an excess of equimolar allylamine and *N*-allylmethylamine solution to **1-$(N_2)_2$** yielded an 85:15 ratio of **1-**

$NH_2CH_2CH=CH_2$ to **1-$NH(Me)CH_2CH=CH_2$**. This ratio suggests that primary amine coordination is favored over secondary amine binding and is consistent with the turnover frequencies presented in Table 3.3. This experiment, coupled with the observation of free and bound amine exchange by EXSY NMR spectroscopy at 23 °C (200 ms mixing time), demonstrated that allylamine is a labile ligand even though it significantly hampers catalytic hydrogenation.

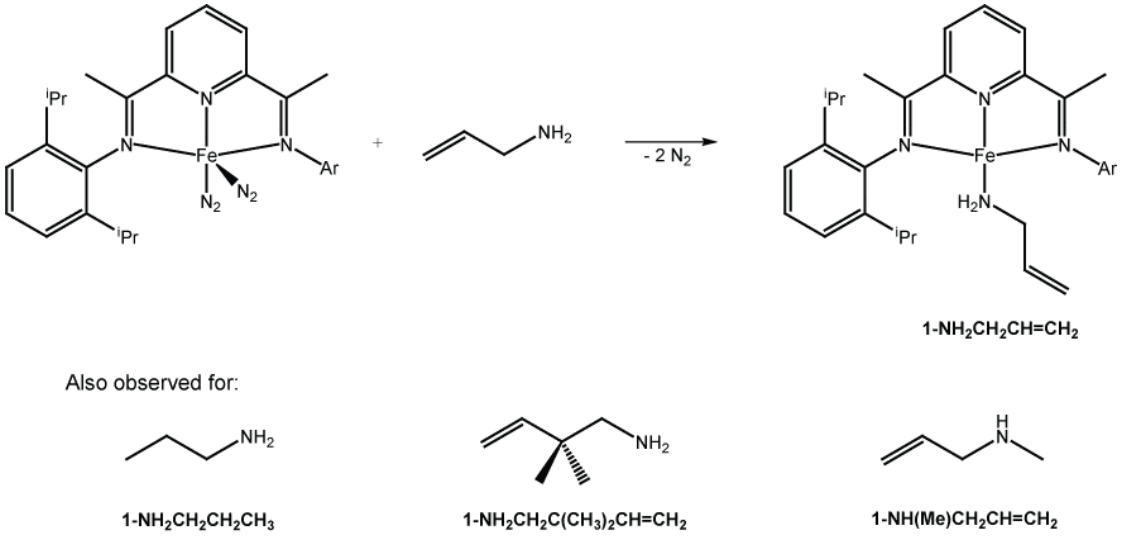

Figure 3.3. Preparation of bis(imino)pyridine iron amine complexes.

Relative amine coordination affinities were also determined as a function of alkyl chain saturation to elucidate if the presence of an olefin assists in amine coordination. Addition of 1 equivalent of both propylamine and allylamine to **1-$(N_2)_2$** resulted in a 2:1 ratio of **1-$NH_2CH_2CH_2CH_3$** to **1-$NH_2CH_2CH=CH_2$** as judged by ^{1}H NMR spectroscopy. This ratio was also obtained upon addition of 1 equivalent of propylamine to **1-$NH_2CH_2CH=CH_2$** or 1 equivalent of allylamine to **1-$NH_2CH_2CH_2CH_3$** (Figure 3.4). This series of experiments establish that binding of the saturated amine is only slightly favored (K_{eq} = 2.0) and suggest that olefin coordination in **1-$NH_2CH_2CH=CH_2$** is negligible.

The ^{1}H and ^{13}C NMR spectroscopic features of these temperature independent paramagnetic (TIP) iron-amine complexes are similar to those observed for **1-NH$_2$^{t}Bu**.[23] For example, **1-NH(Me)CH$_2$CH=CH$_2$** exhibits the number of resonances consistent with a molecule of C_{2v}-symmetry, likely due to fast iron-nitrogen (and possibly N-C) bond rotation on the NMR timescale at 23 °C. The ^{1}H NMR resonances are shifted from their diamagnetic reference values (free ^{iPr}PDI ligand) with the largest deviations observed for the imine methyl groups (-6.55 ppm) and *m*-pyridine resonance (12.62 ppm). Cooling a toluene-d_8 solution of **1-NH(Me)CH$_2$CH=CH$_2$** resulted in decoalesence of the imine methyl resonance at -25 °C, corresponding to a bond rotation barrier of 11.2 kcal/mol at this temperature. In the $\{^{1}H\}^{13}C$ NMR spectra of these complexes, all resonances appear as sharp singlets except for the imine methyl resonance. This resonance typically appears around 40 ppm and is so broad that it can only be observed when line broadening functions are applied. Broadening of this resonance is likely due to electron delocalization through the π-system of the bis(imino)pyridine ligand.[22]

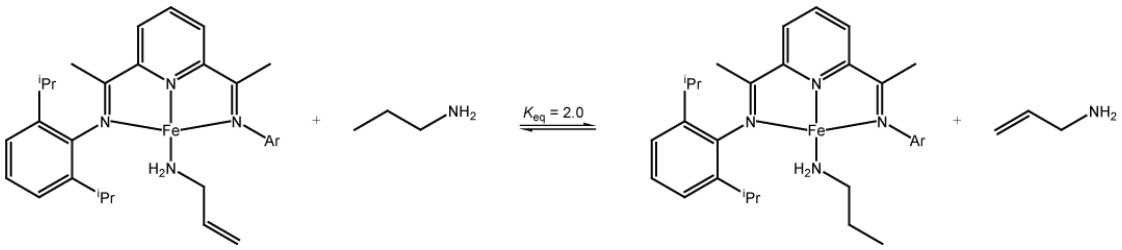

Figure 3.4. Amine exchange at bis(imino)pyridine iron.

To further investigate the slower hydrogenation activity observed for ketone-substituted alkenes, a series of commercially available ketones were added to **1-(N$_2$)$_2$** and their coordination affinity was studied. Addition of 1 equivalent of 5-hexen-2-one to **1-(N$_2$)$_2$** in pentane solution resulted in immediate loss of dinitrogen along with the

formation of (^{iPr}PDI)Fe(OC(Me)(3-butenyl)) (**1-OC(Me)(3-butenyl)**) (Figure 3.5). Using a similar procedure, bis(imino)pyridine iron complexes of (+)-dihydrocarvone (as a mixture of isomers), 2-hexanone, acetophenone, benzylacetone, 2-adamantanone, cyclopropyl methyl ketone, and cyclobutyl methyl ketone were prepared (Figure 3.5). Like the amine compounds, these complexes exhibit ^{1}H NMR spectroscopic features consistent with temperature independent paramagnetism. Diagnostic chemical shifts for these complexes are presented in Table 3.4. As observed for previously reported TIP complexes,[26] the imine methyl resonances are shifted upfield of their diamagnetic reference values. Likewise, the *m*- and *p*-pyridine resonances are shifted downfield of the corresponding free ligand values. One investigated ketone, dicyclohexyl ketone, produced no change in the ^{1}H NMR spectrum of **1-(N_2)$_2$**, likely due to steric crowding.

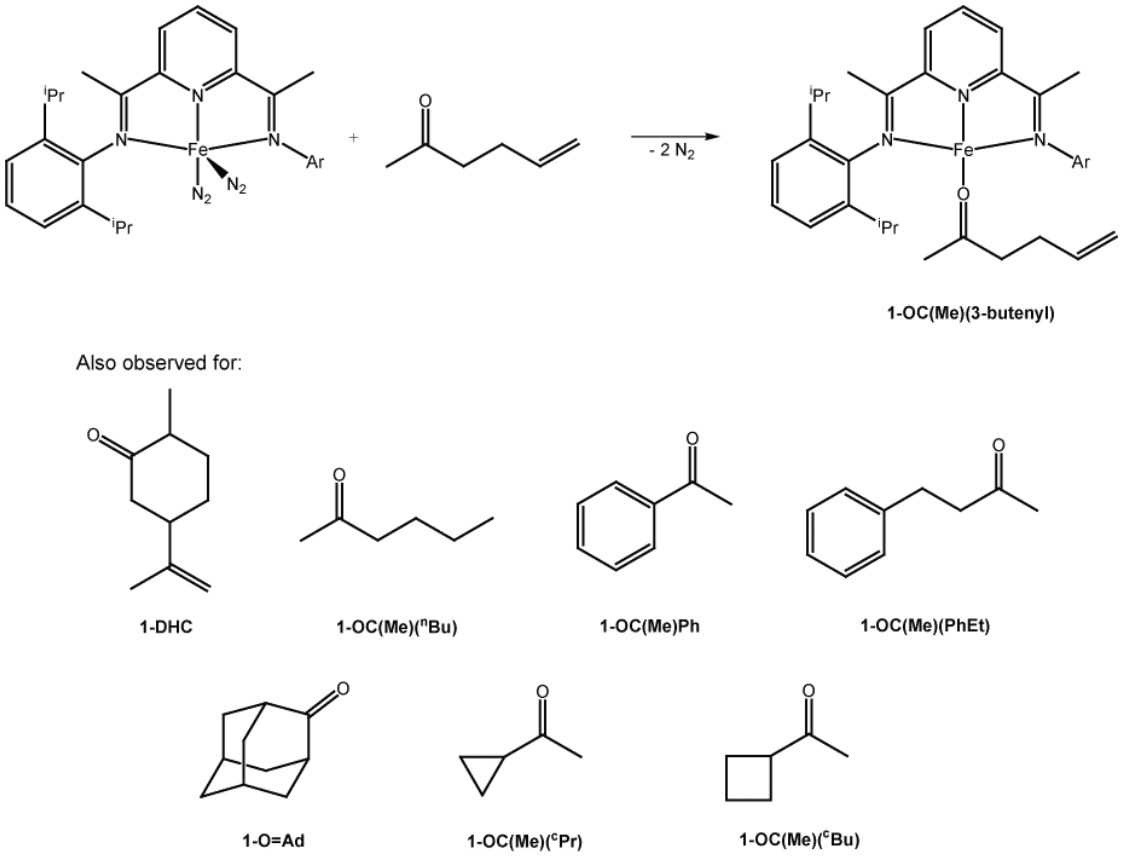

Figure 3.5. Preparation of bis(imino)pyridine iron ketone complexes.

Most of the asymmetrically substituted ketones mentioned above exhibit the number of chelate resonances expected for a C_{2v}-symmetric molecule by ^{1}H NMR spectroscopy at 23 °C, suggesting rapid Fe-O bond rotation under these conditions. Cooling a toluene-d_8 solution of **1-OC(Me)Ph** to -70 °C slowed this Fe-O bond rotation and resulted in decoalescence of the isopropyl resonances. One of these complexes, **1-DHC**, does not undergo fast bond rotation at ambient temperature and exhibits the number of resonances expected for a C_s-symmetric molecule. The tied back cyclic structure of (+)-dihydrocarvone likely hinders the ability of this substrate to rotate quickly within the pocket formed by the bis(imino)pyridine aryl rings.

Table 3.4. Diagnostic benzene-d_6 ^{1}H NMR shifts of newly prepared bis(imino)pyridine complexes that exhibit temperature independent paramagnetism.

Complex	*m-pyr* (ppm)	*p-pyr* (ppm)	N=C*Me* (ppm)
1-$NH_2CH_2CH=CH_2$	12.05	8.77	-6.09
1-$NH_2CH_2CH_2CH_3$	12.12	8.75	-6.09
1-$NH_2CH_2C(Me)_2CH=CH_2$	12.14	8.77	-6.23
1-$NH(Me)CH_2CH=CH_2$	12.62	8.82	-6.55
1-OC(Me)(3-butenyl)	10.49	8.51	-2.87
1-DHC	10.47 10.84	8.46 8.56	-2.89 -3.39
1-OC(Me)(^{n}Bu)	10.59	8.51	-3.07
1-OC(Me)(Ph)	10.05	8.68	-2.23
1-OC(Me)(PhEt)	10.53	8.53	-3.04
1-O=Ad	10.62	8.45	-3.05
1-OC(Me)(^{c}Pr)	10.77	8.53	-3.28
1-OC(Me)(^{c}Bu)	10.68	8.55	-3.22
1-Car	10.37	8.62	-2.59
1-MeOAc	11.67	8.63	-4.88
1-EtOAc	11.61	8.66	-4.67
1-^{i}PrOAc	11.94	8.69	-5.32
1-Valero	11.38	8.60	-4.28
1-DHCou	10.95	8.63	-3.76
1-OC(Me)(NMe_2)	12.33	8.55	-5.25
1-OC(Ph)(NMe_2)	12.07	8.47	-4.58
1-PIP	12.45	8.54	-5.30
1-OC(Me)(N(Me)$CH=CH_2$)	11.89	8.58	-4.86

In an attempt to greater understand the iron-ketone interaction, exchange experiments were conducted to determine whether ketone coordination is labile and reversible. Addition of a stoichiometric amount of 2-hexanone-1,1,1,3,3-d_5 to a benzene solution of either **1-OC(Me)(^{n}Bu)** or **1-OC(Me)(3-butenyl)** resulted in slow exchange over the course of 1 hour at 23 °C as judged by ^{2}H NMR spectroscopy (Figure 3.6). Investigation of this process by EXSY NMR spectroscopy revealed no exchange between free and bound ketone at 23 °C with a mixing time of 500 ms. These studies establish that the relative coordination affinity of ketones to **1-(N_2)$_2$** is much greater than for amines, leading to dramatically decreased rates of hydrogenation in the former case. Evidence for olefin coordination was not observed for **1-OC(Me)(3-butenyl)** in toluene-d_8 solution by ^{1}H NMR spectroscopy and no decrease in symmetry was observed upon cooling the solution to -80 °C.

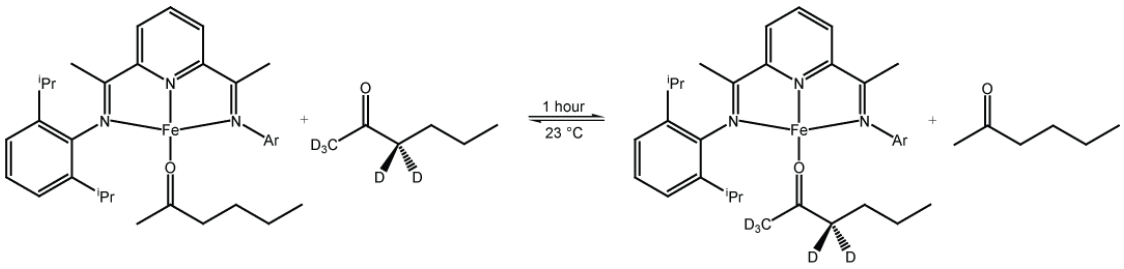

Figure 3.6. Ketone exchange at bis(imino)pyridine iron.

Stoichiometric treatment of **1-(N_2)$_2$** with the α,β-unsaturated ketones presented in Figure 3.1 was also investigated. Performing this reaction either in the absence or presence of 4 atmospheres of H_2 resulted in immediate decomposition of the iron complex and isolation of free ^{iPr}PDI ligand. One notable exception was the addition of (*R*)-carvone to **1-(N_2)$_2$**. In this case, a bis(imino)pyridine iron ketone complex, **1-Car**, exhibiting resonances characteristic of TIP, was observed at early reaction times by ^{1}H NMR spectroscopy. Over the course of 5 minutes at 23 °C, benzene-d_6 solutions of **1-**

Car changed from green to dark brown in color, concurrent with the disappearance of TIP ^{1}H NMR resonances and formation of a complex mixture of paramagnetic products. This substrate may form a more stable complex than the other α-enones because the olefin is trisubstituted, which may temporarily block C-H activation at the β-carbon. Radical chemistry is a more likely cause of these competing decomposition reactions due to the low reduction potential of α-enones relative to the corresponding saturated ketones. For example, the reduction potential of *trans*-4-phenyl-3-buten-2-one in acetonitrile is -2.01 V relative to ferrocene/ferrocenium while that of the saturated molecule, methyl-3-phenylpropionate, does not occur before reduction of the solvent. On the other hand, α,β-unsaturated esters such as *trans*-methylcinnamate and dimethyl itaconate are tolerated by **1-$(N_2)_2$** during hydrogenation (Table 3.2).

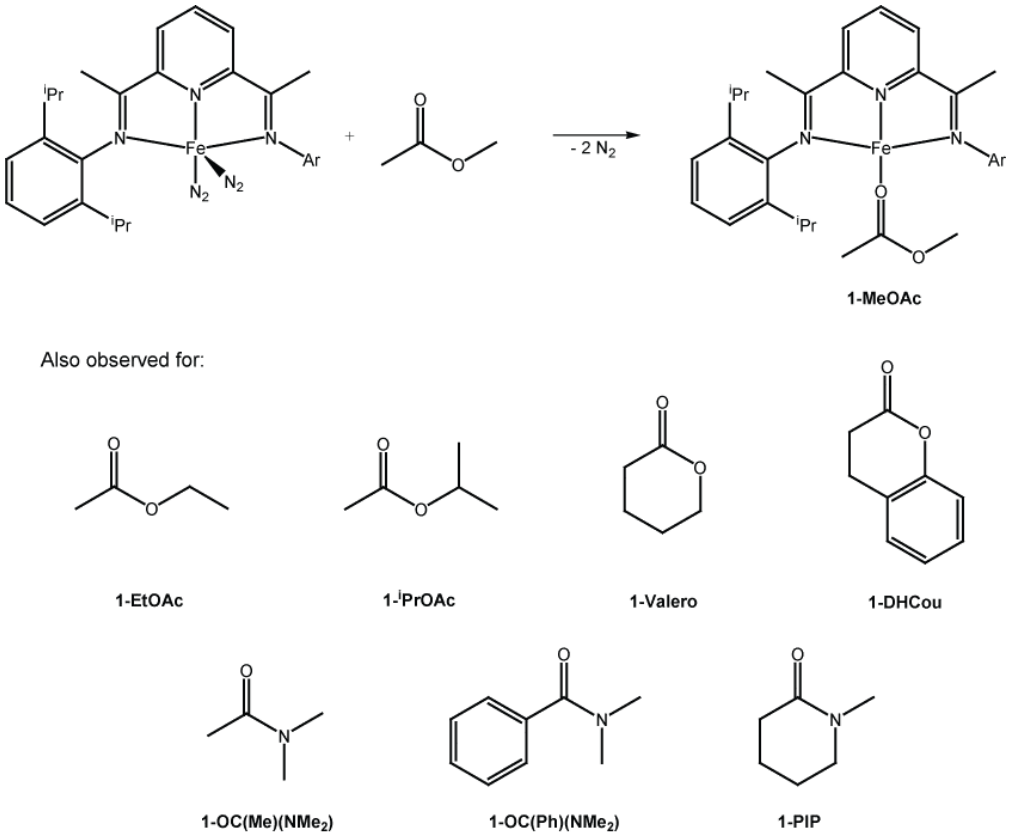

Figure 3.7. Ester and amide TIP complexes of bis(imino)pyridine iron.

Extension of this methodology to the study of esters was met with limited success. Many of the esters that were assayed for olefin hydrogenation did not yield TIP complexes upon reaction with **1-(N_2)$_2$**; however, competing processes were observed and will be discussed in detail in Chapter 4. Complexes exhibiting TIP were observed at early reaction times upon addition of methyl acetate, ethyl acetate, or isopropyl acetate to **1-(N_2)$_2$** (Figure 3.7) and their diagnostic, paramagnetically shifted ^{1}H NMR resonances are presented in Table 3.4. Similar reactivity was observed for δ-valerolactone and dihydrocoumarin, resulting in the isolation of the complexes **1-Valero** and **1-DHCou**, respectively. These TIP complexes proved to be more robust than the alkyl ester complexes, as they persisted for days at 23 °C in benzene-d_6 solution.

Amide addition to **1-(N_2)$_2$** also resulted in the isolation of complexes that exhibit temperature independent paramagnetism by ^{1}H NMR spectroscopy. Bis(imino)pyridine complexes of *N*,*N*-dimethylacetamide (**1-OC(Me)(NMe_2)**), *N*,*N*-dimethylbenzamide (**1-OC(Ph)(NMe_2)**), and *N*-methyl-2-piperidone (**1-PIP**) (Figure 3.7) appeared infinitely stable in solution at ambient temperature, unlike the previously mentioned alkyl esters. The sole amide investigated for hydrogenation activity, *N*-methyl-*N*-vinylacetamide, resulted in the formation of two complexes when added in a stoichiometric amount to **1-(N_2)$_2$**. Because this substrate exists as a mixture of amide rotamers, TIP complex formation (**1-OC(Me)(N(Me)CH=CH_2)**) was observed along with a complex exhibiting paramagnetically broadened resonances shifted over a 35 ppm range. This complex is initially proposed to be **1-(κ^2-Amide)**, where the accessible vinyl substituent is bound to the metal center along with the amide carbonyl.

3.5 Electronic Structure of Neutral Ligand Complexes

The ground state electronic structure of a series of bis(imino)pyridine iron neutral ligand complexes has been described as having an intermediate spin iron(II) center antiferromagnetically coupled to a doubly reduced chelate.[22,23] Due to mixing of a low lying $S = 1$ excited state (Figure 3.8) through spin-orbit coupling, these complexes exhibit temperature independent paramagnetism by ^{1}H NMR spectroscopy. The ^{1}H NMR data presented in Table 3.4, along with the variable temperature spectra taken for many of these complexes, suggests that the same electronic structure description can be applied to all of the aformentioned neutral ligand iron complexes.

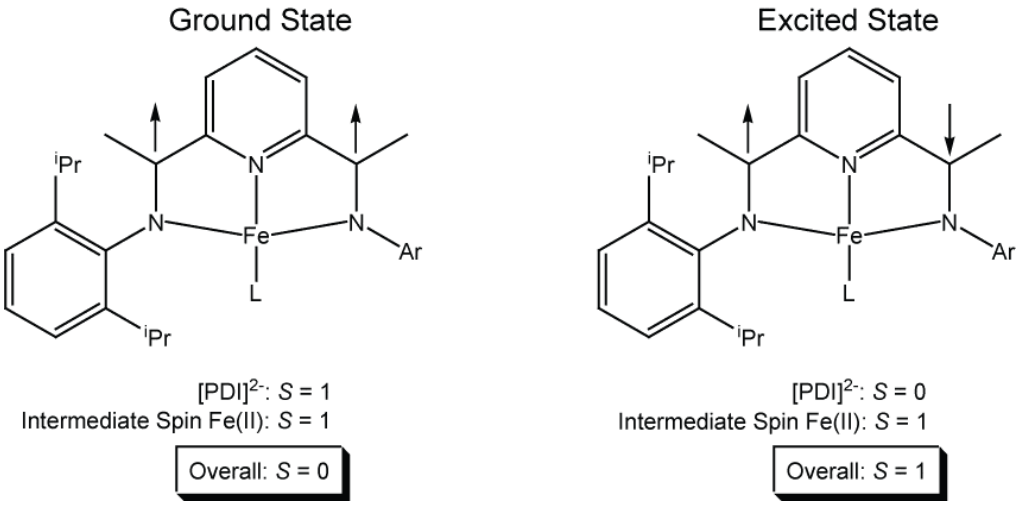

Figure 3.8. Ground and excited state electronic structure of bis(imino)pyridine iron neutral ligand complexes.

However, these spectral features were not observed in all cases. Addition of 1 equivalent of benzophenone to **1-(N_2)$_2$** in benzene-d_6 yielded the complex **1-OC(Ph)$_2$**, which exhibits ^{1}H NMR resonances that suggest a different electronic structure than observed for other bis(imino)pyridine ketone complexes (Figure 3.9). In this case, paramagnetically broadened resonances were observed over a moderately wide (60

ppm) chemical shift range. Again, the in-plane chelate hydrogens were the most shifted from their corresponding free ligand values. The imine methyl group peak was observed upfield at -18.05 ppm while the *p*-pyridine appeared downfield at 36.94 ppm. Cooling a toluene-d_8 solution of **1-OC(Ph)$_2$** revealed that the chemical shifts of these resonances were temperature dependent and that they converged upon the diamagnetic region at lower temperatures (-80 °C). This observation, in conjunction with the lack of observable $^3J_{HH}$ coupling constants, pointed towards a change in electronic structure for **1-OC(Ph)$_2$**.

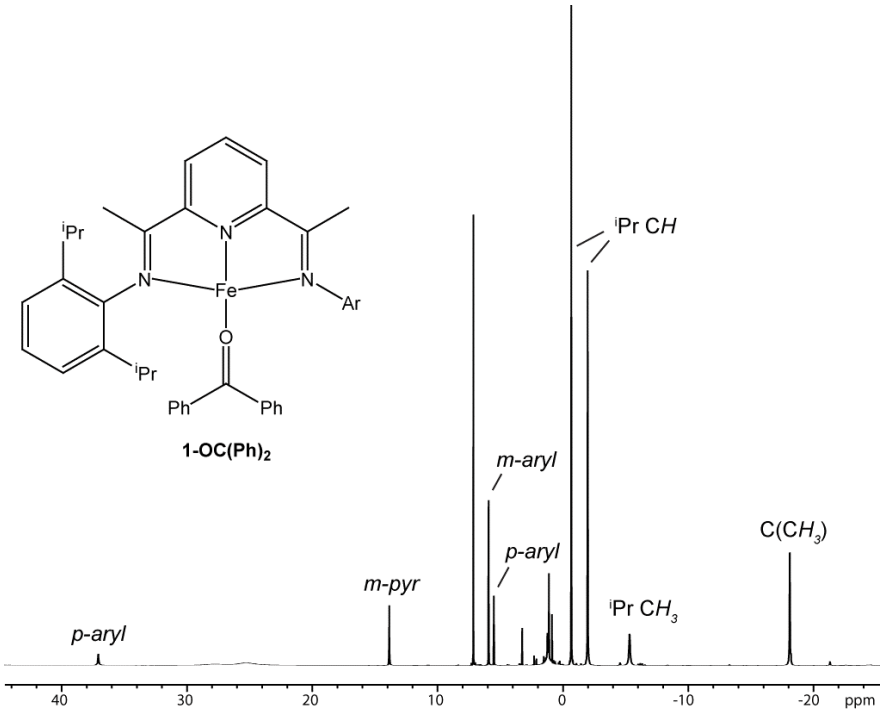

Figure 3.9. ^{1}H NMR spectrum of **1-OC(Ph)$_2$** in benzene-d_6 at 293 K.

Determination of the solid state structure of **1-OC(Ph)$_2$** (Figure 3.10) was accomplished by single crystal X-ray diffraction and selected bond distances and angles are presented in Table 3.5. The geometry about the metal center can best be

described as idealized square planar, with the sum of angles about iron totaling 360 ° and an N(2)-Fe(1)-O(1) bond angle of 179.24(10)°. The phenyl rings are canted with respect to each other and adopt an orthogonal conformation with respect to the bis(imino)pyridine chelate plane. This arrangement is likely due to unfavorable steric interactions with the PDI aryl groups.

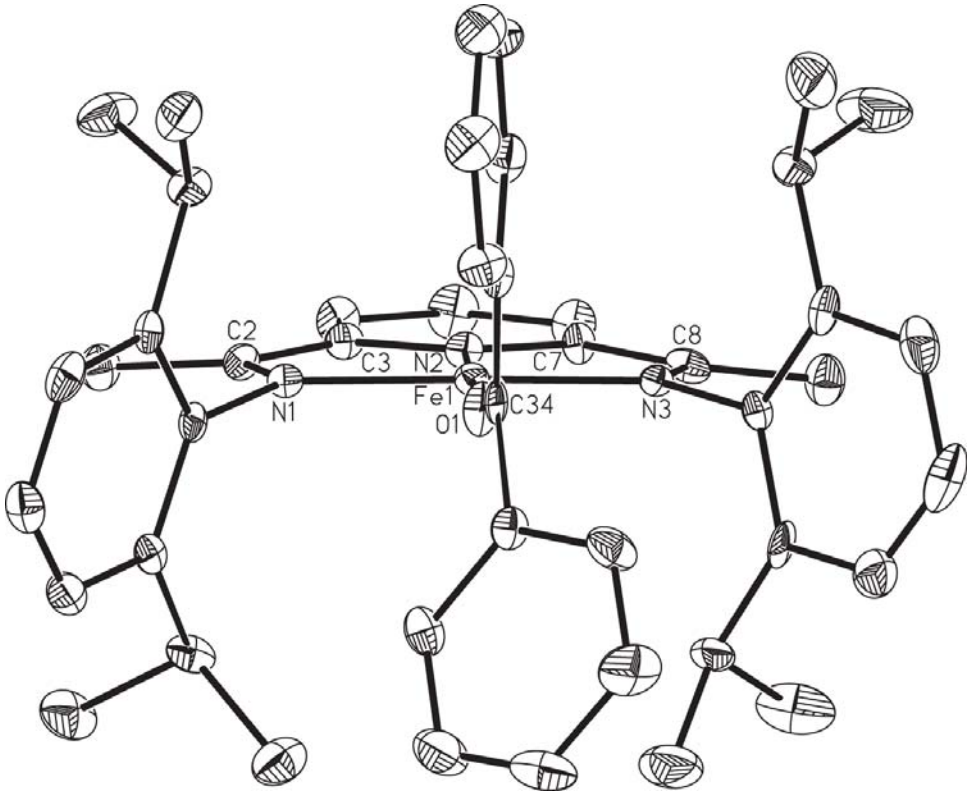

Figure 3.10. Solid state structure of **1-OC(Ph)$_2$** at 30 % probability ellipsoids. Hydrogen atoms omitted for clarity.

Further investigating the metrical parameters of **1-OC(Ph)$_2$** suggests that the bis(imino)pyridine chelate in this complex is doubly reduced.[30] Elongation of the imine N=C bond lengths to 1.342(2), along with the contraction of the C(2)-C(3) and C(7)-C(8) bonds to 1.414(3) Å and 1.411(3) Å, respectively, is indicative of 2 electron bis(imino)pyridine chelate reduction. Interestingly, the O(1)-C(34) bond distance of

1.262(2) Å is elongated compared to the same distance determined for free benzophenone (1.23(1) Å).[31] Another notable feature is the short Fe-O bond length of 1.7924(3) Å. This value is contracted in relation to typical *iron alkoxide* C-O bonds (~1.85 Å) and strongly suggests that the benzophenone ligand is monoreduced. For instance, Holland reported an Fe-O bond distance of 1.8076(16) Å in the iron(II) *β*-diiminate alkoxide complex $L^{Me}FeOCHPh_2$.[32] As expected, the C-O and Fe-O bond distances for an unreduced benzophenone-iron(II) interaction are significantly different than those observed in **1-OC(Ph)$_2$** and have been reported to be 1.256(5) Å and 1.982(3) Å, respectively.[33] Additionally, the Fe(1)-O(1)-C(34) bond angle of 179.15(6) ° for **1-OC(Ph)$_2$** is suggestive of Fe-O double bond character.

Table 3.5. Selected bond distances (Å) and angles (°) for **1-OC(Ph)$_2$**.

Fe(1)-N(1)	1.9113(14)	C(2)-C(3)	1.414(3)
Fe(1)-N(2)	1.8226(15)	C(7)-C(8)	1.411(3)
Fe(1)-N(3)	1.9225(14)	O(1)-C(34)	1.262(2)
Fe(1)-O(1)	1.7924(3)	Fe(1)-O(1)-C(34)	167.05(11)
N(1)-C(2)	1.342(2)	N(1)-Fe(1)-N(2)	80.72(6)
N(3)-C(8)	1.342(2)	N(2)-Fe(1)-O(1)	179.15(6)

Mössbauer spectroscopic investigation of both **1-OC(Me)Ph** and **1-OC(Ph)$_2$** was also conducted to probe for additional evidence of an electronic structure difference between the two complexes. The zero-field spectra of both complexes were recorded at 80 K and are displayed in Figure 3.11. The experimentally determined isomer shifts of 0.313 mm/s and 0.283 mm/s for **1-OC(Me)Ph** and **1-OC(Ph)$_2$**,

respectively, are consistent with values observed for other intermediate spin iron(II) centers.[22,23] The quadrupole splitting observed for these complexes is 0.997 mm/s and 0.531 mm/s respectively. The quadrupole splitting value observed for **1-OC(Ph)$_2$** (0.531 mm/s) is considerably smaller than the value obtained for **1-OC(Me)(Ph)**, and other diamagnetic complexes with doubly reduced PDI ligands (1.42 mm/s on average).[23] This is consistent with removal of electron density along the z-axis, based on the relative orbital energies calculated for **1-(CO)$_2$**, and a ferric metal center.[22] Variable temperature Mössbauer spectroscopy has been used to identify temperature dependent spin states of an iron center,[34] and applying this methodology to **1-OC(Ph)$_2$**, could shed light on the ambient temperature ground state electronic structure of this complex.

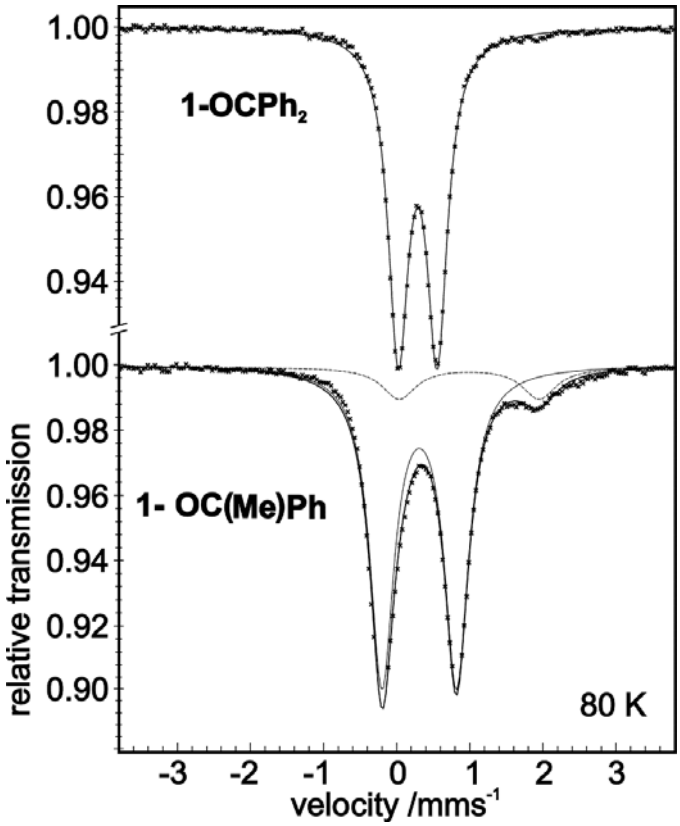

Figure 3.11. ^{57}Fe Mössbauer spectra of **1-OC(Me)Ph** and **1-OC(Ph)$_2$**.

Typically, bis(imino)pyridine iron neutral ligand complexes that exhibit temperature independent magnetism have negligible magnetic moments when freshly prepared. However, the magnetic moment of aged samples of **1-DMAP** has been found to increase as a function of time by SQUID magnetometry.[21] Analysis of these samples by Mössbauer spectroscopy produced no evidence for a second iron species and monitoring samples of **1-DMAP** by ^{1}H NMR specrocsopy in benzene-d_6 solution revealed slow conversion to an NMR silent product. Similarily, the magnetic properties of **1-OC(Ph)$_2$** are not straightforward. The ambient temperature magnetic moment of this complex was measured on freshly prepared samples of **1-OC(Ph)$_2$** and was found to be 1.2(2) μ_B (benzene-d_6). In contrast, measuring the solid state magnetic susceptibility of the same material on a Gouy balance yielded a diamagnetic reading. If the ground state of **1-OC(Ph)$_2$** contained a ferric metal center, as the ^{1}H NMR and Mössbauer spectroscopic properties of this complex suggest, a magnetic susceptibility of at least 1.8 μ_B would be expected.

Similar ^{1}H NMR spectral properties were observed for the complex (^{iPr}PDI)Fe(pyrazine) (**1-Pz**); prepared from straightforward pyrazine addition to **1-(N$_2$)$_2$**. Addition of substoichiometric quantities of pyrazine to **1-(N$_2$)$_2$** resulted in the observation of remaining **1-(N$_2$)$_2$** by ^{1}H NMR spectroscopy, confirming that bimetallic pyrazine binding does not occur due to the steric demands imparted by the PDI aryl substituents. At 293 K, this complex exhibits paramagnetically broadened resonances shifted over a 120 ppm chemical shift range. The imine methyl resonance was observed upfield at -29.59 ppm while the *m*-pyridine resonance was shifted the farthest from its diamagnetic reference value and observed at 78.11 ppm. Although **1-Pz** has not been characterized by Mössbauer spectroscopy, X-ray crystallography, or magnetic studies, preliminary ^{1}H NMR investigation of this complex is suggestive of a similar electronic structure to that of **1-OC(Ph)$_2$**.

3.6 Discussion

Taking all spectral data into account, significant contribution from a ferric oxidation state arising from reduction of the pendant ligand, must be considered when describing the electronic structure of **1-OC(Ph)$_2$** or **1-Pz**. It is likely that the reduction potential of the added substrate is the key factor in determining whether the ferrous oxidation state is accessible. In acetonitrile, the first reduction potential of benzophenone was found to be -2.24 V while that for acetophenone was shifted to -2.46 V (versus Cp_2Fe/Cp_2Fe^+). An even more favorable reduction was observed in the case of pyrazine (-2.19 V),[35] suggesting that a larger ground state contribution from the iron(III) resonance form may give rise to the wider range of ^{1}H NMR resonances observed for **1-Pz** as compared to **1-OC(Ph)$_2$**. The observation of temperature independent paramagnetism for **1-Py**[21] by ^{1}H NMR spectroscopy also supports this hypothesis, as it has a one electron reduction potential of -2.57 V.[35] This metric can be an extremely powerful tool for electronic structure investigation when a second redox active ligand is added to bis(imino)pyridine iron. Interestingly, the α-enones presented in Figure 3.1 have one-electron redox potentials that are easily accessible, likely accounting for the decomposition reactions these substrates induce.

3.6 Conclusion

Bis(imino)pyridine iron has been found to hydrogenate substrates containing amine, ether, ketone, ester, and amide functionalities but was sensitive to their position relative to the olefin. Detailed investigation of the iron-functional group interaction for a wide range of substrates revealed, in most cases, formation of complexes that exhibit temperature independent paramagnetism. For amines and carbonyl containing substrates, the coordination affinity of the functional group was found to be inversely proportional to the observed rate of olefin hydrogenation. In two cases, **1-OC(Ph)$_2$**

and **1-Pz**, evidence for reduction of the substrate and formation of an iron(III) center was observed. Oxidation to the ferrous state is proposed to be a function of the one electron reduction potential of the substrate.

3.8 Experimental Procedures

General Considerations. All air- and moisture-sensitive manipulations were carried out using standard vacuum line, Schlenk and cannula techniques or in an MBraun inert atmosphere dry box containing an atmosphere of purified nitrogen. Solvents for air- and moisture-sensitive manipulations were initially dried and deoxygenated using literature procedures.[36] Hydrogen and deuterium gas were passed through a column containing manganese oxide supported on vermiculite and 4 Å molecular sieves before admission to the high vacuum line. Benzene-d_6 and toluene-d_8 were purchased from Cambridge Isotope Laboratories and dried over 4 Å molecular sieves or titanocene, respectively. **1-$(N_2)_2$** was prepared according to literature procedures.[20] *N*-allylmethylamine, *N*,*N*-dimethylallylamine, propylamine, 2-hexanone, 5-hexen-2-one, 4-hexen-3-one, acetophenone, ethyl acetate, vinyl acetate, allyl acetate, ethyl crotonate, isopropyl acetate, ethyl-3,3-dimethylacrylate, *N*-vinyl-*N*-methyl-acetamide, cyclopropyl methyl ketone, cyclobutyl methyl ketone, *N*,*N*-dimethylacetamide, dicyclohexyl ketone, and (+)-dihydrocarvone as a mixture of isomers were all purchased from Aldrich and dried over calcium hydride for at least 24 hours before being vacuum transferred to a flask containing 4 Å molecular sieves. Allylamine, (-)-carvone, methyl acetate, and *δ*-valerolactone were purchased from Acros and purified in a similar manner. 2-Cyclohexen-1-one was purchased from Fisher Scientific and dried as described above.

Ethyl vinyl ether, and allyl ether were purchased from Aldrich and dried over calcium hydride for 24 hours. Allyl ethyl ether was purchased from Acros and dried

over calcium hydride for 24 hours before use. 4-methyl-1-pentene was vacuum transferred from lithium aluminum hydride after drying overnight. 4-Fluorostyrene, 2,3,4,5,6-pentafluorostyrene, dihydrocoumarin, *N*,*N*-dimethylbenzamide, and pyrazine were purchased from Aldrich and pumped on for approximately 15 minutes on the high vacuum line before use. 1-Methyl-2-piperidone was purchased from Fluka and quickly dried on the high vacuum line. 2-Adamantanone was purchased from Alfa Aesar and dried overnight on the same line before use. Benzylacetone and *trans*-β-methylstyrene were purchased from Aldrich and dried over molecular sieves before use. *trans*-Methyl-cinnamate was purchased from Aldrich, recrystallized from dry pentane at –35 °C, and dried under vacuum. *trans*-Chalcone was purchased from Aldrich and dried under vacuum for 16 hours. After drying, this substrate was recrystallized from a concentrated ethereal solution at -35 °C. Benzophenone was purchased from Fisher Scientific and dried under vacuum for 24 hours. *trans*-4-Phenyl-3-buten-2-one was purchased from Acros and dried *in vacuo* for approximately 1 hour before use. 2-Hexanone-1,1,1,3,3-d_5 was prepared by stirring 2-hexanone in D_2O in the presence of D_2SO_4 and dried with $MgSO_4$ following ether extraction. 1-Amino-2,2-dimethyl-3-butene was prepared arccording to literature procedures.[37]

^{1}H NMR spectra were recorded on Varian Mercury 300, Inova 400 and 500 spectrometers operating at 299.76, 399.78 and 500.62 MHz, respectively. ^{2}H NMR spectra were recorded at 20 °C on Inova 500 and 600 spectrometers operating at 76.85 and 92.07 MHz, respectively. ^{13}C NMR spectra were recorded on the Inova 400 and 500 spectrometers operating at 101.535 or 125.893 MHz, respectively. All ^{1}H and ^{13}C NMR chemical shifts are reported relative to $SiMe_4$ using ^{1}H (residual) and ^{13}C chemical shifts of the solvent as a secondary standard. For complexes exhibiting temperature independent magnetism, many assignments were made based on COSY,

HSQC, and HMBC NMR experiments. Solution magnetic moments were determined by Evans method[38] using a ferrocene standard and are the average value of at least two independent measurements. ^{1}H NMR multiplicity and coupling constants are given where applicable. Peak width at half height is given for paramagnetically broadened resonances. Elemental analyses were performed at Robertson Microlit Laboratories, Inc., in Madison, NJ. Electrochemical measurements were made under a dinitrogen purge with a 3 mm glassy carbon working electrode, Pt wire as a counter electrode, and Ag wire as a reference. Cyclic voltammograms were collected in acetonitrile solution and the reported reduction potentials are referenced relative to ferrocene/ferrocenium.

Single crystals suitable for X-ray diffraction were coated with polyisobutylene oil in a drybox, transferred to a nylon loop and then quickly transferred to the goniometer head of a Bruker X8 APEX2 diffractometer equipped with a molybdenum X-ray tube (λ = 0.71073 Å). Preliminary data revealed the crystal system. A hemisphere routine was used for data collection and determination of lattice constants. The space group was identified and the data were processed using the Bruker SAINT+ program and corrected for absorption using SADABS. The structures were solved using direct methods (SHELXS) completed by subsequent Fourier synthesis and refined by full-matrix least-squares procedures.

Mössbauer data were collected on an alternating constant-acceleration spectrometer. The minimum experimental line width was 0.24 mm s^{-1} (full width at half height). A constant sample temperature was maintained with an Oxford Instruments Variox or an Oxford Instruments Mössbauer-Spectromag 2000 cyrostat. Reported isomer shifts (δ) are referenced to iron metal at 293 K.

General Procedure for the Catalytic Hydrogenation of Amino-Substituted Olefins. A stock solution containing 0.026 g (0.044 mmol) of **1-$(N_2)_2$** and 15.00 g (178.3 mmol) of benzene-d_6 was prepared and stored at -35 °C. Upon thawing to ambient temperature, 0.65 g of the resulting solution was charged into a thick-walled glass vessel. Using a microsyringe, 0.633 mmol of the desired substrate was added and the vessels were quickly sealed. After being submerged in liquid nitrogen, the frozen solutions were treated with 4 atm of dihydrogen. The timer was started when the solutions began to stir upon thawing. The catalytic reactions were quenched by submerging the bomb in liquid nitrogen, evacuating the remaining dihydrogen, and transferring the volatile components of the resulting solution to a J. Young tube for analysis by ^{1}H NMR spectroscopy. Conversions were measured by integrating the residual olefin resonances against their saturated counterparts.

Catalytic deuteration of allylamine. A J. Young tube was charged with 0.012 g (0.020 mmol) of **1-$(N_2)_2$** and approximately 0.65 g of benzene. With a microsyringe, 0.076 g (100 μL, 1.33 mmol) of allylamine was added to the tube. This solution was then submerged in liquid nitrogen, the tube was evacuated, and 4 atm of deuterium was added. The tube was placed in a 65 °C bath for approximately 1 week before the solution was analyzed by ^{2}H NMR spectroscopy.

Catalytic hydrogenation of oxygenated olefins. For each independent trial, a thick-walled glass vessel was charged with a solution containing 0.019 g (0.032 mmol) of **1-$(N_2)_2$** in 0.65 g (7.72 mmol) of benzene-d_6. After standing in a liquid nitrogen chilled cold well for approximately 20 minutes, 0.633 mmol of the desired substrate was added to the vessel. Immediately after addition, the vessel was submerged in liquid nitrogen to prevent reaction of the substrate and catalyst. On the high vacuum line, 4

atm of dihydrogen was added and the solution was warmed to ambient temperature or 65 °C. At the desired reaction time, the vessel was opened to air and the catalyst solution was filtered through a glass frit into an NMR tube. Conversions were determined by integrating the remaining ^{1}H NMR olefin resonances against their saturated analogues.

Catalytic deuteration of 5-hexen-2-one. This reaction was conducted in a similar manner to that of the oxygenated olefins with an identical catalyst loading in benzene solution with 4 atm of deuterium gas. The reaction was opened to air after 90 minutes at 65 °C and the solution was filtered through a glass frit into an NMR tube. Deuterium incorporation was determined by ^{2}H NMR spectroscopy.

Preparation of (^{iPr}PDI)Fe($NH_2CH_2CH=CH_2$) (1-$NH_2CH_2CH=CH_2$). A 20 mL scintillation vial was charged with 0.100 g (0.168 mmol) of **1-$(N_2)_2$** and approximately 10 mL of pentane. With a microsyringe, 0.010 g (13 μL, 0.168 mmol) of allylamine was added to the stirring solution. Upon addition of the amine, dinitrogen evolution was observed and a reddish-brown solution formed. After 20 minutes, the solution was filtered though a frit and the solvent was removed *in vacuo* to yield 0.077 g (77%) of a dark brown solid identified as **1-$NH_2CH_2CH=CH_2$**. Analysis for $C_{36}H_{50}FeN_4$: Calcd C, 72.71; H, 8.48; N, 9.42. Found: C, 72.63; H, 8.77; N, 8.99. ^{1}H NMR (benzene-d_6): δ = 12.05 (d, 7.5 Hz, 2H, *m-pyr*), 8.77 (t, 7.5 Hz, 1H, *p-pyr*), 7.63 (t, 8.0 Hz, 2H, *p-aryl*), 7.24 (d, 8.0 Hz, 4H, *m-aryl*), 5.35 (m, 1H, CH_2CH=CH_2), 4.90 (t, 7.5 Hz, 2H, NH_2CH_2), 4.76 (d, 10.5 Hz, 1H, $CH_2CH=CH_2$), 4.70 (d, 17.0 Hz, 1H, $CH_2CH=CH_2$), 2.78 (sept., 7.0 Hz, 4H, $CH(CH_3)_2$), 1.63 (m, 2H, NH_2CH_2), 1.24 (d, 7.0 Hz, 12H, $CH(CH_3)_2$), -0.34 (d, 7.0 Hz, 12H, $CH(CH_3)_2$), -6.09 (s, 6H, $C(CH_3)$). ^{13}C{^{1}H} NMR (benzene-d_6): δ = 189.45, 165.16, 164.61 (quaternary carbons), 140.00 (*p-pyr*),

137.26 ($CH_2CH=CH_2$), 136.57, 125.25 (*p-aryl*), 124.43 (*m-aryl*), 116.86 ($CH_2CH=CH_2$), 103.09 (*m-pyr*), 44.81 (NH_2CH_2), 39.17 ($C(CH_3)$), 28.53 ($CH(CH_3)_2$), 24.23 ($CH(CH_3)_2$), 23.15 ($CH(CH_3)_2$).

Preparation of (^{iPr}PDI)Fe($NH_2CH_2CH_2CH_3$) (1-$NH_2CH_2CH_2CH_3$). This compound was prepared in a manner similar to **1-$NH_2CH_2CH=CH_2$** with 0.100 g (0.168 mmol) of **1-$(N_2)_2$** and 0.010 g (14 μL, 0.168 mmol) of propylamine to yield 0.075 g (75%) of a dark orange solid identified as **1-$NH_2CH_2CH_2CH_3$**. Analysis for $C_{36}H_{52}N_4Fe$: Calcd C, 72.47; H, 8.78; N, 9.39. Found: C, 72.25; H, 8.35; N, 9.00. ^{1}H NMR (benzene-d_6): δ = 12.12 (d, 7.5 Hz, 2H, *m-pyr*), 8.75 (t, 7.5 Hz, 1H, *p-pyr*), 7.63 (t, 8.0 Hz, 2H, *p-aryl*), 7.24 (d, 8.0 Hz, 4H, *m-aryl*), 4.83 (t, 7.5 Hz, 2H, NH_2CH_2), 2.72 (sept., 7.0 Hz, 4H, $CH(CH_3)_2$), 1.25 (d, 7.0 Hz, 12H, $CH(CH_3)_2$), 0.91 (m, 2H, NH_2CH_2), 0.83 (m, 2H, CH_2CH_3), 0.41 (t, 7.0 Hz, 3H, CH_2CH_3), -0.26 (d, 7.0 Hz, 12H, $CH(CH_3)_2$), -6.09 (s, 6H, $C(CH_3)$). $^{13}C\{^1H\}$ NMR (benzene-d_6): δ = 189.77, 165.29, 164.41, 140.20, 136.38 (*p-pyr*), 125.15 (*p-aryl*), 124.31 (*m-aryl*), 102.95 (*m-pyr*), 43.68 (NH_2CH_2), 38.82 ($C(CH_3)$), 28.48 ($CH(CH_3)_2$), 26.53 (CH_2CH_3), 24.30 ($CH(CH_3)_2$), 23.14 ($CH(CH_3)_2$), 10.80 (CH_2CH_3).

Synthesis of (^{iPr}PDI)Fe($NH_2CH_2C(Me)_2CH=CH_2$) (1-$NH_2CH_2C(Me)_2CH=CH_2$). This compound was prepared in a manner similar to **1-$NH_2CH_2CH=CH_2$** with 0.020 g (0.034 mmol) of **1-$(N_2)_2$** and 0.003 g (4.5 μL, 0.034 mmol) of 1-amino-2,2-dimethyl-3-butene in benzene-d_6 solution. ^{1}H NMR (benzene-d_6): δ = 12.14 (d, 7.5 Hz, 2H, *m-pyr*), 8.77 (t, 7.5 Hz, 1H, *p-pyr*), 7.62 (t, 8.0 Hz, 2H, *p-aryl*), 7.23 (d, 8.0 Hz, 4H, *m-aryl*), 5.40 (m, 1H, $CH=CH_2$), 5.06 (m, 1H, $CH=CH_2$), 4.88 (m, 1H, $CH=CH_2$), 2.75 (sept., 7.0 Hz, 4H, $CH(CH_3)_2$), 1.24 (d, 7.0 Hz, 12H, $CH(CH_3)_2$), 0.44 (s, 6H,

C(C*H*$_3$)$_2$), -0.20 (d, 7.0 Hz, 12H, CH(C*H*$_3$)$_2$), -6.23 (s, 6H, C(C*H*$_3$)), one resonance not located.

Preparation of (^{iPr}PDI)Fe(NH(Me)CH$_2$CH=CH$_2$) (1-NH(Me)CH$_2$CH=CH$_2$). This compound was prepared in a manner similar to **1-NH$_2$CH$_2$CH=CH$_2$** with 0.042 g (0.071 mmol) of **1-(N$_2$)$_2$** and 0.005 g (7 μL, 0.071 mmol) of *N*-allylmethylamine to yield 0.023 g (53 %) of a dark brown solid identified as **1-NH(Me)CH$_2$CH=CH$_2$**. Analysis for $C_{37}H_{52}N_4Fe$: Calcd C, 73.01; H, 8.61; N, 9.20. Found: C, 72.79; H, 8.25; N, 8.96. ^{1}H NMR (benzene-*d*$_6$): δ = 12.62 (d, 8.0 Hz, 2H, *m-pyr*), 8.82 (t, 8.0 Hz, 1H, *p-pyr*), 8.28 (m, 1H, N*H*(CH$_3$)), 7.68 (t, 8.0 Hz, 2H, *p-aryl*), 7.24 (d, 8.0 Hz, 4H, *m-aryl*), 4.99 (m, 1H, CH$_2$C*H*=CH$_2$), 4.92 (d, 10.5 Hz, 1H, CH$_2$CH=C*H*$_2$), 4.75 (d, 17.0 Hz, 1H, CH$_2$CH=C*H*$_2$), 2.16 (m, 2H, NH(C*H*$_2$)), 1.22 (d, 7.0 Hz, 12H, CH(C*H*$_3$)$_2$), 1.02 (d, 7.0 Hz, 3H, NH(C*H*$_3$)), 0.25 (d, 7.0 Hz, 12H, CH(C*H*$_3$)$_2$), -6.55 (s, 6H, C(C*H*$_3$)), one peak not located. ^{13}C{^{1}H} NMR (benzene-*d*$_6$): δ = 192.79, 165.77, 142.46, 137.04, 134.06, 125.50 (*p-aryl*), 124.54 (*m-aryl*), 123.91, 121.22, 103.07 (*m-pyr*), 52.36 (NH*C*H$_2$), 40.93 (C(*C*H$_3$)), 34.31 (NH*C*H$_3$), 28.55 (*C*H(CH$_3$)$_2$), 24.76 (CH(*C*H$_3$)$_2$), 23.22 (CH(*C*H$_3$)$_2$).

Preparation of (^{iPr}PDI)FeOC(Me)(3-butenyl)) (1-OC(Me)(3-butenyl)). With a microsyringe, 0.016 g (20 μL, 0.168 mmol) of 5-hexen-2-one was added to 0.100 g (0.168 mmol) of **1-(N$_2$)$_2$** in approximately 10 mL of pentane. After stirring for 30 minutes, the solution was filtered through Celite and the solvent was evacuated. Recrystallization of the resulting solid from a concentrated pentane solution at -35 °C yielded 0.041 g (38%) of dark brown crystals identified as **1-OC(Me)(3-butenyl)**. Analysis for $C_{39}H_{53}FeN_3O$: Calcd C, 73.69; H, 8.40; N, 6.61. Found: C, 73.43; H, 8.43; N, 6.41. ^{1}H NMR (toluene-*d*$_8$, 20 °C): δ =10.49 (bs, 7.5 Hz, 2H, *m-pyr*), 8.44

(bs, 1H, *p-pyr*), 7.42 (t, 8.0 Hz, 2H, *p-aryl*), 7.14 (d, 8.0 Hz, 4H, *m-aryl*), 5.29 (bs, 1H, CH_2CH=CH_2), 4.83 (bs, 2H, CH_2CH=CH_2), 2.78 (sept., 7.0 Hz, 4H, CH(CH_3)$_2$), 1.44 (bs, 2H, CH_2), 1.20 (d, 7.0 Hz, 12H, CH(CH_3)$_2$), 0.98 (bs, 2H, CH_2), 0.20 (d, 7.0 Hz, 12H, CH(CH_3)$_2$), -2.87 (bs, 6H, C(CH_3)). ^{1}H NMR (toluene-d_8, -60 °C): δ =10.45 (d, 7.5 Hz, 2H, *m-pyr*), 8.55 (t, 7.5 Hz, 1H, *p-pyr*), 7.44 (t, 8.0 Hz, 2H, *p-aryl*), 7.12 (d, 8.0 Hz, 4H, *m-aryl*), 5.30 (m, 1H, CH_2CH=CH_2), 4.89 (d, 11.0 Hz, 1H, CH_2CH=CH_2), 4.85 (d, 17.5 Hz, 1H, CH_2CH=CH_2), 2.74 (sept., 7.0 Hz, 4H, CH(CH_3)$_2$), 1.32 (m, 2H, CH_2), 1.22 (d, 7.0 Hz, 12H, CH(CH_3)$_2$), 0.97 (m, 2H, CH_2), 0.22 (d, 7.0 Hz, 12H, CH(CH_3)$_2$), 0.18 (s, 3H, CO(CH_3)), -2.78 (s, 6H, C(CH_3)). ^{13}C{^{1}H} NMR (toluene-d_8, -60 °C): δ = 205.11 (*C*=O), 171.01, 160.02, 155.51, 139.06, 137.62 (CH_2CH=*C*H_2), 137.12, 131.25 (*p-pyr*), 124.90 (*p-aryl*), 123.53 (*m-aryl*), 115.97 (CH_2*C*H=CH_2), 105.09 (*m-pyr*), 46.96 (*C*H_2CH=CH_2), 31.62 (CO*C*H_3), 30.78 (C(CH_3)), 28.36 (*C*H(CH_3)$_2$), 27.51 (CO*C*H_2), 24.24 (CH(*C*H_3)$_2$), 23.30 (CH(*C*H_3)$_2$).

Preparation of (^{iPr}PDI)Fe(DHC) (1-DHC). This compound was prepared in a manner similar to **1-OC(Me)(3-butenyl)** with 0.100 g (0.168 mmol) of **1-(N_2)$_2$** and 0.025 g (28 μL, 0.168 mmol) of (+)-dihydrocarvone as a mixture of isomers. After filtration, the solvent was removed *in vacuo* and recrystallized from pentane to yield 0.087 g (75%) of a dark purple solid identified as **1-DHC** as a mixture of two diastereomers. Analysis for $C_{43}H_{59}FeN_3O$: Calcd C, 74.87; H, 8.62; N, 6.09. Found: C, 74.80; H, 8.58; N, 5.83. ^{1}H NMR (major diastereomer, benzene-d_6): δ =10.47 (d, 7.5 Hz, 2H, *m-pyr*), 8.46 (t, 7.5 Hz, 1H, *p-pyr*), 7.42 (t, 8.0 Hz, 2H, *p-aryl*), 7.19 (d, 8.0 Hz, 4H, *m-aryl*), 4.63 (s, 1H, C=CH_2), 3.18 (sept., 7.0 Hz, 2H, CH(CH_3)$_2$), 4.52 (s, 1H, C=CH_2), 2.59 (sept., 7.0 Hz, 2H, CH(CH_3)$_2$), 1.83 (m, 2H, *DHC*), 1.50 (s, 3H, DHC CCH_3), 1.21 (d, 7.0 Hz, 6H, CH(CH_3)$_2$), 1.15 (d, 7.0 Hz, 6H, CH(CH_3)$_2$), 0.90-1.07 (m, 6H, *DHC*), 0.56 (d, 7.0 Hz, 6H, CH(CH_3)$_2$), 0.40 (d, 7.0 Hz, DHC CHCH_3),

0.13 (d, 7.0 Hz, 6H, CH(C*H*$_3$)$_2$), -2.89 (s, 6H, C(C*H*$_3$)). ^{1}H NMR (minor diastereomer, benzene-*d*$_6$): δ = 10.84 (d, 7.5 Hz, 2H, *m-pyr*), 8.56 (t, 7.5 Hz, 1H, *p-pyr*), 7.50 (t, 8.0 Hz, 2H, *p-aryl*), 7.20 (d, 8.0 Hz, 4H, *m-aryl*), 4.56 (s, 1H, C=C*H*$_2$), 4.45 (s, 1H, C=C*H*$_2$), 2.82 (sept., 7.0 Hz, 2H, C*H*(CH$_3$)$_2$), 2.50 (m, 2H, *DHC*), 1.43 (s, 3H, DHC CC*H*$_3$), 1.22 (d, 7.0 Hz, 6H, CH(C*H*$_3$)$_2$), 1.19 (d, 7.0 Hz, 6H, CH(C*H*$_3$)$_2$), 0.90-1.07 (m, 6H, *DHC*), 0.36 (d, 7.0 Hz, 6H, CH(C*H*$_3$)$_2$), 0.29 (d, 7.0 Hz, DHC CHC*H*$_3$), 0.18 (d, 7.0 Hz, 6H, CH(C*H*$_3$)$_2$), -3.39 (s, 6H, C(C*H*$_3$)), one peak not located. ^{13}C{^{1}H} NMR (major diastereomer, benzene-*d*$_6$): δ = 210.52 (*C*=O), 171.21, 161.20, 155.18, 147.94, 139.70, 139.10, 130.96 (*p-pyr*), 124.54 (*p-aryl*), 123.74 (*m-aryl*), 123.47 (*m-aryl*), 110.38 (C=*C*H$_2$), 104.31 (*m-pyr*), 46.96 (DHC), 46.16 (DHC), 43.66 (DHC), 30.39 (C(*C*H$_3$)), 28.38 (*C*H(CH$_3$)$_2$), 27.99 (*C*H(CH$_3$)$_2$), 24.29 (CH(*C*H$_3$)$_2$), 23.69 (CH(*C*H$_3$)$_2$), 23.39 (CH(*C*H$_3$)$_2$), 22.48 (CH(*C*H$_3$)$_2$), 20.08 (DHC C*C*H$_3$), 13.53 (DHC CH*C*H$_3$), one peak not located.

Preparation of ^{iPr}PDIFe(OC(Me)(^{n}Bu)) (1-OC(Me)(^{n}Bu)). A 20 mL scintillation vial was charged with 0.100 g (0.168 mmol) of **1-(N$_2$)$_2$** and approximately 10 mL of pentane. While stirring, 0.017 g (21 μL, 0.168 mmol) of 2-hexanone was added by microsyringe and the solution immediately began to evolve N_2 and turn brown. After 20 minutes, the solution was filtered though a frit and the solvent was removed *in vacuo* to yield 0.085 g (79%) of a dark brown solid identified as **1-OC(Me)(^{n}Bu)**. Analysis for $C_{39}H_{55}FeN_3O$: Calcd C, 73.45; H, 8.69; N, 6.59. Found: C, 73.25; H, 8.30; N, 6.46. ^{1}H NMR (benzene-*d*$_6$): δ = 10.59 (d, 7.5 Hz, 2H, *m-pyr*), 8.51 (t, 7.5 Hz, 1H, *p-pyr*), 7.46 (t, 8.0 Hz, 2H, *p-aryl*), 7.16 (d, 8.0 Hz, 4H, *m-aryl*), 2.82 (sept., 7.0 Hz, 4H, C*H*(CH$_3$)$_2$), 1.21 (d, 7.0 Hz, 12H, CH(C*H*$_3$)$_2$), 1.14 (m, 2H, *butyl*), 0.93 (m, 2H, *butyl*), 0.85 (m, 2H, *butyl*), 0.71 (m, 3H, CH$_2$C*H*$_3$), 0.29 (s, 3H, CO(C*H*$_3$)), 0.22 (d, 7.0 Hz, 12H, CH(C*H*$_3$)$_2$), -3.07 (s, 6H, C(C*H*$_3$)). ^{13}C{^{1}H} NMR (benzene-*d*$_6$): δ =

172.82, 160.82, 155.87, 139.11, 132.07 (*p-pyr*), 124.83 (*p-aryl*), 123.51 (*m-aryl*), 104.68 (*m-pyr*), 47.98, 31.84 (CO*C*H_3), 31.41 (bs, C(C*H*$_3$)), 28.43 (*C*H(CH_3)$_2$), 25.87 (*butyl*), 24.32 (CH(*C*H_3)$_2$), 23.37 (CH(*C*H_3)$_2$), 23.35 (*butyl*), 14.16 (CH_2*C*H_3), one peak not located.

Preparation of (^{iPr}PDI)Fe(OC(Me)Ph) (1-OC(Me)Ph). This compound was prepared in a similar manner to **1-OC(Me)(3-butenyl)** with 0.100 g (0.168 mmol) of **1-(N_2)$_2$** and 0.020 g (20 μL, 0.168 mmol) of acetophenone to yield 0.092 g (83%) of a dark green solid identified as **1-OC(Ph)Me**. Analysis for $C_{41}H_{51}FeN_3O$: Calcd C, 74.87; H, 7.82; N, 6.39. Found: C, 75.02; H, 7.41; N, 6.46. ^{1}H NMR (benzene-d_6): δ = 10.05 (d, 7.5 Hz, 2H, *m-pyr*), 8.80 (t, 7.5 Hz, 1H, *p-pyr*), 7.44 (broad s, 1H, *p-phenyl*), 7.42 (t, 8.0 Hz, 2H, *p-aryl*), 7.15 (d, 8.0 Hz, 4H, *m-aryl*), 7.13 (broad s, 2H, *o-phenyl*), 6.69 (broad s, 2H, *m-phenyl*), 2.70 (sept., 7.0 Hz, 4H, C*H*(CH_3)$_2$), 1.19 (d, 7.0 Hz, 12H, CH(C*H*$_3$)$_2$), 0.15 (d, 7.0 Hz, 12H, CH(C*H*$_3$)$_2$), -0.52 (broad s, 3H, COC*H*$_3$), -2.33 (s, 6H, C(C*H*$_3$)). ^{1}H NMR (toluene-d_8, -80 °C): δ = 9.96 (d, 7.5 Hz, 2H, *m-pyr*), 8.68 (t, 7.5 Hz, 1H, *p-pyr*), 7.43 (t, 7.5 Hz, 2H, *p-aryl*), 7.26 (t, 7.5 Hz, 1H, *p-phenyl*), 6.83 (d, 7.0 Hz, 2H, *o-phenyl*), 6.69 (m, 2H, *m-phenyl*), 3.09 (broad s, 2H, C*H*(CH_3)$_2$), 2.27 (broad s, 2H, C*H*(CH_3)$_2$), 1.28 (broad m, 6H, CH(C*H*$_3$)$_2$), 1.18 (broad m, 6H, CH(C*H*$_3$)$_2$), 0.33 (broad s, 6H, CH(C*H*$_3$)$_2$), -0.04 (broad s, 6H, CH(C*H*$_3$)$_2$), -0.11 (s, 3H, COC*H*$_3$), -2.01 (s, 6H, C(C*H*$_3$)), *m-aryl* peak not located. ^{13}C{^{1}H} NMR (benzene-d_6): δ = 166.42, 159.33, 154.74, 139.82, 125.56 (*p-aryl*), 124.01 (*m-aryl*), 107.43 (*m-pyr*), 30.37 (C(C*H*$_3$)), 28.25 (*C*H(CH_3)$_2$), 24.47 (CH(*C*H_3)$_2$), 23.14 (CH(*C*H_3)$_2$), *p-pyr* and *acetophenone* peaks not located.

Preparation of (^{iPr}PDI)Fe(OC(Me)(PhEt)) (1-OC(Me)(PhEt)). This compound was prepared in a manner similar to **1-OC(Me)(3-butenyl)** with 0.100 g (0.168 mmol) of

1-(N_2)$_2$ and 0.025 g (26 μL, 0.168 mmol) of 4-phenyl-2-butanone. The resulting residual solid was recrystallized from pentane at -35 °C to yield 0.030 g (26%) of a dark brown solid identified as **1-OC(Me)(PhEt)**. Analysis for $C_{43}H_{55}FeN_3O$: Calcd C, 75.31; H, 8.08; N, 6.13. Found: C, 74.99; H, 7.86; N, 5.81. ^{1}H NMR (benzene-d_6): δ = 10.53 (d, 7.5 Hz, 2H, *m-pyr*). 8.52 (t, 7.5 Hz, 1H, *p-pyr*), 7.46 (t, 8.0 Hz, 2H, *p-aryl*), 7.17 (d, 8.0 Hz, 4H, *m-aryl*), 7.11 (d, 7.5 Hz, 2H, phenyl), 7.02 (t, 7.5 Hz, 1H, phenyl), 6.90 (d, 7.5 Hz, 2H, phenyl), 2.82 (sept., 7.0 Hz, 4H, C*H*(CH_3)$_2$), 2.07 (m, 2H, CH_2), 1.33 (m, 2H, CH_2), 1.20 (d, 7.0 Hz, 12H, CH(CH_3)$_2$), 0.21 (d, 7.0 Hz, 12H, CH(CH_3)$_2$), 0.17 (s, 3H, CO(CH_3)), -3.04 (s, 6H, C(CH_3)). ^{13}C{^{1}H} NMR (benzene-d_6): δ = 204.77 (*C*=O), 172.32, 160.75, 155.98, 139.29, 131.94, 129.14, 129.03, 127.01, 126.63, 124.98 (*p-aryl*), 123.64 (*m-aryl*), 104.87 (*m-pyr*), 49.32 (*C*H_2), 32.58 (CO*C*H_3), 31.31 (C(*C*H_3)), 29.17 (*C*H_2), 28.44 (*C*H(CH_3)$_2$), 24.30 (CH(*C*H_3)$_2$), 23.39 (CH(*C*H_3)$_2$).

Preparation of (^{iPr}PDI)Fe(O=Ad) (1-O=Ad). This compound was prepared in a similar fashion to **1-OC(Me)(3-butenyl)** with 0.100 g (0.168 mmol) of **1-(N_2)$_2$** and 0.025 g (0.168 mmol) of 2-adamantanone to yield 0.093 g (80%) of a dark purple solid identified as **1-O=Ad**. Analysis for $C_{43}H_{57}FeN_3O$: Calcd C, 75.09; H, 8.35; N, 6.11. Found: C, 75.01; H, 8.62; N, 5.82. ^{1}H NMR (benzene-d_6): δ = 10.62 (d, 7.5 Hz, 2H, *m-pyr*). 8.45 (t, 7.5 Hz, 1H, *p-pyr*), 7.40 (t, 7.5 Hz, 2H, *p-aryl*), 7.19 (d, 7.5 Hz, 4H, *m-aryl*), 2.99 (sept., 7.0 Hz, 4H, C*H*(CH_3)$_2$), 1.63 (broad s, 2H, OC(C*H*)$_2$), 1.36 (broad s, 12H, *adamantyl*), 1.20 (d, 7.0 Hz, 12H, CH(CH_3)$_2$), 0.31 (d, 7.0 Hz, 12H, CH(CH_3)$_2$), -3.05 (s, 6H, C(CH_3)). ^{13}C NMR (benzene-d_6): δ = 172.58, 161.58, 155.25, 139.19, 131.77 (*p-pyr*), 124.68 (*p-aryl*), 123.72 (*m-aryl*), 104.40 (*m-pyr*), 50.30 (OC(*C*H)$_2$), 37.70 (*adamantyl*), 36.31 (*adamantyl*), 31.64 (broad s, C(CH_3)), 28.61 (*C*H(CH_3)$_2$), 27.71 (*adamantyl*), 24.40 (CH(*C*H_3)$_2$), 23.02 (CH(*C*H_3)$_2$), one peak not located.

Observation of (^{iPr}PDI)Fe(OC(Me)(^{c}Pr)) (1-OC(Me)(^{c}Pr)). This complex was prepared in a manner similar to **1-OC(Me)(3-butenyl)** with 0.015 g (0.025 mmol) of **1-$(N_2)_2$** and 0.002 g (2.5 μL, 0.025 mmol) of cyclopropyl methyl ketone in benzene-d_6 solution. ^{1}H NMR (benzene-d_6): δ = 10.78 (d, 7.5 Hz, 2H, *m-pyr*), 8.53 (t, 7.5 Hz, 1H, *p-pyr*), 7.46 (t, 8.0 Hz, 2H, *p-aryl*), 7.16 (m, 4H, *m-aryl*), 2.79 (sept., 7.0 Hz, 2H, C*H*(CH_3)$_2$), 1.23 (d, 7.0 Hz, 12H, CH(C*H*$_3$)$_2$), 0.18 (d, 7.0 Hz, 12H, CH(C*H*$_3$)$_2$), 0.01 (s, 3H, CO(C*H*$_3$)), -3.28 (s, 6H, C(C*H*$_3$)), *cyclopropyl* resonances not located.

Observation of (^{iPr}PDI)Fe(OC(Me)(^{c}Bu)) (1-OC(Me)(^{c}Bu)). This complex was prepared in a manner similar to **1-OC(Me)(3-butenyl)** with 0.015 g (0.025 mmol) of **1-$(N_2)_2$** and 0.002 g (2.75 μL, 0.025 mmol) of cyclobutyl methyl ketone in benzene-d_6 solution. ^{1}H NMR (benzene-d_6): δ = 10.67 (d, 7.5 Hz, 2H, *m-pyr*), 8.55 (t, 7.5 Hz, 1H, *p-pyr*), 7.44 (t, 8.0 Hz, 2H, *p-aryl*), 7.16 (m, 4H, *m-aryl*), 2.76 (sept., 7.0 Hz, 2H, C*H*(CH_3)$_2$), 1.93 (m, 1H, ^{c}*Bu*), 1.60-1.32 (m, 6H, ^{c}*Bu*), 1.22 (d, 7.0 Hz, 12H, CH(C*H*$_3$)$_2$), 0.22 (d, 7.0 Hz, 12H, CH(C*H*$_3$)$_2$), 0.10 (s, 3H, CO(C*H*$_3$)), -3.22 (s, 6H, C(C*H*$_3$)).

Observation of (^{iPr}PDI)Fe(Car) (1-Car). Using a microsyringe, 0.005 g (5.25 μL, 0.034 mmol) of (-)-carvone was added to a solution of **1-$(N_2)_2$** in approximately 0.70 g of benzene-d_6. The resulting bright green solution was quickly filtered through Celite into a J. Young tube and submerged in liquid nitrogen to prevent decomposition. The ^{1}H NMR spectrum of this complex was recorded immediately after thawing. The solution turned dark brown in color during the course of spectral acquisition. ^{1}H NMR (benzene-d_6): δ = 10.37 (d, 7.5 Hz, 2H, *m-pyr*), 8.62 (t, 7.5 Hz, 1H, *p-pyr*), 7.47 (t, 8.0 Hz, 2H, *p-aryl*), 7.26 (d, 8.0 Hz, 4H, *m-aryl*), 6.41 (s, 1H, C=C*H*CH_2), 4.64 (s, 1H,

C=CH_2), 4.56 (s, 1H, C=CH_2), 2.93 (sept., 7.0 Hz, 2H, CH(CH_3)$_2$), 2.61 (m, 2H, CH(CH_3)$_2$ or carvone CH_2), 2.22 (m, 1H, carvone), 1.41 (s, 3H, carvone CH_3), 1.30 (s, 3H, carvone CH_3), 1.25-1.16 (m, 12H, CH(CH_3)$_2$), 0.48 (d, 7.0 Hz, 6H, CH(CH_3)$_2$), 0.09 (d, 7.0 Hz, 6H, CH(CH_3)$_2$), -0.78 (dd, 16 Hz, 1H, COCH_2), -2.59 (s, 6H, C(CH_3)), two peaks not located.

Observation of (^{iPr}PDI)Fe($CH_3O_2CCH_3$) (1-MeOAc). To a solution of 0.020 g (0.025 mmol) of **1-(N_2)$_2$** in approximately 0.7 mL of benzene-d_6, 2.7 μL (0.025 mmol) of methyl acetate was added by microsyringe. The resulting reddish-brown solution was transferred to a J. Young tube and quickly analyzed by ^{1}H NMR spectroscopy. ^{1}H NMR (benzene-d_6): δ = 11.67 (br s, 2H, *m-pyr*), 8.63 (br s, 1H, *p-pyr*), 7.54 (t, 8.0 Hz, 2H, *p-aryl*), 2.57-2.62 (m, 7H, CH(CH_3)$_2$ and OCH_3), 1.21 (d, 7.0 Hz, 12H, CH(CH_3)$_2$), 0.59 (s, 3H, COCH_3), -0.13 (d, 7.0 Hz, 12H, CH(CH_3)$_2$), -4.88 (s, 6H, C(CH_3)), *m-aryl* resonance not located.

Preparation of (^{iPr}PDI)Fe($CH_3O_2CCH_2CH_3$) (1-EtOAc). A 20 mL scintillation vial was charged with 0.080 g (0.135 mmol) of **1-(N_2)$_2$** and approximately 10 mL of diethyl ether. With stirring, 0.012 g (13 μL, 0.135 mmol) of ethyl acetate was added via microsyringe resulting in immediate evolution of N_2 along with a change in color to reddish-brown. After 30 minutes, the solution was filtered though a Celite fitted frit and the solvent was removed *in vacuo* to yield 0.070 g (83%) of a dark brown solid identified as **1-EtOAc**. Analysis for $C_{37}H_{51}FeN_3O_2$: Calcd C, 71.03; H, 8.22; N, 6.72. Found: C, 70.74; H, 7.86; N, 6.97. ^{1}H NMR (toluene-d_8, -60 °C): δ = 11.61 (d, 7.5 Hz, 2H, *m-pyr*), 8.66 (t, 7.0 Hz, 1H, *p-pyr*), 7.50 (t, 8.0 Hz, 2H, *p-aryl*), 7.09 (d, 7.0 Hz, 4H, *m-aryl*), 2.92 (q, 6.0 Hz, 2H, CH_2CH$_3$), 2.52 (sept., 5.5 Hz, 4H, CH(CH_3)$_2$), 1.24 (d, 5.5 Hz, 12H, CH(CH_3)$_2$), 0.81 (t, 6.0 Hz, 3H, CH$_2$CH_3), 0.58 (s, 3H, COCH_3), -

0.12 (d, 5.5 Hz, 12H, CH(C*H*$_3$)$_2$), -4.67 (s, 6H, C(C*H*$_3$)). ^{13}C{^{1}H} NMR (toluene-d_8, -60 °C): δ = 183.41, 181.65, 163.30, 160.00, 137.62, 136.80 (*p-pyr*), 124.53 (*p-aryl*), 123.69 (*m-aryl*), 103.83 (*m-pyr*), 64.22 (*C*H$_2$CH$_3$), 35.39 (C(*C*H$_3$)), 28.29 (*C*H(CH$_3$)$_2$), 23.73 (CH(*C*H$_3$)$_2$), 22.86 (CH(*C*H$_3$)$_2$), 22.33 (CO*C*H$_3$), 13.79 (CH$_2$*C*H$_3$).

Preparation of (^{iPr}PDI)Fe(CH$_3$O$_2$CCH(CH$_3$)$_2$) (1-^{i}PrOAc). This complex was prepared in a manner similar to **1-MeOAc** with 0.015 g (0.025 mmol) of **1-(N$_2$)$_2$** and 0.002 g (2.5 μL, 0.025 mmol) of cyclopropyl methyl ketone in benzene-d_6 solution. Free **1-(N$_2$)$_2$** was also observed by ^{1}H NMR spectroscopy suggesting that acetate exchange causes broadening of the resonances. ^{1}H NMR (benzene-d_6): δ = 11.94 (br s, 2H, *m-pyr*), 8.69 (br s, 1H, *p-pyr*), 7.58 (br s, 2H, *p-aryl*), 2.58 (br s, 4H, C*H*(CH$_3$)$_2$), 0.99 (br s, 12H, CH(C*H*$_3$)$_2$), 0.45 (br s), -0.01 (br s, 12H, CH(C*H*$_3$)$_2$), -5.32 (br s, 6H, C(C*H*$_3$)), several peaks not located.

Preparation of (^{iPr}PDI)Fe(Valerolactone) (1-Valero). This complex was prepared in a manner similar to **1-MeOAc** with 0.015 g (0.025 mmol) of **1-(N$_2$)$_2$** and 0.003 g (2.5 μL, 0.025 mmol) of *δ*-valerolactone in benzene-d_6 solution. ^{1}H NMR (benzene-d_6): δ = 11.38 (d, 7.5 Hz, 2H, *m-pyr*), 8.60 (t, 7.0 Hz, 1H, *p-pyr*), 7.49 (t, 7.5 Hz, 2H, *p-aryl*), 7.16 (m, 4H, *m-aryl*), 2.89 (sept., 7.0 Hz, 4H, C*H*(CH$_3$)$_2$), 1.36 (m, 2H, *valerolactone*), 1.29 (d, 7.0 Hz, 12H, CH(C*H*$_3$)$_2$), 0.77 (m, 2H, *valerolactone*), 0.63 (m, 2H, *valerolactone*), 0.06 (d, 7.0 Hz, 12H, CH(C*H*$_3$)$_2$), -4.28 (s, 6H, C(C*H*$_3$)), one *valerolactone* resonance not located.

Preparation of (^{iPr}PDI)Fe(Dihydrocoumarin) (1-DHCou). This complex was prepared in a manner similar to **1-MeOAc** with 0.015 g (0.025 mmol) of **1-(N$_2$)$_2$** and 0.004 g (3.25 μL, 0.025 mmol) of *δ*-valerolactone in benzene-d_6 solution. ^{1}H NMR

(benzene-d_6): δ = 10.95 (d, 7.5 Hz, 2H, *m-pyr*), 8.63 (t, 7.0 Hz, 1H, *p-pyr*), 7.33 (t, 8.0 Hz, 2H, *p-aryl*), 7.10 (d, 7.0 Hz, 4H, *m-aryl*), 6.81 (m, 1H, *phenyl*), 6.68 (m, 1H, *phenyl*), 6.52 (m, 1H, *phenyl*), 6.44 (m, 1H, *phenyl*), 2.99 (sept., 7.0 Hz, 4H, C*H*(CH_3)$_2$), 1.96 (br t, dihydrocoumarin CH_2), 1.34 (br t, dihydrocoumarin CH_2), 1.27 (d, 7.0 Hz, 12H, CH(CH_3)$_2$), 0.13 (d, 7.0 Hz, 12H, CH(CH_3)$_2$), -3.75 (s, 6H, C(CH_3)).

Observation of (^{iPr}PDI)Fe(OC(Me)(NMe$_2$)) (1-OC(Me)(NMe$_2$)). This complex was prepared in a manner similar to **1-MeOAc** with 0.010 g (0.017 mmol) of **1-(N$_2$)$_2$** and 0.001 g (2 μL, 0.017 mmol) of *N*,*N*-dimethylacetamide in benzene-d_6 solution. ^{1}H NMR (benzene-d_6): δ = 12.33 (d, 7.5 Hz, 2H, *m-pyr*), 8.55 (t, 7.0 Hz, 1H, *p-pyr*), 7.56 (t, 7.5 Hz, 2H, *p-aryl*), 7.14 (m, 4H, *m-aryl*), 2.46 (sept., 7.0 Hz, 4H, C*H*(CH_3)$_2$), 1.96 (s, 6H, N(CH_3)$_2$), 1.22 (d, 7.0 Hz, 12H, CH(CH_3)$_2$), 0.46 (s, 3H, CO(CH_3)), -0.01 (d, 7.0 Hz, 12H, CH(CH_3)$_2$), -5.25 (s, 6H, C(CH_3)).

Observation of (^{iPr}PDI)Fe(OC(Ph)(NMe$_2$)) (1-OC(Ph)(NMe$_2$)). This complex was prepared in a manner similar to **1-MeOAc** with 0.015 g (0.025 mmol) of **1-(N$_2$)$_2$** and 0.004 g (0.025 mmol) of *N*,*N*-dimethylbenzamide in benzene-d_6 solution. ^{1}H NMR (benzene-d_6): δ = 12.07 (d, 7.5 Hz, 2H, *m-pyr*), 8.47 (t, 7.0 Hz, 1H, *p-pyr*), 7.57 (t, 8.0 Hz, 2H, *p-aryl*), 7.18 (d, 8.0 Hz, 4H, *m-aryl*), 6.90 (m, 2H, *phenyl*), 6.40 (m, 2H, *phenyl*), 2.27 (s, 6H, N(CH_3)$_2$), 1.18 (br s, 12H, CH(CH_3)$_2$), 0.09 (br s, 12H, CH(CH_3)$_2$), -4.58 (s, 6H, C(CH_3)), two resonances not located.

Observation of (^{iPr}PDI)Fe(O=C$_6$H$_7$N) (1-PIP). This complex was prepared in a manner similar to **1-MeOAc** with 0.015 g (0.025 mmol) of **1-(N$_2$)$_2$** and 0.003 g (2.75 μL, 0.025 mmol) of 1-methyl-2-piperidone in benzene-d_6 solution. ^{1}H NMR (benzene-d_6): δ = 12.45 (d, 7.5 Hz, 2H, *m-pyr*), 8.54 (t, 7.0 Hz, 1H, *p-pyr*), 7.55 (t, 8.0 Hz, 2H,

p-aryl), 7.14 (m, 4H, *m-aryl*), 2.45 (sept., 7.0 Hz, 4H, C*H*(CH_3)$_2$), 2.37 (m, 2H, CH_2), 1.98 (s, 3H, N(CH_3)), 1.21 (d, 7.0 Hz, 12H, CH(CH_3)$_2$), 1.09 (m, 2H, CH_2), 0.97 (m, 2H, CH_2), 0.60 (m, 2H, CH_2), -0.01 (d, 7.0 Hz, 12H, CH(CH_3)$_2$), -5.30 (s, 6H, C(CH_3)).

Observation of (^{iPr}PDI)Fe(OC(Me)(N(Me)CH=CH$_2$)) (1-OC(Me)(N(Me)CH=CH$_2$)). This complex was prepared in a manner similar to **1-MeOAc** with 0.015 g (0.025 mmol) of **1-(N$_2$)$_2$** and 0.002 g (2.5 μL, 0.025 mmol) of *N*-vinyl-*N*-methylacetamide in benzene-d_6 solution. ^{1}H NMR (benzene-d_6): δ = 11.89 (d, 7.5 Hz, 2H, *m-pyr*), 8.58 (t, 7.0 Hz, 1H, *p-pyr*), 7.53 (t, 7.5 Hz, 2H, *p-aryl*), 7.13 (m, 4H, *m-aryl*), 6.29 (m, 1H, *vinyl*), 5.97 (m, 2H, *vinyl*), 2.49 (sept., 7.0 Hz, 4H, C*H*(CH_3)$_2$), 2.14 (s, 3H, N(CH_3)), 1.22 (d, 7.0 Hz, 12H, CH(CH_3)$_2$), 0.48 (s, 3H, CO(CH_3)), -0.03 (d, 7.0 Hz, 12H, CH(CH_3)$_2$), -4.86 (s, 6H, C(CH_3)). A second product was observed by ^{1}H NMR spectroscopy and has been tentatively assigned as **1- κ^2-Amide.** ^{1}H NMR (benzene-d_6): δ = 17.08 (332 Hz), 13.77 (56 Hz), 11.73 (176 Hz), 11.00 (400 Hz), 8.78 (68 Hz), 6.99 (63 Hz), 6.71 (208 Hz), 0.98 (85 Hz, CH(CH_3)$_2$), 0.91 (88 Hz, CH(CH_3)$_2$), -4.33 (500 Hz, C(CH_3)), -5.16 (503 Hz, C(CH_3)).

Preparation of (^{iPr}PDI)Fe(OCPh$_2$) (1-OCPh$_2$). This compound was prepared in a manner similar to **1-OC(Me)(3-butenyl)** with 0.100 g (0.168 mmol) of **1-(N$_2$)$_2$** and 0.031 g (0.168 mmol) of benzophenone to yield 0.082 g (68%) of a dark green solid identified as **1-OCPh$_2$**. Analysis for $C_{41}H_{51}FeN_3O$: Calcd C, 76.76; H, 7.42; N, 5.84. Found: C, 76.52; H, 7.69; N, 5.62. Magnetic susceptibility: μ_{eff} = 1.2 μ_B (benzene-d_6). Magnetic susceptibility: μ_{eff} = 0.0 μ_B (Gouy Balance). ^{1}H NMR (benzene-d_6): δ = 36.94 (37 Hz, 1H, *p-pyr*), 29.23 (239 Hz, 1H, *phenyl*), 26.66 (290 Hz, 2H, *phenyl*),

13.83 (14 Hz, 2H, *m-pyr*), 5.95 (d, 7.5 Hz, 4H, *m-aryl*), 5.52 (t, 7.5 Hz, 2H, *p-aryl*), -0.65 (7 Hz, 12H, CH(CH_3)$_2$), -1.95 (11 Hz, 12H, CH(CH_3)$_2$), -5.22 (49 Hz, 4H, CH(CH$_3$)$_2$), -18.05 (25 Hz, 6H, C(CH_3)), one *phenyl* peak not located.

Observation of (^{iPr}PDI)Fe(Pz) (1-Pz). This complex was prepared in a manner similar to **1-MeOAc** with 0.015 g (0.025 mmol) of **1-(N$_2$)$_2$** and 0.002 g (2.5 μL, 0.025 mmol) of pyrazine in benzene-d_6 solution. ^{1}H NMR (benzene-d_6): δ = 78.11 (162 Hz, 2H, *m-pyr*), 51.15 (127 Hz, 1H, *p-pyr*), 19.88 (29 Hz), 6.08 (20 Hz), 4.31 (24 Hz), -0.91 (19 Hz, 12H, CH(CH_3)$_2$), -3.76 (26 Hz, 12H, CH(CH_3)$_2$), -10.28 (49 Hz, 4H, CH(CH$_3$)$_2$), -29.60 (150 Hz, 6H, C(CH_3)), one resonance not located.

REFERENCES

[1] Osborn, J. A.; Jardine, F. H.; Young, J. F.; Wilkinson, G. *J. Chem. Soc. A*. **1966**, 1711.

[2] (a) Knowles, W. S.; Sabacky, M. J. *Chem. Commun*. **1968**, 1445. (b) Horner, L.; Siegel, H.; Büthe, H. *Angew. Chem., Int. Ed. Engl*. **1968**, *7*, 942.

[3] Johnson, N. B.; Lennon, I. C.; Moran, P. H.; Ramsden, J. A. *Acc. Chem. Res*. **2007**, *40*, 1291.

[4] Taylor, M. S.; Jacobsen, E. N. *Proc. Natl. Acad. Sci. U. S. Am*., **2004**, *101*, 5368.

[5] Knowles, W. S. *Acc. Chem. Res*. **1983**, *16*, 106.

[6] Noyori, R. *Asymmetric Catalysis in Organic Synthesis*; John Wiley and Sons, Inc., New York, 1994.

[7] Tang, W.; Zhang, X. *Chem. Rev*. **2003**, *103*, 3029.

[8] Lennon, I. C.; Pilkington, C. J. *Synthesis* **2003**, 1639.

[9] Fukatsu, K.; Uchikawa, O.; Kawada, M.; Yamano, T.; Yamashita, M.; Kato, K.; Hirai, K.; Hinuma, S.; Miyamoto, M.; Ohkawa, S. *J. Med. Chem*. **2002**, *45*, 4212.

[10] Enthaler, S.; Junge, K.; Beller, M. *Angew. Chem. Int. Ed*. **2008**, *47*, 3317.

[11] Bolm, C.; Legros, J.; Le Paih, J.; Zani, L. *Chem. Rev*. **2004**, *104*, 6217.

[12] Frankel, E. N.; Emken, E. A.; Peters, H. M.; Davison, V. L.; Butterfield, R. O. *J. Org. Chem*. **1964**, *29*, 3292.

[13] Lynch, T. J.; Banah, M.; Kaesz, H. D.; Porter, C. R. *J. Org. Chem*. **1984**, *49*, 1266.

[14] Schroeder, M. A.; Wrighton, M. S. *J. Am. Chem. Soc*. **1976**, *98*, 551.

[15] Schroeder, M. A.; Wrighton, M. S. *J. Organomet. Chem*. **1977**, *128*, 345.

[16] Miller, M. E.; Grant, E. R. *J. Am. Chem. Soc*. **1984**, *106*, 4635.

[17] Nagorski, H.; Mirbach, M. J. *J. Organomet. Chem*. **1985**, *291*, 199.

[18] Miller, M. E.; Grant. E. R. *J. Am. Chem. Soc*. **1987**, *109*, 7951.

[19] Kismartoni, L. C.; Weitz, E.; Cedeño, D. L. *Organometallics*, **2005**, *24*, 4714.

[20] Bart, S. C.; Lobkovsky, E.; Chirik, P. J. *J. Am. Chem. Soc*. **2004**, *126*, 13794.

[21] Bart, S. C.; Ph.D. Thesis, Cornell University, 2006.

[22] Bart, S. C.; Chlopek, K.; Bill, E.; Bouwkamp, M. W.; Lobkovsky, E.; Neese, F.; Wieghardt, K.; Chirik, P. J. *J. Am. Chem. Soc.* **2006**, *128*, 13901.

[23] Bart, S. C.; Lobkovsky, E.; Bill, E.; Wieghardt, K.; Chirik, P. J. *Inorg. Chem.* **2007**, *46*, 7055.

[24] Casey, C. P.; Guan, H. *J. Am. Chem. Soc.* **2007**, *129*, 5816.

[25] Bianchini, C.; Meli, A.; Peruzzini, M.; Frediani, P.; Bohanna, C.; Esteruelas, M. A.; Oro, L. A. *Organometallics* **1992**, *11*, 138.

[26] Daida, E. J.; Peters, J. C. *Inorg. Chem.* **2004**, *43*, 7474.

[27] Sui-Seng, C.; Freutel, F.; Lough, A. J.; Morris, R. H. *Angew. Chem. Int. Ed.* **2008**, *47*, 940.

[28] Shaikh, N. S.; Enthaler, S.; Junge, K.; Beller, M. *Angew. Chem. Int. Ed.* **2008**, *47*, 2497.

[29] Janvier, P.; Sun, X.; Bienaymé, H.; Zhu, J. *J. Am. Chem. Soc.* **2002**, *124*, 2560.

[30] Knijnenburg, Q.; Gambarotta, S.; Budzelaar, P. H. M. *Dalton Trans.*, **2006**, 5442. 1

[31] Fleischer, E. B.; Sung, N.; Hawkinson, S. *J. Phys. Chem.* **1968**, *72*, 4311.

[32] Vela, J.; Vaddadi, S.; Cundari, T. R.; Smith, J. M.; Gregory, E. A.; Lachicotte, R. J.; Flaschenriem, C. J.; Holland, P. L. *Organometallics* **2004**, *23*, 5226.

[33] Coombs, D. L.; Aldridge, S.; Rossin, A.; Jones, C.; Willock, D. J.; *Organometallics* **2004**, *23*, 2911.

[34] Grunert, C. M.; Reiman, S.; Spiering, H.; Kitchen, J. A.; Brooker, S.; Gütlich, P. *Angew. Chem. Int. Ed.* **2008**, *47*, 2997.

[35] O'Reilly, J. E.; Elving, P. J. *J. Am. Chem. Soc.* **1972**, *94*, 7941.

[36] Pangborn, A. B.; Giardello, M. A.; Grubbs, R. H.; Rosen, R. K.; Timmers, F. J. *Organometallics* **1996**, *15*, 1518.

[37] Casey, C. P.; Vollendorf, N. W.; Haller, K. J. *J. Am. Chem. Soc.* **1984**, *106*, 3754.

[38] Sur, S. K. *J. Magn. Res.* **1989**, *82*, 169.

CHAPTER 4

ETHER AND ESTER CARBON-OXYGEN BOND CLEAVAGE WITH BIS(IMINO)PYRIDINE IRON*

4.1 Abstract

Investigations into the substrate scope of bis(imino)pyridine iron-catalyzed olefin hydrogenation and [$2\pi + 2\pi$] diene cyclization reactions identified C-O bond cleavage as a principal deactivation pathway. Addition of diallyl or allyl ethyl ether to the bis(imino)pyridine iron dinitrogen complex, (^{iPr}PDI)Fe(N_2)$_2$ (^{iPr}PDI = 2,6-(2,6-$^{i}Pr_2$-C_6H_3N=CMe)$_2C_5H_3N$, **1-(N_2)$_2$**), under a dinitrogen atmosphere resulted in facile cleavage of the C-O bond and yielded a mixture of the corresponding paramagnetic iron allyl and alkoxide complexes. Monitoring the catalytic hydrogenation of *trans*-methyl cinnamate *in situ* established ester C-O bond cleavage. Stoichiometric reactions between **1-(N_2)$_2$** and allyl or vinyl acetate, respectively, also resulted in facile C-O oxidative addition. For the latter substrate, a six coordinate diamagnetic bis(imino)pyridine iron vinyl acetate compound was obtained and characterized by X-ray diffraction. Alkyl-substituted esters such as ethyl, pentyl, isopropyl, cyclohexyl, and *tert*-butyl acetate undergo competing ester and acyl C-O bond cleavage accompanied by iron-promoted decarbonylation. Deuterium labeling studies established that reversible C-H activation and chelate cyclometalation occur prior to, but are not a pre-requisite for, C-O bond oxidative addition of ethyl acetate. The molecular and electronic structures of the ether and ester C-O bond cleavage products have been established and demonstrate that ligand, rather than metal, based oxidation accompanies substrate activation.

---

* Parts of this chapter have been accepted for publication in *Organometallics*. Copyright 2008 American Chemical Society.

4.2 Introduction

Oxidative addition is a fundamental transformation in organometallic chemistry and often constitutes a key bond activation step in many stoichiometric reactions and catalytic processes.[1] This two electron redox event typically requires accessible M^n and M^{n+2} oxidation states and is most common with electron rich (*e.g.* d^6 and d^8), late transition metal complexes. For first row ions, oxidative addition of alkyl halides is known to involve radical processes[2] and can result in a two electron oxidation at a single metal center[3] or occur as two one electron oxidations involving two metals.[4,5]

As interest grows in replacing toxic and expensive precious metal catalysts with more cost-effective and benign iron compounds,[6,7] so grows the need to understand the elementary steps, such as oxidative addition, that comprise catalytic turnover and irreversible deactivation pathways.[8] Introduction of redox-active ligands, those that can actively participate in reversible electron transfer chemistry with the metal,[9,10] render oxidative transformations more intriguing as formal electron loss may be either metal or ligand based. Rationally designing compounds that undergo well-understood electron transfer events coupled to oxidative addition may ultimately prove valuable for discovering base metal catalysts that mimic or surpass the reactivity and selectivity often achieved with their second and third row congeners.

As discussed in Chapter 3, our laboratory has reported the synthesis of aryl-substituted bis(imino)pyridine iron dinitrogen compounds, (^{iPr}PDI)Fe(N_2)$_2$ (^{iPr}PDI = 2,6-(2,6-$^{i}Pr_2$-C_6H_3N=CR)$_2$$C_5H_3N$, R = Me, **1-($N_2$)$_2$**;[11] R = Ph, **2-($N_2$)$_2$**),[12] that function as efficient catalysts for the hydrogenation and hydrosilylation of olefins and alkynes at low metal loadings. Subsequently, **1-(N_2)$_2$** was also found to promote the catalytic [$2\pi + 2\pi$] cycloisomerization of α,ω-dienes to yield substituted cyclobutanes.[13] Spectroscopic and computational studies on **1-(N_2)$_2$**[14] and on related neutral ligand

derivatives,[15] such as those described in Chapter 3, have unequivocally established the redox-activity of the bis(imino)pyridine chelate.[16] Thus, **1-$(N_2)_2$** is best described as an intermediate spin, d^6 ferrous center antiferromagnetically coupled to a bis(imino)pyridine diradical dianion.[14]

During the course of our investigations into the substrate scope of catalytic olefin hydrogenation with **1-$(N_2)_2$** (Chapter 3), dramatic substituent effects were observed (Figure 4.1). Diallyl ether was readily hydrogenated to dipropyl ether in the presence of **1-$(N_2)_2$** and 4 atmospheres of dihydrogen. Performing the reaction under a dinitrogen atmosphere, in an attempt to induce $[2\pi + 2\pi]$ cycloaddition, produced no turnover. Likewise, *trans*-methyl cinnamate and dimethyl itaconate were both readily hydrogenated to the corresponding acetoxy-substituted alkane with **1-$(N_2)_2$** and 4 atmospheres of H_2, while allyl and vinyl acetate exhibited no turnover under the same conditions (Figure 4.1).

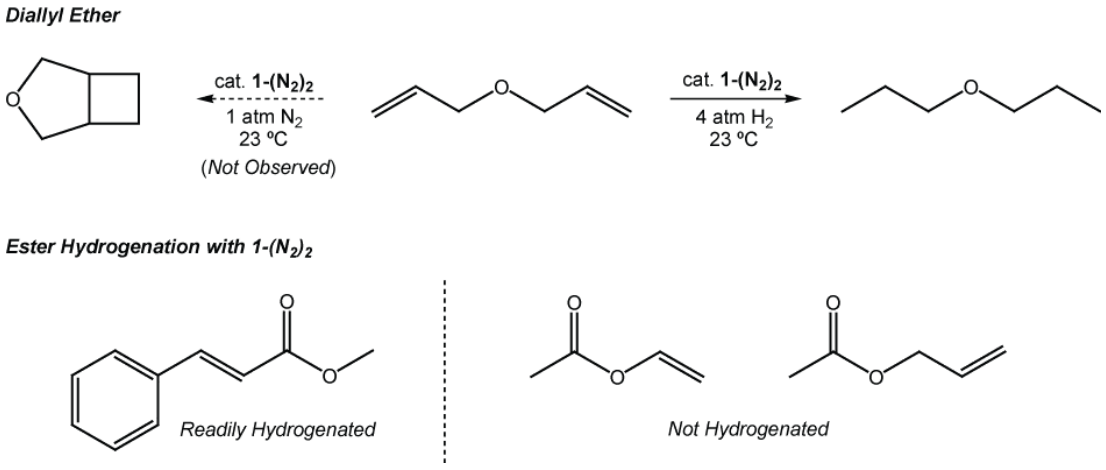

Figure 4.1. Substrate dependent catalytic activity of **1-$(N_2)_2$**.

Here we describe a systematic investigation into the interaction of various ethers, esters, and carboxylated alkenes with **1-$(N_2)_2$**. In addition to identifying important deactivation pathways in catalytic olefin hydrogenation and $[2\pi + 2\pi]$

cycloisomerization processes, these studies provide fundamental insight into oxidative addition chemistry at a reducing iron center bearing a redox active ligand.[17] The complexes presented in Chapter 1, the observation of two one electron bis(imino)pyridine chelate oxidations upon alkyl halide addition to **1-$(N_2)_2$** (Chapter 2), and the previously reported electronic structure determination of related complexes[14] all provide a solid foundation in which to study C-O bond oxidative addition to **1-$(N_2)_2$**.

4.3 Ether Bond Cleavage

The divergent reactivity of diallyl ether observed for catalytic hydrogenation (facile turnover) and [2_{π}+ 2_{π}] cycloisomerization (no turnover) with **1-$(N_2)_2$** prompted further investigation into the substrate-iron interaction. Treatment of a pentane solution of **1-$(N_2)_2$** with 0.5 equivalents of diallyl ether at 23 ºC furnished two iron products, the bis(imino)pyridine iron allyloxide and the iron allyl, **1-$OCH_2CH{=}CH_2$** and **1-Allyl**, respectively (Figure 4.2). As mentioned in Chapter 1, **1-Allyl** was independently synthesized by allylation of **1-Br** with one equivalent of allylmagnesium bromide.

The observation of facile diallyl ether C-O bond cleavage by **1-$(N_2)_2$** under mild conditions prompted additional studies into the scope of the transformation. Addition of 0.5 equivalents of allyl ethyl ether to a pentane solution of **1-$(N_2)_2$** at 23 ºC yielded **1-Allyl** and the bis(imino)pyridine iron ethoxide compound, **1-OEt** (Figure 4.2). These two products were formed exclusively, demonstrating selective and quantitative cleavage of the allylic C-O bond. Independent preparation of the iron allyloxide (Chapter 1) and ethoxide complexes, **1-OAllyl** and **1-OEt**, was accomplished by addition of one equivalent of anhydrous allyl alcohol or ethanol to **1-$(N_2)_2$**, respectively. Based on the data presented in Chapter 1, the electronic structure

of these bis(imino)pyridine iron alkoxide complexes is best described as a high spin ferrous center, antiferromagnetically coupled to a monoreduced chelate. Because alcohol addition to **1-$(N_2)_2$** often resulted in liberation of the bis(imino)pyridine ligand along with the formation of unidentified paramagnetic products (detected by ^{2}H NMR spectroscopy from ethanol-*d* addition), a more reliable route to these complexes was desired, *vide infra*.

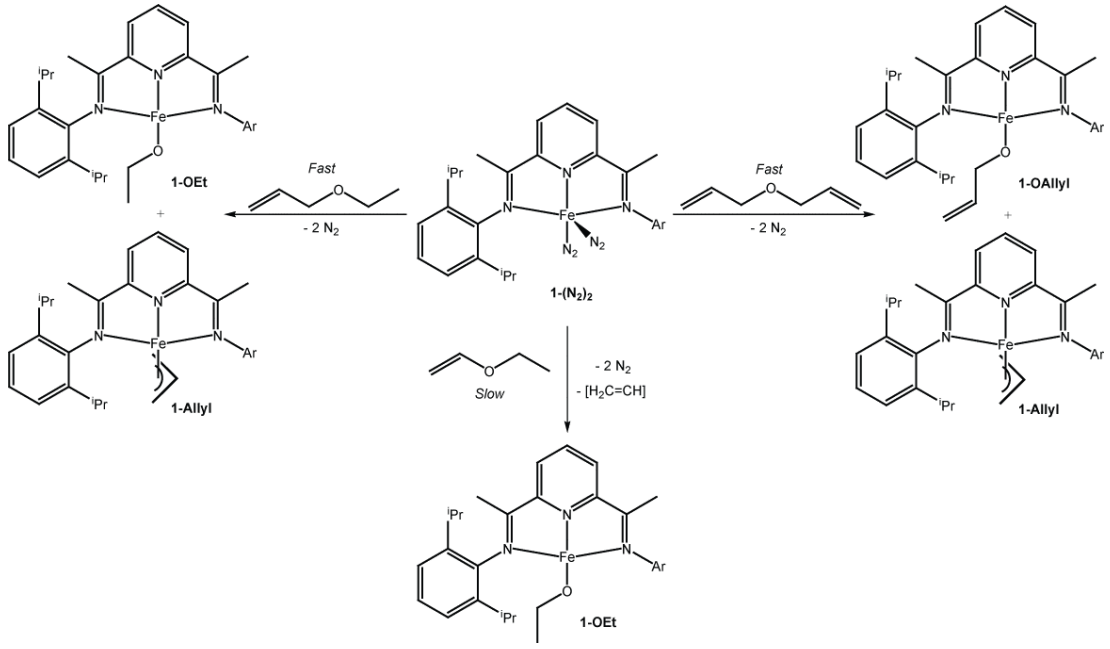

Figure 4.2. Scope of ether C-O bond cleavage with **1-$(N_2)_2$**.

Selective C-O bond cleavage was also observed with ethyl vinyl ether. Stirring a pentane solution of **1-$(N_2)_2$** with one equivalent of ethyl vinyl ether for 24 hours yielded **1-OEt** as the sole, ^{1}H NMR observable iron product (Figure 4.2). To explore whether the putative bis(imino)pyridine iron vinyl complex, **1-Vinyl**, is sufficiently stable to observe by ^{1}H NMR spectroscopy, an independent synthesis was pursued. Because oxidative addition of alkyl bromides to **1-$(N_2)_2$** proved to be a convenient route to four-coordinate bis(imino)pyridine iron alkyls (Chapter 2), this approach was extended to vinyl bromide in an attempt to form the vinyl complex. Addition of 0.5

equivalents of vinyl bromide to **1-$(N_2)_2$** yielded a mixture of the bis(imino)pyridine iron monobromide, **1-Br**, and the desired iron vinyl complex, **1-Vinyl** (Figure 4.3). Unfortunately, **1-Vinyl** was formed in low (~30 %) yield as determined by ^{1}H NMR spectroscopy and attempts to synthesize the compound by salt metathesis of **1-Br** with vinylmagnesium bromide were unsuccessful. Under an inert atmosphere in benzene-d_6 at 23 ºC, **1-Vinyl** persists for over 48 hours after which time ethane, **1-$(N_2)_n$** (n = 1,2), and **1-DH** had formed (Chapter 2). The ^{1}H NMR resonances and half-life established from the independent synthesis of **1-Vinyl** clearly demonstrate that the iron vinyl complex is not a product of ethyl vinyl ether cleavage. Additionally, **1-Isobutenyl** was prepared from the addition of 0.5 equivalents of 1-bromo-2-methylpropene to **1-$(N_2)_2$** and decomposition over the course of 2 days yielded the coupled product diisocrotyl.

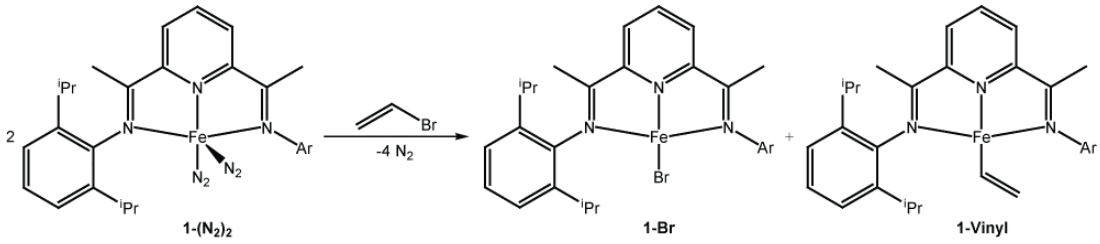

Figure 4.3. Vinyl bromide addition to **1-$(N_2)_2$**.

To probe whether a ^{1}H NMR-silent iron compound accompanied formation of **1-OEt** and accounted for the missing vinyl fragment, **1-$(N_2)_2$** was treated with 0.5 equivalents of ethyl vinyl ether. Monitoring this experiment by ^{1}H NMR spectroscopy established approximately 50% conversion to **1-OEt** with the balance of the iron remaining as **1-$(N_2)_2$**. While accurate quantitation of the relative amounts of paramagnetic versus diamagnetic iron compounds is complicated by the different hydrogen atom relaxation rates, this experiment demonstrated that no other iron compounds accompany **1-OEt** formation from ethyl vinyl ether cleavage. Because no

other organic products (ethane, acetylene, etc.) were observed, the fate of the vinyl fragment remains unknown.

Given the facility with which unsaturated ethers undergo C-O bond cleavage with **1-$(N_2)_2$**, similar chemistry was explored with saturated compounds. No evidence for C-O bond cleavage was obtained upon heating **1-$(N_2)_2$** in the presence of a large excess of diethyl ether or tetrahydrofuran. For the THF experiments, the diamagnetic coordination complex, **1-$(THF)_n$** (n = 1, 2) was observed by ^{1}H NMR spectroscopy in analogy to the previously reported compound with the phenylated backbone.[12]

Addition of excess anisole to a benzene-d_6 solution of **1-$(N_2)_2$** produced no change at 23 ºC. Heating this solution in a sealed tube to 110 ºC for three hours resulted in clean conversion to a new diamagnetic, C_s symmetric iron compound with upfield shifted arene resonances centered at 4.14 (*para*) and 5.46 (*meta*) ppm. These peaks are diagnostic for an η^6-coordinated aryl group (Figure 4.4).[12] The product has therefore been assigned as **1-Aryl**, similar to the structurally characterized compound reported for the bis(imino)pyridine iron complex with a phenyl-substituted backbone.[12] In a control experiment, a benzene-d_6 solution of **1-$(N_2)_2$** was heated to 110 ºC and yielded **1-Aryl**, demonstrating that the anisole plays little, if any, role in arene coordination.

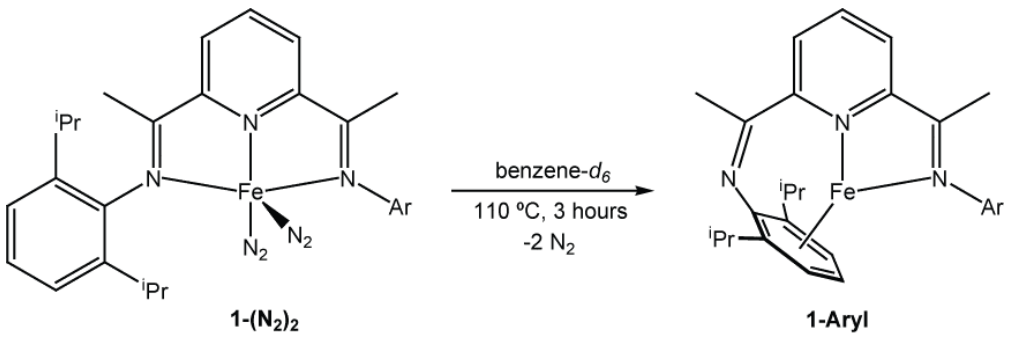

1-$(N_2)_2$ **1-Aryl**

Figure 4.4. Theromolytic preparation of **1-Aryl** from **1-$(N_2)_2$**.

4.4 Cleavage of Ester C-O Bonds

While exploring the scope of ester hydrogenation, certain peculiarities were observed. Substrates such as *trans*-methyl cinnamate and dimethylitaconate were readily hydrogenated under 4 atmospheres of H_2 in the presence of **1-$(N_2)_2$** while other compounds such as vinyl and allyl acetate produced no turnover under the same conditions. For the successful catalytic hydrogenations, relatively high catalyst loadings of 5 mol % were required. In contrast, pure hydrocarbon substrates such as cyclohexene or 1-hexene have been reduced with superior turnover frequencies using only 0.3 mol % of **1-$(N_2)_2$**,[11] suggesting a potential catalyst deactivation pathway with the functionalized substrates.

The possibility of **1-$(N_2)_2$** deactivation by C-O bond cleavage prompted a series of additional experiments whereby the fate of the iron compound was directly studied by ^{1}H NMR spectroscopy. Performing the hydrogenation of *trans*-methyl cinnamate with 10 mol % of **1-$(N_2)_2$** under 4 atmospheres of H_2 in benzene-d_6 established formation of two new paramagnetic iron compounds during the course of catalytic turnover. Both compounds gradually accumulated over time and were the exclusive iron products after hours of hydrogenation. These compounds were identified as the bis(imino)pyridine iron cinnamate and hydrocinnamate compounds, **1-CIN** and **1-H_2CIN**, respectively, arising from ester C-O bond cleavage (Figure 4.5). The hydrogenated carboxylate, **1-H_2CIN**, had been previously prepared from addition of hydrocinnamic acid to **1-$(N_2)_2$** for the electronic structure investigation of bis(imino)pyridine iron acetate complexes (Chapter 1). The formation of **1-CIN** was additionally confirmed by ^{1}H NMR spectroscopy upon stoichiometric addition of *trans*-cinnamic acid to **1-$(N_2)_2$**. Isolating each compound and subjecting it to catalytic hydrogenation conditions produced no turnover, demonstrating that C-O bond cleavage is a competing catalyst deactivation pathway. The hydrogenated compound,

1-H_2CIN derives from C-O bond scission of the reduced product formed during catalytic turnover, as attempts to hydrogenate **1-CIN to 1-H_2CIN** in the presence of **1-$(N_2)_2$** produced no conversion.

Observation of ester C-O bond cleavage under catalytic hydrogenation conditions prompted an additional series of stoichiometric experiments. Addition of 0.5 equivalents of *trans*-methyl cinnamate to a benzene-d_6 solution of **1-$(N_2)_2$** at 23 ºC under a dinitrogen atmosphere resulted in immediate cleavage of the ester C-O bond to yield an equimolar mixture of the bis(imino)pyridine iron cinnamate complex, **1-CIN**, and the iron methyl compound, **1-Me** (Figure 4.5). Exposure of this mixture of products and excess *trans*-methyl cinnamate to 4 atmospheres of H_2 resulted in complete consumption of **1-Me**, forming methane, **1-CIN**, and **1-H_2CIN** and accounts for the observations made during catalytic turnover.

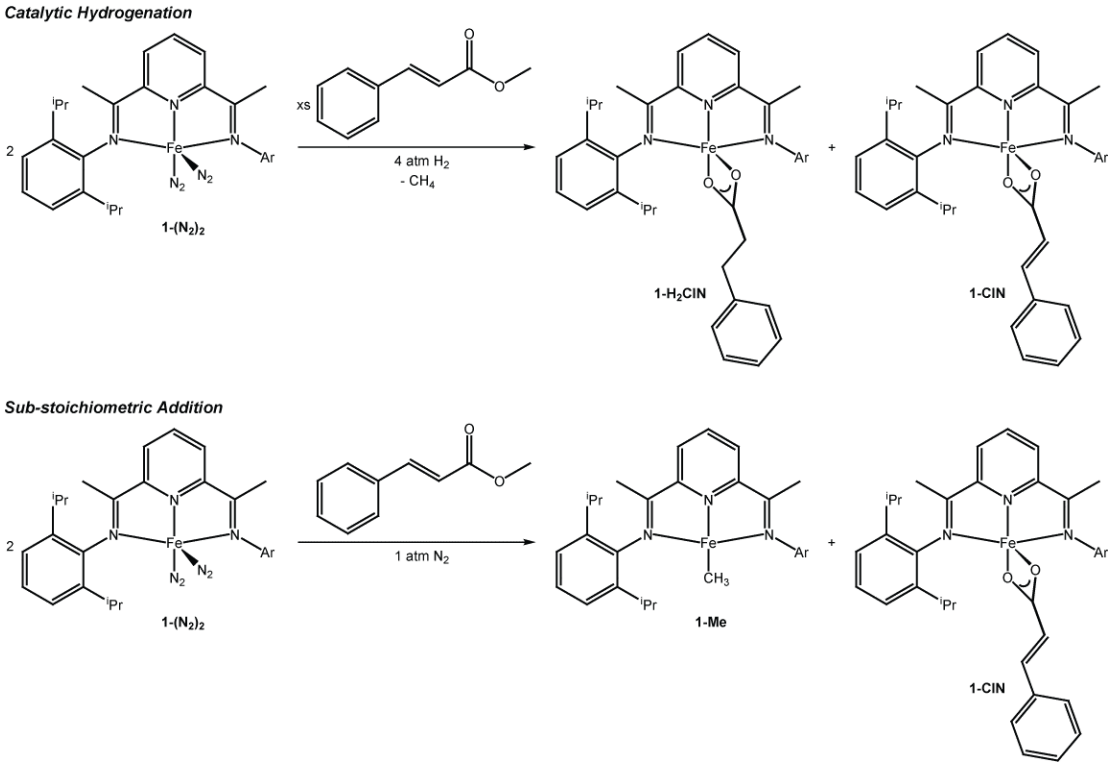

Figure 4.5. C-O bond cleavage of *trans*-methyl cinnamate with **1-$(N_2)_2$**.

The observation of H_2 pressure dependent C-O bond cleavage with *trans*-methyl cinnamate prompted a more detailed investigation into the reaction chemistry of vinyl and allyl acetate with **1-$(N_2)_2$**. Recall from Chapter 3 that these substrates were not hydrogenated using 5 – 10 mol % of **1-$(N_2)_2$** and 4 atmospheres of dihydrogen, suggesting rapid C-O bond cleavage (Figure 4.1). Addition of one equivalent of vinyl acetate or benzoate to a pentane solution of **1-$(N_2)_2$** furnished a bright purple solution of **1-(OAc)(Vinyl)** or **1-(OBz)(Vinyl)**, respectively (Figure 4.6).

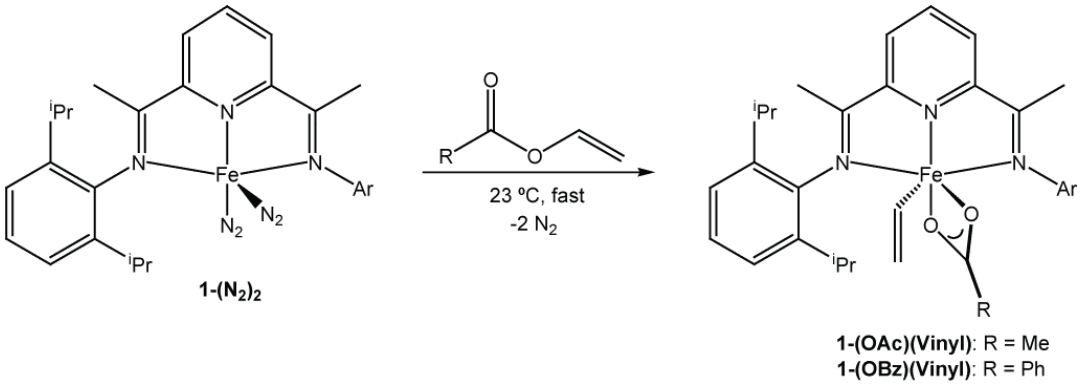

Figure 4.6. Synthesis of **1-(OAc)(Vinyl)** and **1-(OBz)(Vinyl)**.

1-(OAc)(Vinyl) is diamagnetic and was readily characterized by multinuclear (^{1}H and ^{13}C) and two-dimensional NMR spectroscopy. The benzene-d_6 ^{1}H NMR spectrum recorded at 23 ºC exhibits the number of peaks consistent with overall C_s molecular symmetry with a mirror plane equivalencing both sides of the bis(imino)pyridine chelate plane. The β-hydrogens on the vinyl ligand appear as two doublets centered at 4.66 and 1.87 ppm for the *cis* and *trans* (with respect to the iron) hydrogens on the terminal carbon, respectively. The methine hydrogen on the carbon directly attached to the metal appears downfield at 10.07 ppm with a $\{^1H\}^{13}C$ NMR resonance for this position observed at 189.91 ppm. These assignments have been confirmed by COSY, HSQC, and HMBC NMR spectroscopy.

The solid state structure of **1-(OAc)(Vinyl)** was also determined by X-ray diffraction (Figure 4.7) and represents a rare example of a neutral six coordinate bis(imino)pyridine iron compound.[17a] The N(1)-C(2) and N(3)-C(8) bond lengths (Table 4.1) of 1.3127(14) and 1.3103(15) Å are comparable to those observed for compounds with single electron reduction of the bis(imino)pyridine chelate.[16] Similarly, the C(2)-C(3) and C(7)-C(8) distances of 1.4402(16) and 1.4444(15) Å, respectively, are contracted compared to the values of 1.487(3) Å in free ^{iPr}PDI and also support one electron reduction of the bis(imino)pyridine chelate.[16] Two descriptions of the electronic structure accommodate the observed diamagnetic ground state. One possibility is a low spin, d^6 ferrous complex with a neutral bis(imino)pyridine chelate while the other is a low spin, d^5 ferric compound antiferromagnetically coupled to a ^{iPr}PDI radical anion. In the former case, the two electron oxidation occurs at the bis(imino)pyridine ligand, which is oxidized from $[PDI]^{2-}$ to neutral PDI. While the metrical data seems to favor the latter description, care must be taken in over interpreting crystallographic data as ligand field strength and other factors may also influence the bond lengths of the coordinated ^{iPr}PDI. A more definitive electronic structure description of this complex can be deduced from a Mössbauer spectroscopic investigation augmented with open-shell DFT calculations.

Addition of allyl acetate to **1-(N_2)$_2$** at 23 ºC also resulted in rapid cleavage of the ester C-O bond; but in this case, two products, **1-OAc** and **1-Allyl**, were observed (Figure 4.8, top). Free propene (5–10 %) was also observed when the reaction was conducted in a sealed NMR tube. The alkene likely arises from decomposition of **1-Allyl**, as more propene accumulated over the course of one week at 23 ºC.

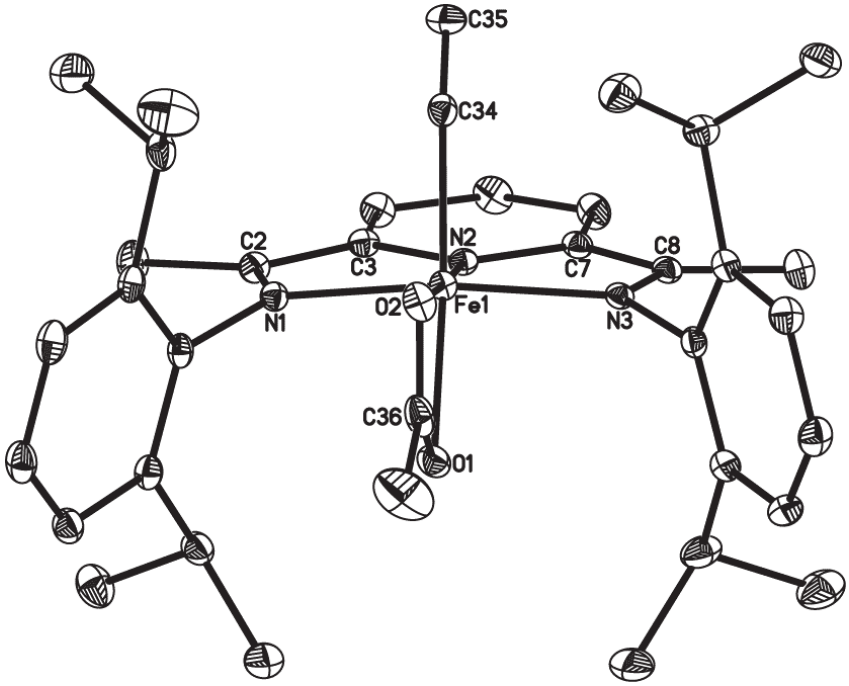

Figure 4.7. Solid-state structure of **1-(OAc)(Vinyl)**. Hydrogen atoms omitted for clarity.

Table 4.1. Selected bond distances (Å) and angles (°) for **1-(OAc)(Vinyl)**.

Fe(1)-N(1)	1.9540(9)	N(3)-C(8)	1.3013(15)
Fe(1)-N(2)	1.7976(9)	C(2)-C(3)	1.4402(16)
Fe(1)-N(3)	1.9504(9)	C(7)-C(8)	1.4444(15)
Fe(1)-O(1)	2.0771(9)	C(34)-C(35)	1.3231(19)
Fe(1)-O(2)	2.0135(8)	N(2)-Fe(1)-O(1)	119.28(4)
Fe(1)-C(34)	1.9942(14)	N(2)-Fe(1)-O(2)	176.81(5)
N(1)-C(2)	1.3127(14)	N(2)-Fe(1)-C(34)	87.31(5)

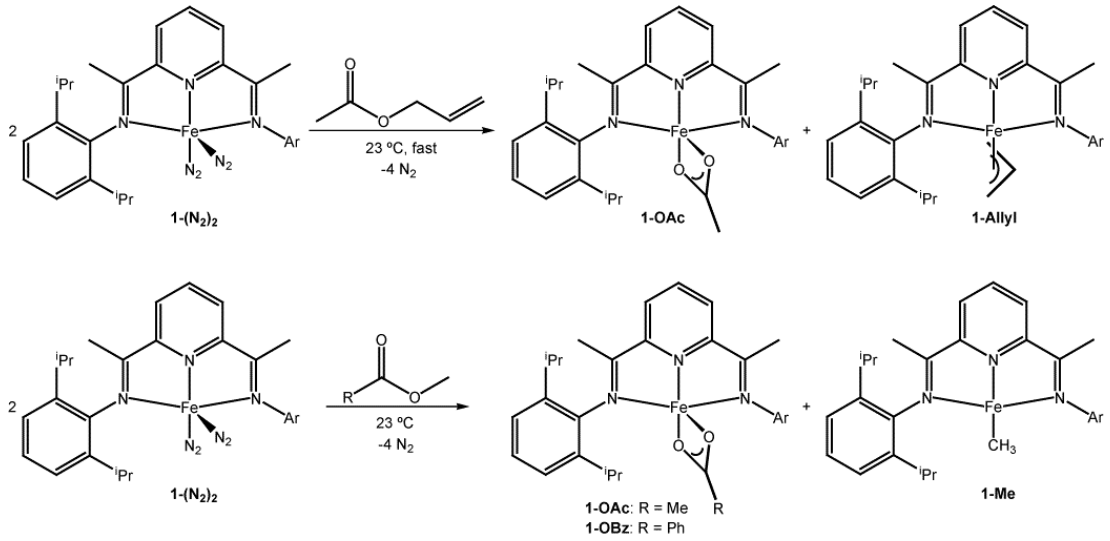

Figure 4.8. Formation of **1-OAc** by ester C-O bond cleavage.

In addition to the unsaturated esters, the possibility of C-O bond cleavage in saturated esters was fully explored. Expanding the scope of methyl ester C-O bond cleavage, addition of methyl acetate to **1-$(N_2)_2$** at 23 ºC resulted in formation of an equimolar ratio of **1-OAc** and **1-Me** over the course of 1 hour (Figure 4.8). As discussed in Chapter 3, careful monitoring of the reaction mixture by ^{1}H NMR spectroscopy revealed that the bis(imino)pyridine iron ester complex, **1-MeOAc**, was formed immediately after mixing. A similar methyl ester cleavage reaction was observed following addition of methyl benzoate to **1-$(N_2)_2$**, resulting in an equimolar mixture of **1-OBz** and **1-Me** (Figure 4.8). In this case, the putative ^{iPr}PDI iron methyl benzoate complex, **1-MeOBz**, was not observed by NMR spectroscopy.

In Chapter 1, the molecular structures of both **1-H_2CIN** and **1-OBz** were presented and examination of the bis(imino)pyridine bond distances suggested a one electron chelate reduction. One important inconsistency was discovered between the two crystal structures; the distances observed for **1-H_2CIN** appeared suggestive of localized chelate reduction (at one imine) while those for **1-OBz** did not. Because the

data set obtained for **1-H_2CIN** was of low quality due to co-crystallization with methyl-3-phenylpropionate, a third crystallographically characterized ^{iPr}PDI iron carboxylate complex was desired to reinforce the electronic structure description of these complexes. To address this concern, single crystals of **1-OAc** were obtained by recrystallization at -35 °C and the molecular structure was determined (Figure 4.9).

For **1-OAc**, the iron is five coordinate with a κ^2-carboxylate, where the O(1)-C(34)-O(2) and iron chelate planes are essentially orthogonal. The central carboxylate carbon, C(34), is nearly symmetrically disposed about the metal. The metrical parameters of the chelate (Table 4.2) confirm that the one electron bis(imino)pyridine reduction observed for these complexes is not localized. The Fe(1)-O(1) bond lengths of 2.0837(16) and 2.116(13) Å for **1-OAc** and **1-OBz** are significantly elongated from typical iron-alkoxide complexes (1.85 Å) and suggest a weaker ligand field imparted by the κ^2-carboxylate, consistent with the data presented in Chapter 1. Similar Fe(1)-O(2) distances of 2.1271(14) and 2.1003(13) Å were observed for **1-OAc** and **1-OBz**, respectively.

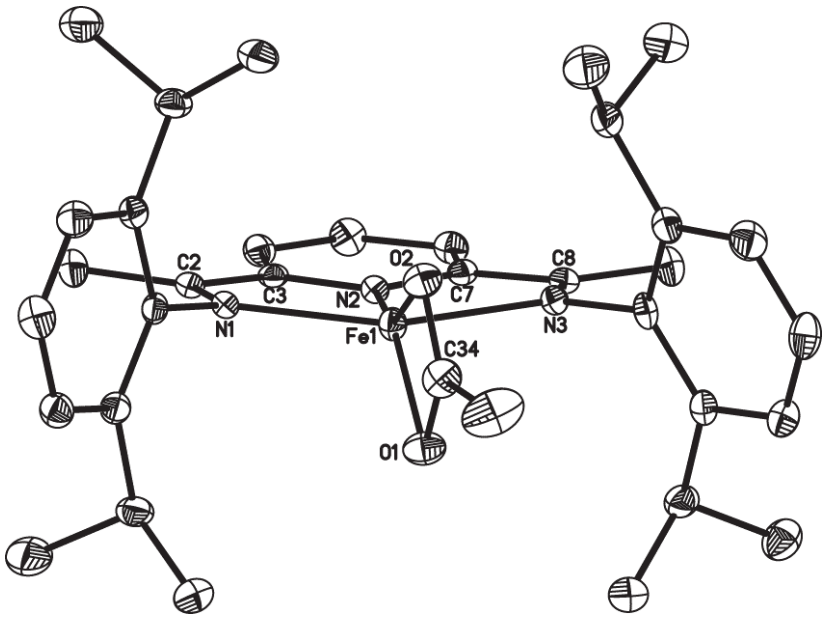

Figure 4.9. Solid-state structure of **1-(OAc)**. Hydrogen atoms omitted for clarity.

Table 4.2. Selected bond distances (Å) and angles (°) for **1-(OAc)**.

Fe(1)-N(1)	2.1085(15)	N(1)-C(2)	1.316(2)
Fe(1)-N(2)	1.9949(17)	N(3)-C(8)	1.302(3)
Fe(1)-N(3)	2.1615(15)	C(2)-C(3)	1.444(3)
Fe(1)-O(1)	2.0837(16)	C(7)-C(8)	1.461(3)
Fe(1)-O(2)	2.1271(14)	N(2)-Fe(1)-O(1)	143.80(6)
Fe(1)-C(34)	2.430(2)	N(2)-Fe(1)-O(2)	152.68(6)

Oxidative addition reactions to reduced iron complexes bearing electronically "non-innocent" bis(imino)pyridine chelates raises the possibility of having ligand rather than metal-based redox events. Related ligand-based oxidative chemistry has been reported by Heyduk and co-workers with group 4 transition metals.[18] In Chapter 2, the oxidative addition of alkyl bromides to **1-(N_2)$_2$** yielded two iron products (**1-Br** and **1-R**) where formal electron loss occurs at the bis(imino)pyridine chelate, maintaining the ferrous oxidation state. Several examples of C-O bond cleavage reported in this chapter follow this general reaction paradigm – oxidative addition to yield two iron complexes with formal oxidation of the ligand, not the metal (Figure 4.10).

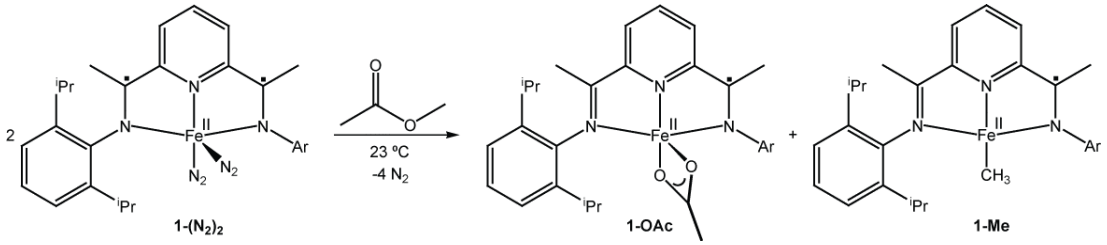

Figure 4.10. Oxidation of the bis(imino)pyridine chelate accompanying ester cleavage.

Although the electronic structure of **1-Allyl** has yet to be fully examined by Mössbauer spectroscopy and DFT calculations, it was concluded in Chapter 1 that the bis(imino)pyridine chelate of this complex is doubly reduced and antiferromagnetically coupled to a ferric metal center. This determination is of special interest when considering the oxidative addition of allyl acetate across two bis(imino)pyridine iron fragments. This substrate remains an interesting exception to the other one electron oxidation reactions because the oxidation of **1-$(N_2)_2$** to **1-OAc** occurs at the ligand, while the oxidation of the same complex to **1-Allyl**, occurs at the metal center (Figure 4.11).

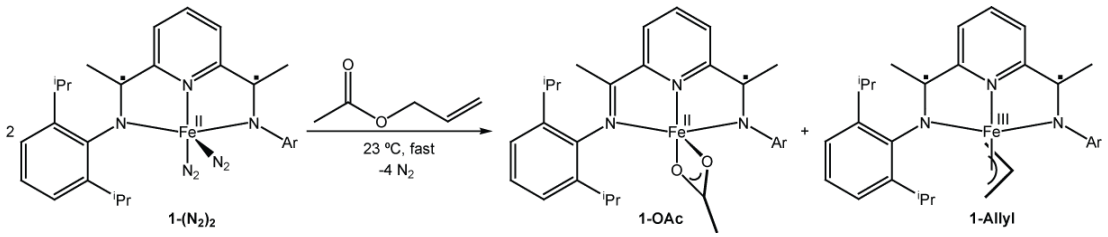

Figure 4.11. Oxidation of one ligand and one metal center upon allyl acetate cleavage with **1-$(N_2)_2$**.

The oxidative addition of vinyl acetate to **1-$(N_2)_2$** provides additional insight into the nature of the bond cleavage event at the reducing iron center. Observation of the six-coordinate **1-(OAc)(Vinyl**) compound demonstrates that oxidative addition can occur at a single iron center and is followed by Fe-C bond homolysis and radical capture to yield the observed products. Several observations support this assertion. Attempts to prepare five-coordinate bis(imino)pyridine iron bis(neopentyl) or neopentyl chloride complexes by ligand substitution reactions resulted in isolation of four-coordinate (^{iPr}PDI)Fe-X compounds, resulting from Fe-C bond homolysis.[19] Likewise, oxidative addition of 5-hexenyl-1-bromide to **1-$(N_2)_2$** yielded **1-Br** along with cyclized iron alkyl products (Chapter 2), consistent with ejection of the 5-hexyl

radical which is known to undergo rapid cyclization.[20,21] In addition, hydrogenation of the vinyl ligand of **1-(OAc)(Vinyl)** in the presence of palladium on carbon or excess **1-$(N_2)_2$** resulted in conversion to **1-OAc**, supporting radical ejection upon conversion to the saturated iron-ethyl intermediate.

Addition of phenyl acetate to **1-$(N_2)_2$** reversed the selectivity of the C-O bond cleavage reaction. Adding one equivalent to a benzene-d_6 solution of **1-$(N_2)_2$** exclusively yielded the products of *acyl* C-O bond cleavage; the iron phenoxide complex, **1-OPh**, and **1-Me** (Figure 4.12). Careful inspection of the diamagnetic region of the ^{1}H NMR spectrum also revealed formation of small quantities **1-$(CO)_2$** accounting for the fate of the carbonyl group.[22] Because acyl bond cleavage is relatively rare,[22] the scope and selectivity of bis(imino)pyridine iron C-O bond cleavage was examined in more detail. Gently heating benzene-d_6 solutions of **1-EtOAc** (Chapter 3) to 65 ºC for 18 hours yielded an equimolar mixture of **1-OAc** and **1-OEt** (Figure 4.13).

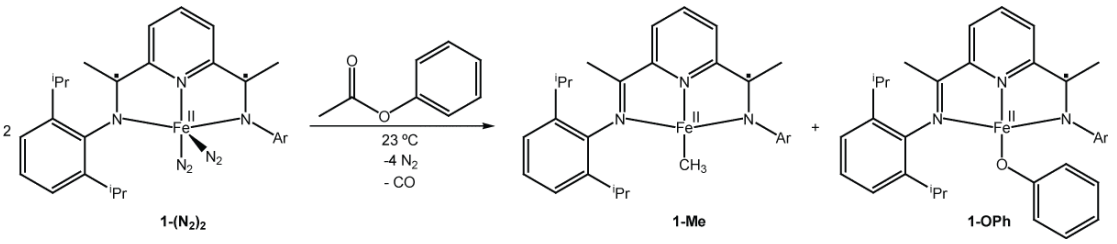

Figure 4.12. Acyl C-O bond cleavage of phenyl acetate at **1-$(N_2)_2$**.

The formation of the iron acetate and ethoxide compounds signals two competing C-O bond cleavage reactions. **1-OAc** is the product of ester C-O bond cleavage while **1-OEt** is the persistent product derived from acyl C-O bond cleavage. Ester C-O bond cleavage would, in principle, also form the bis(imino)pyridine iron ethyl complex, **1-Et**. However, under the more forcing conditions required for ethyl acetate cleavage (18 hours at 65 ºC), **1-Et** would not survive (Chapter 2). For acyl C-O

bond cleavage, the bis(imino)pyridine iron methyl complex, **1-Me**, is the other expected product. This compound was also not observed, and is also too unstable to persist under the conditions required for ethyl acetate cleavage. Control experiments on isolated samples of pure **1-Me** revealed decomposition to an unidentified mixture of products upon heating to 65 ºC. Thus, **1-OAc** and **1-OEt** were the only products thermally robust enough remain after ethyl acetate cleavage.

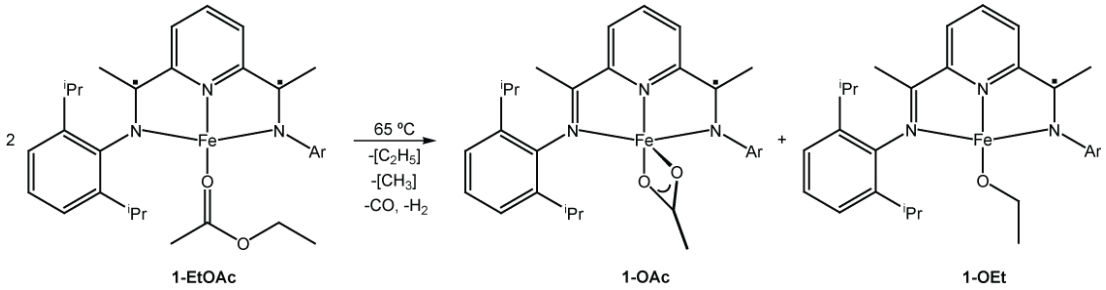

Figure 4.13. Cleavage of ethyl acetate at 65 °C.

In an attempt to observe the putative bis(imino)pyridine iron alkyl products from ethyl acetate cleavage, the reaction was repeated at 23 ºC. The expected products, **1-OAc** and **1-OEt**, were observed over the course of one week. No evidence for the formation of either **1-Me** or **1-Et** was obtained by ^{1}H NMR spectroscopy. The inability to observe **1-Et** is a result of the relative fast rate ($t_{1/2}$ ~ 3 hours) of decomposition of the iron alkyl compared to the slower rate ($t_{1/2}$ ~ 3 days) of the C-O bond cleavage reaction. Because the bis(imino)pyridine iron acyl complex, **1-C(O)Me**, is a likely product following the oxidative addition of the acyl C-O bond of ethyl acetate, attempts were made to evaluate the kinetic stability of such an intermediate. Addition of one atmosphere of carbon monoxide to a benzene-d_6 solution of **1-Me** resulted in immediate formation of **1-(CO)$_2$** along with acetone and methane (~ 5% yield of each). In a related experiment, addition of 0.5 equivalents of

acetyl chloride to a benzene-d_6 solution of **1-$(N_2)_2$** resulted in the formation of **1-Cl** and **1-Me**, consistent with decarbonylation from the putative PDI iron acyl complex.

As part of our studies into substrate scope and selectivity of C-O bond cleavage, the chemistry of ethyl benzoate was explored. Addition of one equivalent of this ester to **1-$(N_2)_2$** at 23 ºC resulted in rapid exclusive cleavage of the ester C-O bond over the course of two hours to furnish **1-Et** and **1-OBz** (Figure 4.14). No products derived from acyl C-O bond cleavage were detected by ^{1}H NMR spectroscopy. This result demonstrates that when ester C-O bond cleavage is sufficiently facile, the alkyl products can be observed by ^{1}H NMR spectroscopy. Thus, it is likely that **1-Et** is formed from ester C-O bond oxidative addition of ethyl acetate but has a rate of decomposition that is faster than the rate of substrate activation.

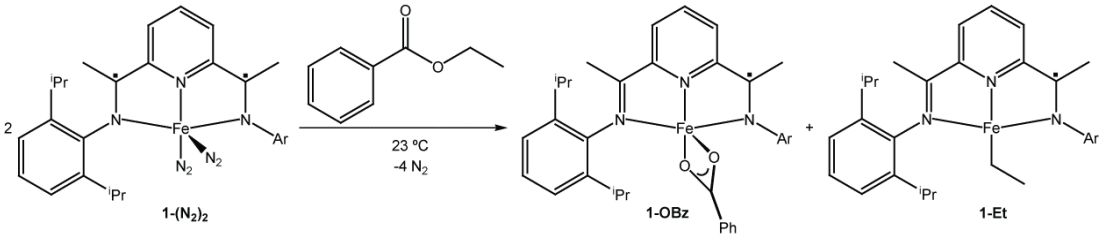

Figure 4.14. Cleavage of ethyl benzoate with **1-$(N_2)_2$** and observation of **1-Et**.

Having demonstrated rare examples of acyl C-O bond cleavage with phenyl and ethyl acetate at ambient temperature, **1-$(N_2)_2$** was treated with other alkyl acetates to assay selectivity. The results of these studies are summarized in Figure 4.15. Because the reactions were conducted at 65 ºC, the corresponding ^{iPr}PDI iron alkyl complexes were not observed. Thus, only the kinetically persistent iron acetate and iron alkoxide compounds were detected by ^{1}H NMR spectroscopy. The product ratios are approximate because they were determined from the integration of paramagnetically broadened and shifted isopropyl methyl resonances.

Observation of acyl C-O bond cleavage in esters suggested that similar chemistry may be possible with formates. Treatment of **1-$(N_2)_2$** with one equivalent of either ethyl or phenyl formate cleanly afforded the desired bis(imino)pyridine iron alkoxide compounds, **1-OEt** and **1-OPh**, respectively (Figure 4.16). As with acyl bond cleavage in esters, examination of the diamagnetic region of the ^{1}H NMR spectrum revealed formation of small quantities of **1-$(CO)_2$**, consistent with decarbonylation. This method represents a clean route to independently synthesize bis(imino)pyridine iron alkoxide complexes.

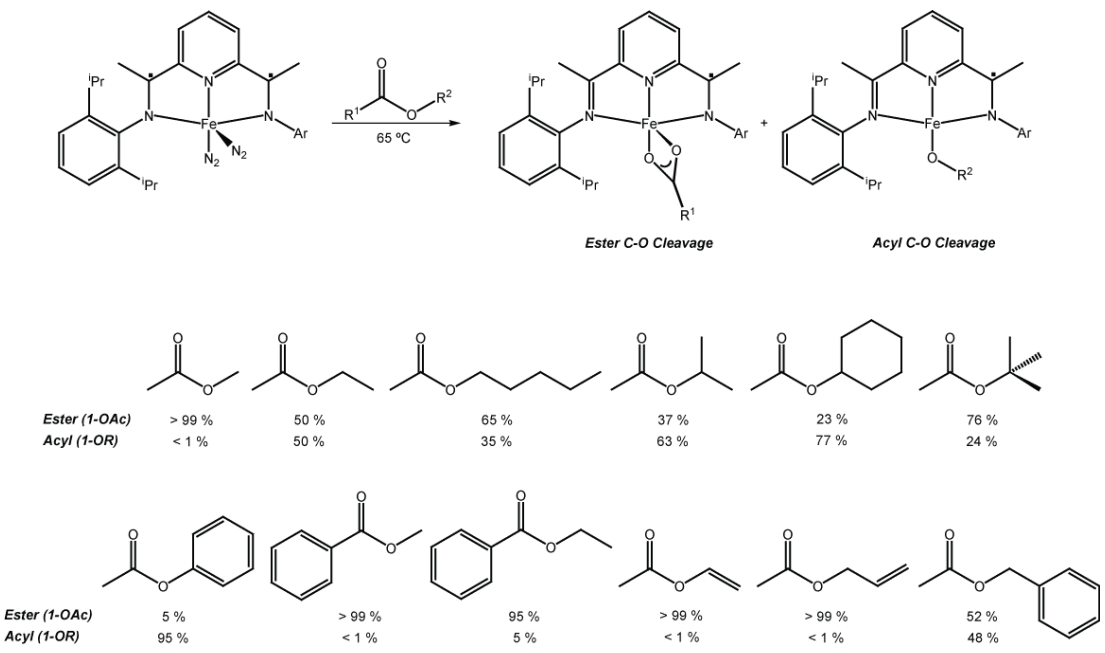

Figure 4.15. Scope of ester and acyl C-O bond cleavage with **1-$(N_2)_2$**.

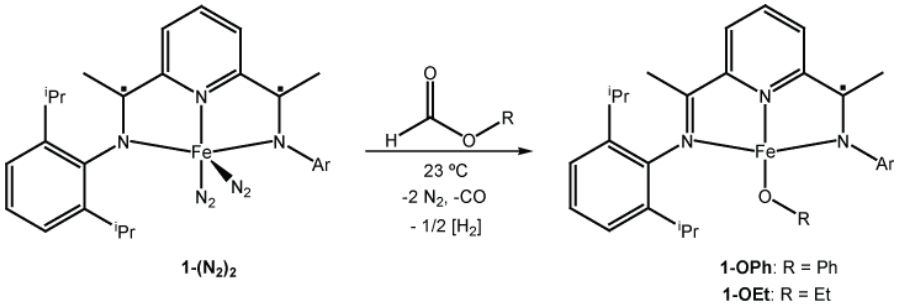

Figure 4.16. Utilization of formates for the preparation of ^{iPr}PDI iron alkoxide complexes.

4.5 Deuterium Labeling Experiments

A series of deuterium labeling experiments were conducted to probe whether C-H(D) activation was competitive with iron-promoted C-O bond cleavage in ester substrates. Addition of methyl acetate-d_6 to a benzene or benzene-d_6 solution of **1-$(N_2)_2$** at 23 ºC resulted in observation of **1-MeOAc-d_6**, as judged by ^{1}H and ^{2}H NMR spectroscopy, in analogy to **1-MeOAc**. Over time, **1-MeOAc-d_6** cleanly converted to an approximately equimolar mixture of **1-OAc-d_3** and **1-CD_3** (Figure 4.17). Because the methyl group of **1-CD_3** (or isotopologues) has not been detected by NMR spectroscopy, chemical degradation experiments were used to determine the isotopic composition of the iron methyl group. Hydrolysis of the product mixture and subsequent analysis of the bis(imino)pyridine ligand by ^{2}H NMR spectroscopy established no deuterium incorporation into the isopropyl methyl substituents. Collection of the liberated methane from protonolysis of the iron methyl complex and analysis by ^{1}H NMR spectroscopy clearly demonstrated that CD_3H was the sole isotopologue of methane formed. A converse experiment was also conducted where natural abundance methyl acetate was added to the deuterium labeled bis(imino)pyridine iron dinitrogen complex, **1*-$(N_2)_2$**, (* denotes deuterium labeling of the isopropyl methyl substituents).[11] In this case, **1*-OAc** and **1*-CH_3** were identified as the sole products. Again, the isotopic composition of the iron methyl group was

assayed by hydrolysis and CH_4 was the only methane isotopologue observed by ^1H NMR spectroscopy.

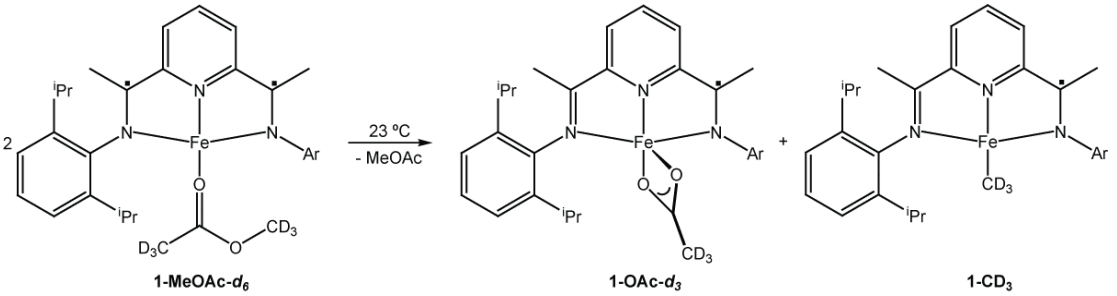

Figure 4.17. Formation of **1-OAc-*d*$_3$** and **1-CD$_3$** from cleavage of methyl acetate-d_6.

Analogous experiments were conducted with isotopologues of ethyl acetate; preparation of 1,2-ethyl acetate-d_2 was accomplished by D_2 addition to vinyl acetate in the presence of a catalytic amount of palladium on carbon. Addition of the isotopically labeled ester to **1-(N$_2$)$_2$** immediately furnished the diamagnetic bis(imino)pyridine iron ethyl acetate complex, **1-EtOAc-*d*$_2$**. As anticipated, the benzene solution ^2H NMR spectrum exhibited two peaks centered at 0.74 and 3.02 ppm for the coordinated ester. Allowing the solution to stand at 23 ºC for 20 minutes revealed isotopic exchange between the isopropyl methyl group of the bis(imino)pyridine chelate and the methylene position of the ester (Figure 4.18). No evidence was obtained for isotopic exchange involving the methyl group of the ester. Warming the solution to 70 ºC for 14 hours yielded the bis(imino)pyridine iron acetate and ethoxide compounds (Figure 4.18). Analysis of the product mixture by ^2H NMR spectroscopy revealed deuterium incorporation in the isopropyl methyl groups of the bis(imino)pyridine ligands in both **1*-OEt** and **1*-OAc** and in the methyl group of the iron ethoxide.

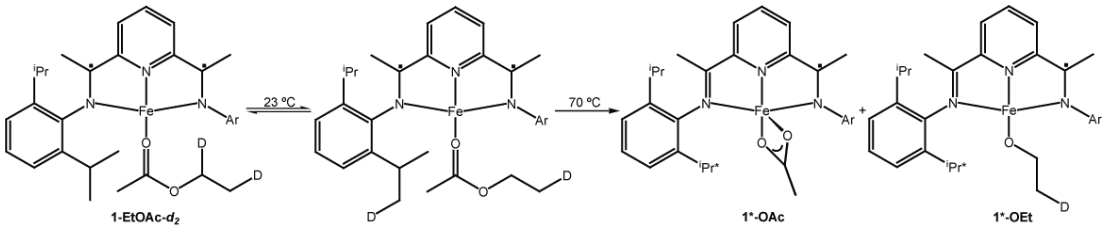

Figure 4.18. Deuterium exchange at the methylene position of ethyl acetate.

The converse experiment was conducted, whereby the deuterium labeled iron dinitrogen compound, **1*-$(N_2)_2$**, was treated with a slight excess of natural abundance ethyl acetate (Figure 4.19, top). Over the course of four hours at 23 ºC, deuterium exchange was observed with the methylene position of both the free and coordinated ester. No evidence was obtained for isotopic exchange into the terminal methyl group. Warming the solution to 65 ºC resulted in C-O bond cleavage and yielded the expected iron acetate and ethoxide compounds, as observed by ^{2}H NMR spectroscopy. To establish the isotopic composition of the acetate and ethoxide ligands, each bis(imino)pyridine iron compound was treated with water and the organic products: bis(imino)pyridine, ethanol, and acetic acid were analyzed by ^{2}H NMR spectroscopy. While no deuterium was detected in the acetic acid, the free ethanol exhibited a peak consistent with isotopic incorporation exclusively in the methylene position.

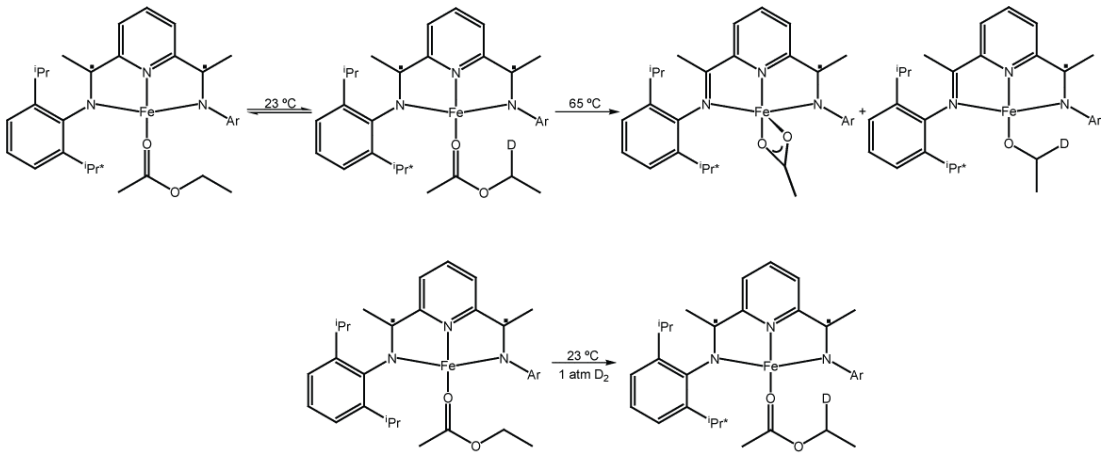

Figure 4.19. Deuterium labeling of ethyl acetate.

In a related experiment, a benzene-d_6 solution of **1-EtOAc** was exposed to four atmospheres of D_2 gas at 23 ºC. Over the course of four hours, isotopic exchange was observed in the isopropyl methyl group of the bis(imino)pyridine chelate of **1-EtOAc**, as well as in the methylene position of the ester (Figure 4.19). When the reaction is carried out with excess ethyl acetate, the deuteration of the methylene is catalytic, demonstrating rapid C-H activation and ligand exchange prior to C-O bond cleavage. The observation of reversible ester coordination is similar to the behavior observed with **1-$(N_2)_2$** with amines and ketones (Chapter 3).

4.6 Discussion

Carbon-oxygen bond oxidative addition reactions are of interest due to their potential application in hydrodeoxygenation (HDO) reactions[23] as well as various cross coupling methodologies used in organic synthesis.[24] Oxidative addition of allylic ethers, carboxylates, carbonates, and halides has enjoyed special utility in the synthesis of metal allyl complexes which can undergo subsequent nucleophilic attack[25,26] or cross-coupling.[27] C-O bond cleavage is well known for second and third row transition metals including palladium,[22,28] rhodium,[29] iridium,[30] ruthenium,[31] zirconium,[32] molybdenum[33] and tantalum.[34,35] For first row metal ions, C-O oxidative addition of both ethers[36,37] and esters[38,39] to Ni(0) has been well-studied and known for some time. Examples with nickel(II) precursors have been reported more recently.[40]

Examples of C-O bond cleavage with well-defined iron compounds are more limited. In a seminal example, Ganem and Small reported the application of ferric chloride to the cleavage of ethereal C-O bonds.[41] A more recent example, described by Plietker and coworkers, applies nitrosylated variants of Collman's reagent[42] for the transesterification of vinyl acetates, phenyl carboxylates and electron poor esters with various alcohols.[43] Iron acyl complexes that do not undergo decarbonylation are

proposed as key intermediates in the catalytic cycle. Direct oxidative addition of carbon-oxygen bonds to electron rich iron(0) compounds has also been reported by Ittel and coworkers. Addition of anisole or methyl benzoate to a transient bis(diphosphine)iron(0) yielded the products of C-O cleavage.[44,45] For methyl benzoate addition, exclusive scission of the ester, not acyl C-O bond, was observed.

Upon examination of the relative rates of **1-$(N_2)_2$** promoted C-O bond cleavage within classes of ethers and esters, several salient trends emerge. Within the family of ester substrates, benzoate esters generally undergo swifter cleavage than the corresponding acetates. Specifically, ethyl benzoate (exclusive ester cleavage) converted to cleavage products over the course of hours at 23 ºC while ethyl acetate (both acyl and ester cleavage) required nearly a week under the same conditions. This effect is likely electronic in origin as the electron withdrawing phenyl group renders the substrate more electrophilic and prone to oxidative cleavage.

Comparison of various substituted acetates also established several important trends. The unsaturated esters, vinyl and allyl acetate, undergo extremely rapid C-O bond cleavage; the reaction was so fast that catalytic hydrogenation was not observed in the presence of **1-$(N_2)_2$** and four atmospheres of dihydrogen. In contrast, C-O bond cleavage in *trans*-methyl cinnamate, while relatively facile under an N_2 atmosphere, was sufficiently slow such that catalytic olefin hydrogenation could be achieved with 5 mol % of **1-$(N_2)_2$** and four atmospheres of dihydrogen (Chapter 3). Eventually, all of the iron converted to catalytically inactive iron carboxylate compounds, establishing C-O bond activation as the principal catalyst deactivation pathway for this class of substrates.

Carbon-oxygen bond cleavage in various allylated substrates also demonstrates the importance of leaving group effects. For diallyl and allyl ethyl ether, the rate of C-O bond cleavage is sufficiently slow such that iron-catalyzed olefin hydrogenation is

observed. As mentioned previously, allyl acetate has not been hydrogenated using our experimental conditions due to the extremely fast rate of C-O bond oxidative addition. This trend is similar to those observed in nickel(0) and palladium(0) chemistry, where allyl acetates undergo more facile oxidative addition than the corresponding allylated ethers.[29,38,39]

It is noteworthy that **1-$(N_2)_2$** promotes *acyl* C-O bond cleavage in alkyl esters. Electron rich Ni(0) compounds[38] promote selective acyl C-O bond cleavage in phenyl acetate but are unreactive toward alkyl-substituted esters. Aryl acetate cleavage reactions are also known with $(dppe)_2Mo(N_2)_2$ (dppe = 1,2-diphenylphosphinoethane),[46] $(Ph_3P)_3RhH$,[47] (η^5-C_5Me_5)RhCl(mdmpp-κP, -κO),[48] $(Ph_3P)_3Ru(CO)_2$,[49] and $Ru_3(CO)_{12}$.[50] In one case, an acyl rhodium complex was isolated following C-O oxidative addition.[51] Using pyridine directing groups, a $Ru_3(CO)_{12}$-catalyzed reductive decarbonylation method has also been developed and has been extended to alkyl-substituted substrates.[52]

Acyl C-O bond cleavage in alkyl esters lacking a directing group, to our knowledge, has not been reported. Thus, the facile C-O bond cleavage of alkyl acetates with **1-$(N_2)_2$** at 65 ºC highlights the reducing potential of a formally iron(II) center with electrons stored in the bis(imino)pyridine chelate. For the alkyl acetates presented in Figure 4.15, a modest trend in selectivity emerges. The smallest member in the series, methyl acetate, undergoes rapid and selective ester C-O bond cleavage, likely due to the steric accessibility of the ester C-O bond. Lengthening the alkyl chain resulted in slower rates as ethyl, pentyl, isopropyl, cyclohexyl, and *tert*-butyl acetate all require heating to 65 ºC or extended reaction times at 23 ºC to reach full conversion. With the exception of *tert*-butyl acetate, the selectivity of acyl bond cleavage increases as the steric protection of the ester C-O bond increases. Thus, for alkyl-substituted acetates, it appears that in the absence of overriding steric effects,

ester C-O bond cleavage is preferred over acyl. The reason for the reversal of kinetic selectivity in the C-O bond cleavage of *tert*-butyl acetate is not known.

Proposed mechanisms for ether, ester, and acyl C-O bond cleavage are presented in Figures 4.20 (ethers) and 4.21 (ester, acyl) and are inspired by those previously reported by Yamamoto for electron rich Ni(0) compounds.[22,36,38,39] Because ether cleavage was only observed with allyl and vinyl-substituted ethers, initial coordination of the alkene of the substrate is proposed.[39] For diallyl and allyl ethyl ethers, S_N2'-type substitution is also plausible and may be preferred. Oxidative addition of the C-O bond yields a five-coordinate iron allyl alkoxide intermediate, in analogy to the structurally characterized, six-coordinate iron vinyl acetate complex, **1-(OAc)(Vinyl)**. Ejection of allyl radical and capture by a reduced iron species, either **1-$(N_2)_2$** or the iron olefin compound, yields the observed products. To have a reduced iron compound available for allyl radical capture, C-O bond cleavage must be the rate-determining step. Circumstantial experimental data support this assertion. Addition of one equivalent of diallyl ether to **1-$(N_2)_2$** yielded an equimolar mixture of **1-Allyl** and **1-$OCH_2CH{=}CH_2$** with unreacted substrate remaining. This suggests that the products do not participate in radical capture. For the case of ethyl vinyl ether cleavage, the olefin compound was observed by ^{1}H NMR spectroscopy immediately after mixing the reagents; C-O bond cleavage occurred over the course of 24 hours at 23 ºC. In general, when the C-O bond cleavage reactions are fast, all of the products of radical capture are observed. When these reactions are slow, as in the case of ethyl vinyl ether, the fate of the ejected organic radical is unknown.

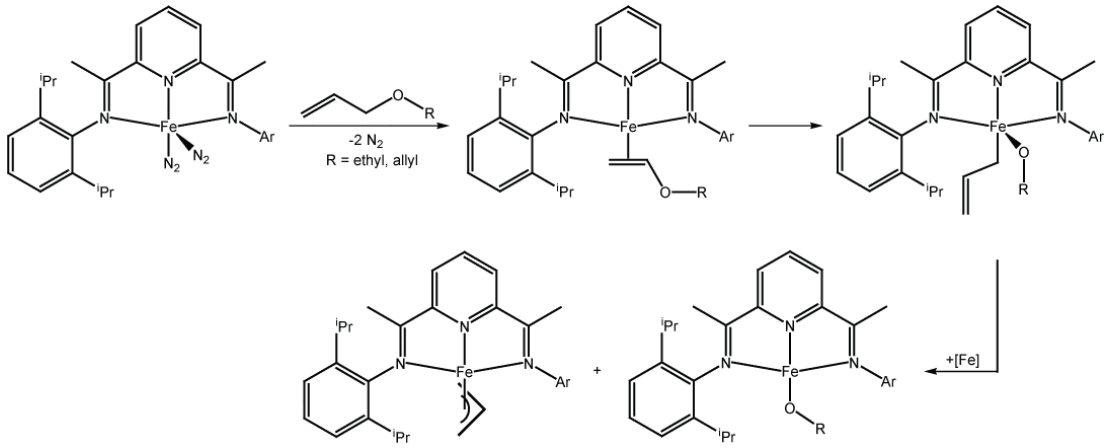

Figure 4.20. Mechanism of ether cleavage with **1-$(N_2)_2$**.

Similar pathways are proposed in Figure 4.21 for ester and acyl C-O bond cleavage. Ethyl acetate is presented as a representative substrate because both ester and acyl scissions were observed. For ester C-O bond cleavage, oxidative addition to yield the six-coordinate iron ethyl acetate complex followed by iron-carbon bond homolysis yields the observed **1-OAc** product. The six-coordinate iron intermediate is proposed based on analogy to isolated **1-(OAc)(Vinyl)**. Ejection of ethyl radical from this compound seems plausible given the previous studies from our laboratory that have demonstrated the propensity of five-coordinate bis(imino)pyridine iron dialkyls to undergo Fe-C homolysis (Chapter 1).[19] For acyl C-O bond cleavage, oxidative addition of the C-O bond forms a five-coordinate intermediate in analogy to **1-(OAc)(Vinyl)**. Decarbonylation followed by Fe-CH_3 homolysis yields the observed product. Observation of **1-Me** and **1-Cl** following treatment of **1-$(N_2)_2$** with $CH_3C(O)Cl$ provides precedent of decarbonylation for bis(imino)pyrdine iron compounds.

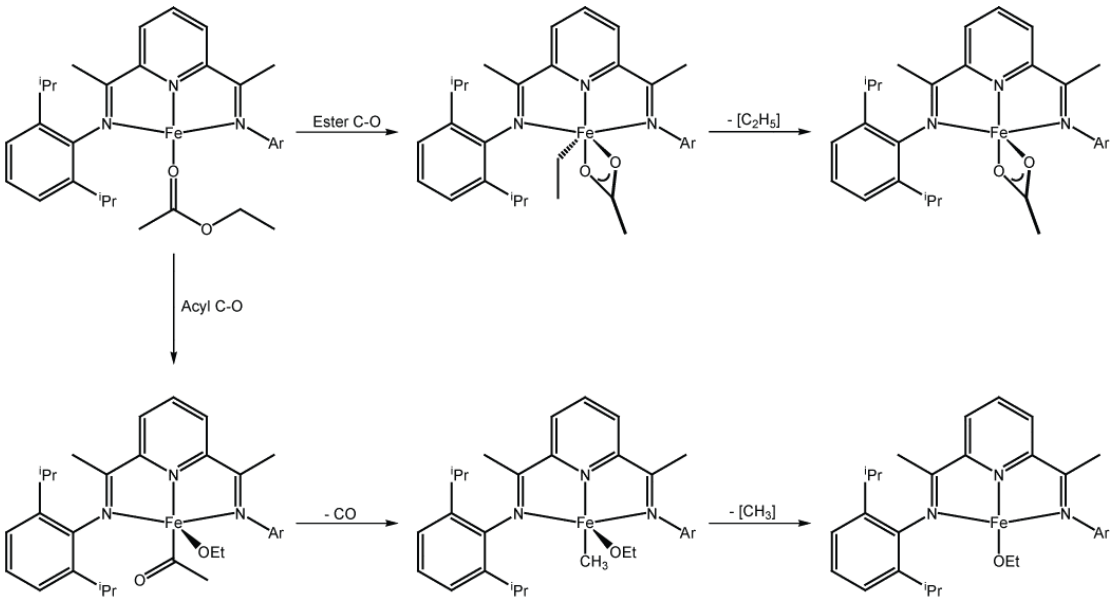

Figure 4.21. Proposed mechanism of ester C-O bond cleavage mediated by **1-$(N_2)_2$**.

Deuterium labeling studies with ethyl acetate also established a competing C-H activation pathway. A proposed mechanism for this transformation, not required for C-O bond cleavage, is presented in Figure 4.22. Recall this reaction is selective - isotopic exchange occurs only between the aryl isopropyl methyl groups on the bis(imino)pyridine chelate and the methylene position of the substrate. The process begins with reversible dissociation-coordination of ethyl acetate to facilitate C-H activation of either the methylene position of the ester or cyclometalation of an isopropyl methyl group of the bis(imino)pyridine chelate. Following formation of the alkyl deuteride, isotopic exchange can occur through cyclometalation, likely by σ-bond metathesis, with either the iron-hydride (deuteride) or alkyl. If the reaction occurs with the iron hydride (deuteride), loss of H-D occurs. Subsequent productive recapture places deuterium in the isopropyl group and hydrogen in the ester completing the isotopic exchange. An alternative σ-bond metathesis pathway involves reaction of the isopropyl methyl group with the iron alkyl, liberating free ethyl acetate,

which following reductive elimination of the iron cyclometalated deuteride and recapture, completes the isotopic exchange. Pathways involving formal oxidative addition and formation of iron(IV) intermediates are also possible but have been deemed less plausible.

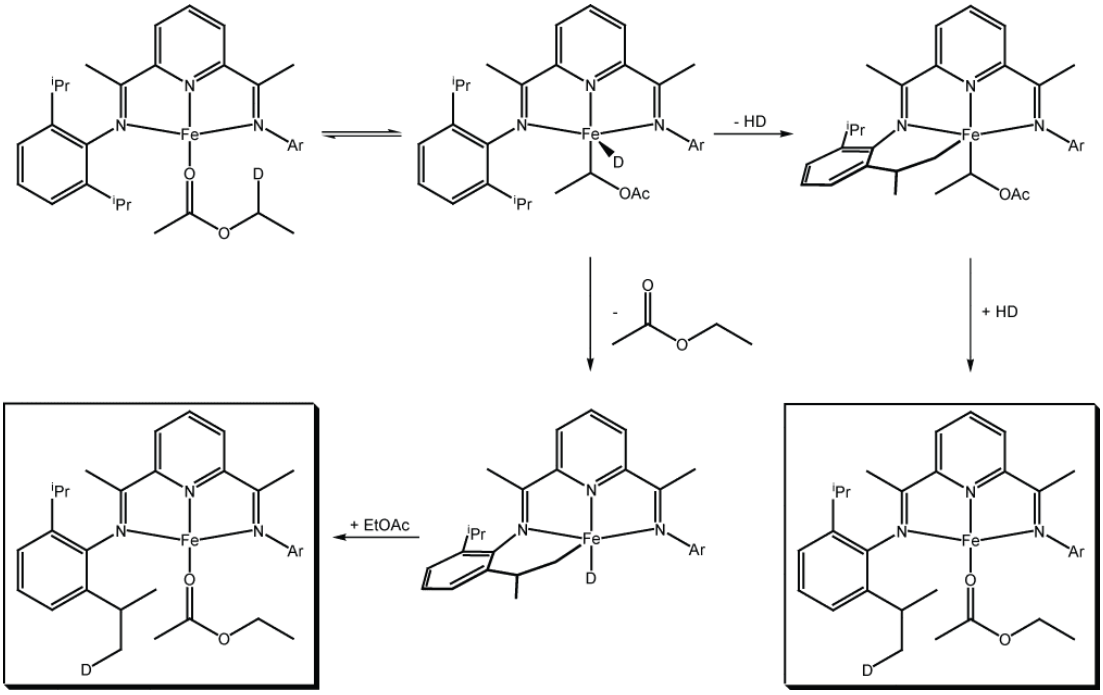

Figure 4.22. Proposed mechanism of deuterium exchange observed for **1-EtOAc**.

The selective isotopic exchange between the methylene position of the ester and the isopropyl methyl groups of the bis(imino)pyridine chelate raises the question as to why this process was not observed with the corresponding iron methyl acetate complex? The lack of a competing C-H activation process for the methyl acetate derivative is accommodated by the relative rates of C-O bond cleavage for the two substrates. Whereas C-O bond cleavage in ethyl acetate occurs over one hour at 65 ºC, methyl acetate cleavage occurs within minutes at 23 ºC. The lack of deuterium exchange with methyl acetate clearly demonstrates that C-H activation can be competitive with C-O cleavage, but is by no means a prerequisite.

4.7 Conclusion

Investigation into the substrate scope of catalytic olefin hydrogenation reactions promoted by the bis(imino)pyridine iron complex, **1-$(N_2)_2$**, established that oxidative addition of carbon-oxygen bonds of ethers and esters is a principal catalyst deactivation pathway. For substrates such as diallyl ether, vinyl ethyl ether, and *trans*-methyl cinnamate, catalytic hydrogenation is competitive with C-O cleavage and conversion to alkane was observed (Chapter 3). For molecules such as allyl and vinyl acetate, C-O cleavage is more rapid than hydrogenation (up to 4 atm of H_2) and no turnover was observed. Exploration of the scope of ester C-O bond cleavage established competing ester and acyl C-O bond cleavage reactions, depending on the specific substrate. Methyl acetate and *trans*-methyl cinnamate underwent exclusive ester C-O bond cleavage while phenyl acetate yielded products from selective acyl C-O bond scission. In alkyl-substituted esters such as ethyl, pentyl, isopropyl, benzyl, cyclohexyl, and *tert*-butyl acetate, competing ester and acyl C-O bond cleavage occurred. In both ethers and esters, oxidative addition of the C-O bond to the reduced bis(imino)pyridine iron complex has been proposed. In all but one case, vinyl acetate, homolysis of the iron-carbon bond from the product of oxidative addition yields the observed products. Further investigation of the electronic structure of several representative products establishes that formal electron loss is generally chelate rather than metal based. In one case, allyl acetate, a one electron chelate oxidation (**1-OAc**) occurs along with oxidation to Fe(III) at a second bis(imino)pyridine iron fragment (**1-Allyl**). Deuterium labeling studies with isotopologues of the iron dinitrogen complex and ethyl acetate establish competing cyclometalation from the 2,6-diisopropyl aryl substituents. Taken together, these studies once again highlight both the chemical and redox-activity of bis(imino)pyridine ligands in reduced iron chemistry.

4.8 Experimental Procedures

General Considerations. All air- and moisture-sensitive manipulations were carried out using standard vacuum line, Schlenk and cannula techniques or in an MBraun inert atmosphere dry box containing an atmosphere of purified nitrogen. Solvents for air- and moisture-sensitive manipulations were initially dried and deoxygenated using literature procedures.[53] Hydrogen and deuterium gas were passed through a column containing manganese oxide supported on vermiculite and 4 Å molecular sieves before admission to the high vacuum line. Benzene-d_6 and toluene-d_8 were purchased from Cambridge Isotope Laboratories and dried over 4 Å molecular sieves or titanocene, respectively. Ethyl acetate, vinyl acetate, allyl acetate, amyl acetate, isopropyl acetate, cyclohexyl acetate, *tert*-butyl acetate, phenyl acetate, methyl benzoate, ethyl formate, isopropyl formate, vinyl bromide, ethyl vinyl ether, allyl ether, and anisole were all purchased from Aldrich and dried over calcium hydride for at least 24 hours before being vacuum transferred onto 4 Å molecular sieves. Methyl acetate and allyl ethyl ether were purchased from Acros and purified in a similar manner. Phenyl formate was purchased from Lancaster and dried over calcium hydride before use.

trans-Methyl-cinnamate was purchased from Aldrich, recrystallized from dry pentane at –35 °C, and dried under vacuum. Hydrocinnamic acid, *trans*-cinnamic acid, and benzoic acid were purchased from Aldrich and dried under vacuum for 16 hours. Allyl alcohol, absolute ethyl alcohol, isopropanol, cyclohexanol, and *tert*-butyl alcohol were purchased from Aldrich and vacuum transferred from sodium before use. Allylmagnesium bromide as a 1.0 M solution in diethyl ether and 10 % palladium on activated carbon were purchased from Aldrich and used as received. Vinylmagnesium bromide as a 0.7 M solution in tetrahydrofuran was purchased from Acros and used as received.

Ethyl acetate-1,2-d_2 was prepared by deuteration of neat vinyl acetate with 10 % palladium on activated carbon under 4 atmospheres of D_2 and vacuum transferred before use. Methyl 3-phenylpropionate was prepared in a similar fashion from *trans*-methyl-cinnamate under 4 atmospheres of H_2. Methyl acetate-d_6 was prepared from D_2SO_4 catalyzed condensation of acetic acid-d_4 and methanol-d_4. The reaction mixture was extracted with *m*-xylene and the methyl acetate-d_6 was collected by short path distillation. Ethyl benzoate was prepared from acid catalyzed condensation of benzoic acid and ethyl alcohol.

^{1}H NMR spectra were recorded on Varian Mercury 300, Inova 400 and 500 spectrometers operating at 299.76, 399.78 and 500.62 MHz, respectively. ^{2}H NMR spectra were recorded at 20 ºC on Inova 500 and 600 spectrometers operating at 76.85 and 92.07 MHz, respectively. ^{13}C NMR spectra were recorded on the Inova 500 spectrometer operating at 125.893 MHz. All ^{1}H and ^{13}C NMR chemical shifts are reported relative to $SiMe_4$ using ^{1}H (residual) and ^{13}C chemical shifts of the solvent as a secondary standard. For diamagnetic complexes, many assignments were made based on COSY, HSQC, and HMBC NMR experiments. Solution magnetic moments were determined by Evans method[54] using a ferrocene standard and are the average value of at least two independent measurements. ^{1}H NMR multiplicity and coupling constants are reported where applicable. Peak width at half height is given for paramagnetically broadened resonances. Elemental analyses were performed at Robertson Microlit Laboratories, Inc., in Madison, NJ.

Single crystals suitable for X-ray diffraction were coated with polyisobutylene oil in a drybox, transferred to a nylon loop and then quickly transferred to the goniometer head of a Bruker X8 APEX2 diffractometer equipped with a molybdenum X-ray tube (λ = 0.71073 Å). Preliminary data revealed the crystal system. A hemisphere routine was used for data collection and determination of lattice constants.

The space group was identified and the data were processed using the Bruker SAINT+ program and corrected for absorption using SADABS. The structures were solved using direct methods (SHELXS) completed by subsequent Fourier synthesis and refined by full-matrix least-squares procedures.

Preparation of (^{iPr}PDI)Fe(OCH_2CH_3) (1-OEt). Method A. This complex was prepared in a manner similar to **1-$OCH_2CH{=}CH_2$** with 0.050 g (0.084 mmol) of **1-$(N_2)_2$** and 5 μL, (0.084 mmol) of ethanol to yield 0.028 g (57%) of a dark brown foam identified as **1-OEt**. **Method B.** A 20 mL scintillation vial was charged with 0.100 g (0.168 mmol) of **1-$(N_2)_2$** and approximately 15 mL of pentane. Using a microsyringe, 0.012 g (14 μL, 0.168 mmol) of ethyl formate was added and the resulting brown solution was allowed to stir for 30 minutes. The solution was filtered through Celite, the solvent was evacuated, and recrystallization of the resulting brown solid from pentane yielded **1-OEt**. Analysis for $C_{35}H_{48}FeN_3O$: Calcd C, 72.15; H, 8.30; N, 7.21. Found: C, 71.94; H, 8.30; N, 6.99. ^{1}H NMR (benzene-d_6, 20 °C): δ = 84.47 (157 Hz, 2H), 71.68 (67 Hz, 3H), -8.49 (28 Hz, 2H, *m-aryl*), -14.43 (19 Hz, 1H, *p-aryl*), -23.41 (23 Hz, 12H, CH(CH_3)$_2$), -36.31 (137 Hz, 12H, CH(CH_3)$_2$), -114.51 (222 Hz, 4H, CH(CH_3)$_2$), -214.04 (130 Hz, 6H, C(CH_3)), two peaks not located.

Preparation of (^{iPr}PDI)Fe($CH{=}CH_2$) (1-Vinyl). Using a calibrated gas bulb, 0.021 mmol of vinyl bromide was transferred to a J. Young NMR tube containing 0.025 g (0.042 mmol) of **1-$(N_2)_2$** and approximately 0.7 mL of benzene-d_6. Upon standing at ambient temperature for 20 min, analysis of the reaction mixture by ^{1}H NMR spectroscopy revealed formation of a mixture of **1-Br** and **1-Vinyl**. ^{1}H NMR (benzene-d_6, 20 °C): δ = 127.07 (221 Hz, 1H, *p-pyr*), 52.84 (45 Hz, 2H, *m-pyr*), -7.37

(32 Hz, 12H, CH(CH_3)$_2$), -12.74 (136 Hz, 12H, CH(CH_3)$_2$), -55.29 (271 Hz, 4H, CH(CH$_3$)$_2$), -141.77 (506 Hz, 6H, C(CH_3)), *aryl* and *vinyl* resonances not located.

Observation of (^{iPr}PDI)Fe(CH$_2$CH(CH$_3$)$_2$) (1-Isobutenyl). This complex was observed upon addition of 0.002 g (1.8 μL, 0.017 mmol) of 1-bromo-2-methylpropene to 0.020 g (0.034 mmol) **1-(N$_2$)$_2$** in approximately 0.7 mL of benzene-d_6. ^{1}H NMR (benzene-d_6, 20 °C): δ = 327.64 (227 Hz, 1H, *p-pyr*), 298.20 (508 Hz, 3H, CH=C(CH_3)$_2$), 236.98 (884 Hz, 3H, CH=C(CH_3)$_2$), 68.38 (99 Hz, 2H, *m-pyr*), -8.92 (38 Hz, 4H, *m-aryl*), -15.46 (34 Hz, 2H, *p-aryl*), -18.19 (44 Hz, 12H, CH(CH_3)$_2$), -24.48 (113 Hz, 12H, CH(CH_3)$_2$), -105.76 (598 Hz, 4H, CH(CH$_3$)$_2$), -181.43 (169 Hz, 6H, C(CH_3)), CH=C(CH$_3$)$_2$ resonance not located.

Preparation of 1-Aryl. To a solution of **1-(N$_2$)$_2$** (0.033 g, 0.056 mmol) in benzene-d_6 (0.7 mL) was added 12 μL (0.057 mmol) of hexamethyldisiloxane. The dark green solution was transferred to an NMR tube fitted with a J. Young adapter and placed in a 95 °C oil bath for 16 h. The resulting burgundy solution was cooled to room temperature, filtered, and solvent and other volatiles were removed *in vacuo*, yielding a pink solid identified as **1-Aryl** (0.023 g, 0.044 mmol, 78%). Similaily, **1-Aryl** was effectively prepared in the presence of a stoichiometric amount of anisole, instead of hexamethyldisiloxane, or in the absence of ether. Analysis for $C_{33}H_{43}N_3Fe$: Calcd: C, 73.73; H, 8.06; N, 7.82. Found: C, 73.69; H, 7.81; N, 7.95. ^{1}H NMR (benzene-d_6): δ = 7.37-7.16 (m, 3H, *pyr*), 6.61 (d, $^3J_{HH}$ = 8.0 Hz, 2H, *m-aryl*), 6.56 (t, $^3J_{HH}$ = 8.0 Hz, 1H, *p-aryl*), 5.46 (d, $^3J_{HH}$ = 5.6 Hz, 2H, η^6-*m-aryl*), 4.12 (t, $^3J_{HH}$ = 5.6 Hz, 1H, η^6-*p-aryl*), 3.36-3.22 (m, 4H, CH(CH$_3$)$_2$), 2.83 (s, 3H, C(CH_3)), 1.46 (d, $^3J_{HH}$ = 6.8 Hz, 6H, CH(CH_3)$_2$), 1.39 (s, 3H, C(CH_3)), 1.26 (d, $^3J_{HH}$ = 6.8 Hz, 6H, CH(CH_3)$_2$), 1.06 (d, $^3J_{HH}$ = 6.8 Hz, 6H, CH(CH_3)$_2$), 0.97 (d, $^3J_{HH}$ = 6.8 Hz, 6H, CH(CH_3)$_2$). ^{13}C{^{1}H}

(benzene-d_6): δ = 170.3, 155.6, 147.0, 146.7, 144.2, 143.3, 141.5, 129.1 (*m-aryl*), 125.9, 124.2, 122.4, 116.7 (*p-aryl*), 79.3 (η^6-*m-aryl*), 78.4 (η^6-*p-aryl*), 28.2 (CH(CH_3)$_2$), 27.6 (CH(CH_3)$_2$), 27.0 (C(CH_3)), 24.9 (CH(CH$_3$)$_2$), 24.7 (CH(CH$_3$)$_2$), 23.4 (CH(CH$_3$)$_2$), 22.4 (CH(CH$_3$)$_2$), 16.3 (C(CH_3)).

Preparation of (^{iPr}PDI)Fe(O_2CCH=CH(Ph)) (1-CIN). A 20 mL vial was charged with 0.050 g (0.084 mmol) of **1-(N_2)$_2$** and approximately 10 mL of pentane. To the solution, 0.013 g (0.084 mmol) of *trans*-cinnamic acid was added and dinitrogen evolution was observed along with a color change from green to brown. The solution was allowed to stir for 2 hours and then filtered through Celite. The solvent was removed *in vacuo* and the residue was recrystallized from pentane at -35 °C to afford 0.036 g (62 %) of a brown solid identified as **1-CIN**. Analysis for $C_{42}H_{50}FeN_3O$: Calcd C, 75.03; H, 7.50; N, 6.25. Found: C, 75.24; H, 7.90; N, 6.32. ^{1}H NMR (benzene-d_6, 20 °C): δ = 372.72 (219 Hz, 1H, *p-pyr*), 159.36 (275 Hz, 1H, COC*H*), 119.25 (294 Hz, 2H, *m-pyr*), 58.80 (191 Hz, 1H, C*H*(C_6H_5)), 27.99 (45 Hz, 2H, *o-phenyl*), 19.01 (16 Hz, 2H, *m-phenyl*), 11.82 (30 Hz, 1H, *p-phenyl*), -3.14 (47 Hz, 2H, *m-aryl*), -16.66 (42 Hz, 1H, *p-aryl*), -19.56 (50 Hz, 12H, CH(CH_3)$_2$), -30.12 (135 Hz, 12H, CH(CH_3)$_2$), -113.05 (524 Hz, 4H, C*H*(CH_3)$_2$), -283.51 (336 Hz, 6H, C(CH_3)).

Preparation of (^{iPr}PDI)Fe(CH=CH_2)(O_2CMe) (1-(OAc)(Vinyl)). A 20 mL vial was charged with 0.200 g (0.337 mmol) of **1-(N_2)$_2$** and approximately 10 mL of pentane. A separate solution of 0.029 g (32 μL, 0.337 mmol) of vinyl acetate in ~ 5 mL of pentane was added slowly dropwise while stirring, resulting in immediate evolution of N_2 along with a change in color to bright purple. After 2 hours, the solution was filtered through Celite and the solvent was removed *in vacuo* to yield a purple residue. Recrystallization from pentane yielded 0.131 g (62 %) of a bright purple solid

identified as **1-(OAc)(Vinyl)**. Analysis for $C_{37}H_{49}FeN_3O_2$: Calcd C, 71.26; H, 7.92; N, 6.74. Found: C, 71.11; H, 7.74; N, 6.61. ^{1}H NMR (benzene-d_6): δ = 10.07 (dd, 16.0 Hz, 7.5 Hz, 1H, C*H*=CH$_2$), 7.43 (d, 7.5 Hz, 2H, *m-pyr*), 7.25 (t, 7.5 Hz, 1H, *p-pyr*), 6.96 (d, 6.0 Hz, 1H, *m-aryl*), 6.95 (d, 6.0 Hz, 1H, *m-aryl*), 4.66 (d, 7.5 Hz, 1H, CH=C*H*$_2$), 3.12 (sept., 7.0 Hz, 2H, C*H*(CH$_3$)$_2$), 1.94 (sept., 7.0 Hz, 2H, C*H*(CH$_3$)$_2$), 1.87 (d, 16.0 Hz, 1H, CH=C*H*$_2$), 1.78 (m, 12H, CH(C*H*$_3$)$_2$ and C(C*H*$_3$)), 1.23 (d, 7.0 Hz, 6H, CH(C*H*$_3$)$_2$), 1.18 (s, 3H, CO$_2$C*H*$_3$), 1.07 (d, 7.0 Hz, 6H, CH(C*H*$_3$)$_2$), 0.80 (d, 7.0 Hz, 6H, CH(C*H*$_3$)$_2$), one peak not located. ^{13}C{^{1}H} NMR (benzene-d_6): δ = 189.91 (*C*H=CH$_2$), 181.48 (*C*O$_2$Me), 163.67 (N=*C*), 144.44 (*aryl*), 143.20, 142.26, 126.89 (*p-aryl*), 124.28 (*m-aryl*), 123.99 (*m-aryl*), 120.79 (*m-py*), 118.39 (*p-py*), 117.14 (CH=*C*H$_2$), 28.54 (*C*H(CH$_3$)$_2$), 28.25 (*C*H(CH$_3$)$_2$), 25.59 (CH(*C*H$_3$)$_2$), 25.07 (CH(*C*H$_3$)$_2$), 24.81 (CH(*C*H$_3$)$_2$), 24.51 (CH(*C*H$_3$)$_2$), 22.42 (CO$_2$*C*H$_3$), 19.20 (C(C*H*$_3$)).

Observation of (^{iPr}PDI)Fe(O$_2$CC$_6$H$_5$)(CH=CH$_2$) (1-(OBz)(Vinyl)). This complex was prepared from the addition of 0.005 g (4.6 μL, 0.034 mmol) of vinyl benzoate to 0.020 g of **1-(N$_2$)$_2$** in approximately 0.7 mL of benzene-d_6. ^{1}H NMR (benzene-d_6): δ = 10.16 (dd, 16.0 Hz, 7.5 Hz, 1H, C*H*=CH$_2$), 7.79 (d, 8.0 Hz, 2H, *aryl/phenyl*), 7.46 (d, 8.0 Hz, 2H, *m-pyr*), 7.28 (t, 8.0 Hz, 1H, *p-pyr*), 7.00 (dd, 8.0 Hz, 1.0 Hz, 2H, *aryl/phenyl*), 6.76 (dd, 8.0 Hz, 1.0 Hz, 2H, *aryl/phenyl*), 4.62 (d, 7.5 Hz, 1H, CH=C*H*$_2$), 3.24 (sept., 7.0 Hz, 2H, C*H*(CH$_3$)$_2$), 2.02 (sept., 7.0 Hz, 2H, C*H*(CH$_3$)$_2$), 1.90 (d, 7.0 Hz, 6H, CH(C*H*$_3$)$_2$), 1.86 (d, 16.0 Hz, 1H, CH=C*H*$_2$), 1.78 (s, 6H, C(C*H*$_3$)), 1.30 (d, 7.0 Hz, 6H, CH(C*H*$_3$)$_2$), 1.06 (d, 7.0 Hz, 6H, CH(C*H*$_3$)$_2$), 0.82 (d, 7.0 Hz, 6H, CH(C*H*$_3$)$_2$), two resonances not located. ^{13}C{^{1}H} NMR (benzene-d_6): δ = 188.19 (*C*H=CH$_2$), 176.41 (*C*O$_2$Me), 165.94, 163.15, 144.18, 142.72, 141.74, 133.97, 130.83, 130.83, 128.85, 127.62, 126.87, 124.04, 123.95, 120.98, 118.76, 117.56, 28.56

($CH(CH_3)_2$), 28.35 ($CH(CH_3)_2$), 25.61 ($CH(CH_3)_2$), 25.23 ($CH(CH_3)_2$), 24.65 ($CH(CH_3)_2$), 24.47 ($CH(CH_3)_2$), 19.27 ($C(CH_3)$).

Preparation of (^{iPr}PDI)Fe(O_2CMe) (1-OAc): Method A. A solution of **1-EtOAc** was prepared in a thick-walled glass vessel by adding 21 μL (0.202 mmol) of ethyl acetate to 10 mL of a pentane solution containing 0.120 g (0.202 mmol) of **1-(N_2)$_2$**. The vessel was sealed and heated to 65 °C in an oil bath for 16 hours. The resulting brown solution was filtered though Celite and the solvent removed *in vacuo* to yield a brown solid. Recrystallization from pentane yielded 0.044 g (36%) of **1-OAc**. **Method B:** A thick-walled glass vessel was charged with 0.100 g (0.170 mmol) of **1-(N_2)$_2$** and approximately 10 mL of pentane. Upon addition of 0.015 g (16 μL, 0.189 mmol) of methyl acetate, the vessel was sealed, submerged in liquid nitrogen, and evacuated on a high vacuum line. After adding 1 atm of dihydrogen, the solution was thawed and stirred for 4 hrs at ambient temperature. The volatiles were removed and the resulting reddish-brown residue was washed through a Celite fitted frit with diethyl ether. The solvent was removed *in vacuo* and recrystallization from pentane at -35 °C afforded spectroscopically pure **1-OAc**. Analysis for $C_{35}H_{46}FeN_3O_2$: Calcd C, 70.46; H, 7.77; N, 7.04. Found: C, 70.25; H, 8.04; N, 6.79. Magnetic susceptibility (benzene-d_6, 20 °C) μ_{eff} = 3.9(2) μ_B. ^{1}H NMR (benzene-d_6, 20 °C): δ = 372.47 (18 Hz, 1H, *p-pyr*), 187.25 (370 Hz, 3H, CO_2CH_3), 119.59 (163 Hz, 2H, *m-pyr*), -3.20 (73 Hz, 2H, *m-aryl*), -16.50 (66 Hz, 1H, *p-aryl*), -19.78 (75 Hz, 12H, $CH(CH_3)_2$), -30.37 (170 Hz, 12H, $CH(CH_3)_2$), -114.95 (525 Hz, 4H, $CH(CH_3)_2$), -284.76 (280 Hz, 6H, $C(CH_3)$).

Preparation of (^{iPr}PDI)Fe(OC_6H_5) (1-OPh). Method A. A 20 vial was charged with 0.050 g (0.084 mmol) of **1-(N_2)$_2$** and 10 mL of pentane. Using a microsyringe, 0.010 g (9 μL, 0.084 mmol) of phenyl formate was added. After 30 minutes the greenish-

brown solution was filtered through Celite and the solcent was evacuated *in vacuo* to yield 0.021 g (40%) of a brown solid identified as **1-OPh**. **Method B.** In a 20 mL scintillation vial, a solution consisting of 0.010 g (0.017 mmol) of **1-(N_2)$_2$** and approximately 0.7 mL of benzene-d_6 was prepared. Upon addition of 0.002 g (0.017 mmol) of phenol, the solution became brown in color within seconds. The solution was filtered through Celite in to a J. Young tube and the formation of **1-OPh** was confirmed by ^{1}H NMR spectroscopy. Analysis for $C_{39}H_{48}FeN_3O$: Calcd C, 74.27; H, 7.67; N, 6.66. Found: C, 74.27; H, 7.68; N, 6.76. ^{1}H NMR (benzene-d_6, 20 °C): δ= 71.02 (224 Hz, 2H, *m-pyr*), 48.99 (535 Hz, *phenyl*), -7.14 (163 Hz, 4H, *m-aryl*), -14.42 (128 Hz, 2H, *p-aryl*), -23.21 (190 Hz, 12H, CH(CH_3)$_2$), -36.72 (290 Hz, 12H, CH(CH_3)$_2$), -113.54 (549 Hz, 4H, CH(CH$_3$)$_2$), -219.17 (293 Hz, 6H, C(CH_3)), 3 resonances not located.

Spectroscopic Identification of 1-O^{n}Pent. This complex was observed along with the formation of **1-OAc** upon cleavage of amyl acetate with **1-(N_2)$_2$**. ^{1}H NMR (benzene-d_6, 20 °C): δ= 87.73 (88 Hz, *pentyl*), 72.76 (79 Hz, 2H, *m-pyr*), 63.36 (*pentyl*), 31.43 (*pentyl*), -8.88 (42 Hz, 4H, *m-aryl*), -14.40 (31Hz, 2H, *p-aryl*), -23.96 (54 Hz, 12H, CH(CH_3)$_2$), -38.92 (269 Hz, 12H, CH(CH_3)$_2$), -117.62 (1004 Hz, 4H, CH(CH$_3$)$_2$), -216.48 (245 Hz, 6H, C(CH_3)), 3 resonances not located.

Spectroscopic Identification of (^{iPr}PDI)Fe(OCHMe$_2$) (1-O^{i}Pr). This complex was observed along with the formation of **1-OAc** upon cleavage of isopropyl acetate with **1-(N_2)$_2$**. The observation of **1-O^{i}Pr** was independently confirmed through addition of either isopropanol or isopropyl formate to **1-(N_2)$_2$**. ^{1}H NMR (benzene-d_6, 20 °C): δ= 86.25 (232 Hz, 6H, OCH(CH_3)$_2$), 68.38 (72 Hz, 2H, *m-pyr*), -8.74 (26 Hz, 4H, *m-aryl*), -14.42 (22 Hz, 2H, *p-aryl*), -22.88 (26 Hz, 12H, CH(CH_3)$_2$), -36.90 (152 Hz,

12H, CH(CH_3)$_2$), -113.00 (373 Hz, 4H, CH(CH$_3$)$_2$), -214.30 (150 Hz, 6H, C(CH_3)), 2 resonances not located.

Spectroscopic Identification of (^{iPr}PDI)Fe(OC$_6$H$_{11}$) (1-OCy). This complex was observed along with the formation of **1-OAc** upon cleavage of cyclohexyl acetate with **1-(N$_2$)$_2$**. The observation of **1-OCy** was independently confirmed through addition of cyclohexanol to **1-(N$_2$)$_2$**. ^{1}H NMR (benzene-d_6, 20 °C): δ = 82.88 (251 Hz, *cyclohexyl*), 68.94 (82 Hz, 2H, *m-pyr*), 62.03 (*cyclohexyl*), 47.79 (128 Hz, *cyclohexyl*), 39.26 (84 Hz, *cyclohexyl*), 28.04 (*cyclohexyl*), -9.00 (26 Hz, 4H, *m-aryl*), -14.46 (20 Hz, 2H, *p-aryl*), -23.14 (29 Hz, 12H, CH(CH_3)$_2$), -36.81 (164 Hz, 12H, CH(CH_3)$_2$), -117.09 (391 Hz, 4H, CH(CH$_3$)$_2$), -214.32 (166 Hz, 6H, C(CH_3)), *p-pyr* resonance not located.

Spectroscopic Identification of (^{iPr}PDI)Fe(OCMe$_3$) (1-O^{t}Bu). This complex was observed along with the formation of **1-OAc** upon cleavage of *tert*-butyl acetate with **1-(N$_2$)$_2$**. The observation of **1-O^{t}Bu** was independently confirmed through addition of *tert*-butyl alcohol to **1-(N$_2$)$_2$**. ^{1}H NMR (benzene-d_6, 20 °C): δ = 84.76 (279 Hz, 9H, C(CH_3)$_3$), 63.98 (72 Hz, 2H, *m-pyr*), -9.24 (23 Hz, 4H, *m-aryl*), -14.63 (27 Hz, 2H, *p-aryl*), -22.34 (27 Hz, 12H, CH(CH_3)$_2$), -36.95 (134 Hz, 12H, CH(CH_3)$_2$), -112.79 (407 Hz, 4H, CH(CH$_3$)$_2$), -213.58 (155 Hz, 6H, C(CH_3)), *p-pyr* resonance not located.

Observation of (^{iPr}PDI)Fe(OCH$_2$Ph) (1-OBenzyl). This complex was observed with **1-OAc** from **1-(N$_2$)$_2$** mediated cleavage of benzyl acetate. ^{1}H NMR (benzene-d_6, 20 °C): δ = 83.79 (648 Hz, 2H, *phenyl*), 75.20 (314 Hz, 2H, *m-pyr*), 29.58 (154 Hz, 2H, *phenyl*), 24.24 (580 Hz, 1H, *phenyl*), -8.54 (193 Hz, 4H, *m-aryl*), -14.44 (203 Hz, 2H, *p-aryl*), -24.40 (207 Hz, 12H, CH(CH_3)$_2$), -39.64 (338 Hz, 12H, CH(CH_3)$_2$), -120.01 (484 Hz, 4H, CH(CH$_3$)$_2$), -221.31 (375 Hz, 6H, C(CH_3)), 2 peaks not located.

REFERENCES

[1] Collman, J. P.; Hegedus, L. S.; Norton, J. R.; Finke R. G. in *Principles and Applications of Organotransition Metal Chemistry*. University Science Books, Mill Valley, CA 1987.

[2] Rossi, R. A.; Pierini, A. B.; Penenory, A. B. *Chem. Rev.* **2003**, *103*, 71.

[3] San Filippo, J., Jr.; Silbermann, J.; Fagan, P. J. *J. Am. Chem. Soc.* **1978**, *100*, 4834.

[4] Spessard, G. O.; Miessler, G. L. *Organometallic Chemistry*, Prentice Hall, Upper Saddle River New Jersey, 1996, pp. 175.

[5] Blaser, H. U.; Halpern, J. *J. Am. Chem. Soc.* **1980**, *102*, 1684.

[6] Bolm, C.; Legros, J.; Le Paih, J.; Zani, L. *Chem. Rev.* **2004**, *104*, 6217.

[7] Enthaler, S.; Junge, K.; Beller, M. *Angew. Chem. Int. Ed.* **2008**, *47*, 3317.

[8] For seminal studies on the oxidative addition of E-X bonds to phosphine-ligated Fe(0) and related complexes see: (a) Klein, H.-F. *Angew. Chem. Int. Ed.* **1980**, *92*, 362. (b) Ittel, S. D.; Tolman, C. A.; English, A. D.; Jesson, J. P. *J. Am. Chem. Soc.* **1976**, *98*, 6073. (c) Tolman, C. A.; Ittel, S. D.; English, A. D.; Jesson, J. P. *J. Am. Chem. Soc.* **1978**, *100*, 4080. (d) Parker, S. F.; Peden, C. H. F.; Barrett, P. H.; Pearson, R. G. *J. Am. Chem. Soc.* **1984**, *106*, 1304.

[9] Jørgensen, C. K. *Coord. Chem. Rev.* **1966**, *1*, 164.

[10] (a) Pierpont, C. G. *Coord. Chem. Rev.* **2001**, *219-221*, 415. (b) Ward, M. D.; McCleverty, J. A.; *J. Chem. Soc. Dalton Trans.* **2002**, 275. (c) Chaudhuri, P.; Verani, C. N.; Bill, E.; Bothe, E.; Weyermüller, T.; Wieghardt, K. *J. Am. Chem. Soc.* **2001**, *123*, 2213.

[11] Bart, S. C.; Lobkovsky, E.; Chirik, P. J. *J. Am. Chem. Soc.* **2004**, *126*, 13794.

[12] Archer, A. M.; Bouwkamp, M. W.; Cortez, M. -P.; Lobkovsky, E.; Chirik, P. J. *Organometallics* **2006**, *25*, 4269.

[13] Bouwkamp, M. W.; Bowman, A. C.; Lobkovsky, E.; Chirik, P. J. *J. Am. Chem. Soc.* **2006**, *128*, 13340.

[14] Bart, S. C.; Chlopek, K.; Bill, E.; Bouwkamp, M. W.; Lobkovsky, E.; Neese, F.; Wieghardt, K.; Chirik, P. J. *J. Am. Chem. Soc.* **2006**, *128*, 13901.

[15] Bart, S. C.; Lobkovsky, E.; Bill, E.; Wieghardt, K.; Chirik, P. J. *Inorg. Chem.* **2007**, *46*, 7055.

[16] Knijnenburg, Q.; Gambarotta, S.; Budzelaar, P. H. M. *Dalton Trans.* **2006**, 5442.

[17] (a) Bianchini, C.; Giambastiani, G.; Rios, I. G.; Mantovani, G.; Meli, A.; Segarra, A. M. *Coord. Chem. Rev.* **2006**, *250*, 1391. (b) Small, B. L.; Brookhart, M.; Bennett, A. M. A. *J. Am. Chem. Soc.* **1998**, *120*, 4049. (c) Britovsek, G. J. P.; Gibson, V. C.;

Kimberley, B. S.; Maddox, P. J.; McTavish, S. J.; Solan, G. A.; White, A. J. P.; Williams, D. J. *Chem. Commun.* **1998**, 849.

[18] (a) Blackmore, K. J.; Lal, N.; Ziller, J. W.; Heyduk, A. F. *J. Am. Chem. Soc.* **2008**, *130*, 2728. (b) Ketterer, N. A.; Fan, H.; Blackmore, K. J.; Yang, X.; Ziller, J. W.; Baik, M. -H.; Heyduk, A. F. *J. Am. Chem. Soc.* **2008**, *130*, 4364.

[19] Fernández, I.; Trovitch, R. J.; Lobkovsky, E.; Chirik, P. J. *Organometallics* **2008**, *27*, 109.

[20] Lal, D.; Griller, D.; Husband, S.; Ingold, K. U. *J. Am. Chem. Soc.* **1974**, *96*, 6355.

[21] Williams, G. M.; Schwartz, J. *J. Am. Chem. Soc.* **1982**, *104*, 1122.

[22] Yamamoto, A.; Kakino, R.; Shimizu, I. *Helv. Chem. Acta* **2001**, *84*, 2996.

[23] Furimsky, E. *Appl. Catal. A: Gen.* **2000**, *199*, 147-190.

[24] Lin, Y. S.; Yamamoto, A. in *Topics in Organometallic Chemistry*, Murai, S., Ed.; Springer-Verlag, Berlin, 1999, Vol 3, pp. 161.

[25] Trost, B.; Verhoven, T. R. in *Comprehensive Organometallic Chemistry*; Wilkinson, G.; Stone, F. G. A.; Abel, A. E. Eds; Pergamon, Oxford, 1982, Vol. 8, pp. 799.

[26] Trost, B. M. *Acc. Chem. Res.* **1980**, *13*, 385.

[27] Waetzig, S. R.; Rayabharapu, D. K.; Weaver, J. D.; Tunge, J. A. *Angew. Chem. Int. Ed.* **2006**, *45*, 4977.

[28] Tsuji, J. in *Palladium Reagents and Catalysts*; Wiley: Chichester, U. K. 1995: pp. 290.

[29] Liou, S.-Y.; van der Boom, M. E.; Ben-David, Y.; Shimon, L. J. W.; Milstein, D. *J. Am. Chem. Soc.* **1998**, *120*, 6531.

[30] Lara, P.; Paneque, M.; Poveda, M. L.; Salazar, V.; Santos, L. L.; Carmona, E. *J. Am. Chem. Soc.* **2006**, *128*, 3512.

[31] Ueno, S.; Mizushima, E.; Chatani, N.; Kakiuchi, F. *J. Am. Chem. Soc.* **2006**, *128*, 16516.

[32] Bradley, C. A.; Veiros, L. F.; Pun, D.; Lobkovsky, E.; Keresztes, I.; Chirik, P. J. *J. Am. Chem. Soc.* **2006**, *128*, 16600.

[33] Faller, J. W.; Linebarrier, D. *Organometallics* **1988**, *7*, 1670.

[34] Bonanno, J. B.; Henry, T. P.; Neithamer, D. R.; Wolczanski, P. T.; Lobkovsky, E. B. *J. Am. Chem. Soc.* **1996**, *118*, 5132.

[35] Kawaguchi, H.; Matsuo, T. *J. Am. Chem. Soc.* **2003**, *125*, 14254.

[36] Yamamoto, T.; Ishizu, J.; Yamamoto, A. *Chem. Lett.* **1979**, 1385.

[37] Eisch, J. J.; Im, K. R. *J. Organomet. Chem.* **1977**, *139*, C51.

[38] Yamamoto, T.; Ishizu, J.; Kohara, T.; Komiya, S.; Yamamoto, A. *J. Am. Chem. Soc.* **1980**, *102*, 3758.

[39] Yamamoto, T.; Ishizu, J.; Yamamoto, A. *J. Am. Chem. Soc.* **1981**, *103*, 6863.

[40] van der Boom, M. E.; Liou, S. Y.; Shimon, L. J. W.; Ben-David, Y.; Milstein, D. *Inorg. Chim. Acta* **2004**, *357*, 4015.

[41] Ganem, B.; Small, V. R., Jr. *J. Org. Chem.* **1974**, *39*, 3728.

[42] Collman, J. P. *Acc. Chem. Res.* **1975**, *8*, 342.

[43] Magens, S.; Erlelt, M.; Jatsch, A.; Plietker, B. *Org. Lett.* **2008**, *10*, 53.

[44] Tolman, C. A.; Ittel, S. D.; English, A. D.; Jesson, J. P. *J. Am. Chem. Soc.* **1979**, *101*, 1742.

[45] Ittel, S. D.; Tolman, C. A.; English, A. D.; Jesson, J. P. *J. Am. Chem. Soc.* **1978**, *100*, 7577.

[46] Tatsumi, T.; Tominaga, H.; Hidai, M.; Uchida, Y. *J. Organomet. Chem.* **1981**, *218*, 177.

[47] Yamamoto, T.; Miyashita, S.; Naito, Y.; Komiya, S.; Ito, T.; Yamamoto, A. *Organometallics* **1982**, *1*, 808.

[48] Yamamoto, Y.; Han, X. –H.; Ma, J. –F. *Angew. Chem. Int. Ed.* **2000**, *39*, 1965.

[49] Hiraki, K.; Kira, S. –I.; Kawano, H. *Bull. Chem. Soc. Jpn.* **1997**, *70*, 1583.

[50] Tatamindani, H.; Yokota, K.; Kakiuchi, F.; Chatani, N. *J. Org. Chem.* **2004**, *69*, 5615.

[51] Grotjahn, D. B.; Joubran, C. *Organometallics* **1995**, *14*, 5171.

[52] Chatani, N.; Tatamindani, H.; Ie, Y.; Kakiuchi, F.; Murai, S. *J. Am. Chem. Soc.* **2001**, *123*, 4849.

[53] Pangborn, A. B.; Giardello, M. A.; Grubbs, R. H.; Rosen, R. K.; Timmers, F. J. *Organometallics* **1996**, *15*, 1518.

[54] Sur, S. K. *J. Magn. Res.* **1989**, *82*, 169.

CHAPTER 5

BIS(DIISOPROPYLPHOSPHINOMETHYL)PYRIDINE IRON COMPLEXES: PREPARATION, REACTIVITY, AND ASSESSMENT OF CATALYTIC HYDROGENATION ACTIVITY*

5.1 Abstract

Preparation of bis(diisopropylphosphinomethyl)pyridine iron dihalide complexes (^{iPr}PNP)FeX_2 (X = Cl, Br; ^{iPr}PNP = 2,6-($^{i}Pr_2PCH_2)_2(C_5H_3N)$) was accomplished through the metallation of ^{iPr}PNP with the desired iron dihalide precursor. Addition of 2 equivalents of $NaBEt_3H$ under an atmosphere of dinitrogen resulted in salt elimination and the formation of the diamagnetic iron dihydride complex (^{iPr}PDI)$FeH_2(N_2)$, where a dinitrogen molecule occupies the sixth coordination site. Phenylsilane addition to (^{iPr}PDI)$FeH_2(N_2)$ resulted in substitution of one iron hydride, exclusively *trans* to the pyridine donor of ^{iPr}PNP, with concomitant liberation of 1 equivalent of H_2. A series of ligand exchange experiments established facile loss of the weakly activated dinitrogen ligand for both complexes. Exposure of either (^{iPr}PDI)$FeH_2(N_2)$ or (^{iPr}PDI)$FeH(SiH_2Ph)(N_2)$ to 4 atmospheres of H_2 resulted in reversible N_2 displacement and formation of the corresponding η^2-dihydrogen complexes. The ^{1}H NMR spectra of both iron hydride dihydrogen complexes suggested rapid exchange between the hydride and η^2-dihydrogen ligands at ambient temperature in benzene-d_6, as further evidenced by deuterium exchange and EXSY NMR studies. Addition of 4 atmospheres of D_2 to (^{iPr}PDI)$FeH(SiH_2Ph)(N_2)$ resulted in fast deuterium incorporation into the iron hydride position along with slower silyl hydrogen exchange. The relative rates of deuterium exchange imply that D_2

* Parts of this chapter have been reproduced with permission from Trovitch, R. J.; Lobkovsky, E.; Chirik, P. J. *Inorg. Chem*. **2006**, *45*, 7252-7260. Copyright 2006 American Chemical Society.

association occurs *trans* to the silyl substituent as well as the intermediacy of an η^2-phenylsilane complex. Both (^{iPr}PDI)FeH_2(N_2) and (^{iPr}PDI)FeH(SiH_2Ph)(N_2) have been identified as active hydrogenation precatalysts; however, low turnover frequencies and facile chelate loss have been identified as major limitations to the catalytic utility of these complexes.

5.2 Introduction

Although the first report of "pincer ligands" appeared in the 1970s,[1] the application of meridonal coordinating ligands in late transition metal chemistry has only recently matured into a remarkably active area of research. Due to their high degree of modularity and ease of preparation,[2] pincer ligands possessing a wide array structural motifs have been introduced. Of particular interest are precious metal complexes containing either chemically innocent[3] or active[4] PNP ligands (shorthand designation for metal bound chelate substituents) that have been shown to mediate useful organic transformations. Most notably, complexes of this sort have been found to catalyze cross coupling reactions[5] as well as amide formation through the dehydrogenative coupling of amines to aldehydes.[6] Fewer complexes featuring PNP ligands are known for first row metals such as Fe, Co, and Ni.[1,7]

As discussed in Chapter 3, there has been an increased impetus among both academic and industrial laboratories to encourage the use of inexpensive and non-toxic first row metal complexes as surrogates for traditional precious metal catalysts. Our group has studied the effect that nitrogen-based, redox-active bis(imino)pyridine ligands have on the ability of reducing iron centers to perform catalytic hydrogenation,[8] hydrosilylation,[9] and [$2\pi + 2\pi$] electrocyclization reactions.[10] Investigation of the catalytically relevant complex (^{iPr}PDI)Fe(N_2)$_2$ (^{iPr}PDI = 2,6-(2,6-$^{i}Pr_2$-C_6H_3N=CMe)$_2$$C_5H_3N$) by Mössbauer spectroscopy, DFT calculations, X-ray

crystallography, and NMR and IR spectroscopies established that the ground state electronic structure of this complex is best described as having an intermediate-spin iron(II) metal center, antiferromagnetically coupled to a doubly reduced bis(imino)pyridine chelate.[11] In the case of [2π + 2π]-cyclization, the shuttling of electrons to and from the ligand has been implicated as an essential feature that allows the metal center to remain in the ferrous oxidation state.[10]

In order to address the role that bis(imino)pyridine redox activity plays in these catalytic processes, the reactivity of a series of PNP iron complexes that lack a conjugated π-system was studied. Although this ligand scaffold relies on phosphine donation rather than imine coordination, raising the barrier to ligand reduction can offer a reasonable assessment of the necessity for π-acidic ligands in neutral iron catalyst development.[12] In this chapter, the characterization of a series of bis(phosphino)pyridine iron complexes and their utility in the hydrogenation and hydrosilylation of unactivated alkenes is discussed.

5.3 Preparation of PNP Iron Complexes

Following preparation of ^{iPr}PNP by literature methods,[13] the corresponding iron dihalide complexes (^{iPr}PNP)FeX_2 (X = Cl, Br; **4-Cl$_2$, 4-Br$_2$**) were synthesized by straightforward complexation of the ligand with either $FeCl_2$ or $FeBr_2$ in tetrahydrofuran solution (Figure 5.1).[14] Both complexes display paramagnetic ^{1}H NMR spectra with ligand resonances spread over a 120 ppm range (Figure 5.2). Consistent with the reported magnetic moment of 5.2(1) μ_B for **4-Cl$_2$**,[14] a solution magnetic moment of 5.1(2) μ_B was measured in chloroform-*d* solution for **4-Br$_2$**. This value is consistent with four unpaired electrons, as would be expected for a high spin iron(II) complex.

With these iron dihalide starting materials in hand, alkali metal reduction in the presence of a weakly coordinating ligand was explored with the goal of isolating a direct analog to **1-(N_2)$_2$**. Unfortunately, attempts to trap such a catalyst precursor with N_2, bis(trimethylsilyl)acetylene, or 1,3-butadiene during the reduction of **4-X_2** with an excess of 0.5% sodium amalgam did not result in the isolation of a tractable organometallic product. Performing the same reduction of either **4-Cl_2** or **4-Br_2** under 1 atmosphere of strongly binding CO; however, did result in the formation of the corresponding diamagnetic iron dicarbonyl complex (^{iPr}PNP)Fe(CO)$_2$ (**4-(CO)$_2$**) (Figure 5.1) based on spectroscopic identification and single-crystal X-ray diffraction.

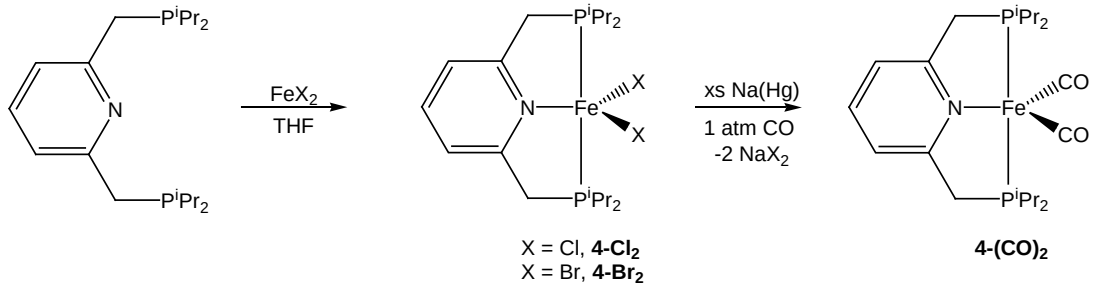

Figure 5.1. Preparation of ^{iPr}PNP iron dihalide starting materials and the reduction of **4-Br_2** under 1 atmosphere of CO.

Isolation of **4-(CO)$_2$** allows a direct comparison of the electronic environments imparted by the PNP and PDI ligands. The solid-state (KBr) infrared spectrum of **4-(CO)$_2$** displays two intense carbonyl stretches centered at 1842 and 1794 cm^{-1}. In comparison, the solid-state stretches for **1-(CO)$_2$** are reported as 1950 and 1894 cm^{-1}, [9] red shifted from **4-(CO)$_2$** by over 100 cm^{-1}. The dramatically lower C-O stretches observed for **4-(CO)$_2$** are consistent with a strongly reducing, formally iron(0), metal center. Although the metal center **1-(CO)$_2$** is also formally zerovalent, **1-(CO)$_2$** is best described as a low spin iron(II) complex with a doubly reduced PDI ligand, greatly

attenuating the reducing capability of the metal center.[11] This difference, coupled with the fact that alkyl phosphines are better sigma donors that imines, explains the drastic difference in the electronic environment imparted at the iron center by the two ligands.

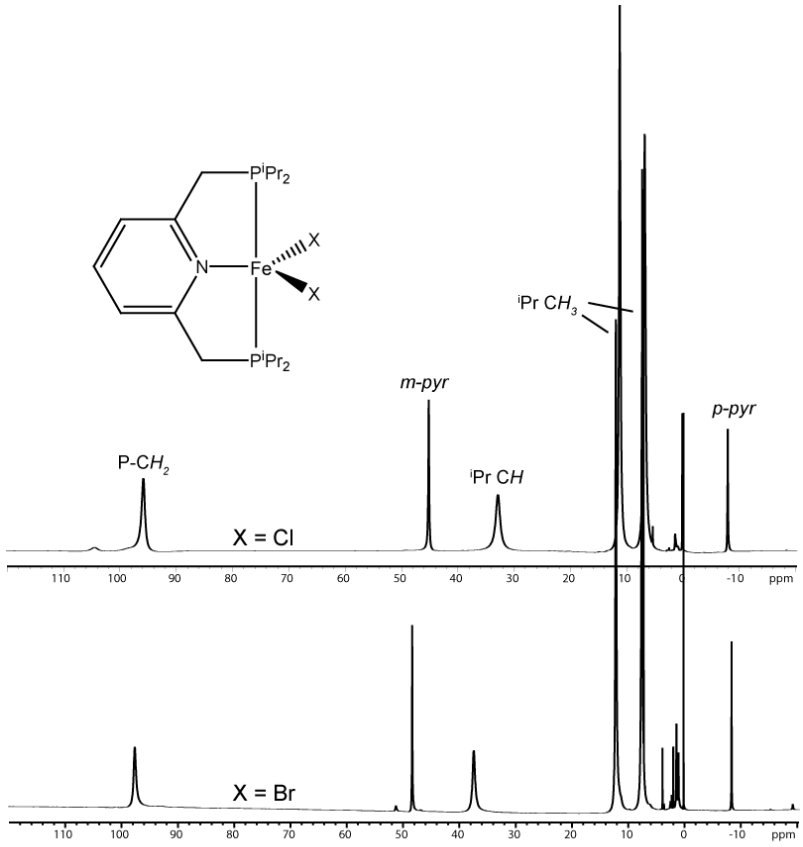

Figure 5.2. ^{1}H NMR spectra of **4-Cl$_2$** and **4-Br$_2$** at 293 K in chloroform-*d*.

Single crystals of **4-(CO)$_2$** suitable for X-ray diffraction were obtained by cooling a concentrated toluene solution of the complex to -35 °C. The solid-state structure (Figure 5.3) and the metrical parameters (Table 5.1) clearly establish the geometry about iron as idealized trigonal pyramidal, possessing C_2-symmetry (Figure 5.3, bottom). The equatorial plane in **4-(CO)$_2$** is defined by the pyridine nitrogen atom and the two carbonyl ligands, with bond angles of 119.91(7)° and 120.04(3)° for C(1)-Fe(1)-C(1A) and C(1)-Fe(1)-N(1), respectively. The axial phosphine ligand arms, with

a crystallographically determined P(1)-Fe(1)-P(1A) angle of 165.990(12)°, are not separated fully by 180° because PNP ligands containing a one atom linker between the pyridine ring and the phosphine typically impart a constrained geometry about the metal center. In comparing the Fe-C bond lengths of both **1-(CO)$_2$**[11] (1.7809(19) Å, 1.7823 (19)) and **4-(CO)$_2$** (1.7325(9) Å), it is apparent that the phosphine substitution and lack of a π-acidic chelate leads to discernable Fe-C bond contraction in **4-(CO)$_2$**, consistent with an increase in metal-carbonyl backbonding.

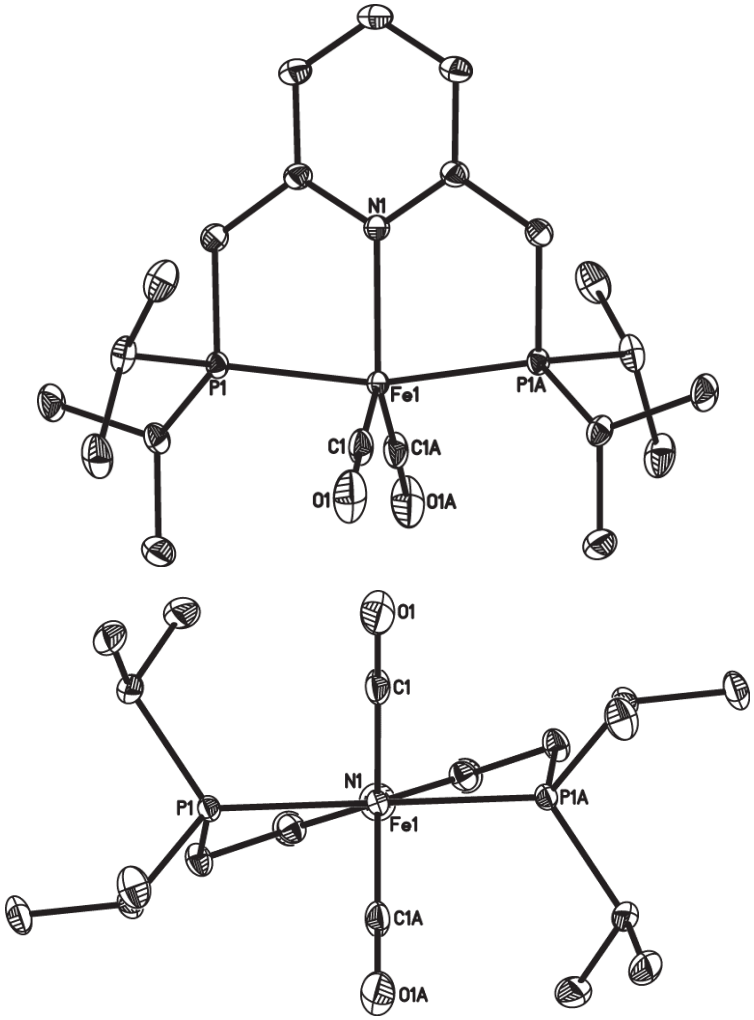

Figure 5.3. Molecular structure of **4-(CO)$_2$** at 30 % probability ellipsoids (top). View of **4-(CO)$_2$** looking down Fe(1)-N(1) bond (bottom). Hydrogen atoms omitted for clarity.

Table 5.1. Selected bond distances (Å) and angles (°) for **4-(CO)$_2$**.

Distance (Å)			Angle (°)
Fe(1)-C(1)	1.7325(9)	P(1)-Fe(1)-P(1A)	165.990(12)
Fe(1)-P(1)	2.1941(2)	C(1)-Fe(1)-C(1A)	119.91(7)
Fe(1)-N(1)	2.0684(8)	N(1)-Fe(1)-P(1)	82.995(6)
C(1)-O(1)	1.1734(11)	C(1)-Fe(1)-N(1)	120.04(3)

The position of the carbonyl ligands relative to the chelate plane is also in stark contrast to the square pyramidal geometry about iron observed in the solid state structure of **1-(CO)$_2$**.[11] This difference in geometry could be due to a lower tendency to backbond to the iron(II) center in **1-(CO)$_2$** as compared to the iron(0) center in **4-(CO)$_2$**. This argument is further supported by the metrical parameters reported for the related, structurally characterized PNP iron dihalide complex, (^{tBu}PNP)FeCl$_2$,[14] containing *tert*-butyl rather than isopropyl phosphine substituents. The molecular geometry in this complex is best described as distorted square planar with a Cl-Fe-Cl angle of 105.1(1). Additionally, the iron atom is lifted out of the chelate plane by 0.552 Å and the Fe-N bond distance is elongated to 2.303(2) Å, compared to 2.0684(8) Å in **4-(CO)$_2$** (Table 5.1). However, recent elucidation of the molecular structure of (^{tBu}PNP)Fe(CO)$_2$[15] has revealed the overall geometry of this complex to be square pyramidal which is likely due to a steric interaction between the *tert*-butyl ligand substituents and carbonyl ligands.

In a second attempt to prepare an iron precatalyst, the possibility of replacing the iron halides with alkyl groups through salt metathesis. Attempts to prepare iron dialkyl complexes that may be active for hydrogenation or hydrosilylation reactions[16] commenced with the addition of alkyllithium reagents to either **4-Cl$_2$** or **4-Br$_2$**.

Although no tractable organometallic product was observed following neosilyllithium addition, the formation of a new paramagnetic product was observed from the addition of either 1 or 2 equivalents of methyllithium to **4-Cl$_2$** (Figure 5.4). This red product has been assigned as the iron methyl chloride (^{iPr}PNP)FeCl(Me) (**4-Cl(Me)**) due to the C_s-symmetry of the complex, as observed by ^{1}H NMR spectroscopy (Figure 5.5). The addition of either 1 or 2 equivalents of phenyllithium to **4-Br$_2$** also yielded paramagnetic reaction mixtures that appeared to have low symmetry by ^{1}H NMR spectroscopy.

Applying a method initially reported by Cámpora[17] and since expanded upon by our group,[18] pincer iron dialkyl complexes could be prepared potentially by straightforward addition of $(py)_2Fe(CH_2SiMe_3)_2$ to the desired chelate. While this possibility has not yet been investigated for ^{iPr}PNP, encouraging results were observed upon addition of the nitrogen analog of this ligand (2,6-(^{i}Pr$_2$NCH$_2$)$_2$(C$_5$H$_3$N)) with $(py)_2Fe(CH_2SiMe_3)_2$.[19]

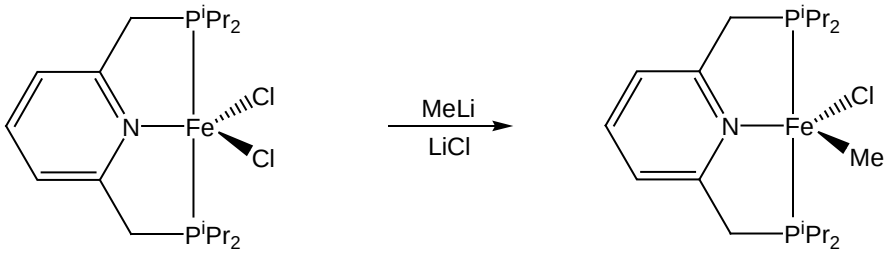

4-Cl$_2$ **4-Cl(Me)**

Figure 5.4. Preparation of **4-Cl(Me)** by salt metathesis.

During the preparation of **1-(N$_2$)$_2$**, it was observed that low yields of this complex could be obtained by adding 2 equivalents of $NaBEt_3H$ to **1-Br$_2$**.[9] In this process, the putative iron dihydride complex loses H_2 and the formally reduced bis(imino)pyridine fragment goes on to coordinate 2 equivalents of dinitrogen.

Applying a similar method to PNP iron chemistry, treatment of an ethereal slurry of either **4-Cl$_2$** or **4-Br$_2$** with 2 equivalents of $NaBEt_3H$ under an atmosphere of N_2 yielded a diamagnetic reddish-orange solid identified as (^{iPr}PNP)FeH_2(N_2) (**4-H$_2$(N$_2$)**) (Figure 5.6). When left in benzene-d_6 solution at ambient temperature for more than a few minutes, chelate liberation and deposition of iron metal began to occur. Loss of the PNP chelate from this complex is likely preceded by loss of either H_2 or N_2; both instances would inherently destabilize the complex.

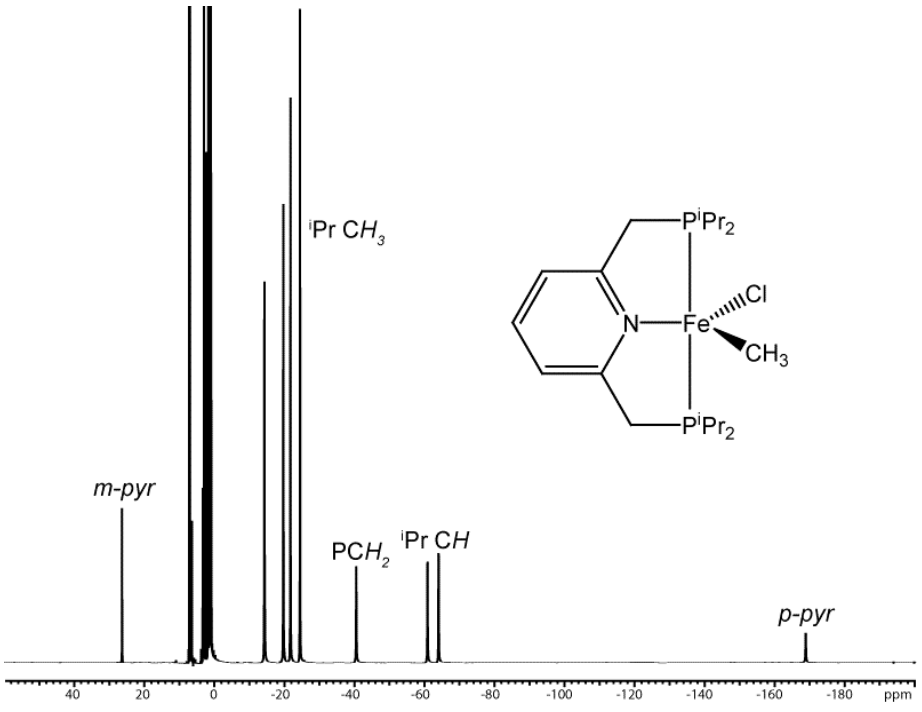

Figure 5.5. ^{1}H NMR spectra of **4-Cl(Me)** at 293 K in benzene-d_6.

Filtration followed by immediate analysis by multinuclear NMR spectroscopy allowed characterization of **4-H$_2$(N$_2$)**. The benzene-d_6 ^{1}H NMR spectrum of this complex at 20 °C displayed two triplets of doublets centered at -17.65 and -12.54 ppm, consistent with the presence of two inequivalent iron hydrides. Similarly, the

proton coupled ^{31}P NMR spectrum exhibited an overlapping doublet of doublets centered at 108.28 ppm, confirming that the phosphine environments were equivalent. Dinitrogen coordination was confirmed by solid-state infrared spectroscopy with the observation of a strong N≡N stretch at 2016 cm^{-1}. The appearance of two inequivalent iron hydrides (lack of C_{2v}-symmetry) ruled out the highly disfavored isomer where the hydrides are in a *trans* configuration. This confirmation is unlikely due to the strong *trans* influence imparted by hydride ligands.[20]

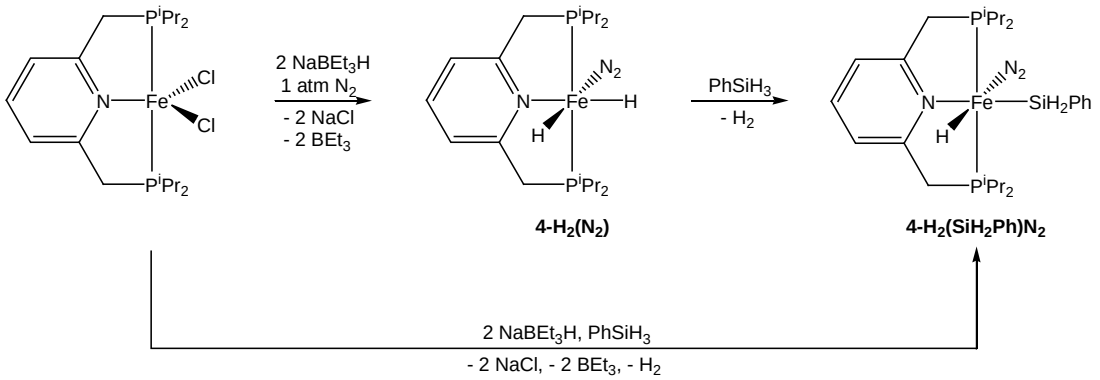

Figure 5.6. Synthetic routes to **4-H$_2$(N$_2$)** and **4-H(SiH$_2$Ph)N$_2$**.

To further assign **4-H$_2$(N$_2$)** as an iron(II) dihydride rather than an iron(0) dihydrogen complex, proton relaxation measurements were conducted at -25 °C in toluene-d_8. A T_1(min) value of 314 ms was measured at 500 MHz, fitting the iron dihydride description.[21] Additionally, the observation of large J_{PH} values of 52.0 and 60.5 Hz confirm that this complex can best be described as a dihydride; η^2-dihydrogen ligands often display little if any coupling to ^{31}P resonances.[21] Even though the iron-hydride resonances appear as a sharp triplet of doublets in the ^{1}H NMR spectrum of **4-H$_2$(N$_2$)**, EXSY NMR experiments (mixing time of 500 ms) revealed rapid exchange between the two positions. This process can either occur through reversible reductive

coupling of the hydrides, followed by fast η^2-dihydrogen σ-bond rotation,[22] or by dinitrogen dissociation and recapture concurrent with the formation of a five-coordinate iron(II) dihydride (Figure 5.7). These experiments highlight that the metal center in these PNP ligated iron complexes remains in the ferrous oxidation state, as stabilized by the highly electron donating properties of the chelate.

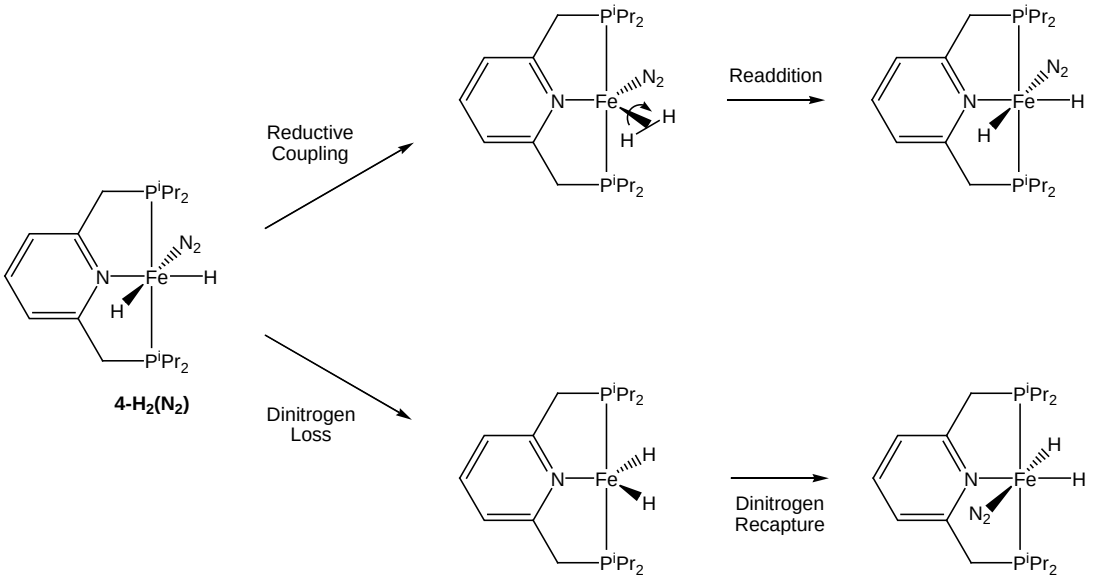

Figure 5.7. Routes of hydride exchange for **4-H_2(N_2)**.

Addition of 1 equivalent of phenylsilane to **4-H_2(N_2)** resulted in the replacement of one hydride ligand with a silyl substituent, yielding a bright orange complex identified as (^{iPr}PNP)FeH(SiH_2Ph)N_2 (**4-H(SiH_2Ph)N_2**) (Figure 5.6). Conveniently, treatment of **4-Cl_2** with 2 equivalents of $NaBEt_3H$ in the presence of phenylsilane generated **4-H(SiH_2Ph)N_2** in good yield. Silyl substitution occured *trans* to the chelate pyridine, as expected from the strong *trans*-influence of both the hydride and the silyl substituents.[23] Unlike **4-H_2(N_2)**, this complex was indefinitely stable at ambient temperature in benzene-d_6. Attempts to perform this substitution with more substituted silanes led to complicated reaction mixtures of undetermined composition.

Examination of **4-H(SiH$_2$Ph)N$_2$** by ^{1}H NMR spectroscopy in benzene-d_6 revealed a triplet at -13.12 ppm with a J_{PH} value of 58 Hz, due to coupling with two equivalent phosphine environments. The proton decoupled ^{31}P NMR spectrum exhibited a single resonance at 96.85 ppm, further establishing equivalence phosphines. As observed for **4-H$_2$(N$_2$)**, chelate isopropyl and backbone methylene resonances consistent with a C_s-symmetric molecule were located by ^{1}H and $\{^1H\}^{13}C$ NMR spectroscopy. In the ^{1}H NMR spectrum, resonances for magnetically inequivalent silane hydrogen atoms were observed as partially overlapping triplets centered at 4.94 ppm.

Similar to **4-H$_2$(N$_2$)**, the relaxation rate of the iron hydride was determined in order to exclude the possibility that this complex can be described as an iron(0) η^2-silane complex. At -50 °C, a T_1(min) value of 368 ms was observed, again consistent with an iron hydride. EXSY NMR spectroscopy, using a 500 ms mixing time, demonstrated that the iron hydride and silyl hydrogens do not exchange on this timescale at ambient temperature. These observations taken together suggest that reversible reductive formation of an iron-silane σ-complex that undergoes fast σ-bond exchange has a higher barrier than the hydride exchange observed for **4-H$_2$(N$_2$)**. Formulation of **4-H(SiH$_2$Ph)N$_2$** as an iron(II) complex further supports the electron donating ability of the PNP chelate to favor oxidative addition.

Confirmation of an octahedral complex with dinitrogen occupying the sixth coordination site was again obtained by infrared spectroscopy. A strong N≡N stretch centered at 2032 cm^{-1}(KBr) was identified, 16 cm^{-1} higher in frequency than that observed for **4-H$_2$(N$_2$)**. This suggests a more electropositive iron center in **4-H(SiH$_2$Ph)N$_2$** than **4-H$_2$(N$_2$)**, rationalizing the observed difference in stability between the two complexes. The dinitrogen stretches of these compounds allow for a fairer approximation of the different electronic environments imparted by the PDI and PNP

ligands, by comparing the two iron(II) complexes. In the solid state, **1-$(N_2)_2$** has dinitrogen stretching frequencies of 2124 and 2053 cm^{-1}, demonstrating that the π-acidic PDI ligand in **1-$(N_2)_2$** clearly fosters two electrons.

The stability of **4-H(SiH_2Ph)N_2** in solution at 23 °C allowed for crystal growth and the determination of the solid-state structure by X-ray diffraction (Figure 5.8). Dinitrogen coordination and the *trans* arrangement of the silyl and pyridine substituents were confirmed and all of the hydrogen atoms, including the iron hydride, were located and refined. The metrical parameters (Table 5.2) reveal a distorted octahedral geometry for this complex, with a P(1)-Fe(1)-P(2) angle of 161.12(2) Å.

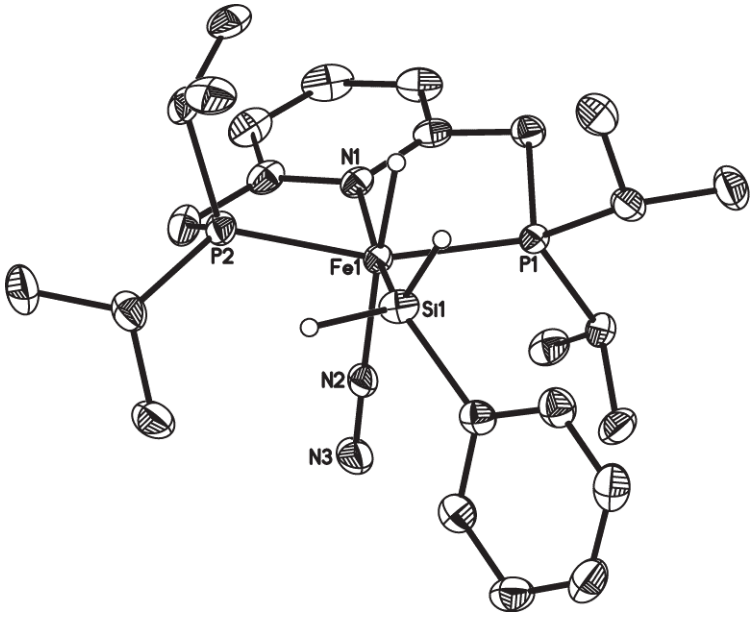

Figure 5.8. Molecular structure of **4-H(SiH_2Ph)N_2** with 30% probability ellipsoids. Hydrogen atoms, expect for the iron-hydride and silicon hydrogens, omitted for clarity.

The iron-hydride is canted towards the silyl ligand with an H(1M)-Fe(1)-Si(1) angle of 76.6(7)°, suggesting a weak silicon-hydrogen interaction. However, the distance between these atoms is 2.420(17) Å, which is significantly outside the sum of the covalent radii of the atoms (~1.45 Å). As expected, the N(2)-N(3) bond distance of

1.120(2) Å is consistent with a weakly activated dinitrogen ligand. The crystallographically determined Fe(1)-H(1M) bond distance of 1.512(19) Å is in the range typically observed for iron-hydrides.[24-26] Importantly, no evidence for pyridine reduction or dearomatization[4,6] is observed in the chelate bond distances, supporting the assertion that PNP acts purely as a σ-donating chelate.

Table 1.2. Metrical parameters for **4-H(SiH$_2$Ph)N$_2$**.

Distance (Å)			Angle (°)
Fe(1)-H(1M)	1.512(19)	P(1)-Fe(1)-P(2)	161.12(2)
Fe(1)-P(1)	2.1823(5)	N(1)-Fe(1)-Si(1)	165.90(4)
Fe(1)-P(2)	2.1817(5)	H(1M)-Fe(1)-N(2)	173.3(7)
Fe(1)-N(1)	2.0370(15)	N(1)-Fe(1)-N(2)	96.82(6)
Fe(1)-Si(1)	2.2718(6)	Si(1)-Fe(1)-N(2)	97.04(5)
Fe(1)-N(2)	1.8002(17)	H(1M)-Fe(1)-P(1)	80.6(7)
N(2)-N(3)	1.120(2)	H(1M)-Fe(1)-P(2)	86.6(7)
Si(1)-H(1M)	2.420(17)	H(1M)-Fe(1)-Si(1)	76.6(7)

A series of ligand substitution reactions were conducted for both **4-H$_2$(N$_2$)** and **4-H(SiH$_2$Ph)N$_2$**. Addition of 4 atmospheres of carbon monoxide to **4-H$_2$(N$_2$)** resulted in immediate formation of **4-(CO)$_2$** along with liberation of H_2 and N_2 (Figure 5.9). On the other hand, monitoring the same addition to **4-H(SiH$_2$Ph)N$_2$** resulted in the formation of a new diamagnetic complex identified as **4-H(SiH$_2$Ph)(CO)** (Figure 5.9). Slow conversion of **4-H(SiH$_2$Ph)(CO)** to **4-(CO)$_2$** under an atmosphere of CO in benzene-d_6 was observed upon heating the reaction mixture to 95°C for weeks. This

difference in reactivity provides evidence that the barrier to reductively eliminate phenylsilane from **4-H(SiH$_2$Ph)(CO)** is much higher than the elimination of dihydrogen from **4-H$_2$(N$_2$)**, correlating to the respective stability of each complex.

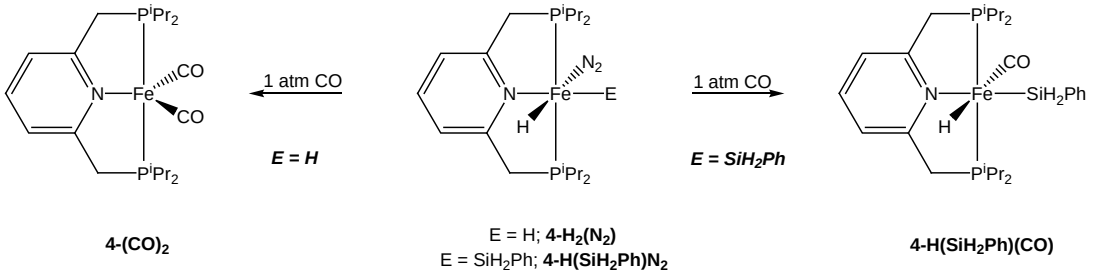

Figure 5.9. Reactivity of **4-H$_2$(N$_2$)** and **4-H(SiH$_2$Ph)N$_2$** towards carbon monoxide.

Evidence for ligand exchange was obtained by infrared spectroscopy, where a strong carbonyl stretch centered at 1879 cm^{-1} was observed. This red shift compared to the stretches observed for **4-(CO)$_2$** correlates with the different metal oxidation state between the two complexes. Similar ^{1}H and ^{31}P NMR features to **4-H(SiH$_2$Ph)N$_2$** were observed for **4-H(SiH$_2$Ph)(CO)**; a triplet (J_{PH} = 55 Hz) centered at -6.41 ppm was observed by ^{1}H NMR spectroscopy along with a proton decoupled singlet at 103.86 ppm in the ^{31}P spectrum.

Additionally, **4-H(SiH$_2$Ph)(CO)** was characterized by single-crystal X-ray diffraction. The molecular structure, with refined iron hydride and silyl hydrogen atoms, is presented in Figure 5.10 and selected metrical parameters are reported in Table 5.3. The distorted octahedral geometry around iron is strikingly similar to that observed in **4-H(SiH$_2$Ph)N$_2$** (Figure 5.8), with a P(1)-Fe(1)-P(2) angle of 160.761(19)°. Again, a weak interaction between the iron hydride and silyl substituent was observed, with a Si(1)-Fe(1)-H(1) angle of 75.9(9)° and Si(1)-H(1) distance of 2.41(2) Å. The C(26)-O(1) bond distance of 1.1635(19) Å is slightly contracted

compared to the carbonyl distances observed for **4-(CO)$_2$** (1.1734(11) Å), as expected for the less reducing iron (II) metal center.

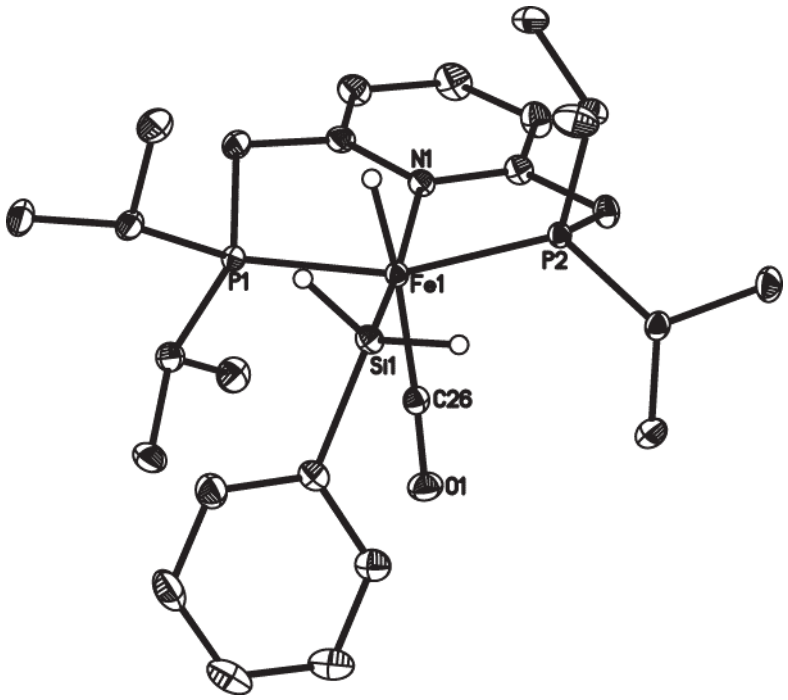

Figure 5.10. Molecular structure of **4-H(SiH$_2$Ph)(CO)** with 30% probability ellipsoids. Hydrogen atoms, expect for the iron-hydride and silicon hydrogens, omitted for clarity.

Treatment of **4-H(SiH$_2$Ph)N$_2$** with a stoichiometric amount of trimethylphosphine also resulted in the liberation of dinitrogen and the formation of (^{iPr}PNP)FeH(SiH$_2$Ph)(PMe$_3$) (**4-H(SiH$_2$Ph)(PMe$_3$)**) as determined by multinuclear NMR spectroscopy and combustion analysis (Figure 5.11). Two-dimensional NOESY NMR spectroscopy was used to determine the overall geometry of this complex. Cross-peaks observed between the iron-hydride and both the silicon and *ortho*-phenyl hydrogens of the silyl ligand, established the same *cis* configuration as observed in the other complexes discussed previously. Accordingly, cross-peaks between the iron-hydride and PMe$_3$ ligand were not observed. In the ^{1}H NMR spectrum of this complex

in benzene-d_6, the iron-hydride resonance centered at -9.97 ppm is expectedly split into a triplet of doublets. However, upon closer examination, the hydride coupling to the *cis* chelate phosphines is 67.0 Hz while coupling to the *trans* PMe_3 ligand is only 21.0 Hz. This abnormality (*trans* J_{PH} values are typically larger for octahedral complexes) is likely a result of the distortion from idealized octahedral geometry observed for this class of compounds. To this end, any deviance of the H-Fe-PMe_3 bond angle from linearity would greatly attenuate the iron-phosphorous coupling constant.

Table 5.3. Selected metrical parameters for **4-H(SiH$_2$Ph)(CO)**.

Distance (Å)			Angle (°)
Fe(1)-H(1M)	1.522(15)	P(1)-Fe(1)-P(2)	160.761(19)
Fe(1)-P(1)	2.1780(5)	N(1)-Fe(1)-Si(1)	167.02(4)
Fe(1)-P(2)	2.1827(4)	H(1M)-Fe(1)-C(26)	166.2(9)
Fe(1)-N(1)	2.0605(13)	N(1)-Fe(1)-C(26)	102.36(6)
Fe(1)-Si(1)	2.2689(5)	Si(1)-Fe(1)-C(26)	90.46(5)
Fe(1)-C(26)	1.7541(16)	H(1M)-Fe(1)-P(1)	81.8(9)
C(26)-O(1)	1.1635(19)	H(1M)-Fe(1)-P(2)	85.6(9)
Si(1)-H(1M)	2.41(2)	H(1M)-Fe(1)-Si(1)	75.9(9)

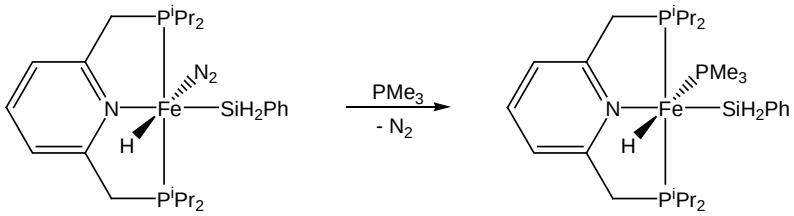

4-H(SiH$_2$Ph)N$_2$ **4-H(SiH$_2$Ph)(PMe$_3$)**

Figure 5.11. Ligand substitution to prepare **4-H(SiH$_2$Ph)(PMe$_3$)**.

The observation of these unusual coupling constants sparked our interest in further examination of the coupling constants of the crystallographically characterized molecules **4-H(SiH$_2$Ph)N$_2$** and **4-H(SiH$_2$Ph)(CO)**, in an attempt to further substantiate this proposal. The ^{13}C labeled isotopologue of **4-H(SiH$_2$Ph)(CO)**, **4-H(SiH$_2$Ph)(**^{13}**CO)**, was prepared from straightforward addition of ^{13}CO to **4-H(SiH$_2$Ph)N$_2$**. This complex allowed determination of the *trans* H-Fe-^{13}C coupling constant of 10.5 Hz. This value is smaller than the *cis* P-Fe-^{13}C coupling constant of 14.0 Hz in the same complex, however, work by Whitesides and Maglio has demonstrated that H-M-^{13}C coupling constants do not necessarily translate to the stereochemistry of the complex.[27] The *cis* H-Fe-Si coupling constants of **4-H(SiH$_2$Ph)N$_2$**, **4-H(SiH$_2$Ph)(CO)**, and **4-H(SiH$_2$Ph)(PMe$_3$)** were determined from the ^{1}H NMR spectra of these complexes and found to be 28.0, 25.0, and 12.5 Hz, respectively. The smaller J_{SiH} value observed for **4-H(SiH$_2$Ph)(PMe$_3$)** may be related to electronic effects imparted by the ligand that occupies the sixth coordination site.

5.4 Evaluation of Catalytic Activity

After studying various ligand substitution reactions and establishing that dinitrogen loss is facile and reductive coupling of X-type ligands occurs for both **4-H$_2$(N$_2$)** and of **4-H(SiH$_2$Ph)N$_2$** at ambient temperature, the catalytic activity of both

complexes was assayed. The hydrogenation and hydrosilylation of unactivated olefins such as 1-hexene and cyclohexene were chosen as initial targets to enable comparison of these PNP species with bis(imino)pyridine iron.[9] Complete hydrogenation (as judged by GC) of 1-hexene using a 0.3 mol % catalyst loading of **4-H_2(N_2)** was accomplished upon stirring for 3 hours at 23 °C. Hydrogenation of 1-hexene with this complex is much slower than for **1-(N_2)$_2$**, where turnover frequencies of greater than 1800 hr^{-1} were observed. Attempts to hydrogenate cyclohexene proved to be even more disappointing. Using the same conditions, only minimal conversion of cyclohexene to cyclohexane (~10 %) after either 6 or 24 hours was observed. Similar conversion at longer reaction times suggests that the rate of catalyst decomposition (as discussed in section 5.3) is competitive with the rate of hydrogenation under these reaction conditions. The hydrosilylation of olefins or alkynes was not accomplished using **4-H(SiH_2Ph)N_2** as a catalyst precursor.

To better understand the observed lack of catalytic competency, the addition of dihydrogen to **4-H_2(N_2)** was studied. Upon adding 4 atmospheres of H_2, gradual disappearance of **4-H_2(N_2)** was noted along with the formation of a new iron-hydride containing complex as evidenced by ^{1}H NMR spectroscopy. The iron-hydride resonance for this newly formed product was observed as a broad singlet ($\Delta\nu_{1/2}$= 12 Hz) at -11.17 ppm, indicative of an iron dihydride dihydrogen complex with rapidly equilibrating hydrogen ligands (Figure 5.12).[26] Cooling this complex, tentatively assigned as **4-H_2(H_2)**, to 193 K in toluene-d_8 solution resulted in gradual broadening of the peak ($\Delta\nu_{1/2}$= 46 Hz) but not resolution of the hydrides. Definitive characterization of this complex was not achieved by NMR spectroscopy, elemental analysis, or X-ray crystallography due to facile PNP chelate loss in solution. Figure 5.12 depicts the η^2-dihydrogen ligand of **4-H_2(H_2)** *trans* to a hydride rather than the chelate pyridine because of the strong *trans* influence of hydride ligands; however, a

structure with *trans* hydrides may be accessed during the course of hydride exchange. Addition of D_2 to **4-H_2(N_2)** resulted in fast isotopic exchange into the iron hydride positions of this complex, suggesting that dinitrogen loss and recapture concurrent with displacement of H_2 or its isotopologues is operative. Exposing either **4-H_2(H_2)** or **4-D_2(D_2)** to 1 atmosphere of N_2 resulted in immediate formation of either **4-H_2(N_2)** or **4-D_2(N_2)**; further demonstrating the preference for π-accepting ligands at the electron rich metal center.

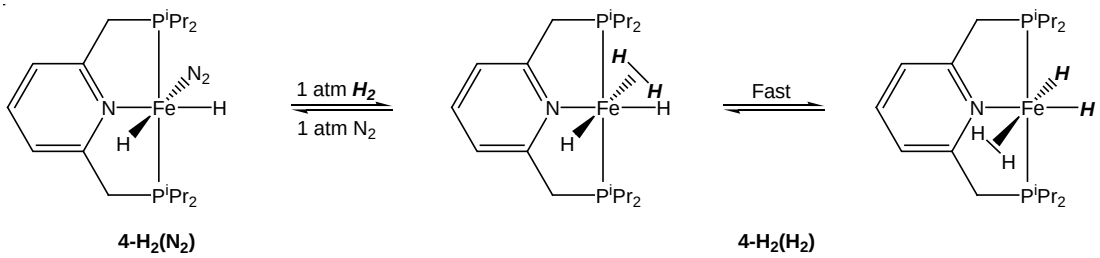

Figure 5.12. Formation of **4-H_2(H_2)** along with iron-hydride equilibration.

In order to circumvent the poor solution stability of **4-H_2(N_2)**, dihydrogen addition to the more robust **4-H(SiH_2Ph)N_2** was explored. Under 4 atmospheres of H_2, the ^{1}H NMR resonances for **4-H(SiH_2Ph)N_2** slowly decreased in intensity over the course of 20 hours as a new set of resonances for **4-H(SiH_2Ph)(H_2)**, including a broad iron hydride resonance at -9.37 ppm corresponding to 3 protons, grew in. Observation of both **4-H(SiH_2Ph)N_2** and **4-H(SiH_2Ph)(H_2)** simultaneously (Figure 5.13) is attributed to slow dissociation of N_2 in this substitution reaction.

As with **1-H_2(H_2)**, the observation of a broad iron-hydride resonance by ^{1}H NMR spectroscopy demonstrates rapid exchange between the iron-hydride and η^2-dihydrogen ligand. The benzene-d_6 EXSY NMR spectrum of this complex conducted with a 500 ms mixing time, established no exchange between the hydride, dihydrogen, or silyl substituents on this timescale. Based on these observations, the isomer where

the hydride and η^2-dihydrogen ligands are *trans* to one another was ruled out as the ground state structure; however, this must be accessible during hydrogen equilibration (Figure 5.13).

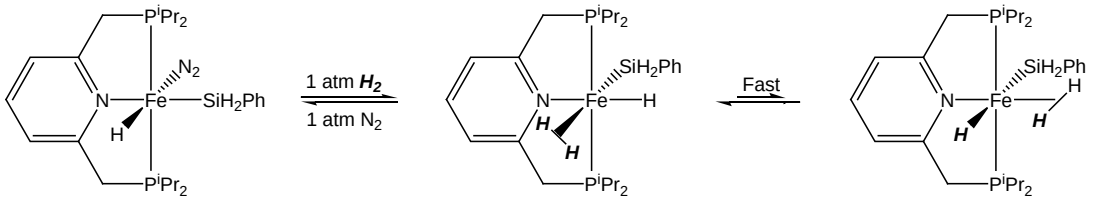

Figure 5.13. Conversion of **4-H(SiH$_2$Ph)N$_2$** to **4-H(SiH$_2$Ph)(H$_2$)** under 4 atmospheres of H_2 in benzene-d_6.

In order to probe the accessibility of a phenylsilane σ-complex, **4-H(SiH$_2$Ph)N$_2$** was treated with 4 atmospheres of D_2. As expected, the iron-hydride resonance in **4-H(SiH$_2$Ph)N$_2$** disappeared rapidly and free H-D gas was observed by ^{1}H NMR spectroscopy. At longer reaction times, the silicon hydrogen resonances for this complex also disappeared, establishing isotopic exchange into this position and intermediacy of a silane σ-complex (Figure 5.14). Dissociation of H-D likely occurs from the coordination site *trans* to the silyl substituent following deuterium exchange into the iron hydride through an intermediate σ-complex, consistent with its observation at early reaction times.

To understand further the inability of **4-H(SiH$_2$Ph)N$_2$** to hydrosilylate olefins or alkynes, addition of large excesses of these substrates was investigated. Adding approximately 50 equivalents of 2-butyne to **4-H(SiH$_2$Ph)N$_2$** in benzene-d_6 at ambient temperature resulted in immediate loss of the ^{iPr}PNP ligand, as determined by ^{1}H and ^{31}P NMR spectroscopy. Evidence for alkyne insertion was obtained by mass spectroscopy and NMR spectroscopy due to the observation of PhSiH(C(CH$_3$)=CH(CH$_3$))$_2$. Large quantities of hexamethylbenzene were also

observed, suggesting that iron catalyzed cyclotrimerization of 2-butyne also occurred throughout the course of the reaction under these conditions.

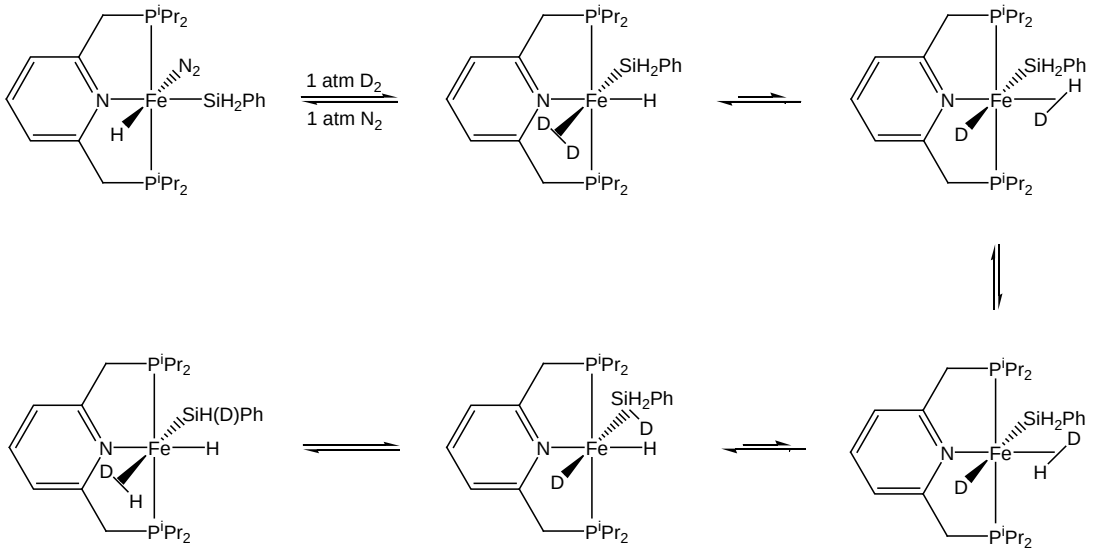

Figure 5.14. Proposed pathway for isotopic exchange in **4-H(SiH$_2$Ph)N$_2$** upon treatment with D_2 gas.

Adding a large excess of either 1-hexene or cyclohexene to **4-H(SiH$_2$Ph)N$_2$** produced no change in the ^{1}H NMR spectrum of this complex over the course of several days at 23 °C. Addition of excess ethylene caused the precipitation of an insoluble organometallic product of unknown composition along with the formation of diethylphenylsilane. This organometallic precipitate, which liberated ^{iPr}PNP upon degradation with water, was unreactive towards olefins or silanes; offering insight into the inability of **4-H(SiH$_2$Ph)N$_2$** to catalyze olefin hydrosilylation.

5.5 Discussion

Although **4-H$_2$(N$_2$)** is an inferior catalyst precursor for the hydrogenation of olefins, there have only been a few phosphine ligated iron complexes reported that mediate this transformation.[28-31] In order to prepare cheap and environmentally benign

alternatives to industrially viable precious metal catalysts; one main objective of this field has been the development of enantioselective iron catalysts, a goal that has only recently been accomplished.[30,31] This work has helped lay the foundation of phosphine-ligated iron hydrogenation catalysis; an area of research truly in its infancy.

The mechanistic investigations conducted in this work shed additional light on what is known about iron-hydride dihydrogen complexes. Most known examples containing this structural motif are cationic bis(diphosphine) compounds in which the hydride and η^2-dihydrogen ligands are in a *trans* configuration.[32-35] Other cationic examples where these ligands are in a *cis* confirmation have been reported and these complexes generally contain tetradentate phosphine ligands.[36-39] One neutral example, most similar to the complexes in this work, is $(Ph_2EtP)_3FeH_2(H_2)$.[40] Variable temperature NMR and neutron diffraction studies established this complex as an iron(II) dihydride dihydrogen complex that exhibits rapid iron hydride exchange on the NMR timescale.[26] A *cis*-effect, or electrostatic interaction between the ligands, has been implicated as the origin of this exchange, rather than a formal oxidation to Fe(IV).[26] It is likely that a similar phenomenon is operative in our system for both **4-$H_2(H_2)$** and **4-$H(SiH_2Ph)(H_2)$**. Although this *cis*-effect concept has not been applied to explain facile exchange between a hydride and silyl substituent, we believe this process occurs and is slightly less favored than the same effect between hydride and η^2-dihydrogen ligands. Also, it is likely that **4-$H_2(H_2)$** hydrogenates 1-hexene by an iron(0)-iron(II) couple rather than relying on a redox-active ligand to keep the metal oxidation state constant.

5.6 Conclusions

A series of catalytically active bis(diisopropylphosphinomethyl)pyridine iron complexes have been prepared and their reactivity has been studied. Infrared

spectroscopy and X-ray crystallographic studies of these complexes, along with ligand substitution reactions, established the highly electron donating properties of the ^{iPr}PNP ligand. Both the iron dihydride and silyl hydride complexes cordinate π-accepting ligands such as dinitrogen or carbon monoxide in the sixth available coordination site, leading to the isolation of the corresponding distorted octahedral Fe (II) complexes. Although poor catalytic activity was observed for these complexes because of competing chelate loss, NMR spectroscopic studies along with deuterium labeling experiments established facile iron hydride exchange with either dihydrogen or phenylsilane. This work ultimately suggests that in the design of new catalytic iron systems, the electronic properties of the ligand are of utmost importance.

5.7 Experimental Procedures

General Considerations. All air- and moisture-sensitive manipulations were carried out using standard vacuum line, Schlenk, and cannula techniques or in an MBraun drybox containing an atmosphere of purified nitrogen. The MBraun drybox was equipped with a cold well designed for freezing samples in liquid nitrogen. Solvents for all air- and moisture-sensitive manipulations were initially dried and deoxygenated using literature procedures.[41] Argon and hydrogen gas were purchased from Airgas Incorporated and passed through a column containing manganese oxide supported on vermiculite and 4 Å molecular sieves before admission to the high vacuum line. Benzene-d_6 was purchased from Cambridge Isotope Laboratories and distilled from 4 Å molecular sieves under an atmosphere of argon and stored over 4 Å molecular sieves and sodium metal. Carbon monoxide was purchased from Aldrich and passed through a liquid-nitrogen cooled trap before use. Ethylene was purchased from Aldrich, passed through a liquid-nitrogen cooled trap, and stored over a slurry of activated MAO in toluene before use. Sodium triethylborohydride was obtained from

Aldrich in a 1.0 M solution in toluene and used as received. Phenylsilane, 1-hexene, cyclohexene, trimethylphosphine, and 2-butyne were purchased from Acros or Aldrich and dried over activated molecular sieves before use. The method used to prepare **1-Cl_2** and **1-Br_2** was initially published by Milstein and co-workers.[14]

^1H, ^{13}C, and ^{31}P NMR spectra were recorded at 399.780 or 500.62, 101.535 or 125.893, and 161.833 or 202.648 MHz, respectively, using Inova 400 and 500 spectrometers. ^1H and $\{^1H\}^{13}C$ NMR chemical shifts are reported in ppm from tetramethylsilane using the chemical shifts of the solvent as a secondary standard. $\{^1H\}^{31}P$ NMR and ^{31}P chemical shifts are reported relative to H_3PO_4 and referenced to an external 85% H_3PO_4 solution. Single crystals suitable from X-ray diffraction were coated with polyisobutylene oil in a drybox and were quickly transferred to the goniometer head of a Bruker X8 APEX2 system equipped with a molybdenum X-ray tube (λ =0.71073 Å). Preliminary data revealed the crystal system. A hemisphere routine was used for data collection and determination of lattice constants. The space group was identified and the data were processed using the Bruker SAINT program and corrected for absorption using SADABS. The structures were solved using direct methods (SHELXS), completed by subsequent Fourier synthesis, and refined by full-matrix least-squares procedures. Elemental analyses were performed at Robertson Microlit Laboratories, Inc. in Madison, NJ.

Preparation of [(2,6-^{i}$Pr_2PCH_2)_2C_5H_3N$]$FeCl_2$ (4-Cl_2). A 500 mL round-bottomed flask was charged with 4.64 g (13.67 mmol) of (2,6-^{i}$Pr_2PCH_2)_2C_5H_3N$ and approximately 150 mL of tetrahydrofuran. While stirring, 1.73g (13.67 mmol) of $FeCl_2$ was added and the yellow mixture turned orange and a precipitate formed within minutes. After stirring for 24 hours, the mixture was washed through a frit with chloroform and the solvent was evacuated. The resulting yellow solid was washed

three times with 20 mL of pentane and dried to yield 6.25 g (98%) **4-Cl_2**. Analysis for $C_{19}H_{35}Cl_2FeNP_2$: Calc. C, 48.95; H, 7.57; N 3.00. Found: C, 48.48; H, 7.50; N, 2.89. Magnetic Susceptibility (chloroform-*d*, 293 K): $\mu_{eff} = 5.5\ \mu_B$. ^{1}H NMR (chloroform-*d*, 293 K): δ = 95.79 (269, 4H, PCH_2), 45.15 (65, 2H, *m-pyr*), 32.86 (325 Hz, 4H, CH(CH_3)$_2$), 11.23 (112 Hz, 12H, CH(CH_3)$_2$)), 6.81 (146 Hz, 12H, CH(CH_3)$_2$)), -7.94 (40 Hz, 1H, *p-pyr*).

Preparation of [(2,6-^{i}Pr_2PCH_2)$_2$$C_5H_3N$]$FeBr_2$ (4-Br_2). This molecule was prepared in a similar manner to **4-Cl_2** with 2.00 g (5.89 mmol) of (2,6-^{i}Pr_2PCH_2)$_2$$C_5H_3N$ and 1.27 g (5.89 mmol) of $FeBr_2$ to yield 3.07 g (94%) of a yellow solid identified as **4-Br_2**. Analysis for $C_{19}H_{35}Br_2FeNP_2$: Calc. C, 41.11; H, 6.36; N 2.52. Found: C, 41.22; H, 6.61; N, 2.46. Magnetic Susceptibility (chloroform-*d*, 293 K): $\mu_{eff} = 5.1\ \mu_B$. ^{1}H NMR (chloroform-*d*, 293 K): δ = 97.52 (194 Hz, 4H, PCH_2), 48.37 (34 Hz, 2H, *m-pyr*), 37.39 (190 Hz, 4H, CH(CH_3)$_2$), 12.18 (79 Hz, 12H, CH(CH_3)$_2$)), 7.58 (91 Hz, 12H, CH(CH_3)$_2$)), -8.36 (20 Hz, 1H, *p-pyr*).

Preparation of [(2,6-^{i}Pr_2PCH_2)$_2$$C_5H_3N$]$Fe(CO)_2$ (4-$(CO)_2$). A dried thick walled reaction vessel was charged with 0.500 g (0.901 mmol) of **4-Br_2** and approximately 50 mL of pentane. An amalgam prepared from 0.104 g (4.51 mmol) of sodium metal and 21.7 g (901 mmol) of mercury was added to the bomb, which was quickly submerged in liquid nitrogen to prevent reaction. An excess of carbon monoxide was admitted to the reaction vessel and the solution warmed to ambient temperature. Within minutes of stirring, the colorless solution turned royal blue in color and the reaction was allowed to stir for 48 hours to ensure complete conversion. The solution was then filtered through Celite with tetrahydrofuran and the solvent was evacuated to yield 0.394 g (97%) of a red solid identified as **4-$(CO)_2$**. Analysis for $C_{21}H_{35}FeNO_2P_2$: Calc. C,

55.89; H, 7.82; N 3.10. Found: C, 55.36; H, 7.65; N, 2.77. ^{1}H NMR (benzene-d_6): δ = 6.55 (t, J_{HH} = 7.0 Hz, 1H, *p-pyr*), 6.34 (d, J_{HH} = 7.0 Hz, 2H, *m-pyr*), 2.79 (m, 4H, PCH_2), 2.16 (m, 4H, CH(CH_3)$_2$), 1.23 (pseudo q, J_{HH} = 6.5 Hz, 12H, CH(CH_3)$_2$), 1.17 (pseudo q, J_{HH} = 6.5 Hz, 12H, CH(CH_3)$_2$). ^{13}C NMR (tetrahydrofuran-d_8): δ = 162.49 (t, J_{PC} = 6.0 Hz, *o-pyr*), 131.15 (s, *p-pyr*), 119.28 (t, J_{PC} = 5.0 Hz, *m-pyr*), 41.15 (t, J_{PC} = 8.5 Hz, PCH$_2$), 28.80 (t, J_{PC} = 10.5 Hz, CH(CH_3)$_2$), 18.74 (s, CH(CH$_3$)$_2$), 18.72 (s, CH(CH$_3$)$_2$). {^{1}H}^{31}P NMR (tetrohydrofuran-d_8): δ = 109.59 (s). IR (KBr): ν_{CO} = 1794, 1842 cm^{-1}.

Characterization of [(2,6-^{i}Pr$_2$PCH$_2$)$_2$C$_5$H$_3$N]FeCl(Me) (4-Cl(Me)). A 25 mL round-bottomed flask was charged with 0.100 g (0.216 mmol) of **4-Cl$_2$** and approximately 10 mL of pentane. A second solution of 0.432 mmol of methyllithium in 5 mL of pentane was added slowly dropwise. After about 1 hour, the red solution was filtered through Celite and the solvent was evacuated. ^{1}H NMR spectroscopy revealed peaks consistent with **4-Cl(Me)**. ^{1}H NMR (benzene-d_6, 293 K): δ = 26.33 (17 Hz, 2H, *m-pyr*), -14.33 (35 Hz, 6H, CH(CH_3)$_3$), -19.72 (29 Hz, 6H, CH(CH_3)$_3$), -21.74 (24 Hz, 6H, CH(CH_3)$_3$), -24.47 (21 Hz, 6H, CH(CH_3)$_3$), -40.54 (44 Hz, 4H, PCH_2), -60.89 (45 Hz, 2H, CH(CH_3)$_3$), -64.05 (42 Hz, 2H, CH(CH_3)$_3$), -169.16 (116 Hz, 1H, *p-pyr*).

Preparation of [(2,6-^{i}Pr$_2$PCH$_2$)$_2$C$_5$H$_3$N]FeH$_2$(N$_2$) (4-H$_2$(N$_2$)). A 100 mL round-bottomed flask was charged with 1.00 g (2.16 mmol) of **4-Cl$_2$** and approximately 50 mL of diethyl ether. This mixture was chilled in a liquid nitrogen cooled cold well for 15 minutes and then thawed. While stirring, 0.542 g (4.32 mmol) of sodium triethylborohydride (from 1.0 M solution in toluene) was added slowly dropwise and the reaction mixture immediately turned dark purple in color. After stirring for 1 hour,

the solution was filtered through Celite and the solvent was evacuated. The resulting residue was washed three times with diethyl ether to yield 0.333 g (36%) of a reddish-orange solid identified as **4-$H_2(N_2)$**. Analysis for $C_{19}H_{37}FeN_3P_2$: Calc. C, 53.66; H, 8.77; N 9.88. Found: C, 53.95; H, 8.46; N, 10.18. ^{1}H NMR (benzene-d_6): δ = 6.63 (t, J_{HH} = 7.0 Hz, 1H, *p-pyr*), 6.48 (d, J_{HH} = 7.0 Hz, 2H, *m-pyr*), 3.05 (m,1H, PCH_2), 3.08 (m,1H, PCH_2), 2.91 (m,1H, PCH_2), 2.88 (m,1H, PCH_2), 2.29 (m, 2H, CH(CH_3)$_2$), 1.94 (m, 2H, CH(CH_3)$_2$), 1.31 (m, 12H, CH(CH_3)$_2$), 1.21 (pseudo q, J_{HH} = 7.0 Hz, 6H, CH(CH_3)$_2$), 0.91 (pseudo q, J_{HH} = 7.0 Hz, 6H, CH(CH_3)$_2$), -12.54 (td, J_{HH} = 21.5 Hz, J_{PH} = 60.5 Hz, 1H, Fe-H), -17.65 (td, J_{HH} = 21.5 Hz, J_{PH} = 52.0 Hz, 1H, Fe-H). ^{13}C NMR (benzene-d_6): δ = 164.47 (t, J_{PC} = 6.0 Hz, *o-pyr*), 130.57 (s, *p-pyr*), 118.07 (t, J_{PC} = 4.5 Hz, *m-pyr*), 41.70 (t, J_{PC} = 5.5 Hz, PCH$_2$), 27.77 (t, J_{PC} = 6.5 Hz, CH(CH_3)$_2$), 26.74 (t, J_{PC} = 14.0 Hz, CH(CH_3)$_2$), 20.15 (s, CH(CH$_3$)$_2$), 20.04 (s, CH(CH$_3$)$_2$), 19.22 (s, CH(CH$_3$)$_2$), 19.06 (s, CH(CH$_3$)$_2$). {^{1}H}^{31}P NMR (benzene-d_6): δ = 108.28 (s). ^{31}P NMR (benzene-d_6): δ = 108.28 (t, J_{PH} = 52.0 Hz). IR (KBr): ν_{NN} = 2016 cm^{-1}.

Preparation of [(2,6-^{i}Pr$_2$PCH$_2$)$_2$C$_5$H$_3$N]FeH(SiH$_2$Ph)(N$_2$) (4-H(SiH$_2$Ph)(N$_2$)). A 100 mL round-bottomed flask was charged with 0.635 g (1.36 mmol) of **4-Cl_2**, 0.147 g (1.36 mmol) of phenylsilane, and approximately 60 mL of diethyl ether. After chilling the solution in a cold well for 15 minutes, 0.332 g (2.73 mmol) of sodium triethylborohydride (from 1.0 M solution in toluene) was added slowly dropwise while stirring. After 3 hours, the orange reaction mixture was filtered through Celite and the solvent was evacuated. Recrystallization of the resulting residue from pentane at -35 °C yielded 0.588 g (81 %) of an orange solid identified as **4-H(SiH_2Ph)(N_2)**. Analysis for $C_{25}H_{43}FeN_3P_2Si$: Calc. C, 56.49; H, 8.15; N 7.91. Found: C, 56.53; H, 8.37; N, 7.64. ^{1}H NMR (benzene-d_6): δ = 8.15 (m, 2H, *o-phenyl*), 7.35 (m, 2H, *m-phenyl*), 7.23 (m, 1H, *p-phenyl*), 6.68 (t, J_{HH} = 7.5 Hz, 1H, *p-pyr*), 6.48 (d, J_{HH} = 7.5 Hz, 2H, *m-*

pyr), 4.94 (td, J_{HH} = 1.0 Hz, J_{PH} = 5.5 Hz, 2H, Si*H*$_2$), 2.99 (m, 1H, PC*H*$_2$), 2.95 (m, 1H, PC*H*$_2$), 2.73 (m, 1H, PC*H*$_2$), 2.69 (m, 1H, PC*H*$_2$), 2.39 (m, 2H, C*H*(CH$_3$)$_2$), 2.16 (m, 2H, C*H*(CH$_3$)$_2$), 1.26 (m, 12H, CH(C*H*$_3$)$_2$), 0.94 (pseudo q, J_{HH} = 7.0 Hz, 6H, CH(C*H*$_3$)$_2$), 0.64 (pseudo q, J_{HH} = 7.0 Hz, 6H, CH(C*H*$_3$)$_2$), -13.12 (t, J_{PH} = 57.5 Hz, 1H, Fe-*H*). ^{13}C NMR (benzene-d_6): δ =163.33 (t, J_{PC} = 5.5 Hz, *o-pyr*), 149.48 (s, *ipso-phenyl*), 136.29 (s, *o-phenyl*), 132.78 (s, *p-pyr*), 127.57 (s, *m-phenyl*), 126.79 (s, *p-phenyl*), 118.84 (t, J_{PC} = 4.0 Hz, *m-pyr*), 38.47 (t, J_{PC} = 5.0 Hz, P*C*H$_2$), 27.48 (t, J_{PC} = 7.5 Hz, *C*H(CH$_3$)$_2$), 25.47 (t, J_{PC} = 14.0 Hz, *C*H(CH$_3$)$_2$), 19.20 (s, CH(*C*H$_3$)$_2$), 18.92 (s, CH(*C*H$_3$)$_2$), 18.32 (s, CH(*C*H$_3$)$_2$), 17.87 (s, CH(*C*H$_3$)$_2$). {^{1}H}^{31}P NMR (benzene-d_6): δ = 96.85 (s). IR (KBr): ν_{NN} = 2032 cm^{-1}.

Preparation of [(2,6-^{i}Pr$_2$PCH$_2$)$_2$C$_5$H$_3$N]FeH(SiH$_2$Ph)(CO) (4-H(SiH$_2$Ph)(CO)). To a thick-walled reaction vessel, 0.200 g of **4-H(SiH$_2$Ph)(N$_2$)** and approximately 50 mL of pentane was added. The bomb was submerged in liquid nitrogen, evacuated, and an excess of carbon monoxide was added. After 3 hours of stirring at room temperature, the reaction mixture was green in color. The bomb was evacuated after 48 hours of stirring and the residue was washed twice with 20 mL of pentane. Recrystallization from diethyl ether at -35 °C yielded 0.117 g (56%) of an olive green solid identified as **4-H(SiH$_2$Ph)(CO)**. Analysis for $C_{26}H_{43}FeNOP_2Si$: Calc. C, 58.75; H, 8.15; N, 2.64. Found: C, 58.50; H, 8.03; N, 2.76. ^{1}H NMR (benzene-d_6): δ = 8.21 (d, J_{HH} = 7.5Hz, 2H, *o-phenyl*), 7.33 (t, J_{HH} = 7.5 Hz, 2H, *m-phenyl*), 7.22 (t, J_{HH} = 7.5Hz, 1H, *p-phenyl*), 6.66 (t, J_{HH} = 7.5 Hz, 1H, *p-pyr*), 6.40 (d, J_{HH} = 7.5 Hz, 2H, *m-pyr*), 4.94 (td, J_{HH} = 2.0 Hz, J_{PH} = 5.0 Hz, 2H, Si*H*$_2$), 2.90 (m, 1H, PC*H*$_2$), 2.86 (m, 1H, PC*H*$_2$), 2.76 (m, 1H, PC*H*$_2$), 2.72 (m, 1H, PC*H*$_2$), 2.24 (m, 2H, C*H*(CH$_3$)$_2$), 2.14 (m, 2H, C*H*(CH$_3$)$_2$), 1.35 (pseudo q, J_{HH} = 7.0 Hz, 6H, CH(C*H*$_3$)$_2$), 1.26 (pseudo q, J_{HH} = 7.0 Hz, 6H, CH(C*H*$_3$)$_2$), 0.96 (pseudo q, J_{HH} = 7.0 Hz, 6H, CH(C*H*$_3$)$_2$), 0.67 (pseudo q,

J_{HH} = 7.0 Hz, 6H, CH(C*H*$_3$)$_2$), -6.41 (t, J_{PH} = 55.2 Hz, 1H, Fe-*H*). ^{13}C NMR (benzene-*d*$_6$): δ = 162.86 (t, J_{PC} = 5.5 Hz, *o-pyr*), 149.37 (s, *ipso-phenyl*), 136.38 (s, *o-phenyl*), 133.17 (s, *4-pyr*), 127.52 (s, *m-pyr*), 126.13 (s, *p-phenyl*), 118.69 (t, J_{PC} = 4.5 Hz, *m-pyr*), 39.50 (t, J_{PC} = 6.5 Hz, P*C*H$_2$), 27.00 (t, J_{PC} = 10.0 Hz, *C*H(CH$_3$)$_2$), 25.39 (t, J_{PC} = 13.0 Hz, *C*H(CH$_3$)$_2$), 19.18 (s, CH(*C*H$_3$)$_2$), 18.61 (s, CH(*C*H$_3$)$_2$), 18.03 (s, CH(*C*H$_3$)$_2$), 17.63 (s, CH(*C*H$_3$)$_2$). $\{^1H\}^{31}$P NMR (benzene-*d*$_6$): δ = 103.86 (s). IR (KBr): ν_{CO} = 1879 cm^{-1}.

Preparation of [(2,6-^{i}Pr$_2$PCH$_2$)$_2$C$_5$H$_3$N]FeH(SiH$_2$Ph)(P(CH$_3$)$_3$) (4-H(SiH$_2$Ph)(P(CH$_3$)$_3$)). To a thick-walled reaction vessel, 0.040 g of **4-H(SiH$_2$Ph)(N$_2$)** and approximately 50 mL of diethyl ether was added. The bomb was submerged in liquid nitrogen, evacuated on a high vacuum line, and 1 equivalent of P(CH$_3$)$_3$ was added using a calibrated gas bulb. The mixture was warmed to ambient temperature and allowed to stir for 72 hours. The resulting purple solution was washed through a frit fitted with Celite and the volatiles were removed *in vacuo* to yield 0.035 g (80%) of a dark purple solid identified as **4-H(SiH$_2$Ph)(P(CH$_3$)$_3$)**. Analysis for C$_{28}$H$_{52}$FeNOP$_3$Si: Calc. C, 58.03; H, 9.04; N, 2.42. Found: C, 57.87; H, 9.29; N, 2.31. ^{1}H NMR (benzene-*d*$_6$): δ = 8.32 (d, J_{HH} = 7.5Hz, 2H, *o-phenyl*), 7.53 (t, J_{HH} = 7.5 Hz, 2H, *m- phenyl*), 7.21 (t, J_{HH} = 7.5Hz, 1H, *p-phenyl*), 6.53 (t, J_{HH} = 7.5 Hz, 1H, *p-pyr*), 6.41 (d, J_{HH} = 7.5 Hz, 2H, *m-pyr*), 4.94 (q, J_{PH} = 7.0 Hz, 2H, Si*H*$_2$), 3.05 (m, 1H, PC*H*$_2$), 3.01 (m, 1H, PC*H*$_2$), 2.62 (m, 1H, PC*H*$_2$), 2.58 (m, 1H, PC*H*$_2$), 2.43 (m, 2H, C*H*(CH$_3$)$_2$), 2.16 (m, 2H, C*H*(CH$_3$)$_2$), 1.39 (pseudo q, J_{HH} = 6.5 Hz, 6H, CH(C*H*$_3$)$_2$), 1.29 (pseudo q, J_{HH} = 6.5 Hz, 6H, CH(C*H*$_3$)$_2$), 1.10 (d, J_{PH} = 5.5 Hz, 9H, P(C*H*$_3$)$_3$), 1.07 (pseudo q, J_{HH} = 6.5 Hz, 6H, CH(C*H*$_3$)$_2$), 0.97 (pseudo q, J_{HH} = 6.5 Hz, 6H, CH(C*H*$_3$)$_2$), -9.97 (td, J_{PH} (PMe$_3$) = 21.0 Hz, J_{PH} (P^{i}Pr$_2$) = 67.0 Hz, 1H, Fe-*H*). ^{13}C NMR (benzene-*d*$_6$): δ = 164.13 (t, J_{PC} = 5.5 Hz, *o-pyr*), 150.78 (m, *ipso-phenyl*),

137.66 (s, *o-phenyl*), 128.68 (s, *p-pyr*), 127.06 (s, *m-phenyl*), 126.48 (s, *p-phenyl*), 117.45 (t, J_{PC} = 5.0 Hz, *m-pyr*), 44.26 (t, J_{PC} = 3.0 Hz, P*C*H_2), 32.17 (m, *C*H(CH_3)$_2$), 28.94 (m, *C*H(CH_3)$_2$), 22.15 (d, J_{PC} = 17.0 Hz, P(*C*H_3)$_3$), 20.90 (s, CH(*C*H_3)$_2$), 20.63 (s, CH(*C*H_3)$_2$), 20.11 (s, CH(*C*H_3)$_2$), 19.89 (s, CH(*C*H_3)$_2$). $\{^1H\}^{31}P$ NMR (benzene-d_6): δ = 86.49 (d, J_{PP} = 18.0 Hz , *P*^{i}Pr$_2$), 9.83 (t, J_{PP} = 18.0 Hz, *P*Me_3). $\{C\mathit{H}\}^{31}P$ NMR (benzene-d_6): δ = 86.49 (dd, J_{PP} = 18.0 Hz, J_{PH} = 67.0 Hz, *P*^{i}Pr$_2$), 9.83 (pseudo q, J_{PP} = 18.0 Hz, J_{PH} = 21.0 Hz, *P*Me_3).

Observation of [(2,6-^{i}Pr$_2$PCH$_2$)$_2$C$_5$H$_3$N]FeH(SiH$_2$Ph)(H$_2$) (4-H(SiH$_2$Ph)(H$_2$)). A J. Young tube was charged with 0.010 g (0.02 mmol) of **4-H(SiH$_2$Ph)(N$_2$)** and approximately 0.5 mL of benzene-d_6. The tube was submerged in liquid nitrogen and evacuated on a high-vacuum line. At this temperature, 1 atmosphere of H_2 was admitted and the tube was sealed, thawed, and shaken. Monitoring the reaction by multinuclear NMR spectroscopy established growth of **4-H(SiH$_2$Ph)(H$_2$)** over the course of hours at 23 °C. ^1H NMR (benzene-d_6): δ = 8.23 (d, J_{HH} = 7.5 Hz, 2H, *o-phenyl*), 7.33 (t, J_{HH} = 7.5 Hz, 2H, *m-phenyl*), 7.21 (t, J_{HH} = 7.5 Hz, 1H, *p-phenyl*), 6.68 (t, J_{HH} = 8.0 Hz, 1H, *p-pyr*), 6.45 (d, J_{HH} = 8.0 Hz, 2H, *m-pyr*), 5.54 (m, 2H, Si*H*$_2$), 2.84 (m, 4H, PC*H*$_2$), 2.04 (m, 4H, C*H*(CH_3)$_2$), 1.14 (pseudo q, J_{HH} = 7.0 Hz, 12H, CH(C*H*$_3$)$_2$), 0.94 (pseudo q, J_{HH} = 7.0 Hz, 12H, CH(C*H*$_3$)$_2$), -9.37 (br s, 3H, Fe-H). $\{^1H\}^{31}P$ NMR (benzene-d_6): δ = 108.36 (s).

REFERENCES

[1] Dahlhoff, W. V.; Nelson, S. M *J. Chem. Soc. A* **1971**, *13*, 2184.

[2] Benito-Garagorri, D.; Kirchner, K. *Acc. Chem. Res.* **2008**, *41*(2), 201.

[3] (a) Clarke, Z. E.; Maragh, P. T.; Dasgupta, T. P.; Gusev, D. G.; Lough, A. J.; Abdur-Rashid, K. *Organometallics*, **2006**, *25*, 4113. (b) Weng, W.; Guo, C.; Gelenligil,-Cetin R.; Foxman, B. M.; Ozerov, O. V. *Chem. Commun.* **2006**, 197.

[4] Zhang, J.; Leitus, G.; Ben-David, Y.; Milstein, D. *J. Am. Chem. Soc.* **2005**, *127*, 10840.

[5] Huang, M.-H.; Liang, L.-C. *Organometallics*, **2004**, *23*, 2813.

[6] Gunanathan, C.; Ben-David, Y.; Milstein, D. *Science* **2007**, *317*, 790.

[7] Representative examples for Fe: (a) Benito-Garagorri, D; Wiedermann, J.; Pollak, M.; Mereiter, K.; Kirchner, K. *Organometallics* **2007**, *26*, 217. (b) Benito-Garagorri, D.; Becker, E.; Wiedermann, J.; Lackner, W.; Pollack, M.; Mereiter, K.; Kisala, J.; Kirchner, K. *Organometallics* **2006**, *25*, 1900. For Co: (c) Fout, A. R.; Basuli, F.; Fan, H.; Tomaszewski, J.; Huffman, J. C.; Baik, M.-H.; Mindiola, D. J. *Angew. Chem. Int. Ed.* **2006**, *45*, 3291. For Ni: (d) Fan, L.; Ozerov, O. V. *Chem. Commun.* **2005**, 4450. (e) Adhikari, D.; Huffman, J. C.; Mindiola, D. J. *Chem. Commun.* **2007**, *43*, 4489.

[8] Bart, S. C.; Hawrelak, E. J.; Lobkovsky, E.; Chirik, P. J. *Organometallics* **2005**, *24*, 5518.

[9] Bart, S. C.; Lobkovsky, E.; Chirik, P. J. *J. Am. Chem. Soc.* **2004**, 126, 13794.

[10] Bouwkamp, M. W.; Bowman, A. C.; Lobkovsky, E.; Chirik, P. J. *J. Am. Chem. Soc.* **2006**, *128*, 13340.

[11] Bart, S. C.; Chlopek, K.; Bill, E.; Bouwkamp, M. W.; Lobkovsky, E.; Nesse, F.; Wieghardt, K.; Chirik, P. J. *J. Am. Chem. Soc.* **2006**, *128*, 13901.

[12] PCP ligand reduction has been observed: Frech, C. M.; Ben-David, Y.; Weiner, L.; Milstein, D. *J. Am. Chem. Soc.* **2006**, *128*, 7128.

[13] Jansen, A.; Pitter, S. *Montasch. Chem.* **1999**, *130*, 783.

[14] Zhang, J.; Gandelman, M.; Herrman, D.; Leitus, G.; Shimon, L. J. W.; Ben-David, Y.; Milstein, D. *Inorg. Chim. Acta* **2006**, *359*, 1955.

[15] Pelczar, E. M.; Emge, T. J.; Krogh-Jespersen, K.; Goldman, A. S. *Private communication*.

[16] Tondreau, A. M.; Lobkovsky, E.; Chirik, P. J. *Org. Lett.* **2008**, *10*, 2789.

[17] Cámpora, J.; Naz, A. M.; Palma, P.; Álverez, E.; Reyes, M. L. *Organometallics* **2005**, *24*, 4878.

[18] Fernández, I.; Trovitch, R. J.; Lobkovsky, E.; Chirik, P. J. *Organometallics* **2008**, *27*, 109.

[19] Trovitch, R. J.; Chirik, P. J. *Unpublished results*.

[20] Collman, J. P.; Hegedus, L. S.; Norton, J. R.; Finke, R. G. *Principles and Applications of Organotransition Metal Chemistry*, 2nd Ed. University Science, 1987.

[21] Kubas, G. J. *Acc. Chem. Res.* **1988**, *21*, 120.

[22] Eckert, J.; Kubas, G. J. *J. Phys. Chem.* **1993**, *97*, 2378.

[23] Dioumaev, V. K.; Procopio, L. J.; Caroll, P. J.; Berry, D. H. *J. Am. Chem. Soc.* **2003**, *125*, 8043.

[24] Ricci, J. S.; Koetzle, T. F.; Bautista, M. T.; Hofstede, T. M.; Morris, R. H.; Sawyer, J. F.; *J. Am. Chem. Soc.* **1989**, *111*, 8823.

[25] Ho, N. N.; Bau, R.; Mason, S. A. *J. Organomet. Chem.* **2003**, *676*, 85.

[26] Van Der Sluys, L. S.; Eckert, J.; Eisenstein, O.; Hall, J. H.; Huffman, J. C.; Jackson, S. A.; Koetzle, T. F.; Kubas, G. J.; Vergamini, P. J.; Caulton, K. G. *J. Am. Chem. Soc.* **1990**, *112*, 4831.

[27] Whitesides, G. M.; Maglio, G. *J. Am. Chem. Soc.* **1969**, *91*, 4980.

[28] Bianchini, C.; Meli, A.; Peruzzini, M.; Frediani, P.; Bohanna, C.; Esteruelas, M. A.; Oro, L. A. *Organometallics* **1992**, *11*, 138.

[29] Daida, E. J.; Peters, J. C. *Inorg. Chem.* **2004**, *43*, 7474.

[30] Sui-Seng, C.; Freutel, F.; Lough, A. J.; Morris, R. H. *Angew. Chem. Int. Ed.* **2008**, *47*, 940.

[31] Shaikh, N. S.; Enthaler, S.; Junge, K.; Beller, M. *Angew. Chem. Int. Ed.* **2008**, *47*, 2497.

[32] Gilbertson, J. D.; Szymczak, N. K.; Tyler, D. R. *Inorg. Chem.* **2004**, *43*, 3341.

[33] Morris, R. H.; Sawyer, J. F.; Shiralian, M.; Zubkowski, J. D. *J. Am. Chem. Soc.* **1985**, *107*, 5581.

[34] Bautista, M.; Earl, K. A.; Morris, R. H.; Sella, A. *J. Am. Chem. Soc.* **1987**, *109*, 3780.

[35] Helleren, C. A.; Henderson, R. A.; Leigh, G. J. *J. Chem. Soc., Dalton Trans.* **1999**, 1213.

[36] Field, L. D.; Li, H. L.; Messerle, B. A.; Smernik, R. J.; Turner, P. *Dalton Trans.* **2004**, 1418.

[37] Bampos, N.; Field, L. D. *Inorg. Chem.* **1990**, *29*, 587.

[38] Jia, G.; Drouin, S. D.; Jessop, P. G.; Lough, A. J.; Morris, R. H. *Organometallics* **1993**, *12*, 906.

[39] Bianchini, C.; Peruzzini, M.; Zanobini, F. *J. Organomet. Chem.* **1988**, 354, C19.

[40] Aresta, M.; Giannoccaro, P.; Rossi, M.; Sacco, A *Inorg. Chim. Acta* **1971**, *5*, 115.

[41] Pangborn, A. B.; Giardello, M. A.; Grubbs, R. H.; Rosen, R. K.; Timmers, F. J. *Organometallics* **1996**, *15*, 1518.

APPENDIX A

PRELIMINARY INVESTIGATIONS

A.1 Electronic Structure Determination of (^{Et}PDI)$_2$Fe

Over the last decade, major strides have been made towards accurately describing the electronic structure of complexes that bear redox-active ligands. Bond distances determined by X-ray crystallography are diagnostic for determining electronic structure; however, many other forms of spectroscopy (EPR, electrochemistry, etc.) can be utilized along with magnetochemistry and DFT calculations to augment these determinations. Mössbauer spectroscopy provides a unique advantage to determining the electronic structure of iron complexes; ^{57}Fe is by far the most studied nuclei using this technique.[1] This extremely powerful spectroscopic method offers insight into the covalency and spin-state of organometallic iron complexes, and comparing a series of complexes bearing the same ligand framework can offer information about the oxidation state of iron for each complex.[2]

In 2000, Wieghardt and co-workers described the molecular and electronic structure of a series of bis(pyridine-2,6-diimine) complexes, [(^{OMe}PDI)$_2$M][PF$_6$]$_n$ (^{OMe}PDI = 2,6-((4-OMe-C$_6$H$_4$)N=CMe)$_2$C$_6$H$_3$N; n = 0,1,2,3; M = Mn, Fe, Co, Ni, Cu, Zn).[3] In this report, the cationic complexes for each metal were prepared and the reduced forms of these complexes were generated electrochemically and characterized *in situ*. For iron, the diamagnetic bis(ligand) complex [(^{OMe}PDI)$_2$Fe][PF$_6$]$_2$ was crystallographically characterized and was described as having a ferrous metal center with two neutral bis(imino)pyridine ligands through investigation of the chelate bond distances (Figure A.1).[4] Also, the average Fe-N$_{py}$ and Fe-N$_{imine}$ bond distances of

1.868(1) Å and 1.987(1) Å, respectively, were consistent with the distances observed for the diamagnetic, low spin complex, $[(terpy)_2Fe][ClO_4]_2$.[5]

Additionally, $[(^{OMe}PDI)_2Fe][PF_6]_2$ was investigated by Mössbauer spectroscopy. At 80 K, this complex displayed a symmetrical quadrupole doublet with an isomer shift (δ) of 0.235 mm·s^{-1} and a quadrupole splitting (ΔE_Q) of 1.081 mm·s^{-1}.[3] This isomer shift is consistent with values observed for other dicationic, low spin, and octahedral iron complexes bearing *N*-donor ligands.[6,7] Taken together $[(^{OMe}PDI)_2Fe][PF_6]_2$ and $[(terpy)_2Fe][ClO_4]_2$ suggest that low spin octahedral ferrous centers bearing two C_{2v}–symmetric ligand environments should have an isomer shift between 0.2 and 0.3 mm·s^{-1} and a ΔE_Q value of approximately 1.1 mm·s^{-1}.[6]

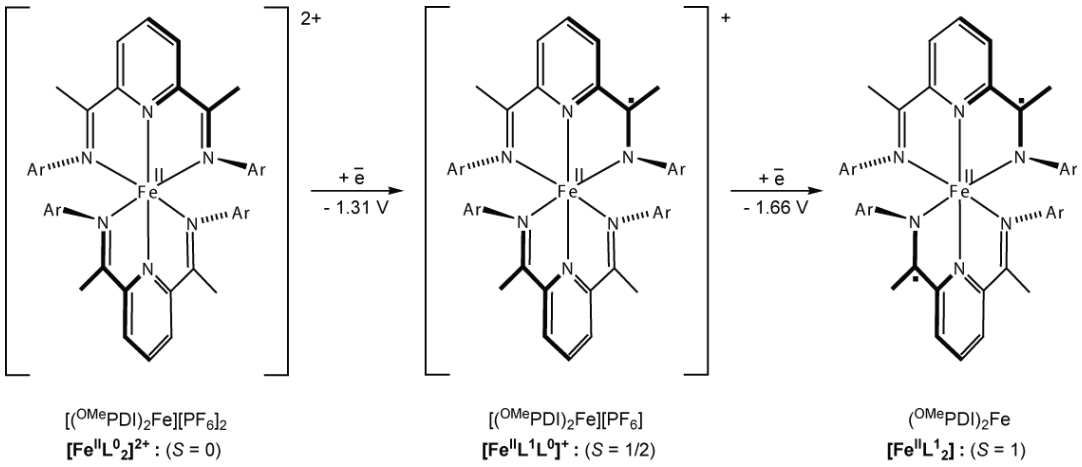

Figure A.1. Previously reported electronic structure of $[(^{OMe}PDI)_2Fe][PF_6]_2$ and electrochemically related complexes. Potentials are given verses Fc/Fc^+ in acetonitrile.

In the same report, $[(^{OMe}PDI)_2Fe][PF_6]$ was electrochemically prepared in acetonitrile solution at -20 °C and investigated by X-band EPR spectroscopy. The evidence of a "slightly rhombic, almost isotropic" signal with small *g*-value deviations led the authors to conclude that this complex consisted of a low spin ferrous metal center that was antiferromagnetically coupled to one anionic bis(imino)pyridine ligand ($S = 1/2$) (Figure A.1).[3] The neutral complex, $(^{OMe}PDI)_2Fe$, was accessed at a potential

of -1.66 V (vs. Fc^{+}/Fc) in acetonitrile solution and the electronic spectrum was recorded. With no further experimental data (the compounds were not isolated), the authors concluded that this complex likely contained a *low spin* ferrous ion and two singly reduced bis(imino)pyridine ligands (Figure A.1).[3] Because neither $[(^{OMe}PDI)_2Fe][PF_6]$ or $(^{OMe}PDI)_2Fe$ were isolated, these complexes were not investigated by Mössbauer spectroscopy or magnetometry.

Recent attempts to expand the reduction chemistry of $(^{iPr}PDI)FeBr_2$ (^{iPr}PDI = 2,6-((2,6-$^{i}Pr_2$-C_6H_3)N=CMe)$_2C_6H_3N$, **1-Br$_2$**) to less sterically demanding dihalide precursors, as a way to prepare more accessible iron centers for catalysis, have resulted in formation of bis(ligand) complexes instead of dinitrogen complexes. One ligand set that was investigated contained isopropyl groups (^{iPr}APDI) in place of the bulky 2,6-diisopropylaryl substituents. Reduction of $(^{iPr}APDI)FeBr_2$ with excess 0.5 % sodium amalgam in pentane solution resulted in the formation of $(^{iPr}APDI)_2Fe$ rather than the desired bis(dinitrogen) complex. This reduction product was characterized by X-ray crystallography and the solid-state structure is presented in Figure A.2.

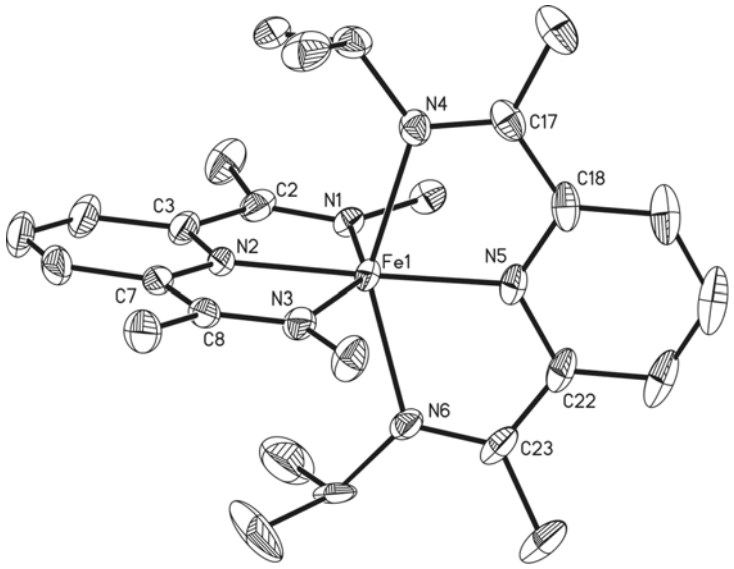

Figure A.2. Solid-state structure of $(^{iPr}APDI)_2Fe$ at 30 % probability ellipsoids. Hydrogen atoms and four isopropyl methyl groups omitted for clarity.

The metrical parameters (Table A.1) for this complex are consistent with a partially localized, one electron reduction of each bis(imino)pyridine ligand.[4] The average N_{imine}-C_{imine} and C_{imine}-C_{ispo} distances were found to be 1.308 Å and 1.441 Å, respectively. Although this crystal structure confirms that there is a single electron reduction at each ligand, as originally proposed,[3] closer inspection of the average Fe-N_{py} and Fe-N_{imine} distances of 2.021 Å and 2.237 Å, respectively, offered the first clue that this complex high, rather than low-spin.

Table A.1. Selected bond distances (Å) and angles (°) for (^{iPr}APDI)$_2$Fe. Values in brackets obtained from open-shell DFT calculations.

Fe(1)-N(1)	2.252(2), [2.232]	N(4)-C(23)	1.312(3), [1.325]
Fe(1)-N(2)	2.0180(17), [2.041]	N(6)-C(29)	1.304(3), [1.325]
Fe(1)-N(3)	2.2506(19), [2.275]	C(2)-C(3)	1.431(3), [1.462]
Fe(1)-N(4)	2.259(2), [2.266]	C(7)-C(8)	1.457(4), [1.464]
Fe(1)-N(5)	2.0236(18), [2.042]	C(23)-C(24)	1.426(3), [1.463]
Fe(1)-N(6)	2.1846(18), [2.234]	C(28)-C(29)	1.450(4), [1.463]
N(1)-C(2)	1.316(3), [1.326]	N(1)-Fe(1)-N(4)	94.99(7), [93.39]
N(3)-C(8)	1.299(3), [1.299]	N(2)-Fe(1)-N(5)	176.90(8), [177.42]

The solid-state magnetic moment of (^{iPr}APDI)$_2$Fe was found to be 2.4(1) μ_B (Guoy Balance) and the average of six Evans method determinations was 2.9(6) μ_B (benzene-d_6, 293 K), both consistent with an $S = 1$ complex. The ^{1}H NMR of (^{iPr}APDI)$_2$Fe displayed resonances over a 380 ppm range that were much broader and less informative than the peaks typically observed for paramagnetic bis(imino)pyridine iron complexes (Chapter 1). Electrochemical and UV-visible data were also collected

for this complex, confirming that neutral bis(ligand) compound was spectroscopically identical to the complex that was generated *in situ* by Wieghardt and co-workers.[3]

The metrical parameters of (^{iPr}APDI)$_2$Fe were effectively reproduced with a broken symmetry geometry optimization where each bis(imino)pyridine ligand was assumed to be monoreduced (Table A.1).[8] A classic d-orbital splitting diagram was determined with a (4,2) broken symmetry calculation where one unpaired electron was placed on each ligand and four on the metal center. The spin-density for each orbital is presented in Figure A.3. The overlap integral (S) between each ligand-based orbital with the metal center was determined to be approximately 0.4 (Figure A.3). The percentage of each orbital that is metal-based is presented in brackets.

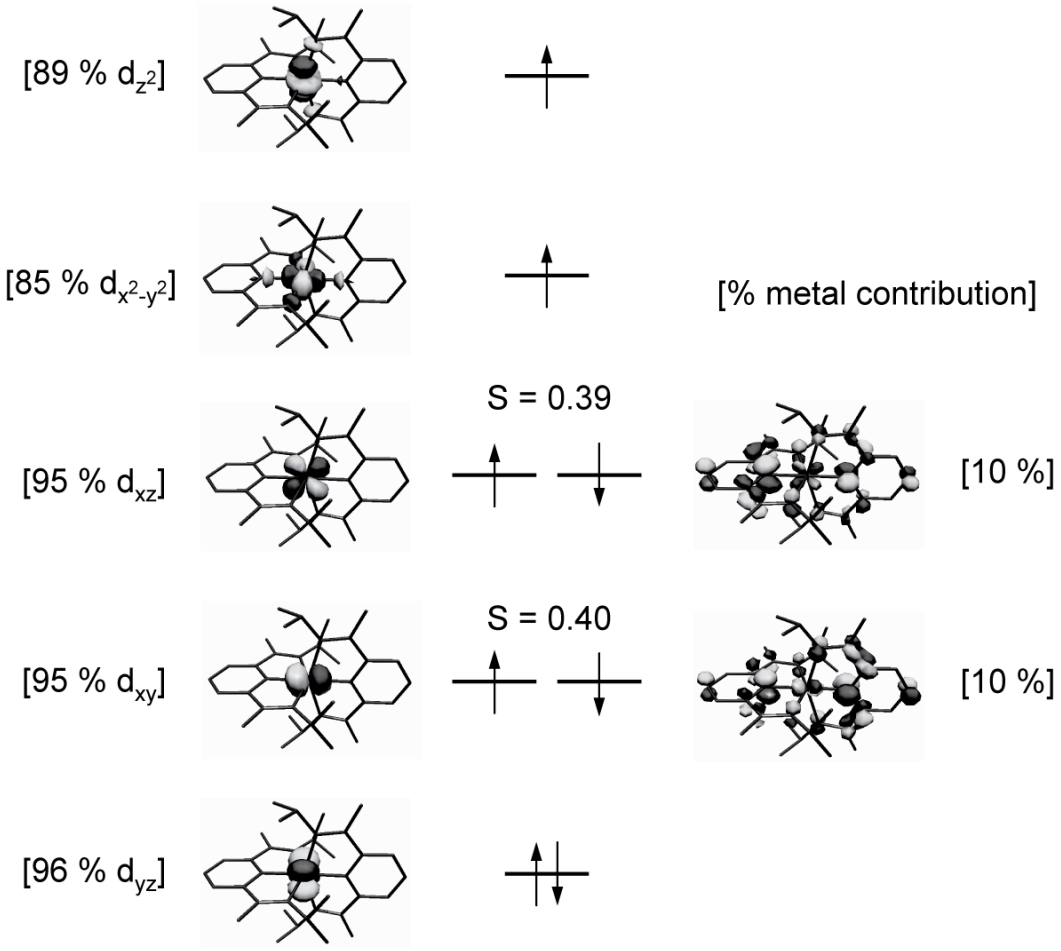

Figure A.3. Ligand- and metal-based orbitals computed for (^{iPr}APDI)$_2$Fe.

The ligand-based orbitals presented in Figure A.3 clearly show antibonding character along the imine bond and bonding character between the imine and ipso carbons, a feature highlighted in the molecular structures of bis(imino)pyridine complexes.[4] The overall unpaired spin density for (^{iPr}APDI)$_2$Fe was additionally computed and is presented in Figure A.4. As expected for a high spin d^6 metal center, the unpaired spin density on iron was found to be approximately four electrons while the ligand-based electron density, of the opposite sign, sums to approximately two electrons – one on each ligand.

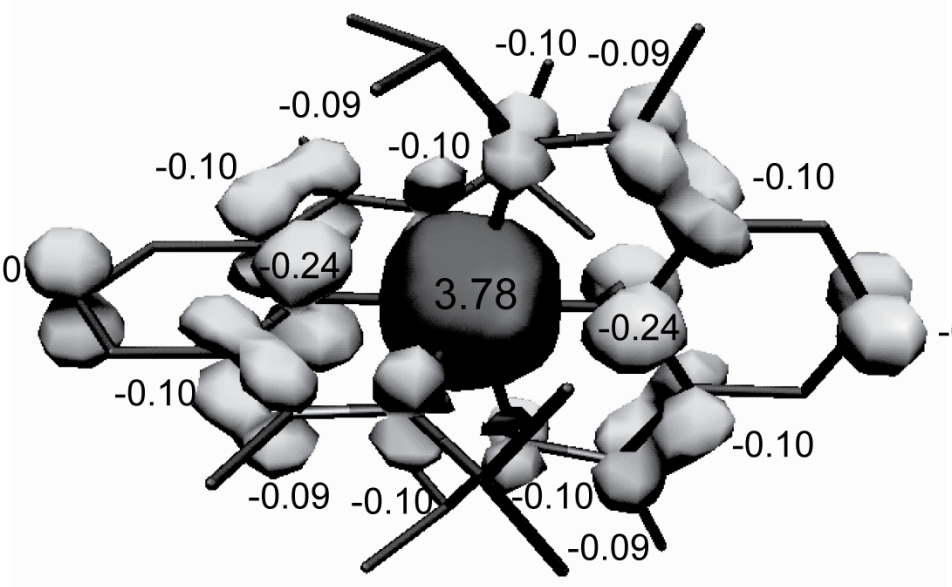

Figure A.4. Computationally determined unpaired spin density plot for (^{iPr}APDI)$_2$Fe.

This complex was also investigated by zero-field Mössbauer spectroscopy and the resulting spectrum is displayed in Figure A.5. At 80 K, the isomer shift of this complex was found to be 0.93 mm·s^{-1}, confirming the presence of a high spin ferrous center.[1] The quadrupole splitting for this complex was barely discernable at 0.24 mm·s^{-1} and is more narrow than the values observed for the low spin ferrous examples discussed previously.[5,6] Density functional theory reasonably predicted the Mössbauer

parameters of this complex at $\delta = 0.82$ mm·s^{-1} and $\Delta E_Q = 1.22$ mm·s^{-1}.[9] Generally, quadrupole splitting values are poorly replicated computationally, while the isomer shifts can be predicted to within 0.2 mm·s^{-1}.[10]

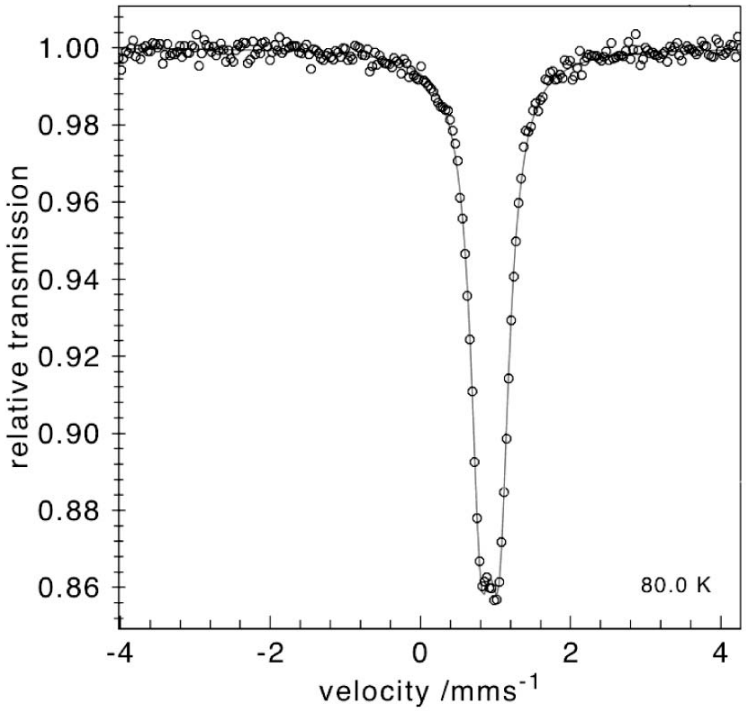

Figure A.5. Zero-field Mössbauer spectrum of (^{iPr}APDI)$_2$Fe at 80 K.

In analogy to (^{iPr}APDI)FeBr$_2$, reduction of (^{Et}PDI)FeBr$_2$ (^{Et}PDI = 2,6-((2,6-Et$_2$-C$_6$H$_3$)N=CMe)$_2$C$_6$H$_3$N, **2-Br$_2$**) with excess 0.5 % sodium amalgam also yielded an undesired bis(ligand) product, **2-(^{Et}PDI)** (Figure A.6). Suprisingly, reducing the steric pressure of the PDI 2,6-aryl substituents by replacing the isopropyl groups with ethyl groups resulted in a complete change in reactivity, preventing the formation of a bis(dinitrogen) complex and favoring bis(ligand) formation. Higher yields of this complex were obtained by performing the reduction of the dibromide in the presence of an extra equivalent of ^{Et}PDI (Figure A.6). Like (^{iPr}APDI)$_2$Fe, this complex also

displays extremely broad and paramagnetically shifted ^{1}H NMR resonances. Crystals of **2-(^{Et}PDI)** suitable for X-ray diffraction were obtained upon cooling a concentrated pentane solution to -35 °C. The solid-state structure of this bis(ligand) complex (Figure A.7) can best be described as tetrahedral with two weakly coordinated imine arms. The metrical parameters of **2-(^{Et}PDI)** are consistent with two highly localized, singly reduced bis(imino)pyridine ligands (Table A.2).[4]

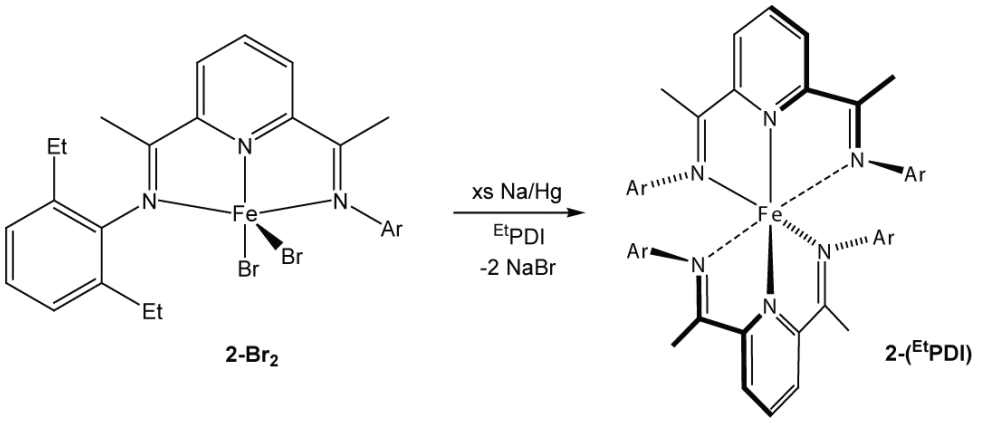

Figure A.6. Preparation of **2-(^{Et}PDI)** from sodium amalgam reduction of **2-Br$_2$**.

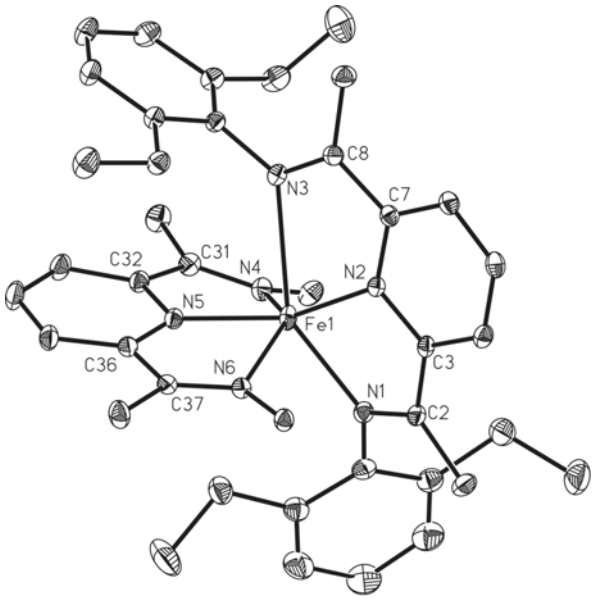

Figure A.7. Solid-state structure of **2-(^{Et}PDI)** at 30 % probability ellipsoids. Hydrogen atoms and two diethylaryl groups omitted for clarity.

Table A.2. Selected bond distances (Å) and angles (°) for **2-(^{Et}PDI)**. Values in brackets obtained from open-shell DFT calculations.

Fe(1)-N(1)	2.1246(16), [2.157]	N(6)-C(37)	1.291(2), [1.314]
Fe(1)-N(2)	1.9853(15), [1.984]	C(2)-C(3)	1.435(3), [1.453]
Fe(1)-N(3)	2.5579(16), [2.517]	C(7)-C(8)	1.478(3), [1.467]
Fe(1)-N(4)	2.1098(16), [2.124]	C(31)-C(32)	1.435(3), [1.453]
Fe(1)-N(5)	1.9864(15), [1.991]	C(36)-C(37)	1.481(3), [1.469]
Fe(1)-N(6)	2.6096(16), [2.589]	N(1)-Fe(1)-N(2)	78.99(6), [78.9]
N(1)-C(2)	1.332(2), [1.340]	N(4)-Fe(1)-N(5)	79.44(6), [79.8]
N(3)-C(8)	1.291(2), [1.317]	N(1)-Fe(1)-N(4)	101.15(6), [97.5]
N(4)-C(31)	1.334(3), [1.341]	N(2)-Fe(1)-N(5)	138.95(6), [145.6]

Although the ^{1}H NMR spectrum of this compound suggested that it had the same electronic structure as (^{iPr}APDI)$_2$Fe, magnetic data was also collected for **2-(^{Et}PDI)** to provide further support for this assumption. Due to the ease of synthesis and outstanding crystallinity of this complex, SQUID magnetic data was collected for three independently prepared samples of **2-(^{Et}PDI)**. The magnetic susceptibility of this complex was reproducible and ranged from 1.8 μ_B to 3.2 μ_B between 5 and 300 K (Figure A.8), consistent with a high spin ferrous complex antiferromagnetically coupled to two singly reduced chelates (S = 1). Fitting the magnetic data yielded the following spin Hamiltonian parameters: g = 2.084, $|D|$ = 9.3 cm^{-1}, and E/D = 0.008, consistent with a high-spin ferrous ion in a tetrahedral ligand field.

This electronic structure claim was again augmented with open-shell DFT calculations. To a rough approximation, the metrical parameters of **2-(^{Et}PDI)** were

effectively reproduced by a (4,2) broken symmetry geometry optimization where each bis(imino)pyridine ligand was assumed to be monoreduced.[7] The relative orbital energies along with their spin-densities are presented in Figure A.9. The overlap integral (S) between each ligand-based orbital with the metal center was determined to be approximately 0.4, similar to (^{iPr}APDI)$_2$Fe (Figure A.9). The metal-based percentage of each orbital is presented in brackets. The overall unpaired spin density for **2-(^{Et}PDI)** was additionally computed and is presented in Figure A.10. As observed in the crystal structure, the spin density plot reveals localized reduction at both bis(imino)pyridine ligands and two relatively unreduced imine arms.

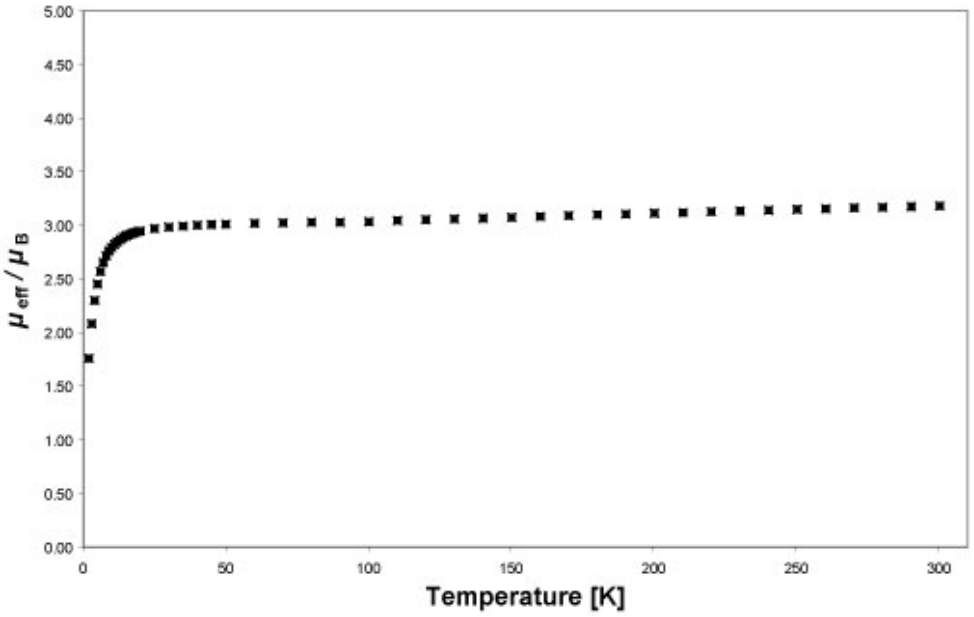

Figure A.8. Variable temperature solid-state magnetic data for **2-(^{Et}PDI)**.

The Mössbauer spectrum of **2-(^{Et}PDI)** is considerably different than the one obtained for (^{iPr}APDI)$_2$Fe. It is composed of two different isomers that display similar isomer shifts and slightly different quadrupole splittings (Figure A.11). The κ^2-configuration of each chelate creates the possibility of having 2 isomers; however, this phenomenon could either stem from the crystallization of two distinct aryl group

rotamers or *cis* verses *trans* orientation of the weakly coordinated imines across the dimer. At this point, the first explanation is favored but this hypothesis can only be validated by obtaining the solid-state structure of the second isomer. At 80 K, the isomer shifts observed for **2-(**^{Et}**PDI)** were 0.91 mm·s^{-1} (58 %) and 0.92 mm·s^{-1} (42%) with ΔE_Q values of 1.53 mm·s^{-1} and 1.95 mm·s^{-1}, respectively. The experimental isomer shift values confirm the presence of a high spin ferrous center in this complex.[1] A Mössbauer spectrum was collected on a second batch of **2-(**^{Et}**PDI)** to ensure that one of the two signals was not due to an impurity. As expected, the same signals were observed in exactly the same ratio.

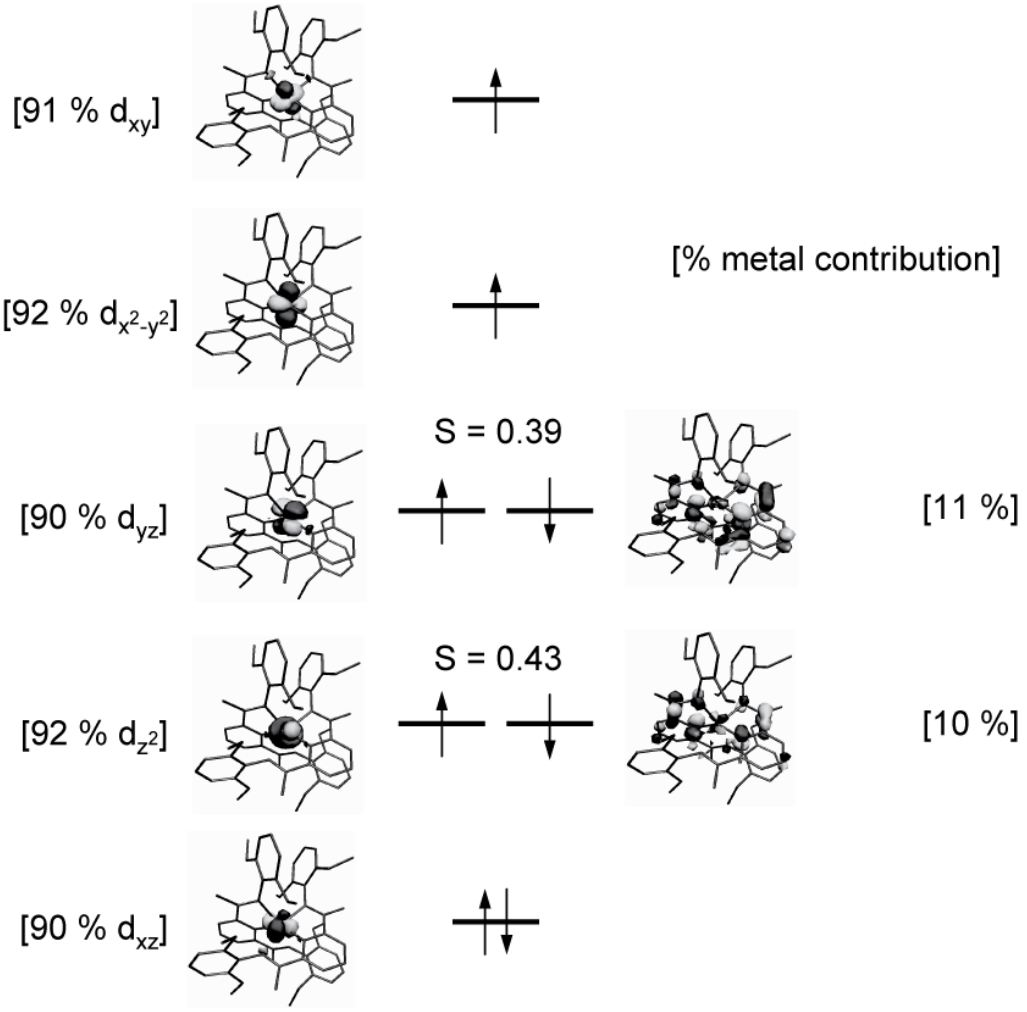

Figure A.9. Ligand- and metal-based orbitals computed for **2-(**^{Et}**PDI)**.

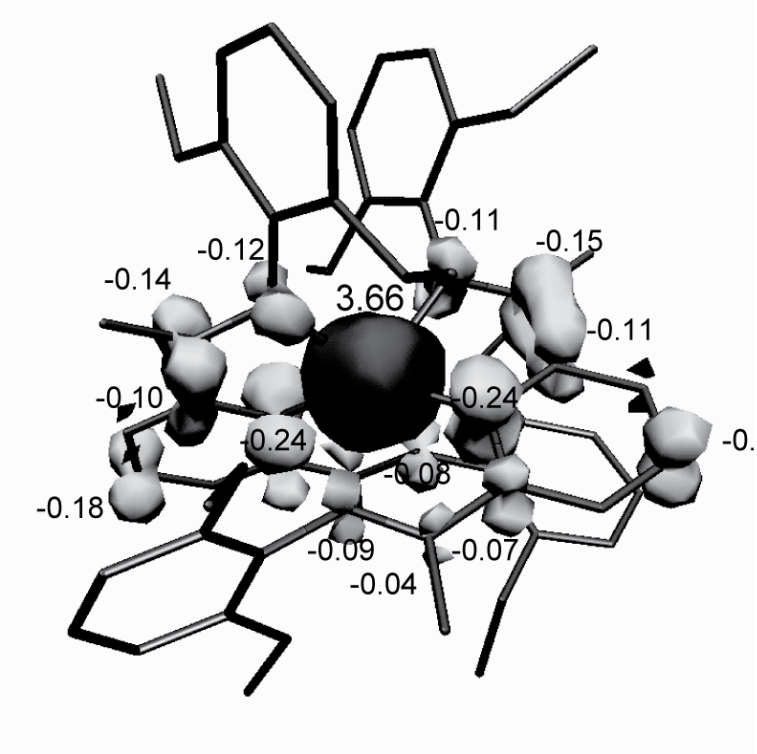

Figure A.10. Computationally determined unpaired spin density plot for **2-(**^{Et}**PDI)**.

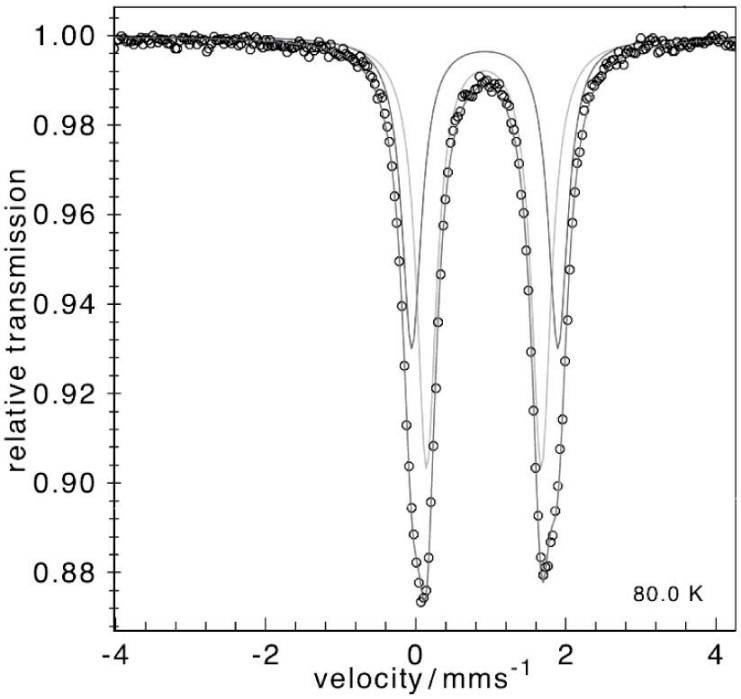

Figure A.11. Zero-field Mössbauer spectrum of **2-(**^{Et}**PDI)** at 80 K.

Taking both the experimental and computational data into account, (^{iPr}APDI)$_2$Fe and (^{Et}PDI)$_2$Fe are described as having high spin iron(II) centers that are antiferromagnetically coupled to two monoreduced bis(imino)pyridine ligands. In preparing these complexes from their cationic counterparts, reduction occurs at the ligand rather than the metal center, allowing retention of the ferrous oxidation state. This chelate reduction also causes a spin change at the metal center from low to high spin, providing a classic example of how reduction of a redox-active ligand can greatly influence its inherent field strength.

A.2 Addition of Bidentate and Terdentate Ligands to (^{iPr}PDI)Fe(N_2)$_2$

The electronic structure determination of iron complexes was extended to include cases where ligand reduction could occur either at the bis(imino)pyridine chelate or a second redox-active ligand. As described in Chapter 1, the reducing iron complex (^{iPr}PDI)Fe(N_2)$_2$ (^{iPr}PDI = 2,6-((2,6-^{i}Pr$_2$-C$_6$H$_3$)N=CMe)$_2$C$_6$H$_3$N, **1-(N_2)$_2$**) can best be though of as having an iron(II) center that is antiferromagnetically coupled to a bis(imino)pyridine diradical.[8] While this was partially explored in Chapter 3 with the addition of benzophenone or pyrazine to **1-(N_2)$_2$**, these ligands simply allowed contributions from an iron(III) metal center rather than oxidation of the bis(imino)pyridine ligand. Because ligands with electronic characteristics similar to the bis(imino)pyridines were desired, the coordination of *N*-donor redox-active ligands, such as 2,2'-bipyridine and 2,2':6',2''-terpyridine, to bis(imino)pyridine iron were explored.

Stoichiometric addition of 2,2'-bipyridine to a toluene solution of **1-(N_2)$_2$** at ambient temperature resulted in the immediate formation of a deep blue solution. Removal of the solvent afforded the bis(imino)pyridine iron bipyridine complex, **1-Bpy**, in high yield (94 %). This complex was fully characterized by ^{1}H and ^{13}C NMR

spectroscopy and exhibited resonances between 0.7 and 8.8 ppm, the range expected for a diamagnetic, low-spin bis(imino)pyridine iron complex.[8,11] Additional evidence for this electronic structure description was obtained by X-ray diffraction. The solid-state structure of **1-Bpy** (Figure A.11) reveals a nearly idealized square planar geometry about iron and is consistent with two electron reduction of the chelate, with N_{imine}-C_{imine} and C_{imine}-C_{ipso} bond distances of 1.360(4)/1.351(4) Å and 1.408(5)/1.410(5) Å, respectively (Table A.3).[4,11] Inspection of the iron-nitrogen bond distances to both ligands (Table A.3) reveals that these distances are similar to those previously described for low-spin iron(II) dicationic complexes.[3,5] Even though this bond length comparison does not take bis(imino)pyridine ligand reduction into account, it is important to note that the Fe(1)-N(4) and Fe(1)-N(5) distances are relatively short at 1.923(3) Å and 1.954(3) Å, respectively (Table A.3). For high-spin iron bipyridine complexes, the Fe-N bond lengths are typically 0.16 to 0.22 Å longer than their low-spin counterparts.[12]

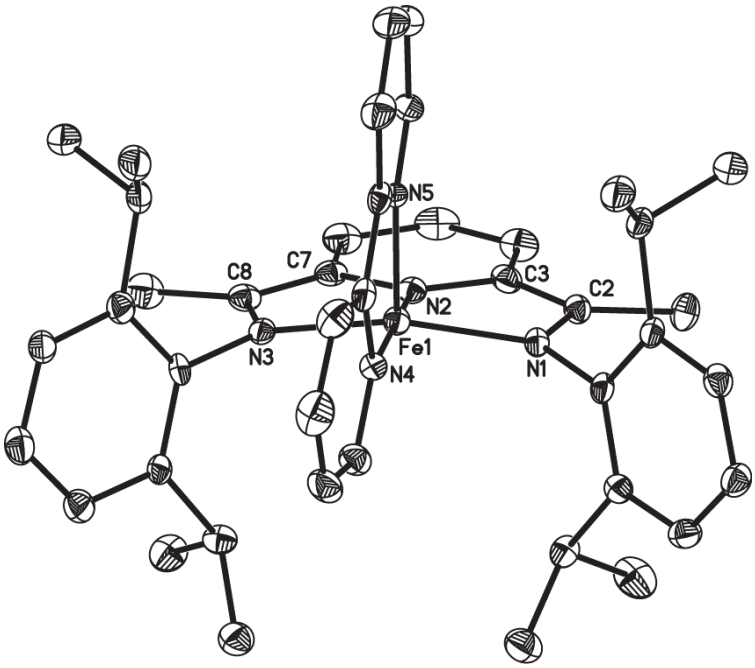

Figure A.11. Molecular structure of **1-Bpy** at 30 % probability ellipsoids. Hydrogen atoms omitted for clarity.

Table A.3. Selected bond distances (Å) and angles (°) for **1-Bpy**.

Fe(1)-N(1)	1.938(3)	N(5)-C(19)	1.354(4)
Fe(1)-N(2)	1.840(3)	C(10)-C(11)	1.370(5)
Fe(1)-N(3)	1.938(3)	C(11)-C(12)	1.406(5)
Fe(1)-N(4)	1.932(3)	C(12)-C(13)	1.361(5)
Fe(1)-N(5)	1.954(3)	C(13)-C(14)	1.392(5)
N(1)-C(2)	1.360(4)	C(14)-C(15)	1.431(5)
N(3)-C(8)	1.351(4)	C(15)-C(16)	1.402(5)
C(2)-C(3)	1.408(5)	C(16)-C(17)	1.365(5)
C(7)-C(8)	1.401(5)	C(17)-C(18)	1.375(5)
N(4)-C(10)	1.347(4)	C(18)-C(19)	1.389(5)
N(4)-C(14)	1.387(4)	N(2)-Fe(1)-N(4)	173.39(12)
N(5)-C(15)	1.355(4)	N(2)-Fe(1)-N(5)	105.38(12)

Importantly, there is also cyrstallographic evidence for reduction of the bipyridine ligand when compared to the distances in $[Fe(bpy)_3](PF_6)_2$ and $[Fe(bpy)_3][Fe(CN)_5NO]$, where little reduction is expected.[12-14] The bipyridine C(14)-C(15) distance of 1.431(5) in **1-Bpy** is significantly contracted compared to the same distance in either cationic complex (1.474 Å for average of six bond lengths).[12-14] Additionally, the bipyridine N-C and C-C ring distances are an average of 1.361 Å and 1.383 Å for **1-Bpy**, both elongated from the average values of 1.346 Å and 1.372 Å observed for $[Fe(bpy)_3](PF_6)_2$.[12,13] The observed bipyridine reduction could be due to a

contribution from a resonance form of **1-Bpy** where the bipyridine (α-diimine) ligand is doubly reduced.[15] This observation could also result from an Fe(IV) resonance form contribution where both chelates are doubly reduced. A third electronic structure description where the bipyridine ligand is singly reduced and antiferromagnetically coupled to a low-spin ferrous center is also possible and cannot be ruled out.

Crystallographic evidence for reduction of the 2,2'-bipyridine ligand in **1-Bpy** prompted the addition of 2,2':6',2''-terpyridine to **1-$(N_2)_2$**., as it has one electron reduction potential (-1.51 V verses Fc/Fc^+) that is more easily accessible than bipyridine (-1.60 V verses Fc/Fc^+).[15] In the absence of ligand reduction, terpyridine addition to **1-$(N_2)_2$** could result in a formal 20 electron, 6-coordinate complex. Stoichiometric addition of terpyridine to **1-$(N_2)_2$** in toluene solution and subsequent workup resulted in isolation of the desired complex, **1-Tpy**, as a reddish-purple solid. Investigation by ^{1}H NMR spectroscopy suggested that **1-Tpy** has a different electronic structure than **1-Bpy**, as paramagnetically broadened resonances were observed over a 370 ppm range. This spectrum was readily assigned; the imine methyl resonance was observed at -147.63 ppm and the 2,6-disubstituted *p*-pyridine resonances of both ligands were located at 219.11 and 196.38 ppm. The solution magnetic susceptibility of this complex was determined to be 2.7(2) μ_B in benzene-d_6 at ambient temperature. Additionally, the solid state moment of this complex was found to be 2.4(1) μ_B (Gouy balance). Both determinations are strikingly similar to the values observed for the bis(ligand) complexes discussed in Section A.1 and are consistent with an $S = 1$ complex.

To determine whether or not this was indeed a 6-coordinate complex (a 5-coordinate, high-spin (tpy)Fe(κ^2-PDI) complex where the κ^2-PDI ligand is doubly reduced was a second possibility), crystals of **1-Tpy** suitable for X-ray diffraction were grown from a concentrated pentane solution at -35 °C. The molecular structure

of **1-Tpy** was found to have a 6-coordinate, nearly idealized octahedral geometry about iron (Figure A.12). Selected metrical parameters for this complex are presented in Table A.4 along with a side view of the terpyridine ligand in Figure A.13.

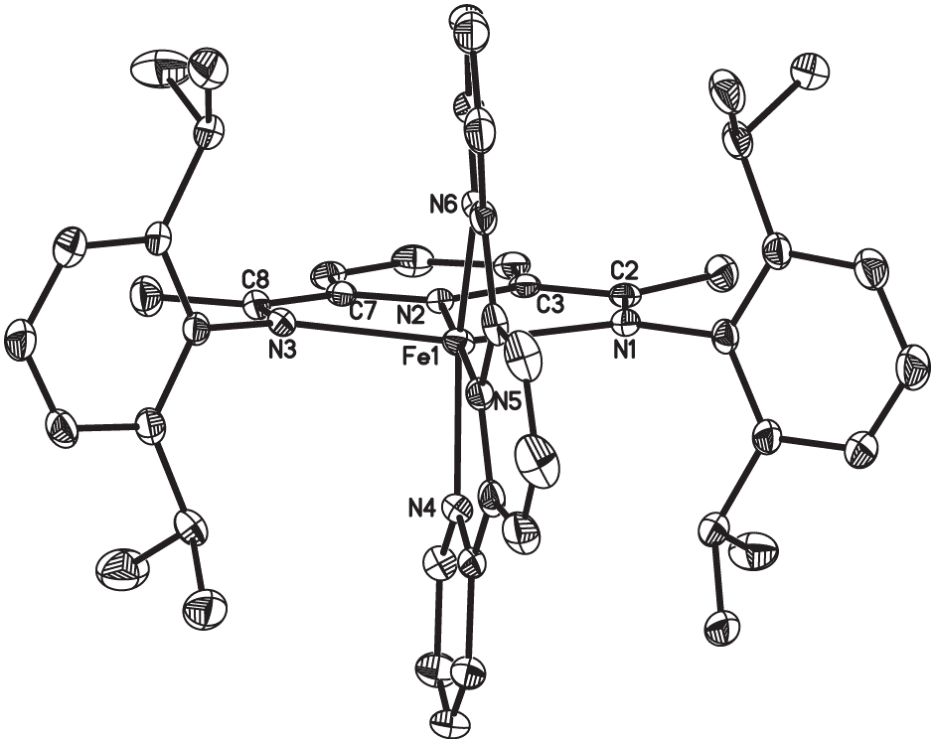

Figure A.12. Molecular structure of **1-Tpy** at 30 % probability ellipsoids. Hydrogen atoms omitted for clarity.

The metrical parameters of the bis(imino)pyridine ligand are consistent with single electron reduction with N_{imine}-C_{imine} and C_{imine}-C_{ipso} distances of 1.297(3)/ 1.307(3) Å and 1.452(3)/ 1.451(3) Å, respectively.[4] Considerably longer bonds between the metal center and both chelates are observed for **1-Tpy** (Table A.4) than for **1-Bpy** (Table A.3), highlighting the spin state difference between the two complexes. Investigation of the terpyridine ligand distances suggests a one electron reduction at this chelate also. The ring-linking C-C bonds in **1-Tpy** at 1.443(4) Å are contracted from the free ligand average value of 1.49 Å,[16] as well as the average value

reported for $[Fe(terpy)_2]^{2+}$ (1.466 Å).[17] Additionally, the average aromatic N-C and C-C bond distances for **1-Tpy** of 1.362 Å and 1.382 Å are elongated from the average $[Fe(terpy)_2]^{2+}$ values of 1.346 Å and 1.373 Å, respectively. [17]

Table A.4. Selected bond distances (Å) and angles (°) for **1-Tpy**.

Fe(1)-N(1)	2.3174(19)	C(34)-C(35)	1.371(4)
Fe(1)-N(2)	1.994(2)	C(35)-C(36)	1.387(5)
Fe(1)-N(3)	2.3007(18)	C(36)-C(37)	1.346(5)
Fe(1)-N(4)	2.144(2)	C(37)-C(38)	1.411(4)
Fe(1)-N(5)	2.024(2)	C(38)-C(39)	1.443(4)
Fe(1)-N(6)	2.094(2)	C(39)-C(40)	1.381(4)
N(1)-C(2)	1.297(3)	C(40)-C(41)	1.391(5)
N(3)-C(8)	1.307(3)	C(41)-C(42)	1.383(4)
C(2)-C(3)	1.452(3)	C(42)-C(43)	1.385(4)
C(7)-C(8)	1.451(3)	C(43)-C(44)	1.443(4)
N(4)-C(34)	1.352(4)	C(44)-C(45)	1.406(4)
N(4)-C(38)	1.361(3)	C(45)-C(46)	1.368(4)
N(5)-C(39)	1.372(3)	C(46)-C(47)	1.382(5)
N(5)-C(43)	1.367(3)	C(47)-C(48)	1.374(4)
N(6)-C(44)	1.362(3)	N(2)-Fe-N(5)	175.99(8)
N(6)-C(48)	1.356(3)	N(4)-Fe-N(6)	151.01(9)

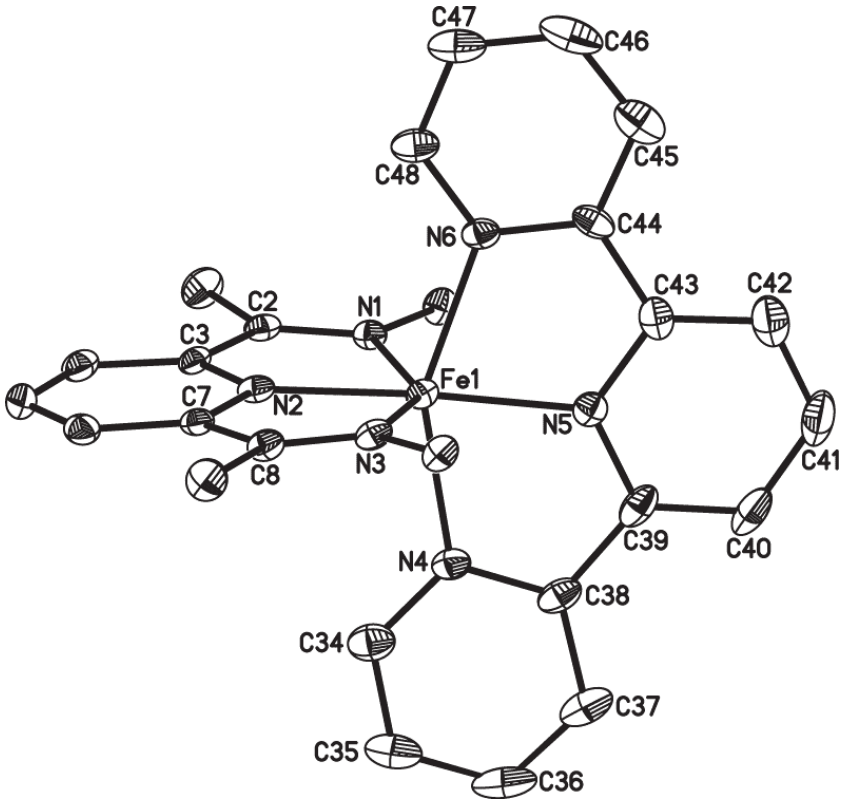

Figure A.13. Side view of the solid-state structure of **1-Tpy** at 30 % probability ellipsoids. Hydrogen atoms and 2,6-diisopropylaryl groups removed for clarity.

The electronic absorption spectra of **1-Bpy** and **1-Tpy** were also investigated due to the intense color of these complexes. As expected, these compounds exhibited spectra dominated by charge transfer bands (Figure A.14). For these complexes, at least three charge transfer bands were observed and each compound appears to have an additional high energy band at approximately 350 nm. Dicationic iron complexes bearing bipyridine and terpyridine ligands have been investigated for utility in photochemical water splitting reactions; however, extremely short excited state lifetimes[18,19] and complications from readily accessible d-d transitions have been identified as major obstacles.[20] Although dicationic versions of **1-Bpy** and **1-Terpy** may be promising for this application, the moisture sensitivity of the neutral

complexes renders them inadequate even though they display a wide range of charge transfer bands.[20]

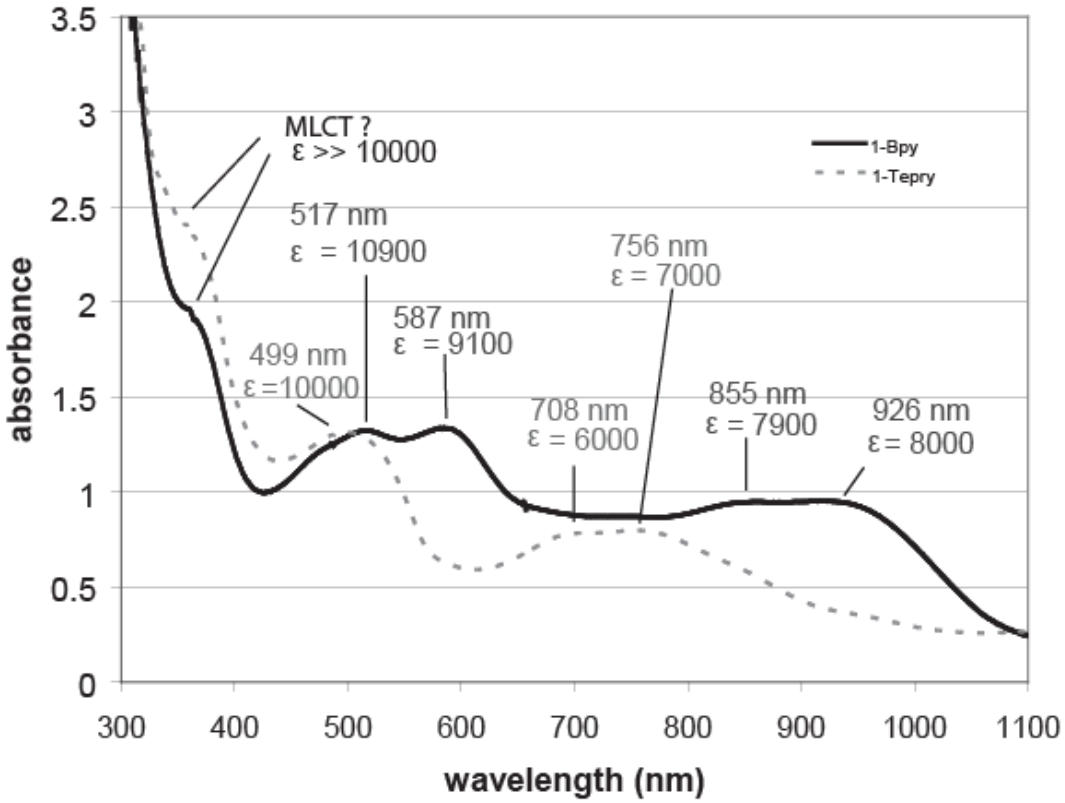

Figure A.14. Metal to ligand charge transfer bands in the absorption spectra of **1-Bpy** and **1-Tpy**.

In summary, the electronic structures of **1-Bpy** and **1-Tpy** have been investigated and a striking anomaly has been identified. In changing the chelating ligand from 2,2'-bipyridine to 2,2':6',2''-terpyridine, the coordination number was increased and the ligand field strengthened. However, the iron(II) center counterintuitively went from low-spin to high-spin upon introduction of the terdentate ligand. This comparison, coupled with the bis(ligand) cases presented in Section A.1, truly highlights how ligand reduction can drastically influence the field strength of the ligand itself and alter the overall electronic configuration of an organometallic complex.

A.3 Identification of Catalyst Deactivation Pathways for α-Diimine Iron Catalyzed Olefin Hydrogenation

Upon discovering that (^{iPr}DI)Fe(η^2,η^2-1,5-C_8H_{12}) (^{iPr}DI = [(2,6-$(CH(CH_3)_2)_2$-C_6H_3)N=C(CH_3)-(CH_3)C=N(2,6-$(CH(CH_3)_2)_2$-C_6H_3)) (**5-COD**) and (^{iPr}DI)Fe(η^2-C_8H_{14}) (**5-COE**) (Figure A.15) were effective precatalysts for the hydrogenation of 1-hexene,[21] a comprehensive study of substrate scope was carried out. Employing 1.0 mol % loadings of either **5-COD** or **5-COE**, the scope of unfunctionalized olefin hydrogenation (1.23 M solutions in pentane) was investigated at 23 °C under 4 atmospheres of H_2 (Table A.5). While **5-COD** was investigated for each substrate shown in Table A.5. Results for **5-COE** mediated hydrogenation are reported below those observed for **5-COD** where applicable.

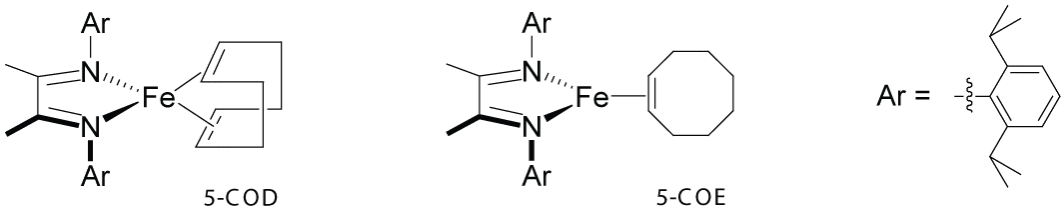

Figure A.15. α-Diimine based iron hydrogenation precatalysts.

Notably, both catalysts readily hydrogenated terminal or cyclic olefins. In the case of limonene, complete conversion of the *gem*-disubstituted olefin was observed under the standard conditions with **5-COD** after 1 day along with minor amounts of trisubstituted olefin hydrogenation. Remarkably, these precatalysts were able to efficiently hydrogenate 2-methyl-2-butene (Table A.5). Due to catalyst death, *vide infra*, only minimal conversions were observed for the hydrogenation of a tetrasubstituted olefin, 2,3-dimethyl-2-butene, with both **5-COD** and **5-COE**.

Table A.5. Unfunctionalized olefin hydrogenation with **5-COD** (top values) and **5-COE** (bottom values).

Substrate	Time (min)	% Conversion	TOF (hr^{-1})
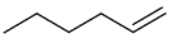	210 180	> 98 > 98	28.6 33.3
	330 270	> 98 > 98	18.2 22.2
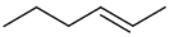	570	> 98	10.5
	720	> 98	8.3
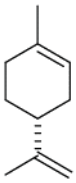	1440	> 98	4.2
	1440 1440	86 > 98	3.6 4.2
	1440 1440	15 18	0.6 0.7

For substrates where **5-COD** and **5-COE** were each employed, **5-COE** was the slightly more active precatalyst. The observation that **5-COD** converts to **5-COE** under 1 atmosphere of hydrogen in cyclohexane-d_{12} solution,[21] offers insight into this phenomenon. Quenching **5-COD** mediated hydrogenations of 1-hexene and cyclohexene at early reaction times revealed very low conversions during the first hour of the reaction by gas chromatography. These observations taken together suggest that there is a relatively slow pre-activation period for the conversion of **5-**

COD to **5-COE** and/or the active catalytic species. Additionally, **5-COD** did not was not active for the hydrosilylation of 1,5-cyclooctadiene, even at elevated temperatures.

The ability of **5-COD** to hydrogenate a series of functionalized substrates was also investigated (Table A.6). Using a 10 mol % catalyst loading of **5-COD** under 4 atmospheres of H_2 at ambient temperature, effective conversion of allylamine to propylamine was observed after 24 hours. Partial hydrogenation of 3-cyclohexene-1-carboxylic acid methyl ester was also observed; however, no hydrogenation of dimethyl itaconate or carvone was observed after 24 hours under these reaction conditions. A more thorough investigation into the reaction chemistry of these substrates with **5-COD** may shed light on the observed selectivity.

Table A.6. Hydrogenation of functionalized olefins with **5-COD**.

Substrate	Time (min)	% Conversion	TOF (hr^{-1})
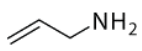	1440	> 98	4.2
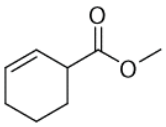	1440	63	2.6
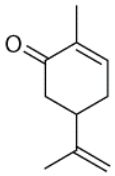	1440	0	N/A
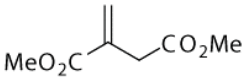	1440	0	N/A

A series of labeling experiments was also conducted to provide further insight into the catalytic hydrogenation process. Performing the deuteration of 1-butene or *cis*-2-butene under 4 atmospheres of D_2 with 5.0 mol % of **5-COD** in benzene solution

allowed the detection of chain-walking by ^{2}H NMR spectroscopy (Figure A.16). For 1-butene, a 2:3 ratio of terminal to internal deuterium incorporation was observed, consistent with a small amount of isomerization. Deuterium incorporation into the methyl groups of butane was also observed from the reduction of *cis*-2-butene. Deuteration of 2,3-dimethyl-2-butene yielded only a small amount of deuterium incorporation into the methyl groups of 2,3-dimethylbutane, while most of the deuterium label was observed in the methine position (Figure A.16). In a similar fashion to other hydrogenation catalysts, deuterium addition occurred with a *syn* orientation across the *exo* face of norbornene.[22]

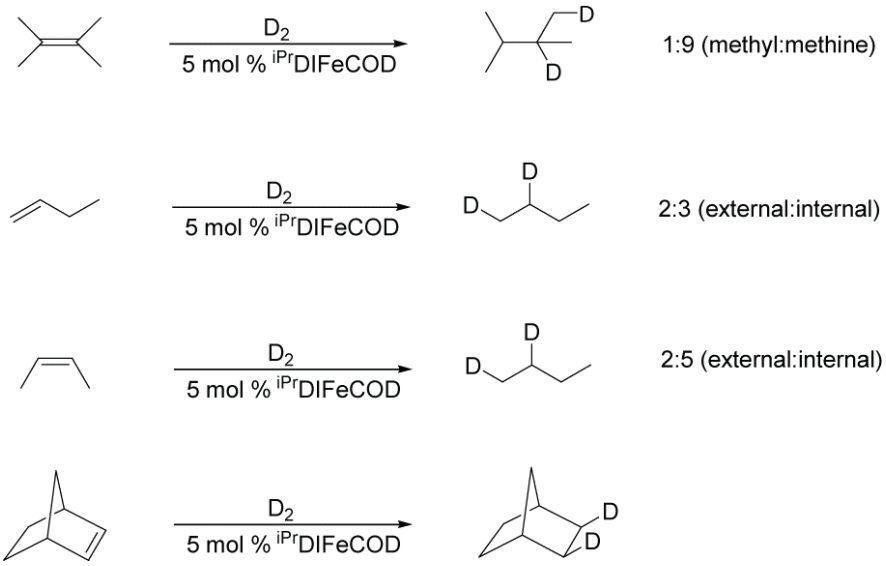

Figure A.16. Deuteration of butenes and norbornene with 5.0 mol % solutions of **5-COD** in benzene.

In an attempt to fully hydrogenate 2,3-dimethyl-2-butene, standard conditions were employed using either **5-COE** or **5-COD** and the solutions were allowed to sit for days. Unfortunately, increasing the reaction time did not result in higher conversions to 2,3-dimethylbutane, but rather, the formation of a new catalytically inactive organometallic along with cyclooctene and cyclooctane. This complex was

identified by X-ray crystallography as the dimer of (^{iPr}DI)Fe (**5$_2$**), where the iron center is coordinated in an η^6-fashion to the diisopropyl aryl group of a second (^{iPr}DI)Fe fragment (Figure A.17). Additionally, exposing solutions of **5-COD** or **5-COE** to 4 atmospheres of hydrogen in the absence of substrate allowed full characterization of this diamagnetic product.

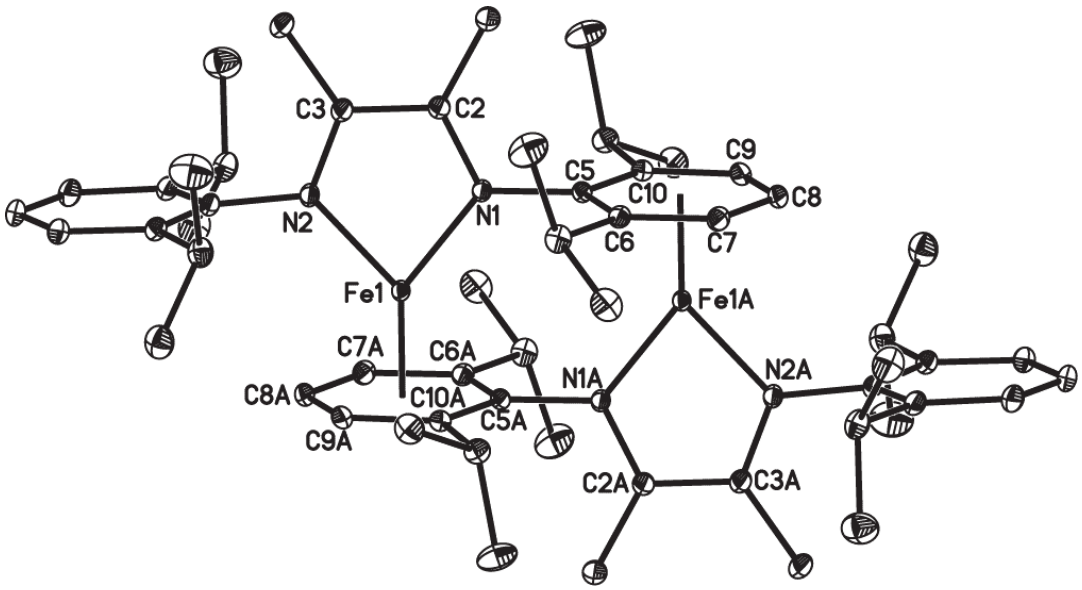

Figure A.17. Molecular structure of **5$_2$** at 30 % probability ellipsoids. Hydrogen atoms omitted for clarity.

The observation of this catalyst deactivation product was not entirely unexpected. Previous attempts to reduce **5-Cl$_2$** in aromatic solvents such as toluene or benzene resulted in the formation of the corresponding η^6-coordinated solvent complexes.[21] Additionally, addition of aromatic substrates to α-diimine iron η^2-acetylene complexes resulted in the immediate displacement of the acetylene ligand with the substrate phenyl group. At first glance, this η^6-arene coordination appears to be thermodynamically favored because it formally results in the formation of an 18 electron, Fe(0) complex. Closer inspection of the metrical parameters of **5$_2$** (Table

A.7) reveal significant contributions from the ene-diamide resonance form of the α-diimine ligand.[21] A cystallographically characterized zirconium complex with two doubly reduced α-diimine ligands has been reported with N_{imine}-C_{imine} and C_{imine}-C_{imine} bond distances of 1.405(3) Å and 1.359(4) Å, respectively.[23] Computationally determined values for α-diimine are as follows: $[DI]^0$: N_{imine}-C_{imine} = 1.29 Å, C_{imine}-C_{imine} = 1.47 Å; $[DI]^-$: N_{imine}-C_{imine} = 1.35 Å, C_{imine}-C_{imine} = 1.40 Å; $[DI]^{2-}$: N_{imine}-C_{imine} = 1.40 Å, C_{imine}-C_{imine} = 1.36 Å.[24]

Table A.7. Selected bond distances (Å) and angles (°) for $\mathbf{5_2}$.

Fe(1)-N(1)	1.9022(9)	N(2)-C(3)	1.3481(14)
Fe(1)-N(2)	1.8934(9)	C(2)-C(3)	1.3897(15)
N(1)-C(2)	1.3549(16)	N(1)-Fe(1)-N(2)	80.94(4)

Because α-diimine ligands can be easily modified at the ligand backbone or imine substituents, modifications of the ^{iPr}DI ligand framework were explored in an attempt to produce more efficient iron hydrogenation catalysts. First, modification of the ligand backbone to include an acenaphthyl moiety was investigated. In a similar fashion to **5-COD**, ^{iPr}ADIFe(η^2,η^2-1,5-C_8H_{12}) (**6-COD**) was prepared by reduction of $\mathbf{6\text{-}Cl_2}$ with excess 0.5 % Na/Hg amalgam in the presence of 10 equivalents of 1,5-cyclooctadiene (Figure A.18, top). In analogy to the the reactivity observed with $\mathbf{5\text{-}Cl_2}$,[21] isolation of an ^{iPr}ADI iron η^2-acetylide complex (**6-(TMSCCTMS)**) was accomplished when this reduction was conducted in the presence of 3 equivalents of bis(trimethylsilyl)acetylene (Figure A.18, bottom).

The catalytic competency of **6-COD** was investigated by conducting the hydrogenation of 1-hexene under the same conditions that were used for **5-COD**

mediated olefin hydrogenation. Unfortunately, poor conversion (7 % after 2 hours) of 1-hexene to hexane was observed when **6-COD** was used as the catalyst precursor. This result was sufficiently discouraging to warrant further reactivity studies, although the low conversion at early reaction times could be an artifact of catalyst pre-activation. Attempts to prepare **6-COE** by reduction of **6-Cl$_2$** in the presence of excess (10 equivalents) of cyclooctene were unsuccessful.

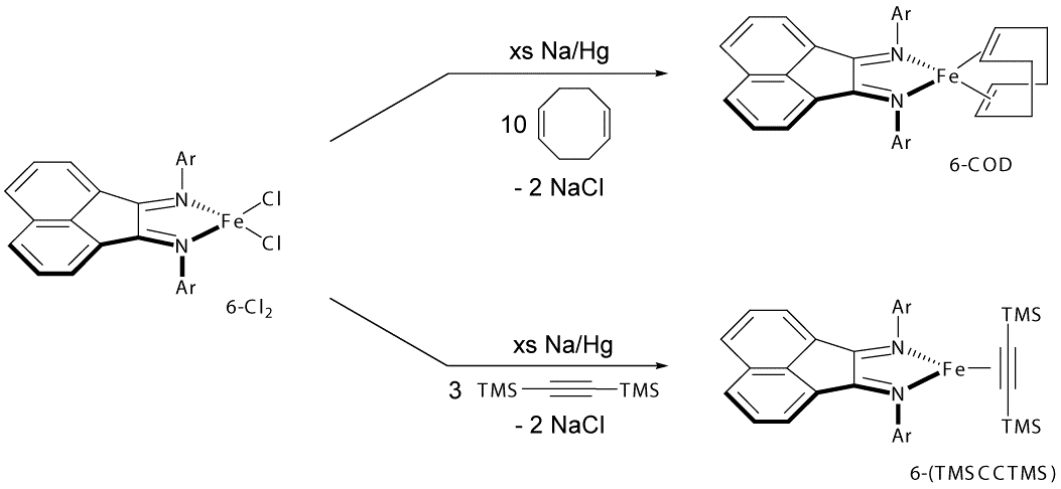

Figure A.18. Preparation of ^{iPr}ADI iron complexes.

Modifications were also made at the imine substituent in the search for more active precatalysts. Upon replacing the diisopropyl aniline with mesityl aniline during ligand preparation, ^{Mes}DI was complexed with iron dichloride in tetrahydrofuran solution according to literature procedures.[25] The resulting dichloride, (^{Mes}DI)FeCl$_2$ (**7-Cl$_2$**), was crystallographically characterized (Figure A.19) and the metrical parameters are presented in Table A.8. Both the N_{imine}-C_{imine} and C_{imine}-C_{imine} bond lengths are consistent with the neutral, α-diimine form of the ligand with distances of 1.2846(12)/1.2810(13) Å and 1.5085(14) Å, respectively.

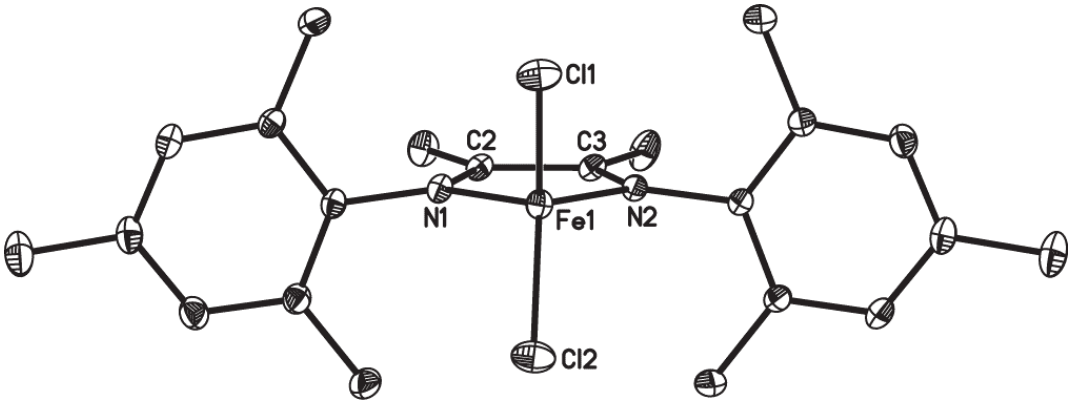

Figure A.19. Solid-state structure of **7-Cl_2** at 30% probability ellipsoids. Hydrogen atoms omitted for clarity.

Table A.8. Selected bond distances (Å) and angles (°) for **7-Cl_2**.

Fe(1)-N(1)	2.1083(8)	N(1)-C(2)	1.2846(12)
Fe(1)-N(2)	2.1154(9)	N(2)-C(3)	1.2810(13)
Fe(1)-Cl(1)	2.2381(4)	C(2)-C(3)	1.5085(14)
Fe(1)-Cl(2)	2.2230(5)	N(1)-Fe(1)-N(2)	76.02(3)

Reduction of either **7-Cl_2** with excess 0.5 % sodium amalgam in pentane resulted in the formation of the bis α-diimine ligand complex **7-^{Mes}DI**. Complexes of this type have been previously observed[21,26] and have been described as having two singly reduced chelates that are antiferromagnetically coupled to a high spin ferrous ion.[27] They exhibit diagnostic ^{1}H NMR spectra with paramagnetically broadened resonances shifted over a 300 ppm range (Figure A.20).[21] The resonance for the imine methyl groups of these complexes, appearing at approximately –250 ppm, is the most shifted from its diamagnetic reference value due to a Fermi contact interaction with the high spin metal center.

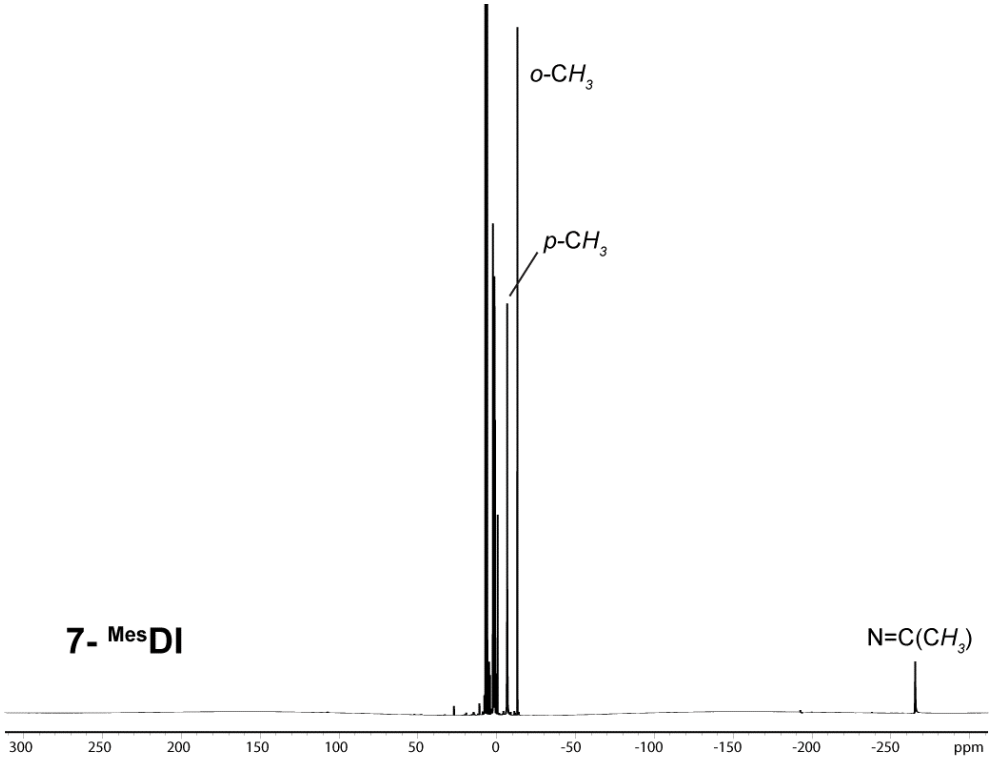

Figure A.20. ^{1}H NMR spectrum of **7-^{Mes}DI** in benzene-d_6 at 20 °C.

Reduction of **7-Cl$_2$** in the presence of trapping reagents was also explored. Attempts to prepare **7-(TMSCCTMS)** or **7-COD** by reduction of **7-Cl$_2$** in the presence of either 3 equivalents of bis(trimethylsilyl)acetylene or cyclooctadiene were unsuccessful and instead resulted in the formation of the bis(ligand) complex, **7-^{Mes}DI**. In fact, observation of **7-COD** was only accomplished by ^{1}H NMR spectroscopy upon conducting the reduction of **7-Cl$_2$** in *neat 1,5-cyclooctadiene*. Even when employing these conditions, this complex could not be isolated as **7-^{Mes}DI** was identified as a major side product (~50 %). Conducting the same reduction in neat benzene; however, allowed formation of the η^6-arene complex, **7-(C$_6$H$_6$)** (Figure A.21), which has been previously described for in the ^{iPr}DI system.

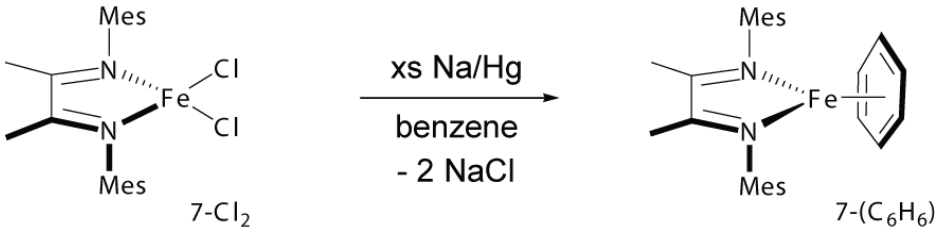

Figure A.21. Reduction of **7-Cl$_2$** with excess 0.5 % sodium amalgam in benzene.

In an attempt to prepare an asymmetric olefin hydrogenation catalyst containing an *α*-diimine ligand framework, bulky chiral amines with substituted *sec*-phenethyl moieties were incorporated into the ligand framework (Figure A.22).[28] Condensation of these amines with acenaphthenequinone has been previously accomplished,[29] and the resulting chiral DI ligands have been utilized for nickel catalyzed, isospecific polymerization of *trans*-2-butene[29] and copolymerization of *α*-olefins.[30,31] This class of ligand provides a second benefit in the development of an *α*-diimine iron catalyst; the steric bulk of the *sec*-phenethyl substituent could potentially disfavor catalyst degradation through formation of a bis(ligand) complex.

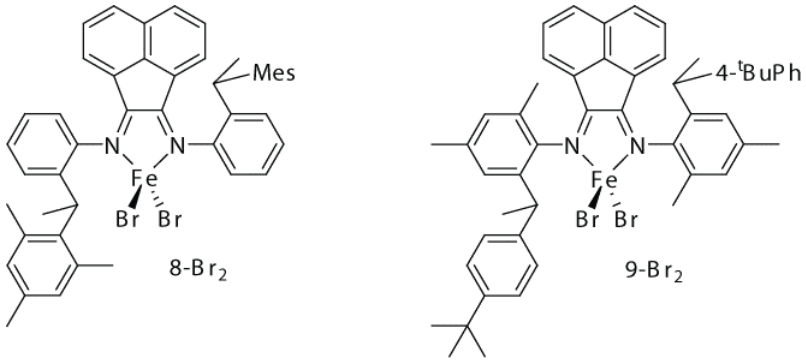

Figure A.22. Chiral *C$_2$*-symmetric *α*-diimine iron dibromide complexes.

The *α*-diimine iron dibromide complexes, **8-Br$_2$** and **9-Br$_2$** (Figure A.22), were readily prepared upon metallation of the ligand with $FeBr_2$ in tetrahydrofuran. Because

it was found to be an effective trapping ligand in the reduction of **5-Cl$_2$** and **6-Cl$_2$**, the reduction of each C_2-symmetric complex was conducted in the presence of excess 1,5-cyclooctadiene. Unfortunately, reduction of **8-Br$_2$** in benzene solution with excess 0.5 % sodium amalgam in the presence of 10 equivalents of 1,5-cyclooctadiene did not result in the formation of **8-COD**. Inspection of the diamagnetic region of the ^{1}H NMR spectrum of the resulting material revealed the formation of **8-Aryl**, where a ligand mesityl group coordinates in an η^6-fashion to the metal center (Figure A.23). The η^6-arene hydrogen ^{1}H NMR resonances (η^6-*m*-mesityl) were located at 4.47 and 5.16 ppm, as iron η^6-arene hydrogens are typically shifted upfield.[21]

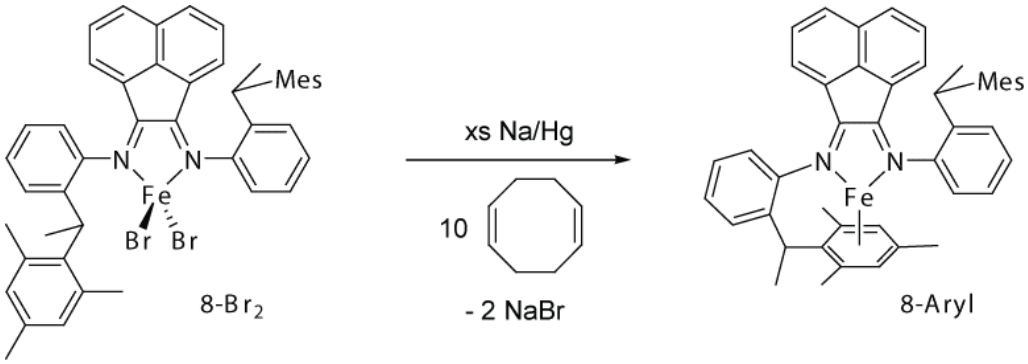

Figure A.23. Preparation of **8-Aryl** from reduction of **8-Br$_2$**.

This product was additionally characterized by X-ray crystallography. The solid-state structure of **8-Aryl** (Figure A.24) confirmed intramolecular η^6-arene coordination and selected metrical parameters for this complex are presented in Table A.8. The metrical parameters of the α-diimine ligand appear consistent with the ene-diamide resonance form of the ligand with N_{imine}-C_{imine} and C_{imine}-C_{imine} distances of 1.3557(12)/1.3363(12) Å and 1.4100(13) Å, respectively. The N(1)-Fe(1)-N(2) bond angle of 83.44(3) ° was similar to the same angle of 80.94(4) ° observed for **5$_2$**.

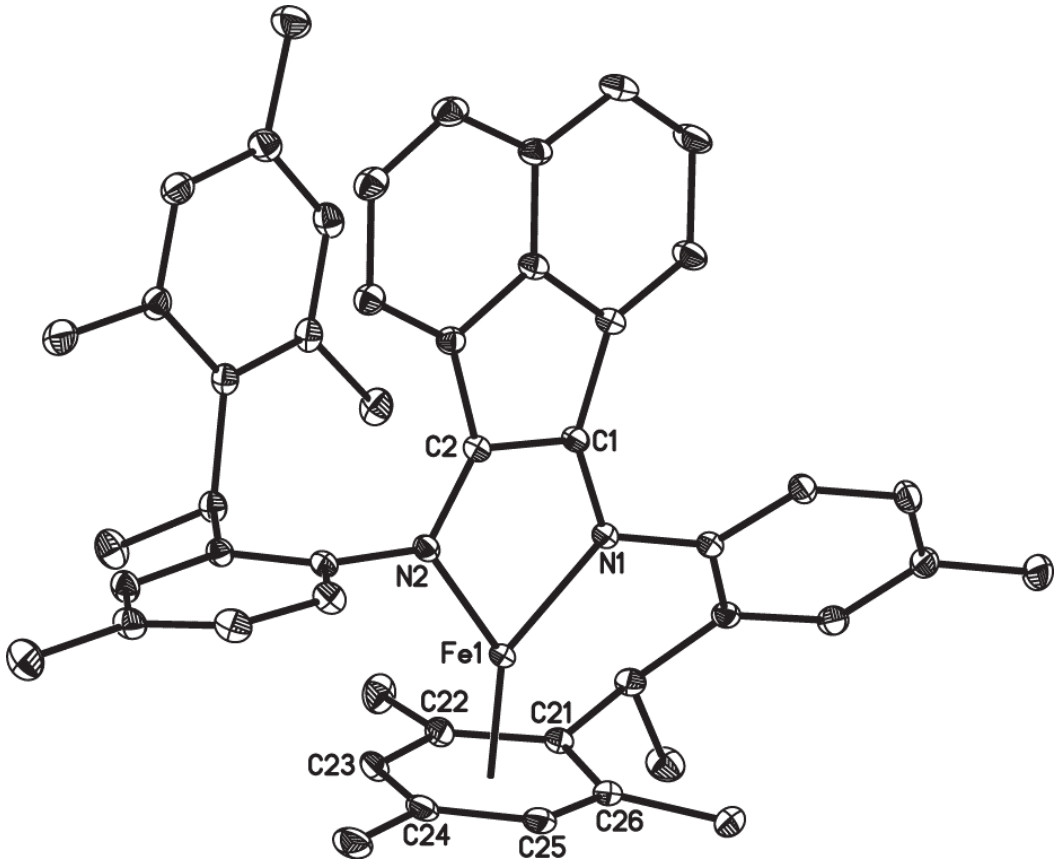

Figure A.24. Molecular structure of **8-Aryl** at 30 % probablility ellipsoids. Hydrogen atoms omitted for clarity.

Table A.7. Selected bond distances (Å) and angles (°) for **8-Aryl**.

Fe(1)-N(1)	1.9114(8)	N(2)-C(2)	1.3363(12)
Fe(1)-N(2)	1.8977(9)	C(1)-C(2)	1.4100(13)
N(1)-C(1)	1.3557(12)	N(1)-Fe(1)-N(2)	83.44(3)

Similar reactivity was observed for the reduction of **9-Br$_2$** in the presence of 20 equivalents of 1,5-cyclooctadiene with excess 0.5 % sodium amalgam. In this case, however, allowing the reduction to proceed for 24 hours resulted in the formation of

an equimolar mixture of **9-Aryl** and **9-^{2,4,6}DI**, the undesired bis(ligand) complex. Allowing the same reduction to stir for 4 days resulted in the observation of only **9-^{2,4,6}DI**. Although bis(ligand) formation was not observed upon reduction of **8-Br$_2$**, allowing the reduction stir for longer reaction times (more than 36 hours), may produce a similar outcome. Unfortunately, both η^6-arene complexes, **8-Aryl** and **9-Aryl**, were not active precatalysts for the hydrogenation or hydrosilylation of 1-hexene.

In order to prepare an asymmetric α-diimine ligated iron hydrogenation catalyst, close attention must be paid to two important aspects of ligand design. The steric influence of the imine substituents must be substantially large in order to prevent the formation of catalytically inactive bis(ligand) iron complexes. Additionally, upon reduction of the iron dihalide precursors or generation of α-diimine iron(0) *in situ*, aromatic ligand substituents and aryl-containing substrates[21] must be avoided.

A.4 Experimental Procedures

Preparation of (^{iPr}APDI)$_2$Fe ((^{iPr}APDI)$_2$Fe). (0.636 g, 1.38 mmol) was suspended in toluene (20 mL), and added to an amalgam of sodium metal (0.159 g, 6.92 mmol) in mercury (31.80 g, 159 mmol) and toluene (100 mL), yielding a dark green solid. After recrystallization from toluene and pentane, a dark green crystalline solid identified as **(^{iPr}APDI)$_2$Fe** (0.276 g, 0.505 mmol, 73%, based on ^{iPr}APDI) was obtained. Crystals suitable for X-ray diffraction studies were grown from a solution of **(^{iPr}APDI)$_2$Fe** in toluene and pentane at -35 °C. Anal. Calcd for $C_{30}H_{46}N_6Fe$: C, 65.92; H, 8.48; N, 15.38. Found: C, 57.26; H, 7.36; N, 11.89. ^{1}H NMR (benzene-d_6, 293 K): δ = 225.4 (1040 Hz), 87.57 (392 Hz), 81.25 (368 Hz), -18.17 (177 Hz), -158.4 (1394 Hz). Magnetic susceptibility: μ_{eff} = 2.9(6) μ_B (benzene-d_6, 293 K); μ_{eff} = 2.4(1) μ_B (Gouy Balance, 293 K).

Preparation of (^{Et}PDI)$_2$Fe (2-(^{Et}PDI)). A 250 mL round bottomed flask was charged with mercury (25.0 g, 124.6 mmol) and approximately 100 mL of pentane. Sodium metal (0.125 g, 5.4 mmol) was added slowly, in small pieces, to the mercury with stirring, and the resulting amalgam was stirred for 20 min to ensure complete dissolution of the metal. A slurry of **2-Br$_2$** (0.500 g, 0.78 mmol) in pentane (10 mL) was added along with ^{Et}PDI (0.331 g, 0.78 mmol), and the capped solution was stirred for 24 h at ambient temperature. The solution was filtered through Celite and pentane and other volatiles were removed in vacuo. The resulting brown solid was recrystallized twice from a concentrated pentane solution, yielding dark brown crystals identified as **2-(^{Et}PDI)** (0.387 g, 0.427 mmol, 55% based on Fe). Lower yields of this complex were obtained when the reduction of **2-Br$_2$** was carried out in the absence of ^{Et}PDI. Crystals suitable for X-ray diffraction studies were grown from a solution of **2-(^{Et}PDI)** in pentane at -35 °C. Anal. Calcd. for $C_{58}H_{70}N_6Fe$: C, 76.80; H, 7.78; N, 9.27. Found: C, 76.49; H, 7.65; N, 8.73. Magnetic susceptibility: μ_{eff} = 2.7(2) μ_B (benzene-d_6, 293 K); μ_{eff} = 3.2 μ_B (SQUID, 300 K). ^{1}H NMR (benzene-d_6, 293 K): δ = 166.3 (7602 Hz), 58.7 (5291 Hz), 1.42 (359 Hz), -0.49 (186 Hz).

Preparation of (^{iPr}PDI)Fe(2,2'-bipyridine) (1-Bpy). A 20 mL scintillation vial was charged with 0.100 g (0.168 mmol) of **1-(N$_2$)$_2$** and approximately 10 mL of toluene. While stirring, a solution of 0.026 g (0.168 mmol) of 2,2'-bipyridine in approximately 5 mL of toluene was added and evolution of N_2 occurred along with a change in color from green to blue. After 1 hour, the solution was filtered through Celite and the solvent was removed *in vacuo* to yield 0.110 g (94%) of a dark blue solid identified as **1-Bpy**. Analysis for $C_{43}H_{51}FeN_5$: Calc. C, 74.45; H, 7.41; N, 10.09. Found: C, 74.14; H, 7.76; N, 9.87. ^{1}H NMR (benzene-d_6): δ = 8.82 (d, 8.0 Hz, 1H, *p-pyr*), 7.78 (t, 8.0 Hz, 2H, *m-pyr*), 7.23 (d, 8.0 Hz, 2H, *bpy*), 6.95 (t, 7.5 Hz, 2H, *p-aryl*), 6.87 (d, 7.5 Hz,

4H, *m-aryl*), 6.80 (t, 7.5 Hz, 2H, *bpy*), 6.43 (d, 6.5 Hz, 2H, *bpy*), 6.01 (t, 6.5 Hz, 2H, *bpy*), 2.10 (sept., 7.0 Hz, 4H, C*H*$(CH_3)_2$), 1.50 (s, 6H, C(C*H*$_3$)), 0.98 (d, 7.0 Hz, 12H, CH(C*H*$_3$)$_2$), 0.72 (d, 7.0 Hz, 12H, CH(C*H*$_3$)$_2$). ^{13}C NMR (benzene-d_6): δ =164.24, 156.13, 153.71, 151.98, 147.56, 141.29, 126.10, 124.97, 123.77, 122.89, 121.89, 120.32, 114.04, 28.23 (*C*H$(CH_3)_2$), 25.48 (CH(*C*H$_3$)$_2$), 25.18 (CH(*C*H$_3$)$_2$), 21.67(*C*(CH_3)).

Preparation of (^{iPr}PDI)Fe(2,2':6',2''-terpyridine) (1-Tpy). This complex was prepared in a manner similar to **1-Bpy** with 0.100 g (0.168 mmol) of **1-$(N_2)_2$** and 0.039 g (0.167 mmol) of 2,2':6',2''-terpyridine to yield 0.085 g (66%) of a dark reddish-purple solid identified as **1-Tpy**. Analysis for $C_{48}H_{54}FeN_6$: Calcd C, 74.79; H, 7.06; N, 10.90. Found: C, 75.01; H, 7.25; N, 10.71. Magnetic susceptibility: μ_{eff} = 2.7(2) μ_B (benzene-d_6, 293 K), μ_{eff} = 2.4(1) μ_B (Gouy balance). ^{1}H NMR (benzene-d_6, 293 K): δ = 219.11 (786 Hz, 1H, ^{iPr}PDI or Tpy *p-pyr*), 196.38 (915 Hz, 1H, ^{iPr}PDI or Tpy *p-pyr*), 108.59 (2239 Hz, 2H, *tpy*), 94.36 (318 Hz, 2H, *tpy*), 83.61 (193 Hz, 2H, *tpy*), 65.50 (250 Hz, 2H, ^{iPr}PDI or Tpy *m-pyr*), 64.31 (259 Hz, 2H, ^{iPr}PDI or Tpy *m-pyr*), 41.50 (127 Hz, 2H, *tpy*), 4.31 (39 Hz, 4H, C*H*$(CH_3)_2$), -1.51 (68 Hz, 12H, CH(C*H*$_3$)$_2$), -3.35 (105 Hz, 12H, CH(C*H*$_3$)$_2$), -147.63 (834 Hz, 6H, C(C*H*$_3$)).

Preparation of [{(2,6-$(CH(CH_3)_2)_2$-C_6H_3)N=C(CH_3)-(CH_3)C=N(μ-η^6-2,6-$(CH(CH_3)_2)_2$-C_6H_3)}Fe]$_2$ ($\mathbf{5_2}$). A dried thick-walled reaction vessel was charged with 1.00 g (0.18 mmol) of **5-COD** and approximately 70 mL of pentane. The vessel was placed on a high vacuum line where it was completely submerged in liquid nitrogen and evacuated. One atmosphere of hydrogen was added and the reaction mixture was warmed to ambient temperature and stirred for 48 hours. The volatiles were removed *in vacuo* and 0.048 g (59%) of a reddish-brown solid identified as **$\mathbf{5_2}$** was obtained by

recrystallization from pentane. Anal. Calcd. for $C_{56}H_{80}Fe_2N_4$: C, 73.03; H, 8.76; N, 6.08. Found: C, 73.05; H, 8.94; N, 5.76. ^{1}H NMR (benzene-d_6): δ = 0.76 (s, 6H, N=C(CH_3)), 0.85 (d, 6.8 Hz, 12H, CH(CH_3)$_2$), 0.91 (s, 6H, N=C(CH_3)), 1.08 (d, 6.8 Hz, 12H, CH(CH_3)$_2$), 1.69 (d, 6.8 Hz, 12H, CH(CH_3)$_2$), 1.74 (d, 6.8 Hz, 12H, CH(CH_3)$_2$), 3.95 (sept, 6.8 Hz, 4H, CH(CH$_3$)$_2$), 4.04 (sept, 6.8 Hz, 4H, CH(CH$_3$)$_2$), 4.43 (t, 6.8 Hz, 2H, *p*-(*μ*-η^6-*aryl*)), 5.90 (d, 6.8 Hz, 4H, *m*-(*μ*-η^6-*aryl*), 7.35 (d, 6.8 Hz, *m-aryl*), 7.41 (t, 6.8 Hz, 2H, *p-aryl*). ^{13}C NMR (benzene-d_6): δ = 18.72 (*C*H(CH$_3$)$_2$), 21.63 (*C*H(CH$_3$)$_2$), 24.53 (CH(*C*H$_3$)$_2$), 24.82 (CH(*C*H$_3$)$_2$), 25.21 (CH(*C*H$_3$)$_2$), 25.44 (CH(*C*H$_3$)$_2$), 27.85 (N=C(*C*H$_3$)), 28.08 (N=C(*C*H$_3$)), 76.10 (*μ*-η^6-*aryl*), 82.93 (*μ*-η^6-*aryl*), 97.48 (*μ*-η^6-*aryl*), 117.08 (*μ*-η^6-*aryl*), 123.43 *(aryl)*, 123.49 (*aryl*), 125.74 (*aryl*), 141.86 (*aryl*), 143.83 (N=*C*(CH$_3$)), 144.51 (N=*C*(CH$_3$)).

Preparation of [(2,6-(CH(CH$_3$)$_2$)$_2$-C$_6$H$_3$)N=C(An)-(An)C=N(2,6-(CH(CH$_3$)$_2$)$_2$-C$_6$H$_3$)]Fe(η^2-η^2-1,5,-C$_8$H$_{12}$) (6-COD). While stirring, 0.500 g (0.795 mmol) of [(2,6-(CH(CH$_3$)$_2$)$_2$-C$_6$H$_3$)N=C(An)-(An)C=N(2,6-(CH(CH$_3$)$_2$)$_2$-C$_6$H$_3$)]FeCl$_2$ (**6-Cl$_2$**) was added to a 250 mL round-bottomed flask containing 0.092 g (3.98 mmol) of Na, 18.4 g (91.7 mmol) of Hg, 0.859 g (7.95 mmol) of 1,5-cyclooctadiene, and approximately 100 mL of pentane. After stirring for 72 hours, the reaction mixture was filtered through Celite, the solvent was removed in vacuo, and the resulting brownish-green solid was recrystallized from pentane to afford 0.287 g (50%) of **6-COD**. Anal. Calcd. for $C_{44}H_{52}FeN_2$: C, 79.50; H, 7.88; N, 4.21. Found: C, 79.68; H, 7.87; N, 4.12. ^{1}H NMR (benzene-d_6) δ = -185.9 (638 Hz), -62.7 (307 Hz), -7.1 (22 Hz), -4.2 (15 Hz), -0.4 (56 Hz), 0.2 (27 Hz), 3.8 (18 Hz), 5.0 (6 Hz), 50.6 (52 Hz), 56.3 (36 Hz), 272.9 (2 Hz).

Preparation of [(2,6-(CH(CH$_3$)$_2$)$_2$-C$_6$H$_3$)N=C(An)-(An)C=N(2,6-(CH(CH$_3$)$_2$)$_2$-C$_6$H$_3$)]Fe(η^2-(CH$_3$)$_3$SiC≡CSi(CH$_3$)$_3$) (6-(TMSCCTMS)). While stirring, 0.150 g (0.239 mmol) of **6-Cl$_2$** was added to a 25 mL round-bottomed flask containing 0.028 g (1.195 mmol) of Na, 5.6 g (27.9 mmol) of Hg, 0.122 g (0.717 mmol) of (CH$_3$)$_3$SiC≡CSi(CH$_3$)$_3$, and approximately 20 mL of pentane. After stirring for 48 hours, the reaction mixture was filtered through Celite, the solvent was removed *in vacuo*, and the resulting brownish-green solid was recrystallized from pentane to afford 0.072 g (41%) of **6-(TMSCCTMS)**. Anal. Calcd. for C$_{44}$H$_{58}$FeN$_2$Si$_2$: C, 72.70; H, 8.04; N, 3.85. Found: C, 72.42; H, 8.00; N, 3.72. ^{1}H NMR (benzene-*d*$_6$) δ = -42.6 (141 Hz), -38.2 (280 Hz), -23.2 (30 Hz), 1.0 (14 Hz), 6.2 (83 Hz), 71.5 (30 Hz), 78.8 (127 Hz).

Preparation of [(2,4,6-(CH$_3$)$_3$-C$_6$H$_2$)N=C(CH$_3$)-(CH$_3$)C=N(2,4,6-(CH$_3$)$_3$-C$_6$H$_2$)]FeCl$_2$ (7-Cl$_2$). A dried 500 mL round-bottomed flask was charged with 5.00 g (15.5 mmol) of (2,4,6-(CH$_3$)$_3$-C$_6$H$_2$)N=C(CH$_3$)-(CH$_3$)C=N(2,4,6-(CH$_3$)$_3$-C$_6$H$_2$), 1.90 g (15.5 mmol) of FeCl$_2$, and approximately 200 mL of tetrahydrofuran. The solution immediately turned green in color and was stirred for 24 hours. The solvent was removed *in vacuo* and the remaining red residue was collected by filtration with pentane. After washing with an additional 20 mL of pentane, 5.84 g (84%) of a reddish-brown solid identified as **7-Cl$_2$** was obtained. Anal. Calc. for C$_{22}$H$_{28}$Cl$_2$FeN$_2$: C, 59.08; H, 6.31; N, 6.26. Found: C, 59.44; H, 6.27; N, 5.81.

Preparation of [(2,4,6-(CH$_3$)$_3$-C$_6$H$_2$)N=C(CH$_3$)-(CH$_3$)C=N(2,4,6-(CH$_3$)$_3$-C$_6$H$_2$)]$_2$Fe (7-^{Mes}DI). A 20 mL scintillation vial was charged with 0.052 g (2.24 mmol) of sodium metal, 10.4 g (51.8 mmol) of mercury, and approximately 12 mL of pentane. While stirring, 0.200 g (0.488 mmol) of **7-Cl$_2$** was added. After stirring for 1 hour, the

solution was filtered through Celite and the solvent was removed *in vacuo* to yield 0.104 g (67%) of a yellowish-brown solid identified as **7-^{Mes}DI**. Anal. Calc. for $C_{44}H_{56}FeN_4$: C, 75.84; H, 8.10; N 8.04. Found: C, 75.24; H, 8.70; N, 8.04. ^{1}H NMR (benzene-d_6): δ = -265.84 (97.24, 12H, N=C(CH_3)), -13.l9 (19.23, 8H, *aryl*), -6.71 (58.71, 24H, *o*-CH_3), 5.90 (16.92, 12H, *p*-CH_3).

Preparation of [(2,4,6-(CH$_3$)$_3$-C$_6$H$_2$)N=C(CH$_3$)-(CH$_3$)C=N(2,4,6-(CH$_3$)$_3$-C$_6$H$_2$)]Fe(η^6-C$_6$H$_6$) (7-C$_6$H$_6$). While stirring, 0.334 g (0.747 mmol) of **7-Cl$_2$** was added to a 250 mL round-bottomed flask containing 0.086 g (3.74 mmol) of Na, 17.2 g (85.8 mmol) of Hg, and approximately 100 mL of benzene. The olive green solution became bright orange in color after stirring at ambient temperature for 48 hours. The reaction mixture was decanted and filtered though Celite and the filtrate collected. The solvent was removed *in vacuo* and the resulting solid recrystallized from pentane yielded 0.117 g (34%) of a deep red solid identified as **7-(C$_6$H$_6$)**. Anal. Calc. for $C_{28}H_{34}FeN_2$: C, 74.01; H, 7.54; N, 6.16. Found: C, 74.29; H, 7.25; N, 6.29. ^{1}H NMR (benzene-d_6): δ = 1.05 (s, 6H, N=C(CH_3)), 2.27 (s, 12H, *o*-CH_3), 2.35 (s, 6H, *p*-CH_3), 4.82 (s, 6H, C$_6H_6$), 7.00 (s, 4H, *m-aryl*). ^{13}C NMR (benzene-d_6): δ = 15.64 (*p*-*C*H$_3$), 18.28 (*o*-*C*H$_3$), 21.22 (N=C(*C*H$_3$)), 81.47 (*C$_6$*H$_6$), 128.68 (*aryl*), 130.39 (*aryl*), 133.32 (*aryl*), 142.03 (*aryl*), 154.58 (N=*C*(CH$_3$)).

Preparation of *rac*-[2-CH(CH$_3$)(2,4,6-(CH$_3$)$_3$-C$_6$H$_2$)-4-CH$_3$-C$_6$H$_3$N=C(An)-(An)C=NC$_6$H$_3$-2-CH(CH$_3$)(2,4,6-(CH$_3$)$_3$-C$_6$H$_2$)-4-CH$_3$]FeBr$_2$ (8-Br$_2$). A 250 mL round-bottomed flask was charged with 0.562 g (0.862 mmol) of *rac*-[2-CH(CH$_3$)(2,4,6-(CH$_3$)$_3$-C$_6$H$_2$)-4-CH$_3$-C$_6$H$_3$N=C(An)-(An)C=NC$_6$H$_3$-2-CH(CH$_3$)(2,4,6-(CH$_3$)$_3$-C$_6$H$_2$)-4-CH$_3$], 0.186 g (0.862 mmol) of FeBr$_2$, and approximately 150 mL of tetrahydrofuran. A green solution resulted within a few

minutes of stirring and the reaction was allowed to proceed for 24 hours. The solution was filtered though a frit and the solvent was removed *in vacuo* to yield 0.517 g (69%) of a tan solid identified as **8-Br$_2$**. Anal. Calcd. for $C_{48}H_{58}Br_2FeN_2$: C, 66.38; H, 5.57; N, 3.23. Found: C, 65.86; H, 5.30; N, 2.89.

Preparation of [2-CH(CH$_3$)(η^6-2,4,6-(CH$_3$)$_3$-C$_6$H$_2$)-4-CH$_3$-C$_6$H$_3$N=C(An)-(An)C=NC$_6$H$_3$-2-CH(CH$_3$)(2,4,6-(CH$_3$)$_3$-C$_6$H$_2$)-4-CH$_3$]Fe (8-Aryl). A 100 mL round-bottomed flask was charged with 0.190 g (0.219 mmol) of **8-Br$_2$** and approximately 50 mL of benzene. While stirring, an amalgam prepared from 0.025 g of sodium (1.09 mmol) and 5 g of mercury was added to the flask. The solution slowly turned purple in color and was allowed to stir for 36 hours. At that time, the solution was filtered through Celite and the solvent was evacuated to yield a purple solid identified as **8-Aryl**. Anal. Calcd. for $C_{48}H_{52}FeN_2$: C, 81.34; H, 6.83; N, 3.95. Found: C, 81.31; H, 6.96; N, 3.73. ^{1}H NMR (benzene-d_6): δ = 7.84 (d, 8.0 Hz, 1H, *aryl*), 7.72 (s, 1H, *aryl*), 7.57 (d, 8.0 Hz, 1H, *aryl*), 7.54 (s, 1H, *aryl*), 7.42 (d, 8.0 Hz, 1H, *aryl*), 7.25 (d, 8.0 Hz, 1H, *aryl*), 7.14 (s, 1H, *aryl*), 7.06 (d, 8.0 Hz, 1H, *aryl*), 6.99 (d, 8.0 Hz, 1H, *aryl*), 6.95 (t, 8.0 Hz, 1H, *aryl*), 6.74 (d, 8.0 Hz, 1H, *aryl*), 6.48 (t, 8.0 Hz, 1H, *aryl*), 6.05 (s, 1H, *aryl*), 5.99 (d, 8.0 Hz, 1H, *aryl*), 5.72 (q, 7.5 Hz, 1H, C*H*CH$_3$), 5.57 (s, 1H, *aryl*), 5.16 (s, 1H, η^6-*aryl*), 4.91 (q, 7.5 Hz, 1H, C*H*CH$_3$), 4.47 (s, 1H, η^6-*aryl*), 2.54 (s, 3H, *methyl*), 2.43 (s, 3H, *methyl*), 2.22 (s, 3H, *methyl*), 2.19 (s, 3H, *methyl*), 1.85 (d, 7.5 Hz, 3H, CHC*H$_3$*), 1.83 (s, 3H, *methyl*), 1.79 (d, 7.5 Hz, 3H, CHC*H$_3$*), 1.56 (s, 3H, *methyl*), a.45 (s, 3H, *methyl*), 1.18 (s, 3H, *methyl*).

REFERENCES

[1] Dickson, D. P. E.; Barry, F. J. Mössbauer Spectroscopy, Cambridge University Press: Cambridge, 1986.

[2] Chirik P. J. *Angew*. *Chem*. *Int*. *Ed*. **2006**, *45*, 6956.

[3] de Bruin, B.; Bill, E.; Bothe, E.; Weyhermüller, T.; Wieghardt, K. *Inorg*. *Chem*. **2000**, *39*, 2936.

[4] Knijnenburg, Q.; Gambarotta, S.; Budzelaar, P. H. M. *Dalton Trans*. **2006**, 5442.

[5] Baker, A. T.; Goodwin, H. A. *Aust*. *J*. *Chem*. **1985**, *38*, 207.

[6] Epstein, L. M. *J*. *Phys*. *Chem*. **1964**, *40*, 435.

[7] Collins, R. L.; Pettit, R.; Baker, W. A., Jr. *J*. *Inorg*. *Nucl*. *Chem*. **1966**, *28*, 1001.

[8] Bart, S. C.; Chlopek, K.; Bill, E.; Bouwkamp, M. W.; Lobkovsky, E.; Neese, F.; Wieghardt, K. W.; Chirik, P. J. *J*. *Am*. *Chem*. *Soc*. **2006**, *128*, 13901.

[9] Sinnecker, S.; Slep, L. D.; Bill, E.; Neese, F. *Inorg*. *Chem*. **2005**, *44*, 2245.

[10] Neese, F. *Inorg*. *Chim*. *Acta* **2002**, *337*, 181.

[11] Bart, S. C.; Lobkovsky, E.; Bill, E.; Wieghardt, K.; Chirik, P. J. *Inorg*. *Chem*. **2007**, *46*, 7055.

[12] Daku, L. M. L.; Vargas, A.; Hauser, A.; Fouqueau, A.; Casida, M. E. *Chem*. *Phys*. *Chem*. **2005**, *6*, 1393.

[13] Dick, S. *Krystallogr*.*-New Cryst*. *Struct*. **1998**, *213*, 356.

[14] García Posse, M. E.; Juri, M. A.; Aymonino, P. J.; Piro, O. E.; Negri, H. A.; Castellano, E. E. *Inorg*. *Chem*. **1984**, *23*, 948.

[15] Braterman, P. S.; Song, J.-I.; Peacock, R. D. *Inorg*. *Chem*. **1992**, *31*, 555.

[16] Bessel, C. A.; See, R. F.; Jameson, D. L.; Churchill M. R.; Takeuchi, K. J. *J*. *Chem*. *Soc*., *Dalton Trans*. **1992**, 3217.

[17] Kabir, M. K.; Tobita, H.; Matsuo, H.; Nagayoshi, K.; Yamada, K.; Adachi, K.; Sugiyama, Y.; Kitagawa, S.; Kawata, S. *Cryst*. *Growth Des*. **2003**, *3*, 795.

[18] Winkler, J. R.; Sutin, N. *Inorg*. *Chem*. **1987**, *26*, 220.

[19] Creutz, C.; Chou, M.; Netzel, T. L.; Okumura, M.; Sutin, N. *J*. *Am*. *Chem*. *Soc*. **1980**, *102*, 1309.

[20] Meyer, T. J. *Acc*. *Chem*. *Res*. **1989**, *22*, 163.

[21] Bart, S. C.; Hawrelak, E. J.; Lobkovsky, E.; Chirik, P. J. *Organometallics* **2005**, *24*, 5518.

[22] Bart, S. C.; Lobkovsky, E.; Chirik, P. J. *J. Am. Chem. Soc.* **2004**, *126*, 13794.

[23] Stanciu, C.; Jones, M. E.; Fanwick, P. E.; Abu-Omar, M. M. *J. Am. Chem. Soc.* **2007**, *129*, 12400.

[24] Wieghardt, K. *Personal Communication*.

[25] Bart, S. C.; Hawrelak, E. J.; Schmisseur, A. K.; Lobkovsky, E.; Chirik, P. J. *Organometallics* **2004**, *23*, 237.

[26] tom Dieck, H.; Bruder, H. *Chem. Commun.* **1977**, 24.

[27] Muresan, N.; Lu, C. C.; Ghosh, M.; Peters, J. C.; Abe, M.; Henling, L. M.; Weyhermöller, T.; Bill, E.; Wieghardt, K. *Inorg. Chem.* **2008**, *47*, 4579.

[28] Cherian, A. E.; Domski, G. J.; Rose, J. M.; Lobkovsky, E. B.; Coates, G. W. *Org. Lett.* **2005**, *23*, 5135.

[29] Cherian, A. E.; Lobkovsky, E. B.; Coates, G. W. *Chem. Commun.* **2003**, *20*, 2566.

[30] Cherian, A. E.; Rose, J. M.; Lobkovsky, E. B.; Coates, G. W. J. Am. Chem. Soc. **2005**, *127*, 13770.

[31] Rose, J. M.; Cherian, A. E.; Coates, G. W. *J. Am. Chem. Soc.* **2006**, *128*, 4186.

APPENDIX B

INVESTIGATION OF PDI IRON COMPLEXES BY EPR SPECTROSCOPY

General Procedure: A 2 mM solution of each complex was prepared in a 60:40 toluene:pentane solvent mixture. Each sample was cooled by quickly submerging a loaded EPR tube (~ 2 cm sample height) in liquid nitrogen for less than one second and quickly pulling it back out several times. When cold, the tube was left in liquid nitrogen for approximately one minute, at which time it was transferred to a liquid nitrogen cooled dewar located in the resonator of a Bruker EPR spectrometer. Data was recorded at 77 K with a modulation amplitude of 2 mT and an attenuation of 1 mW. Additional data was collected at 5 K for the monohalide complexes when no signal was observed at 77 K. Simulations were conducted using the W95EPR software package.

Table B.1. Compilation of EPR data for compounds discussed in this manuscript.

Compound	Simulated *g*-values [line widths]
1-CC^{t}Bu(py)	2.275[20], 2.050[11], 2.019[12]
1-CCPh(py)	2.255[16], 2.063[8], 2.035[10]
1-Ph(Et_2O)	2.224[14], 2.1258[12], 2.0765[12]
1-Np(py)	2.23[27], 2.024[21]
1-Cl(py)	1.845[72], 3.04[85], 5.10[30]
1-Br(py)	1.895[92], 3.25[113], 5.05[45]

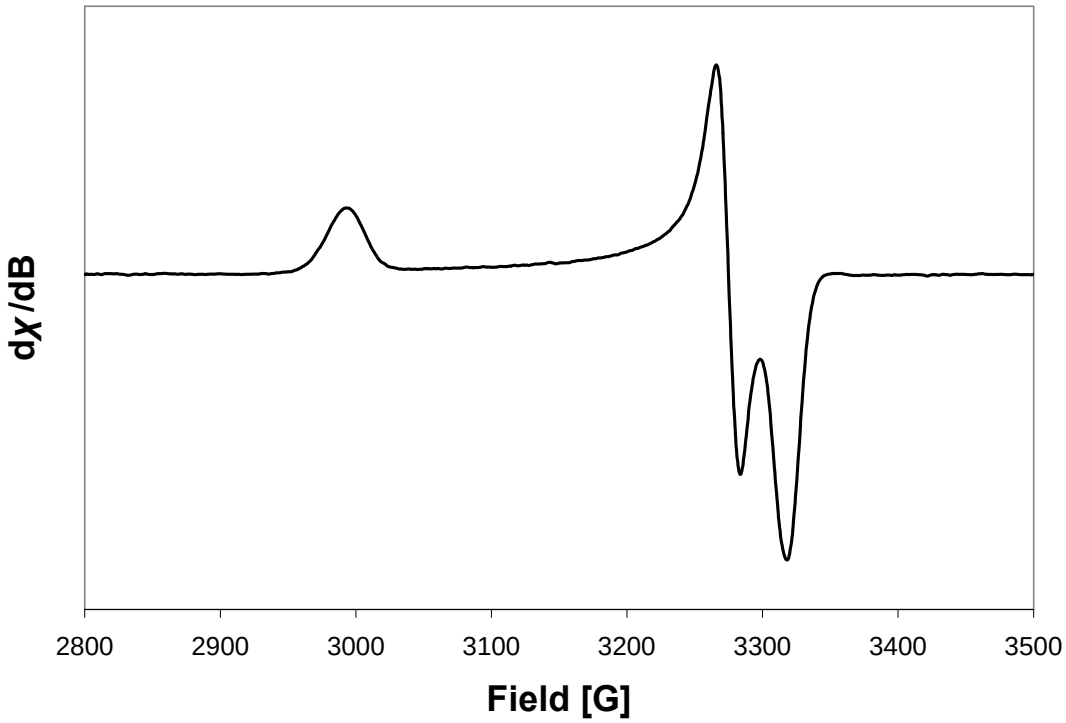

Figure B.1. EPR spectrum of **1-CCPh(py)** at 77 K.

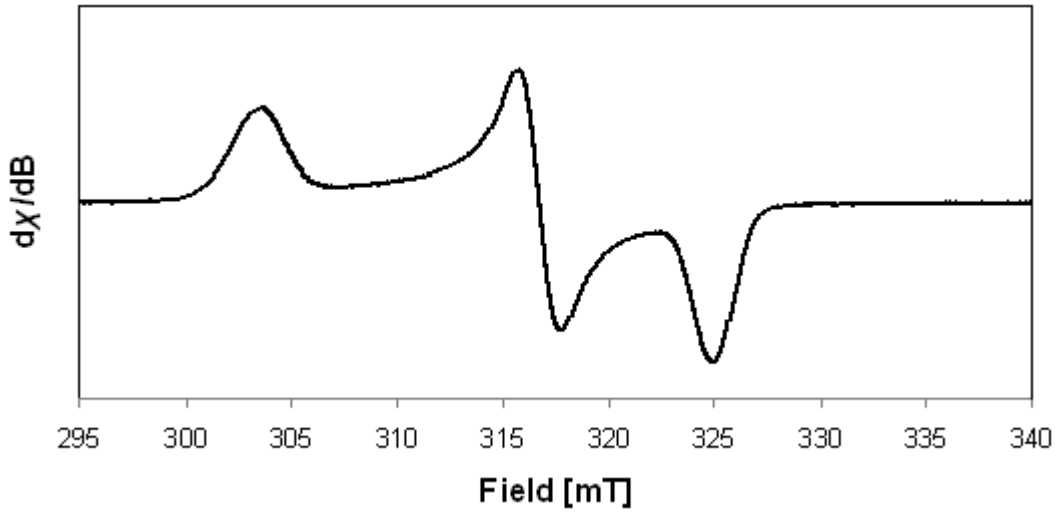

Figure B.2. EPR spectrum of **1-Ph(Et_2O)** at 77 K.

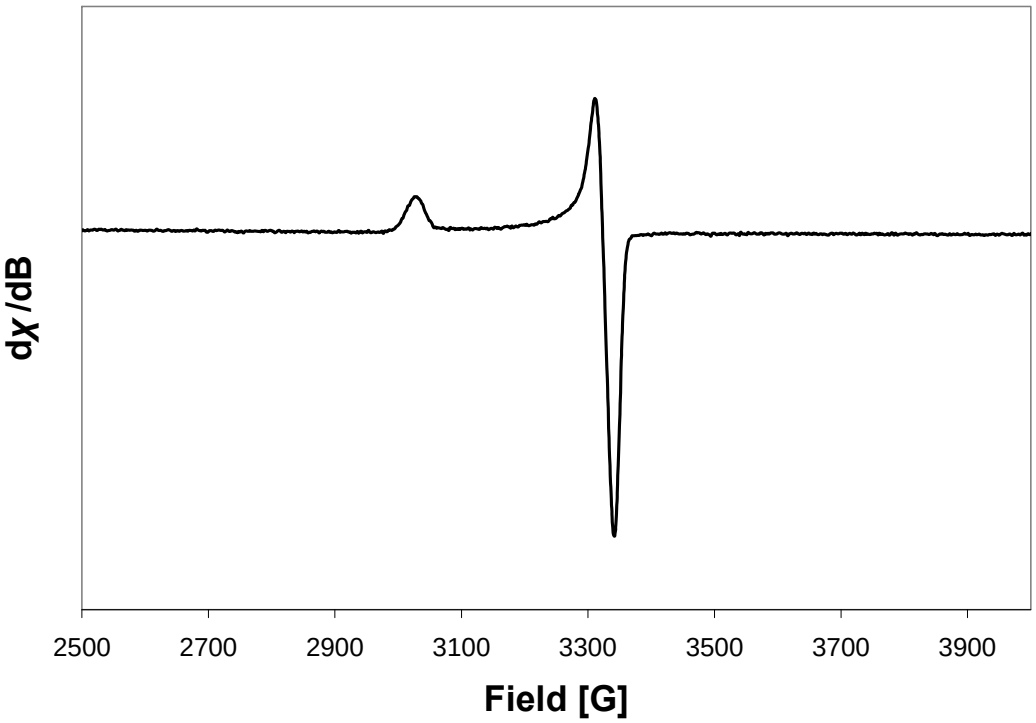

Figure B.3. EPR spectrum of **1-Np(py)** at 77 K.

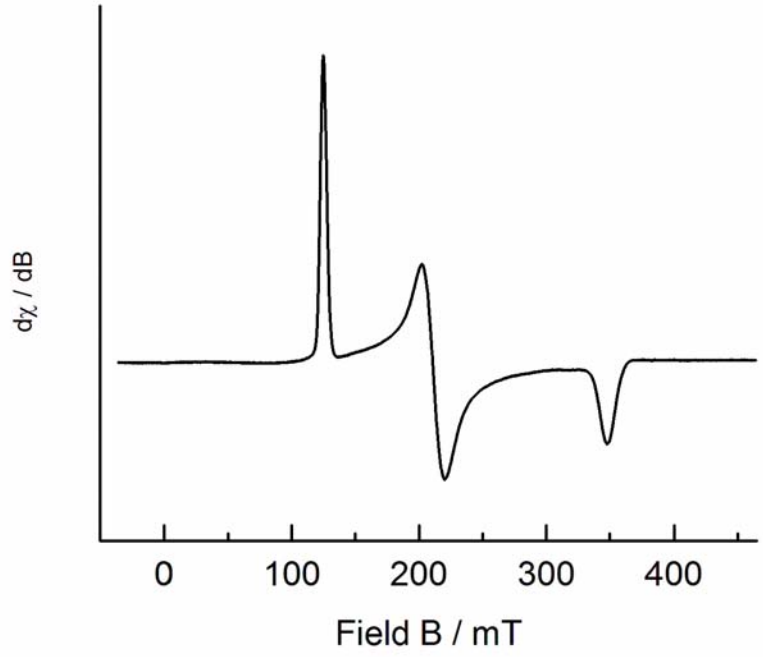

Figure B.4. EPR spectrum of **1-Cl(py)** at 5 K.

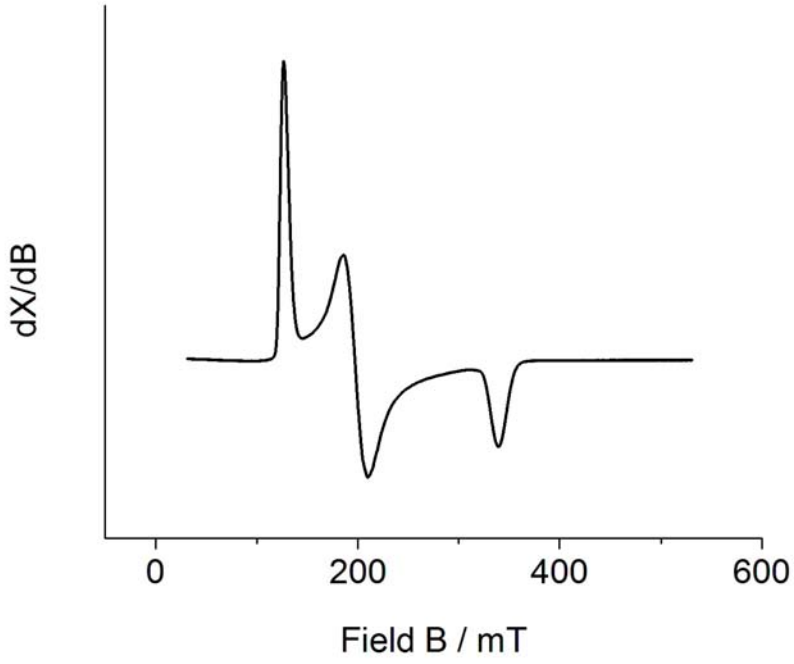

Figure B.5. EPR spectrum of **1-Br(py)** at 5 K.

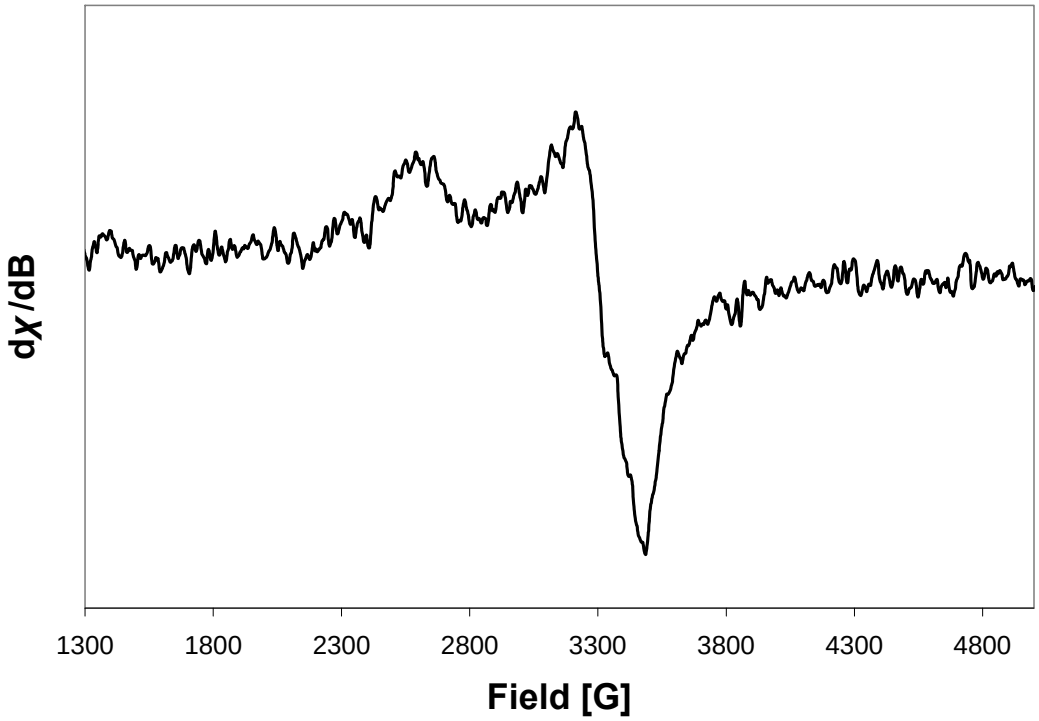

Figure B.6. EPR spectrum of **1-Allyl** at 77 K.

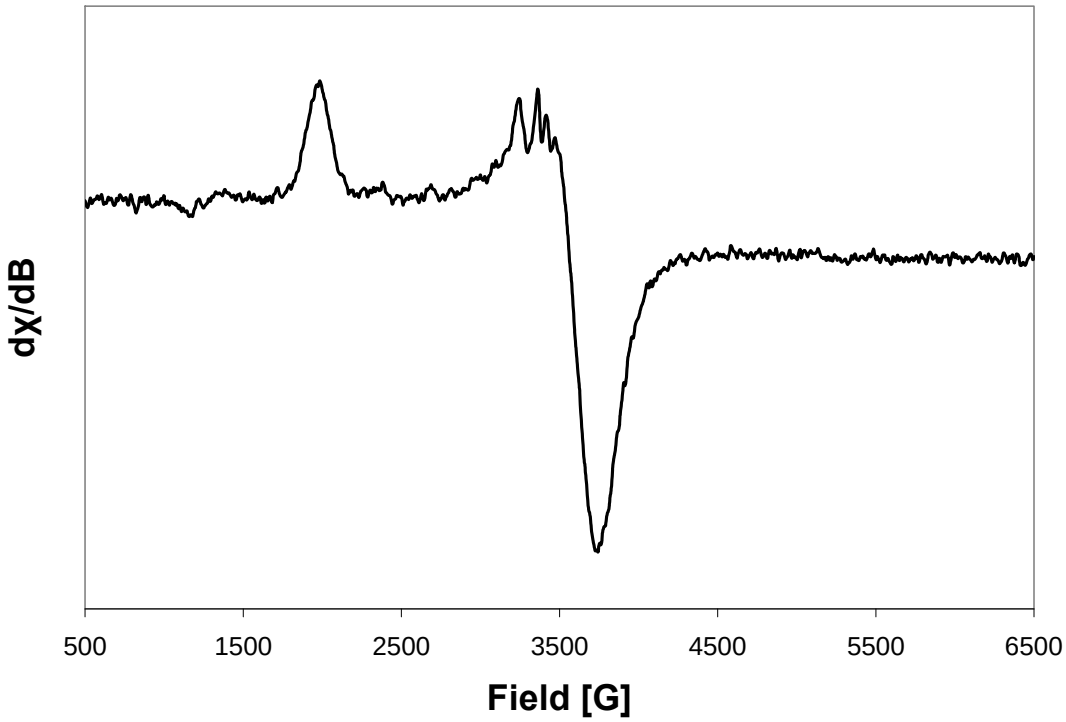

Figure B.7. EPR spectrum of **1-CCPh** at 77 K.

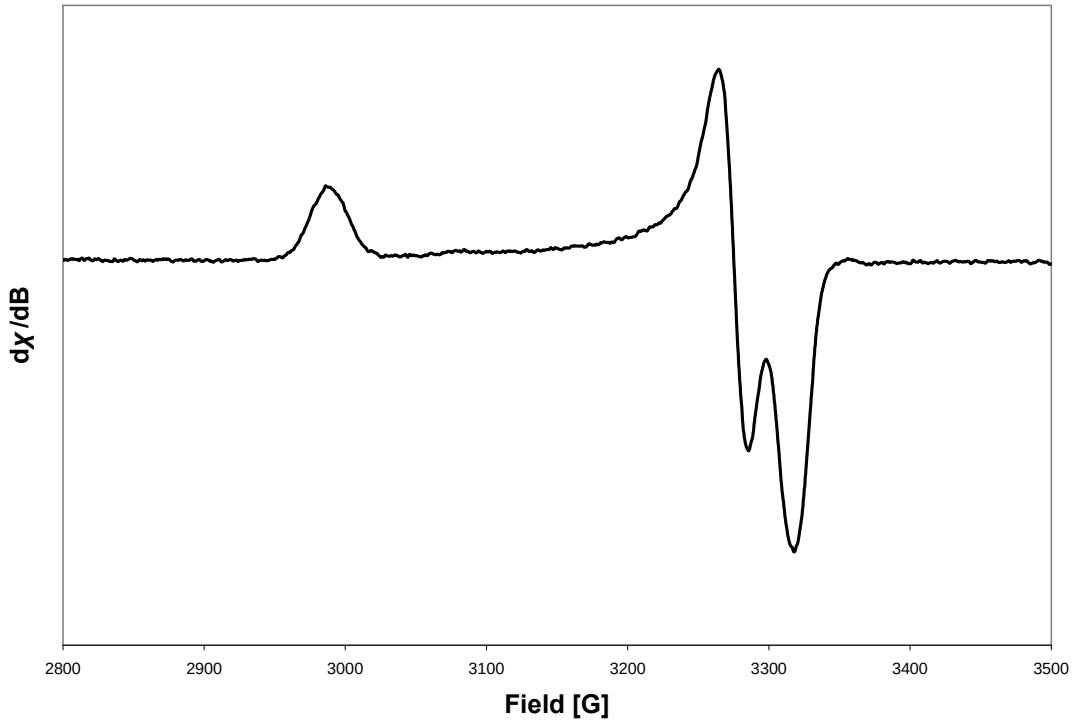

Figure B.8. EPR spectrum of **1-CC^{t}Bu(py)** at 77 K.

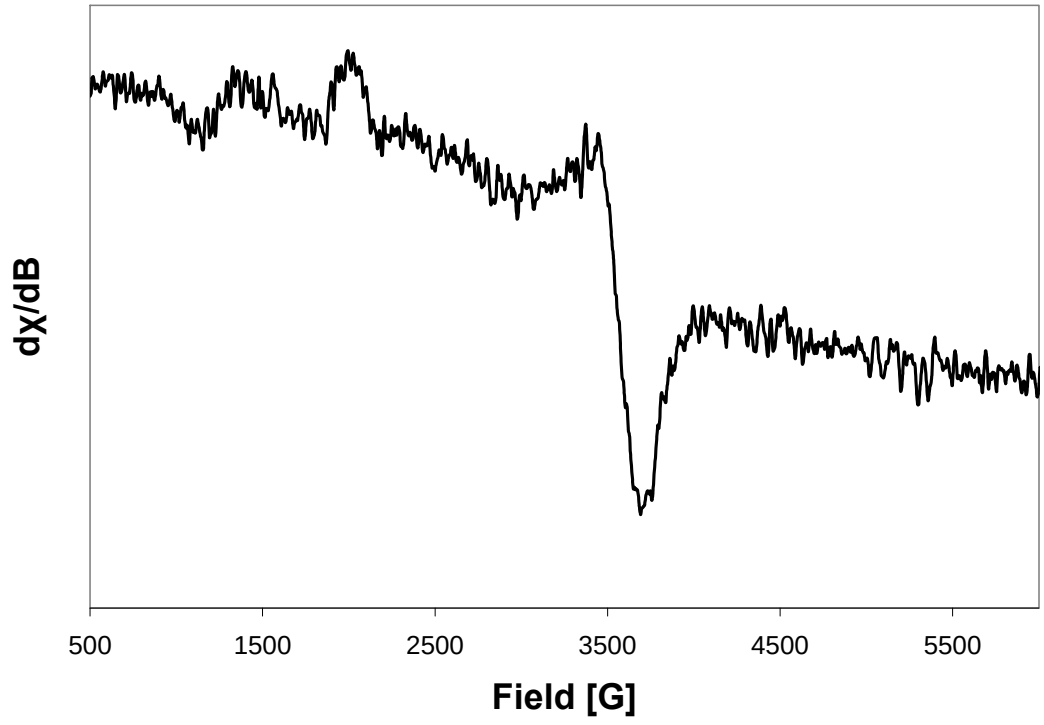

Figure B.9. EPR spectrum of **1-CC^{t}Bu** at 77 K.

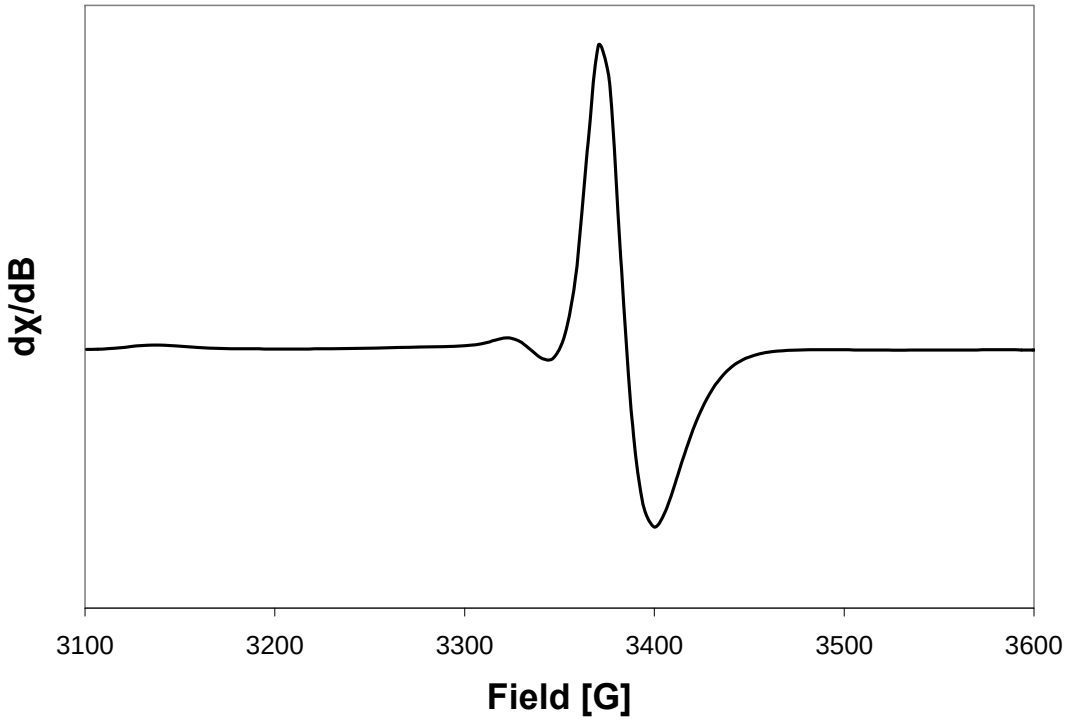

Figure B.10. EPR spectrum of **1-Me(py)** at 77 K.

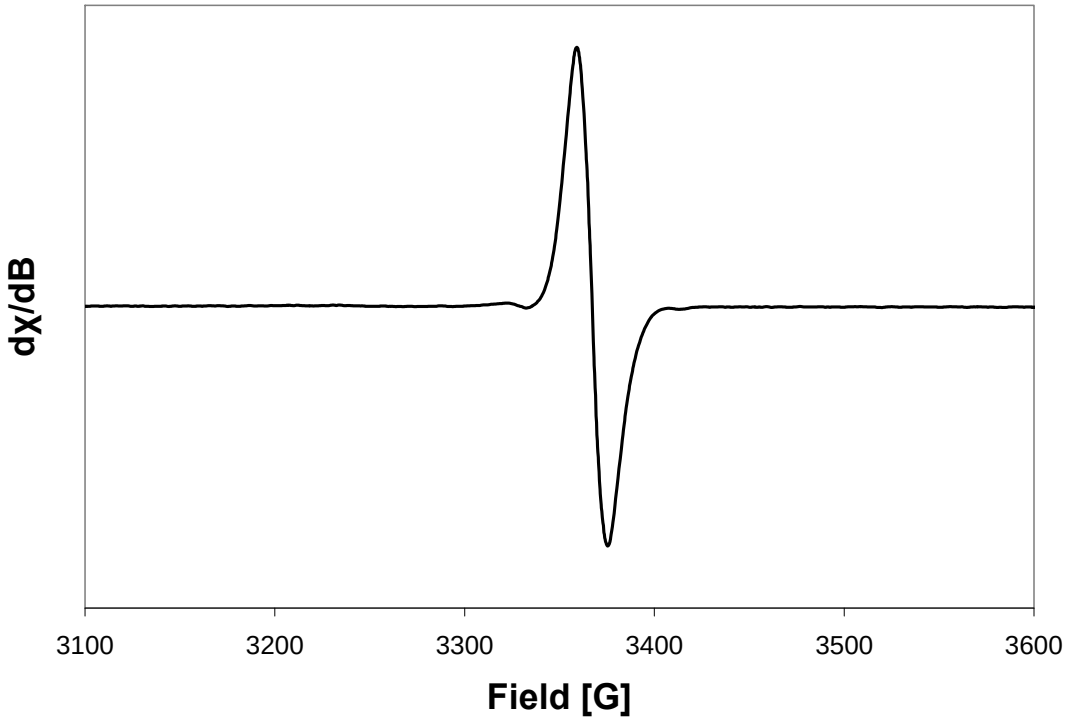

Figure B.11. EPR spectrum of **1-^{i}Bu(py)** at 77 K.

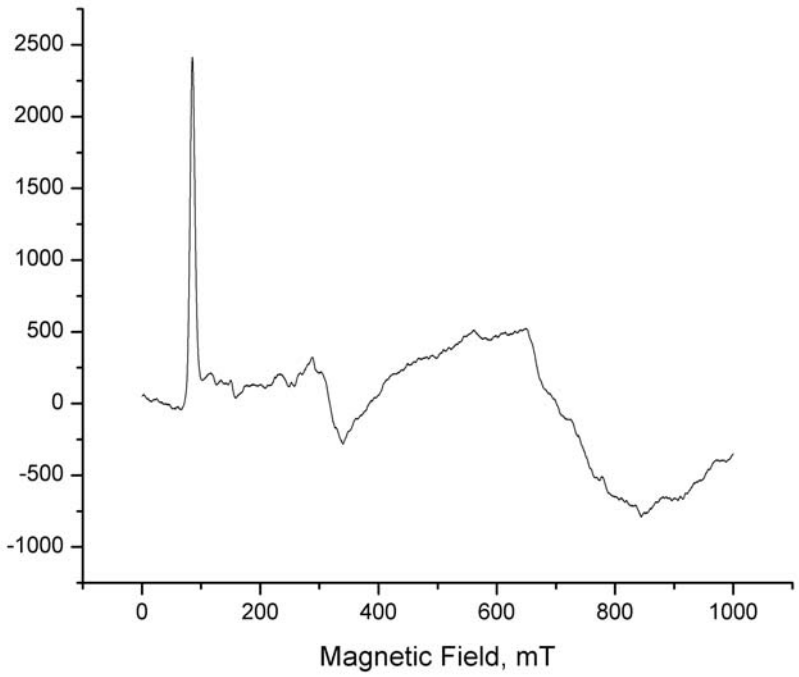

Figure B.10. EPR spectrum of **1-Br** at 5 K.

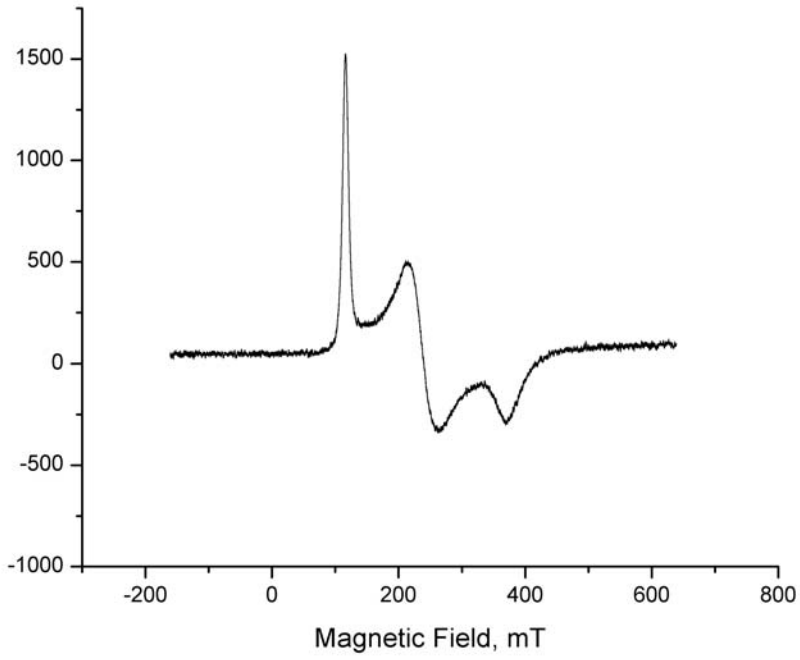

Figure B.12. EPR spectrum of **1-Br(Et_2O)** at 5 K.

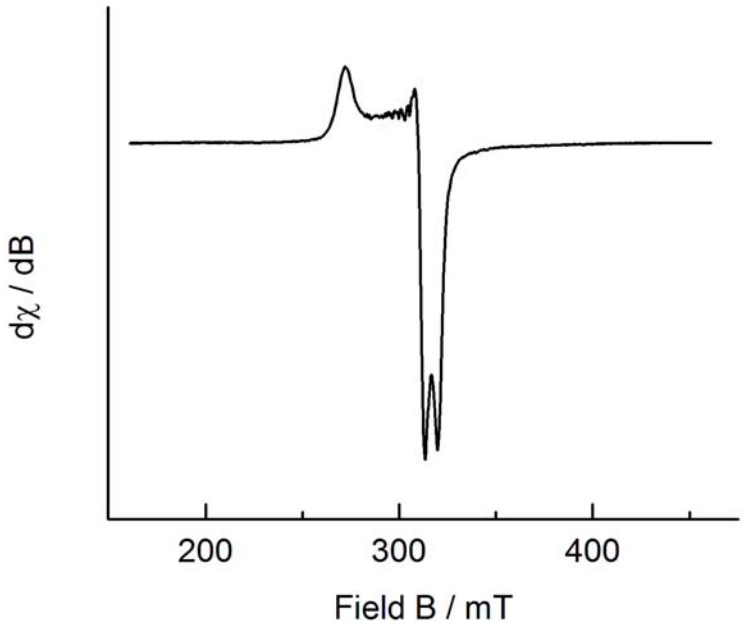

Figure B.13. EPR spectrum of **1-(FBF_3)(Et_2O)** at 5 K.

APPENDIX C

CRYSTAL STRUCTURE DATA

Table C.1. Compilation of X-ray data for compounds discussed in this manuscript.

Compound	CU X-Ray ID	Location
2-Cl(Et_2O)	rt1	*Chem*. *Commun*. **2005**, 3406.
7-Cl_2	rt2	Appendix C
5_2	rt3	Appendix C
8-Aryl	rt4	Appendix C
4-$(CO)_2$	rt6	*Inorg*. *Chem*. **2006**, *45*, 7252.
4-H(SiH_2Ph)(N_2)	rt9	*Inorg*. *Chem*. **2006**, *45*, 7252.
4-H(SiH_2Ph)(CO)	rt11	*Inorg*. *Chem*. **2006**, *45*, 7252.
(^{iPr}PDI)Ti(C_4H_6)	rt13	Appendix C
1-$OCPh_2$	rt15	*Organometallics* **2008**, *27*, 1470.
1-Bpy	rt16a	Appendix C
1-H_2CIN	rt22	Appendix C
2-Np	rt24	*Organometallics* **2008**, *27*, 109.
1-(FBF_3)(Et_2O)	rt25	Appendix C
1-(OAc)(Vinyl)	rt28	*Accepted Organometallics*
1-OBz	rt30	*Accepted Organometallics*
1-OAc	rt32	*Accepted Organometallics*
1-Allyl	rt34	*Accepted Organometallics*
1-Br(THF)	rt35	*JACS* DOI: 10.1021/ja803296f
1-CC^{t}Bu	rt38	Appendix C
1-Tpy	rt40	Appendix C
1-CCPh	rt41	Appendix C

Table C.2. Crystal data and structure refinement for **7-Cl_2**.

Identification code	rt2	
Empirical formula	C22 H28 Cl2 Fe N2	
Formula weight	447.21	
Temperature	173(2) K	
Wavelength	0.71073 Å	
Crystal system	Monoclinic	
Space group	P2(1)/c	
Unit cell dimensions	a = 12.5819(17) Å	α= 90°.
	b = 14.5340(19) Å	β= 90.498(7)°.
	c = 14.201(2) Å	γ = 90°.
Volume	2596.8(6) $Å^3$	
Z	4	
Density (calculated)	1.144 Mg/m^3	
Absorption coefficient	0.794 mm^{-1}	
F(000)	936	
Crystal size	0.45 x 0.35 x 0.15 mm^3	
Theta range for data collection	1.62 to 35.09°.	
Index ranges	-20<=h<=20, -23<=k<=23, -22<=l<=22	
Reflections collected	49552	
Independent reflections	11231 [R(int) = 0.0266]	
Completeness to theta = 35.09°	97.5 %	
Absorption correction	Semi-empirical from equivalents	
Max. and min. transmission	0.8902 and 0.7164	
Refinement method	Full-matrix least-squares on F^2	
Data / restraints / parameters	11231 / 0 / 356	
Goodness-of-fit on F^2	1.076	
Final R indices [I>2sigma(I)]	R1 = 0.0374, wR2 = 0.1207	
R indices (all data)	R1 = 0.0459, wR2 = 0.1249	
Largest diff. peak and hole	0.505 and -0.468 $e.Å^{-3}$	

Table C.3. Atomic coordinates (x 10^4) and equivalent isotropic displacement parameters ($Å^2$x 10^3) for **7-Cl_2**. U(eq) is defined as one third of the trace of the orthogonalized U^{ij} tensor.

	x	y	z	U(eq)
Fe(1)	1145(1)	6396(1)	7222(1)	22(1)
Cl(1)	1836(1)	5312(1)	8165(1)	39(1)
Cl(2)	835(1)	6018(1)	5727(1)	41(1)
N(1)	-144(1)	7119(1)	7807(1)	22(1)
N(2)	1748(1)	7738(1)	7440(1)	21(1)
C(1)	-723(1)	8552(1)	8568(1)	30(1)
C(2)	51(1)	7940(1)	8095(1)	21(1)
C(3)	1145(1)	8303(1)	7877(1)	22(1)
C(4)	1416(1)	9272(1)	8128(1)	36(1)
C(5)	-1205(1)	6759(1)	7865(1)	22(1)
C(6)	-1498(1)	6245(1)	8657(1)	23(1)
C(7)	-2537(1)	5919(1)	8683(1)	28(1)
C(8)	-3255(1)	6080(1)	7956(1)	30(1)
C(9)	-2920(1)	6575(1)	7177(1)	31(1)
C(10)	-1895(1)	6927(1)	7119(1)	27(1)
C(11)	-725(1)	6064(1)	9441(1)	30(1)
C(12)	-4368(1)	5713(1)	7990(2)	45(1)
C(13)	-1559(1)	7489(1)	6283(1)	37(1)
C(14)	2761(1)	8021(1)	7093(1)	21(1)
C(15)	2802(1)	8373(1)	6180(1)	23(1)
C(16)	3795(1)	8587(1)	5820(1)	27(1)
C(17)	4721(1)	8447(1)	6338(1)	30(1)
C(18)	4644(1)	8097(1)	7242(1)	30(1)
C(19)	3670(1)	7882(1)	7638(1)	26(1)
C(20)	1814(1)	8526(1)	5610(1)	32(1)
C(21)	5781(1)	8691(1)	5930(1)	44(1)
C(22)	3599(1)	7509(1)	8620(1)	38(1)

Table C.4. Bond lengths [Å] and angles [°] for **7-Cl$_2$**.

Fe(1)-N(1)	2.1083(8)	C(3)-N(2)-C(14)	121.03(8)
Fe(1)-N(2)	2.1154(9)	C(3)-N(2)-Fe(1)	116.65(7)
Fe(1)-Cl(2)	2.2230(5)	C(14)-N(2)-Fe(1)	122.28(6)
Fe(1)-Cl(1)	2.2381(4)	N(1)-C(2)-C(1)	125.25(9)
N(1)-C(2)	1.2846(12)	N(1)-C(2)-C(3)	115.52(8)
N(1)-C(5)	1.4374(12)	C(1)-C(2)-C(3)	119.14(9)
N(2)-C(3)	1.2810(13)	N(2)-C(3)-C(4)	125.83(9)
N(2)-C(14)	1.4311(12)	N(2)-C(3)-C(2)	114.88(8)
C(1)-C(2)	1.4842(14)	C(4)-C(3)-C(2)	119.20(9)
C(2)-C(3)	1.5085(14)	C(10)-C(5)-C(6)	122.68(9)
C(3)-C(4)	1.4916(15)	C(10)-C(5)-N(1)	117.86(9)
C(5)-C(10)	1.3859(15)	C(6)-C(5)-N(1)	119.45(9)
C(5)-C(6)	1.4007(14)	C(7)-C(6)-C(5)	117.19(10)
C(6)-C(7)	1.3914(15)	C(7)-C(6)-C(11)	121.65(10)
C(6)-C(11)	1.4954(16)	C(5)-C(6)-C(11)	121.16(9)
C(7)-C(8)	1.3856(17)	C(8)-C(7)-C(6)	121.96(10)
C(8)-C(9)	1.3879(17)	C(7)-C(8)-C(9)	118.72(10)
C(8)-C(12)	1.4987(17)	C(7)-C(8)-C(12)	121.30(12)
C(9)-C(10)	1.3915(16)	C(9)-C(8)-C(12)	119.97(12)
C(10)-C(13)	1.5047(16)	C(8)-C(9)-C(10)	121.73(11)
C(14)-C(19)	1.3898(15)	C(5)-C(10)-C(9)	117.69(10)
C(14)-C(15)	1.3960(14)	C(5)-C(10)-C(13)	121.41(10)
C(15)-C(16)	1.3898(15)	C(9)-C(10)-C(13)	120.89(11)
C(15)-C(20)	1.4933(16)	C(19)-C(14)-C(15)	122.30(9)
C(16)-C(17)	1.3877(18)	C(19)-C(14)-N(2)	119.84(9)
C(17)-C(18)	1.3852(18)	C(15)-C(14)-N(2)	117.70(9)
C(17)-C(21)	1.5014(17)	C(16)-C(15)-C(14)	117.63(10)
C(18)-C(19)	1.3888(15)	C(16)-C(15)-C(20)	120.96(10)
C(19)-C(22)	1.4991(17)	C(14)-C(15)-C(20)	121.40(9)
N(1)-Fe(1)-N(2)	76.02(3)	C(17)-C(16)-C(15)	121.75(10)
N(1)-Fe(1)-Cl(2)	111.72(3)	C(18)-C(17)-C(16)	118.66(10)
N(2)-Fe(1)-Cl(2)	115.30(3)	C(18)-C(17)-C(21)	120.98(13)
N(1)-Fe(1)-Cl(1)	114.28(3)	C(16)-C(17)-C(21)	120.34(12)
N(2)-Fe(1)-Cl(1)	115.11(3)	C(17)-C(18)-C(19)	121.85(10)
Cl(2)-Fe(1)-Cl(1)	117.477(15)	C(18)-C(19)-C(14)	117.79(10)
C(2)-N(1)-C(5)	119.63(8)	C(18)-C(19)-C(22)	121.16(10)
C(2)-N(1)-Fe(1)	116.34(7)	C(14)-C(19)-C(22)	121.05(10)
C(5)-N(1)-Fe(1)	123.99(6)		

Table C.5. Crystal data and structure refinement for $\mathbf{5_2}$.

Identification code	rt3	
Empirical formula	C28 H40 Fe N2	
Formula weight	460.47	
Temperature	173(2) K	
Wavelength	0.71073 Å	
Crystal system	Triclinic	
Space group	P-1	
Unit cell dimensions	a = 10.1476(11) Å	α= 72.739(5)°.
	b = 10.7372(11) Å	β= 85.026(5)°.
	c = 12.3048(14) Å	γ = 75.048(5)°.
Volume	1236.9(2) $Å^3$	
Z	2	
Density (calculated)	1.236 Mg/m^3	
Absorption coefficient	0.627 mm^{-1}	
F(000)	496	
Crystal size	0.30 x 0.20 x 0.05 mm^3	
Theta range for data collection	1.73 to 31.40°.	
Index ranges	-14<=h<=14, -15<=k<=15, -17<=l<=17	
Reflections collected	36876	
Independent reflections	8000 [R(int) = 0.0325]	
Completeness to theta = 31.40°	98.0 %	
Absorption correction	Semi-empirical from equivalents	
Max. and min. transmission	0.9693 and 0.8343	
Refinement method	Full-matrix least-squares on F^2	
Data / restraints / parameters	8000 / 0 / 440	
Goodness-of-fit on F^2	1.070	
Final R indices [I>2sigma(I)]	R1 = 0.0309, wR2 = 0.0864	
R indices (all data)	R1 = 0.0396, wR2 = 0.0899	
Largest diff. peak and hole	0.523 and -0.428 $e.Å^{-3}$	

Table C.6. Atomic coordinates (x 10^4) and equivalent isotropic displacement parameters ($Å^2$x 10^3) for **5_2**. U(eq) is defined as one third of the trace of the orthogonalized U^{ij} tensor.

	x	y	z	U(eq)
Fe(1)	1732(1)	8934(1)	839(1)	14(1)
N(1)	-77(1)	9172(1)	1441(1)	15(1)
N(2)	2123(1)	7949(1)	2378(1)	17(1)
C(1)	-1510(1)	8611(1)	3231(1)	26(1)
C(2)	-198(1)	8571(1)	2569(1)	19(1)
C(3)	1044(1)	7879(1)	3094(1)	19(1)
C(4)	1129(1)	7137(1)	4334(1)	27(1)
C(5)	-1331(1)	9929(1)	867(1)	15(1)
C(6)	-1813(1)	11320(1)	811(1)	17(1)
C(7)	-3040(1)	12048(1)	229(1)	20(1)
C(8)	-3770(1)	11427(1)	-270(1)	21(1)
C(9)	-3279(1)	10071(1)	-226(1)	20(1)
C(10)	-2060(1)	9288(1)	347(1)	17(1)
C(11)	-1083(1)	12035(1)	1363(1)	22(1)
C(12)	-1351(2)	13542(1)	767(1)	31(1)
C(13)	-1475(2)	11853(2)	2619(1)	41(1)
C(14)	-1615(1)	7805(1)	429(1)	22(1)
C(15)	-2109(1)	7470(1)	-562(1)	28(1)
C(16)	-2136(2)	6957(1)	1530(1)	37(1)
C(17)	3442(1)	7304(1)	2862(1)	18(1)
C(18)	4037(1)	5965(1)	2881(1)	21(1)
C(19)	5290(1)	5339(1)	3416(1)	26(1)
C(20)	5932(1)	6011(1)	3914(1)	28(1)
C(21)	5352(1)	7339(1)	3860(1)	25(1)
C(22)	4111(1)	8015(1)	3323(1)	20(1)
C(23)	3364(1)	5207(1)	2331(1)	25(1)
C(24)	4365(2)	4483(2)	1586(1)	35(1)
C(25)	2700(2)	4205(2)	3200(1)	40(1)
C(26)	3524(1)	9486(1)	3255(1)	25(1)
C(27)	2897(2)	9678(2)	4381(2)	47(1)
C(28)	4588(2)	10311(1)	2864(1)	32(1)

Table C.7. Bond lengths [Å] for $\mathbf{5_2}$.

Fe(1)-N(2)	1.8934(9)	C(12)-H(12A)	0.996(19)
Fe(1)-N(1)	1.9022(9)	C(13)-H(13C)	0.95(2)
Fe(1)-C(9)#1	2.0872(11)	C(13)-H(13B)	0.89(2)
Fe(1)-C(7)#1	2.0980(11)	C(13)-H(13A)	1.03(2)
Fe(1)-C(8)#1	2.1007(11)	C(14)-C(15)	1.5264(17)
Fe(1)-C(5)#1	2.1053(10)	C(14)-C(16)	1.5286(18)
Fe(1)-C(10)#1	2.1156(11)	C(14)-H(14)	0.961(14)
Fe(1)-C(6)#1	2.1198(10)	C(15)-H(15C)	0.968(16)
N(1)-C(2)	1.3549(14)	C(15)-H(15B)	0.940(18)
N(1)-C(5)	1.4358(12)	C(15)-H(15A)	0.922(17)
N(2)-C(3)	1.3481(14)	C(16)-H(16C)	1.01(2)
N(2)-C(17)	1.4297(13)	C(16)-H(16B)	0.94(2)
C(1)-C(2)	1.4974(16)	C(16)-H(16A)	0.892(18)
C(1)-H(1C)	0.965(16)	C(17)-C(22)	1.3993(16)
C(1)-H(1B)	0.973(17)	C(17)-C(18)	1.4018(15)
C(1)-H(1A)	0.963(17)	C(18)-C(19)	1.3942(15)
C(2)-C(3)	1.3897(15)	C(18)-C(23)	1.5107(17)
C(3)-C(4)	1.4951(16)	C(19)-C(20)	1.3755(19)
C(4)-H(4C)	0.92(2)	C(19)-H(19)	0.946(16)
C(4)-H(4B)	0.95(2)	C(20)-C(21)	1.3798(19)
C(4)-H(4A)	0.968(19)	C(20)-H(20)	0.959(15)
C(5)-C(10)	1.4273(15)	C(21)-C(22)	1.3917(15)
C(5)-C(6)	1.4296(14)	C(21)-H(21)	0.914(16)
C(5)-Fe(1)#1	2.1053(10)	C(22)-C(26)	1.5168(16)
C(6)-C(7)	1.4125(14)	C(23)-C(25)	1.524(2)
C(6)-C(11)	1.5127(15)	C(23)-C(24)	1.5260(19)
C(6)-Fe(1)#1	2.1197(10)	C(23)-H(23)	0.984(14)
C(7)-C(8)	1.3953(17)	C(24)-H(24C)	0.987(17)
C(7)-Fe(1)#1	2.0981(11)	C(24)-H(24B)	0.92(2)
C(7)-H(7)	0.940(14)	C(24)-H(24A)	0.96(2)
C(8)-C(9)	1.3981(16)	C(25)-H(25C)	0.968(18)
C(8)-Fe(1)#1	2.1007(11)	C(25)-H(25B)	0.970(19)
C(8)-H(8)	0.930(16)	C(25)-H(25A)	1.01(2)
C(9)-C(10)	1.4134(14)	C(26)-C(27)	1.522(2)
C(9)-Fe(1)#1	2.0871(11)	C(26)-C(28)	1.5275(19)
C(9)-H(9)	0.919(15)	C(26)-H(26)	0.919(15)
C(10)-C(14)	1.5126(15)	C(27)-H(27C)	0.87(2)
C(10)-Fe(1)#1	2.1156(11)	C(27)-H(27B)	1.04(2)
C(11)-C(12)	1.5275(17)	C(27)-H(27A)	0.94(2)
C(11)-C(13)	1.5300(19)	C(28)-H(28C)	0.991(18)
C(11)-H(11)	0.954(14)	C(28)-H(28B)	0.919(19)
C(12)-H(12C)	0.926(19)	C(28)-H(28A)	0.945(18)
C(12)-H(12B)	0.963(16)		

Table C.8. Angles [°] for $\mathbf{5_2}$.

N(2)-Fe(1)-N(1)	80.94(4)	C(2)-C(3)-C(4)	121.81(10)
N(2)-Fe(1)-C(9)#1	107.49(4)	C(3)-C(4)-H(4C)	114.0(12)
N(1)-Fe(1)-C(9)#1	143.03(4)	C(3)-C(4)-H(4B)	110.6(11)
N(2)-Fe(1)-C(7)#1	109.49(4)	H(4C)-C(4)-H(4B)	111.3(16)
N(1)-Fe(1)-C(7)#1	141.66(4)	C(3)-C(4)-H(4A)	112.3(11)
C(9)#1-Fe(1)-C(7)#1	70.78(5)	H(4C)-C(4)-H(4A)	107.0(16)
N(2)-Fe(1)-C(8)#1	95.53(4)	H(4B)-C(4)-H(4A)	100.8(16)
N(1)-Fe(1)-C(8)#1	176.35(4)	C(10)-C(5)-C(6)	121.30(9)
C(9)#1-Fe(1)-C(8)#1	39.00(5)	C(10)-C(5)-N(1)	119.56(9)
C(7)#1-Fe(1)-C(8)#1	38.82(5)	C(6)-C(5)-N(1)	119.13(9)
N(2)-Fe(1)-C(5)#1	178.27(4)	C(10)-C(5)-Fe(1)#1	70.63(6)
N(1)-Fe(1)-C(5)#1	99.82(4)	C(6)-C(5)-Fe(1)#1	70.77(6)
C(9)#1-Fe(1)-C(5)#1	70.97(4)	N(1)-C(5)-Fe(1)#1	131.50(7)
C(7)#1-Fe(1)-C(5)#1	70.88(4)	C(7)-C(6)-C(5)	118.09(10)
C(8)#1-Fe(1)-C(5)#1	83.73(4)	C(7)-C(6)-C(11)	118.87(9)
N(2)-Fe(1)-C(10)#1	138.75(4)	C(5)-C(6)-C(11)	123.03(9)
N(1)-Fe(1)-C(10)#1	112.25(4)	C(7)-C(6)-Fe(1)#1	69.61(6)
C(9)#1-Fe(1)-C(10)#1	39.30(4)	C(5)-C(6)-Fe(1)#1	69.68(6)
C(7)#1-Fe(1)-C(10)#1	84.62(4)	C(11)-C(6)-Fe(1)#1	133.50(8)
C(8)#1-Fe(1)-C(10)#1	71.04(4)	C(8)-C(7)-C(6)	121.09(10)
C(5)#1-Fe(1)-C(10)#1	39.53(4)	C(8)-C(7)-Fe(1)#1	70.69(6)
N(2)-Fe(1)-C(6)#1	141.59(4)	C(6)-C(7)-Fe(1)#1	71.26(6)
N(1)-Fe(1)-C(6)#1	111.44(4)	C(8)-C(7)-H(7)	120.8(8)
C(9)#1-Fe(1)-C(6)#1	84.61(4)	C(6)-C(7)-H(7)	118.0(9)
C(7)#1-Fe(1)-C(6)#1	39.13(4)	Fe(1)#1-C(7)-H(7)	129.1(9)
C(8)#1-Fe(1)-C(6)#1	70.80(4)	C(7)-C(8)-C(9)	120.37(10)
C(5)#1-Fe(1)-C(6)#1	39.55(4)	C(7)-C(8)-Fe(1)#1	70.49(6)
C(10)#1-Fe(1)-C(6)#1	72.02(4)	C(9)-C(8)-Fe(1)#1	69.97(6)
C(2)-N(1)-C(5)	115.54(8)	C(7)-C(8)-H(8)	120.3(10)
C(2)-N(1)-Fe(1)	115.76(7)	C(9)-C(8)-H(8)	118.9(10)
C(5)-N(1)-Fe(1)	128.68(7)	Fe(1)#1-C(8)-H(8)	126.3(10)
C(3)-N(2)-C(17)	116.74(9)	C(8)-C(9)-C(10)	121.22(10)
C(3)-N(2)-Fe(1)	116.48(7)	C(8)-C(9)-Fe(1)#1	71.02(6)
C(17)-N(2)-Fe(1)	126.76(7)	C(10)-C(9)-Fe(1)#1	71.44(6)
C(2)-C(1)-H(1C)	110.8(10)	C(8)-C(9)-H(9)	120.1(9)
C(2)-C(1)-H(1B)	111.7(10)	C(10)-C(9)-H(9)	118.7(9)
H(1C)-C(1)-H(1B)	111.0(14)	Fe(1)#1-C(9)-H(9)	129.5(9)
C(2)-C(1)-H(1A)	112.3(10)	C(9)-C(10)-C(5)	117.91(10)
H(1C)-C(1)-H(1A)	106.4(13)	C(9)-C(10)-C(14)	119.20(10)
H(1B)-C(1)-H(1A)	104.3(14)	C(5)-C(10)-C(14)	122.83(9)
N(1)-C(2)-C(3)	113.51(9)	C(9)-C(10)-Fe(1)#1	69.27(6)
N(1)-C(2)-C(1)	125.57(10)	C(5)-C(10)-Fe(1)#1	69.85(6)
C(3)-C(2)-C(1)	120.92(10)	C(14)-C(10)-Fe(1)#1	134.88(8)
N(2)-C(3)-C(2)	113.30(9)	C(6)-C(11)-C(12)	112.77(10)
N(2)-C(3)-C(4)	124.89(10)	C(6)-C(11)-C(13)	112.25(11)

Table C.8. (continued)

C(12)-C(11)-C(13)	107.93(11)	C(19)-C(20)-H(20)	117.8(9)
C(6)-C(11)-H(11)	104.3(8)	C(21)-C(20)-H(20)	122.4(9)
C(12)-C(11)-H(11)	110.7(9)	C(20)-C(21)-C(22)	121.16(12)
C(13)-C(11)-H(11)	108.8(9)	C(20)-C(21)-H(21)	122.5(10)
C(11)-C(12)-H(12C)	109.0(12)	C(22)-C(21)-H(21)	116.3(10)
C(11)-C(12)-H(12B)	114.5(9)	C(21)-C(22)-C(17)	118.32(11)
H(12C)-C(12)-H(12B)	107.8(14)	C(21)-C(22)-C(26)	119.63(10)
C(11)-C(12)-H(12A)	108.7(10)	C(17)-C(22)-C(26)	122.05(10)
H(12C)-C(12)-H(12A)	108.2(15)	C(18)-C(23)-C(25)	112.40(11)
H(12B)-C(12)-H(12A)	108.4(14)	C(18)-C(23)-C(24)	111.79(11)
C(11)-C(13)-H(13C)	109.6(13)	C(25)-C(23)-C(24)	109.66(12)
C(11)-C(13)-H(13B)	109.2(12)	C(18)-C(23)-H(23)	108.0(8)
H(13C)-C(13)-H(13B)	112.1(18)	C(25)-C(23)-H(23)	107.2(8)
C(11)-C(13)-H(13A)	106.5(13)	C(24)-C(23)-H(23)	107.6(8)
H(13C)-C(13)-H(13A)	109.1(18)	C(23)-C(24)-H(24C)	111.3(10)
H(13B)-C(13)-H(13A)	110.2(17)	C(23)-C(24)-H(24B)	107.9(13)
C(10)-C(14)-C(15)	112.95(10)	H(24C)-C(24)-H(24B)	107.7(16)
C(10)-C(14)-C(16)	111.31(10)	C(23)-C(24)-H(24A)	108.7(12)
C(15)-C(14)-C(16)	107.74(11)	H(24C)-C(24)-H(24A)	109.0(15)
C(10)-C(14)-H(14)	104.6(8)	H(24B)-C(24)-H(24A)	112.3(17)
C(15)-C(14)-H(14)	110.8(8)	C(23)-C(25)-H(25C)	109.1(11)
C(16)-C(14)-H(14)	109.4(8)	C(23)-C(25)-H(25B)	111.3(11)
C(14)-C(15)-H(15C)	114.4(9)	H(25C)-C(25)-H(25B)	106.4(15)
C(14)-C(15)-H(15B)	107.3(11)	C(23)-C(25)-H(25A)	109.9(11)
H(15C)-C(15)-H(15B)	106.7(14)	H(25C)-C(25)-H(25A)	110.5(16)
C(14)-C(15)-H(15A)	110.9(10)	H(25B)-C(25)-H(25A)	109.6(15)
H(15C)-C(15)-H(15A)	106.4(13)	C(22)-C(26)-C(27)	112.22(12)
H(15B)-C(15)-H(15A)	111.1(14)	C(22)-C(26)-C(28)	112.04(10)
C(14)-C(16)-H(16C)	107.5(12)	C(27)-C(26)-C(28)	109.29(12)
C(14)-C(16)-H(16B)	110.2(13)	C(22)-C(26)-H(26)	104.7(9)
H(16C)-C(16)-H(16B)	114.3(17)	C(27)-C(26)-H(26)	107.6(9)
C(14)-C(16)-H(16A)	109.2(11)	C(28)-C(26)-H(26)	110.8(9)
H(16C)-C(16)-H(16A)	111.4(16)	C(26)-C(27)-H(27C)	108.4(13)
H(16B)-C(16)-H(16A)	104.1(16)	C(26)-C(27)-H(27B)	106.3(13)
C(22)-C(17)-C(18)	121.15(10)	H(27C)-C(27)-H(27B)	115.4(18)
C(22)-C(17)-N(2)	119.31(10)	C(26)-C(27)-H(27A)	109.2(12)
C(18)-C(17)-N(2)	119.54(10)	H(27C)-C(27)-H(27A)	108.4(17)
C(19)-C(18)-C(17)	118.19(11)	H(27B)-C(27)-H(27A)	109.0(17)
C(19)-C(18)-C(23)	120.01(10)	C(26)-C(28)-H(28C)	111.5(10)
C(17)-C(18)-C(23)	121.79(10)	C(26)-C(28)-H(28B)	112.4(11)
C(20)-C(19)-C(18)	121.22(11)	H(28C)-C(28)-H(28B)	107.9(14)
C(20)-C(19)-H(19)	120.8(10)	C(26)-C(28)-H(28A)	110.1(11)
C(18)-C(19)-H(19)	118.0(10)	H(28C)-C(28)-H(28A)	106.1(14)
C(19)-C(20)-C(21)	119.87(11)	H(28B)-C(28)-H(28A)	108.6(15)

Table C.9. Crystal data and structure refinement for **8-Aryl**.

Identification code	rt4	
Empirical formula	C52 H58 Fe N2 O	
Formula weight	782.85	
Temperature	173(2) K	
Wavelength	0.71073 Å	
Crystal system	Triclinic	
Space group	P1	
Unit cell dimensions	a = 11.8418(8) Å	α= 108.154(3)°.
	b = 13.1152(9) Å	β= 104.645(4)°.
	c = 15.1165(10) Å	γ = 103.542(4)°.
Volume	2029.5(2) $Å^3$	
Z	2	
Density (calculated)	1.281 Mg/m^3	
Absorption coefficient	0.413 mm^{-1}	
F(000)	836	
Crystal size	0.45 x 0.35 x 0.30 mm^3	
Theta range for data collection	1.51 to 32.81°.	
Index ranges	-17<=h<=17, -19<=k<=19, -22<=l<=22	
Reflections collected	67696	
Independent reflections	14810 [R(int) = 0.0292]	
Completeness to theta = 32.81°	98.3 %	
Absorption correction	Semi-empirical from equivalents	
Max. and min. transmission	0.8860 and 0.8358	
Refinement method	Full-matrix least-squares on F^2	
Data / restraints / parameters	14810 / 0 / 605	
Goodness-of-fit on F^2	1.054	
Final R indices [I>2sigma(I)]	R1 = 0.0364, wR2 = 0.1011	
R indices (all data)	R1 = 0.0454, wR2 = 0.1066	
Largest diff. peak and hole	0.630 and -0.342 e.$Å^{-3}$	

Table C.10. Atomic coordinates (x 10^4) and equivalent isotropic displacement parameters ($Å^2$x 10^3) for **8-Aryl**. U(eq) is defined as one third of the trace of the orthogonalized U^{ij} tensor.

	x	y	z	U(eq)
Fe(1)	7146(1)	8612(1)	3968(1)	17(1)
N(1)	7344(1)	7347(1)	4283(1)	17(1)
N(2)	8311(1)	8362(1)	3338(1)	18(1)
C(1)	8138(1)	6908(1)	3919(1)	18(1)
C(2)	8684(1)	7497(1)	3412(1)	18(1)
C(3)	9504(1)	6951(1)	3032(1)	19(1)
C(4)	10273(1)	7137(1)	2511(1)	23(1)
C(5)	10892(1)	6349(1)	2241(1)	27(1)
C(6)	10742(1)	5404(1)	2471(1)	27(1)
C(7)	9945(1)	5186(1)	3006(1)	23(1)
C(8)	9648(1)	4229(1)	3258(1)	30(1)
C(9)	8825(1)	4123(1)	3746(1)	31(1)
C(10)	8248(1)	4947(1)	4026(1)	26(1)
C(11)	8526(1)	5900(1)	3808(1)	19(1)
C(12)	9368(1)	5985(1)	3285(1)	19(1)
C(13)	6856(1)	6957(1)	4930(1)	18(1)
C(14)	5675(1)	6953(1)	4968(1)	19(1)
C(15)	5282(1)	6577(1)	5644(1)	23(1)
C(16)	6004(1)	6231(1)	6293(1)	24(1)
C(17)	7176(1)	6275(1)	6265(1)	24(1)
C(18)	7595(1)	6637(1)	5600(1)	21(1)
C(19)	5535(1)	5841(1)	7011(1)	31(1)
C(20)	4835(1)	7332(1)	4289(1)	21(1)
C(21)	5521(1)	8425(1)	4224(1)	20(1)
C(22)	5330(1)	8473(1)	3264(1)	23(1)
C(23)	6148(1)	9392(1)	3187(1)	26(1)
C(24)	7141(1)	10254(1)	4012(1)	26(1)
C(25)	7274(1)	10218(1)	4954(1)	24(1)
C(26)	6447(1)	9356(1)	5080(1)	21(1)
C(27)	3663(1)	7413(1)	4517(1)	31(1)
C(28)	4264(1)	7628(1)	2338(1)	32(1)
C(29)	8008(1)	11216(1)	3918(1)	36(1)
C(30)	6606(1)	9481(1)	6131(1)	26(1)
C(31)	8783(1)	8981(1)	2805(1)	18(1)
C(32)	8126(1)	8710(1)	1799(1)	18(1)
C(33)	8554(1)	9470(1)	1386(1)	23(1)
C(34)	9634(1)	10419(1)	1905(1)	25(1)
C(35)	10309(1)	10611(1)	2871(1)	26(1)
C(36)	9877(1)	9909(1)	3322(1)	23(1)
C(37)	10053(1)	11214(1)	1425(1)	37(1)
C(38)	6978(1)	7642(1)	1207(1)	20(1)
C(39)	7276(1)	6539(1)	864(1)	19(1)
C(40)	6742(1)	5645(1)	1123(1)	21(1)
C(41)	7075(1)	4670(1)	900(1)	25(1)
C(42)	7866(1)	4506(1)	377(1)	26(1)
C(43)	8308(1)	5347(1)	58(1)	27(1)

Table C.10. (continued)

C(44)	8039(1)	6358(1)	293(1)	24(1)
C(45)	6035(1)	7732(1)	355(1)	30(1)
C(46)	5781(1)	5677(1)	1610(1)	28(1)
C(47)	8231(1)	3456(1)	174(1)	36(1)
C(48)	8623(1)	7207(1)	-85(1)	34(1)
O(1S)	5406(1)	9357(1)	-1327(1)	52(1)
C(1S)	3401(2)	8643(2)	-1298(2)	61(1)
C(2S)	4344(2)	8362(2)	-1721(1)	49(1)
C(3S)	6406(2)	9166(2)	-1622(1)	53(1)
C(4S)	7418(2)	10271(2)	-1269(1)	55(1)

Table C.11. Bond lengths [Å] for **5_2**.

Fe(1)-N(2)	1.8977(9)	C(20)-C(21)	1.5187(14)
Fe(1)-N(1)	1.9114(8)	C(20)-C(27)	1.5304(15)
Fe(1)-C(21)	2.0315(10)	C(21)-C(26)	1.4285(14)
Fe(1)-C(22)	2.0800(11)	C(21)-C(22)	1.4341(14)
Fe(1)-C(23)	2.1097(10)	C(22)-C(23)	1.4153(16)
Fe(1)-C(25)	2.1119(10)	C(22)-C(28)	1.5055(16)
Fe(1)-C(26)	2.1263(10)	C(23)-C(24)	1.4045(18)
Fe(1)-C(24)	2.1354(10)	C(24)-C(25)	1.4101(16)
N(1)-C(1)	1.3557(12)	C(24)-C(29)	1.4984(16)
N(1)-C(13)	1.4181(12)	C(25)-C(26)	1.4085(15)
N(2)-C(2)	1.3363(12)	C(26)-C(30)	1.5034(14)
N(2)-C(31)	1.4287(12)	C(31)-C(36)	1.3883(14)
C(1)-C(2)	1.4100(13)	C(31)-C(32)	1.4073(13)
C(1)-C(11)	1.4735(13)	C(32)-C(33)	1.3961(13)
C(2)-C(3)	1.4616(13)	C(32)-C(38)	1.5243(13)
C(3)-C(4)	1.3737(14)	C(33)-C(34)	1.3926(15)
C(3)-C(12)	1.4190(14)	C(34)-C(35)	1.3863(17)
C(4)-C(5)	1.4189(15)	C(34)-C(37)	1.5062(15)
C(5)-C(6)	1.3726(17)	C(35)-C(36)	1.3859(15)
C(6)-C(7)	1.4238(16)	C(38)-C(39)	1.5323(15)
C(7)-C(12)	1.3957(14)	C(38)-C(45)	1.5332(15)
C(7)-C(8)	1.4156(16)	C(39)-C(44)	1.4082(14)
C(8)-C(9)	1.3711(18)	C(39)-C(40)	1.4115(13)
C(9)-C(10)	1.4210(16)	C(40)-C(41)	1.3923(15)
C(10)-C(11)	1.3771(14)	C(40)-C(46)	1.5046(15)
C(11)-C(12)	1.4264(14)	C(41)-C(42)	1.3827(17)
C(13)-C(18)	1.3987(14)	C(42)-C(43)	1.3839(16)
C(13)-C(14)	1.4134(14)	C(42)-C(47)	1.5036(17)
C(14)-C(15)	1.3981(14)	C(43)-C(44)	1.3961(16)
C(14)-C(20)	1.5235(14)	C(44)-C(48)	1.5102(15)
C(15)-C(16)	1.3892(16)	O(1S)-C(3S)	1.415(2)
C(16)-C(17)	1.3879(16)	O(1S)-C(2S)	1.416(2)
C(16)-C(19)	1.5048(15)	C(1S)-C(2S)	1.483(3)
C(17)-C(18)	1.3855(14)	C(3S)-C(4S)	1.485(3)

Table C.12. Angles [°] for $\mathbf{5_2}$.

N(2)-Fe(1)-N(1)	83.44(3)	C(5)-C(6)-C(7)	120.10(10)
N(2)-Fe(1)-C(21)	160.90(4)	C(12)-C(7)-C(8)	116.61(10)
N(1)-Fe(1)-C(21)	92.20(4)	C(12)-C(7)-C(6)	116.45(10)
N(2)-Fe(1)-C(22)	125.78(4)	C(8)-C(7)-C(6)	126.91(10)
N(1)-Fe(1)-C(22)	115.85(4)	C(9)-C(8)-C(7)	119.81(10)
C(21)-Fe(1)-C(22)	40.81(4)	C(8)-C(9)-C(10)	122.75(11)
N(2)-Fe(1)-C(23)	103.73(4)	C(11)-C(10)-C(9)	119.29(10)
N(1)-Fe(1)-C(23)	153.27(4)	C(10)-C(11)-C(12)	117.12(9)
C(21)-Fe(1)-C(23)	72.53(4)	C(10)-C(11)-C(1)	137.53(10)
C(22)-Fe(1)-C(23)	39.48(4)	C(12)-C(11)-C(1)	105.25(8)
N(2)-Fe(1)-C(25)	124.60(4)	C(7)-C(12)-C(3)	123.51(9)
N(1)-Fe(1)-C(25)	127.48(4)	C(7)-C(12)-C(11)	124.39(9)
C(21)-Fe(1)-C(25)	72.44(4)	C(3)-C(12)-C(11)	112.02(9)
C(22)-Fe(1)-C(25)	84.73(4)	C(18)-C(13)-C(14)	118.62(9)
C(23)-Fe(1)-C(25)	69.62(4)	C(18)-C(13)-N(1)	119.22(9)
N(2)-Fe(1)-C(26)	158.98(4)	C(14)-C(13)-N(1)	122.03(8)
N(1)-Fe(1)-C(26)	99.41(4)	C(15)-C(14)-C(13)	117.99(9)
C(21)-Fe(1)-C(26)	40.11(4)	C(15)-C(14)-C(20)	120.25(9)
C(22)-Fe(1)-C(26)	71.84(4)	C(13)-C(14)-C(20)	121.75(9)
C(23)-Fe(1)-C(26)	83.12(4)	C(16)-C(15)-C(14)	123.35(10)
C(25)-Fe(1)-C(26)	38.82(4)	C(17)-C(16)-C(15)	117.69(9)
N(2)-Fe(1)-C(24)	102.14(4)	C(17)-C(16)-C(19)	121.30(10)
N(1)-Fe(1)-C(24)	165.60(4)	C(15)-C(16)-C(19)	120.99(11)
C(21)-Fe(1)-C(24)	86.60(4)	C(18)-C(17)-C(16)	120.65(10)
C(22)-Fe(1)-C(24)	71.82(5)	C(17)-C(18)-C(13)	121.64(10)
C(23)-Fe(1)-C(24)	38.63(5)	C(21)-C(20)-C(14)	113.02(8)
C(25)-Fe(1)-C(24)	38.78(4)	C(21)-C(20)-C(27)	110.66(9)
C(26)-Fe(1)-C(24)	70.65(4)	C(14)-C(20)-C(27)	114.65(9)
C(1)-N(1)-C(13)	120.58(8)	C(26)-C(21)-C(22)	119.13(9)
C(1)-N(1)-Fe(1)	113.46(6)	C(26)-C(21)-C(20)	121.50(9)
C(13)-N(1)-Fe(1)	125.53(6)	C(22)-C(21)-C(20)	119.02(9)
C(2)-N(2)-C(31)	119.41(8)	C(26)-C(21)-Fe(1)	73.52(6)
C(2)-N(2)-Fe(1)	113.68(6)	C(22)-C(21)-Fe(1)	71.42(6)
C(31)-N(2)-Fe(1)	126.91(6)	C(20)-C(21)-Fe(1)	120.56(7)
N(1)-C(1)-C(2)	113.75(8)	C(23)-C(22)-C(21)	118.62(10)
N(1)-C(1)-C(11)	138.02(9)	C(23)-C(22)-C(28)	117.90(10)
C(2)-C(1)-C(11)	107.90(8)	C(21)-C(22)-C(28)	123.41(10)
N(2)-C(2)-C(1)	115.64(8)	C(23)-C(22)-Fe(1)	71.39(6)
N(2)-C(2)-C(3)	134.51(9)	C(21)-C(22)-Fe(1)	67.78(6)
C(1)-C(2)-C(3)	109.75(8)	C(28)-C(22)-Fe(1)	135.87(8)
C(4)-C(3)-C(12)	118.76(9)	C(24)-C(23)-C(22)	122.55(10)
C(4)-C(3)-C(2)	136.31(9)	C(24)-C(23)-Fe(1)	71.67(6)
C(12)-C(3)-C(2)	104.91(8)	C(22)-C(23)-Fe(1)	69.13(6)
C(3)-C(4)-C(5)	118.55(10)	C(23)-C(24)-C(25)	117.80(10)
C(6)-C(5)-C(4)	122.59(10)	C(23)-C(24)-C(29)	122.03(11)

Table C.12. (continued)

C(25)-C(24)-C(29)	120.13(11)	C(36)-C(35)-C(34)	120.49(10)
C(23)-C(24)-Fe(1)	69.69(6)	C(35)-C(36)-C(31)	120.68(10)
C(25)-C(24)-Fe(1)	69.71(6)	C(32)-C(38)-C(39)	113.70(8)
C(29)-C(24)-Fe(1)	134.33(8)	C(32)-C(38)-C(45)	114.03(8)
C(26)-C(25)-C(24)	121.93(10)	C(39)-C(38)-C(45)	111.92(8)
C(26)-C(25)-Fe(1)	71.15(6)	C(44)-C(39)-C(40)	117.95(9)
C(24)-C(25)-Fe(1)	71.52(6)	C(44)-C(39)-C(38)	123.87(9)
C(25)-C(26)-C(21)	119.38(9)	C(40)-C(39)-C(38)	118.18(9)
C(25)-C(26)-C(30)	116.81(9)	C(41)-C(40)-C(39)	119.81(10)
C(21)-C(26)-C(30)	123.81(9)	C(41)-C(40)-C(46)	117.51(9)
C(25)-C(26)-Fe(1)	70.04(6)	C(39)-C(40)-C(46)	122.65(10)
C(21)-C(26)-Fe(1)	66.37(5)	C(42)-C(41)-C(40)	122.45(10)
C(30)-C(26)-Fe(1)	137.22(7)	C(41)-C(42)-C(43)	117.30(10)
C(36)-C(31)-C(32)	120.24(9)	C(41)-C(42)-C(47)	120.95(11)
C(36)-C(31)-N(2)	118.25(9)	C(43)-C(42)-C(47)	121.74(11)
C(32)-C(31)-N(2)	121.39(8)	C(42)-C(43)-C(44)	122.37(11)
C(33)-C(32)-C(31)	117.26(9)	C(43)-C(44)-C(39)	119.80(10)
C(33)-C(32)-C(38)	122.31(9)	C(43)-C(44)-C(48)	115.97(10)
C(31)-C(32)-C(38)	120.41(8)	C(39)-C(44)-C(48)	124.23(10)
C(34)-C(33)-C(32)	122.81(10)	C(3S)-O(1S)-C(2S)	113.55(13)
C(35)-C(34)-C(33)	118.21(9)	O(1S)-C(2S)-C(1S)	108.73(15)
C(35)-C(34)-C(37)	121.10(10)	O(1S)-C(3S)-C(4S)	109.61(14)
C(33)-C(34)-C(37)	120.69(11)		

Table C.13. Crystal data and structure refinement for **(^{iPr}PDI)Ti(C_4H_6)**.

Identification code	rt13	
Empirical formula	C74 H98 N6 Ti2	
Formula weight	1167.38	
Temperature	173(2) K	
Wavelength	0.71073 Å	
Crystal system	Monoclinic	
Space group	P2(1)/c	
Unit cell dimensions	a = 15.3274(9) Å	α= 90°.
	b = 20.7076(11) Å	β= 101.401(2)°.
	c = 21.0803(11) Å	γ = 90°.
Volume	6558.7(6) Å^3	
Z	4	
Density (calculated)	1.182 Mg/m^3	
Absorption coefficient	0.290 mm^{-1}	
F(000)	2512	
Crystal size	0.50 x 0.35 x 0.15 mm^3	
Theta range for data collection	1.36 to 24.48°.	
Index ranges	-17<=h<=17, -24<=k<=24, -24<=l<=23	
Reflections collected	58116	
Independent reflections	10850 [R(int) = 0.0537]	
Completeness to theta = 24.48°	99.6 %	
Absorption correction	Semi-empirical from equivalents	
Max. and min. transmission	0.9578 and 0.8687	
Refinement method	Full-matrix least-squares on F^2	
Data / restraints / parameters	10850 / 0 / 968	
Goodness-of-fit on F^2	1.052	
Final R indices [I>2sigma(I)]	R1 = 0.0401, wR2 = 0.1012	
R indices (all data)	R1 = 0.0654, wR2 = 0.1121	
Largest diff. peak and hole	0.290 and -0.362 e.Å^{-3}	

Table C.14. Atomic coordinates (x 10^4) and equivalent isotropic displacement parameters (Å^{2}x 10^3) for **(^{iPr}PDI)Ti(C_4H_6)**. U(eq) is defined as one third of the trace of the orthogonalized U^{ij} tensor.

	x	y	z	U(eq)
Ti(1)	6431(1)	357(1)	3648(1)	25(1)
Ti(2)	1540(1)	662(1)	1401(1)	25(1)
N(1)	6070(1)	-437(1)	2906(1)	26(1)
N(2)	6486(1)	734(1)	2781(1)	22(1)
N(3)	6690(1)	1327(1)	3820(1)	27(1)
N(4)	2491(1)	682(1)	767(1)	26(1)
N(5)	2700(1)	929(1)	1950(1)	22(1)
N(6)	1293(1)	786(1)	2366(1)	25(1)
C(1)	5911(2)	-741(1)	1748(1)	40(1)
C(2)	6105(1)	-286(1)	2309(1)	27(1)
C(3)	6338(1)	374(1)	2217(1)	24(1)
C(4)	6381(2)	635(1)	1628(1)	28(1)
C(5)	6572(2)	1297(1)	1575(1)	30(1)
C(6)	6690(1)	1665(1)	2116(1)	27(1)
C(7)	6647(1)	1401(1)	2723(1)	23(1)
C(8)	6754(2)	1723(1)	3297(1)	27(1)
C(9)	6909(3)	2437(1)	3349(2)	44(1)
C(10)	5789(2)	-1079(1)	3044(1)	28(1)
C(11)	4889(2)	-1176(1)	3052(1)	30(1)
C(12)	4628(2)	-1789(1)	3208(1)	36(1)
C(13)	5231(2)	-2286(1)	3344(1)	41(1)
C(14)	6099(2)	-2186(1)	3326(1)	40(1)
C(15)	6414(2)	-1585(1)	3177(1)	35(1)
C(16)	4196(2)	-648(1)	2881(1)	34(1)
C(17)	3722(2)	-697(1)	2170(1)	52(1)
C(18)	3504(2)	-650(1)	3312(2)	51(1)
C(19)	7381(2)	-1514(1)	3133(2)	49(1)
C(20)	8019(2)	-1778(2)	3727(2)	65(1)
C(21)	7568(2)	-1852(2)	2527(2)	81(1)
C(22)	6913(2)	1633(1)	4447(1)	27(1)
C(23)	7812(2)	1698(1)	4746(1)	31(1)
C(24)	8012(2)	1977(1)	5353(1)	36(1)
C(25)	7359(2)	2197(1)	5658(1)	38(1)
C(26)	6480(2)	2146(1)	5356(1)	35(1)
C(27)	6238(2)	1866(1)	4748(1)	29(1)
C(28)	8559(2)	1495(1)	4413(1)	45(1)
C(29)	9099(2)	2073(2)	4277(2)	88(1)
C(30)	9186(2)	1001(2)	4790(2)	73(1)
C(31)	5263(2)	1838(1)	4424(1)	36(1)
C(32)	4949(2)	2483(1)	4111(1)	57(1)
C(33)	4654(2)	1627(1)	4879(1)	50(1)
C(34)	7352(3)	-273(2)	4265(1)	52(1)
C(35)	7034(2)	123(1)	4717(1)	49(1)
C(36)	6140(2)	263(1)	4680(1)	45(1)
C(37)	5444(2)	37(2)	4193(1)	47(1)
C(38)	4063(2)	902(2)	660(1)	42(1)

Table C.14. (continued)

C(39)	3329(1)	846(1)	1030(1)	26(1)
C(40)	3473(1)	981(1)	1695(1)	23(1)
C(41)	4279(2)	1143(1)	2081(1)	27(1)
C(42)	4345(2)	1275(1)	2731(1)	30(1)
C(43)	3594(2)	1225(1)	2993(1)	30(1)
C(44)	2783(1)	1053(1)	2612(1)	24(1)
C(45)	1989(2)	970(1)	2831(1)	27(1)
C(46)	1937(2)	1076(2)	3527(1)	44(1)
C(47)	2287(1)	553(1)	81(1)	28(1)
C(48)	2326(2)	-83(1)	-138(1)	34(1)
C(49)	2086(2)	-188(2)	-801(1)	48(1)
C(50)	1838(2)	313(2)	-1230(1)	57(1)
C(51)	1812(2)	926(2)	-1008(1)	48(1)
C(52)	2033(2)	1066(1)	-351(1)	36(1)
C(53)	2639(2)	-639(1)	311(1)	40(1)
C(54)	2083(2)	-1251(1)	146(2)	64(1)
C(55)	3613(2)	-799(2)	327(1)	57(1)
C(56)	2014(2)	1761(1)	-129(1)	44(1)
C(57)	2770(2)	2154(2)	-311(2)	85(1)
C(58)	1144(2)	2099(2)	-404(2)	68(1)
C(59)	456(1)	681(1)	2557(1)	27(1)
C(60)	-165(2)	1189(1)	2499(1)	31(1)
C(61)	-970(2)	1068(2)	2682(1)	43(1)
C(62)	-1167(2)	481(2)	2917(1)	46(1)
C(63)	-556(2)	-6(2)	2972(1)	42(1)
C(64)	264(2)	80(1)	2794(1)	33(1)
C(65)	41(2)	1854(1)	2272(1)	39(1)
C(66)	-737(2)	2162(1)	1808(1)	63(1)
C(67)	349(2)	2305(1)	2843(1)	54(1)
C(68)	922(2)	-471(1)	2880(1)	47(1)
C(69)	1271(2)	-599(2)	3605(2)	82(1)
C(70)	523(3)	-1086(1)	2554(2)	83(1)
C(71)	319(6)	1108(6)	948(4)	40(2)
C(72)	412(3)	652(4)	485(3)	43(2)
C(73)	633(5)	21(4)	631(4)	42(2)
C(74)	814(8)	-232(6)	1255(5)	46(3)
C(71')	527(5)	1157(5)	705(4)	39(2)
C(72')	21(3)	717(4)	1021(2)	35(2)
C(73')	224(4)	84(3)	1152(2)	37(2)
C(74')	975(8)	-235(5)	995(5)	44(3)

Table C.15. Bond lengths [Å] for **(^{iPr}PDI)Ti(C_4H_6)**.

Ti(1)-N(2)	2.0054(17)	C(15)-C(19)	1.511(4)
Ti(1)-N(3)	2.0674(18)	C(16)-C(18)	1.526(3)
Ti(1)-C(34)	2.158(3)	C(16)-C(17)	1.535(4)
Ti(1)-C(37)	2.175(3)	C(19)-C(20)	1.528(4)
Ti(1)-N(1)	2.2615(18)	C(19)-C(21)	1.533(4)
Ti(1)-C(35)	2.311(3)	C(22)-C(27)	1.402(3)
Ti(1)-C(36)	2.314(3)	C(22)-C(23)	1.403(3)
Ti(2)-N(5)	1.9986(17)	C(23)-C(24)	1.383(3)
Ti(2)-C(74')	2.152(10)	C(23)-C(28)	1.516(3)
Ti(2)-C(71)	2.135(9)	C(24)-C(25)	1.370(4)
Ti(2)-C(71')	2.172(8)	C(25)-C(26)	1.375(4)
Ti(2)-N(6)	2.1582(17)	C(26)-C(27)	1.388(3)
Ti(2)-N(4)	2.1628(18)	C(27)-C(31)	1.516(3)
Ti(2)-C(74)	2.149(12)	C(28)-C(30)	1.515(4)
Ti(2)-C(72')	2.311(5)	C(28)-C(29)	1.515(4)
Ti(2)-C(73')	2.314(5)	C(31)-C(32)	1.525(4)
Ti(2)-C(72)	2.322(5)	C(31)-C(33)	1.527(3)
Ti(2)-C(73)	2.330(6)	C(34)-C(35)	1.413(4)
N(1)-C(2)	1.307(3)	C(35)-C(36)	1.388(4)
N(1)-C(10)	1.444(3)	C(36)-C(37)	1.407(4)
N(2)-C(3)	1.384(3)	C(38)-C(39)	1.495(3)
N(2)-C(7)	1.413(3)	C(39)-C(40)	1.403(3)
N(3)-C(8)	1.392(3)	C(40)-C(41)	1.380(3)
N(3)-C(22)	1.444(3)	C(41)-C(42)	1.381(3)
N(4)-C(39)	1.339(3)	C(42)-C(43)	1.376(3)
N(4)-C(47)	1.443(3)	C(43)-C(44)	1.387(3)
N(5)-C(40)	1.399(3)	C(44)-C(45)	1.395(3)
N(5)-C(44)	1.400(3)	C(45)-C(46)	1.500(3)
N(6)-C(45)	1.353(3)	C(47)-C(48)	1.401(3)
N(6)-C(59)	1.435(3)	C(47)-C(52)	1.403(3)
C(1)-C(2)	1.495(3)	C(48)-C(49)	1.389(3)
C(2)-C(3)	1.436(3)	C(48)-C(53)	1.507(4)
C(3)-C(4)	1.366(3)	C(49)-C(50)	1.379(4)
C(4)-C(5)	1.412(3)	C(50)-C(51)	1.357(4)
C(5)-C(6)	1.353(3)	C(51)-C(52)	1.389(3)
C(6)-C(7)	1.406(3)	C(52)-C(56)	1.517(4)
C(7)-C(8)	1.363(3)	C(53)-C(55)	1.523(4)
C(8)-C(9)	1.497(3)	C(53)-C(54)	1.529(4)
C(10)-C(11)	1.398(3)	C(56)-C(58)	1.517(4)
C(10)-C(15)	1.410(3)	C(56)-C(57)	1.526(4)
C(11)-C(12)	1.390(3)	C(59)-C(64)	1.394(3)
C(11)-C(16)	1.519(3)	C(59)-C(60)	1.407(3)
C(12)-C(13)	1.374(4)	C(60)-C(61)	1.387(3)
C(13)-C(14)	1.355(4)	C(60)-C(65)	1.510(3)
C(14)-C(15)	1.391(3)	C(61)-C(62)	1.369(4)

Table C.15. (continued)

C(62)-C(63)	1.364(4)	C(71)-C(72)	1.385(13)
C(63)-C(64)	1.392(3)	C(72)-C(73)	1.368(12)
C(64)-C(68)	1.510(3)	C(73)-C(74)	1.393(16)
C(65)-C(67)	1.523(4)	C(71')-C(72')	1.443(10)
C(65)-C(66)	1.525(4)	C(72')-C(73')	1.363(10)
C(68)-C(70)	1.517(4)	C(73')-C(74')	1.422(13)
C(68)-C(69)	1.537(4)		

Table C.16. Angles [°] for **(^{iPr}PDI)Ti(C_4H_6)**.

N(2)-Ti(1)-N(3)	74.92(7)	C(71')-Ti(2)-C(72')	37.4(3)
N(2)-Ti(1)-C(34)	130.12(11)	N(6)-Ti(2)-C(72')	88.16(14)
N(3)-Ti(1)-C(34)	113.63(11)	N(4)-Ti(2)-C(72')	122.76(14)
N(2)-Ti(1)-C(37)	139.38(10)	C(74)-Ti(2)-C(72')	62.3(4)
N(3)-Ti(1)-C(37)	109.46(10)	N(5)-Ti(2)-C(73')	155.52(15)
C(34)-Ti(1)-C(37)	86.45(14)	C(74')-Ti(2)-C(73')	36.9(3)
N(2)-Ti(1)-N(1)	72.58(7)	C(71)-Ti(2)-C(73')	58.3(4)
N(3)-Ti(1)-N(1)	147.18(7)	C(71')-Ti(2)-C(73')	67.4(3)
C(34)-Ti(1)-N(1)	91.13(10)	N(6)-Ti(2)-C(73')	88.17(13)
C(37)-Ti(1)-N(1)	92.53(9)	N(4)-Ti(2)-C(73')	122.25(13)
N(2)-Ti(1)-C(35)	152.81(10)	C(74)-Ti(2)-C(73')	28.3(4)
N(3)-Ti(1)-C(35)	90.37(9)	C(72')-Ti(2)-C(73')	34.3(3)
C(34)-Ti(1)-C(35)	36.66(11)	N(5)-Ti(2)-C(72)	156.16(17)
C(37)-Ti(1)-C(35)	66.88(12)	C(74')-Ti(2)-C(72)	59.2(4)
N(1)-Ti(1)-C(35)	121.22(8)	C(71)-Ti(2)-C(72)	35.9(3)
N(2)-Ti(1)-C(36)	160.15(9)	C(71')-Ti(2)-C(72)	29.2(3)
N(3)-Ti(1)-C(36)	88.99(8)	N(6)-Ti(2)-C(72)	122.96(14)
C(34)-Ti(1)-C(36)	66.88(12)	N(4)-Ti(2)-C(72)	88.22(14)
C(37)-Ti(1)-C(36)	36.36(10)	C(74)-Ti(2)-C(72)	66.1(4)
N(1)-Ti(1)-C(36)	121.60(8)	C(72')-Ti(2)-C(72)	34.82(18)
C(35)-Ti(1)-C(36)	34.93(10)	C(73')-Ti(2)-C(72)	48.3(2)
N(5)-Ti(2)-C(74')	135.3(4)	N(5)-Ti(2)-C(73)	154.3(2)
N(5)-Ti(2)-C(71)	137.7(3)	C(74')-Ti(2)-C(73)	25.2(3)
C(74')-Ti(2)-C(71)	87.0(5)	C(71)-Ti(2)-C(73)	65.5(4)
N(5)-Ti(2)-C(71')	134.1(3)	C(71')-Ti(2)-C(73)	63.3(4)
C(74')-Ti(2)-C(71')	87.8(4)	N(6)-Ti(2)-C(73)	122.23(17)
C(71)-Ti(2)-C(71')	17.68(19)	N(4)-Ti(2)-C(73)	87.88(17)
N(5)-Ti(2)-N(6)	73.85(7)	C(74)-Ti(2)-C(73)	35.9(4)
C(74')-Ti(2)-N(6)	110.2(2)	C(72')-Ti(2)-C(73)	50.6(2)
C(71)-Ti(2)-N(6)	93.9(2)	C(73')-Ti(2)-C(73)	34.43(19)
C(71')-Ti(2)-N(6)	110.2(2)	C(72)-Ti(2)-C(73)	34.2(3)
N(5)-Ti(2)-N(4)	73.86(7)	C(2)-N(1)-C(10)	118.99(18)
C(74')-Ti(2)-N(4)	92.2(2)	C(2)-N(1)-Ti(1)	116.18(14)
C(71)-Ti(2)-N(4)	110.7(2)	C(10)-N(1)-Ti(1)	124.82(13)
C(71')-Ti(2)-N(4)	93.02(19)	C(3)-N(2)-C(7)	117.01(17)
N(6)-Ti(2)-N(4)	147.69(7)	C(3)-N(2)-Ti(1)	123.02(14)
N(5)-Ti(2)-C(74)	134.2(4)	C(7)-N(2)-Ti(1)	119.92(13)
C(74')-Ti(2)-C(74)	17.2(2)	C(8)-N(3)-C(22)	115.18(17)
C(71)-Ti(2)-C(74)	85.7(5)	C(8)-N(3)-Ti(1)	118.33(14)
C(71')-Ti(2)-C(74)	91.7(5)	C(22)-N(3)-Ti(1)	126.12(13)
N(6)-Ti(2)-C(74)	93.2(2)	C(39)-N(4)-C(47)	117.51(18)
N(4)-Ti(2)-C(74)	108.8(2)	C(39)-N(4)-Ti(2)	117.24(14)
N(5)-Ti(2)-C(72')	155.07(16)	C(47)-N(4)-Ti(2)	125.22(13)
C(74')-Ti(2)-C(72')	66.9(4)	C(40)-N(5)-C(44)	116.87(17)
C(71)-Ti(2)-C(72')	24.5(3)	C(40)-N(5)-Ti(2)	121.50(13)

Table C.16. (continued)

C(44)-N(5)-Ti(2)	121.59(14)	C(25)-C(26)-C(27)	121.2(2)
C(45)-N(6)-C(59)	117.39(18)	C(26)-C(27)-C(22)	118.4(2)
C(45)-N(6)-Ti(2)	117.21(14)	C(26)-C(27)-C(31)	119.4(2)
C(59)-N(6)-Ti(2)	125.39(13)	C(22)-C(27)-C(31)	122.2(2)
N(1)-C(2)-C(3)	114.64(19)	C(30)-C(28)-C(29)	108.6(3)
N(1)-C(2)-C(1)	124.8(2)	C(30)-C(28)-C(23)	113.8(2)
C(3)-C(2)-C(1)	120.5(2)	C(29)-C(28)-C(23)	111.0(2)
C(4)-C(3)-N(2)	122.6(2)	C(27)-C(31)-C(32)	111.1(2)
C(4)-C(3)-C(2)	123.9(2)	C(27)-C(31)-C(33)	113.5(2)
N(2)-C(3)-C(2)	113.49(18)	C(32)-C(31)-C(33)	110.0(2)
C(3)-C(4)-C(5)	120.2(2)	C(35)-C(34)-Ti(1)	77.57(17)
C(6)-C(5)-C(4)	118.4(2)	C(36)-C(35)-C(34)	123.5(3)
C(5)-C(6)-C(7)	121.7(2)	C(36)-C(35)-Ti(1)	72.63(16)
C(8)-C(7)-C(6)	126.8(2)	C(34)-C(35)-Ti(1)	65.77(15)
C(8)-C(7)-N(2)	113.25(18)	C(35)-C(36)-C(37)	124.6(3)
C(6)-C(7)-N(2)	119.94(19)	C(35)-C(36)-Ti(1)	72.44(15)
C(7)-C(8)-N(3)	113.56(19)	C(37)-C(36)-Ti(1)	66.45(15)
C(7)-C(8)-C(9)	122.5(2)	C(36)-C(37)-Ti(1)	77.19(16)
N(3)-C(8)-C(9)	123.9(2)	N(4)-C(39)-C(40)	114.38(19)
C(11)-C(10)-C(15)	121.5(2)	N(4)-C(39)-C(38)	124.2(2)
C(11)-C(10)-N(1)	118.01(19)	C(40)-C(39)-C(38)	121.4(2)
C(15)-C(10)-N(1)	120.4(2)	C(41)-C(40)-N(5)	121.32(19)
C(12)-C(11)-C(10)	117.7(2)	C(41)-C(40)-C(39)	125.7(2)
C(12)-C(11)-C(16)	119.6(2)	N(5)-C(40)-C(39)	113.00(18)
C(10)-C(11)-C(16)	122.6(2)	C(40)-C(41)-C(42)	121.0(2)
C(13)-C(12)-C(11)	121.3(3)	C(43)-C(42)-C(41)	118.7(2)
C(14)-C(13)-C(12)	120.2(2)	C(42)-C(43)-C(44)	120.9(2)
C(13)-C(14)-C(15)	122.0(2)	C(43)-C(44)-C(45)	125.5(2)
C(14)-C(15)-C(10)	117.2(2)	C(43)-C(44)-N(5)	121.2(2)
C(14)-C(15)-C(19)	119.3(2)	C(45)-C(44)-N(5)	113.23(18)
C(10)-C(15)-C(19)	123.4(2)	N(6)-C(45)-C(44)	114.12(19)
C(11)-C(16)-C(18)	113.1(2)	N(6)-C(45)-C(46)	124.3(2)
C(11)-C(16)-C(17)	110.9(2)	C(44)-C(45)-C(46)	121.6(2)
C(18)-C(16)-C(17)	109.3(2)	C(48)-C(47)-C(52)	121.4(2)
C(15)-C(19)-C(20)	113.1(2)	C(48)-C(47)-N(4)	119.4(2)
C(15)-C(19)-C(21)	110.8(3)	C(52)-C(47)-N(4)	119.2(2)
C(20)-C(19)-C(21)	109.0(2)	C(49)-C(48)-C(47)	117.3(2)
C(27)-C(22)-C(23)	120.73(19)	C(49)-C(48)-C(53)	120.0(2)
C(27)-C(22)-N(3)	120.21(19)	C(47)-C(48)-C(53)	122.7(2)
C(23)-C(22)-N(3)	119.1(2)	C(50)-C(49)-C(48)	121.7(3)
C(24)-C(23)-C(22)	118.3(2)	C(51)-C(50)-C(49)	120.1(3)
C(24)-C(23)-C(28)	119.6(2)	C(50)-C(51)-C(52)	121.3(3)
C(22)-C(23)-C(28)	122.1(2)	C(51)-C(52)-C(47)	118.2(2)
C(25)-C(24)-C(23)	121.6(2)	C(51)-C(52)-C(56)	119.3(2)
C(24)-C(25)-C(26)	119.8(2)	C(47)-C(52)-C(56)	122.6(2)

Table C.16. (continued)

C(48)-C(53)-C(55)	111.6(2)	C(67)-C(65)-C(66)	109.3(2)
C(48)-C(53)-C(54)	113.4(2)	C(64)-C(68)-C(70)	112.3(2)
C(55)-C(53)-C(54)	109.0(2)	C(64)-C(68)-C(69)	110.0(2)
C(52)-C(56)-C(58)	112.9(2)	C(70)-C(68)-C(69)	109.6(3)
C(52)-C(56)-C(57)	111.5(2)	C(72)-C(71)-Ti(2)	79.4(5)
C(58)-C(56)-C(57)	108.1(2)	C(73)-C(72)-C(71)	123.3(6)
C(64)-C(59)-C(60)	120.8(2)	C(73)-C(72)-Ti(2)	73.2(3)
C(64)-C(59)-N(6)	119.9(2)	C(71)-C(72)-Ti(2)	64.7(4)
C(60)-C(59)-N(6)	119.2(2)	C(72)-C(73)-C(74)	124.4(7)
C(61)-C(60)-C(59)	117.6(2)	C(72)-C(73)-Ti(2)	72.6(3)
C(61)-C(60)-C(65)	120.4(2)	C(74)-C(73)-Ti(2)	64.9(5)
C(59)-C(60)-C(65)	121.9(2)	C(73)-C(74)-Ti(2)	79.1(6)
C(62)-C(61)-C(60)	122.2(3)	C(72')-C(71')-Ti(2)	76.5(4)
C(63)-C(62)-C(61)	119.3(3)	C(71')-C(72')-C(73')	125.3(6)
C(62)-C(63)-C(64)	121.6(3)	C(71')-C(72')-Ti(2)	66.1(4)
C(63)-C(64)-C(59)	118.4(2)	C(73')-C(72')-Ti(2)	73.0(3)
C(63)-C(64)-C(68)	119.2(2)	C(74')-C(73')-C(72')	124.3(6)
C(59)-C(64)-C(68)	122.4(2)	C(74')-C(73')-Ti(2)	65.3(4)
C(60)-C(65)-C(67)	111.1(2)	C(72')-C(73')-Ti(2)	72.7(3)
C(60)-C(65)-C(66)	113.5(2)	C(73')-C(74')-Ti(2)	77.7(5)

Table C.17. Crystal data and structure refinement for **1-Bpy**.

Identification code	rt16a	
Empirical formula	C43 H51 Fe N5	
Formula weight	693.74	
Temperature	173(2) K	
Wavelength	0.71073 Å	
Crystal system	Monoclinic	
Space group	C2/c	
Unit cell dimensions	a = 22.503(3) Å	α= 90°.
	b = 18.2414(19) Å	β= 99.393(3)°.
	c = 22.395(3) Å	γ = 90°.
Volume	9069.5(18) $Å^3$	
Z	8	
Density (calculated)	1.016 Mg/m^3	
Absorption coefficient	0.363 mm^{-1}	
F(000)	2960	
Crystal size	0.50 x 0.30 x 0.02 mm^3	
Theta range for data collection	1.44 to 23.28°.	
Index ranges	-24<=h<=24, -20<=k<=17, -24<=l<=24	
Reflections collected	31188	
Independent reflections	6510 [R(int) = 0.1193]	
Completeness to theta = 23.28°	99.9 %	
Absorption correction	Semi-empirical from equivalents	
Max. and min. transmission	0.9928 and 0.8394	
Refinement method	Full-matrix least-squares on F^2	
Data / restraints / parameters	6510 / 0 / 442	
Goodness-of-fit on F^2	0.776	
Final R indices [I>2sigma(I)]	R1 = 0.0466, wR2 = 0.0906	
R indices (all data)	R1 = 0.1102, wR2 = 0.1005	
Largest diff. peak and hole	0.245 and -0.248 $e.Å^{-3}$	

Table C.18. Atomic coordinates (x 10^4) and equivalent isotropic displacement parameters ($Å^2$x 10^3) for **1-Bpy**. U(eq) is defined as one third of the trace of the orthogonalized U^{ij} tensor.

	x	y	z	U(eq)
Fe(1)	2109(1)	2852(1)	2434(1)	24(1)
N(1)	2158(1)	2628(1)	3286(1)	24(1)
N(2)	2831(1)	2359(1)	2569(2)	23(1)
N(3)	2196(1)	2599(1)	1612(1)	24(1)
N(4)	1312(1)	3270(2)	2242(1)	25(1)
N(5)	2320(1)	3892(2)	2471(1)	23(1)
C(1)	2856(2)	2209(2)	4231(2)	35(1)
C(2)	2700(2)	2373(2)	3568(2)	25(1)
C(3)	3098(2)	2210(2)	3161(2)	29(1)
C(4)	3675(2)	1913(2)	3275(2)	38(1)
C(5)	3977(2)	1765(2)	2793(2)	41(1)
C(6)	3696(2)	1892(2)	2196(2)	37(1)
C(7)	3119(2)	2183(2)	2092(2)	27(1)
C(8)	2738(2)	2329(2)	1539(2)	28(1)
C(9)	2929(2)	2147(2)	942(2)	40(1)
C(10)	795(2)	2894(2)	2080(2)	33(1)
C(11)	254(2)	3221(3)	1866(2)	42(1)
C(12)	224(2)	3989(3)	1823(2)	50(1)
C(13)	738(2)	4382(2)	1995(2)	40(1)
C(14)	1280(2)	4028(2)	2202(2)	27(1)
C(15)	1857(2)	4373(2)	2353(2)	25(1)
C(16)	1969(2)	5129(2)	2374(2)	40(1)
C(17)	2544(2)	5390(2)	2503(2)	43(1)
C(18)	3010(2)	4896(2)	2618(2)	41(1)
C(19)	2891(2)	4148(2)	2602(2)	31(1)
C(20)	1692(2)	2708(2)	3652(2)	25(1)
C(21)	1626(2)	3362(2)	3969(2)	26(1)
C(22)	1188(2)	3387(2)	4338(2)	32(1)
C(23)	820(2)	2795(2)	4405(2)	34(1)
C(24)	882(2)	2163(2)	4080(2)	33(1)
C(25)	1312(2)	2115(2)	3705(2)	26(1)
C(26)	2027(2)	4024(2)	3942(2)	30(1)
C(27)	1654(2)	4730(2)	3800(2)	44(1)
C(28)	2468(2)	4119(2)	4530(2)	44(1)
C(29)	1369(2)	1394(2)	3363(2)	28(1)
C(30)	1677(2)	808(2)	3799(2)	51(1)
C(31)	756(2)	1108(2)	3056(2)	43(1)
C(32)	1746(2)	2687(2)	1078(2)	26(1)
C(33)	1342(2)	2114(2)	909(2)	24(1)
C(34)	919(2)	2186(2)	388(2)	35(1)
C(35)	887(2)	2814(2)	38(2)	39(1)
C(36)	1279(2)	3387(2)	223(2)	33(1)
C(37)	1708(2)	3335(2)	733(2)	32(1)
C(38)	1367(2)	1396(2)	1259(2)	29(1)
C(39)	740(2)	1092(2)	1303(2)	40(1)
C(40)	1736(2)	826(2)	959(2)	42(1)

Table C.18. (continued)

C(41)	2140(2)	3982(2)	894(2)	36(1)
C(42)	2611(2)	4013(2)	475(2)	46(1)
C(43)	1794(2)	4712(2)	861(2)	46(1)

Table C.19. Bond lengths [Å] for **1-Bpy**.

Fe(1)-N(2)	1.840(3)	C(15)-C(16)	1.402(5)
Fe(1)-N(4)	1.932(3)	C(16)-C(17)	1.365(5)
Fe(1)-N(1)	1.938(3)	C(17)-C(18)	1.375(5)
Fe(1)-N(3)	1.938(3)	C(18)-C(19)	1.389(5)
Fe(1)-N(5)	1.954(3)	C(20)-C(25)	1.395(4)
N(1)-C(2)	1.360(4)	C(20)-C(21)	1.410(4)
N(1)-C(20)	1.440(4)	C(21)-C(22)	1.387(4)
N(2)-C(7)	1.376(4)	C(21)-C(26)	1.514(4)
N(2)-C(3)	1.389(4)	C(22)-C(23)	1.384(4)
N(3)-C(8)	1.351(4)	C(23)-C(24)	1.383(5)
N(3)-C(32)	1.444(4)	C(24)-C(25)	1.384(4)
N(4)-C(10)	1.347(4)	C(25)-C(29)	1.538(4)
N(4)-C(14)	1.387(4)	C(26)-C(28)	1.525(4)
N(5)-C(19)	1.354(4)	C(26)-C(27)	1.541(4)
N(5)-C(15)	1.355(4)	C(29)-C(31)	1.530(4)
C(1)-C(2)	1.500(4)	C(29)-C(30)	1.534(4)
C(2)-C(3)	1.408(5)	C(32)-C(33)	1.397(4)
C(3)-C(4)	1.392(5)	C(32)-C(37)	1.407(5)
C(4)-C(5)	1.392(5)	C(33)-C(34)	1.387(4)
C(5)-C(6)	1.400(5)	C(33)-C(38)	1.522(4)
C(6)-C(7)	1.387(5)	C(34)-C(35)	1.383(5)
C(7)-C(8)	1.410(5)	C(35)-C(36)	1.388(5)
C(8)-C(9)	1.507(5)	C(36)-C(37)	1.374(5)
C(10)-C(11)	1.370(5)	C(37)-C(41)	1.532(5)
C(11)-C(12)	1.406(5)	C(38)-C(39)	1.532(4)
C(12)-C(13)	1.361(5)	C(38)-C(40)	1.552(4)
C(13)-C(14)	1.392(5)	C(41)-C(42)	1.528(5)
C(14)-C(15)	1.431(5)	C(41)-C(43)	1.538(5)

Table C.20. Angles [°] for **1-Bpy**.

N(2)-Fe(1)-N(4)	173.39(12)	N(4)-C(14)-C(15)	112.8(3)
N(2)-Fe(1)-N(1)	80.05(13)	C(13)-C(14)-C(15)	125.9(4)
N(4)-Fe(1)-N(1)	101.81(12)	N(5)-C(15)-C(16)	120.1(3)
N(2)-Fe(1)-N(3)	79.46(13)	N(5)-C(15)-C(14)	113.6(3)
N(4)-Fe(1)-N(3)	96.68(12)	C(16)-C(15)-C(14)	126.3(4)
N(1)-Fe(1)-N(3)	152.51(11)	C(17)-C(16)-C(15)	120.6(4)
N(2)-Fe(1)-N(5)	105.38(12)	C(16)-C(17)-C(18)	118.6(4)
N(4)-Fe(1)-N(5)	80.60(13)	C(17)-C(18)-C(19)	120.1(4)
N(1)-Fe(1)-N(5)	100.84(11)	N(5)-C(19)-C(18)	121.1(4)
N(3)-Fe(1)-N(5)	102.12(11)	C(25)-C(20)-C(21)	119.8(3)
C(2)-N(1)-C(20)	116.9(3)	C(25)-C(20)-N(1)	118.9(3)
C(2)-N(1)-Fe(1)	115.6(2)	C(21)-C(20)-N(1)	121.2(3)
C(20)-N(1)-Fe(1)	127.5(2)	C(22)-C(21)-C(20)	118.2(3)
C(7)-N(2)-C(3)	120.8(3)	C(22)-C(21)-C(26)	118.9(3)
C(7)-N(2)-Fe(1)	120.1(3)	C(20)-C(21)-C(26)	122.9(3)
C(3)-N(2)-Fe(1)	119.0(3)	C(23)-C(22)-C(21)	122.3(3)
C(8)-N(3)-C(32)	117.8(3)	C(24)-C(23)-C(22)	118.7(3)
C(8)-N(3)-Fe(1)	115.7(2)	C(23)-C(24)-C(25)	120.9(4)
C(32)-N(3)-Fe(1)	126.4(2)	C(24)-C(25)-C(20)	120.1(3)
C(10)-N(4)-C(14)	117.2(3)	C(24)-C(25)-C(29)	118.7(3)
C(10)-N(4)-Fe(1)	126.1(3)	C(20)-C(25)-C(29)	121.2(3)
C(14)-N(4)-Fe(1)	116.3(2)	C(21)-C(26)-C(28)	111.4(3)
C(19)-N(5)-C(15)	119.5(3)	C(21)-C(26)-C(27)	111.6(3)
C(19)-N(5)-Fe(1)	124.0(3)	C(28)-C(26)-C(27)	109.8(3)
C(15)-N(5)-Fe(1)	116.5(2)	C(31)-C(29)-C(30)	109.2(3)
N(1)-C(2)-C(3)	112.9(3)	C(31)-C(29)-C(25)	111.9(3)
N(1)-C(2)-C(1)	125.0(3)	C(30)-C(29)-C(25)	110.1(3)
C(3)-C(2)-C(1)	121.8(3)	C(33)-C(32)-C(37)	120.2(3)
N(2)-C(3)-C(4)	119.6(3)	C(33)-C(32)-N(3)	118.6(3)
N(2)-C(3)-C(2)	110.8(3)	C(37)-C(32)-N(3)	121.2(3)
C(4)-C(3)-C(2)	129.5(4)	C(34)-C(33)-C(32)	119.0(3)
C(3)-C(4)-C(5)	119.5(4)	C(34)-C(33)-C(38)	118.5(3)
C(4)-C(5)-C(6)	120.4(4)	C(32)-C(33)-C(38)	122.5(3)
C(7)-C(6)-C(5)	119.3(4)	C(35)-C(34)-C(33)	121.3(4)
N(2)-C(7)-C(6)	120.2(3)	C(34)-C(35)-C(36)	118.9(4)
N(2)-C(7)-C(8)	110.0(3)	C(37)-C(36)-C(35)	121.5(4)
C(6)-C(7)-C(8)	129.7(4)	C(36)-C(37)-C(32)	119.0(4)
N(3)-C(8)-C(7)	113.3(3)	C(36)-C(37)-C(41)	118.3(3)
N(3)-C(8)-C(9)	125.5(3)	C(32)-C(37)-C(41)	122.6(3)
C(7)-C(8)-C(9)	121.1(3)	C(33)-C(38)-C(39)	112.8(3)
N(4)-C(10)-C(11)	123.5(4)	C(33)-C(38)-C(40)	109.3(3)
C(10)-C(11)-C(12)	119.1(4)	C(39)-C(38)-C(40)	110.4(3)
C(13)-C(12)-C(11)	118.5(4)	C(42)-C(41)-C(37)	111.2(3)
C(12)-C(13)-C(14)	120.5(4)	C(42)-C(41)-C(43)	109.6(3)
N(4)-C(14)-C(13)	121.1(3)	C(37)-C(41)-C(43)	111.1(3)

Table C.21. Crystal data and structure refinement for **1-H_2CIN**.

Identification code	rt22	
Empirical formula	C42 H52 Fe N3 O2	
Formula weight	686.72	
Temperature	173(2) K	
Wavelength	0.71073 Å	
Crystal system	Orthorhombic	
Space group	P2(1)2(1)2(1)	
Unit cell dimensions	a = 14.809(10) Å	α= 90°.
	b = 20.418(17) Å	β= 90°.
	c = 29.82(2) Å	γ = 90°.
Volume	9018(12) $Å^3$	
Z	8	
Density (calculated)	1.012 Mg/m^3	
Absorption coefficient	0.366 mm^{-1}	
F(000)	2936	
Crystal size	0.30 x 0.20 x 0.10 mm^3	
Theta range for data collection	1.21 to 22.21°.	
Index ranges	-15<=h<=13, -18<=k<=21, -31<=l<=31	
Reflections collected	33765	
Independent reflections	11224 [R(int) = 0.1716]	
Completeness to theta = 22.21°	99.0 %	
Absorption correction	Semi-empirical from equivalents	
Max. and min. transmission	0.9643 and 0.8980	
Refinement method	Full-matrix least-squares on F^2	
Data / restraints / parameters	11224 / 855 / 845	
Goodness-of-fit on F^2	0.727	
Final R indices [I>2sigma(I)]	R1 = 0.0627, wR2 = 0.1061	
R indices (all data)	R1 = 0.1709, wR2 = 0.1240	
Absolute structure parameter	0.02(2)	
Largest diff. peak and hole	0.422 and -0.312 $e.Å^{-3}$	

Table C.22. Atomic coordinates (x 10^4) and equivalent isotropic displacement parameters ($Å^2$x 10^3) for **1-H_2CIN**. U(eq) is defined as one third of the trace of the orthogonalized U^{ij} tensor.

	x	y	z	U(eq)
Fe(1)	-7904(1)	1364(1)	9288(1)	34(1)
O(1)	-8564(2)	2122(1)	8924(1)	45(1)
O(2)	-9053(2)	1102(1)	8915(1)	41(1)
N(1)	-8489(2)	1517(2)	9937(1)	28(1)
N(2)	-7020(2)	974(1)	9721(1)	20(1)
N(3)	-6776(2)	1124(2)	8888(1)	32(1)
C(1)	-8367(2)	1314(2)	10740(1)	45(1)
C(2)	-8068(2)	1291(2)	10271(1)	22(1)
C(3)	-7185(2)	971(2)	10168(1)	21(1)
C(4)	-6599(2)	705(2)	10466(1)	28(1)
C(5)	-5794(2)	406(2)	10308(1)	27(1)
C(6)	-5623(2)	450(2)	9853(1)	28(1)
C(7)	-6233(2)	727(2)	9566(1)	20(1)
C(8)	-6119(2)	810(2)	9101(1)	25(1)
C(9)	-5257(2)	574(2)	8860(1)	39(2)
C(10)	-9365(2)	1837(2)	9974(1)	32(1)
C(11)	-9394(2)	2512(2)	9961(1)	33(1)
C(12)	-10235(2)	2813(2)	10001(1)	43(2)
C(13)	-11006(3)	2452(2)	10011(2)	44(2)
C(14)	-10964(2)	1811(2)	10027(1)	41(1)
C(15)	-10156(2)	1452(2)	10004(1)	28(1)
C(16)	-8551(2)	2939(2)	9950(1)	36(1)
C(17)	-8581(2)	3465(2)	9598(1)	52(2)
C(18)	-8398(2)	3230(2)	10414(1)	59(2)
C(19)	-10161(2)	723(2)	9987(1)	42(1)
C(20)	-10652(3)	453(2)	9588(1)	63(2)
C(21)	-10541(3)	426(2)	10407(1)	62(2)
C(22)	-6719(2)	1267(2)	8424(1)	22(1)
C(23)	-6498(2)	1939(2)	8313(1)	45(1)
C(24)	-6504(2)	2081(2)	7873(1)	57(2)
C(25)	-6712(3)	1629(3)	7550(1)	69(2)
C(26)	-6937(3)	1001(2)	7663(1)	62(2)
C(27)	-6942(3)	801(2)	8111(1)	49(1)
C(28)	-6256(3)	2425(2)	8663(2)	52(2)
C(29)	-5217(3)	2545(3)	8675(2)	120(3)
C(30)	-6701(3)	3074(2)	8594(2)	73(2)
C(31)	-7145(3)	96(2)	8228(1)	52(2)
C(32)	-6597(3)	-433(2)	7989(2)	94(2)
C(33)	-8180(3)	-28(2)	8153(1)	72(2)
C(34)	-9104(3)	1710(2)	8810(1)	38(1)
C(35)	-9928(3)	1899(2)	8527(1)	53(2)
C(36)	-10246(3)	2569(2)	8611(2)	64(2)
C(37)	-11136(3)	2718(3)	8346(1)	61(2)
C(38)	-11033(3)	3009(2)	7935(2)	64(2)
C(39)	-11791(3)	3171(2)	7674(2)	77(2)
C(40)	-12626(3)	3015(2)	7854(1)	75(2)

Table C.22. (continued)

C(41)	-12706(3)	2740(3)	8254(2)	99(2)
C(42)	-11937(3)	2582(3)	8495(2)	81(2)
Fe(2)	-5459(1)	-1294(1)	10574(1)	33(1)
O(3)	-5985(2)	-2069(1)	10957(1)	47(1)
O(4)	-6685(2)	-1127(1)	10912(1)	47(1)
N(4)	-4432(2)	-888(2)	10975(1)	26(1)
N(5)	-4580(2)	-923(1)	10134(1)	15(1)
N(6)	-5971(2)	-1569(2)	9935(1)	27(1)
C(43)	-2994(2)	-258(2)	11001(1)	44(2)
C(44)	-3786(2)	-596(2)	10766(1)	24(1)
C(45)	-3847(2)	-603(2)	10291(1)	21(1)
C(46)	-3219(2)	-341(2)	10001(1)	31(1)
C(47)	-3327(2)	-432(2)	9541(1)	29(1)
C(48)	-4082(2)	-783(2)	9387(1)	31(1)
C(49)	-4692(2)	-1018(2)	9688(1)	23(1)
C(50)	-5522(2)	-1370(2)	9585(1)	23(1)
C(51)	-5804(2)	-1463(2)	9105(1)	39(2)
C(52)	-4406(2)	-950(2)	11450(1)	31(1)
C(53)	-4979(3)	-560(2)	11711(1)	42(1)
C(54)	-4948(3)	-649(2)	12174(1)	54(2)
C(55)	-4421(3)	-1118(2)	12358(1)	55(2)
C(56)	-3906(3)	-1530(2)	12099(1)	47(2)
C(57)	-3868(2)	-1453(2)	11627(1)	34(1)
C(58)	-5544(3)	-34(2)	11506(1)	47(2)
C(59)	-5003(3)	621(2)	11463(1)	60(2)
C(60)	-6439(3)	93(2)	11744(1)	68(2)
C(61)	-3327(3)	-1928(2)	11357(1)	52(2)
C(62)	-3752(3)	-2608(2)	11356(1)	68(2)
C(63)	-2315(3)	-1964(2)	11524(1)	74(2)
C(64)	-6811(2)	-1912(2)	9895(1)	28(1)
C(65)	-7627(2)	-1561(2)	9846(1)	26(1)
C(66)	-8415(3)	-1944(2)	9825(1)	30(1)
C(67)	-8446(3)	-2599(2)	9846(1)	47(2)
C(68)	-7608(2)	-2927(2)	9900(1)	37(1)
C(69)	-6802(2)	-2585(2)	9922(1)	27(1)
C(70)	-7701(3)	-827(2)	9826(1)	40(1)
C(71)	-8019(2)	-614(2)	9367(1)	59(2)
C(72)	-8277(2)	-551(2)	10204(1)	56(2)
C(73)	-5922(2)	-2990(2)	9969(1)	36(1)
C(74)	-5693(3)	-3285(2)	9515(1)	72(2)
C(75)	-5975(3)	-3482(2)	10336(1)	49(2)
C(76)	-6613(3)	-1720(2)	11053(1)	45(1)
C(77)	-7404(3)	-1943(2)	11350(1)	74(2)
C(78)	-7905(3)	-2497(3)	11160(1)	82(2)
C(79)	-8618(3)	-2747(3)	11483(2)	65(2)
C(80)	-9393(3)	-2391(3)	11565(2)	64(2)
C(81)	-10042(3)	-2607(3)	11867(2)	79(2)
C(82)	-9886(3)	-3182(3)	12074(1)	66(2)
C(83)	-9128(3)	-3575(3)	12005(2)	89(2)
C(84)	-8485(3)	-3322(2)	11699(1)	68(2)

Table C.23. Bond lengths [Å] for **1-H_2CIN**.

Fe(1)-N(2)	2.005(3)	C(31)-C(33)	1.570(5)
Fe(1)-O(2)	2.102(3)	C(34)-C(35)	1.534(5)
Fe(1)-N(3)	2.109(3)	C(35)-C(36)	1.468(6)
Fe(1)-O(1)	2.127(3)	C(36)-C(37)	1.567(6)
Fe(1)-N(1)	2.143(3)	C(37)-C(42)	1.297(6)
Fe(1)-C(34)	2.383(4)	C(37)-C(38)	1.370(6)
O(1)-C(34)	1.209(5)	C(38)-C(39)	1.405(6)
O(2)-C(34)	1.281(5)	C(39)-C(40)	1.385(6)
N(1)-C(2)	1.264(4)	C(40)-C(41)	1.324(6)
N(1)-C(10)	1.457(4)	C(41)-C(42)	1.386(6)
N(2)-C(7)	1.351(4)	Fe(2)-N(5)	1.998(3)
N(2)-C(3)	1.356(4)	Fe(2)-O(3)	2.101(3)
N(3)-C(8)	1.327(4)	Fe(2)-O(4)	2.104(3)
N(3)-C(22)	1.419(4)	Fe(2)-N(4)	2.104(3)
C(1)-C(2)	1.466(4)	Fe(2)-N(6)	2.127(3)
C(2)-C(3)	1.494(5)	Fe(2)-C(76)	2.391(4)
C(3)-C(4)	1.356(5)	O(3)-C(76)	1.205(5)
C(4)-C(5)	1.421(5)	O(4)-C(76)	1.286(5)
C(5)-C(6)	1.383(5)	N(4)-C(44)	1.287(4)
C(6)-C(7)	1.366(5)	N(4)-C(52)	1.422(5)
C(7)-C(8)	1.408(5)	N(5)-C(45)	1.350(4)
C(8)-C(9)	1.542(5)	N(5)-C(49)	1.356(4)
C(10)-C(11)	1.379(5)	N(6)-C(50)	1.304(4)
C(10)-C(15)	1.412(5)	N(6)-C(64)	1.433(4)
C(11)-C(12)	1.395(5)	C(43)-C(44)	1.530(5)
C(11)-C(16)	1.525(5)	C(44)-C(45)	1.422(5)
C(12)-C(13)	1.359(5)	C(45)-C(46)	1.377(5)
C(13)-C(14)	1.311(5)	C(46)-C(47)	1.393(5)
C(14)-C(15)	1.406(5)	C(47)-C(48)	1.405(5)
C(15)-C(19)	1.490(6)	C(48)-C(49)	1.360(5)
C(16)-C(17)	1.503(5)	C(49)-C(50)	1.456(5)
C(16)-C(18)	1.523(5)	C(50)-C(51)	1.501(5)
C(19)-C(20)	1.499(5)	C(52)-C(57)	1.403(5)
C(19)-C(21)	1.502(5)	C(52)-C(53)	1.401(5)
C(22)-C(27)	1.373(5)	C(53)-C(54)	1.391(5)
C(22)-C(23)	1.448(6)	C(53)-C(58)	1.492(6)
C(23)-C(24)	1.344(5)	C(54)-C(55)	1.352(6)
C(23)-C(28)	1.484(6)	C(55)-C(56)	1.374(6)
C(24)-C(25)	1.369(6)	C(56)-C(57)	1.419(5)
C(25)-C(26)	1.368(7)	C(57)-C(61)	1.493(6)
C(26)-C(27)	1.398(6)	C(58)-C(60)	1.527(5)
C(27)-C(31)	1.511(6)	C(58)-C(59)	1.564(6)
C(28)-C(30)	1.495(6)	C(61)-C(62)	1.525(6)
C(28)-C(29)	1.559(6)	C(61)-C(63)	1.580(5)
C(31)-C(32)	1.527(6)	C(64)-C(69)	1.376(5)

Table C.23. (continued)

C(64)-C(65)	1.412(5)	C(73)-C(74)	1.521(5)
C(65)-C(66)	1.407(5)	C(76)-C(77)	1.538(5)
C(65)-C(70)	1.504(5)	C(77)-C(78)	1.466(6)
C(66)-C(67)	1.339(5)	C(78)-C(79)	1.519(6)
C(67)-C(68)	1.419(5)	C(79)-C(84)	1.354(7)
C(68)-C(69)	1.385(5)	C(79)-C(80)	1.379(6)
C(69)-C(73)	1.550(5)	C(80)-C(81)	1.391(6)
C(70)-C(71)	1.511(5)	C(81)-C(82)	1.346(7)
C(70)-C(72)	1.521(5)	C(82)-C(83)	1.395(6)
C(73)-C(75)	1.489(5)	C(83)-C(84)	1.417(6)

Table C.24. Angles [°] for **1-H_2CIN**.

N(2)-Fe(1)-O(2)	140.23(12)	C(12)-C(11)-C(16)	118.7(4)
N(2)-Fe(1)-N(3)	75.75(12)	C(10)-C(11)-C(16)	123.2(3)
O(2)-Fe(1)-N(3)	106.40(11)	C(13)-C(12)-C(11)	120.8(4)
N(2)-Fe(1)-O(1)	156.61(12)	C(14)-C(13)-C(12)	120.2(4)
O(2)-Fe(1)-O(1)	62.83(11)	C(13)-C(14)-C(15)	124.0(4)
N(3)-Fe(1)-O(1)	104.18(12)	C(14)-C(15)-C(10)	114.7(4)
N(2)-Fe(1)-N(1)	74.96(12)	C(14)-C(15)-C(19)	121.2(3)
O(2)-Fe(1)-N(1)	100.86(11)	C(10)-C(15)-C(19)	123.9(3)
N(3)-Fe(1)-N(1)	149.75(11)	C(17)-C(16)-C(18)	111.1(3)
O(1)-Fe(1)-N(1)	99.72(11)	C(17)-C(16)-C(11)	113.6(3)
N(2)-Fe(1)-C(34)	171.70(14)	C(18)-C(16)-C(11)	109.0(3)
O(2)-Fe(1)-C(34)	32.42(13)	C(15)-C(19)-C(20)	113.5(3)
N(3)-Fe(1)-C(34)	108.75(13)	C(15)-C(19)-C(21)	112.1(3)
O(1)-Fe(1)-C(34)	30.43(13)	C(20)-C(19)-C(21)	109.4(3)
N(1)-Fe(1)-C(34)	101.26(13)	C(27)-C(22)-N(3)	120.4(4)
C(34)-O(1)-Fe(1)	86.6(3)	C(27)-C(22)-C(23)	123.9(4)
C(34)-O(2)-Fe(1)	86.0(2)	N(3)-C(22)-C(23)	115.5(3)
C(2)-N(1)-C(10)	122.9(3)	C(24)-C(23)-C(22)	115.1(4)
C(2)-N(1)-Fe(1)	117.4(2)	C(24)-C(23)-C(28)	123.0(4)
C(10)-N(1)-Fe(1)	119.6(2)	C(22)-C(23)-C(28)	121.9(4)
C(7)-N(2)-C(3)	119.3(3)	C(23)-C(24)-C(25)	123.0(5)
C(7)-N(2)-Fe(1)	119.5(2)	C(26)-C(25)-C(24)	120.9(4)
C(3)-N(2)-Fe(1)	121.2(2)	C(25)-C(26)-C(27)	120.6(4)
C(8)-N(3)-C(22)	121.4(3)	C(22)-C(27)-C(26)	116.5(4)
C(8)-N(3)-Fe(1)	115.1(2)	C(22)-C(27)-C(31)	123.5(4)
C(22)-N(3)-Fe(1)	123.5(2)	C(26)-C(27)-C(31)	119.9(4)
N(1)-C(2)-C(1)	126.2(3)	C(23)-C(28)-C(30)	112.9(4)
N(1)-C(2)-C(3)	115.4(3)	C(23)-C(28)-C(29)	111.1(4)
C(1)-C(2)-C(3)	118.4(3)	C(30)-C(28)-C(29)	107.4(4)
C(4)-C(3)-N(2)	122.1(3)	C(27)-C(31)-C(32)	117.5(4)
C(4)-C(3)-C(2)	126.8(3)	C(27)-C(31)-C(33)	108.3(3)
N(2)-C(3)-C(2)	111.0(3)	C(32)-C(31)-C(33)	109.8(3)
C(3)-C(4)-C(5)	119.4(3)	O(1)-C(34)-O(2)	124.5(4)
C(6)-C(5)-C(4)	116.8(3)	O(1)-C(34)-C(35)	120.3(4)
C(7)-C(6)-C(5)	121.4(3)	O(2)-C(34)-C(35)	115.1(4)
N(2)-C(7)-C(6)	120.7(3)	O(1)-C(34)-Fe(1)	63.0(2)
N(2)-C(7)-C(8)	113.3(3)	O(2)-C(34)-Fe(1)	61.60(19)
C(6)-C(7)-C(8)	126.0(3)	C(35)-C(34)-Fe(1)	175.3(3)
N(3)-C(8)-C(7)	116.1(3)	C(36)-C(35)-C(34)	113.4(4)
N(3)-C(8)-C(9)	122.4(3)	C(35)-C(36)-C(37)	111.5(4)
C(7)-C(8)-C(9)	121.4(3)	C(42)-C(37)-C(38)	120.1(4)
C(11)-C(10)-C(15)	122.1(3)	C(42)-C(37)-C(36)	123.6(4)
C(11)-C(10)-N(1)	118.3(3)	C(38)-C(37)-C(36)	116.3(4)
C(15)-C(10)-N(1)	119.6(3)	C(37)-C(38)-C(39)	120.6(4)
C(12)-C(11)-C(10)	117.8(4)	C(40)-C(39)-C(38)	116.4(4)

Table C.24. (continued)

C(41)-C(40)-C(39)	121.8(4)	C(57)-C(52)-N(4)	117.0(3)
C(40)-C(41)-C(42)	119.5(5)	C(53)-C(52)-N(4)	119.2(3)
C(37)-C(42)-C(41)	121.6(5)	C(54)-C(53)-C(52)	117.2(4)
N(5)-Fe(2)-O(3)	152.19(11)	C(54)-C(53)-C(58)	121.2(4)
N(5)-Fe(2)-O(4)	144.60(12)	C(52)-C(53)-C(58)	121.3(4)
O(3)-Fe(2)-O(4)	62.71(11)	C(55)-C(54)-C(53)	121.0(4)
N(5)-Fe(2)-N(4)	75.70(12)	C(54)-C(55)-C(56)	121.7(4)
O(3)-Fe(2)-N(4)	104.82(12)	C(55)-C(56)-C(57)	120.8(4)
O(4)-Fe(2)-N(4)	106.78(12)	C(52)-C(57)-C(56)	115.6(4)
N(5)-Fe(2)-N(6)	75.15(12)	C(52)-C(57)-C(61)	125.3(3)
O(3)-Fe(2)-N(6)	98.97(12)	C(56)-C(57)-C(61)	119.0(4)
O(4)-Fe(2)-N(6)	99.38(11)	C(53)-C(58)-C(60)	114.7(3)
N(4)-Fe(2)-N(6)	150.55(11)	C(53)-C(58)-C(59)	111.2(4)
N(5)-Fe(2)-C(76)	174.91(13)	C(60)-C(58)-C(59)	109.8(3)
O(3)-Fe(2)-C(76)	30.25(13)	C(57)-C(61)-C(62)	111.7(4)
O(4)-Fe(2)-C(76)	32.47(13)	C(57)-C(61)-C(63)	111.7(3)
N(4)-Fe(2)-C(76)	108.73(14)	C(62)-C(61)-C(63)	110.4(4)
N(6)-Fe(2)-C(76)	100.58(14)	C(69)-C(64)-C(65)	121.4(3)
C(76)-O(3)-Fe(2)	88.3(3)	C(69)-C(64)-N(6)	118.3(3)
C(76)-O(4)-Fe(2)	86.1(2)	C(65)-C(64)-N(6)	120.2(4)
C(44)-N(4)-C(52)	120.2(3)	C(66)-C(65)-C(64)	115.6(4)
C(44)-N(4)-Fe(2)	116.4(2)	C(66)-C(65)-C(70)	119.4(3)
C(52)-N(4)-Fe(2)	123.4(2)	C(64)-C(65)-C(70)	124.9(3)
C(45)-N(5)-C(49)	120.5(3)	C(67)-C(66)-C(65)	125.5(4)
C(45)-N(5)-Fe(2)	118.7(2)	C(66)-C(67)-C(68)	116.6(4)
C(49)-N(5)-Fe(2)	120.7(2)	C(69)-C(68)-C(67)	121.4(4)
C(50)-N(6)-C(64)	121.9(3)	C(64)-C(69)-C(68)	119.5(4)
C(50)-N(6)-Fe(2)	117.0(2)	C(64)-C(69)-C(73)	123.2(3)
C(64)-N(6)-Fe(2)	120.9(2)	C(68)-C(69)-C(73)	117.3(4)
N(4)-C(44)-C(45)	115.6(3)	C(71)-C(70)-C(72)	113.0(3)
N(4)-C(44)-C(43)	123.9(3)	C(71)-C(70)-C(65)	110.2(3)
C(45)-C(44)-C(43)	120.5(3)	C(72)-C(70)-C(65)	112.4(3)
N(5)-C(45)-C(46)	121.0(3)	C(75)-C(73)-C(74)	113.6(4)
N(5)-C(45)-C(44)	113.6(3)	C(75)-C(73)-C(69)	112.5(3)
C(46)-C(45)-C(44)	125.4(4)	C(74)-C(73)-C(69)	108.6(3)
C(45)-C(46)-C(47)	119.1(3)	O(3)-C(76)-O(4)	122.9(4)
C(46)-C(47)-C(48)	118.8(3)	O(3)-C(76)-C(77)	123.3(4)
C(49)-C(48)-C(47)	119.6(4)	O(4)-C(76)-C(77)	113.8(4)
C(48)-C(49)-N(5)	121.0(3)	O(3)-C(76)-Fe(2)	61.5(2)
C(48)-C(49)-C(50)	126.5(3)	O(4)-C(76)-Fe(2)	61.4(2)
N(5)-C(49)-C(50)	112.5(3)	C(77)-C(76)-Fe(2)	175.1(3)
N(6)-C(50)-C(49)	114.5(3)	C(78)-C(77)-C(76)	113.1(4)
N(6)-C(50)-C(51)	125.6(3)	C(77)-C(78)-C(79)	111.4(4)
C(49)-C(50)-C(51)	119.9(3)	C(84)-C(79)-C(80)	119.7(4)
C(57)-C(52)-C(53)	123.4(4)	C(84)-C(79)-C(78)	119.4(4)

Table C.24. (continued)

C(80)-C(79)-C(78)	120.9(5)	C(81)-C(82)-C(83)	124.9(5)
C(79)-C(80)-C(81)	121.5(5)	C(82)-C(83)-C(84)	115.3(5)
C(82)-C(81)-C(80)	117.1(5)	C(79)-C(84)-C(83)	121.6(5)

Table C.25. Crystal data and structure refinement for **1-(FBF_3)(Et_2O)**.

Identification code	rt25	
Empirical formula	C37 H53 B F4 Fe N3 O	
Formula weight	698.48	
Temperature	143(2) K	
Wavelength	0.71073 Å	
Crystal system	Triclinic	
Space group	P-1	
Unit cell dimensions	a = 10.846(3) Å	α= 82.929(9)°.
	b = 11.882(4) Å	β= 79.064(9)°.
	c = 19.482(6) Å	γ = 62.895(9)°.
Volume	2192.5(11) $Å^3$	
Z	2	
Density (calculated)	1.058 Mg/m^3	
Absorption coefficient	0.388 mm^{-1}	
F(000)	742	
Crystal size	0.40 x 0.20 x 0.05 mm^3	
Theta range for data collection	1.93 to 23.35°.	
Index ranges	-12<=h<=12, -13<=k<=13, -21<=l<=21	
Reflections collected	30510	
Independent reflections	6145 [R(int) = 0.0782]	
Completeness to theta = 23.35°	96.5 %	
Absorption correction	Semi-empirical from equivalents	
Max. and min. transmission	0.9809 and 0.8603	
Refinement method	Full-matrix least-squares on F^2	
Data / restraints / parameters	6145 / 0 / 428	
Goodness-of-fit on F^2	0.987	
Final R indices [I>2sigma(I)]	R1 = 0.0589, wR2 = 0.1467	
R indices (all data)	R1 = 0.0884, wR2 = 0.1575	
Extinction coefficient	0.0073(7)	
Largest diff. peak and hole	0.700 and -0.408 $e.Å^{-3}$	

Table C.26. Atomic coordinates (x 10^4) and equivalent isotropic displacement parameters ($Å^2$x 10^3) for **1-(FBF_3)(Et_2O)**. U(eq) is defined as one third of the trace of the orthogonalized U^{ij} tensor.

	x	y	z	U(eq)
Fe(1)	7801(1)	887(1)	2171(1)	27(1)
F(1)	9638(1)	981(1)	2266(1)	35(1)
F(2)	11292(2)	1236(2)	1435(1)	50(1)
F(4)	11918(2)	120(2)	2439(1)	63(1)
F(3)	11331(2)	-693(2)	1635(1)	51(1)
O(1)	6808(2)	1988(2)	3057(1)	34(1)
N(1)	6982(2)	2249(2)	1321(1)	25(1)
N(2)	8284(2)	-149(2)	1353(1)	26(1)
N(3)	8328(2)	-1005(2)	2629(1)	30(1)
B(1)	11121(3)	366(4)	1925(2)	40(1)
C(1)	7095(3)	2528(3)	30(2)	41(1)
C(2)	7376(2)	1775(2)	698(1)	27(1)
C(3)	8116(2)	401(2)	699(1)	27(1)
C(4)	8538(2)	-313(2)	117(1)	32(1)
C(5)	9155(3)	-1624(3)	203(2)	38(1)
C(6)	9299(2)	-2187(2)	864(1)	34(1)
C(7)	8860(2)	-1452(2)	1440(1)	30(1)
C(8)	8826(2)	-1893(2)	2160(1)	30(1)
C(9)	9244(3)	-3261(2)	2350(2)	47(1)
C(10)	6109(2)	3596(2)	1366(1)	28(1)
C(11)	6697(2)	4388(2)	1440(1)	30(1)
C(12)	5799(3)	5681(2)	1546(1)	38(1)
C(13)	4372(3)	6162(3)	1579(2)	43(1)
C(14)	3828(3)	5343(3)	1482(2)	45(1)
C(15)	4641(2)	4073(2)	1374(1)	33(1)
C(16)	8261(2)	3910(2)	1417(2)	35(1)
C(17)	8611(3)	3978(3)	2131(2)	41(1)
C(18)	8859(3)	4608(3)	853(2)	45(1)
C(19)	3986(3)	3257(3)	1247(2)	45(1)
C(20)	2978(3)	3118(3)	1884(2)	64(1)
C(21)	3198(3)	3766(3)	612(2)	60(1)
C(22)	8081(2)	-1363(2)	3362(1)	30(1)
C(23)	9058(3)	-1583(3)	3802(2)	35(1)
C(24)	8730(3)	-1864(3)	4509(2)	44(1)
C(25)	7464(3)	-1870(3)	4777(2)	50(1)
C(26)	6510(3)	-1639(3)	4340(2)	51(1)
C(27)	6796(3)	-1395(3)	3619(2)	40(1)
C(28)	10446(3)	-1558(3)	3523(2)	40(1)
C(29)	11591(3)	-2854(3)	3297(2)	72(1)
C(30)	10960(3)	-1059(3)	4036(2)	57(1)
C(31)	5745(3)	-1194(3)	3153(2)	48(1)
C(32)	5316(3)	-2272(4)	3219(2)	83(1)
C(33)	4478(4)	39(4)	3283(2)	93(1)
C(34)	7535(3)	1809(3)	3652(1)	41(1)
C(35)	6803(3)	1537(3)	4336(2)	57(1)
C(36)	5369(3)	2950(3)	3138(2)	54(1)

Table C.26. (continued)

C(37)	5188(4)	4206(3)	3281(2)	79(2)

Table C.27. Bond lengths [Å] for **1-(FBF_3)(Et_2O)**.

Fe(1)-N(2)	1.977(2)	C(10)-C(15)	1.423(3)
Fe(1)-F(1)	2.0890(16)	C(11)-C(12)	1.411(3)
Fe(1)-O(1)	2.1027(18)	C(11)-C(16)	1.517(3)
Fe(1)-N(3)	2.169(2)	C(12)-C(13)	1.376(4)
Fe(1)-N(1)	2.177(2)	C(13)-C(14)	1.393(5)
F(1)-B(1)	1.484(3)	C(14)-C(15)	1.376(4)
F(2)-B(1)	1.371(4)	C(15)-C(19)	1.503(5)
F(4)-B(1)	1.364(4)	C(16)-C(18)	1.520(4)
F(3)-B(1)	1.350(4)	C(16)-C(17)	1.529(4)
O(1)-C(36)	1.446(3)	C(19)-C(20)	1.537(4)
O(1)-C(34)	1.465(3)	C(19)-C(21)	1.540(4)
N(1)-C(2)	1.312(3)	C(22)-C(23)	1.402(4)
N(1)-C(10)	1.445(3)	C(22)-C(27)	1.404(4)
N(2)-C(3)	1.362(3)	C(23)-C(24)	1.394(4)
N(2)-C(7)	1.383(3)	C(23)-C(28)	1.513(4)
N(3)-C(8)	1.330(3)	C(24)-C(25)	1.376(4)
N(3)-C(22)	1.449(3)	C(25)-C(26)	1.374(4)
C(1)-C(2)	1.484(4)	C(26)-C(27)	1.404(4)
C(2)-C(3)	1.454(3)	C(27)-C(31)	1.507(4)
C(3)-C(4)	1.378(4)	C(28)-C(30)	1.522(5)
C(4)-C(5)	1.389(4)	C(28)-C(29)	1.525(4)
C(5)-C(6)	1.378(4)	C(31)-C(33)	1.490(4)
C(6)-C(7)	1.381(4)	C(31)-C(32)	1.534(5)
C(7)-C(8)	1.437(4)	C(34)-C(35)	1.495(4)
C(8)-C(9)	1.493(4)	C(36)-C(37)	1.470(5)
C(10)-C(11)	1.389(4)		

Table C.28. Angles [°] for **1-(FBF_3)(Et_2O)**.

N(2)-Fe(1)-F(1)	105.62(7)	N(3)-C(8)-C(7)	115.9(2)
N(2)-Fe(1)-O(1)	165.93(8)	N(3)-C(8)-C(9)	123.6(2)
F(1)-Fe(1)-O(1)	88.43(7)	C(7)-C(8)-C(9)	120.4(2)
N(2)-Fe(1)-N(3)	76.42(9)	C(11)-C(10)-C(15)	121.3(2)
F(1)-Fe(1)-N(3)	98.13(7)	C(11)-C(10)-N(1)	119.8(2)
O(1)-Fe(1)-N(3)	101.37(8)	C(15)-C(10)-N(1)	118.9(2)
N(2)-Fe(1)-N(1)	75.13(8)	C(10)-C(11)-C(12)	118.5(2)
F(1)-Fe(1)-N(1)	104.18(7)	C(10)-C(11)-C(16)	122.4(2)
O(1)-Fe(1)-N(1)	102.43(7)	C(12)-C(11)-C(16)	119.1(3)
N(3)-Fe(1)-N(1)	147.59(9)	C(13)-C(12)-C(11)	121.6(3)
B(1)-F(1)-Fe(1)	135.18(18)	C(12)-C(13)-C(14)	118.1(3)
C(36)-O(1)-C(34)	114.8(2)	C(15)-C(14)-C(13)	123.4(3)
C(36)-O(1)-Fe(1)	123.60(17)	C(14)-C(15)-C(10)	117.1(3)
C(34)-O(1)-Fe(1)	121.57(13)	C(14)-C(15)-C(19)	120.3(2)
C(2)-N(1)-C(10)	117.6(2)	C(10)-C(15)-C(19)	122.5(2)
C(2)-N(1)-Fe(1)	114.92(15)	C(11)-C(16)-C(18)	112.0(2)
C(10)-N(1)-Fe(1)	127.46(16)	C(11)-C(16)-C(17)	111.4(2)
C(3)-N(2)-C(7)	119.5(2)	C(18)-C(16)-C(17)	110.8(2)
C(3)-N(2)-Fe(1)	120.89(17)	C(15)-C(19)-C(20)	113.1(3)
C(7)-N(2)-Fe(1)	119.58(17)	C(15)-C(19)-C(21)	111.4(3)
C(8)-N(3)-C(22)	118.5(2)	C(20)-C(19)-C(21)	108.9(2)
C(8)-N(3)-Fe(1)	113.84(17)	C(23)-C(22)-C(27)	121.8(3)
C(22)-N(3)-Fe(1)	127.40(16)	C(23)-C(22)-N(3)	120.5(2)
F(3)-B(1)-F(4)	112.7(3)	C(27)-C(22)-N(3)	117.6(2)
F(3)-B(1)-F(2)	112.3(3)	C(24)-C(23)-C(22)	117.8(3)
F(4)-B(1)-F(2)	111.2(3)	C(24)-C(23)-C(28)	120.5(3)
F(3)-B(1)-F(1)	107.9(3)	C(22)-C(23)-C(28)	121.6(2)
F(4)-B(1)-F(1)	106.3(2)	C(25)-C(24)-C(23)	121.5(3)
F(2)-B(1)-F(1)	106.0(2)	C(26)-C(25)-C(24)	120.0(3)
N(1)-C(2)-C(3)	114.6(2)	C(25)-C(26)-C(27)	121.3(3)
N(1)-C(2)-C(1)	125.0(2)	C(26)-C(27)-C(22)	117.5(3)
C(3)-C(2)-C(1)	120.3(2)	C(26)-C(27)-C(31)	119.7(3)
N(2)-C(3)-C(4)	121.6(2)	C(22)-C(27)-C(31)	122.8(3)
N(2)-C(3)-C(2)	113.1(2)	C(23)-C(28)-C(30)	113.6(2)
C(4)-C(3)-C(2)	125.2(2)	C(23)-C(28)-C(29)	112.1(3)
C(3)-C(4)-C(5)	118.9(3)	C(30)-C(28)-C(29)	108.8(2)
C(6)-C(5)-C(4)	119.9(3)	C(33)-C(31)-C(27)	111.0(3)
C(5)-C(6)-C(7)	120.2(2)	C(33)-C(31)-C(32)	110.1(3)
C(6)-C(7)-N(2)	119.9(2)	C(27)-C(31)-C(32)	113.5(3)
C(6)-C(7)-C(8)	126.4(2)	O(1)-C(34)-C(35)	114.0(3)
N(2)-C(7)-C(8)	113.4(2)	O(1)-C(36)-C(37)	114.3(3)

Table C.29. Crystal data and structure refinement for **1-CC^{t}Bu**.

Identification code	rt38	
Empirical formula	C39 H52 Fe N3	
Formula weight	618.69	
Temperature	173(2) K	
Wavelength	0.71073 Å	
Crystal system	Monoclinic	
Space group	P2(1)/n	
Unit cell dimensions	a = 13.5303(6) Å	α= 90°.
	b = 14.9138(6) Å	β= 98.110(2)°.
	c = 18.0729(9) Å	γ = 90°.
Volume	3610.4(3) Å^3	
Z	4	
Density (calculated)	1.138 Mg/m^3	
Absorption coefficient	0.446 mm^{-1}	
F(000)	1332	
Crystal size	0.40 x 0.25 x 0.20 mm^3	
Theta range for data collection	1.77 to 24.74°.	
Index ranges	-15<=h<=15, -17<=k<=13, -21<=l<=21	
Reflections collected	24143	
Independent reflections	6150 [R(int) = 0.0473]	
Completeness to theta = 24.74°	99.5 %	
Absorption correction	Semi-empirical from equivalents	
Max. and min. transmission	0.9160 and 0.8416	
Refinement method	Full-matrix least-squares on F^2	
Data / restraints / parameters	6150 / 108 / 435	
Goodness-of-fit on F^2	1.083	
Final R indices [I>2sigma(I)]	R1 = 0.0673, wR2 = 0.1713	
R indices (all data)	R1 = 0.0997, wR2 = 0.1925	
Largest diff. peak and hole	1.625 and -0.755 e.Å^{-3}	

Table C.30. Atomic coordinates (x 10^4) and equivalent isotropic displacement parameters ($Å^2$x 10^3) for **1-CC^{t}Bu**. U(eq) is defined as one third of the trace of the orthogonalized U^{ij} tensor.

	x	y	z	U(eq)
Fe(1)	495(1)	890(1)	1913(1)	30(1)
N(1)	1664(2)	1395(2)	1582(1)	32(1)
N(2)	705(2)	70(2)	1179(1)	27(1)
N(3)	-591(2)	55(2)	1996(1)	32(1)
C(1)	2959(3)	1262(3)	737(2)	45(1)
C(2)	2052(2)	980(2)	1059(2)	31(1)
C(3)	1510(2)	173(2)	803(2)	30(1)
C(4)	1692(2)	-450(2)	268(2)	35(1)
C(5)	1057(3)	-1166(2)	111(2)	34(1)
C(6)	229(2)	-1257(2)	493(2)	33(1)
C(7)	72(2)	-647(2)	1028(2)	29(1)
C(8)	-673(2)	-627(2)	1522(2)	32(1)
C(9)	-1460(3)	-1338(3)	1493(2)	48(1)
C(10)	2081(2)	2253(2)	1860(2)	33(1)
C(11)	2787(2)	2273(2)	2503(2)	35(1)
C(12)	3106(3)	3105(2)	2790(2)	44(1)
C(13)	2733(3)	3880(2)	2455(2)	42(1)
C(14)	2030(3)	3853(2)	1834(2)	44(1)
C(15)	1685(3)	3045(2)	1524(2)	41(1)
C(16)	3200(3)	1418(3)	2898(2)	45(1)
C(17)	4320(3)	1314(4)	2871(3)	79(2)
C(18)	3004(4)	1409(3)	3709(2)	66(1)
C(19)	872(3)	3046(3)	853(2)	58(1)
C(20)	-74(3)	3450(4)	1026(3)	92(2)
C(21)	1213(5)	3478(3)	181(2)	85(2)
C(22)	-1250(2)	101(2)	2558(2)	38(1)
C(23)	-934(3)	-286(3)	3255(2)	47(1)
C(24)	-1581(3)	-248(3)	3787(2)	66(1)
C(25)	-2491(3)	182(4)	3638(3)	74(2)
C(26)	-2764(3)	606(4)	2961(2)	69(1)
C(27)	-2148(3)	581(3)	2401(2)	53(1)
C(28)	71(3)	-741(3)	3436(2)	49(1)
C(29)	687(3)	-333(4)	4117(3)	73(1)
C(30)	0(4)	-1741(3)	3505(3)	83(2)
C(31)	-2442(3)	1047(3)	1666(2)	59(1)
C(32)	-3464(4)	818(4)	1286(3)	85(2)
C(33)	-2359(4)	2063(4)	1776(3)	96(2)
C(34)	314(3)	1703(2)	2693(2)	44(1)
C(35)	226(3)	2237(3)	3184(2)	49(1)
C(36)	114(7)	2824(6)	3772(6)	52(2)
C(37)	496(11)	2434(8)	4532(6)	118(4)
C(38)	-1001(6)	3059(7)	3794(7)	101(3)
C(39)	645(8)	3737(6)	3724(6)	86(3)
C(36')	47(14)	2959(13)	3761(10)	92(4)
C(38')	-825(10)	2549(11)	4138(8)	116(4)
C(37')	1041(11)	2897(12)	4336(8)	140(5)

Table C.30. (continued)

C(39')	-97(17)	3816(10)	3351(11)	157(6)

Table C.31. Bond lengths [Å] for **1-CC^{t}Bu**.

Fe(1)-N(2)	1.855(2)	C(16)-C(18)	1.526(6)
Fe(1)-C(34)	1.902(4)	C(16)-C(17)	1.531(5)
Fe(1)-N(1)	1.921(3)	C(19)-C(20)	1.487(7)
Fe(1)-N(3)	1.948(3)	C(19)-C(21)	1.503(6)
N(1)-C(2)	1.301(4)	C(22)-C(23)	1.396(5)
N(1)-C(10)	1.459(4)	C(22)-C(27)	1.405(5)
N(2)-C(3)	1.371(4)	C(23)-C(24)	1.390(5)
N(2)-C(7)	1.374(4)	C(23)-C(28)	1.513(5)
N(3)-C(8)	1.325(4)	C(24)-C(25)	1.380(6)
N(3)-C(22)	1.445(4)	C(25)-C(26)	1.381(6)
C(1)-C(2)	1.492(5)	C(26)-C(27)	1.400(6)
C(2)-C(3)	1.451(4)	C(27)-C(31)	1.501(6)
C(3)-C(4)	1.388(4)	C(28)-C(30)	1.500(6)
C(4)-C(5)	1.374(5)	C(28)-C(29)	1.514(6)
C(5)-C(6)	1.404(5)	C(31)-C(32)	1.495(6)
C(6)-C(7)	1.366(4)	C(31)-C(33)	1.530(7)
C(7)-C(8)	1.437(5)	C(34)-C(35)	1.211(5)
C(8)-C(9)	1.499(5)	C(35)-C(36)	1.400(11)
C(10)-C(11)	1.397(4)	C(35)-C(36')	1.541(16)
C(10)-C(15)	1.399(5)	C(36)-C(37)	1.514(14)
C(11)-C(12)	1.390(5)	C(36)-C(39)	1.549(13)
C(11)-C(16)	1.528(5)	C(36)-C(38)	1.555(13)
C(12)-C(13)	1.367(5)	C(36')-C(39')	1.48(3)
C(13)-C(14)	1.366(5)	C(36')-C(38')	1.57(2)
C(14)-C(15)	1.382(5)	C(36')-C(37')	1.58(2)
C(15)-C(19)	1.519(5)		

Table C.32. Angles [°] for **1-CC^{t}Bu**.

N(2)-Fe(1)-C(34)	177.77(14)	C(10)-C(15)-C(19)	122.5(3)
N(2)-Fe(1)-N(1)	79.68(11)	C(18)-C(16)-C(11)	110.7(3)
C(34)-Fe(1)-N(1)	100.26(13)	C(18)-C(16)-C(17)	109.7(3)
N(2)-Fe(1)-N(3)	80.05(11)	C(11)-C(16)-C(17)	111.6(3)
C(34)-Fe(1)-N(3)	99.92(13)	C(20)-C(19)-C(21)	111.5(4)
N(1)-Fe(1)-N(3)	159.68(11)	C(20)-C(19)-C(15)	112.4(4)
C(2)-N(1)-C(10)	119.5(3)	C(21)-C(19)-C(15)	112.1(4)
C(2)-N(1)-Fe(1)	118.2(2)	C(23)-C(22)-C(27)	122.7(3)
C(10)-N(1)-Fe(1)	122.2(2)	C(23)-C(22)-N(3)	118.2(3)
C(3)-N(2)-C(7)	120.4(3)	C(27)-C(22)-N(3)	119.0(3)
C(3)-N(2)-Fe(1)	119.5(2)	C(24)-C(23)-C(22)	117.6(4)
C(7)-N(2)-Fe(1)	120.1(2)	C(24)-C(23)-C(28)	120.2(4)
C(8)-N(3)-C(22)	119.2(3)	C(22)-C(23)-C(28)	122.2(3)
C(8)-N(3)-Fe(1)	115.8(2)	C(25)-C(24)-C(23)	121.1(4)
C(22)-N(3)-Fe(1)	124.8(2)	C(24)-C(25)-C(26)	120.4(4)
N(1)-C(2)-C(3)	112.9(3)	C(25)-C(26)-C(27)	121.1(4)
N(1)-C(2)-C(1)	126.0(3)	C(26)-C(27)-C(22)	117.0(4)
C(3)-C(2)-C(1)	121.0(3)	C(26)-C(27)-C(31)	121.2(4)
N(2)-C(3)-C(4)	120.1(3)	C(22)-C(27)-C(31)	121.9(3)
N(2)-C(3)-C(2)	109.6(3)	C(30)-C(28)-C(23)	113.4(4)
C(4)-C(3)-C(2)	130.3(3)	C(30)-C(28)-C(29)	111.4(4)
C(5)-C(4)-C(3)	119.8(3)	C(23)-C(28)-C(29)	111.8(3)
C(4)-C(5)-C(6)	119.5(3)	C(32)-C(31)-C(27)	114.4(4)
C(7)-C(6)-C(5)	119.9(3)	C(32)-C(31)-C(33)	109.4(4)
C(6)-C(7)-N(2)	120.2(3)	C(27)-C(31)-C(33)	109.7(4)
C(6)-C(7)-C(8)	130.3(3)	C(35)-C(34)-Fe(1)	177.7(3)
N(2)-C(7)-C(8)	109.4(3)	C(34)-C(35)-C(36)	177.4(6)
N(3)-C(8)-C(7)	114.6(3)	C(34)-C(35)-C(36')	175.1(8)
N(3)-C(8)-C(9)	124.1(3)	C(36)-C(35)-C(36')	6.6(10)
C(7)-C(8)-C(9)	121.3(3)	C(35)-C(36)-C(37)	112.9(8)
C(11)-C(10)-C(15)	121.2(3)	C(35)-C(36)-C(39)	114.0(8)
C(11)-C(10)-N(1)	119.4(3)	C(37)-C(36)-C(39)	106.6(9)
C(15)-C(10)-N(1)	119.0(3)	C(35)-C(36)-C(38)	111.8(7)
C(12)-C(11)-C(10)	118.0(3)	C(37)-C(36)-C(38)	105.8(9)
C(12)-C(11)-C(16)	119.8(3)	C(39)-C(36)-C(38)	105.2(8)
C(10)-C(11)-C(16)	122.2(3)	C(39')-C(36')-C(35)	106.7(13)
C(13)-C(12)-C(11)	120.8(3)	C(39')-C(36')-C(38')	120.1(16)
C(14)-C(13)-C(12)	120.7(3)	C(35)-C(36')-C(38')	102.8(12)
C(13)-C(14)-C(15)	120.9(3)	C(39')-C(36')-C(37')	114.8(17)
C(14)-C(15)-C(10)	118.3(3)	C(35)-C(36')-C(37')	101.8(12)
C(14)-C(15)-C(19)	119.1(3)	C(38')-C(36')-C(37')	108.3(14)

Table C.33. Crystal data and structure refinement for **1-Tpy**.

Identification code	rt40	
Empirical formula	C48 H54 Fe N6	
Formula weight	770.82	
Temperature	173(2) K	
Wavelength	0.71073 Å	
Crystal system	Monoclinic	
Space group	P2(1)/c	
Unit cell dimensions	a = 12.1322(15) Å	α= 90°.
	b = 25.354(3) Å	β= 122.078(6)°.
	c = 16.1051(15) Å	γ = 90°.
Volume	4197.6(8) $Å^3$	
Z	4	
Density (calculated)	1.220 Mg/m^3	
Absorption coefficient	0.400 mm^{-1}	
F(000)	1640	
Crystal size	0.40 x 0.25 x 0.15 mm^3	
Theta range for data collection	1.91 to 25.35°.	
Index ranges	-14<=h<=14, -30<=k<=30, -18<=l<=19	
Reflections collected	28643	
Independent reflections	7690 [R(int) = 0.0942]	
Completeness to theta = 25.35°	100.0 %	
Absorption correction	Semi-empirical from equivalents	
Max. and min. transmission	0.9425 and 0.8565	
Refinement method	Full-matrix least-squares on F^2	
Data / restraints / parameters	7690 / 0 / 602	
Goodness-of-fit on F^2	1.007	
Final R indices [I>2sigma(I)]	R1 = 0.0544, wR2 = 0.1019	
R indices (all data)	R1 = 0.1126, wR2 = 0.1222	
Largest diff. peak and hole	0.545 and -0.395 $e.Å^{-3}$	

Table C.34. Atomic coordinates (x 10^4) and equivalent isotropic displacement parameters ($Å^2$x 10^3) for **1-Tpy**. U(eq) is defined as one third of the trace of the orthogonalized U^{ij} tensor.

	x	y	z	U(eq)
Fe(1)	7281(1)	1377(1)	3508(1)	26(1)
N(1)	6198(2)	884(1)	2079(1)	24(1)
N(2)	8637(2)	1163(1)	3232(1)	24(1)
N(3)	9212(2)	1673(1)	4832(1)	27(1)
N(4)	6697(2)	2127(1)	2786(1)	30(1)
N(5)	5864(2)	1632(1)	3715(1)	28(1)
N(6)	7080(2)	763(1)	4288(1)	28(1)
C(1)	6570(2)	372(1)	927(2)	38(1)
C(2)	6974(2)	717(1)	1812(2)	26(1)
C(3)	8329(2)	875(1)	2402(2)	24(1)
C(4)	9244(2)	765(1)	2171(2)	31(1)
C(5)	10517(2)	945(1)	2758(2)	35(1)
C(6)	10828(2)	1229(1)	3587(2)	31(1)
C(7)	9913(2)	1331(1)	3830(2)	25(1)
C(8)	10185(2)	1607(1)	4709(2)	28(1)
C(9)	11565(2)	1794(1)	5404(2)	41(1)
C(10)	4823(2)	748(1)	1483(2)	28(1)
C(11)	3967(2)	1112(1)	780(2)	34(1)
C(12)	2657(3)	983(1)	224(2)	45(1)
C(13)	2191(3)	515(1)	349(2)	52(1)
C(14)	3036(3)	163(1)	1044(2)	42(1)
C(15)	4372(2)	267(1)	1622(2)	33(1)
C(16)	4435(2)	1626(1)	605(2)	38(1)
C(17)	4701(3)	1586(1)	-210(2)	55(1)
C(18)	3501(3)	2085(1)	396(2)	45(1)
C(19)	5241(3)	-149(1)	2352(2)	39(1)
C(20)	4804(3)	-293(1)	3053(2)	53(1)
C(21)	5274(3)	-651(1)	1830(2)	48(1)
C(22)	9512(2)	1928(1)	5732(2)	29(1)
C(23)	9922(2)	1628(1)	6580(2)	32(1)
C(24)	10315(3)	1893(1)	7451(2)	45(1)
C(25)	10298(3)	2431(1)	7506(2)	43(1)
C(26)	9825(3)	2719(1)	6663(2)	42(1)
C(27)	9415(2)	2481(1)	5758(2)	33(1)
C(28)	9950(3)	1028(1)	6590(2)	45(1)
C(29)	11257(3)	808(1)	6860(3)	77(1)
C(30)	9549(3)	789(1)	7246(2)	62(1)
C(31)	8905(3)	2828(1)	4866(2)	40(1)
C(32)	9985(3)	3130(1)	4861(2)	68(1)
C(33)	7861(3)	3206(1)	4755(2)	58(1)
C(34)	7240(3)	2371(1)	2342(2)	41(1)
C(35)	6862(3)	2858(1)	1911(2)	54(1)
C(36)	5884(3)	3116(1)	1952(2)	58(1)
C(37)	5312(3)	2886(1)	2381(2)	48(1)
C(38)	5723(2)	2381(1)	2806(2)	34(1)
C(39)	5187(2)	2086(1)	3278(2)	35(1)

Table C.34. (continued)

C(40)	4098(3)	2222(1)	3296(2)	49(1)
C(41)	3696(3)	1900(1)	3785(3)	60(1)
C(42)	4390(3)	1448(1)	4248(2)	49(1)
C(43)	5465(2)	1320(1)	4199(2)	33(1)
C(44)	6242(2)	849(1)	4594(2)	31(1)
C(45)	6183(3)	494(1)	5240(2)	47(1)
C(46)	6946(3)	51(1)	5540(2)	56(1)
C(47)	7765(3)	-44(1)	5205(2)	49(1)
C(48)	7809(3)	317(1)	4586(2)	37(1)

Table C.35. Bond lengths [Å] for **1-Tpy**.

Fe(1)-N(2)	1.994(2)	C(14)-C(15)	1.401(3)
Fe(1)-N(5)	2.024(2)	C(15)-C(19)	1.514(3)
Fe(1)-N(6)	2.094(2)	C(16)-C(17)	1.512(4)
Fe(1)-N(4)	2.144(2)	C(16)-C(18)	1.531(4)
Fe(1)-N(3)	2.3007(18)	C(19)-C(20)	1.525(4)
Fe(1)-N(1)	2.3174(19)	C(19)-C(21)	1.539(4)
N(1)-C(2)	1.297(3)	C(22)-C(23)	1.403(4)
N(1)-C(10)	1.457(3)	C(22)-C(27)	1.410(4)
N(2)-C(3)	1.390(3)	C(23)-C(24)	1.392(4)
N(2)-C(7)	1.386(3)	C(23)-C(28)	1.522(4)
N(3)-C(8)	1.307(3)	C(24)-C(25)	1.368(4)
N(3)-C(22)	1.445(3)	C(25)-C(26)	1.370(4)
N(4)-C(34)	1.352(4)	C(26)-C(27)	1.401(4)
N(4)-C(38)	1.361(3)	C(27)-C(31)	1.509(4)
N(5)-C(43)	1.367(3)	C(28)-C(30)	1.506(5)
N(5)-C(39)	1.372(3)	C(28)-C(29)	1.511(4)
N(6)-C(48)	1.356(3)	C(31)-C(32)	1.523(4)
N(6)-C(44)	1.362(3)	C(31)-C(33)	1.521(4)
C(1)-C(2)	1.515(3)	C(34)-C(35)	1.371(4)
C(2)-C(3)	1.452(3)	C(35)-C(36)	1.387(5)
C(3)-C(4)	1.374(4)	C(36)-C(37)	1.346(5)
C(4)-C(5)	1.392(3)	C(37)-C(38)	1.411(4)
C(5)-C(6)	1.382(4)	C(38)-C(39)	1.443(4)
C(6)-C(7)	1.383(4)	C(39)-C(40)	1.381(4)
C(7)-C(8)	1.451(3)	C(40)-C(41)	1.391(5)
C(8)-C(9)	1.514(3)	C(41)-C(42)	1.383(4)
C(10)-C(11)	1.400(3)	C(42)-C(43)	1.385(4)
C(10)-C(15)	1.403(4)	C(43)-C(44)	1.443(4)
C(11)-C(12)	1.386(4)	C(44)-C(45)	1.406(4)
C(11)-C(16)	1.508(4)	C(45)-C(46)	1.368(4)
C(12)-C(13)	1.375(4)	C(46)-C(47)	1.382(5)
C(13)-C(14)	1.371(4)	C(47)-C(48)	1.374(4)

Table C.36. Angles [°] for **1-Tpy**.

N(2)-Fe(1)-N(5)	175.99(8)	N(3)-C(8)-C(7)	117.0(2)
N(2)-Fe(1)-N(6)	107.75(8)	N(3)-C(8)-C(9)	125.5(2)
N(5)-Fe(1)-N(6)	76.09(8)	C(7)-C(8)-C(9)	117.4(2)
N(2)-Fe(1)-N(4)	101.15(8)	C(11)-C(10)-C(15)	121.1(2)
N(5)-Fe(1)-N(4)	74.97(9)	C(11)-C(10)-N(1)	118.4(2)
N(6)-Fe(1)-N(4)	151.01(9)	C(15)-C(10)-N(1)	120.5(2)
N(2)-Fe(1)-N(3)	74.95(8)	C(12)-C(11)-C(10)	118.1(3)
N(5)-Fe(1)-N(3)	106.22(8)	C(12)-C(11)-C(16)	119.9(2)
N(6)-Fe(1)-N(3)	94.18(7)	C(10)-C(11)-C(16)	121.9(2)
N(4)-Fe(1)-N(3)	95.36(7)	C(13)-C(12)-C(11)	121.8(3)
N(2)-Fe(1)-N(1)	74.45(7)	C(14)-C(13)-C(12)	119.7(3)
N(5)-Fe(1)-N(1)	104.64(7)	C(13)-C(14)-C(15)	121.2(3)
N(6)-Fe(1)-N(1)	90.57(7)	C(14)-C(15)-C(10)	118.1(2)
N(4)-Fe(1)-N(1)	95.12(7)	C(14)-C(15)-C(19)	117.9(2)
N(3)-Fe(1)-N(1)	149.02(7)	C(10)-C(15)-C(19)	124.0(2)
C(2)-N(1)-C(10)	118.9(2)	C(11)-C(16)-C(17)	112.3(2)
C(2)-N(1)-Fe(1)	112.16(14)	C(11)-C(16)-C(18)	112.9(2)
C(10)-N(1)-Fe(1)	128.98(16)	C(17)-C(16)-C(18)	109.6(2)
C(3)-N(2)-C(7)	117.4(2)	C(15)-C(19)-C(20)	111.7(3)
C(3)-N(2)-Fe(1)	121.70(14)	C(15)-C(19)-C(21)	111.2(2)
C(7)-N(2)-Fe(1)	120.78(17)	C(20)-C(19)-C(21)	109.0(2)
C(8)-N(3)-C(22)	116.30(19)	C(23)-C(22)-C(27)	120.1(2)
C(8)-N(3)-Fe(1)	111.99(15)	C(23)-C(22)-N(3)	120.3(2)
C(22)-N(3)-Fe(1)	131.68(16)	C(27)-C(22)-N(3)	119.6(2)
C(34)-N(4)-C(38)	117.9(2)	C(24)-C(23)-C(22)	118.2(2)
C(34)-N(4)-Fe(1)	125.43(18)	C(24)-C(23)-C(28)	118.6(3)
C(38)-N(4)-Fe(1)	116.59(18)	C(22)-C(23)-C(28)	123.1(2)
C(43)-N(5)-C(39)	118.8(2)	C(25)-C(24)-C(23)	122.6(3)
C(43)-N(5)-Fe(1)	119.84(17)	C(24)-C(25)-C(26)	118.6(3)
C(39)-N(5)-Fe(1)	120.86(19)	C(25)-C(26)-C(27)	122.1(3)
C(48)-N(6)-C(44)	118.5(2)	C(26)-C(27)-C(22)	118.1(2)
C(48)-N(6)-Fe(1)	124.8(2)	C(26)-C(27)-C(31)	118.6(2)
C(44)-N(6)-Fe(1)	116.37(16)	C(22)-C(27)-C(31)	123.3(2)
N(1)-C(2)-C(3)	117.5(2)	C(30)-C(28)-C(29)	109.3(3)
N(1)-C(2)-C(1)	124.9(2)	C(30)-C(28)-C(23)	113.3(3)
C(3)-C(2)-C(1)	117.6(2)	C(29)-C(28)-C(23)	112.7(3)
C(4)-C(3)-N(2)	121.7(2)	C(27)-C(31)-C(32)	112.3(2)
C(4)-C(3)-C(2)	124.3(2)	C(27)-C(31)-C(33)	112.0(3)
N(2)-C(3)-C(2)	114.0(2)	C(32)-C(31)-C(33)	110.3(2)
C(3)-C(4)-C(5)	120.9(2)	N(4)-C(34)-C(35)	123.7(3)
C(6)-C(5)-C(4)	117.6(3)	C(34)-C(35)-C(36)	117.8(3)
C(5)-C(6)-C(7)	121.5(2)	C(37)-C(36)-C(35)	120.4(3)
C(6)-C(7)-N(2)	121.0(2)	C(36)-C(37)-C(38)	119.8(3)
C(6)-C(7)-C(8)	124.4(2)	N(4)-C(38)-C(37)	120.3(3)
N(2)-C(7)-C(8)	114.6(2)	N(4)-C(38)-C(39)	114.0(2)

Table C.36. (continued)

C(37)-C(38)-C(39)	125.6(3)	C(42)-C(43)-C(44)	125.6(3)
N(5)-C(39)-C(40)	121.1(3)	N(6)-C(44)-C(45)	120.3(3)
N(5)-C(39)-C(38)	113.0(2)	N(6)-C(44)-C(43)	114.3(2)
C(40)-C(39)-C(38)	125.9(3)	C(45)-C(44)-C(43)	125.3(3)
C(39)-C(40)-C(41)	119.5(3)	C(46)-C(45)-C(44)	119.8(3)
C(40)-C(41)-C(42)	119.8(3)	C(45)-C(46)-C(47)	119.7(3)
C(41)-C(42)-C(43)	119.0(3)	C(48)-C(47)-C(46)	118.7(3)
N(5)-C(43)-C(42)	121.8(3)	N(6)-C(48)-C(47)	122.8(3)
N(5)-C(43)-C(44)	112.6(2)		

Table C.37. Crystal data and structure refinement for **1-CCPh**.

Identification code	rt41	
Empirical formula	C41 H48 Fe N3	
Formula weight	638.67	
Temperature	173(2) K	
Wavelength	0.71073 Å	
Crystal system	Monoclinic	
Space group	P2(1)/n	
Unit cell dimensions	a = 12.3966(6) Å	α= 90°.
	b = 17.6656(8) Å	β= 96.720(2)°.
	c = 16.4638(8) Å	γ = 90°.
Volume	3580.7(3) $Å^3$	
Z	4	
Density (calculated)	1.185 Mg/m^3	
Absorption coefficient	0.452 mm^{-1}	
F(000)	1364	
Crystal size	0.60 x 0.40 x 0.04 mm^3	
Theta range for data collection	1.95 to 25.35°.	
Index ranges	-13<=h<=14, -21<=k<=17, -19<=l<=17	
Reflections collected	28797	
Independent reflections	6537 [R(int) = 0.0412]	
Completeness to theta = 25.35°	100.0 %	
Absorption correction	Semi-empirical from equivalents	
Max. and min. transmission	0.9821 and 0.7730	
Refinement method	Full-matrix least-squares on F^2	
Data / restraints / parameters	6537 / 9 / 442	
Goodness-of-fit on F^2	1.033	
Final R indices [I>2sigma(I)]	R1 = 0.0444, wR2 = 0.0990	
R indices (all data)	R1 = 0.0713, wR2 = 0.1095	
Largest diff. peak and hole	0.277 and -0.302 $e.Å^{-3}$	

Table C.38. Atomic coordinates (x 10^4) and equivalent isotropic displacement parameters ($Å^2$x 10^3) for **1-CCPh**. U(eq) is defined as one third of the trace of the orthogonalized U^{ij} tensor.

	x	y	z	U(eq)
Fe(1)	9031(1)	3621(1)	1386(1)	38(1)
N(1)	9689(1)	3020(1)	589(1)	41(1)
N(2)	8778(1)	4252(1)	495(1)	37(1)
N(3)	8271(1)	4433(1)	1865(1)	35(1)
C(1)	10143(2)	2960(1)	-848(1)	63(1)
C(2)	9679(2)	3329(1)	-145(1)	46(1)
C(3)	9153(2)	4049(1)	-225(1)	44(1)
C(4)	8967(2)	4519(1)	-901(1)	53(1)
C(5)	8405(2)	5187(1)	-843(1)	57(1)
C(6)	8028(2)	5394(1)	-113(1)	47(1)
C(7)	8229(2)	4919(1)	561(1)	39(1)
C(8)	7943(1)	5008(1)	1375(1)	36(1)
C(9)	7345(2)	5681(1)	1636(1)	49(1)
C(10)	10058(2)	2246(1)	717(1)	44(1)
C(11)	11123(2)	2091(1)	1033(1)	54(1)
C(12)	11419(2)	1338(1)	1149(2)	62(1)
C(13)	10689(2)	761(1)	974(1)	65(1)
C(14)	9642(2)	930(1)	685(1)	63(1)
C(15)	9297(2)	1672(1)	551(1)	52(1)
C(16)	11945(2)	2715(1)	1248(2)	69(1)
C(17)	12363(2)	2710(2)	2155(2)	96(1)
C(18)	12883(2)	2672(2)	731(2)	79(1)
C(19)	8054(5)	1914(4)	287(4)	54(2)
C(20)	7277(6)	1505(4)	783(4)	79(2)
C(21)	7757(6)	1799(5)	-621(4)	104(3)
C(19')	8182(6)	1789(4)	239(4)	71(2)
C(20')	7475(6)	1639(5)	917(5)	115(3)
C(21')	7783(5)	1362(3)	-536(3)	84(2)
C(22)	8112(2)	4452(1)	2718(1)	37(1)
C(23)	7178(2)	4133(1)	2971(1)	46(1)
C(24)	7106(2)	4097(1)	3810(1)	55(1)
C(25)	7921(2)	4359(1)	4363(1)	62(1)
C(26)	8825(2)	4676(1)	4097(1)	67(1)
C(27)	8948(2)	4735(1)	3272(1)	48(1)
C(28)	6259(2)	3826(1)	2365(1)	65(1)
C(29)	5155(2)	4150(2)	2500(2)	108(1)
C(30)	6240(2)	2970(1)	2403(2)	92(1)
C(31)	9952(2)	5084(2)	2988(1)	64(1)
C(32)	10081(2)	5912(2)	3220(2)	80(1)
C(33)	10967(2)	4652(2)	3301(2)	90(1)
C(34)	9362(2)	2974(1)	2315(1)	45(1)
C(35)	9634(2)	2557(1)	2892(1)	44(1)
C(36)	10007(2)	2049(1)	3546(1)	46(1)
C(37)	9951(2)	2240(2)	4354(1)	71(1)
C(38)	10343(2)	1749(2)	4977(2)	92(1)
C(39)	10766(2)	1069(2)	4802(2)	93(1)

Table C.38. (continued)

C(40)	10835(2)	874(2)	4006(2)	89(1)
C(41)	10460(2)	1357(1)	3382(2)	63(1)

Table C.39. Bond lengths [Å] for **1-CCPh**.

Fe(1)-N(2)	1.8401(14)	C(15)-C(19)	1.610(6)
Fe(1)-C(34)	1.915(2)	C(16)-C(17)	1.522(4)
Fe(1)-N(3)	1.9329(15)	C(16)-C(18)	1.522(3)
Fe(1)-N(1)	1.9407(15)	C(19)-C(21)	1.512(8)
N(1)-C(2)	1.325(2)	C(19)-C(20)	1.516(8)
N(1)-C(10)	1.449(2)	C(19')-C(21')	1.515(7)
N(2)-C(7)	1.370(2)	C(19')-C(20')	1.521(8)
N(2)-C(3)	1.370(2)	C(22)-C(27)	1.391(3)
N(3)-C(8)	1.330(2)	C(22)-C(23)	1.395(3)
N(3)-C(22)	1.441(2)	C(23)-C(24)	1.395(3)
C(1)-C(2)	1.499(3)	C(23)-C(28)	1.524(3)
C(2)-C(3)	1.429(3)	C(24)-C(25)	1.360(3)
C(3)-C(4)	1.385(3)	C(25)-C(26)	1.370(3)
C(4)-C(5)	1.381(3)	C(26)-C(27)	1.388(3)
C(5)-C(6)	1.389(3)	C(27)-C(31)	1.511(3)
C(6)-C(7)	1.390(3)	C(28)-C(30)	1.514(3)
C(7)-C(8)	1.436(3)	C(28)-C(29)	1.524(4)
C(8)-C(9)	1.491(3)	C(31)-C(33)	1.510(3)
C(10)-C(11)	1.388(3)	C(31)-C(32)	1.516(3)
C(10)-C(15)	1.391(3)	C(34)-C(35)	1.218(3)
C(11)-C(12)	1.387(3)	C(35)-C(36)	1.436(3)
C(11)-C(16)	1.514(3)	C(36)-C(37)	1.381(3)
C(12)-C(13)	1.371(3)	C(36)-C(41)	1.384(3)
C(13)-C(14)	1.362(3)	C(37)-C(38)	1.387(3)
C(14)-C(15)	1.388(3)	C(38)-C(39)	1.356(4)
C(15)-C(19')	1.433(7)	C(39)-C(40)	1.366(4)

Table C.40. Angles [°] for **1-CCPh**.

N(2)-Fe(1)-C(34)	177.43(8)	C(10)-C(15)-C(19')	124.6(3)
N(2)-Fe(1)-N(3)	80.23(6)	C(14)-C(15)-C(19)	124.1(3)
C(34)-Fe(1)-N(3)	100.76(7)	C(10)-C(15)-C(19)	117.7(3)
N(2)-Fe(1)-N(1)	80.66(7)	C(19')-C(15)-C(19)	8.6(4)
C(34)-Fe(1)-N(1)	98.36(7)	C(11)-C(16)-C(17)	111.6(2)
N(3)-Fe(1)-N(1)	160.88(6)	C(11)-C(16)-C(18)	111.7(2)
C(2)-N(1)-C(10)	119.30(16)	C(17)-C(16)-C(18)	110.7(2)
C(2)-N(1)-Fe(1)	115.61(13)	C(21)-C(19)-C(20)	111.8(5)
C(10)-N(1)-Fe(1)	124.67(12)	C(21)-C(19)-C(15)	110.2(5)
C(7)-N(2)-C(3)	120.95(16)	C(20)-C(19)-C(15)	112.1(5)
C(7)-N(2)-Fe(1)	119.81(12)	C(15)-C(19')-C(21')	115.8(5)
C(3)-N(2)-Fe(1)	119.24(13)	C(15)-C(19')-C(20')	109.0(5)
C(8)-N(3)-C(22)	120.37(15)	C(21')-C(19')-C(20')	111.8(5)
C(8)-N(3)-Fe(1)	116.63(12)	C(27)-C(22)-C(23)	121.96(17)
C(22)-N(3)-Fe(1)	122.90(11)	C(27)-C(22)-N(3)	118.15(17)
N(1)-C(2)-C(3)	113.92(17)	C(23)-C(22)-N(3)	119.66(16)
N(1)-C(2)-C(1)	124.16(19)	C(22)-C(23)-C(24)	117.79(18)
C(3)-C(2)-C(1)	121.89(18)	C(22)-C(23)-C(28)	122.07(17)
N(2)-C(3)-C(4)	119.83(19)	C(24)-C(23)-C(28)	120.13(19)
N(2)-C(3)-C(2)	110.52(16)	C(25)-C(24)-C(23)	121.3(2)
C(4)-C(3)-C(2)	129.63(18)	C(24)-C(25)-C(26)	119.7(2)
C(5)-C(4)-C(3)	119.63(19)	C(25)-C(26)-C(27)	122.1(2)
C(4)-C(5)-C(6)	120.53(19)	C(22)-C(27)-C(26)	117.2(2)
C(5)-C(6)-C(7)	119.0(2)	C(22)-C(27)-C(31)	121.38(17)
N(2)-C(7)-C(6)	120.03(17)	C(26)-C(27)-C(31)	121.46(19)
N(2)-C(7)-C(8)	110.29(15)	C(30)-C(28)-C(23)	110.1(2)
C(6)-C(7)-C(8)	129.67(18)	C(30)-C(28)-C(29)	110.6(2)
N(3)-C(8)-C(7)	113.04(16)	C(23)-C(28)-C(29)	112.7(2)
N(3)-C(8)-C(9)	124.20(16)	C(27)-C(31)-C(33)	111.9(2)
C(7)-C(8)-C(9)	122.76(16)	C(27)-C(31)-C(32)	112.5(2)
C(11)-C(10)-C(15)	121.51(19)	C(33)-C(31)-C(32)	109.99(19)
C(11)-C(10)-N(1)	120.75(17)	C(35)-C(34)-Fe(1)	176.11(18)
C(15)-C(10)-N(1)	117.67(18)	C(34)-C(35)-C(36)	176.5(2)
C(12)-C(11)-C(10)	117.74(19)	C(37)-C(36)-C(41)	118.1(2)
C(12)-C(11)-C(16)	120.4(2)	C(37)-C(36)-C(35)	121.4(2)
C(10)-C(11)-C(16)	121.85(19)	C(41)-C(36)-C(35)	120.49(19)
C(13)-C(12)-C(11)	121.8(2)	C(38)-C(37)-C(36)	120.5(2)
C(14)-C(13)-C(12)	119.2(2)	C(39)-C(38)-C(37)	120.4(3)
C(13)-C(14)-C(15)	121.7(2)	C(38)-C(39)-C(40)	119.8(3)
C(14)-C(15)-C(10)	118.0(2)	C(39)-C(40)-C(41)	120.5(3)
C(14)-C(15)-C(19')	117.4(3)	C(40)-C(41)-C(36)	120.7(2)